Development of Control Strategies for Digital Displacement Units

Pedersen, Niels Henrik

DOI (link to publication from Publisher):
10.54337/aau301506073

Publication date:
2018

Document Version
Publisher's PDF, also known as Version of record

DEVELOPMENT OF CONTROL STRATEGIES FOR DIGITAL DISPLACEMENT UNITS

BY
NIELS HENRIK PEDERSEN

DISSERTATION SUBMITTED 2018

AALBORG UNIVERSITY
DENMARK

Development of Control Strategies for Digital Displacement Units

Ph.D. Dissertation

Niels Henrik Pedersen

Dissertation submitted October 24, 2018

Dissertation submitted:	October 24, 2018
PhD supervisor:	Prof. Torben Ole Andersen, Aalborg University, Aalborg, Denmark
Assistant PhD supervisor:	Assistant Prof. Per Johansen, Aalborg University, Aalborg, Denmark
PhD committee:	B.Sc., M.Sc., PhD Birgitte Bak-Jensen (chairman) Aalborg University
	Associate Professor Jerome Jeoffroy University of Southern Denmark (SDU)
	D.Eng. Victor Juliano De Negri Federal University of Santa Catarina
PhD Series:	Faculty of Engineering and Science, Aalborg University
Department:	Department of Energy Technology

ISSN (online): 2446-1636
ISBN (online): 978-87-7210-345-7

Published by:
Aalborg University Press
Langagervej 2
DK – 9220 Aalborg Ø
Phone: +45 99407140
aauf@forlag.aau.dk
forlag.aau.dk

Printed in Denmark by Rosendahls, 2018

Preface

This dissertation has been carried out at the Department of Energy Technology at Aalborg University in the period Sep. 2015 - October. 2018. The work has been submitted to the Faculty of Engineering and Science at Aalborg University in partial fulfillment of the requirements for the degree of Doctor of Philosophy and is submitted in the paper collection format. The thesis has been a part of the HyDrive research project which is funded by Innovation Fund Denmark (Project No. 1305-00038B).

I would like to thank in particular, but not exclusively:

My supervisor, Prof. Torben O. Andersen, for the opportunity in doing this research, as well as the inspiring discussions and great moral support throughout this work.

My co-supervisor Assistant Prof. Per Johansen for countless long and inspiring discussions on different aspects regarding control of digital displacement units, as well as always being willing to provide valuable feedback.

The offices colleagues during my time as a Ph.d. student, Remzija Ćerimagić, Uffe S. Freiberg and Esben Bach-Soerensen for the many enjoyable and fun hours. Thanks for being able to follow their interesting projects as well.

The remaining staff at the Fluid Power and Mechatronics Section at the Department of Energy Technology for providing a great working environment. Thanks for making the conference trips around the world highly enjoyable and memorable.

Finally, I want to thank my girlfriend and family for their patience, support and encouragement during the research period.

Niels Henrik Pedersen
Aalborg University, October 24, 2018

List of Publications

This dissertation has been submitted for assessment in partial fulfillment of the Ph.D. degree. The dissertation is based on the submitted or published scientific papers below. Parts of the papers are used directly or indirectly in the extended summary of the dissertation and referred to as e.g. [Paper **A**]. Co-author statements have been made available to the assessment committee through The Doctoral School of Engineering and Science. The main body of this dissertation is based on the contents of the following papers:

A **Niels H. Pedersen**, Per Johansen and Torben O. Andersen, "Challenges with Respect to Control of Digital Displacement Hydraulic Units". *Modeling, Identication and Control, Vol. 39, No. 2*, 2018, doi:10.4173/mic.2018.2.4.

B **Niels H. Pedersen**, Per Johansen and Torben O. Andersen, "Analysis of Suitable Operation Strategies and the Non-Smooth Effects of Digital Displacement Units", Submitted to *The 10th Workshop on Digital Fluid Power*, Linz, Austria, 2019. Status: Awaiting acceptance.

C **Niels H. Pedersen**, Per Johansen and Torben O. Andersen, "Feedback Control of Pulse-Density Modulated Digital Displacement Transmission using a Continuous Approximation". *Submitted to IEEE/ASME Transactions on Mechatronics*, October 12, 2017. Status: Under 3rd revision.

D **Niels H. Pedersen**, Per Johansen and Torben O. Andersen, "LQR Feedback Control Development for Wind Turbines Featuring a Digital Fluid Power Transmission System". In *Proc. of the 9th Fluid Power Net International Ph.D. Symp. on Fluid Power*, Florianópolis, Brazil, 2016, ISBN: 978-0-7918-5047-3, doi:10.1115/FPNI2016-1537.

E **Niels H. Pedersen**, Per Johansen and Torben O. Andersen, "Optimal Control of a Wind Turbine with Digital Fluid Power Transmission". *Nonlinear Dynamics*, Springer, 2018, doi:10.1007/s11071-017-3896-0.

F **Niels H. Pedersen**, Per Johansen and Torben O. Andersen, "Event-Driven Control of a Speed Varying Digital Displacement Machine". In *Proc. of the Bath/ASME Symposium on Fluid Power and Motion Control*, Sarasota, USA, 2017, ISBN: 978-0-7918-5833-2, doi:10.1115/FPMC2017-4260.

G **Niels H. Pedersen**, Per Johansen and Torben O. Andersen, "Model Predictive Control and Discrete Analysis of Partial Stroke Operated Digital Displacement Machine". In *Proc. of the IEEE Global Fluid Power Society PhD Symposium*, Samara, Russia, 2018, ISBN: 978-1-5386-4785-1, doi:10.1109/GFPS.2018.8472366

H **Niels H. Pedersen**, Per Johansen, Anders H. Hansen and Torben O. Andersen, "Model Predictive Control of Low-Speed Partial Stroke Operated Digital Displacement Pump Unit". *Modeling, Identication and Control, Vol 39, No. 3*, 2018, doi:10.4173/mic.2018.3.3.

I **Niels H. Pedersen**, Per Johansen, Lasse Schmidt, Rudolf Scheidl and Torben O. Andersen, "Control and Performance Analysis of a Digital Direct Hydraulic Cylinder Drive". Submitted to *International Journal of Fluid Power*, June 14, 2018. Status: Under review.

J **Niels H. Pedersen**, Per Johansen, Rudolf Scheidl and Torben O. Andersen, "Non-Linear Hybrid Control Oriented Modelling of a Digital Displacement Machine". In *Proc. of 9th Workshop on Digital Fluid Power*, Aalborg, Denmark, 2017.

K **Niels H. Pedersen**, Per Johansen and Torben O. Andersen, "Four Qudrant Hybrid Control Oriented Dynamical System Model of Digital Displacement Units". In *Proc. of the Bath/ASME Symposium on Fluid Power and Motion Control*, Bath, UK, 2018.

L **Niels H. Pedersen**, Per Johansen and Torben O. Andersen, "Investigation of Concepts and Operation Strategies for a Wind Turbine with a Digital Fluid Power Transmission", 2017. Status: Not submitted

In addition to the papers above, the following paper has also been written during the Ph.D. period:

- **Niels H. Pedersen**, Soeren C. Jensen, Rico H. Hansen, Anders H. Hansen and Torben O. Andersen, "Control of an Energy Efficient Hydraulic Cylinder Drive with Multiple Pressure Lines". Submitted to *Modeling, Identication and Control*, May 29, 2018. Status: Under review.

Abstract

To cope with the ever-increasing demand for energy efficient and reliable fluid power solutions, research within newly emerging digital hydraulic concepts is conducted in both academia and industry. A high potential digital fluid power concept is the so-called digital displacement technology, where numerous pressure chambers are controlled individually by electromechanical actuated on/off valves to obtain the desired displacement throughput. The feature of controlling the pressure chambers individually enables efficient reduction in the committed displacement, since pressure chambers may be held inactive in an idling mode which entails very low losses. The technology is assessed to have potential as being the core component of future transmission solution for high power renewable energy take-off systems in e.g. wind and wave energy. Furthermore, the digital hydraulic concept may lead to a paradigm shift within hydraulic drives where the technology may directly replace conventional fluid power pump and motor units. The present thesis concerns development of control strategies for digital displacement fluid power machines which is an important aspect with respect to successfully market deployment of the technology.

The present work focuses on development of control design models of digital displacement (DD) units, enabling dynamical analysis and control synthesis. The models must describe the important dynamics of the machine with respect to system wide control, where one or more DD units are utilized in a hydraulic application. It is desired that the models can describe the fundamental machine characteristics independent of operation conditions, i.e. speed, displacement fraction, direction of motion, pumping or motoring, etc. Furthermore, it is beneficial that the models are simple, and the applied control theory is relatively uncomplicated and well known. This enables model-based feedback control design without very complex and time-consuming algorithms. However, these two objectives often come with a compromise, where a more general description often lead to a more complex model and control algorithms, and vice versa. Therefore, models with a variety of complexity and physical accuracy are developed, where the simplest are limited

to only apply under certain operation conditions.

A preliminary study is conducted to identify the control challenges related to such non-smooth dynamical system. The study shows that the dynamics of the machine is highly dependent on the applied operation and control strategy. Furthermore, it is found that within a limited operation region, the fundamental dynamical behavior may be described by both continuous and discrete approximations. Control synthesis for such systems are well known and methods related to both linear and nonlinear systems may be applied. Controller synthesis based on both deterministic and stochastic optimal state feedback control, as well as model predictive strategies has been applied to obtain the desired performance.

More complex dynamical system theories have been studied in the aim of obtaining a more accurate and general control design model description. Since the system dynamics is governed by nonlinear continuous differential equations and the valves are limited to being either open or closed and may only be altered in discrete intervals, the system dynamics belongs to the class of hybrid dynamical systems. Hybrid dynamical system theory can describe the dynamics of such system comprising both nonlinear continuous and non-smooth discrete elements. However, the control law for such system is based on stability proofs relating to both nonlinear continuous and discrete stability theory. The analysis and control synthesis for hybrid systems are in general considered quite complex even for relatively simple systems.

The research documented in this dissertation has contributed with an investigation of the underlying challenges related to control of a complex dynamical system comprising of nonlinear, continuous, discrete, binary and operation altering dynamical elements. The developed control design models are meant as the foundation in the process of designing feedback controllers for digital displacement units. Since the presented analysis tools are independent on which application the machine is used in, only a minor effort has been put into optimized control performance for a specific applications.

Resumé

For at imødekomme den stadigt stigende efterspørgsel af energieffektive og pålidelige hydrauliske løsninger udføres der forskning inden for nyudviklede digitale hydrauliske koncepter, både akademisk og industrielt. Et digitalt hydraulisk koncept med højt potentiale er den såkaldte digitale fortrængnings teknologi, hvor adskillige trykkamre styres individuelt ved brug af elektromagnetisk aktuerede ventiler for at opnå den ønskede fortrængning. Funktionen med at styre trykkamrene individuelt muliggør en effektiv reduktion i den ønskede fortrængning, da trykkamre kan holdes inaktive i tomgangstilstand, hvilket medfører meget lave tab. Teknologien vurderes at have et potentiale som den fremtidige hovedkomponent i energi effektive drivsystem til vedvarende energi applikationer, f.eks. vind- og bølgeenergi. Desuden kan det digitale hydrauliske koncept føre til et paradigmeskifte inden for hydrauliske drev, hvor teknologien direkte kan udskifte konventionelle hydraulik pumper og motorenheder. Den foreliggende afhandling omhandler udvikling af regulerings strategier til disse digital hydrauliske maskiner, hvilket betragtes som et vigtigt aspekt med hensyn på succesfuld markeds implementering af teknologien.

Dette arbejde fokuserer på udvikling af modeller af digitale fortrængning (DD) enheder, der muliggør dynamisk analyse og regulator design. Modellerne skal beskrive maskinens vigtigste dynamik med hensyn til systemstyring, hvor en eller flere DD-enheder anvendes i en hydraulisk applikation. Det er ønsket, at modellerne er i stand til at beskrive de grundlæggende maskinegenskaber uafhængige af driftsbetingelser, dvs. hastighed, fortrængnings forhold, bevægelsesretning, pumpe eller motor operation, osv. Det er endvidere gavnligt, at modellerne er enkle, og den anvendte reguleringsteori er forholdsvis ukompliceret og velkendt, således at modelbaseret regulator design kan udføres uden meget komplekse og tidskrævende algoritmer. Disse to mål kommer ofte med et kompromis, hvor en mere generel beskrivelse ofte fører til en mere kompleks model samt regulerings algoritmer og omvendt. Derfor udvikles modeller med varierende kompleksitet og fysisk

nøjagtighed, hvor de mest enkle er begrænset til visse driftsforhold.

En indledende undersøgelse udføres for at identificere reguleringsudfordringerne i forbindelse med et sådant ikke-glat dynamisk system og viser, at maskinens dynamik er stærkt afhængig af den anvendte drift og regulerings strategi. Undersøgelsen viser, at den grundlæggende dynamiske opførsel inden for en begrænset operationsregion kan beskrives af både kontinuerlige og diskrete tilnærmelser. Regulator design til sådanne systemer er velkendt, og metoder relateret til både lineære og ikke-lineære systemer kan anvendes. Kontrol design baseret på både deterministisk og stokastisk optimering, samt model forudsigende strategier er blevet anvendt.

Mere komplekse dynamiske systemteorier er blevet undersøgt med det formål at opnå en mere præcis og generel modelbeskrivelse til regulator design. Da systemdynamikken består af ikke-lineær kontinuerlige differentialligninger, og ventilerne er begrænset til at være enten åbne eller lukkede og kun kan ændres i diskrete intervaller, tilhører systemdynamikken hybrid systemer. Hybrid dynamisk systemteori er i stand til at beskrive dynamikken af et sådant system, der omfatter både ikke-lineære kontinuerlige og ikke glatte diskrete elementer. Regulator design for et sådant system er imidlertid baseret på stabilitetsbeviser, der omfatter både ikke-lineær kontinuerlig og diskret stabilitetsteori. Analyse- og regulator design for hybridsystemer anses generelt for at være forholdsvis komplekse, selv for relativt enkle systemer.

Forskningen dokumenteret i denne afhandling har bidraget med en undersøgelse af de underliggende komplikationer relateret til regulering af et komplekst dynamisk system bestående af ikke-lineære, kontinuerlige, diskrete, binære og hukommelseselementer. De præsenterede modeller skal ses som fundamentet i processen med at udfører modelbaseret tilbagekoblings regulering af digitale fortrængnings enheder. Kun en mindre indsats er derfor blevet lagt i optimal ydeevne af specifikke applikationer, da de præsenterede analyseværktøjer er uafhængige af i hvilken applikation maskinen anvendes.

Contents

Part I

Extended Summary

Chapter 1

Introduction

The main objective of this thesis is development of control strategies for digital displacement machines (DDMs), where the primary focus is put towards strategies that utilizes model based feedback control design. The DDM is an emerging type of digital fluid power pump-motor unit, which has the potential of becoming the solution for future hydraulic drives and transmissions. The prospective application utilization of these machines spans widely due to their high power density and modular construction yielding great scalability and efficiency. With the estimation that wind energy is one of the leading resources in the future energy systems, the DDM technology may lead to a breakthrough in hydrostatic transmission as the solution for increasingly large wind turbine drive trains [59, 77]. A special focus is hence made on utilization of DDMs in a hydrostatic wind turbine transmission. This chapter serves as an introduction to the digital displacement machine and its operation principle and gives an overview of the development of the digital displacement technology.

1.1 Digital Displacement Machine Fundamentals

The DDM technology differs in various ways when comparing to conventional variable displacement fluid power machines (typically axis-piston type, gear type or radial piston type), where the main difference lies in the way that oil displacement to the high- and low-pressure manifold is controlled. In digital displacement units multiple hydraulic cylinders are connected to a common eccentric cam shaft (or cam ring), which employs a reciprocating piston motion similar to the radial piston type machine. The fundamental difference is that oil-displacement between the pressure chambers and the manifolds is individually controlled by fast electro-magnetically actuated on/off valves. Precise timing of the valve switchings is thus the key to obtain high efficien-

cies and great control performance independent of operation conditions. A fundamental description of the DDM is based on the simplified sketch of the radial piston type machine shown in Fig. 1.1.

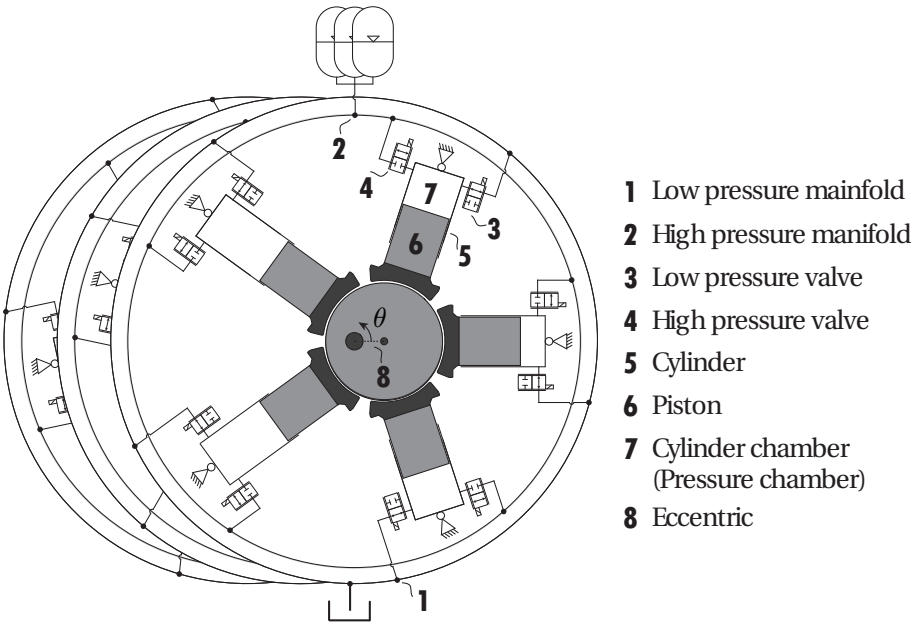

Fig. 1.1: Illustration of the radial piston type digital displacement machine. The shown design has three modules with five cylinders in each module [Paper **A,B,G,H,K**].

It is seen that the cylinders are radially distributed around the eccentric shaft, which results in a reciprocating piston motion being angular shifted with respect to each other. The core feature of the digital displacement technology is that each pressure chamber may be controlled individually by the electro-magnetically actuated and leakage free seat valves. A more detailed illustration of a single cylinder and the configuration of the valves is shown in Fig. 1.2. The high pressure valve (HPV) is of type normally closed, while the low pressure valve (LPV) is of type normally open. In case of a failure, a spring ensures that the valves are in the original configuration, where the chamber is depressurized. By manipulating the state of the high- and low-pressure valves accordingly to the piston position each pressure chamber may be reconfigured individually to operate in one of the three modes; pumping, motoring and idling. Additionally, there are two distinct operation strategies, namely full- and partial stroke. In full stroke, the decision of operation mode is done on a stroke-by-stroke basis at a specific piston position and the chosen mode is maintained throughout the full stroke. In partial stroke operation, only a fraction of the full stroke is used while the machine

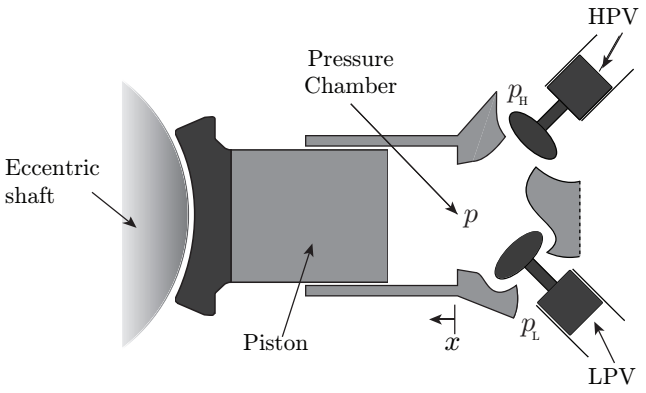

Fig. 1.2: Illustration of the individual pressure chamber and the configuration of the corresponding valves [Paper **A,B,C,H,I,J,K**].

is idling in the remaining part. An illustration of the three operation modes with a full stroke strategy is shown in Fig. 1.3.

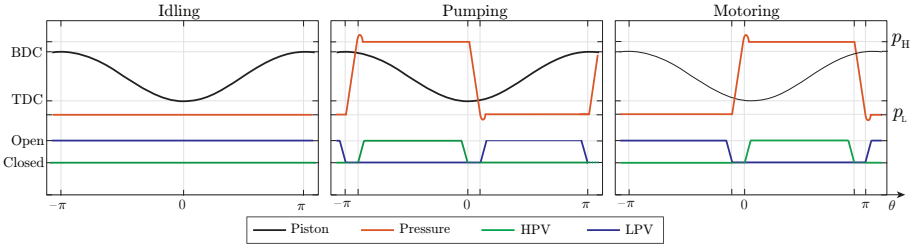

Fig. 1.3: Illustration of the three operation modes of the digital displacement machine, being pumping, motoring and idling [Paper **B**].

A full stroke strategy is considered the simplest, since the state (open or closed) of the HPV and LPV may only be changed at specific piston positions. Since the piston position is kinematically determined by the shaft angle, the valve states are changed at specific local shaft angles located near either top dead center (TDC) or bottom dead center (BDC). To understand the working principle, descriptions of the three operation modes are made:

- **Idling:** The LPV is kept open and the HPV is kept closed during the full revolution cycle. As a result, the chamber pressure is maintained low, while oil is displaced to and from the low-pressure manifold. This way the net displacement is zero and due to the low chamber pressure, the losses are very low in idling mode.

- **Pumping:** The LPV is closed just prior to BDC, such that a pressure buildup is created due to fluid compression as the piston moves towards TDC. As the chamber pressure exceeds the high pressure, the HPV is passively opened due to pressure force and a pressurized fluid flow is created towards the high pressure manifold. At TDC the HPV is again closed and as the volume increases right after, the pressure decreases below the low pressure. As a result of the created suction effect, the LPV is passively opened and maintained open during piston contraction, until the cycle is repeated. Alternatively, based on the machine design (pump only), a passive check-valve may be used as the HPV. Using such setup only gives a minor shift to the shown timing scheme without changing the working principle.

- **Motoring:** Is approximately a reflection of the pumping mode around zero angle, where the LPV is closed near ahead of TDC. This results in a chamber pressurization used for passive opening of the HPV at TDC. As the chamber volume is increased when moving towards BDC, pressurized fluid is withdrawn from the high pressure line and used as the driving mechanism of the piston and common shaft. Near ahead of BDC, the HPV is closed and due to the suction effect created by the pressure decrease, a passive opening of the LPV is generated. The LPV is afterwards held open during the upstroke, until the cycle is repeated. Contrary to pumping mode, motoring requires active closing of both valves.

In full stroke operation the altering of valve states is made in the proximity of either TDC or BDC, where the flow rates are low. Since both the pressure difference across the valves and the flow rates are low, the losses and the required actuation power are reduced to a minimum. The machine displacement throughput is seen to be determined by the ratio of active chambers (pumping or motoring), why the machine displacement throughput per revolution is quantized by the number of pressure chambers.

In partial pumping stroke operation, the LPV is closed at a later piston position, such that the displacement fraction is reduced to the desired value. Similarly, in partial motoring stroke operation the HPV is closed at an earlier position, such that the desired displacement fraction is obtained. This feature yields the possibility of obtaining any displacement fraction during each stroke for every cylinder. Despite that the valve states are still altered at low pressure difference, it may occur at large fluid flows which brings increased losses as well as flow/pressure spikes. In addition, the complexity of achieving precise valve control is increased as the flow rates and closing angles are varying. A more detailed description of the operation modes is made in Chap. 2 concerning control complications with respect to these machines.

How the actuation forces that are necessary to obtain the desired valve opening and closing characteristics are generated is considered out of scope of this thesis. For more information about this, Roemer [67] and Noergaard [52] have made a tremendous contribution to the design and optimization of these valves for improving the machine efficiency and obtain great valve performance.

1.2 Development of Digital Displacement Machines

The following provides an overview of the research and development related to the digital displacement technology. The overview includes the most significant works carried out in both industry and academia.

The concept behind the digital displacement (DD) technology was established at Edinburgh University in the 1980s by a team of researchers led by Stephen Salter. The initial work were originated in the development of an energy efficient power take-off system for renewable energy applications, from which ideas and possibilities were published in 1984 [70]. The first patent on the DD technology was filed in 1989 (acc. 1994) for the pump design [71], followed by the motor design in 1990 (acc. 1995) [72]. This led to the founding of the company Artemis Intelligent Power Ltd. (AIP) in 1994, which continued to develop the technology. The first constructed DD unit was made at 18 cc/rev scale [63], and was later upscaled to a simple 1.5 kW demonstrator [39]. With focus on demonstrating the potential of the DD concept, AIP has applied it in a wide range of different applications; wind turbine transmissions, wave power take-off systems, commercial vehicles (cars and buses) and off-road vehicles (excavators and heavy equipment) [76, 83]. During the years AIP has been involved with several major industrial partners with the aim of improving and commercializing the technology. Since 1998 AIP has been working with Sauer Danfoss (now Danfoss Power Solutions) on mobile DD equipment and off-road vehicles [63, 89]. In 1999 the company Dana became involved, with the aim of developing hydraulic hybrid vehicle transmissions [63]. This partnership lasted until 2006 where Bosch Rexroth overtook the license and are of today still an active partner. In 2008 the DD technology was demonstrated in a BMW 530i and showed promising fuel savings of up to 50 %. Following this, AIP has been developing a retrofittable hybrid transmission for a city bus based on the DD technology showing up to 27 % energy consumption reduction [82]. Despite the large amount of research regarding the digital displacement technology, only one product has made its market appearance and was introduced in 2015. This product is a 12-piston 96 cc/rev DD pump with operation speeds of up to 1800 rpm and pressures up to 350 bar. An illustration and a picture of the E-dyn 96 cc/rev DD pump is shown in Fig. 1.4. The 12 cylinders are arranged in three mod-

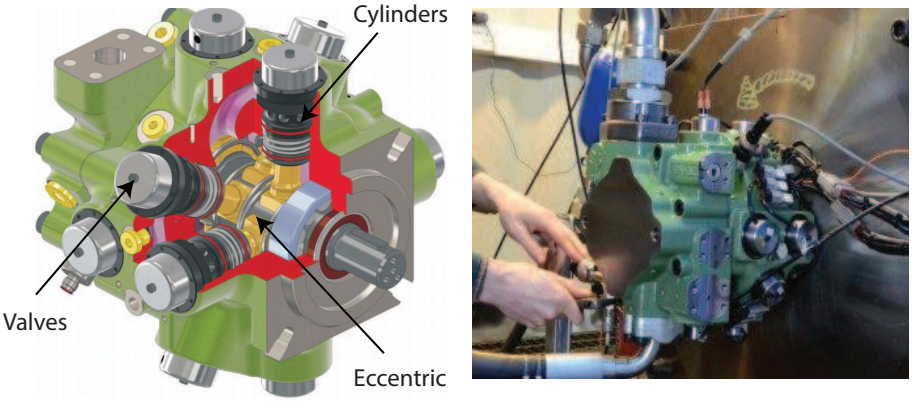

Fig. 1.4: Illustration and picture of the E-dyn 99 cc/rev DD pump [42,44].

ules of four and comprises of electrically actuated solenoid valves. However, the DD unit is limited to pumping operation due to the HPV being a passive check-valve. In early 2017, it was announced that a project for developing digital displacement hybrid rail transmission is in progress, where a three month test period has started in December 2017 [68]. Recently in 2018, AIP has unveiled its plans for using the DD technology in the aeospace industry [43].

The plans for development of a large scale DD wind turbine hydrostatic transmission were established in the early years of the DD technology and a paper has been published on the subject in 2006 [62]. A 1.5 MW wind turbine transmission with a 1 MNm DD pump and two 800kW DD motors running at 1500 rpm was tested in 2009 [63]. In 2010 Mitsubishi Heavy Industries (MHI) acquired AIP with the intention of developing a large scale fluid power transmission system for wind turbines [22]. Plans for a 7 MW hydrostatic DD based wind turbine transmission were announced in 2013 [50] [87] and in 2015 the complete system was tested in Scotland [23]. The 7 MW turbine drive train prototype comprises of a 7 MW slow-rotating ($\omega < 15$ rpm) digital cam-ring pump attached to the turbine rotor and two 3.5 MW fast-rotating ($\omega > 1000$ rpm) digital radial piston motors. Fig. 1.5 shows a picture of the turbine drive train set-up. Published results regarding operation of the transmission are very limited, but it has been reported that the total efficiency of the transmission is 94 % (98 % and 96 % for the pump and motor respectively) in a wide operation range [49]. Also, in 2015 MHI deployed a 7 MW digital hydrostatic transmission at Yokoshima, Japan for further testing of the technology. However, no results have been made publicly available. An undergoing project at AIP as of 2017 concern the implementation of the DD technology in wave power take-off systems [41,55].

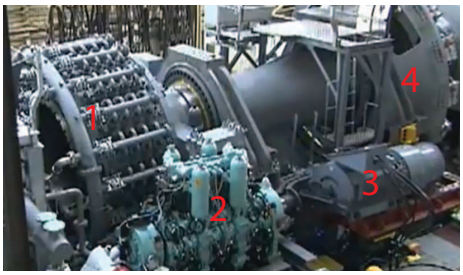

Fig. 1.5: 7 MW wind turbine transmission based on the digital displacement technology [76].

Another commercial company with research activities related to the DD technology is Diinef A/S and Chapdrive A/S, whose main focus is on low-speed high-torque machines, with valves that are capable of opening against large pressure forces [5, 36, 85]. A planned application is for large offshore winch drives, which has resulted in the forming of the project Digiwin [7].

Research related to the digital displacement technology has also been explored in academia, where focus has been on various subcomponent of the DD machine. Initially as mentioned, the fundamental development of the DD technology began at Edinburgh University, Scotland, starting in the 1980s. Two Ph.d. dissertations were published in the 1990s at the University of Edinburgh on the fundamentals of the digital displacement machine [8, 61]. An industrial Ph.d. dissertation between Edinburgh University and AIP regarding the fundamentals of a digital displacement hydrostatic transmission systems was published in 2007 [3]. Several other research institutions have made contributions to the development of the technology. Purdue University, US, has conducted research regarding digital displacement motor and pump concepts, where focus has mainly been on development of operation strategies and valve timing control [20,21,47,48]. Tampere University of Technology, Finland, has been developing a hydraulic power management system (DHPMS) similar to the digital displacement pump-motor concept with multiple independently controlled outlets [14,15,17,18]. The main focus has been on development of an energy efficient digital flow control unit and special effort has been put in the development of the fast switching valves for the technology [29, 37, 88].

Research on the digital displacement machines has also been conducted at Agder University, Norway, lately. Special attention has been on offshore applications with high power requirement. Work on drilling and winch drives have been investigated and it is expected that the DDM is a viable machine solution for energy efficiency improvement of these systems [12, 53, 54].

Since 2010 the Department of Energy Technology at Aalborg University (AAU), Denmark, has performed research and development of the DD tech-

nology, where the first initial experimental studies were conducted on a 1-piston digital pump prototype [66]. Further research included design and optimization of the electromagnetic valve actuation system, wear and reliability studies, as well as the tribological interface and fluid mechanics related to the digital machine [24, 67]. A drawing of a 7.3 MW digital displacement motor that has been designed at AAU is shown in Fig. 1.6.

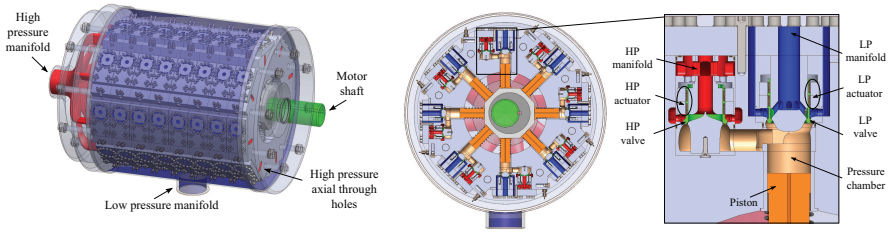

Fig. 1.6: Drawing of the radial piston type digital displacement motor designed at AAU with 64 cylinders and nominal speed of 1500 rpm [67].

The depicted DD motor comprises of eight radially distributed cylinders banks with eight cylinders in each bank. The focus of the research has mainly been on the design and optimization of the fast switching digital valves. The shown design resulted in a valve with a measured response time of 1.8-2.9 ms and a pressure drop below 0.5 bar at a flow rate of 600 l/min. Successfully deployment of the digital hydraulic machines is highly dependent on the performance and reliability of these valves. Several research institutes are focusing on highly efficient and fast actuation valves, which may be candidates for usage in the DD units. Amongst others, Linz center of mechatronics and Johannes Keppler university of Linz, Austria have been a long-time contributor in the development of such digital valves. Alternative DD pump-motor concepts, which relies on robust mechanical valves relative to the seemingly more fragile electronically controlled valves are also being explored [19, 64, 86].

The mentioned milestones in the research and development of the digital displacement technology are summarized in the illustration shown in Fig. 1.7.

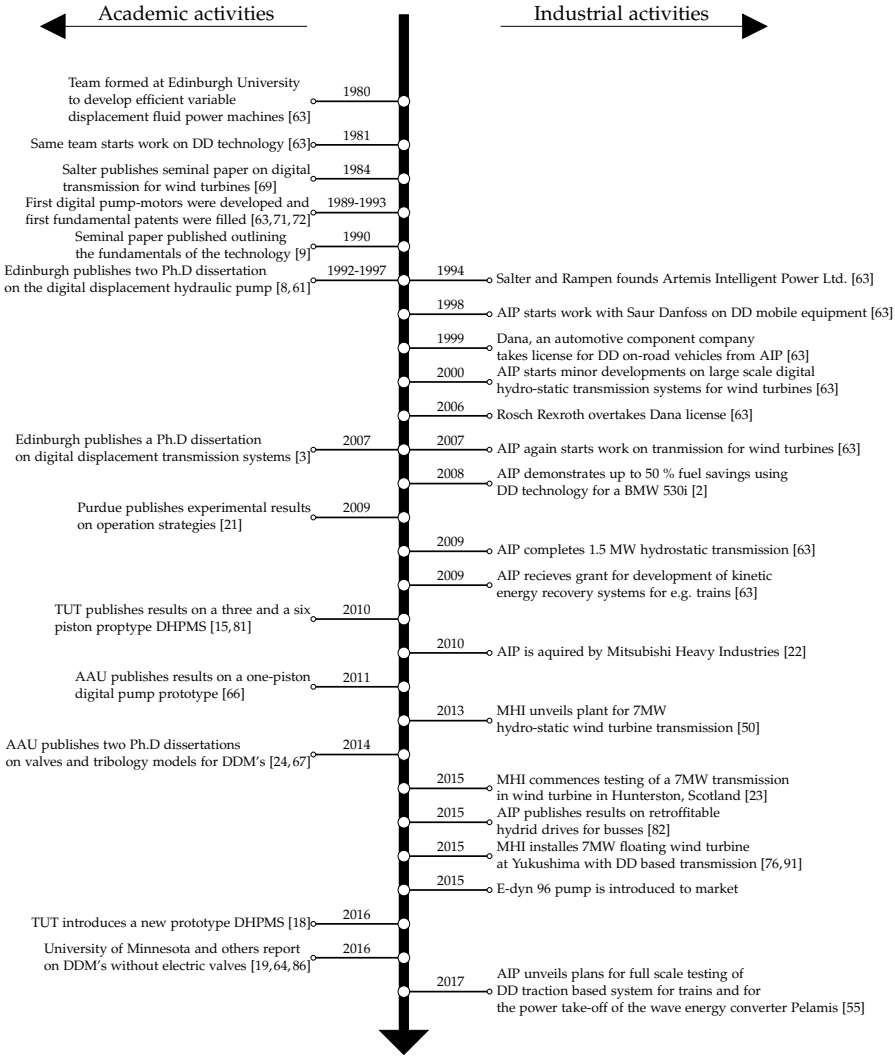

Fig. 1.7: Summarization of the milestones regarding research and development of digital displacement machines. The timeline is made with inspiration from Noergaard [52].

1.3 Features of Digital Displacement Units

The digital displacement technology has the potential of becoming the preferred technology for future hydraulic pump and motor units due to a high number of valuable features. Several of these features have already been mentioned and are further explained in the following, together with several other advantages of the DD technology.

Efficiency

A key feature is the high efficiency that the technology enables compared to conventional fluid power machines. The high efficiency is the result of having very low losses of idling cylinders and only switching the valve states at low pressure difference and low flow rates (full-stroke), as well as having near zero leakage flow through the seat valves. The ability to idle cylinders individually at low pressure enables an efficient reduction of the power throughput. As a result, significantly improved energy efficiencies are obtained at lower displacement ratios compared to conventional fluid power pump-motor units. Controlling the displacement by the ratio of activated pressure chambers has shown efficiencies above 90 % even at part-load operation as shown in Fig. 1.8.

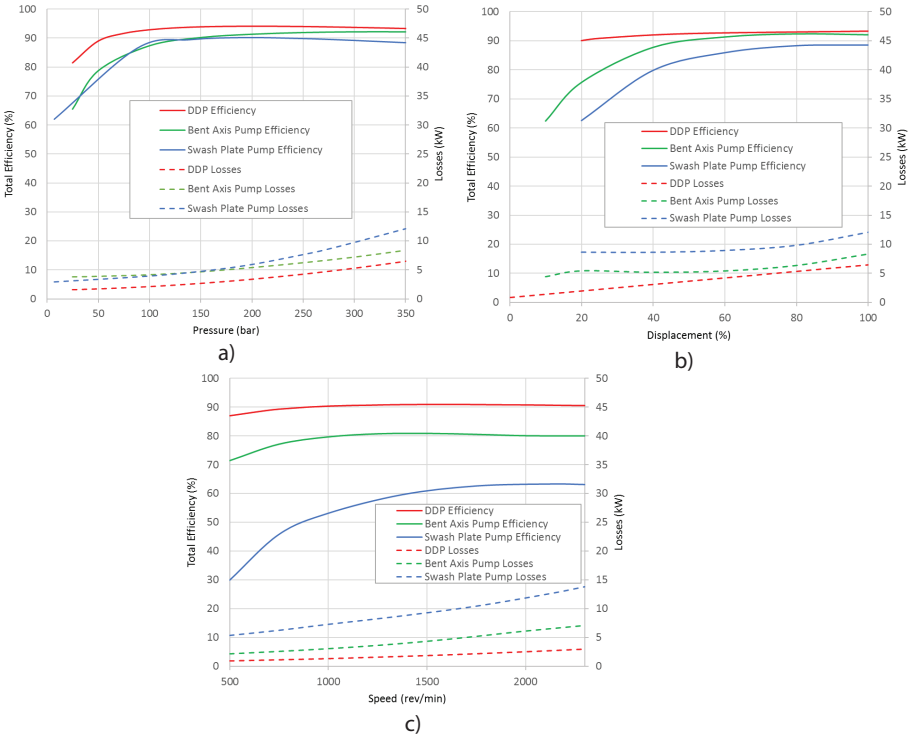

Fig. 1.8: Efficiency map comparison of conventional hydraulic pump pumps and the digital displacement pump. a) 100 % displacement, 1800 rpm. b) 350 bar, 1800 rpm. c) 350 bar, 25 % displacement [90].

It is evident that the efficiency map for a digital displacement machine is significantly higher than those for conventional fluid power machines. At full displacement the DDM has a peak efficiency of approx. 95 %, while at

20 % displacement the machine efficiency is approx. 90 %. It is seen that in approx. 80 % of the shown operation range, the efficiencies are above 90 %, making the DD units a strong competitor to electrical machines in high power applications.

Scalability, Redundancy and Reliability

Due to the modular construction with numerous identical pressure chambers, the scalability of the machine is superb compared to conventional hydraulic units. Additional pressure chambers may simply be added to increase the power rating, whereby the same operation curves are obtained at a lager power rating. This feature omits the requirement to develop new larger cylinders and valves to increase the power rating, which likely increases the development and production costs.

The modular construction directly provides great redundancy, since the operation of the machine is sustained in the case of a pressure chamber failure. Considering the failure of a single pressure chamber, the remaining chambers are still functional, such that the machine functionality is maintained at a fractional lower peak power. Since the machine comprises of many smaller components, a malfunctioned valve may be replaced easily by hand and does not require large and heavy equipment. As a result, the maintenance cost may be lowered for e.g. off-shore wind turbines, which have very high costs related to downtime due to failed components.

The digital displacement unit has the potential of having high reliability, since hydraulic components are known to be robust and operate under rough conditions. However, the small and seemingly fragile electromagnetically actuated valves challenge this feature, which makes them the bottleneck with respect to reliability. Therefore, development of reliable valves is also considered an important research topic with respect to successfully deployment of the technology.

Other Important Features

The digital displacement machine comes with several other features, some of which are worth mentioning are listed below:

- Extensive controllability, where flow, pressure, torque, power, speed and position control is possible.
- Fast response (at high shaft speed) from zero to full oil displacement in half of a revolution.
- Reliable load holding due to the use of leakage free seat valves.
- Requires less cooling due to the higher efficiency.

Since control development for the DDM is the main objective of this work, the first two features are noteworthy and are discussed throughout the remainder of the thesis. Of course, there are several drawbacks related to the technology, where some worth mentioning are; non-smooth output containing a large quantity of ripples, seemingly fragile valves, complex control and distinctive sound pattern. However, since the work hours spent on developing and improving the technology is very limited compared to the work hours spent on electrical rotary machines, there is a large potential of improving the technology. Therefore, one may consider the mentioned problems for challenges rather than drawbacks.

1.4 Aims and Focus of Research

The overall aim of this thesis is the development of control strategies for digital displacement units. Especially, focus is drawn towards control of digital displacement machines in a hydrostatic transmission for a wind turbine which is a high potential application for the technology.

The research is primarily focused on development of control design models that allow for dynamical system analysis and model-based feedback control synthesis. It is considered a crucial task to be able to analyze the system's dynamical behavior if something goes wrong (instability, resonance, limit cycles, malfunctioned pressure chamber, strange behavior, etc.). Therefore, heuristic control methods are not considered, and the research is made with focus on the mathematical framework for describing the system dynamics with respect to control. Simple control structures and methods that are well known, such as linear time invariant (LTI) or discrete linear time invariant (DLTI) are considered beneficial with respect to potential usage in the industry. However, such strategies are often limited to be valid in a minor operation range, why more advanced and general models are demanded.

Therefore, the research is structured such that simple approaches are attempted where possible and the complexity of control design models and strategies are increased based on the difficulty of the control problem and the requirements to the system. Unfortunately, no experimental work has been conducted since a test-setup of the DDM has not been available during the dissertation. However, the developed control models and strategies are validated through simulation models describing the physical system behavior, which has been experimentally verified for a single pressure chamber.

1.5 Main Contributions

The main contributions of this research are:

- Identification of control challenges related to full-stroke and partial-stroke operated digital displacement machines.
- Identification of control challenges related to the design and the application use of the digital displacement machines.
- Development of control design models describing the fundamental dynamics of the digital displacement machines. These models (continuous, discrete and hybrid dynamical system models) allows for dynamic analysis and controller design.
- Development of control strategies related to full-stroke and partial-stroke operated digital displacement machines. This includes usage of modulation strategies for handling the digital behavior.
- Development of control strategies related to application use of digital displacement machines. This thesis has a special focus towards hydrostatic transmission for wind turbines, but also direct cylinder drive applications are considered.
- Control design procedures for controller synthesis. However, only a minor effort has been put into synthesis of controllers for optimal performance, since the work considers a general framework and not one single specific application.

1.6 Reading Guidelines

Chap. 2 presents an investigation of the control challenges related to both full- and partial stroke operation and provides suggestion when to apply which strategy. Also, control related challenges with respect to the design and application use of the DD units are investigated. Understanding the control challenges is considered important for a successful development of control strategies and control design models. The majority of this work is also documented in [Paper **A**].

Chap. 3 provides a review of the state-of-the-art control strategies for the DDM and investigates the dynamical behavior and digital effects of the machine, which is based on the work published in [Paper **B**]. Furthermore, control design models of the DDM is developed based on continuous [Paper **C**], discrete [Paper **D**,**E**,**F**] and hybrid dynamical system theory [Paper **J**,**K**].

The validity and limitations of the individual models are discussed, such that the models may be applied accordingly. Both control strategies for full and partial stroke operation are proposed and suggestions when to apply which strategy are provided. Only a brief overview of the control models and strategies are given, while references to published papers on the given subject are provided for more detailed informations.

Chap. 4 discusses the applicability and limitations of the developed control design models. Suggestions on control design methods are provided and a brief description of the mathematical design framework is given [Paper **D**,**E**,**F**,**G**,**H**]. Several proposals on further important aspect related to this work are provided, since additional research within control of DDMs is required to enhance the technology further.

Chapter 2

DDM Control Challenges

Often the control problem for a dynamical system (continuous or discrete) is related to choosing the most suitable control strategy and then tune the controller with respect to the desired performance criteria. Since control of the digital displacement technology is a relatively unexplored field, an important initial step is to identify the control challenges related to the non-smooth machine behavior and the application it is used in. The identification of control challenges is meant as a foundation in the development of control design models. Instead of deriving a complex model for investigation of the control challenges, a relatively simple model with idealized behavior is used, which maintains the fundamental dynamics and all the challenges with respect to machine level control.

2.1 Establishment of Mathematical Model

The derivation of the relatively simple mathematical model is based on the illustration of the digital displacement machine shown in Fig. 1.1 and the single pressure chamber shown in Fig. 1.2.

The piston displacement, x, for a single pressure chamber is kinematically described as function of the shaft angle by

$$x_i = r_\mathrm{e}\ (1 - \cos(\theta_i)) \qquad \theta_\mathrm{i} = \theta + \frac{2\,\pi}{N_\mathrm{c}}\,(i-1) \qquad i \in \{1, \ldots, N_\mathrm{c}\} \tag{2.1}$$

where N_c is the number of cylinders and r_e is the eccentric radius, such that the piston stroke length is $\bar{x} = 2\,r_\mathrm{e}$. The cylinder chamber volume, V, and its

time derivative are then described by

$$V_i = \frac{V_\mathrm{d}}{2}\,(1-\cos(\theta_i)) + V_0 \qquad \dot{V}_i = \frac{V_\mathrm{d}}{2}\,\sin(\theta_i)\,\dot{\theta} \tag{2.2}$$

where V_0 is the minimum chamber volume and $V_\mathrm{d} = 2\,r_\mathrm{e}\,A_\mathrm{p}$ is the displacement volume, where A_p is the piston area. The cylinder pressure dynamics is described by the continuity equation and given to be

$$\dot{p}_i = \frac{\beta_\mathrm{e}}{V_\mathrm{i}}\,\left(Q_{\mathrm{H},i} - Q_{\mathrm{L},i} - \dot{V}_i\right) \tag{2.3}$$

where Q_H and Q_L are the flows through the high and low pressure valve respectively and β_e is the effective bulk modulus being considered constant. The oil-flows through the valves are described by the orifice equation and given to be

$$\begin{aligned} Q_{\mathrm{L},i} &= \frac{\bar{x}_\mathrm{L}}{k_\mathrm{f}}\,\sqrt{|p_i - p_\mathrm{L}|}\,\mathrm{sign}\,(p_i - p_\mathrm{L}) \\ Q_{\mathrm{H},i} &= \frac{\bar{x}_\mathrm{H}}{k_\mathrm{f}}\,\sqrt{|p_\mathrm{H} - p_i|}\,\mathrm{sign}\,(p_\mathrm{H} - p_i) \end{aligned} \tag{2.4}$$

where k_f is the valve flow coefficient, while $\bar{x}_\mathrm{L} \in [0,1]$ and $\bar{x}_\mathrm{H} \in [0,1]$ are normalized valve plunger positions. The torque from each pressure chamber is derived to be given by

$$\tau_i = \frac{d\,V_i\,(\theta_i)}{d\theta}\,p_i = \frac{V_\mathrm{d}}{2}\,\sin(\theta_i)\,p_i \tag{2.5}$$

The parameter values used in the simulation model do not change the dynamical behavior significantly. For this particular simulation the values provided in Tab. 2.1 are utilized.

Table 2.1: Parameter values for the digital displacement machine simulation model.

Parameter	Symbol	Value	Unit
Eccentric radius	r_e	25	mm
Piston area	A_p	30.7	cm^2
Minimum chamber volume	V_0	153.4	cm^3
Effective bulk modulus	β_e	12000	bar
Valve flow coefficient	k_f	1e6	$\mathrm{m}^3/\sqrt{\mathrm{Pa}}$
Low pressure	p_L	20	bar
High pressure	p_H	300	bar
Rotational speed	$\dot{\theta}$	100	rpm

The dynamics of the pressure chamber is illustrated by a polar phase plot of the pressure trajectories for a full and a partial stroke operation and are shown in Fig. 2.1.

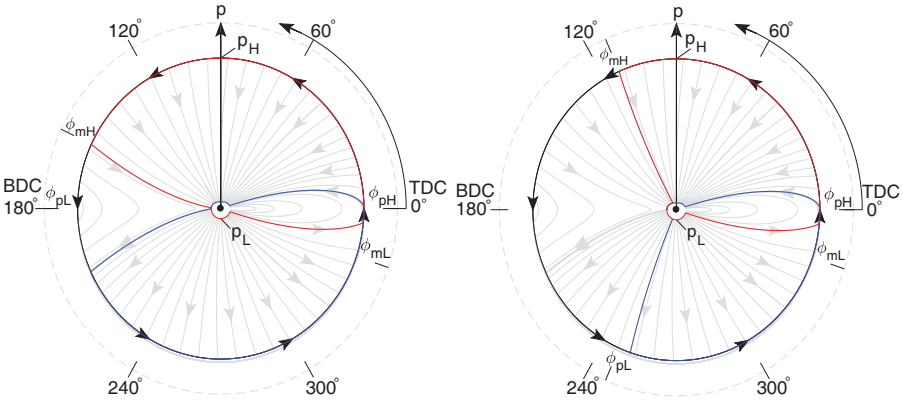

(a) Full stroke operation phase plot. **(b)** Partial stroke operation phase plot.

Fig. 2.1: Polar phase plot of the pressure trajectories of a single pressure chamber. Red trajectory indicates a motoring stroke and blue trajectory indicates a pumping stroke [Paper **A**,**B**,**K**].

The motoring strokes (full and partial) are initiated by closing the LPV at ϕ_{mL} shortly before TDC, which results in a pressurization due to piston extension. As the pressure increases above the high pressure, the HPV is passively opened at TDC due to the generated pressure force. The motoring stroke is ended by closing the HPV at ϕ_{mH}, which results in a depressurization due to piston retraction. As the pressure decreases below the low pressure, the LPV is passively opened due to the generated suction force. The pumping operation is seen to be a reflected version of the motoring stroke around a horizontal line between BDC and TDC. The pumping stroke is initiated by closing the LPV at ϕ_{pL} and due to piston retraction, the pressure is increased towards TDC and results in a passive opening of the HPV. Therefore, the first part of the pumping stroke generates no flow and torque, while the last part of the motoring stroke generates no flow and torque.

In the following investigation of control challenges, a quasi-static scenario is considered, where the pressure build-up in a chamber takes place instantaneously. The chamber pressure is hence allowed to jump between low and high pressure momentarily. This simplification is valid when describing the fundamental machine dynamics, since the pressure build up as function of the shaft angle is fast as seen in Fig. 2.1. As a result of the simplification, $Q_{\mathrm{H}} \vee Q_{\mathrm{L}} = \dot{V}_{\mathrm{c}}$, depending on whether the high or low pressure valve is open. From the above model description, the flow and torque throughput as

function of the displacement volume are given by

$$\mathcal{D}_i = \frac{V_\mathrm{d}}{2} \sin(\theta_i)\ \bar{u}_i \qquad Q_{\mathrm{H},i} = \mathcal{D}_i\, \dot{\theta}_i \qquad \tau_i = \mathcal{D}_i\, p_i \tag{2.6}$$

where $\mathcal{D}$ is the displacement volume and $\bar{u} \in \{0, 1\}$ describes whether the pressure chamber is active or inactive. It is seen that the flow and torque throughput are highly nonlinear functions. Additionally, the input, $\bar{u}$, may only be altered at certain angles as identified in Fig. 2.1.

The description of the displacement throughput is used in the following analysis to examine the operation principle of the digital displacement machine. The control challenges for full- and partial stroke operation are vastly different, since the system behavior is changed based on the operation strategy. Therefore, the control challenges for the two operation strategies are investigated separately.

2.1.1 Full Stroke Operation

In full stroke operation, the decision to either pump or idle during piston extension is made on a stroke-by-stroke basis once for every revolution at a fixed angle. Similarly, the decision to either motor or idle during piston retraction is made once every revolution at a fixed angle. (ϕ_mL and ϕ_pL for motoring and pumping respectively). An illustration of the decision angles is shown in Fig. 2.2.

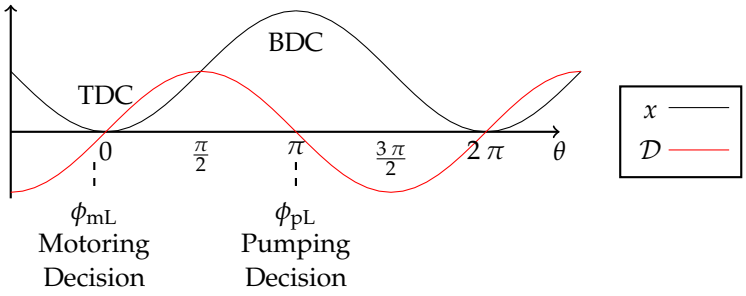

Fig. 2.2: Illustration of the decision angles for pump and motoring using full stroke operation.

It is seen that the decision to either motor or idle (motoring decision) is made at ϕ_mL shortly ahead of TDC and the decision to either pump or idle (pumping decision) is done at ϕ_pL located at BDC. An illustration of the control sampling scheme and displacement responses are shown in Fig. 2.3 for a DDM with 5 cylinders.

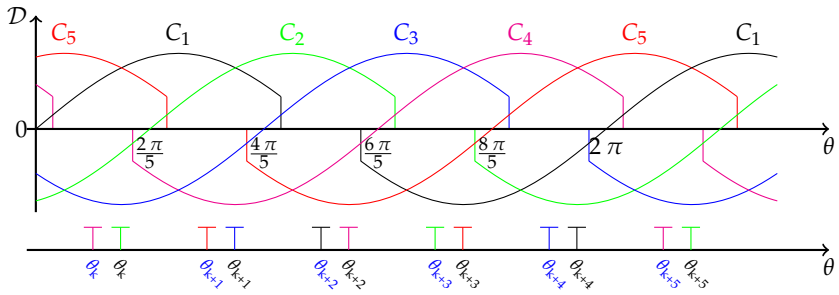

Fig. 2.3: Displacement response and control decision scheme of a full stroke operated DDM using both pumping and motoring strokes. Black samples are for motoring and blue samples are for pumping [Paper **A**].

If the DDM is to supply pressurized fluid as a pump, only the decisions to either pump or idle are made (blue samples). Similar, if the DDM is to operate as a hydraulic motor, only the decisions to either motor or idle are made (black samples). Considering the DDM to operate exclusively as either a motor or pump, a control decision is made for every cylinder at every $2\,\pi\,/\,N_\mathrm{c}$ rad. The synchronous decision angle results in an asynchronous decision time if the machine speed is varying. If the machine is to both pump and motor, only a periodic synchronous decision in the angle domain is obtained. Furthermore, it is seen that the displacement responses are different for the motoring and pumping decision, since the last part of the motoring stroke is not used, while the first part of the pumping stroke is not used.

The control problem is further complicated if the machine is to operate in all four quadrants (Pumping and motoring in both directions of motion), since operation in both direction of motion changes the decision sampling scheme. This is illustrated in Fig. 2.4 with steep changes in the rotational speed between clockwise and counter-clockwise direction of motion. It is seen that if the direction of motion is changed during a motoring stroke, the remaining part of the stroke is committed as pumping. Additionally, the subsequent sample is also for a motoring stroke, but since the direction of motion is reverse, the decision angle ahead of TDC is now located at $\phi^{-}_{\mathrm{mL}} = 2\,\pi - \phi^{+}_{\mathrm{mL}}$.

One interesting control phenomenon occurs when the speed of the machine is zero and the shaft is stationary. At standstill the system is uncontrollable, since the next control update never occurs. Therefore, an external torque is required to bring the machine into motion and is thus also required at startup.

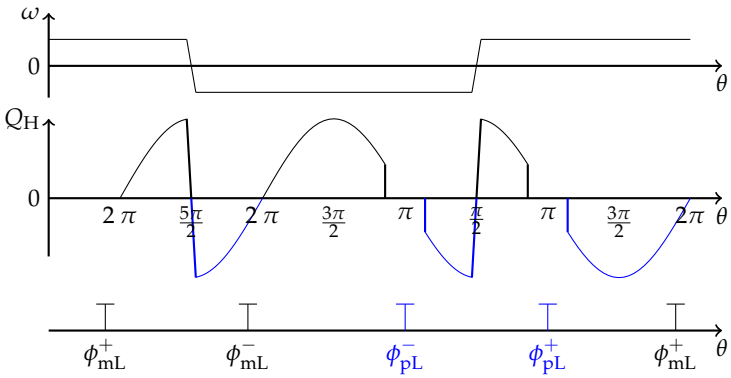

Fig. 2.4: Illustration of response and sampling scheme with motion in both directions. ω is the rotational shaft speed. [Paper **A**].

2.1.2 Partial Stroke Operation

As an alternative to controlling the displacement throughput in discrete steps determined by the ratio of activated cylinders in full stroke operation, the displacement resolution may be increased by utilizing partial stroke operation. Partial stroke operation is characterized by using a continuous fraction of the full stroke for every cylinder. Three different partial stroke operation strategies exist which are illustrated in Fig. 2.5 for pumping.

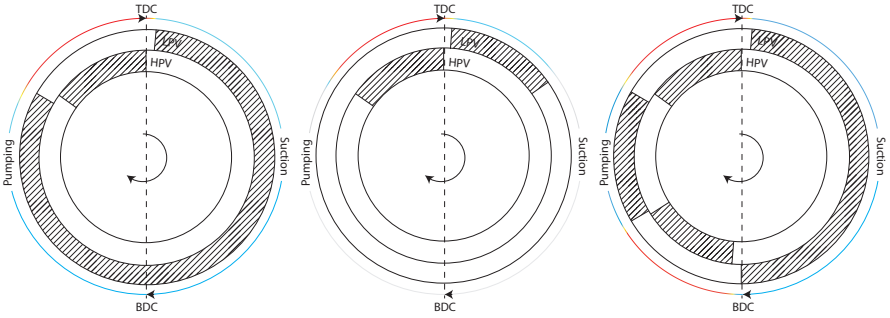

(a) Conventional flow-diverting pumping. **(b)** Flow-limited pumping. **(c)** Sequential flow-diverting pumping.

Fig. 2.5: Partial stroke operation methods: Black hatched area indicates an open valve and white area a closed valve. The outer colored circle represent the pressure level in the chamber. Red is high pressure, blue is low pressure and gray is cavitation pressure. Made with inspiration from [20].

Using the conventional flow-diverting strategy (FDS) shown in Fig. 2.5a, the LPV is closed later in the pumping period to reduce the displacement output compared to full stroke. Although the valve state has to be altered at

higher flow rates compared to full stroke, the pressure difference across the valve is maintained low.

The flow-limiting strategy (FLS) shown in Fig. 2.5b relies on cavitating the pressure chamber by closing the LPV during the suction part at an angle ϕ. As the pressure again rises during the pumping part, the HPV is passively opened at an angle approximately equal to $2\,\pi - \phi$. This strategy entails lower losses due to the marginally lower pressure level. However, reducing the pressure below atmospheric pressure may introduce further complications, such as additional mechanical- and fluid wear [20, 21, 51]. Additionally, a large delay is introduced since the decision is taken in the first part of the revolution and the output is generated in the last part.

In the sequential flow-diverting strategy (SFDS) shown in Fig. 2.5c, the strategy is similar to that in Fig. 2.5a, but the active pumping part is divided into segments. In this example the pumping stroke is divided into two parts, but the strategy may be extended to comprise of multiple parts. This strategy increases the control update rate, since several decisions may be taken for every stroke. Additionally, switchings at high flow rates located at the midpoint between BDC and TDC may be avoided if a displacement fraction of approx. 50 % is desired. However, the method costs more actuation energy since it is required to open the LPV against high pressure difference. Therefore, larger valves that can open/close against high pressure difference are required compared to the other strategies.

The partial stroke methods are also applicable for motoring operation, which are illustrated in Fig. 2.6.

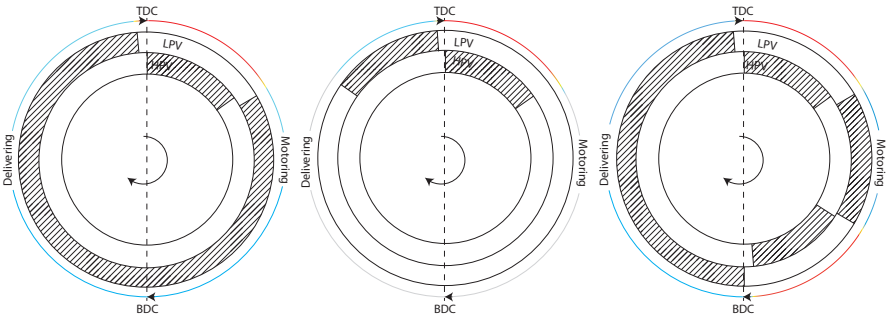

(a) Conventional flow-diverting motoring. **(b)** Flow-limited motoring. **(c)** Sequential flow-diverting motoring.

Fig. 2.6: Partial stroke operation methods: Black hatched area indicates an open valve and white area a closed valve. The outer colored circle represent the pressure level in the chamber. Red is high pressure, blue is low pressure and gray is cavitation pressure. Made with inspiration from [20].

Partial Stroke Control Challenges

The challenges with respect to control of a partial-stroke operated DDM are very different than those identified for full stroke operation. The displacement response in partial stroke operation is peculiar when compared to the response of a conventional dynamical system. This is due to the input being a state altering angle, ϕ that scales the width of the response, rather than a conventional system which input scales the magnitude of the response. To normalize the input, an input variable change is made, such that the input is a displacement fraction $\eta \in [0, 1]$. The input transformation is done by considering the committed displacement fraction for a motoring stroke by use of (2.2).

$$\eta = \frac{V(\phi)}{V(\pi)} = \frac{\frac{V_d}{2}\ (1 - \cos(\phi))}{\frac{V_d}{2}\ (1 - \cos(\pi))} = \frac{(1 - \cos(\phi))}{2} \tag{2.7}$$

The resulting input transformation is then given by

$$\phi(\eta) = \operatorname{acos}(1 - 2\,\eta) \qquad\qquad \eta \in [0,\ 1] \tag{2.8}$$

How the displacement response of the DD unit depends on the input is illustrated in Fig. 2.7.

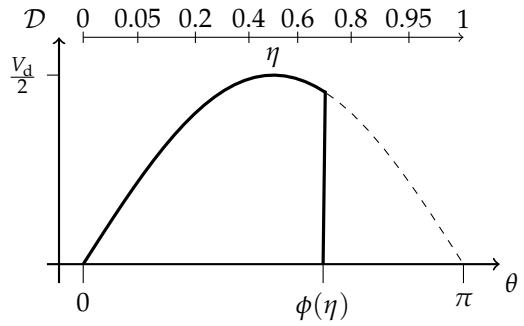

Fig. 2.7: Displacement response as function of the input, $\eta = 0.7$ for conventional partial stroke operation [Paper **A**,**B**].

This highly non-smooth system behavior introduces control challenges, since the input changes the impulse response. In theory, it is possible to change the input, η, continuously until the local shaft angle has exceeded the state changing angle, $\theta_i >= \phi(\eta)$, where the HPV is closed. This yields a high degree of freedom, but also complicates control further since the impulse response is unknown when initiated.

A partial stroke strategy is seen to yield a continuous displacement throughput over a revolution, but that the instantaneous output value for each chamber is determined by the shaft angle and may therefore not be controlled. Considering an angle average displacement over a full revolution, there is an infinite number of combinations that yields the same combined displacement. This is illustrated in Fig. 2.8 where the same integrated displacements (50 %) are committed over a full revolution with two vastly different activation patterns.

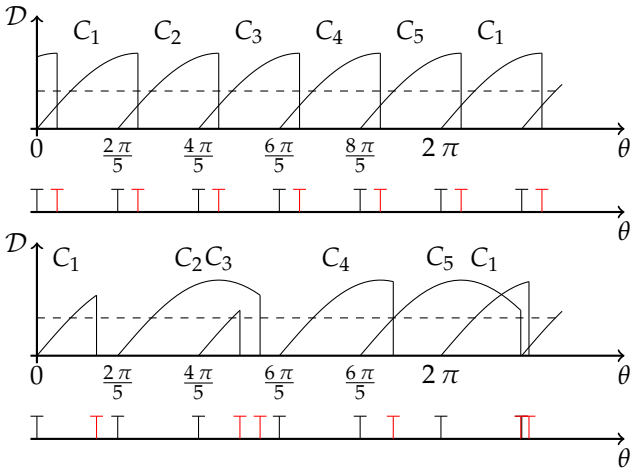

Fig. 2.8: Output displacement response and control decision scheme of a partial stroke operated DDM, using only motoring strokes [Paper **A**].

The top strategy commits 50 % displacement for each pressure chamber and is considered the most simple approach. The bottom strategy is chosen arbitrarily to give a total displacement of 50 % over a full revolution and is seen to be much more sophisticated. Since the flow is largest as the midstroke, the pressure spikes and energy cost due to switching is also largest at this point. Therefore, it may be beneficial to avoid switching near maximum flow rates. However, including the energy and pulsation cost in the control strategy further increases the control complexity.

Sequential Partial Stroke Control Challenges

In sequential partial stroke, the valves are opened and closed independently of the shaft position. Thereby, the control update rate may be significantly increased and is only constrained by the valve actuation time. An illustration of two arbitrary sequential partial stroke operations are shown in Fig. 2.9.

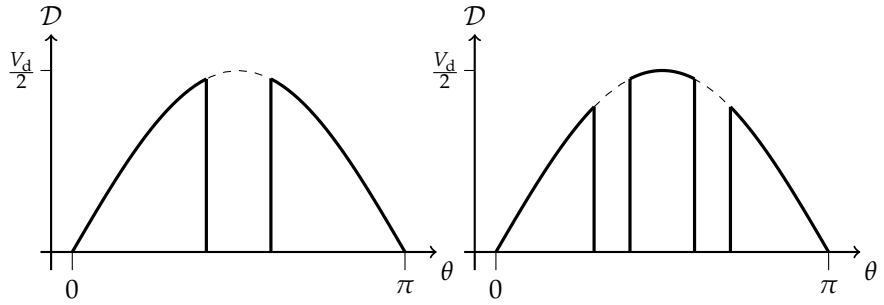

Fig. 2.9: Examples of response yielding a displacement fraction of, $\eta = 0.7$, with sequential partial stroke [Paper **A**].

Although the obtainable displacement fraction during a revolution is continuous and the control update rate may be high, it is not possible to obtain continuous control of the committed displacement. Even if it is theoretically possible to activate and deactivate the pressure chambers infinitely fast, the instantaneous displacement for each pressure chamber is a fixed value depending on the shaft angle as shown in Fig. 2.7. Considering a DD motor, the maximum number of cylinders that may be active simultaneously is $N_{\max} = \text{ceil}\,(N_c/2)$. Since each chamber may be either active or inactive, there is a maximum of $2^{N_{\max}}$ possible displacement combinations for each angle. An illustration of the combinations as function of the shaft angle are shown in Fig. 2.10.

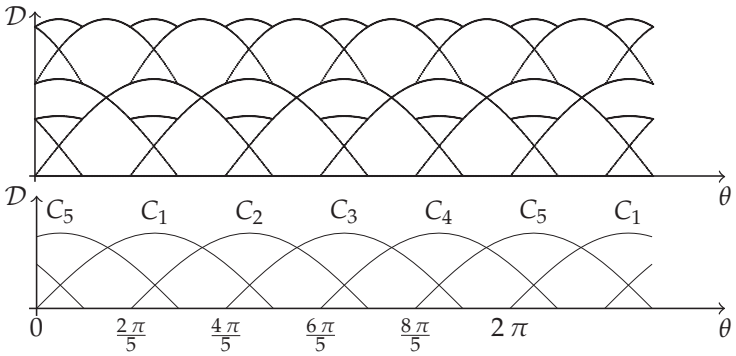

Fig. 2.10: Illustration of the displacement combinations as function of the shaft angle with 5 cylinders [Paper **A**].

With 5 cylinders there are either $2^2 = 4$ or $2^3 = 8$ combinations to choose between at each angle. The shown example is a best-case scenario where the pressure chambers are activated and deactivated instantaneously and very high number of times during a stroke. The intersection points between curves

shown in the top figure are non-unique points, where the same displacement is obtained by two different combinations. If the pressure chambers may both use motoring and pumping strokes, the number of combinations becomes 2^{N_c} and may both take positive and negative values.

2.1.3 Discussion of Operation Methods

To provide an overview of when to use what operation strategy, a summary of the characteristics, advantages and disadvantages of the different strategies are listed in the table below [Paper **A**]:

Machine features

Pressure and shaft dynamics	Non linear continuous differential equations	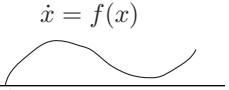
Control input type	Binary (active or inactive)	

Operation strategy features

	Full stroke	**Partial Stroke**	**Sequential Partial stroke**	
Valve type and requirements	Only capable of opening against low pressure difference	Only capable of opening against low pressure difference	Capable of opening against high pressure difference	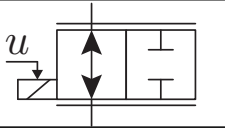
Control update rate	Proportional to the shaft speed and once every revolution at a fixed angle for both pumping and motoring	Proportional to the shaft speed and once every revolution at a variable angle for both pumping and motoring	Approx. continuous, but constrained by the actuation time	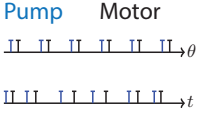
Displacement resolution	Proportional to the number of cylinders over one revolution and non-existent instantaneously	Continuous over one revolution and non-existent instantaneously	Continuous over one revolution, but proportional to the number of cylinders instantaneously with discrete levels being angle dependent	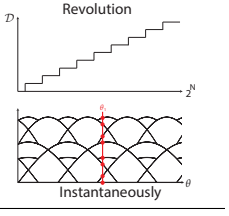

Chamber impulse response time	Proportional to the shaft speed (half of a revolution)	Scaled by the input and proportional to the shaft speed (up to half of a revolution).	The time between each actuation decision	
Machine response time (0 to max displacement)	Proportional to the shaft speed (half of a revolution)	Proportional to the shaft speed (up to half of a revolution)	Instantaneously (limited by the actuation time)	
Pumping vs motoring	Impulse response is different (first part of pumping is not used and last part of motoring is not used)	Impulse response is different (first part of pumping is not used and last part of motoring is not used)	Similarly	
Change of rotation direction	Pumping becomes motoring and vice versa. Angle of control decision changes.	Pumping becomes motoring and vice versa. Angle of control decision changes.	Pumping becomes motoring and vice versa	
Energy cost and pressure spikes	Very low due to no pressure difference across the valve and no flow at switching	Dependent on the angle where the chamber is deactivated. Largest at mid-point between BDC and TDC	Dependent on the angle where the chamber is deactivated. Largest at mid-point between BDC and TDC.	

- **Full stroke:** Is the favorable choice for high-speed machine operation, where energy efficiency is important. Furthermore, it is considered the simplest strategy since valve state changes are done at fixed angles.
- **Partial stroke (FDS):** Is the favorable choice for relatively low speed machine operation, where both tracking performance and energy efficiency are important.
- **Partial stroke (FLS):** Is not considered favorable, since relying on cavitation is in general something to avoid for hydraulic systems. Additionally, the strategy introduces a varying delay of up to half of a revolution which preferably should also be avoided.
- **Sequential partial stroke:** Is the favorable choice for very low speed operation, where control tracking performance is important and energy efficiency is of less importance.

Although, that the advantages and disadvantages of each method are speed dependent, it may also be beneficial to use a full stroke strategy at low speed if tracking performance is not very important, but simplicity and energy efficiency are. Similar, it may be beneficial to use a partial stroke strategy at high speed, if tracking performance is very important, but simplicity and energy efficiency are not.

Based on the above analysis it may seem favorable to utilize a combination of full- and partial stroke operation if the machine is to operate in a wide range of speeds. However, a combination of full and partial stroke operation is simply a partial stroke operation, since a full stroke is also a possible choice when utilizing a partial stroke strategy. Using the sequential partial stroke strategy where several state changes may be made during each stroke also covers the conventional partial stroke strategy, since a possible choice is to only do one state change or none at all (full stroke). However, this does not mean that it is advantageous to use the SFDS independent of the operation speed, since the SFDS strategy requires large valves capable of opening against high pressure and the control complexity may be severely increased if the optimal control choices are e.g. only full strokes.

2.2 Application Control Challenges

In addition to the identified control challenges for an individual DDM, there may be introduced additional challenges when the machine is used in a hydraulic application. Two high potential applications for the digital displacement technology are in hydrostatic transmission systems and direct cylinder drive concepts.

2.2.1 Hydrostatic Transmission

A hydrostatic transmission is a potential alternative to conventional mechanical gearbox transmissions in e.g. off-road vehicles, winch drives and wind turbines [7, 62, 89]. Since the dynamical behavior of the digital machines is vastly more complex than for conventional hydraulic pump-motor units, the control challenges are further increased when using multiple DDMs in a hydrostatic transmission. An identification of this is covered by a further investigation into a hydrostatic wind turbine transmission and a hydraulic winch drive.

Wind turbine transmission

An illustration of a hydrostatic wind turbine transmission comprising two digital displacement machines is shown in Fig. 2.13. The transmission is essentially working as a variable gear, since the speed of the rotor shaft and generator shaft is completely decoupled.

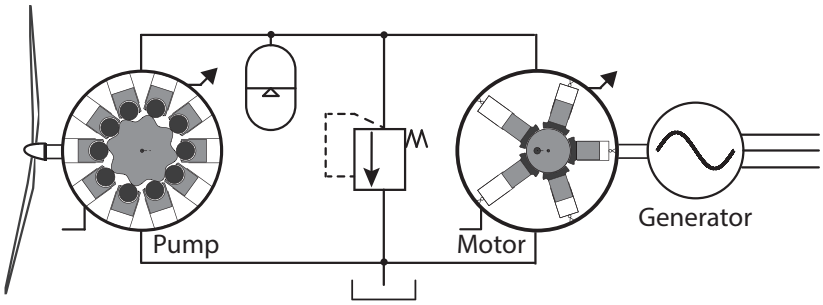

Fig. 2.11: Digital fluid power transmission for a wind turbine [Paper **A**].

The wind turbine transmission comprises a DD pump unit being driven by the low speed rotor shaft ($\omega < 15\,\text{rpm}$). The pump supplies pressurized fluid to the DD motor driving the high speed electrical generator ($\omega > 1000\,\text{rpm}$). To get a large volumetric output in a compact design of the low speed pump, a multi-lobe cam-ring design is used [62, 76]. This design increases the number of strokes per shaft revolution by the number of lobes on the outer circumference. As a result, the control update rate and volumetric output resolution is proportionally increased by the number of lobes.

The turbine rotor and electrical generator is only rotating in one direction and the power flow is only in one direction. Therefore, the pump is solely using a pumping strategy and the motor is solely using a motoring strategy. The wind turbine has a cut-in wind speed, which corresponds to the pump rotating at approximately 58 % of its rated speed (corresponding to $\omega \approx 7\,\text{rpm}$) as identified in [Paper **K**]. With a relative high number of lobes (>

12 [45, 46, 76]), the minimum angular speed is $\omega > 84$ rpm for the pump cylinders. Additionally, the generator is controlled to maintain its rated speed ($\omega > 1000$ rpm), such that both DD machines have a control decision rate that is relatively high. With a relatively high control update rate and energy efficiency being a top priority, it is considered favorable to use a full-stroke control strategy for both machines in a wind turbine transmission.

Considering the hydrostatic transmission shown in Fig. 2.11, there are two machines with different speeds and a different number of actuation decisions per revolution. To illustrate the actuation decisions for the two machines, a downscaled 5 decisions per. revolution pump and a 3 decisions per. revolution motor are considered and shown in Fig. 2.12. (For the purpose of illustration, the radial piston design is shown for the pump also).

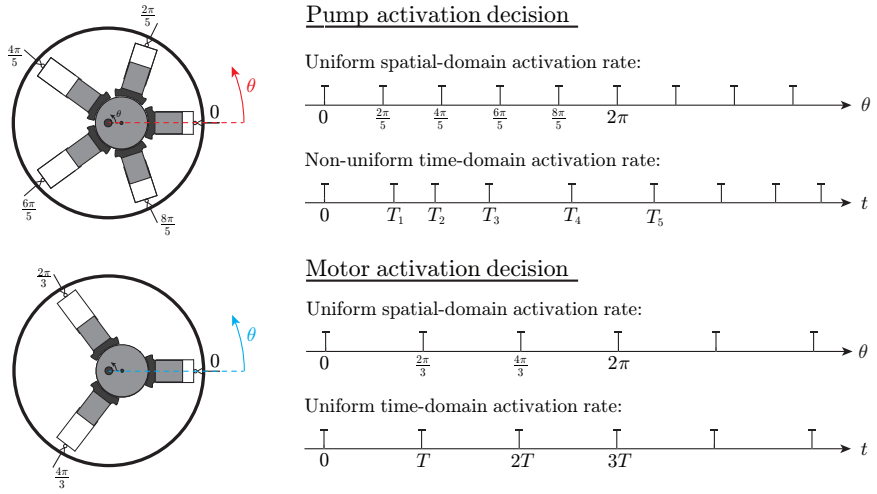

Fig. 2.12: Illustration of the activation decisions scheme for a variable speed DD pump and fixed speed DD motor presented as function of the angle (spatial-domain) and time [27].

An arbitrary and exaggerated speed profile is used for the digital displacement pump for the purpose of illustration. When combining the two control decision schemes, it is seen that the combined scheme becomes non-uniform in both the time and spatial domain. However, the combined activation decision scheme is periodic synchronous for every revolution in the angle domain. The system is hence a multi-rate sampled control system, which is often considered complex with respect to dynamical analysis and control design.

Winch Drive System / Vehicle Transmission

A winch drive system is different in several aspects compared to the turbine transmission, since it has to be able to reverse the direction of motion and possibly also reverse the direction of the power flow (similar to vehicle transmissions). By reversing the power flow direction, it is theoretically possible to recuperate energy by the electrical motor running in generator mode. An illustration of a digital hydrostatic winch drive is shown in Fig. 2.13.

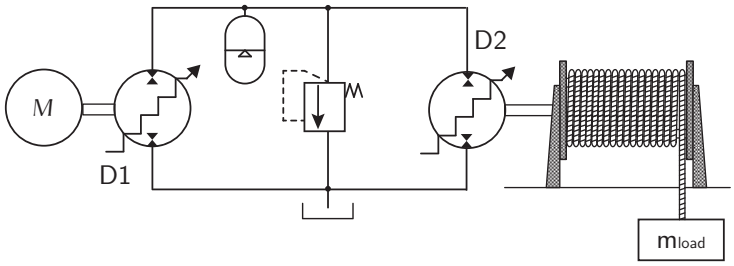

Fig. 2.13: Digital fluid power transmission for a which system [53].

When hoisting the load, the DD unit, D2, is operated as a motor, while the DD unit, D1, is operated as a pump driven by the electrical motor. When lowering the load, the operation is revered and the machine, D2, is operated as a pump driven by the load due to gravity. The high pressure fluid can then be stored in the hydraulic accumulators and consumed again during hoisting. Alternatively, the unit, D1, can be driven as a motor, while the electrical motor runs in generator mode. Transiently it is even possible to lower the load while the machine, D2, operates in motoring mode to accelerate the lowering. The ultimate hydraulic transmission system comprises of two DDMs that are able to both pump and motor in both direction of motions in a four-quadrant operation.

Combining the control challenges related to a single DDM operating in all four-quadrants with the challenges related to having multiple DDMs interconnect through pressure lines results in great challenges with respect to dynamical model based feedback control.

2.2.2 Direct Cylinder Drive

The digital displacement technology also has a large potential for use as a direct cylinder drive, since individual separate metering control of multiple cylinders and energy regeneration is possible. A conceptional drawing of a multi cylinder direct drive system with one single DD unit is illustrated in Fig. 2.14. Each main cylinder rod and piston side is connected to each individual module of a single DD unit. This gives the possibility of individual

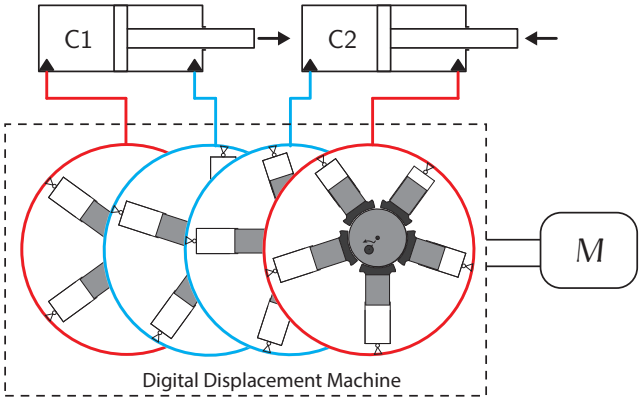

Fig. 2.14: Conceptional drawing of a multi cylinder digital displacement controlled direct drive. (Red illustrates pumping and blue illustrates motoring) [Paper **A**].

meter-in meter-out cylinder control by its respective module. In the case of piston extension, a high pressure is created on the piston side by a pumping module (Shown with red for cylinder C_1). Simultaneously, the return flow on the rod side is supplying the motoring module and thus regenerating energy to the common shaft (Shown with blue for cylinder C_1). By changing the pumping module to a motoring module and the motoring module to a pumping module, enables piston movement in the opposite direction as illustrated for the second cylinder, C_2. Since reverse operation is not required with the proposed setup, a fixed high-speed electrical motor may be used to drive the DDM. Therefore, a full stroke operation strategy seems suitable, but partial stroke methods are also considered valid to yield a smoother output, especially at low displacements.

If a cylinder experiences a light load, while another cylinder has a large load, it is possible to reconfigure the setup using electrically actuated on/off valves. Thereby, several modules may be connected to the cylinder with a high load. On a conceptional level at least, it is possible to reconfigure the system online, which however requires more components and changes the systems dynamical behavior accordingly. As a result, the control problem becomes significantly more complex.

2.2.3 Alternative Machine Construction and Configuration

The digital displacement technology features many interesting possibilities with respect to design and configuration. Several of these ideas are discussed to identify the possibilities and related control challenges.

Multiple Individual Outlets

An alternative design for the digital displacement machine concept is through the use of pressure chambers with multiple individual outlets. This way, a single pressure chamber is able to supply flow to both the piston and rod side of a direct cylinder drive. This concept corresponds to the Digital Hydraulic Power Management System (DHPMS) developed at Tampere Unversity [16]. A conceptional drawing of a direct cylinder drive system with one single DD unit having multiple individual outlets is illustrated in Fig. 2.15.

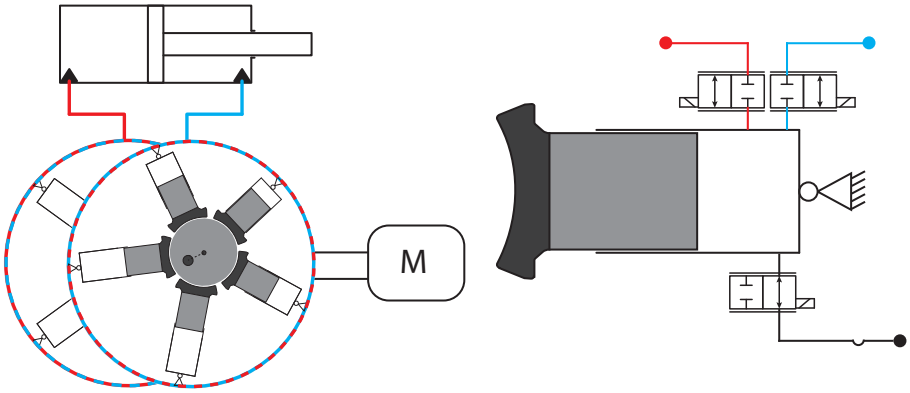

Fig. 2.15: Conceptional drawing of a digital displacement direct cylinder drive with individual inlets/outlets [Paper **A**].

With the shown configuration every DD cylinder chamber is able to both supply and receive flow from both the piston and rod side of the main cylinder. As a result, the control decision update rate is doubled with respect to the concept shown in Fig. 2.14 when using the same number of cylinders. Opposite to the concept shown in Fig. 2.14, fluid may be directly displaced from the piston to the rod side of the main cylinder and vice versa. Energy regeneration is thus achieved by fluid reallocation rather than through the torque as with the other concept. The proposed concept does however require multiple high pressure valves and the DD chamber sizes cannot be matched with the differential cylinder area ratio.

The concept introduces additional control challenges, since a control decision is now to determine whether the pressure chamber should be inactive (idling) or active towards the piston or rod side. Additional high pressure valves may be used to further increase the number of outlets to supply additional cylinders, which further increases the complexity and production cost.

Multiple Sized Cylinders

Since a full stroke operation is the simplest and most energy efficient strategy, but has a poor displacement resolution, it may be beneficial to utilize an alternative machine design with multiple sized pressure chambers. To reduce the machine costs, it is desired to have a low number of pressure chambers with a high displacement volume. However, to increase the displacement resolution and control update rate, it is desired to have a high number of cylinders with a small displacement volume. A compromise is to use variable sized pressure chambers, where the small chambers are used to yield a smoother displacement throughput.

Having multiple sized pressure chambers increases the control complexity significantly, since the displacement response from the individual pressure chamber has different magnitudes depending on the chamber size. Additionally, the control activation decisions become asynchronous with respect to the shaft angle. One design proposal is to have fewer large cylinders in one module and more smaller cylinders in another module and so forth as illustrated in Fig. 2.16.

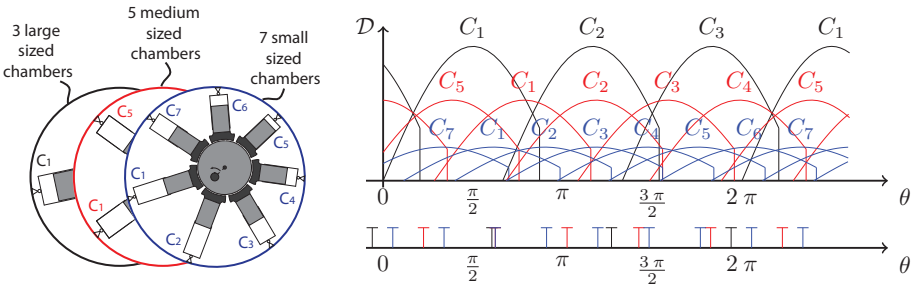

Fig. 2.16: Conceptional drawing of a digital hydraulic direct cylinder drive with multiple sized pressure chambers [Paper **A**].

It is seen that the variable size chambers in each module results in an asynchronous activation decision scheme and that the displacement response from the cylinders in the different modules has variable magnitudes depending on the size of the displacement chamber. How the eccentric is rotated for each module also plays a direct role with respect to which angles the individual actuation decisions are made for the respective module. The sampling scheme of each module (black, blue or red) may thus be shifted with respect to each other based on the eccentric orientation for the individual modules. The sampling scheme is however always periodic synchronous for every revolution.

In theory, cylinders with different pressure chamber sizes may be located in the same module, e.g. one module with 5 different sized pressure cham-

bers. This construction may however impose other problems, such as uneven load distribution, complicated construction, etc.

2.3 Summary

As presented, the challenges and complexity with respect to development of dynamic control design models are highly dependent on the DD unit(s) configuration, applied operation strategy and the application which it is used in.

The alternative machine designs may be used in all the presented applications. For a digital displacement transmission with four-quadrant operating DD units, each having multiple sized chambers and possibly multiple outlets, the challenges with respect to model-based control development may become very difficult. As mentioned, it is even possible to reconfigure the outlet manifold connections of modules online with electrical actuated on/off valves, which further complicates the control. The investigation hence indicates that it might be nearly impossible to develop a unified dynamical control design model, which covers all the presented control related challenges. Therefore, it is considered beneficial to develop models for specific scenarios and thereby divide the control problem into multiple subproblems to reduce the complexity.

Chapter 3

Development of Control Strategies and Models

The goal with respect to control of digital displacement units is to be able to perform dynamic system analysis and model-based feedback control independent of the operation strategy, design configuration and in which application the machine(s) is used. This is considered a very challenging task, since the presented investigation show that the dynamics comprises of a broad class of components (linear, nonlinear, continuous, discrete, time-varying and binary inputs, as well as state-dependent, multi-rate and asynchronous control updates, etc.). Furthermore, the dynamical behavior is changed based on the machine configuration and chosen operation strategy.

3.1 State-of-the-art Control Strategies

The published results with respect to control of digital displacement units are very limited and are mostly based on open-loop methods and often limited to simplified load conditions at fixed speed operation. However, several publications have been made regarding both flow, pressure, torque and velocity control of digital displacement machines. Research within development of control strategies for DD units has been conducted both in academia and industry. A brief overview of the current state-of-the-art control strategies for digital displacement units is provided in the following.

The earliest published control strategies are based on the research results from Edinburgh University obtained during the development process of the machine technology. Ehsan et al. (2000) [9] presents several control strategies based on a full stroke valve timing control (VTC) method. The VTC handles the task of providing signals for the actuation valves at the optimal shaft

angle based on the desired operation mode (pumping, motoring or idling). Initially, a simple ternary control mode is described, where the decision to pump, motor or idle the next cylinder is determined by a ternary code table (containing +1, -1, 0) corresponding to the operation mode. The method is simple and robust, while being strong for repetitive control and rapid change in demands where a controller might be too slow. However, the method is open loop and a quantization error has to be accounted for in time. The authors subsequently propose both a pressure and a flow control strategy based on a decision making algorithm. The decision to idle or activate the next cylinder is based on an estimation of already committed displacements and the load flow in a look-ahead angle, together with the displacement necessary to maintain the reference. In the flow control method, the accumulated quantization error is taken into account and minimized. Although the methods are simple and show promising results, they do not include any system dynamics. Heikkila and Linjama (2013) [16] extends the look-ahead displacement estimation technique by including an estimated valve delay and compression/decompression time. Sondre et al. (2017) [53,54] applies a similar displacement estimation control strategy for a digital hydraulic which drive system, where a PID controller is used in an outer loop for disturbance rejection and to remove eventual steady state errors.

Armstrong and Yuan (2006) [1] describes a multi-level control strategy for speed control of a digital fluid power motor. The outer control level consist of a simple PI velocity controller, while the inner control level identifies the optimal cylinder actuation sequence, based on an estimate of the torque output using all the possible combination of active/inactive chambers. The transient behavior and number of switching events are not considered when determining the optimal combination sequence. However, an improved method where the slope of the torque curve for a cylinder chamber is considered is proposed.

Xubin Song (2008) [80] presents a five-level flow control method for a fixed speed digital displacement pump/motor unit in an active vehicle suspension system. The control algorithm converts the flow demand into a series of sequential valve control commands. The five-level control commands consist of a full and partial stroke pumping mode, full and partial stroke motoring mode and an idling mode. The control sequence is determined by a preprogrammed decision scheme representing the optimum decisions.

Johansen and Roemer (2011) [66] investigates several control strategies for a DD pump. Both full and partial stroke methods based on look-ahead volume estimation techniques in a closed loop configuration are presented. The same authors present a full stroke delta-sigma pulse-density modulation method for flow control [25] (2015). In the strategy, the load pressure is measured and used to scale the displacement reference based on offline simulation results. The modulator then converts the scaled displacement ref-

erence needed to maintain the load pressure to a pulse train, determining whether the current cylinder should pump or idle. Johansen et al. (2017) [26] proposes a flow control method for a fixed speed DD pump using partial stroke operation, where the control design is based on a discrete linear time invariant (DLTI) model. The DLTI model is constructed by considering the sum of committed displacement responses from the individual chambers between each actuation decision. The controller sets a displacement reference for each cylinder chamber from where a local VTC converts the displacement reference to a closing angle for the low pressure valve. To account for the load pressure influence on the output flow, the load pressure is measured and used to scale the reference based on offline simulation results. Yigen (2012) [92] performs flow control of a DDP utilizing an internal model controller and a smith predictor to account for the actuation time delay. The control design is based on a discrete transfer function obtained through system identification methods.

Sniegucki et al. (2013,2016) [78, 79] present an optimal torque control strategy. A mixed logical dynamic (MLD) system representation is used to describe the nonlinear and discrete phenomenas of the digital machine. The MLD representation is then used to set up a constrained optimization problem. The optimization objective is chosen as a summed weighting of set-point derivation, frequency content and number of switching events. Since an active cylinder influences the output for a significant angle interval, the prediction horizon ensures that the constraints are not violated in the look-ahead angle. Simulation result show reduced torque ripples and improved steady state accuracy compared to pulse-width and pulse-density modulation techniques. A large drawback of the method is however the large computational time of 2 s. on average pr. decision, making the method only usable for offline optimization.

A vastly different control strategy based on "creep-mode" operation is presented by Larsen et al - Diinef (2018) [34]. The strategy relies on closing all pressure chamber valves (both the HPV and LPV) and with some arbitrary load, each pressure chamber obtains an equilibrium pressure. Clockwise rotation is then achieved by connecting a pressure chamber that yields positive torque to the high pressure manifold or a chamber that yields negative torque to the low pressure manifold. Similarly, counter-clockwise rotation is done by connecting the pressure chamber to the opposite pressure manifolds. This results in a minor shaft movement, where after a new equilibrium is obtained and a new decision is taken. The strategy hence allows for an accurate control of the shaft angle, but no dynamics is considered and thus leaves potential for further exploration of the method.

In addition to the above presented research results, several patents have also been published on the subject of controlling digital displacement machines. The patents are mainly from Artemis Intelligent Power Ltd. (AIP

A/S), Sauer Danfoss ApS (now Danfoss Power Solutions), and Mitsubishi Heavy Industry (MHI). The patents are in general methods that have a great similarity with the above presented modulation techniques and displacement estimation strategies [4, 31, 32, 40, 60]. Furthermore, several methods for reducing ripples and evenly distribute the load for reduced fatigue is patented [38, 46]. However, similar for all of the strategies is that no dynamics is considered.

The mentioned milestones regarding research and development of control strategies for the digital displacement technology is summarized in the illustration shown in Fig. 3.1.

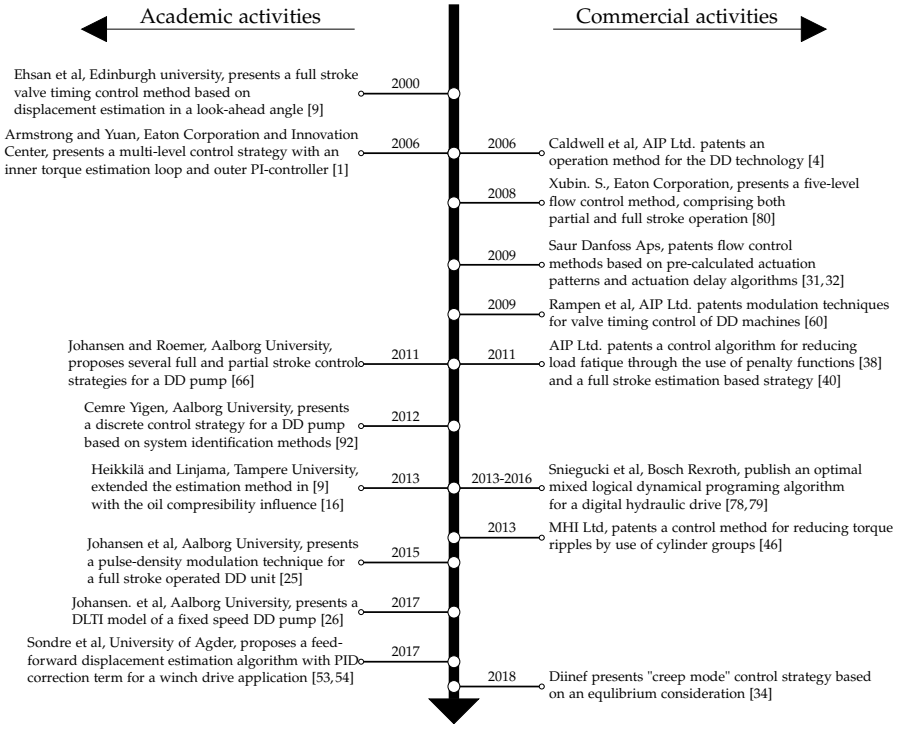

Fig. 3.1: Summarization of the milestones regarding research and development of control strategies for digital displacement machines. The timeline is made with inspiration from Noergaard [52].

3.2 Investigation of the Digital Effect and Dynamics

Often the state-of-the-art control strategies neglects the transient behavior when developing the control system for the DDM. Depending on how the

machine is constructed and operated, this simplification may or may not be justified. To investigate if its acceptable to omit the DDM when designing the control system for the actuated plant, an investigation of the digital effect is conducted. This investigation also serves to provide a deeper understanding of the DDM dynamics and may thus aid in the establishment of control design models.

The analysis of the digital effects is made by simulating the response of a pulse modulated DDM connected to a first order continuous plant. The DDM effect is determined by comparing the response with the response of an identical first order plant being actuated by an ideal pump/motor. The ideal pump/motor is described by a unity gain with infinitely fast dynamics and thus correspond to neglecting it. The system under investigation is illustrated in Fig. 3.2 for a full stroke operated machine with pulse-density modulation (PDM).

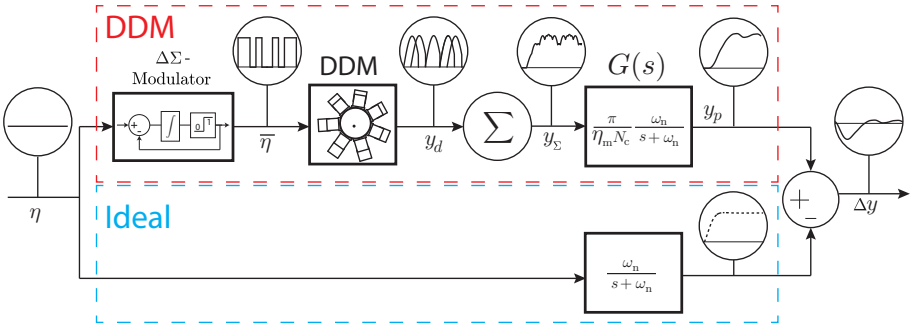

Fig. 3.2: Strategy for investigation of the digital effect [Paper **B**].

It is seen that a constant displacement fraction, $\eta \in [0,1]$, is given to a PDM, that generates a binary actuation sequence, $\bar{\eta} \in \{0,1\}$, for the individual cylinders. The DDM output is simplified to be sine wave pulses for each active chamber, y_d, which is considered a valid representation of the torque and flow characteristics for this investigation. The displacement output of the DDM is scaled with a constant $\pi/(\eta_\mathrm{m}\, N_\mathrm{c})$ to normalize the output for comparison to the ideal actuated plant. $\eta_\mathrm{m} = 0.96$ is the maximum displacement fraction of a full-stroke and takes into account that the last minor fraction of a motoring stroke is not used to allow for passive LPV opening. The sum of sine wave pulses, y_Σ, is given as input to a continuous first order plant with eigen-frequency, ω_n. This plant represents either the pressure or shaft speed

dynamics and are given by

$$G_{\mathrm{p}}(s) = \frac{p(s)}{Q(s)} = \frac{\frac{\beta_{\mathrm{e}}}{V}}{s + \underbrace{\frac{\beta_{\mathrm{e}}}{V} k_{\mathrm{L}}}_{\omega_{\mathrm{n}}}} \qquad G_{\tau}(s) = \frac{\omega(s)}{\tau(s)} = \frac{\frac{1}{J}}{s + \underbrace{\frac{d}{J}}_{\omega_{\mathrm{n}}}} \tag{3.1}$$

where β_{e} is the effective fluid bulk modulus, V is the pressure line volume, k_{L} is the fluid leakage coefficient, J is the mechanical shaft inertia and d is the viscous friction coefficient. It is evident that ω_{n} represents the inertness of the system and is expected to greatly influence the digital effect on the output, y_{p}, due to the filtering property.

The effect of the DDM is investigated by taking the difference, Δy, between the plant response with the DDM and that being actuated by an ideal pump/motor. The same strategy has also been applied for a partial stroke operated machine with pulse-width modulation (PWM). The responses are shown in Fig. 3.3 for a DDM with 5 cylinders and a displacement fraction of $\eta = 0.5$. It is seen that the differences in the plant responses, y_{p}, are an initial delay angle, θ_{d} and ripples in the response actuated by the DDM. The size of this delay and the energy in the steady state part of the difference signal, Δy, gives a measure of the digital effect of the DDM. If this digital effect is below a certain threshold, it is considered valid to neglect its dynamics when designing the control system. The digital effect is however a function of several variables, being the number of cylinders, displacement fraction, rotational speed and the plant eigen-frequency. It is possible to reduce the number of variables by one when considering a relative frequency, ω_{r}, defined by

$$\omega_{\mathrm{r}} = \frac{\omega_{\mathrm{n}}}{\omega} \tag{3.2}$$

where ω is the rotational speed of the DDM. The relative frequency exploits that the response in the angle domain is identical for a constant ω_{r} and hence describes the relative bandwidth between the DDM and plant. The squared average energy in the steady-state response of the difference signal, Δy, is evaluated for 10 full revolutions given by

$$E = \frac{1}{20\,\pi} \int_{\theta_0}^{\theta_0 + 20\,\pi} \Delta_{\mathrm{y}}(\theta)^2 d\theta \tag{3.3}$$

where θ_0 is the initial angle during steady state operation. The resulting energy and time delay are shown in Fig. 3.4 and Fig. 3.5 for a PDM operated DDM and in Fig. 3.6 and Fig. 3.7 for a PWM operated DDM respectively.

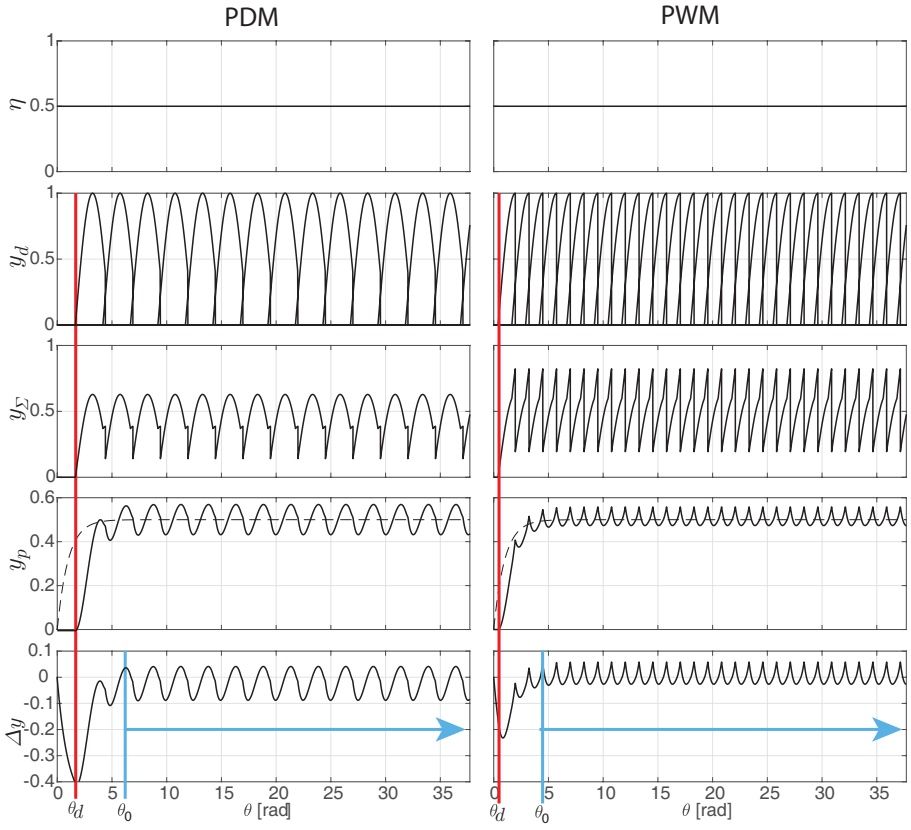

Fig. 3.3: Simulation results for analysis of the digital effect. Red line indicates the DDM response delay and the blue line indicates the initial steady state angle [Paper **B**].

It is seen that the steady state energy for PDM operation is drastically decreasing for a higher number of cylinders, since the response contains more but significant smaller ripples as the number of cylinders increases. The energy is also drastically decreasing for a lower relative frequency, since the digital machine dynamics is increasingly filtered by the plant. Furthermore, the energy is seen to be almost symmetric around $\eta = 0.5$, since activating a single chamber yields the same absolute ripple as deactivating a single chamber.

The time delay for PDM operation is in general seen to be reduced for a higher number of cylinders and higher rotational speed of the DDM. The time delay is actually inverse proportional to the speed of the machine and number of cylinders, since the delay is the angle to the next activation decision for the subsequent cylinder. Therefore, if the displacement fractions and rotational speed is going towards zero, the time delay goes towards infinity.

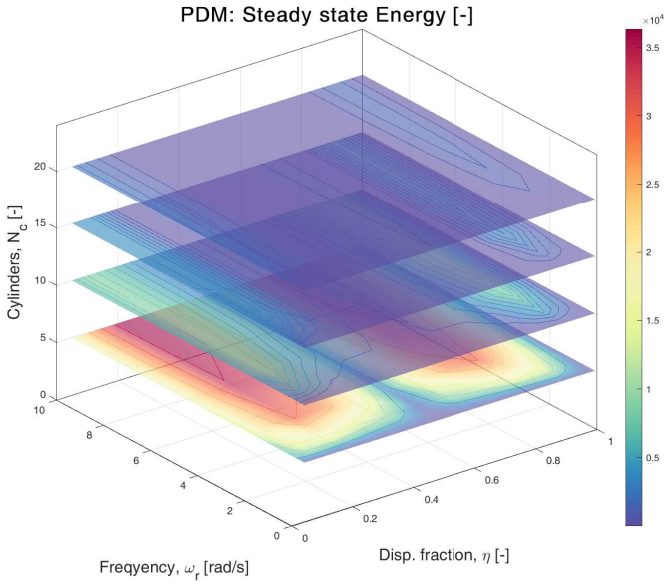

Fig. 3.4: Energy in difference signal as function of number of cylinders, relative frequency and displacement [Paper **B**].

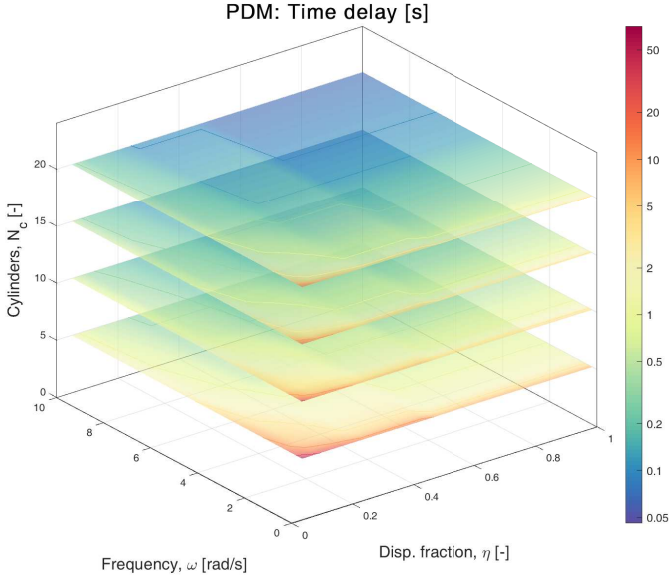

Fig. 3.5: Time delay as function of number of cylinders, rotation speed and displacement [Paper **B**].

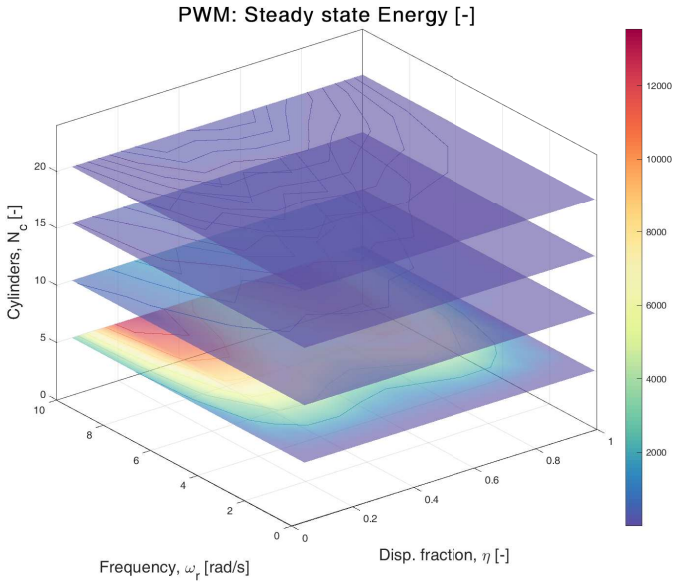

Fig. 3.6: Energy in difference signal as function of number of cylinders, relative frequency and displacement [Paper **B**].

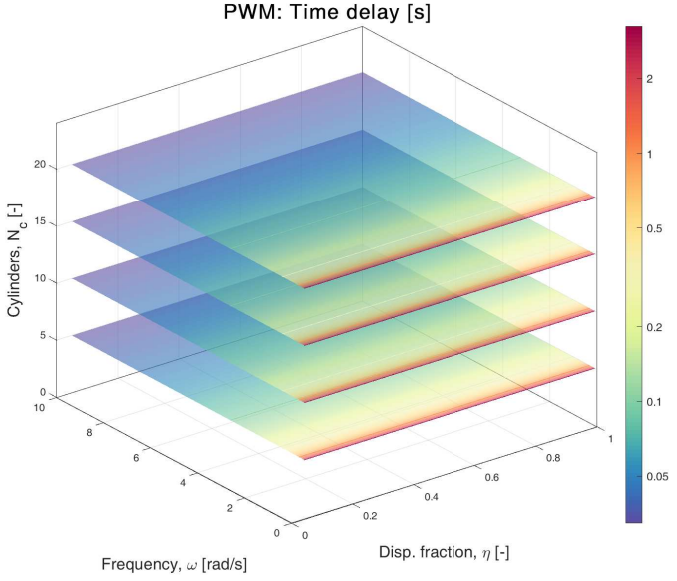

Fig. 3.7: Time delay as function of number of cylinders, rotation speed and displacement [Paper **B**].

The minimum delay occurs if the first cylinder is activated, which occurs if $\eta(0) \geq 0.5$.

The simulation conducted for the PWM operation show a lower energy level in general but has a similar tendency as for the PDM operation. However, the correlation between displacement fraction and energy is difficult to interpret from the results, since the number of cylinders has a high influence. Although, for a relatively high number of cylinders ($N_c \geq 15$), the highest energy is for a displacement fraction of $\eta = 0.5$, since the output is ended at the maximum point on the sine wave. The time-delay is seen to be constant with respect to the number of cylinders and displacement fractions (considering motoring operation), since the first cylinder is always activated. Since the delay is a constant angle, the time-delay is proportional to the speed of the machine as seen. For pumping operation, the delay is reduced proportional to the displacement fraction.

The investigation show that the digital effect is reduced for an increasing number of cylinders, higher rotational speed and slower plant dynamics. Additionally, the minimum delay occurs for all displacement fractions with PWM operation and for displacement fractions above $\eta(0) \geq 0.5$ in PDM operation. The results clearly reveal that the dynamics of the DDM should not be neglected in cases where the steady-state energy and/or the time-delay is high, since it may cause severe reduction in control performance and especially a large time-delay may lead to instability.

3.3 Dynamical Control Design Model Development

It is evident that only a very limited number of the state-of-the-art control strategies include the transient behavior of the digital displacement machines and those methods are in general based on simple approximations and/or simplified operation and load conditions. Since it is considered an important objective to be able to perform dynamical analysis with respect to stability, controller synthesis and study of failure mechanism, control methods not based on dynamical models are considered out of scope of this thesis. Alternative control strategies that do not require a dynamical model representation of the system are open-loop estimation methods, fuzzy logic control, ternary mode control, hysteresis control, etc. In classical control theory, there are two branches of dynamical systems, namely continuous and discrete time systems. Linear control theory in both branches is well established and used both academically and industrially. Also, non-linear control theory has been thoroughly studied and stability analysis for control design is developed, especially for continuous time systems. As identified, the digital displacement machine has dynamics relating to both branches, since non-linear continuous dynamics are switched in discrete events. Such system belongs to the class

of hybrid dynamical systems. Although, hybrid dynamical system theory enables an accurate description of the system dynamics, the design of stabilizing feedback control laws is a difficult task. Therefore, instead of deriving a general mathematical model that covers all combinations of machine configurations and operation strategies, simpler models and control methods that are only valid under certain conditions are developed. An overview of the possible settings and operation conditions that greatly influence the control design model are shown in Fig. 3.8.

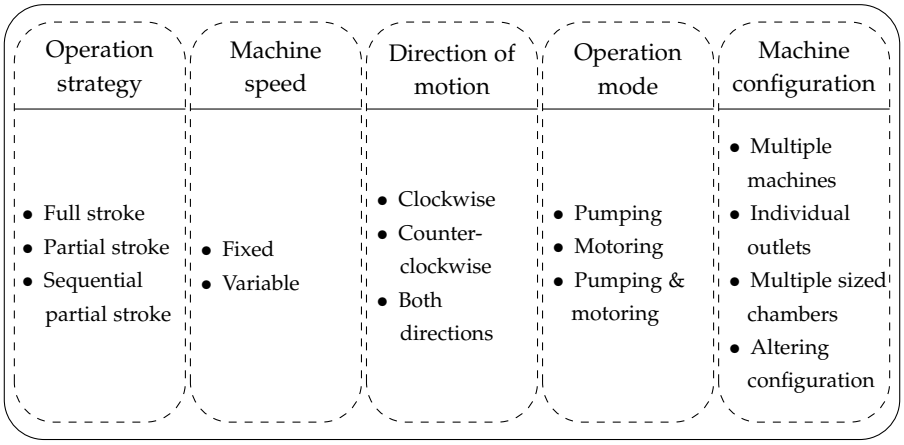

Fig. 3.8: Overview of the different configurations that greatly influence the control challenges.

Proposals on how the different branches of dynamical theory may be exploited and enable model-based control design for digital displacement machines are provided in this chapter. The solution strategy is to initially develop control strategies for the simpler operation methods and configurations and expand the machine(s) complexity of configuration and operation method as solutions proposals are made. The chapter is structured such that each branch of dynamical systems, i.e. continuous, discrete and hybrid is investigated and the limitation of applicability for each branch is discussed. Since the solution proposals are only described briefly, references to papers are made for a more detailed description of the strategy.

3.4 Continuous Dynamical Approximation

Although the dynamics of each pressure chamber of the DDM is continuous, the inputs are binary (active or inactive) and updated discretely, the machine dynamics may be approximated to be continuous by exploiting methods from digital electronics. As reviewed in the state-of-the-art section, both

pulse-width modulation (PWM) and pulse-density modulation (PDM) techniques are used to convert a continuous signal $u(t) \in \mathbb{R}$ into a digital signal. The analog signal hence corresponds to a duty-cycle which for the PDM technique result in a binary actuation sequence $\bar{u}(k) \in \{0,1\}$ and for the PWM technique $\eta(k) = u(t)$ for each pressure chamber. The displacement step response using both a PDM and a PWM technique is illustrated in Fig. 3.9 for a DDM with 5 and 20 cylinders. The displacement references are $u(t) = \{0.1\ 0.2\ 0.4\ 0.6\ 0.8\ 1\}$.

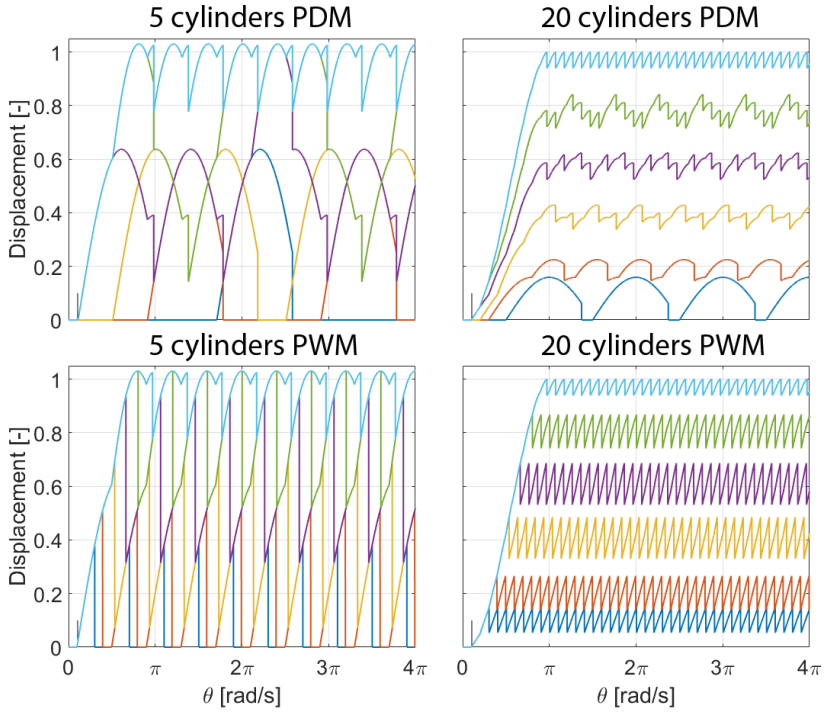

Fig. 3.9: Step response for various displacements using delta-sigma modulation and pulse-density modulation [Paper **A**].

Using the PDM strategy, it is seen that for a high number of cylinders at high displacements, the step response resembles a continuous response with minor ripples in the angle domain as expected. The response has an initial delay, due to the actuation decision being made ahead of the active stroke part and has a response time of approximately half of a revolution, $\theta_{\text{resp}} \approx \pi$. Using a PWM strategy, the response resembles a slew-rate limited continuous response with ripples. The slew-rate limited alike behavior is caused by the response angle is given by $\theta_{\text{resp}} \approx \phi(\eta)$. The response is fitted to a continuous transfer function by use of a spatial domain Laplace transformation defined

as

$$F(\bar{s}) = \bar{\mathcal{L}}\{f(\theta)\} = \int_0^\infty e^{-\bar{s}\,\theta} f(\theta) d\theta$$
$$G(\bar{s}) = \frac{\eta(\bar{s})}{u(\bar{s})} = K \frac{\omega_\mathrm{n}^2}{\bar{s}^2 + 2\,\zeta\,\omega_\mathrm{n}\,\bar{s} + \omega_\mathrm{n}^2} e^{-\bar{s}\,\theta_\mathrm{d}} \tag{3.4}$$

where θ_d, K, ω_n and ζ are the approximated delay angle, dc-gain, eigen-frequency and damping coefficient. A comparison of the continuous model approximation with the non-linear mathematical model is shown in Fig. 3.10.

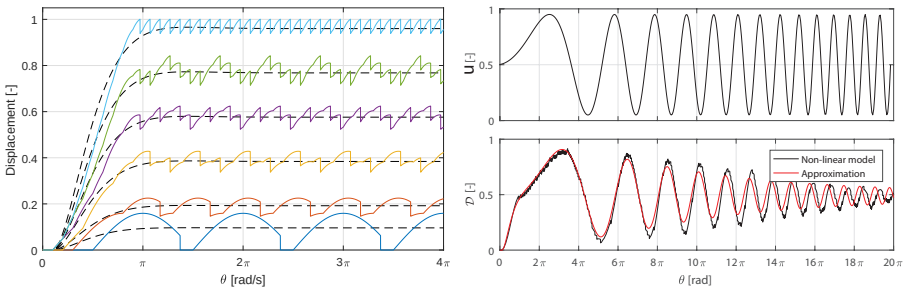

(a) Various step response comparison with 20 cylinders.

(b) Variable frequency comparison with 42 cylinders.

Fig. 3.10: Comparison of continuous model approximation with non-linear model [Paper **C**].

It is seen that the transient response of the approximation crosses the physical response and that the steady state response of the approximation is an average value of the physical. For amplitude and frequency varying displacement fractions, it is seen that the approximated model response slightly lags the non-linear response at low frequencies, but slightly leads at high frequencies. Similarly, the approximated gain is lower than the non-linear at low frequencies, but higher at high frequencies. Therefore, it is not considered possible to make a significantly more accurate linear model if it must be valid in a broad range of frequencies.

To analyze the continuous method further, a frequency response comparison is made. Since the physical system behavior is non-smooth and has a large quantity of ripples, a frequency response band is conducted. This band is constructed by considering the maximum and minimum value of the gain and phase, such that the physical response is always within this band. The response band has been made by applying a high number of inputs with varying amplitudes and offsets, $u(t) = A\,\sin(\omega\,t) + B$. The maximum and minimum values are determined by the method illustrated in Fig. 3.11a. The resulting frequency response is shown in Fig. 3.11b

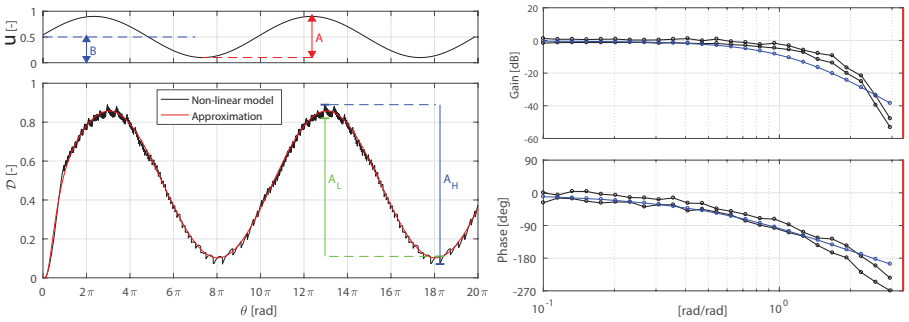

(a) Evaluation method for determine maximum and minimum gain and phase.

(b) Frequency response comparison of approximation method.

Fig. 3.11: Frequency response comparison between the non-linear and continuous approximation model [Paper **C**].

A_{L} and A_{H} represents the identified minimum and maximum gain respectively. Similarly has the maximum and minimum phase been identified based on a high number of periods. The resulting frequency response of the continuous model is seen to be within the response band at low frequencies. However, it is seen that the approximation is less accurate at higher frequencies where both the gain and phase cross the response band. Since the system is discretely controlled, the sampling effect has a large influence at higher frequencies, making a continuous approximation insufficient. The red line in Fig. 3.11b illustrates the Nyquist frequency and is the maximum frequency where the approximation may be considered valid.

The above machine dynamics has been described in the angle domain and to couple the machine dynamics with the remaining system dynamics (pressure line, mechanical shaft, load, etc.) and thereby enable classical control, a conversion to the time domain is necessary. Conversion from the angle to the time domain is done by the relationship given as

$$d\theta = \omega(t)dt \leftrightarrow dt = \frac{1}{\omega(\theta)}d\theta \tag{3.5}$$

Using this relation yields the time transfer function given by

$$G(s) = \frac{\eta(s)}{u(s)} = K\frac{\omega^2(s)\,\omega_{\mathrm{n}}^2}{s^2 + 2\,\zeta\,\omega(s)\,\omega_{\mathrm{n}}\,s + \omega^2(s)\,\omega_{\mathrm{n}}^2}\,e^{-s\,\frac{\theta_{\mathrm{d}}}{\omega(s)}} \tag{3.6}$$

Since the shaft speed, $\omega(t)$, is a time varying state, the system becomes non-linear in the time-domain for varying speed operation. The eigen-frequency is seen to be proportional to the shaft speed, which corresponds well with the previous described machine characteristics. Frequency responses of the

continuous approximation in the time domain at varying shaft speeds are shown in Fig. 3.12

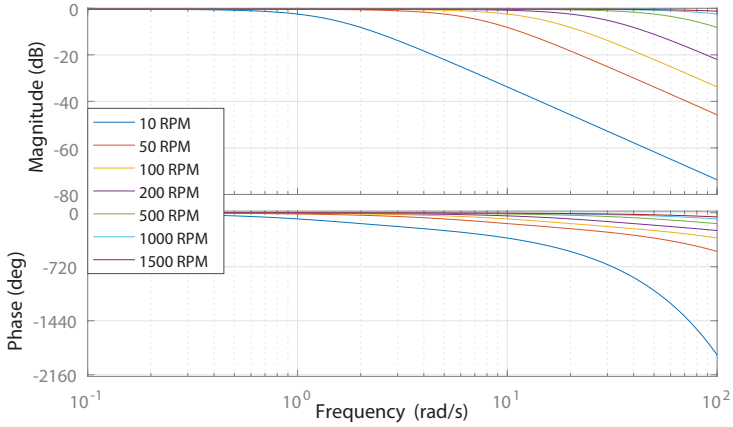

Fig. 3.12: Frequency responses of the continuous approximation in the time domain at varying shaft speeds [Paper **C**].

It is evident that if linear control theory is applied, linearization is required by choosing a steady state operation speed. To ensure stability the speed of the machine must be above the linearization speed to avoid additional unmodeled phase. Since the approximation only represents the low frequency fundamental characteristics of the DDM dynamics, the method is limited in use for control design. However, for a DDM with a relative high number of cylinders operated at relatively large displacements and speeds, the strategy is considered sufficient to ensure stability.

Summarization:

- Simple dynamical model and subsequently well-known control design methods.
- Only applicable to pulse-density and pulse-width modulation techniques.
- Is an angle average approximation, which average output matches the physical system output.
- Does not describe the discrete sampling effect and the non-smooth ripple dynamics.
- Reduced accuracy for a lower number of cylinders.
- Reduced accuracy for lower displacement with full stroke operation

- Only valid up to a certain excitation frequency (where the discrete effect is no longer neglectable).
- Yields a nonlinear model in the time domain if the shaft speed is varying.
- In case of applying linear control, the minimum speed has to be lower bounded by the linearization speed to ensure stability.

3.5 Discrete Dynamical Approximation

Since the DDM is a discretely actuated continuous system, a discrete approximation may be made by considering a sample-and-hold system, similar to conventional discrete control of a continuous plant. Considering the pressure build-up in each chamber to be significantly faster than the remaining machine dynamics, the flow and torque may be approximated by

$$\begin{aligned} Q_{\mathrm{H}} &\approx \frac{dV(\theta)}{d\theta}\,\frac{d\theta}{dt} = \frac{V_{\mathrm{d}}}{2}\,\sin(\theta)\,\dot{\theta} = \mathcal{D}(\theta)\,\dot{\theta} \\ \tau &= \frac{dV(\theta)}{d\theta}\,p \approx \frac{V_{\mathrm{d}}}{2}\,\sin(\theta)\,p = \mathcal{D}(\theta)\,p \end{aligned} \tag{3.7}$$

The flow and torque are seen to be described as function of the displacement like a conventional fluid power machine, but where the displacement is a function of the shaft angle.

3.5.1 Full Stroke Operation

The discrete model is established by considering the displacement throughput between samples and is given by the change in chamber volume divided by the constant sampling angle. This discretization method is initially proposed by Johansen et al. [26]. The discrete displacement fraction is given as

$$\mathcal{D}[k] = \frac{\Delta V[k]}{\theta_{\mathrm{s}}} = \frac{\left(V\left(\theta[k+1]\right) - V\left(\theta[k]\right)\right)\,N_{\mathrm{c}}}{2\,\pi} \tag{3.8}$$

where $\theta_{\mathrm{s}} = 2\,\pi/N_{\mathrm{c}}$ is the sampling angle. Considering a motoring stroke, the angles where a control decision is made are given by

$$\theta[k] = \phi_{\mathrm{mL}} + \theta_{\mathrm{s}}\,(k-1) \qquad\qquad i \in \{1, ..., N_{\mathrm{c}}\} \tag{3.9}$$

where ϕ_{mL} is the angle where the LPV is closed and the decision whether to idle or motor for the given chamber is made. For the motor flow, the

displacement fractions are evaluated by

$$\Delta V[k] = \begin{cases} 0 & \theta[k], \theta[k+1] \notin [0\,; \phi_{\mathrm{mH}}] \\ V(\theta[k+1]) - V(\theta[k]) & \theta[k], \theta[k+1] \in [0\,; \phi_{\mathrm{mH}}] \\ V(\theta[k+1]) - V(0) & \theta[k] < 0 < \theta[k+1] \\ V(\phi_{\mathrm{mH}}) - V(\theta[k]) & \theta[k] < \phi_{\mathrm{mH}} < \theta[k+1] \end{cases} \tag{3.10}$$

where ϕ_{mH} is the angle where the HPV is closed and the active part of the motoring stroke is ended. It is seen that only a displacement is output between $\theta \in [0, \phi_{\mathrm{mH}}]$. The resulting displacement response of the full stroke discrete motor approximation is shown in Fig. 2.3 for a DDM with 15 cylinders.

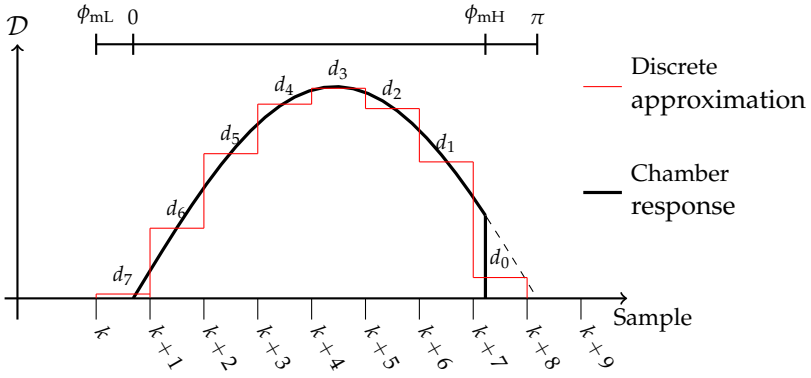

Fig. 3.13: Discretization of displacement response for a motoring stroke [Paper **A**].

As seen, the discrete approximation is increasingly accurate for a higher number of cylinders, since the quantization resolution is increased proportionally. The shown displacement fractions are given by $d_{\mathrm{k}} = \mathcal{D}[7-k]$ and are used to establish a linear discrete transfer function given by

$$G(z) = \frac{\mathcal{D}(z)}{u(z)} = \frac{d_7\, z^7 + d_6\, z^6 + \cdots + d_1\, z + d_0}{z^7} \tag{3.11}$$

Since each chamber may either be active or inactive, $u(k) \in \{0, 1\}$, this type of system is very different compared to a conventional discrete control system where $u(t) \in \mathbb{R}$. In state space form the transfer function may be written as

memory states given by

$$\underbrace{\begin{bmatrix} u(k) \\ u(k-1) \\ u(k-2) \\ \vdots \\ u(k-m+1) \end{bmatrix}}_{z_{\mathrm{u}}(k+1)} = \underbrace{\begin{bmatrix} 0 & 0 & \cdots & 0 & 0 \\ 1 & 0 & \cdots & 0 & 0 \\ 0 & 1 & \cdots & 0 & 0 \\ \vdots & \vdots & \ddots & \vdots & \vdots \\ 0 & 0 & \cdots & 1 & 0 \end{bmatrix}}_{A_{\mathrm{u}}} \underbrace{\begin{bmatrix} u(k-1) \\ u(k-2) \\ \vdots \\ u(k-m+1) \\ u(k-m) \end{bmatrix}}_{z_{\mathrm{u}}(k)} + \underbrace{\begin{bmatrix} 1 \\ 0 \\ 0 \\ \vdots \\ 0 \end{bmatrix}}_{B_{\mathrm{u}}} u(k) \tag{3.12}$$

$$\mathcal{D}(k) = \underbrace{\begin{bmatrix} \mathcal{D}[1] & \mathcal{D}[2] & \ldots & \mathcal{D}[m] \end{bmatrix}}_{C_{\mathrm{u}}} z_{\mathrm{u}}(k) + \underbrace{\mathcal{D}[0]}_{D_{\mathrm{u}}} u(k) \tag{3.13}$$

where $m = 6$ is the number of states necessary to describe the full stroke. The motor flow is then obtained as $Q(k) = \mathcal{D}(k)\,\dot{\theta}(k)$.

To describe the torque in (3.7) requires a discrete representation of the chamber pressure. The pressure dynamics may be split up in a fast and a slow dynamical component given by [79]

$$\dot{p} = \frac{\beta_{\mathrm{e}}}{V(\theta)} \left(\underbrace{Q_{\mathrm{H}} - Q_{\mathrm{L}}}_{\text{fast}} - \underbrace{\dot{V}(\theta, \dot{\theta})}_{\text{slow}} \right) \tag{3.14}$$

Neglecting the fast transient flow dynamics and describing the pressure build-up as function of the shaft angle yields

$$\frac{dp}{dt}\frac{dt}{d\theta} = \frac{dp}{d\theta} = -\frac{\beta_{\mathrm{e}}}{V(\theta)}\frac{dV(\theta)}{d\theta} = \underbrace{-\frac{\beta_{\mathrm{e}}}{\frac{V_{\mathrm{d}}}{2}\,(1-\cos(\theta)) + V_0}\,\frac{V_{\mathrm{d}}}{2}\sin(\theta)}_{f_{\mathrm{p}}(\theta)} \tag{3.15}$$

A discrete representation of the chamber pressure may then be written as

$$p(k+1) = \begin{cases} p_{\mathrm{H}} & if \quad (\bar{x}_{\mathrm{L}} = 0 \wedge \bar{x}_{\mathrm{H}} = 1) \vee p(k+1) > p_{\mathrm{H}} \\ p(k) + f_{\mathrm{p}}(\theta[k]) & if \quad \bar{x}_{\mathrm{L}} = 0 \wedge \bar{x}_{\mathrm{H}} = 0 \\ p_{\mathrm{L}} & if \quad (\bar{x}_{\mathrm{L}} = 1 \wedge \bar{x}_{\mathrm{H}} = 0) \vee p(k+1) < p_{\mathrm{L}} \end{cases} \tag{3.16}$$

By normalizing the discrete pressure by $p(k) = \bar{p}(k)\,p_{\mathrm{H}}(k)$, the torque output of the discrete model is given by $\tau(k) = \mathcal{D}(k)\,\bar{p}(k)\,p_{\mathrm{H}}(k)$. The discrete model is validated by comparing its response to the response of the nonlinear model presented in Chap. 2. The valve dynamics in the non-linear model has been

modeled as a simple first order system given by

$$\frac{\bar{x}_\mathrm{L}}{u_\mathrm{L}} = \frac{1}{\tau_\mathrm{v}\, s + 1} \qquad \frac{\bar{x}_\mathrm{H}}{u_\mathrm{H}} = \frac{1}{\tau_\mathrm{v}\, s + 1} \tag{3.17}$$

where $u_\mathrm{L} \wedge u_\mathrm{H} \in \{0, 1\}$ is the valve input and $\tau_\mathrm{v} = 2\,\mathrm{ms}$ is the valve time constant. The response comparison is shown in Fig. 3.14 for a DD motor with 42 cylinders.

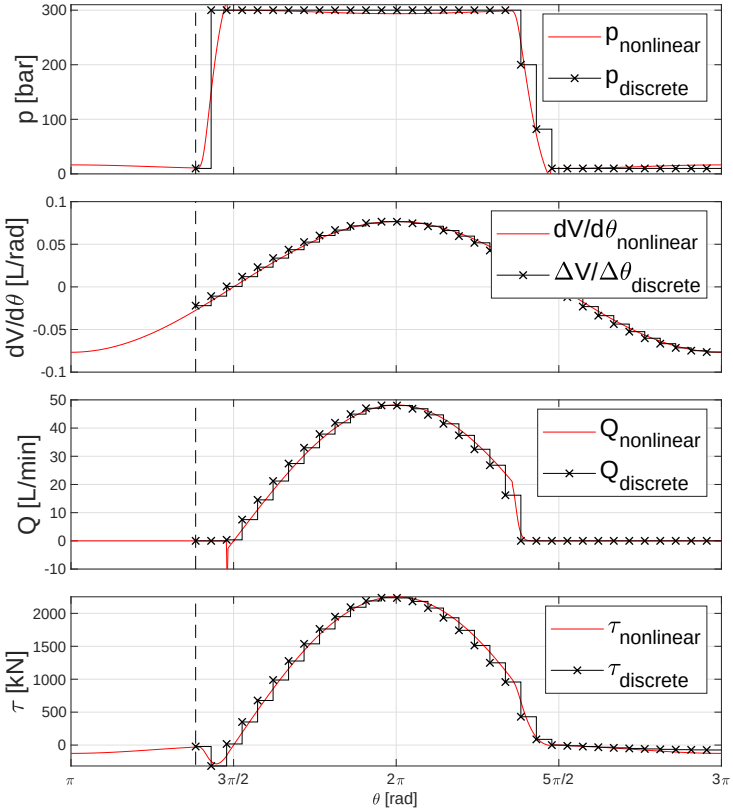

Fig. 3.14: Comparison of nonlinear and discrete approximation response. $\dot{\theta} = 100\,\mathrm{rpm}$, $p_\mathrm{H} = 300\,\mathrm{bar}$, $p_\mathrm{L} = 10\,\mathrm{bar}$.

It is seen that the discrete approximation is fairly accurate for a high number of cylinders. However, for a low cylinder number, the pressure jumps directly between high and low pressure, such that the torque may be described as $\tau(k) = \mathcal{D}(k)\, p_\mathrm{H}$.

Utilizing a pulse-density modulator to generate the binary input sequence introduces a high non-linearity due to the quantizer given by

$$u(k) = \begin{cases} 1 & \text{if} \quad \eta(k) \geq 0.5 \\ 0 & \text{if} \quad \eta(k) < 0.5 \end{cases} \tag{3.18}$$

where $\eta(k)$ is the displacement fraction reference. Since control theory for nonlinear discrete control systems is complex, it is often favorable to pursue a linear strategy. In linear control of electrical systems, the nonlinearity caused by the quantizer is commonly described by considering a dc-component combined with an additive noise input, $u(k) = \eta(k) + n(k)$ [65]. Where $n(k)$ is the noise input with intensity $I \in [0, 0.5]$. When omitting the noise term, this corresponds to a duty-cycle ratio approximation, which is the commonly used strategy in control of electrical systems. However, the major difference is that the sampling rate is very high in electrical systems, but is speed dependent for a DDM. An examination of the duty-cycle ratio approximation is done by comparing the nonlinear response with the linear. The resulting responses are shown in Fig. 3.15 for an input of $\eta(k) = 1/3$. The discretization is not shown for simplicity of illustration.

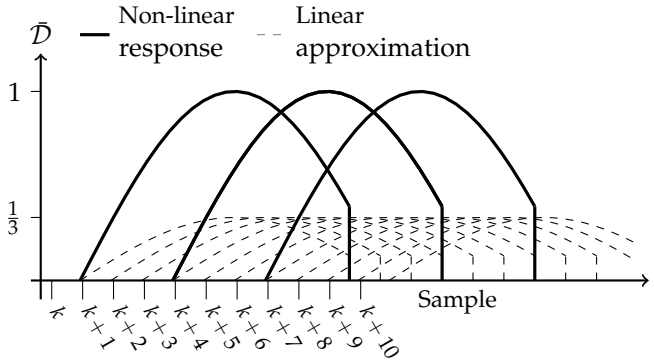

Fig. 3.15: Discretization of displacement response [Paper **I**].

The linear duty cycle approximation is seen to result in an angle average description of the output. Although that the integrated output of the linear model matches the nonlinear response, it is significantly smoother. The linear approximation is also seen to be increasingly inaccurate for lower displacements, where the highly non-smooth pulsating behavior is not very well captured. As a result, one should be carefully when applying this strategy for machines with a low number of cylinders and for operation at low displacements.

Variable Speed Operation

An additional challenge is introduced if a variable speed DDM is to actuate a continuous time plant, which is very often the case. The constant control decision rate in the angle domain result in a varying decision rate in the time domain for speed varying machine operation. To enable classical discrete control of such system, by having a constant decision rate, requires a transformation of the continuous time equations to the angle domain by

$$\frac{dx}{dt} = f(x(t)) \qquad \frac{dx}{d\theta} = \frac{1}{\omega(\theta)}\frac{dx}{dt} \longrightarrow \frac{dx}{d\theta} = \frac{1}{\omega(\theta)} f(x(\theta)) \tag{3.19}$$

where $f(x(t))$ described the continuous plant dynamics with state x. Conversion from the time to the angle domain is seen to introduce a nonlinearity through the multiplication of the reciprocal shaft speed. Like the continuous approximation, a steady state operation speed may be chosen as linearization point and the speed of the machine has to be above this value to maintain the stability margins. After linearization, the plant may afterwards be discretized by the decision angle when considering a sample-and-hold input from the discrete approximated DDM model.

3.5.2 Partial Stroke Operation

For partial stroke operation, only a part of the full stroke is used, which introduces additional complications seen from a partial stroke discrete approximation shown in Fig. 3.16.

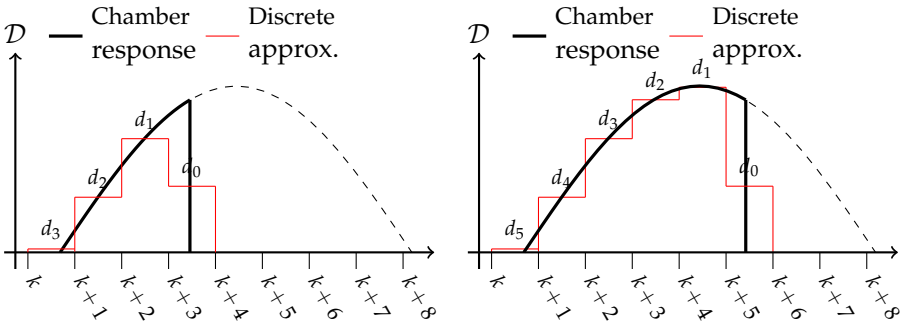

Fig. 3.16: Left: Discrete approximation with $\eta = 0.3$. Right: Discrete approximation with $\eta = 0.7$ [Paper **G**].

It is seen that the displacement is committed over less samples and the number of samples is depending on the input displacement fraction. As a result, the transfer function model order and coefficients are functions of the

displacement fraction input. The resulting transfer functions for the illustrated examples are given to be

$$G_1(z) = \frac{d_3\, z^3 + \cdots + d_1\, z + d_0}{z^3} \qquad G_2(z) = \frac{d_5\, z^5 + \cdots + d_1\, z + d_0}{z^5} \tag{3.20}$$

Since the displacement fraction is a varying input, the discrete model structure is an input dependent angle varying system. By further allowing the closing angle of the HPV (displacement fraction) to be changed until the HPV is closed, yields an unknown impulse response when the stroke is initiated. This is considered a tough control challenge and does not comply with any classical control theory. How the system dynamics varies depending on the input as illustrated by the frequency response shown in Fig. 3.17.

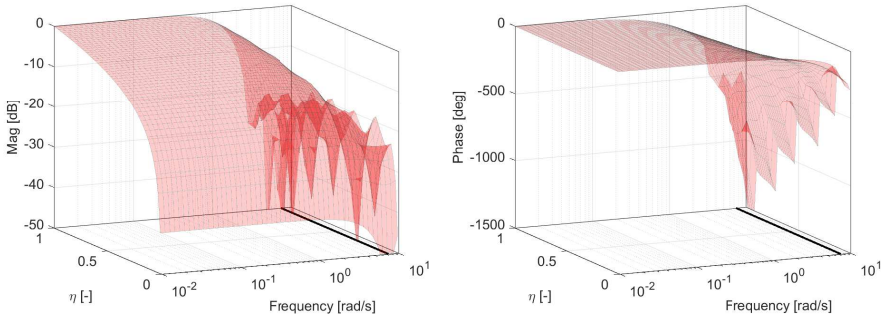

(a) Magnitude as function of displacement fraction and frequency.

(b) Phase as function of displacement fraction and frequency.

Fig. 3.17: Frequency response as function of the displacement fraction input [Paper **G**].

It is seen that the worst-case phase contribution occurs for a full stroke, $\eta = 1$, and thus represents a worst case scenario with respect to the phase contribution. Using a strategy where the displacement fraction is fixed when the stroke is initialized greatly simplifies the control problem. A conservative angle invariant model is obtained by choosing a linearization point of $\eta = 1$, which result in an angle average approximation where the integrated output over a full stroke matches the physical response. The angle average approximation is illustrated in Fig. 3.18.

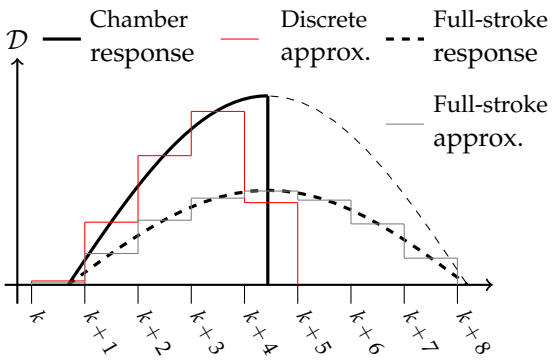

Fig. 3.18: Discretization of displacement response, where $\eta = 0.5$ corresponding to half of a stroke. A full stroke $\eta = 1$, with $u = 0.5$ yields the angle average committed displacement as if $\eta = 0.5$ and $u = 1$ [Paper **G**].

It is seen that the angle average approximation is increasingly inaccurate for lower displacement fractions, where a significantly smoother response is obtained. However, the presented model is considered the best possible when considering a DLTI approximation.

Summarization:

- Relatively simple dynamical model approach and well-known control design strategies in the linear case.
- Does describe the discrete sampling effect and the non-smooth ripple dynamics.
- Valid in a broad frequency range (up to the Nyquist frequency).
- Reduced accuracy for a lower number of cylinders.
- Results in a nonlinear model if the shaft speed is varying.
- Results in a time varying model when using partial stroke operation.
- In case of applying linear control, the minimum speed has to be higher than the linearization speed to maintain the stability margins.
- In case of a linear approximation, it is increasingly inaccurate for lower displacements.

3.6 Hybrid Dynamical System

Since the non-smooth dynamics of the digital displacement machine comprises of both continuous time dynamics and discrete switching events, the

system is essentially a hybrid dynamical system. Although the continuous and discrete approximations are applicable in certain operation regions, their applicability is limited, especially if linear control theory is considered. To more accurately capture the machine dynamics and allow for analysis and control design in a broader range of situations, hybrid dynamical system theory is deemed necessary.

The class of hybrid dynamical system comprises several sub-classes with different structures, which describes the non-smooth interactions differently. The choice of hybrid class model is often based on the type of switching phenomena for the given system. Mention-worth classes are; switched systems, impulsive systems, hybrid automatons, petri nets, discrete event dynamical systems, etc. However, in general all of the different branches may be described through a hybrid dynamical notation.

A hybrid dynamical system comprises both continuous differential (flow) equations and discrete difference (jump) equations [10, 73, 75, 84]. A hybrid system is in generality formulated by

$$\mathcal{H}: \quad \begin{cases} \dot{x} & \in F(x,u), & x \in C, \\ x^{+} & \in G(x,u), & x \in D \\ y & = h(x,u) \end{cases} \tag{3.21}$$

where $\dot{x}$ is the state time derivative and x^{+} is the state value after a jump. u and y are the input and output respectively. The system dynamics is described by the following maps and sets:

- The flow set: C
- The flow map: F
- The jump set: D
- The jump map: G
- The output map: h

As long as x belongs to the flow set, C, it is described by the differential inclusion given by the flow map, F and when x belongs to the jump set, D, it is described by the difference inclusion given by the jump map G. The dynamical behavior of a hybrid system is illustrated in Fig. 3.19.

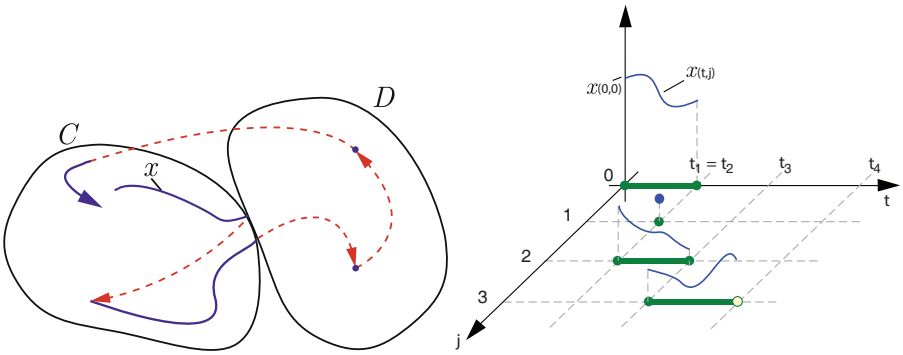

(a) State behavior of a hybrid dynamical system. Modified from [10].

(b) Solution behavior of a hybrid dynamical system. Modified from [10].

Fig. 3.19: Dynamical behavior of a hybrid dynamical system.

The left figure illustrates how the state evolves in accordance with the continuous flow map when it belongs to the flow set and how the state discretely jumps based on the jump map when reaching the jump set. The right figure illustrates the solution domain of a hybrid system, where t is the time and j is a counter for every jump caused by triggering the jump set. Contrary to conventional discrete control of continuous systems where the time generates the jumps, also a combination of the states may generate a jump for hybrid systems.

3.6.1 Hybrid DDM Model

Hybrid models are intuitive and enables an accurate description of the DDM dynamics. However, the same behavior may be obtained with numerous model structures depending on how the switching phenomenas and state evolving are modeled. With respect to control it is desired to have a relatively simple model which only captures the fundamental characteristics and thereby significantly reduces the control design complexity. This section presents a physical intuitive model which includes the pressure chamber dynamics and therefore is relatively accurately, as well as a simper model only applicable for full stroke operation.

Physical intuitive model

The physical intuitive model is established by describing the dynamics of each individual pressure chamber by the corresponding differential equations. The flow map and set for a single pressure chamber is given by (3.22)

in correspondence with the model presented in Sec. 2.1.

$$\left.\begin{aligned}
\dot{\theta} &= \omega \\
\dot{p}_\mathrm{i} &= \frac{\beta_\mathrm{e}}{V_\mathrm{i}} \left(Q_{\mathrm{H,i}} - Q_{\mathrm{L,i}} - \dot{V}_\mathrm{i}\right) \\
V_\mathrm{i} &= \frac{V_\mathrm{d}}{2} \left(1 - \cos(\theta_\mathrm{i})\right) + V_0 \\
\dot{V}_\mathrm{i} &= \frac{V_\mathrm{d}}{2} \sin(\theta_\mathrm{i})\, \omega \\
Q_{\mathrm{L,i}} &= \frac{x_{\mathrm{L,i}}}{k_\mathrm{f}} \sqrt{|p_\mathrm{i} - p_\mathrm{L}|}\, \mathrm{sign}\left(p_\mathrm{i} - p_\mathrm{L}\right) \\
Q_{\mathrm{H,i}} &= \frac{x_{\mathrm{H,i}}}{k_\mathrm{f}} \sqrt{|p_\mathrm{H} - p_\mathrm{i}|}\, \mathrm{sign}\left(p_\mathrm{H} - p_\mathrm{i}\right) \\
\dot{x}_{\mathrm{L,i}} &= \frac{1}{\tau_\mathrm{v}} \left(u_{\mathrm{L,i}} - x_{\mathrm{L,i}}\right) \\
\dot{x}_{\mathrm{H,i}} &= \frac{1}{\tau_\mathrm{v}} \left(u_{\mathrm{H,i}} - x_{\mathrm{H,i}}\right) \\
\dot{u}_{\mathrm{L,i}} &= 0 \\
\dot{u}_{\mathrm{H,i}} &= 0 \\
\dot{q}_\mathrm{i} &= 0
\end{aligned}\right\} \quad (x_\mathrm{i}, u_\mathrm{i}) \in \underbrace{\mathbb{R}^n \setminus D_\mathrm{i}}_{C_\mathrm{i}} \qquad (3.22)$$

where $x_\mathrm{i} = \begin{bmatrix}\theta & p_\mathrm{i} & x_{\mathrm{L,i}} & x_{\mathrm{H,i}} & u_{\mathrm{L,i}} & x_{\mathrm{H,i}} & q_\mathrm{i}\end{bmatrix}^T$ are the states. The i'th entry indicates that there should be a state for each pressure chamber. The valves dynamics are modeled as a first order system with time constant τ_v. $u_\mathrm{L} \in \{0, 1\}$ and $u_\mathrm{H} \in \{0, 1\}$ are the valve inputs (active or inactive). The state q is introduced to identify which mode the chamber operates in and is used to set-up a hybrid automaton representation. Additional states describing the shaft acceleration, high pressure dynamics, etc. may also be included similarly to how the shaft angle state is included.

The digital valve actuation dynamics is described by considering the hybrid automaton shown in Fig. 3.20. The three modes are seen to be idle, compression and pressurization. Two mode switching functions are defined as $\lambda_\mathrm{H} = F_\mathrm{H} - (p_\mathrm{H} - p)\, A_\mathrm{v}$ and $\lambda_\mathrm{L} = F_\mathrm{L} - (p - p_\mathrm{L})\, A_\mathrm{v}$ and are used to construct the jump maps. The mode switching function are described by considering the force equilibrium illustrated in Fig. 3.21.

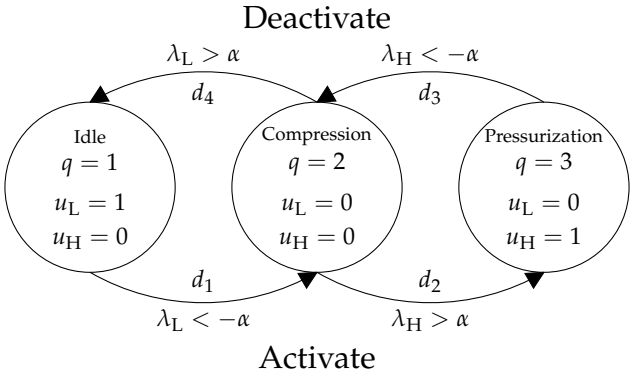

Fig. 3.20: Hybrid Automaton representation of valve control of the digital displacement machine [Paper **K**].

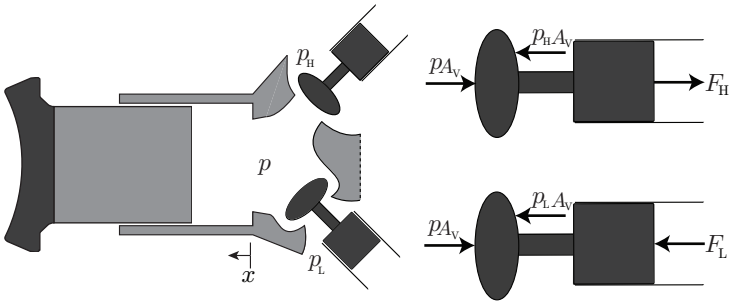

Fig. 3.21: DDM chamber model and force equilibrium used to construct the switching functions.

The system inputs are the valve forces, $u = \begin{bmatrix} F_H & F_L \end{bmatrix}^T$ for the high and low pressure valve respectively. A_v is the effective valve area that the pressure is generating a force on. The effective valve area is simplified to be the same on both sides of the valve. Since the valve areas are truly not identically on both sides, different areas should be used to increase the model accuracy. The mode switching functions hence generates jumps based on the relation between the force input and the force generated by the pressure difference across the valve.

To transfer from idle mode to compression mode, the LPV is closed by a force $F_L < -\alpha$. In compression mode a pressure build up is created due to fluid compression and when $(p - p_H) A_v > \alpha$ the HPV is passively opened due to the generated pressure force. Similar transitions are made to deactivate the pressure chamber, where the HPV is actively closed and the LPV is

passively opened. The constant α creates a minor hysteresis band around the switching point, to avoid numerous jumps subsequently between modes.

The hybrid automaton representation is used to set-up the jump maps and sets and are given by

$$
\left.\begin{aligned} \theta^+ &= \theta \\ p_{\mathrm{i}}^+ &= p_{\mathrm{i}} \\ x_{\mathrm{L,i}}^+ &= x_{\mathrm{L,i}} \\ x_{\mathrm{H,i}}^+ &= x_{\mathrm{H,i}} \end{aligned}\right\} \quad (x_{\mathrm{i}}, u_{\mathrm{i}}) \in D_{\mathrm{i}} \qquad D_{\mathrm{i}} = D_{\mathrm{q1,i}} \cup D_{\mathrm{q2,i}} \cup D_{\mathrm{q3,i}}
$$

$$
\left.\begin{aligned} u_{\mathrm{L,i}}^+ &= 1 \\ u_{\mathrm{H,i}}^+ &= 0 \\ q_{\mathrm{i}}^+ &= 1 \end{aligned}\right\} \quad \underbrace{(x_{\mathrm{i}}, u_{\mathrm{i}}) \in d_{4,\mathrm{i}} \wedge q_{\mathrm{i}} = 2}_{D_{\mathrm{q1,i}}} \tag{3.23}
$$

$$
\left.\begin{aligned} u_{\mathrm{L,i}}^+ &= 0 \\ u_{\mathrm{H,i}}^+ &= 0 \\ q_{\mathrm{i}}^+ &= 2 \end{aligned}\right\} \quad \underbrace{((x_{\mathrm{i}}, u_{\mathrm{i}}) \in d_{1,\mathrm{i}} \wedge q_{\mathrm{i}} = 1) \vee ((x_{\mathrm{i}}, u_{\mathrm{i}}) \in d_{3,\mathrm{i}} \wedge q_{\mathrm{i}} = 3)}_{D_{\mathrm{q2,i}}}
$$

$$
\left.\begin{aligned} u_{\mathrm{L,i}}^+ &= 0 \\ u_{\mathrm{H,i}}^+ &= 1 \\ q_{\mathrm{i}}^+ &= 3 \end{aligned}\right\} \quad \underbrace{(x_{\mathrm{i}}, u_{\mathrm{i}}) \in d_{2,\mathrm{i}} \wedge q_{\mathrm{i}} = 2}_{D_{\mathrm{q3,i}}}
$$

Three jump maps and sets are required for each pressure chamber to describe the three modes as seen. Since each pressure chamber requires 6 states, the model becomes increasingly larger for a higher number of cylinders. It is seen that only the valve input states, u_{L} and u_{H} and the mode state q are updated on a jump, while the remaining states values are continuous and therefore maintains their values. Simulation results for the presented hybrid dynamical model of the DDM is shown in Fig. 3.22 for both pumping and motoring strokes. The simulations are done by use of the Hybrid Equations Toolbox v2.04 for Matlab. It is seen that the hybrid model yields a rather accurate description of the DDM dynamics, where also the pressure and valve dynamics is included. Although it is not shown, the model is also valid for operation in both directions of motion, partial stroke and sequential partial stroke operation [Paper **K**].

Despite the physical accuracy of the hybrid model, it is considered challenging to utilize it for stability analysis and control design. This is due to the quite large number of states, as well as multiple jump maps and sets. Additionally, an infinite number of sizes and shapes of the force input yields the same response, while the actuation energy may be very different. The presented hybrid dynamical model is made in a general description where control design is made through stability analysis using Lyapunov functions

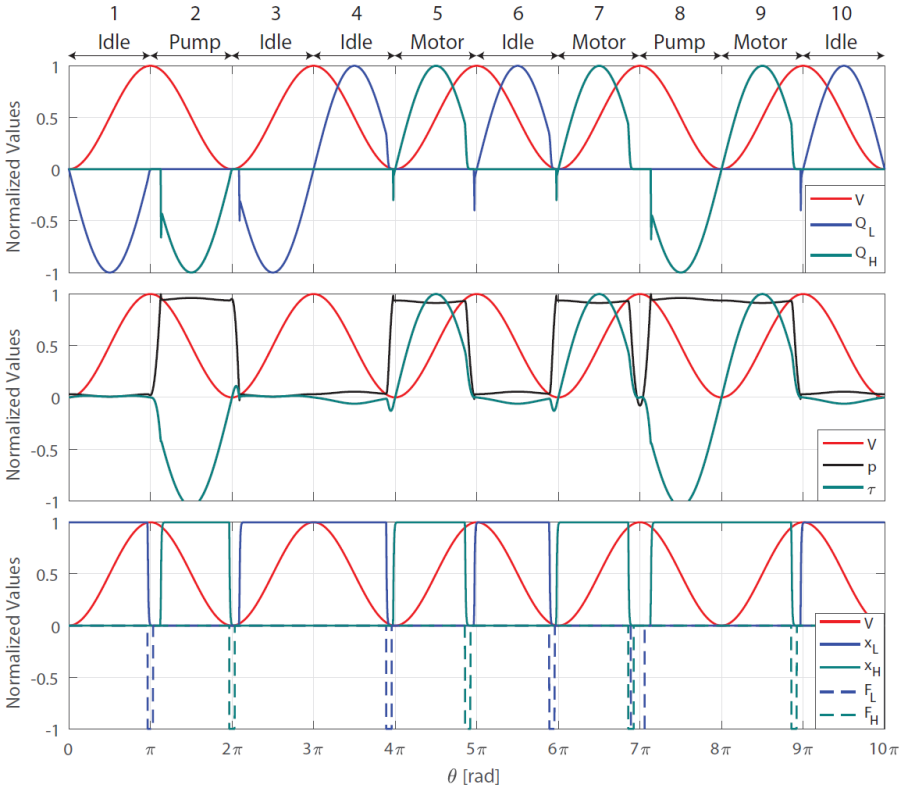

Fig. 3.22: Simulation of a pumping, idling and motoring strokes of the digital displacement machine. $\dot{\theta} = 100\,\text{rpm}$, $p_\text{H} = 300\,\text{bar}$, $p_\text{L} = 10\,\text{bar}$, $\tau_\text{v} = 2\text{ms}$, $\alpha = 50\text{N}$ and $A_\text{v} = 0.317\,\text{cm}^2$ [Paper **K**].

and passivity theorems [10,73,75,84]. Due to the model complexity, it is considered a very tough mathematical task to derive control algorithms based on the presented model.

As mentioned earlier a partial or sequential partial stroke method are considered most suitable for relatively low speed operation. Since energy consumption, as well as torque and pressure pulsations are desired to be minimum, a model predictive strategy is considered highly favorable for partial stroke methods at low speeds. The presented hybrid model is not directly applicable for model predictive control and demands a reformulation. Sniegucki (2016) [78] has made a tremendous contribution with respect to model predictive control using discretization of DDM dynamics with binary inputs. However, a discrete model requires motion in the same shaft direction to have a monotonic increasing control decision scheme. Since numerous hydraulic systems requires pumps and motors operating in two or

more quadrants, models as the above presented may be a necessity for such system.

Full stroke model

Stability based control design for hybrid systems is assessed to have the highest potential for high speed operation using a full stroke strategy. Therefore, a much simpler hybrid dynamical model is proposed for full stroke operation in a single quadrant (pumping or motoring in one direction of motion). With a full stroke method, the system is a sample-and-hold control system with a constant decision angle. Such system is modeled by timers for hybrid dynamical systems. As an example, a sample-and-hold feedback control system for a continuous plant may be modeled as a hybrid system on the form given by

$$\left.\begin{aligned}\dot{x} &= -0.1\,x + u\\ \dot{\chi} &= 1\\ \dot{z} &= 0\end{aligned}\right\}\quad \chi \in [0,1]$$

$$\left.\begin{aligned}x^+ &= x\\ \chi^+ &= 0\\ z^+ &= u = -0.4\,x\end{aligned}\right\}\quad \chi = 1 \tag{3.24}$$

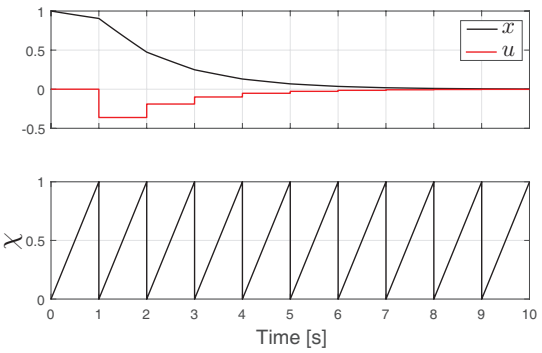

Fig. 3.23: Example of hybrid dynamical sample-and-hold control model and response [Paper **J**].

A first order continuous plant is seen to be discretely controlled by the control law $u = -0.4\,x$, which input is held constant between samples. The timer χ counts the time between samples and generates the control update and subsequently resets when reaching the sample time (jump map) of $1\,s$.

For the full stroke operated DDM, an input decision is taken at a constant angle for every cylinder. When a decision of an active stroke is taken, the response is affected for the next half of a revolution where the subsequent decisions are taken meanwhile. This is illustrated in Fig. 3.24 by the sampling scheme of a DD motor with 42 cylinders. It is seen that there is an initial delay of θ_d lasting for a few samples and it takes m samples to describe the full stroke. The memory effect is described by introducing an input decision

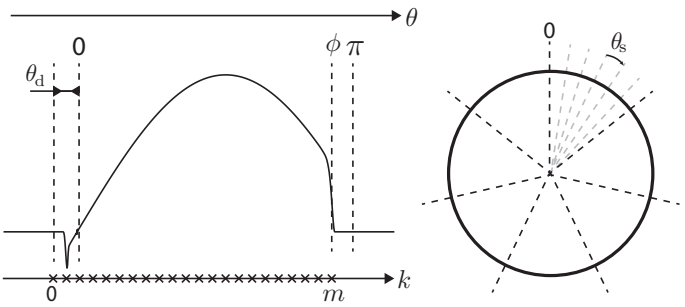

Fig. 3.24: Sampling scheme for DD motor with 42 cylinders. [Paper **I**].

state vector defined as

$$z_{\mathrm{u}}^{+} = \begin{bmatrix} z_{\mathrm{u}}(k) & z_{\mathrm{u}}(k-1) & \dots & z_{\mathrm{u}}(k-m) \end{bmatrix}^{T} \tag{3.25}$$

where $z_{\mathrm{u}} \in \{0,1\}$ contains the previous input decisions. The memory states for the input are updated linearly by the matrix-vector representation given by

$$\underbrace{\begin{bmatrix} z_{\mathrm{u}}(k) \\ z_{\mathrm{u}}(k-1) \\ z_{\mathrm{u}}(k-2) \\ \vdots \\ z_{\mathrm{u}}(k-m) \end{bmatrix}}_{z_{\mathrm{u}}^{+}} = \underbrace{\begin{bmatrix} 0 & 0 & \cdots & 0 & 0 \\ 1 & 0 & \cdots & 0 & 0 \\ 0 & 1 & \cdots & 0 & 0 \\ \vdots & \vdots & \ddots & \vdots & \vdots \\ 0 & 0 & \cdots & 1 & 0 \end{bmatrix}}_{A_{\mathrm{u}}} \underbrace{\begin{bmatrix} z_{\mathrm{u}}(k-1) \\ z_{\mathrm{u}}(k-2) \\ \vdots \\ z_{\mathrm{u}}(k-m) \\ z_{\mathrm{u}}(k-m-1) \end{bmatrix}}_{z_{\mathrm{u}}} + \underbrace{\begin{bmatrix} 1 \\ 0 \\ 0 \\ \vdots \\ 0 \end{bmatrix}}_{B_{\mathrm{u}}} u(k) \tag{3.26}$$

The hybrid formulation is described by (3.27) where an angle timer is used to trigger the jump map and thereby accounts for variable speed operation.

$$\left.\begin{aligned} \dot{\theta} &= \omega \\ \dot{\chi} &= \omega \\ \dot{z}_{\mathrm{u}} &= 0 \\ \dot{z}_{\theta} &= 0 \end{aligned}\right\} \; \chi \in [0, \theta_{\mathrm{s}}] \quad \left\{\begin{aligned} \theta^{+} &= \theta \\ \chi^{+} &= 0 \\ z_{\mathrm{u}}^{+} &= A_{\mathrm{u}}\, z_{\mathrm{u}} + B_{\mathrm{u}}\, u \\ z_{\theta}^{+} &= \theta \end{aligned}\right\} \; \chi = \theta_{\mathrm{s}} \tag{3.27}$$

where $u \in \{0,1\}$ and θ_{s} is the constant sampling angle. The state z_{θ} contains the angle where the newest sample has been taken and is used to shift the output map accordingly. By neglecting the fast chamber pressure dynamics,

the flow and torque throughput may be described as

$$Q_{\mathrm{m}}(t) = \sum_{i=1}^{N_{\mathrm{c}}} Q_{\mathrm{H},i}(t) \approx \frac{V_{\mathrm{d}}}{2}\,\omega(t)\,\sum_{i=n}^{m} \sin\left(\theta(t) - \underbrace{z_\theta + \theta_{\mathrm{s}}\,(i-1) - \theta_{\mathrm{d}}}_{\theta_{\mathrm{shift}}}\right) z_{\mathrm{u},i}$$
$$\tau_{\mathrm{m}}(t) = \sum_{i=1}^{N_{\mathrm{c}}} \tau_i(t) \approx \frac{V_{\mathrm{d}}}{2}\,p_{\mathrm{H}}(t)\,\sum_{i=n}^{m} \sin\left(\theta(t) - \underbrace{z_\theta + \theta_{\mathrm{s}}\,(i-1) - \theta_{\mathrm{d}}}_{\theta_{\mathrm{shift}}}\right) z_{\mathrm{u},i} \tag{3.28}$$

where Q_{m} and τ_{m} are the total flow and torque throughput of the DDM and constitutes the output map $y = [Q_{\mathrm{m}}\ \tau_{\mathrm{m}}]^T$. The n'th sample is the first sample after the delay, θ_{d}, with a displacement output. The shifting angle, θ_{shift}, is updated accordingly to the shaft angle to generate the correct sine waves.

The full stroke hybrid model is validated by comparing its response to that of a nonlinear model similar to that with a response shown in Fig. 3.22. A radial piston motor comprising 42 cylinders and a multi-lobe cam-ring pump comprising 100 cylinders and 25 lobes for a 5 MW transmission have been simulated. The impulse responses are obtained by simulation in the Hybrid Equations Toolbox v2.04 for Matlab and are shown in Fig. 3.25.

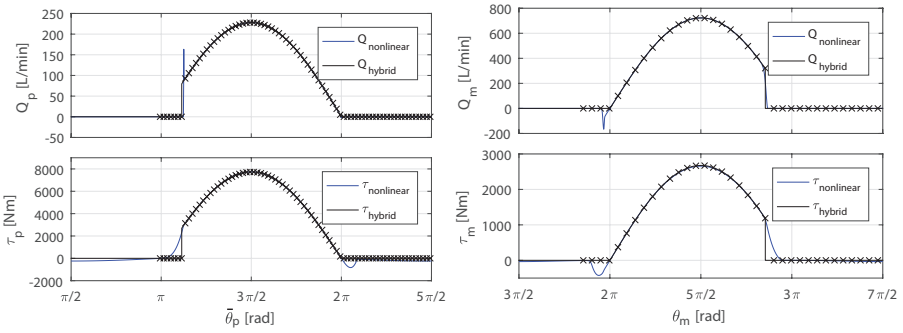

(a) Pump **(b)** Motor

Fig. 3.25: Validation of the full stroke hybrid model of the flow and torque model of the DDM. $p_{\mathrm{H}} = 350\,\mathrm{bar}$ and $\omega = 1500\,\mathrm{rpm}$ for the motor and $\omega = 9.1\,\mathrm{rpm}$ for the pump [Paper **J**].

Fairly accurate approximation responses are seen with minor deviates in the beginning and end of the stroke due to neglecting of the pressure dynamics. This hybrid model is also increasingly accurate for a higher number of cylinders, since the output map is discretized by the number of cylinders. However, a model improvement could be made by utilizing another description of the displacement for the first and last sample of the active stroke part.

A further model simplification is made by considering a constant output between samples similar to the discrete model presented in Sec. 3.5.1. The resulting state model representation is similar to that in (3.27) and the only difference is that the sampling angle state is omitted. The resulting hybrid state model thus becomes

$$\left.\begin{aligned}\dot{\theta} &= \omega \\ \dot{\chi} &= \omega \\ \dot{z}_\mathrm{u} &= 0\end{aligned}\right\} \; \chi \in [0, \theta_\mathrm{s}] \quad \left\{\begin{aligned}\theta^+ &= \theta \\ \chi^+ &= 0 \\ z_\mathrm{u}^+ &= A_\mathrm{u}\, z_\mathrm{u} + B_\mathrm{u}\, u\end{aligned}\right\} \; \chi = \theta_\mathrm{s} \tag{3.29}$$

The output map is generated by the sum of individual displacement fractions obtained by the procedure presented in Sec. 3.5.1. The output map is given to be

$$\begin{aligned}\mathcal{D} &= \underbrace{\begin{bmatrix}\mathcal{D}[0] & \mathcal{D}[1] & \mathcal{D}[2] & \cdots & \mathcal{D}[m]\end{bmatrix}}_{C}\, z_\mathrm{u} \\ y &= \begin{bmatrix}Q_\mathrm{m} & \tau_\mathrm{m}\end{bmatrix}^T = \begin{bmatrix}\omega\, C\, z_\mathrm{u} & p_\mathrm{H}\, C\, z_\mathrm{u}\end{bmatrix}^T\end{aligned} \tag{3.30}$$

The response of the hybrid model is again compared to the nonlinear model representing the physical system. The simulation results are shown in Fig. 3.26.

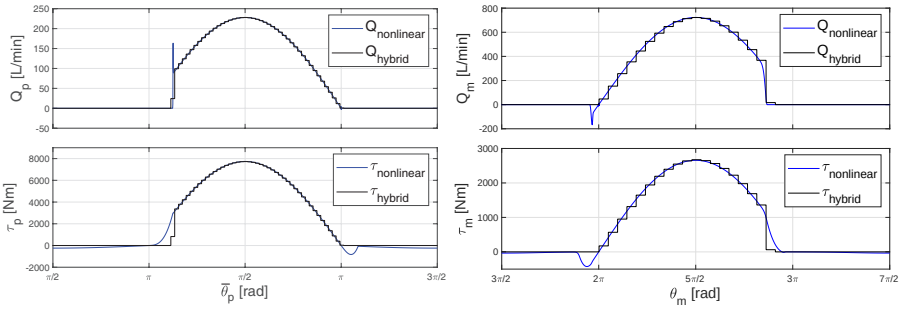

(a) Pump **(b)** Motor

Fig. 3.26: Validation of the full stroke hybrid model of the flow and torque model of the DDM. $p_\mathrm{H} = 350\,\mathrm{bar}$ and $\omega = 1500\,\mathrm{rpm}$ for the motor and $\omega = 9.1\,\mathrm{rpm}$ for the pump.

The simulated responses are identically to that obtained with the discrete linear model, when assuming that the pressure jumps directly between high and low pressure. A more precise torque approximation may thus be obtained by also discretization the chamber pressure dynamics as described in (3.16).

The hybrid model is capable of capturing the nonlinearity in the output map where states are multiplied, as well as the position dependent sampling

and the quantizer effect. Additionally, it enables description of eventually nonlinearities in the application dynamics.

Summarization:

- Intuitive and possibly accurate model, where the complexity is greatly dependent on the chosen level of accuracy.
- Does describe the discrete sampling effect and the non-smooth ripple dynamics.
- Does describe the nonlinear continuous dynamics
- Reduced accuracy for a lower number of cylinders for the two full stroke models
- Difficult and complex control design based on nonlinear stability analysis.

Chapter 4

Application Control Synthesis

With a variety of different dynamical model representations, it is not evident when to use which model for control design and how to perform controller synthesis. As identified, several of the presented models are only valid under certain conditions and their complexity with respect to use for control design are vastly different. Additionally, the application utilization has a large impact on the challenges with respect to synthesizing the controllers. Therefore, the following chapter describes and discusses control design methods based on the presented dynamical model.

4.1 Low Speed - Partial Stroke Operation

For low speed operation it is found favorable in Sec. 2.1.3 to use a partial stroke operation method combined with model prediction control (MPC). This gives the possibility to optimize the control performance relative to the energy cost and generated pressure/torque pulsations caused by valve switchings. Since the continuous partial stroke model approximation (featuring a pulse-width-modulation technique) is not applicable for MPC, the strategy is only considered feasible for partial stroke operation if the goal is to use the simplest strategy. In this thesis, a conventional discrete model based MPC strategy is investigated for control of the partial stroke operated DDM.

4.1.1 Discrete Linear MPC:

Since the input of a partial stroke operated DDM scales the width of the response and not the amplitude, the discrete model is input dependent with unity amplitude as identified in Sec. 3.5.2. A model predictive strategy for partial stroke operation is proposed in Paper **G** and is written as

$$\begin{aligned} \eta^* &= \underset{\eta^* \in [0,\eta_{\max}]}{\arg\min} \left\{ J_1^T\, J_1 + W_1\, J_2^T\, J_2 \right\} \\ J_1 &= \sum_{k=1}^{p} \left(y[k] - y_{\text{ref}}[k] \right) \qquad J_2 = \sum_{k=1}^{p} \frac{d}{d\theta} V(\phi(\eta[k]))) \\ y[k] &= C(\eta[k])\, x[k] + D(\eta[k]) \qquad x[k+1] = A(\eta[k])\, x[k] + B(\eta[k]) \end{aligned} \tag{4.1}$$

where p is the number of samples in the prediction horizon, $\eta^* \in [0, \eta_{\max}]$ is the optimal input. The prediction horizon is chosen as the number of samples necessary to describe a full stroke (approx. $N_c/2$) and $\eta_{\max} \approx 0.96$ is the maximum displacement fraction corresponding to a full stroke. J_1 and J_2 are the functions to minimize and represent the reference tracking error and the switching energy (pulsation magnitude) respectively. W_1 is a weighting parameter specifying the relative importance between tracking performance and energy/pulsation reduction. A simple representation is made of the energy and pressure/torque pulsation term, where it is assumed that the energy and pulsation magnitude is proportional to the flow level when switching.

The dynamical state model is obtained by rewriting the transfer function representation in (3.20). The model with output $y = Q_m \vee \tau_m$ is seen to be varying and depends on the optimal solution η^*. Such problem is possible to solve through various optimization methods but does not belong to classical MPC, since the input to the model is always unity. Additionally, stability proof of such problem may be very hard to find if it even exists.

To obtain a discrete linear time invariant (DLTI) MPC problem, the conservative linearization approach shown in Fig. 3.18 may be used to obtain a linear model and apply classical MPC. The linearization approach result in the state space form given by (4.2) and has the impulse response shown in Fig. 3.13.

$$y[k] = C\, x[k] + D\, u[k] \qquad x[k+1] = A\, x[k] + B\, u[k] \tag{4.2}$$

An illustration of the DLTI MPC strategy for a 15 cylinder DDM is illustrated in Fig. 4.1. The decision for the 5'th cylinder $c5$ is taken at sample $k = 1$, where the decision for the previous cylinders are fixed. The MPC algorithm estimates the optimal displacement fractions for the subsequent cylinders in the prediction horizon of a full stroke. The choice of suitable solving algo-

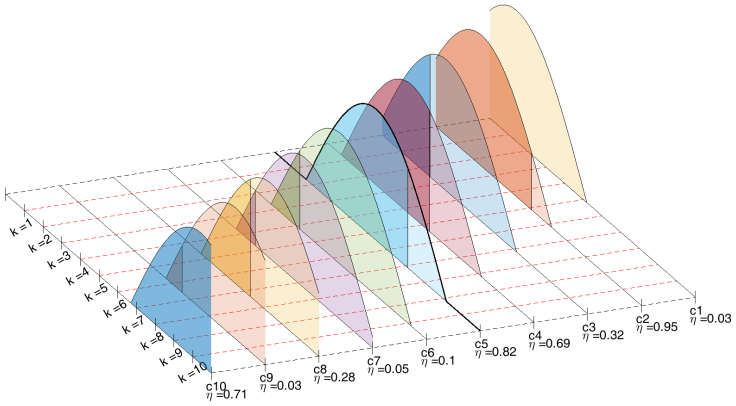

Fig. 4.1: Illustration of the model predictive control strategy for partial stroke operation [Paper **G**].

rithm for the optimization problem has not been investigated in this thesis, since no specific application has been studied. The objective is of course to identify the global minimum (or the lowest possible objective function value) and have a low computational time, such that the algorithm is suitable for online implementation.

It is clear that the DLTI MPC strategy does not allow a re-decision of the displacement fraction, since the HPV closing angle is determined in the beginning of the stroke. Being able to make a re-decision is expected to increase the tracking performance due to a reduced phase in the control system. Additionally, it is also expected to reduce the energy consumption and pulsation magnitude. Therefore, research into more advanced MPC strategies with online solving capability is desired.

Several more advanced classes of MPC are considered feasible for the presented models in Chap. 3, but additional alternative MPC strategies may likely exist.

- Advanced discrete MPC (Discrete): nonlinear, robust, adaptive etc. The methods feature a discrete model where the optimal input is found through optimization in a finite prediction horizon [30].
- Mixed Logical Dynamical Programming (Hybrid): Optimal control strategy involving a discrete model, as well as discrete valued states, constraints and logic elements. This makes it possible to include the special type of input when solving for the optimal input in the prediction horizon. Additionally, constraints to the closing and opening of valves may be implemented in the control structure [13, 28].
- Lyanunov based MPC (Hybrid): Deals with hybrid systems, where the state equations are solved in the prediction horizon from where the op-

timal input is found through stability proofs featuring Lyapunov Control Functions (LCF) [35].

Each method has its own advantages and disadvantages related to complexity, accuracy, computational time, etc. A Mixed Logical Dynamical (MLD) system representation and control strategy for a fixed speed DDM has been demonstrated and show promising results [78]. However, due to the high computational time, the speed of the machine has to be very low for online implementation. Lyapunov based MPC for hybrid systems is considered a tough mathematical problem, since it relies on finding a Lyapunov control function that ensures that the energy dissipates for every sample (jump) [35]:

$$... \leq V_{\text{MPC}}(x_{k+1}) \leq V_{\text{MPC}}(x_k) \leq ... \leq V_{\text{MPC}}(x_0) \tag{4.3}$$

where V_{MPC} is a Lyapunov control function fulfilling the required criterias. Although that the strategies are rather complex, such methods are demanded and further research is required.

4.1.2 Sequential Partial Stroke

In sequential partial stroke, the valves may be switched multiple times and at any angle during a stroke. However, to obtain a constant sampling angle required for conventional MPC, a strategy where the valves are only switched at discrete angles is proposed. This greatly simplifies the control problem, since the MPC problem becomes time invariant.

The proposed strategy divides a full stroke into discrete steps, where the valves may only be switched at the discrete angles. Since the strategy is considered for very low speed operation, the valve switching time is fast compared to the time it takes to perform a full stroke. Therefore, the switching dynamics is neglected and the input is a displacement fraction. By dividing the stroke into discrete steps, every cylinder may either be active or inactive for every step.

Since it is desired to be able to switch the pressure chambers on and off in the beginning and at the end of the stroke, a full revolution is divided into the same number of parts as there is cylinders. A comparison between the discrete model and the nonlinear model is shown in Fig. 4.2 for a 10 cylinder DDM. Large valves capable of opening against a high pressure difference are used. It is seen that the same cylinder is subsequently switched on and off at every discrete decision angle. It is seen that the nonlinear model has severe torque and flow spikes due to the high pressure difference when switching the valves. It is clear that it cost the most energy to switch the valves when opening against high pressure difference at large flows. The energy cost function hence penalize the valves that opens against the highest pressure difference at a large flow rate [Paper **H**].

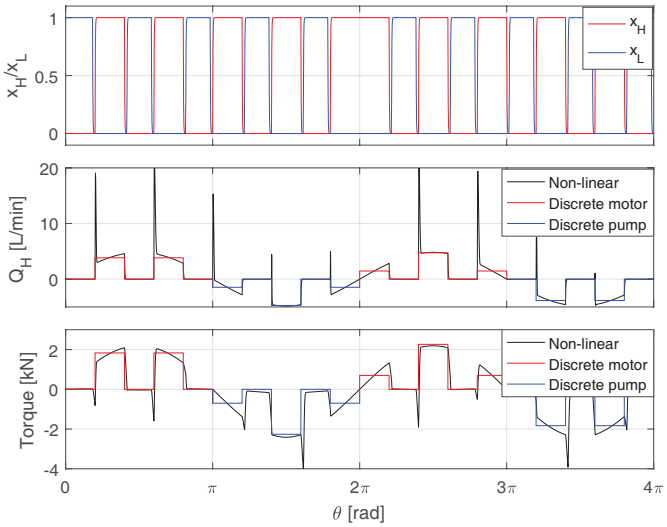

Fig. 4.2: Comparison between DLTI and nonlinear model, $\omega = 10\,\text{rpm}$, $p_\text{H} = 300\,\text{bar}$ [Paper **H**].

Since every cylinder can be either active or inactive, there are $2^{N_\text{c}} = 1024$ combinations for every decision, whose tracking performance and energy consumption may be very different. By only allowing the machine to either motor or pump the number of combinations is reduced to $(2^{N_\text{c}}/2) = 32$. The discrete displacement fraction are shown in Fig. 4.3 for a DD pump.

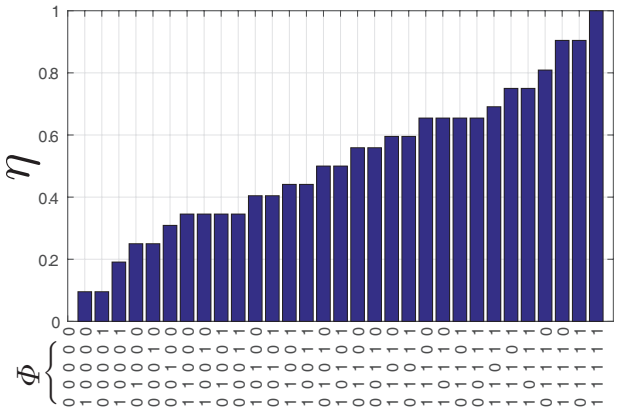

Fig. 4.3: Discrete displacement fraction inputs [Paper **H**].

Since the input is chosen from a set of discrete values, the optimization algorithm has to be capable of handling a discrete valued optimization problem. The discrete model of the DDM becomes that in (4.4) and is very simple

since there is no memory effect.

$$y[k] = D\,u[k] \quad u[k] \in \eta \tag{4.4}$$

Although the DDM model is simple, a discrete dynamical representation is introduced when the machine is combined with the controlled plant dynamics. An illustration of the sequential partial stroke MPC strategy for a 10 cylinder DDM is illustrated in Fig. 4.4.

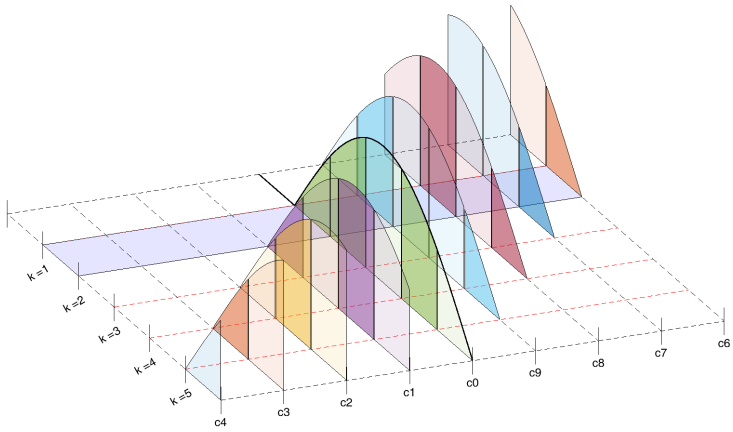

Fig. 4.4: Illustration of the chamber actuation decisions in the prediction horizon [Paper **H**].

The MPC strategy is seen to predict which valves that should be active (solid color) and which should be inactive (transparent color) in the prediction horizon. Since the model of the sequential partial stroke operated DDM comprises no dynamical effects, an improvement of the method is obtained by increasing the control decision frequency by an integer number, while maintaining online computation capability. One of the major drawback of the presented method is the severe flow/pressure/torque spikes, which suggest the use of a more advanced MPC strategy where valve switching pattern and pressure chamber dynamics are included.

4.2 High Speed - Full Stroke Operation

For full stroke operation, all the presented models are applicable for control design. However, the models are different in many aspects with their own advantages and disadvantages and should hence be applied accordingly. Since the choice of control design method is highly dependent on the model and application use, a comparison of the models presented in Chap. 3 is made in Tab. 4.2.

Full stroke	**Continuous Approximation**	**Discrete Approximation**	**Hybrid 1: Physical accurate**	**Hybrid 2: Nonlinear $\mathcal{D}$**	**Hybrid 3: Linear $\mathcal{D}$**
Number of states	2	$\approx N_c/2$	$6N_c$	$\approx N_c/2+3$	$\approx N_c/2+2$
Number of inputs	1	1	$2N_c$	1	1
Nonlinearities	Eigenfrequency proportional to speed and the output map	Sampling freq. proportional to speed, quantizer and the output map	Chamber flow, chamber pressure, state jumps and output map	State jumps, quantizer, displacement $\mathcal{D}$ and output map	State jumps, quantizer and output map
Accuracy	Reduced accuracy for lower number of cylinders, lower displacement and higher excitation frequencies	Reduced accuracy for lower number of cylinders	Always accurate	Reduced accuracy for lower number of cylinders	Reduced accuracy for lower number of cylinders
Validity	Multiple machines and four-quadrant operation	Single machine and one-quadrant operation	Multiple machines and four-quadrant operation	Multiple machines and one-quadrant operation	Multiple machines and one-quadrant operation
Control design difficulty	Simple when linearized, Moderate when nonlinear	Simple when linearized, Difficult when nonlinear	Extremely difficult	Very difficult	Very difficult

Based on the above comparison, suitable control design methods are discussed for the different models. Additionally, an assessment of when to use each model is provided. It is considered beneficial to use the simplest strategies as long as their accuracy and validity meets the requirements.

4.2.1 Continuous Approximation Model

Although the model is applicable for four-quadrant operation, its limited accuracy at low displacements makes it unsuitable for operation in more than one-quadrant. Since the discrete model is significantly more accurate than the continuous model, its applicability is limited. However, the discrete model seems unsuitable for describing the combined sampling domain for varying speed DD machines in a fluid power transmission. Therefore, the model is assessed to have the greatest potential for a transmission system with multiple DDMs operating in one quadrant at relatively high displacements.

One such application is a wind turbine transmission with a DD pump connected to the turbine rotor and a DD motor connected to an electrical generator, see [Paper **L**] for operation curves. An illustration of the digital fluid power transmission for a wind turbine is shown in Fig. 4.5.

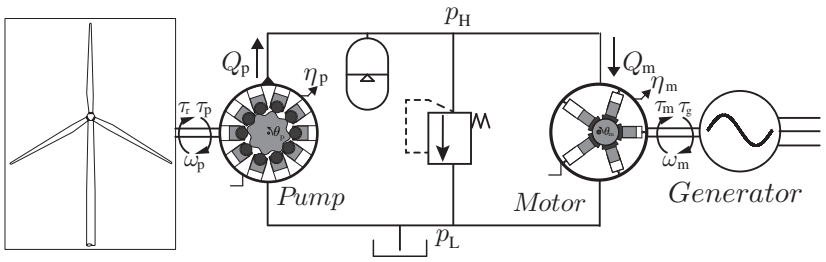

Fig. 4.5: Illustration of a digital fluid power transmission for a wind turbine [Paper **A**].

The transmission dynamics may be described relatively simple by (4.5) when considering constant oil stiffness and neglecting the pressure drop in the transmission line.

$$\begin{aligned}
\dot{\omega}_\mathrm{p} &= -\frac{d_\mathrm{p}}{J_\mathrm{p}}\,\omega_\mathrm{p} - \frac{1}{J_\mathrm{p}}\,\Delta p\,\tilde{V}_\mathrm{p}\,\eta_\mathrm{p} + \frac{1}{J_\mathrm{p}}\,\tau_\mathrm{r} \\
\dot{\Delta p} &= -\frac{\beta_\mathrm{e}}{V_\mathrm{L}}\,k_\mathrm{L}\,\Delta p + \frac{\beta_\mathrm{e}}{V_\mathrm{L}}\,\tilde{V}_\mathrm{p}\,\omega_\mathrm{p}\,\eta_\mathrm{p} - \frac{\beta_\mathrm{e}}{V_\mathrm{L}}\,\tilde{V}_\mathrm{m}\,\omega_\mathrm{m}\,\eta_\mathrm{m} \\
\dot{\omega}_\mathrm{m} &= -\frac{d_\mathrm{m}}{J_\mathrm{m}}\,\omega_\mathrm{m} + \frac{1}{J_\mathrm{m}}\,\Delta p\,\tilde{V}_\mathrm{m}\,\eta_\mathrm{m} - \frac{1}{J_\mathrm{m}}\,\tau_\mathrm{g}
\end{aligned} \tag{4.5}$$

where J_p and J_m are moments of inertia, d_p and d_m are viscous damping coefficients, $\tilde{V}_\mathrm{p}$ and $\tilde{V}_\mathrm{m}$ are the volumetric output per radians for the pump

and motor respectively. k_{L} is the leakage coefficient, V_{L} is the high pressure transmission line volume, βe is the effective bulk modulus and $\Delta p = p_{\mathrm{H}} - p_{\mathrm{L}}$ is the pressure difference. The parameter values for the transmission based on the 5 MW NREL wind turbine are found in Paper **C**.

The dynamical influence of the digital displacement machines in the transmission is analyzed by a frequency response showing the singular values. A comparison between the transmission system dynamics where the DDM is modeled by the continuous approximation and where an ideal pump and motor are assumed (omitted dynamics) is shown in Fig. 4.6.

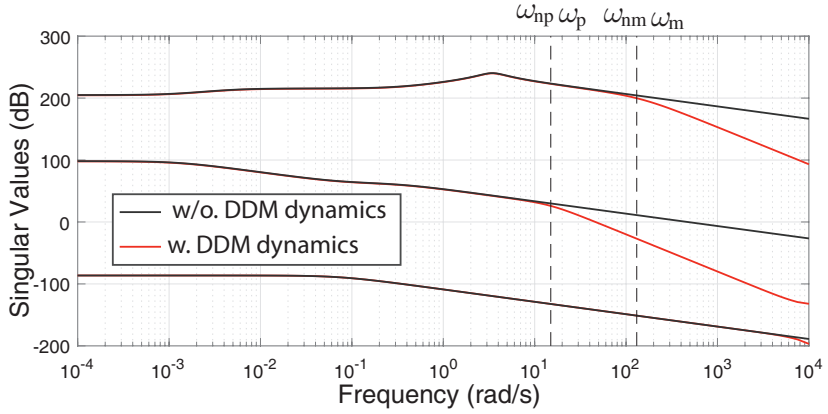

Fig. 4.6: Singular values analysis of a digital fluid power transmission with and without the DDM dynamics [Paper **C**].

ω_{np} and ω_{nm} are the estimated transfer function eigen-frequencies of the approximation for the pump and motor respectively. ω_{p} and ω_{m} are the lowest shaft speed of the pump and motor respectively and thus yields the lowest system bandwidth. Since the closed-loop excitation frequency is relatively low for the large mechanical system, the dynamics of the digital displacement machines may be neglected during control synthesis, making the continuous model dispensable. Therefore, it is considered that the usefulness of the continuous approximation model is very limited.

If the DDM is operated at lower speeds where the dynamics cannot be neglected, the model may be used in conjunction with an observer to estimate the non-measurable states of the DDM. Since the transmission has at least 3 states and each DDM comprises of 2 states, the relatively large number of states complicates the use of nonlinear control strategies. Therefore, a linear control design strategy based on the Linear Quadratic Gaussian (LQG) algorithm is suggested. The control challenge is hence reduced to specifying

the weighing matrices Q and R for the optimal control problem given as

$$\mathcal{J} = \int_0^\infty \left(x^T \, Q \, x + u^T \, R \, u \right) \tag{4.6}$$

where Q and R are weighting matrices for the states and input energy respectively [58]. To avoid additionally phase in the control system, the lowest machine speed is again used as linearization point.

4.2.2 Discrete Approximation Model

The discrete approximation model is more accurate than the continuous approximation model but is only applicable for single-quadrant operation and for a system with a single DDM. Therefore, the strategy is most suitable for system where conventional fluid power pumps/motors are replaced by DDMs, e.g. cylinder drives.

The binary input to the full stroke operated DDM, together with the output map are severe nonlinearities in the plant dynamics. If it is required to include the nonlinearities, it is assessed to be beneficial to utilize a hybrid model formulation instead of the discrete approximation. This is justified by the control theory being similar, but the hybrid formulation is more accurate. If nonlinear control is pursued the objective is to show stability through a Lyapunov Control function (LCF) given again to be

$$... \leq V(x_{k+1}) \leq V_{\text{LCF}}(x_k) \leq ... \leq V_{\text{LCF}}(x_0) \tag{4.7}$$

Numerous alternative strategies where the nonlinear dynamics is approximated also exist [6, 33, 57].

Due to the relatively simple and structured design procedure, linear control theory is considered favorable for control of a discrete plant with a relatively large number of states. However, it introduces another restriction to the controlled plant. Linearly, the quantizer that generates the binary input is treated as a duty cycle ratio with an additive noise source. By neglecting the noise source, the linear model is inaccurate at low displacements as shown in Fig. 3.15. Since a hydraulic pump is often operated in the whole displacement range, the inaccurate model description at low displacements may cause problems with respect to control performance and stability. Additionally, it is often found that the dynamics of the DDM may be neglected when the linear model is analyzed if the machine is operated at a fixed high speed. However, this does not necessary mean that the dynamics is neglectable, since the input to the linear model is limited to be binary, which introduces a significantly delay in the response for lower displacements [Paper **B**].

Since the full stroke method is favorable for high speed operation, it is not considered a problem to utilize a linear discrete method for variable speed operation. Additionally unmodeled phase is avoided by choosing the lowest operation speed as the linearization point. Furthermore, since the model is increasingly accurate for a higher number of cylinders, a high number of cylinders is expected when applying the discrete approximation method. Therefore, the number of states ($\approx N_c/2$) is large and optimal control theory is again considered favorable. The control design is hence reduced to choosing the weighting matrices Q and R for the states and input respectively. The objective function to minimize when applying discrete optimal control is given by [58]

$$\mathcal{J} = \sum_{k=1}^{\infty} \Big(x(k)^T \, Q \, x(k) + u(k)^T \, R \, u(k) \Big) \tag{4.8}$$

The stochastic Linear Quadrant Gaussian (LQG) algorithm enables the inclusion of the additive quantizer disturbance source compared to the Linear Quadrant Regulator (LQR) algorithm. However, it has been found that the control performance, where the controllers have been designed by the two strategies are indistinguishable [Paper **D**]. This is caused by the binary states of the DDM are all being estimated to be the duty cycle ratio, where after the generated control input $u \in [0, 1]$ is quantized to be binary, $\bar{u} \in \{0, 1\}$.

4.2.3 Hybrid Dynamical model

Two similar full stroke hybrid models have been proposed and are considered sufficiently simple to be used for control synthesis. However, since control law establishment and stability proof for control of hybrid dynamical systems are considered a difficult task, this section briefly describes the related challenges and control theory. The following section presents a simplified and engineering intuitive description of the stability based control synthesis of hybrid system. A more mathematical description is given in several publications [10, 73–75, 84].

Establishment of control laws for hybrid dynamical systems are normally done through stability proof by Lyapunov Control Functions (LCF). Stability theory for hybrid systems combines the theories of stability for nonlinear continuous and discrete systems. The main difference is that instead of driving all the states to zero in conventional nonlinear control theory, the objective is to drive the states to a closed set $\mathcal{A}$. This set consist of a subset, $\mathcal{S}$, containing all values for the logic states, timer states, sampling and mode states, etc. which are always bounded and stable. Additionally, it comprises the subset, $\mathcal{P}$, containing the equilibrium point for those states for which values may diverge and should be driven to zero. For the DDM system, these states are

the plant states actuated by the DDM, e.g. shaft angle, shaft velocity, pressure etc. The definition of the closed set $\mathcal{A} = \mathcal{S} \bigcup \mathcal{P}$ is shown in Fig. 4.7.

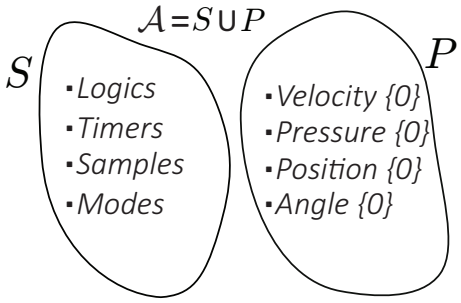

Fig. 4.7: Definition of the compact $\mathcal{A}$ comprising all values of the bounded and stable states, as well as the zero value for the states to be stabilized.

Stability Theory for Hybrid Dynamical Systems

The objective is to obtain a system which is Uniformly Globally pre-Asymptotically Stable (UGpAS) with respect to the set $\mathcal{A}$. The definition of UGpAS is similar to that of conventional nonlinear systems and is illustrated in Fig. 4.8.

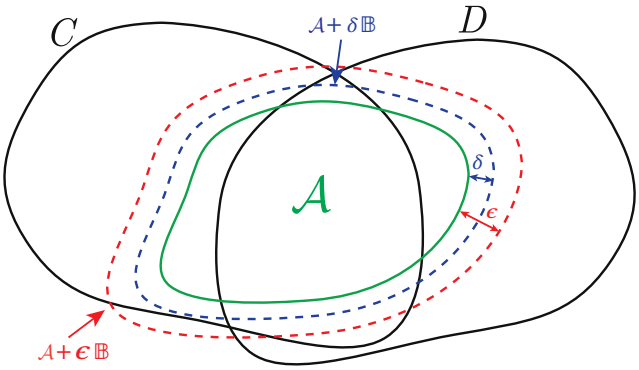

Fig. 4.8: Illustration of stability of hybrid dynamical systems.

The illustration shows the set $\mathcal{A}$ having a ball $\mathcal{B}$ with distance δ and a ball with distance ϵ around it. These sets are used to define the UGpAS properties of the hybrid system defined as

Definition: (Uniformly Globally pre-Asymptotically Stability) Given $\mathcal{H}$ and a closed set $\mathcal{A} \subset \mathbb{R}^n$, we say that $\mathcal{A}$ is asymptotically stable if it is both

- (S) Stable: for each $\epsilon > 0$ there exist $\delta > 0$ such that each maximal solution ϕ to $\mathcal{H}$ with $|\phi(0,0)|_{\mathcal{A}} \leq \delta$, satisfies $|\phi(t,j)|_{\mathcal{A}} \leq \epsilon$ for all $(t,j) \in dom\, \phi$. With definition $|x|_{\mathcal{A}} = \min\{x - y| : y \in \mathcal{A}\}$
- (A) Pre-attractive: there exist $\epsilon > 0$ such that every maximal solution ϕ to $\mathcal{H}$ with $|\phi(0,0)|_{\mathcal{A}} \leq \epsilon$, is bounded and the complete solution converges to $\mathcal{A}$, that is

$$\lim_{(t,j)\in dom\,\phi, t+j\to\infty} |\phi(t,j)|_{\mathcal{A}} \to 0 \tag{4.9}$$

  The set $\mathcal{A}$ is said to be pre-asymptotically stable if its stable and pre-attractive. Asymptotic stability is said to be *global* when the attractivity property holds for every point in D and every point in the closure of C. It is *uniformly* if the time to converge to the set $\mathcal{A}$ is uniform with respect to a compact set of initial conditions $\phi(0,0)$ [10, 11, 73, 75].

where maximal solution is defined as the solution domain of ϕ that can not be extended. The proof of pre-asymptotically stability may be established by a Lyapunov Control Function (LCF), $V(x)$, that is continuous differential and ensures that the energy in the system dissipates along the solution trajectory. The condition for pre-asymptotically stability in the sense of Lyapunov theory is defined as

Definition: The set $\mathcal{A}$ is pre-asymptotically stable if there exist a Lyapunov-function candidate V for $(\mathcal{H}, \mathcal{A})$ such that

$$\begin{aligned} \langle \nabla V(x), f \rangle < 0 \quad \forall x \in C \setminus \mathcal{A}, \forall f \in F(x) \\ V(g(x)) - V(x) < 0 \quad \forall x \in D \setminus \mathcal{A}, \forall g \in G(x) \end{aligned} \tag{4.10}$$

then the set $\mathcal{A}$ is pre-asymptotically stable [10].

$$\langle \nabla V(x), f \rangle = \frac{d}{dt} V(\phi(t)) = \nabla V(x) \bullet f(x) | x = \phi(t) \tag{4.11}$$

UGpAS is shown by introducing a class $\mathcal{K}_\infty$ function, ensuring that the convergence to the set $\mathcal{A}$ is uniform. The sufficient Lyapunov condition for UPGAS is defined as

Definition: Let $\mathcal{H} = (C, F, D, G)$ be a hybrid system and let $\mathcal{A} \subset \mathbb{R}^n$ be closed. If V is a Lyapunov function candidate for $\mathcal{H}$ and there exist $\alpha_1, \alpha_2 \in \mathcal{K}_\infty$, and a continuous positive definite function $\rho : \mathbb{R} \to \mathbb{R}_{\geq 0}$ such that

$$\begin{aligned}
&\bullet \quad \alpha_1(|x|_{\mathcal{A}}) \leq V(x) \leq \alpha_2(|x|_{\mathcal{A}}) && \forall x \in C \cup D \cup G(D) \\
&\bullet \quad \langle \nabla V(x), f(x) \rangle \leq -\rho(|x|_{\mathcal{A}}) && \forall x \in C, f \in F(x) \\
&\bullet \quad V(g(x)) - V(x) \leq -\rho(|x|_{\mathcal{A}}) && \forall x \in D, g \in G(x)
\end{aligned} \tag{4.12}$$

Then $\mathcal{A}$ is Uniformly Globally Pre-Asymptotically Stable for $\mathcal{H}$ [11].

where the class $\mathcal{K}_\infty$ is defined to be a function that is continuous, strictly increasing and unbounded, as well as evaluates to zero in zero. The objective is hence to find the functions $V, \alpha_1, \alpha_2, \rho$. Such functions for numerous non-smooth systems have been proposed, which includes sample-and-hold control systems [10,11,73,75]. Relaxed conditions for UGpAS based on LCFs exist, where e.g. the jump or flow map may give an increase in energy, as long as the total energy decrease during a certain period. However, these relaxed conditions are not shown in this dissertation to keep the content short in the summary.

Control Challenges for the DDM Hybrid Models

It is seen that the objective is to ensure that the energy dissipates both during flows and jumps. For the full stroke hybrid model, several complications with respect to finding the Lyapunov control function exist. The state models for the full stroke operated DDM given in (3.28) and (3.29) comprise of numerous logic states (angle sampler, angle timer and previous binary inputs). Hence, for a fixed speed machine the system is always stable since all states belongs to the closed set $\mathcal{A}$. However, for a variable speed DDM the machine speed requires stabilizing. Additionally, for a DDM that actuates a continuous plant, the states of the continuous plant need stabilization. To illustrate the control problem, a simple system is considered in Fig. 4.9 where a fixed speed DDM is controlling the pressure in the high pressure line where an orifice is implemented as flow restriction.

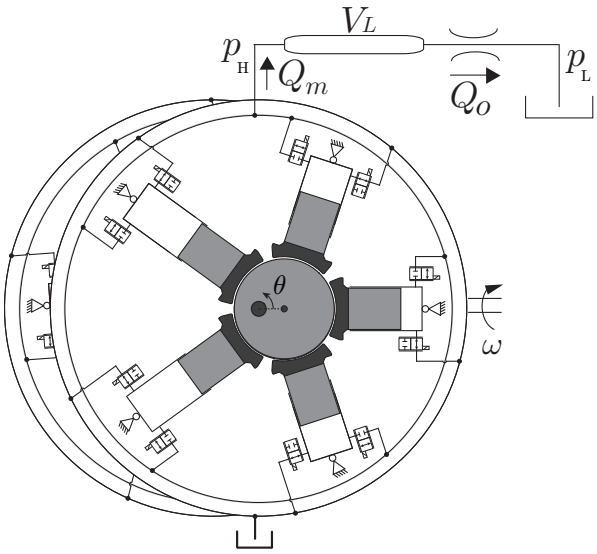

Fig. 4.9: Illustration of simple system where a DDM is controlling the pressure in the high pressure line. [Paper **G**].

Considering the hybrid model in (3.29), where constant displacement between samples is assumed, then the model of the system to be controlled becomes

$$\left.\begin{aligned} \dot{\theta} &= \omega \\ \dot{p}_{\mathrm{H}} &= \frac{\beta_{\mathrm{e}}}{V_{\mathrm{L}}}\left(\omega\, C\, z_{\mathrm{u}} - k_{\mathrm{qo}}\sqrt{p}_{\mathrm{H}}\right) \\ \dot{\chi} &= \omega \\ \dot{z}_{\mathrm{u}} &= 0 \end{aligned}\right\} \chi \in [0, \theta_{\mathrm{s}}] \quad \left.\begin{aligned} \theta^{+} &= \theta \\ p_{\mathrm{H}}^{+} &= p_{\mathrm{H}} \\ \chi^{+} &= 0 \\ z_{\mathrm{u}}^{+} &= A_{\mathrm{u}}\, z_{\mathrm{u}} + B_{\mathrm{u}}\, u \end{aligned}\right\} \chi = \theta_{\mathrm{s}} \tag{4.13}$$

where $Q_{\mathrm{m}} = \omega\, C\, z_{\mathrm{u}}$ and $Q_{\mathrm{o}} = k_{\mathrm{qo}}\sqrt{p_{\mathrm{H}}}$, the low pressure p_{L} is assumed to be zero and k_{qo} is the orifice flow coefficient. The definition of the set $\mathcal{A}$ for the states $x = \begin{bmatrix}\theta & p_{\mathrm{H}} & \chi & z_{\mathrm{u}}\end{bmatrix}$ is given by $\mathcal{A} = \{\mathcal{R}\} \times \{0\} \times \{\mathcal{R}\} \times \{\mathcal{R}\}$, indicating that the objective is to show uniform convergence to zero for the pressure state, p_{H}. The main challenge is that the input is limited to be binary, $u \in \{0, 1\}$. Therefore, it is very difficult to ensure that the energy always dissipates by (4.12). An approach to overcome this challenge is to consider a duty cycle ratio as input. However, by doing this the accuracy of the model is severely reduced and corresponds to linearizing the discrete approximation of the DDM. Published research where a disturbance input is considered to scale all inputs to binary values (similar to the linear description of the quantizer) has been considered for a similar system [56]. The main difference

is that the control input is continuous updated and not discretely as for the DDM system. Another approach is to apply relaxed conditions, where the energy is allowed to increase momentarily if the total energy over a certain period is decreased [11]. However, the complexity of theory for relaxed conditions is greatly increased. This explains why it has not been possible to establish a proof of stability for a full stroke operated DDM in this dissertation. However, the presented hybrid models may be an inspiration for further work with respect to control development.

Chapter 5

Closing remarks

5.1 Conclusion

This dissertation concerns model based development of control strategies for digital displacement machines (DDMs). The main contributions are the identification of the many challenges related to control of the DDMs, as well as development of control design models allowing for dynamical analysis and feedback control synthesis.

The many control challenges related to the non-smooth behavior of the machine has been investigated with the purpose of clarifying suitable operation and control strategies. The findings shows that the control challenges are highly dependent on the operation strategy (full stroke, partial stroke or sequential partial stroke), machine design (number of cylinders, output connections, pressure chamber orientation and size, etc.) and application use (motoring, pumping, direction of motion, multiple machines, etc.). Since the DDM dynamically behaves significantly different depending on its settings, there are many sub-challenges to be solved with respect to development of control strategies.

An investigation is conducted to examine the effects of the DDM by comparing the response of a first order plant actuated by a DDM to the response of the same plant actuated by an ideal pump/motor unit. The results shows that the time delay and energy in the steady state ripples are reduced for a higher number of cylinders and faster shaft speed. Hence, the results indicates that the dynamics of the DDM should not be always be omitted to ensure stability, which has been done by the majority of state-of-the-art control strategies.

Since the dynamics of each pressure chamber of the DDM is continuous and the actuation of it is made discretely, the system dynamics belongs to the class of hybrid dynamical systems. Due to the complexity in establishing

feedback stabilizing control laws for such nonlinear system with switching elements, approximation models are initially applied which are valid in a limited amount of situations. Both continuous and discrete approximations has been developed and allows for use of classical control design methods. Both deterministic and stochastic optimal control methods, as well as model predictive control strategies have been used to synthesize controllers. However, in this thesis a limited effort has been spent on control design and optimized control performance since no specific application is considered.

Due to the approximation models only being valid in a limited number of situations, several hybrid dynamical models of the DDM have been developed, where one is very accurate in describing the machine dynamics on a pressure chamber level, while the others are simpler and only captures the fundamental dynamics of a full stroke operated machine. Development of stabilizing feedback control laws of hybrid dynamical system is considered difficult even for relatively simple systems. The DDM is not considered to be a simple system, since its dynamics contains nonlinear continuous, discrete, binary and switching elements being both dependent on the input and states. Furthermore, since the dynamics highly depends on the machine settings, a general framework in control development is considered very challenging and is yet to be solved.

5.2 Further Work

This thesis only briefly investigates the three branches of dynamical control (continuous, discrete and hybrid) with respect to the three operation modes (full, partial and sequential partial stroke). Only linear control theory has been pursued with the continuous and discrete strategies, but nonlinear strategies are likely to improve the validity of the strategies and the control performance and is thus open for further exploration.

The input dependent discrete model is assessed to have a great potential for model predictive control (MPC), but has an unconventional model structure with a varying model structure and unity input. In this thesis an angle average MPC strategy has been applied for a low speed and partial stroke operated DDM. However, an improved performance is expected with more complex MPC structures featuring the input dependent discrete model.

Since the applicability of the continuous and discrete approximation are applicable in a limited number of situations, there is a high incentive to further explore hybrid dynamical theory with respect to modeling and control of the digital machines. Proper tools for analyzing and developing control laws for four-quadrant operated machines and multiple machines in a transmission are in high demand and requires further research. Similarly, control methods for DDMs with multiple sized pressure chambers and/or multiple

individual outlet connections has not been investigated in this thesis and therefore requires further investigation.

References

[1] B. S. R. Armstrong and Q. Yuan, "Multi-level control of hydraulic gerotor motors and pumps," *Proc. of the american control conference, Minnesota, USA*, 2006.

[2] Autoblog, "Artemis intelligent power demostrates hydraulic hybrid bmw 530i w/video," Accessed: 11/13-2017 2009. [Online]. Available: https://www.autoblog.com/2009/02/26/artemis-intelligent-power-demostrates-hydraulic-hybrid-bmw-530i/

[3] N. J. Caldwell, "Digital displacement hydrostatic transmission systems," Ph.D. dissertation, Edinburgh University, 2007.

[4] N. J. Caldwell, W. H. Rampen, S. Almond, and P. Jonathan, "Fluid-working machine and operating method," European Patent EP1 537 333B1, 2006.

[5] P. Chapple, P. N. Lindholdt, and H. B. Larsen, "An approach to digital distributor valves in low speed pumps and motors," *Proc. of the ASME/BATH Symposium on Fluid Power and Motion Control, Bath, UK*, 2014.

[6] L. Chen and K. Narendra, "Identification and control of a nonlinear discrete-time system based on its linearization: a unified framework." *IEEE Transaction on Neural Networks*, 2004.

[7] Digiwin, "Research project on digital hydraulic winch systems." [Online]. Available: https://www.digiwin.info/

[8] M. Ehsan, "A new type of malone engine with digital-displacement hydraulic drive," Ph.D. dissertation, University of Edinburgh, 1997.

[9] M. Ehsan, W. Rampen, and S. Salter, "Modeling of digital-displacement pump-motors and their application as hydraulic drives for nonuniform loads," *Journal of Dynamic Systems, Measurement and Control, vol. 122, no. 1, pp. 210–215*, 2000.

[10] R. Goebel, R. G. Sanfelice, and A. R. Teel, "Hybrid dynamical systems - robust stability and control for systems that combine continuous time and discrete time dynamics," *IEEE control systems magazine*, 2009.

[11] ——, *Hybrid Dynamical Systems - Modeling, Stability and Robustness*. Princeton, 2012.

[12] D. Hagen, W. Pawlus, M. Ebbesen, and T. Andersen, "Feasibility study of electromechanical cylinder drivetrain for offshore mechatronic systems," *Modeling, Identification and Control, Vol. 38, No. 2, pp. 59–77*, 2017.

[13] K. Halbaoui, M. F. Belazreg, D. Boukhetala, and M. H. Belhouchat, *Modeling and Predictive Control of Nonlinear Hybrid Systems Using Mixed Logical Dynamical Formalism*. Springer, 2016.

[14] M. Heikkilä, M. Huova, J. Tammisto, K. Huhtala, and M. Linjama, "Experimental evaluation of a piston-type digital pump-motortransformer with two independent outlets," *Proc. of the ASME/Bath Symp. on Fluid Power and Motion Control, Bath, UK*, 2010.

[15] ——, "Digital hydraulic power management system – measured characteristics of a second prototype," *Proc. of the Eighth Workshop on Digital Fluid Power, Tampere, Finland*, 2016.

[16] M. Heikkilä and M. Linjama, "Displacement control of a mobile crane using a digital hydraulic power management system," *Mechatronics, Volume 23, Issue 4*, 2013.

[17] ——, "Hydraulic energy recovery in displacement controlled digital hydraulic system," *Proc. of the 13th Scandinavian International Conference on Fluid Power, Sweden*, 2013.

[18] M. Heikkilä, J. Tammisto, M. Huova, K. Huhtala, and M. Linjama, "Experimental evaluation of a digital hydraulic power management system," *Proc. of the Third Workshop on Digital Fluid Power, October 13 - 14, 2010, Tampere, Finland*, 2010.

[19] T. Helmus, F. Breidi, and J. Lumkes, "Simulation of a variable displacement mechanically actuated digital pump unit," *Proc. of the eighth workshop on digital fluid power, Tampere, Finland*, 2016.

[20] M. A. Holland, "Design of digital pump/motors and experimental validation of operating strategies," Ph.D. dissertation, Purdue University, 2012.

[21] M. A. Holland, G. Wilfong, K. J. Merrill, and J. Lumkes, "Experimental evaluation of digital pump/motor operating strategies with a single-piston pump/motor," *Proc. of the 52nd National Conference on Fluid Power, Las Vegas, US*, 2011.

[22] M. H. Industries, "Mhi acquires artemis intelligent power, a uk venture company, to secure unique hydraulic power drive technology," 2010, accessed: 11/13-2017. [Online]. Available: http://www.mhi.com/news/story/1012031389.html

[23] ——, "Ceremony held to mark the launch of verification testing of world's first digital hydraulic drive train for offshore wind turbines at hunterston test centre in the uk," 2015, accessed: 11/13-2017. [Online]. Available: http://www.mhi.com/news/story/1502051871.html

[24] P. Johansen, "Tribodynamic modeling of digital fluid power motors," Ph.D. dissertation, Department of Energy Technology, Aalborg University, 2014.

[25] P. Johansen, D. B. Roemer, T. O. Andersen, and H. C. Pedersen, "Delta-sigma modulated displacement of a digital fluid power pump," *Proc. of the 7th workshop on digital fluid power, Linz, Austria*, 2015.

[26] ——, "Discrete linear time invariant analysis of digital fluid power pump flow control," *Journal of Dynamic Systems, Measurement and Control*, 2017.

[27] P. Junker, T.-E. Lindberg, and K. B. Nielsen, "Development of multirate model and analysis of applicability to wind turbine digital fluid power transmissions," Master's thesis, Aalborg University, 2017.

[28] S. Karaman, R. G. Sanfelice, and E. Frazzoli, "Optimal control of mixed logical dynamical systems with linear temporal logic specifications," *Proc. of the 47th IEEE Conference on Decision and Control*, 2008.

[29] M. Ketonen and M. Linjama, "High flowrate digital hydraulic valve system," *Proc. of the Ninth Workshop on Digital Fluid Power, Aalborg, Denmark*, 2017.

[30] B. Kouvaritakis, *Model Predictive Control*. Springer, 2015.

[31] O. Kuttler and J. H. Nestler, "Method of controlling a cyclically commutated hydraulic pump," European Patent EP2 055 944A1, 2009.

[32] ——, "Method of operating a fluid working machine," European Patent EP2 055 943A1, 2009.

[33] D. S. Laila, "Design and analysis of nonlinear sampled-data control systems," Ph.D. dissertation, Department of Electrical and Electronic Engineering - The University of Melbourne, 2003.

[34] H. B. Larsen, M. Kjelland, A. Holland, and P. N. Lindholdt, "Digital hydraulic winch drives," *Proc. of the Bath/ASME Symposium on Fluid Power and Motion Control*, 2018.

[35] M. Lazar, W. P. M. H. Heemels, S. Weiland, and A. Bemporad, "Stabilizing model predictive control of hybrid systems," *IEEE Transaction on Automatic Control*, 2006.

[36] P. Lindholdt and H. B. Larsen, "Digital distributor valves in low speed motors - practical approach," *Proc. of the Ninth Workshop on Digital Fluid Power, Aalborg, Denmark*, 2017.

[37] M. Linjama, M. Paloniitty, L. Tiainen, and K. Huhtala, "Mechatronic design of digital hydraulic micro valve package," *Proc. of the 2nd International Conference of Dynamics and Vibroacoustics of Machines, Samara, Russia*, 2014.

[38] A. I. P. Ltd., "Fluid working machine and method for operating fluid working machines," Great Britain Patent GB2 477 997, 2011.

[39] ——, "History," 2017, accessed 11/13-2017. [Online]. Available: http://www.artemisip.com/company/history/

[40] ——, "Fluid working machine and methods," U.S. Patent US20 110 268 590, 2011.

[41] ——, "Edinburgh technology duo secure £2.5 million to turn wave power into electricity," 2017, accessed: 11/13-2017. [Online]. Available: http://www.artemisip.com/edinburgh-technology-duo-secure-2-5-million-turn-wave-power-electricity/

[42] ——, "Technology," 2017. [Online]. Available: http://www.artemisip.com/technology/

[43] ——, "Digital displacement pump to end 'guilty secrets' of aerospace hydraulic systems," 2018. [Online]. Available: https://www.wearefinn.com/topics/posts/digital-displacement-pump-to-end-guilty-secrets-of-aerospace-hydraulic-systems/

[44] ——, "E-dyn 96 series digital displacement pump datasheet," Accessed 21/6 2017, http://www.artemisip.com/wp-content/uploads/2015/11/E-dyn-96IH-RP-Datasheet-120515.pdf.

[45] M. H. I. Ltd., "Energy extraction device, group of energy extraction devices and operating methods," U.S. Patent US 2013/0 221 676 A1, 2013.

[46] ——, "Method of controlling hydraulic machine to reduce torque ripple and/or bearing side load," U.S. Patent US 2013/0 205 763 A1, 2013.

[47] K. J. Merrill, "Modeling and analysis of active valve control of a digital pump-motor," Ph.D. dissertation, Purdue University, 2012.

[48] K. J. Merrill, M. A. Holland, and J. J. Lumkes, "Efficiency analysis of a digital pump/motor as compared to a valve plate design," *Proc. of the 7th International Fluid Power Conference, Aachen, Germany*, 2010.

[49] W. P. Monthly, "Mitsubishi launches 7mw turbine," 2012, accessed: 11/13-2017. [Online]. Available: https://www.windpowermonthly.com/article/1109873/mitsubishi-launches-7mw-turbine

[50] W. Monthly, "Mitsubishi to unveil 7mw offshore turbine," 2011, accessed 11/13-2017. [Online]. Available: https://www.windpowermonthly.com/article/1106330/mitsubishi-unveil-7mw-offshore-turbine

[51] M. Nieling, F. Fronczak, and N. Beachley, "Design of a virtually variable displacement pump/motor," *Proc. of the 50th National Conference on Fluid Power, Las Vegas, USA*, 2005.

[52] C. Noergaard, "Design, optimization and testing of valves for digital displacement machines," Ph.D. dissertation, Department of Energy Technology. Aalborg University, 2017.

[53] S. Nordaas, M. K. Ebbesen, and T. O. Andersen, "Feasibility study of a digital hydraulic winch drive system," *Proc. of the Ninth Workshop on Digital Fluid Power, Aalborg, Denmark*, 2017.

[54] ——, "The potential of a digital hydrulic winch drive system," *Proc. of the Ninth Workshop on Digital Fluid Power, Aalborg, Denmark*, 2017.

[55] Q. I. Offshore, "Quoceant partner with artemis intelligent power in innovative project to provide improved power take-off for the marine energy industry," 2015, accessed: 13/11-2017. [Online]. Available: https://www.quoceant.com/single-post/2015/07/31/Quoceant-partner-with-Artemis-Intelligent-Power-in-innovative-project

[56] R. N. on Yuh Yanashita and D. Tsubakino, "Higher-order sliding-mode control for binary input by using implicit lyapunov function," *IFAC paper archive*, 2015.

[57] R. Ordonez and K. M. Passino, "Control of discrete time nonlinear systems with a time-varying structure," *Automatica 39*, 2003.

[58] I. Postlethwaite and S. Skogestad, *Multivariable Feedback Control: Analysis and Design*, 2nd, Ed. JOHN WILEY & SONS, 2005.

[59] Powermag, "Iea: Wind power could supply 18 percent of world's power by 2050." [Online]. Available: http://www.powermag.com/iea-wind-power-could-supply-18-of-worlds-power-by-2050/

[60] W. Rampen, U. Bernhard, P. Stein, M. Fielding, and N. Caldwell, "Digital hydraulic pump/motor torque modulation system and apparatus," U.S. Patent US 2009/0 317 266 A1, 2009.

[61] W. Rampen, "The digital displacement hydraulic piston pump," Ph.D. dissertation, University of Edinburgh, 1992.

[62] ——, "Gearless transmissions for large wind turbines – the history and future of hydraulic drives." *Bremen*, 2006.

[63] ——, "The development of digital displacement technology," Fluid Power and Motion Control, 2010.

[64] M. B. Rannow, P. Y. Li, and T. R. Chase, "Discrete piston pump/motor using a mechanical rotary valve control mechanism," *Proc. of the eighth workshop on digital fluid power, Tampere, Finland*, 2016.

[65] J. D. Reiss, "Understanding sigma-delta modulation: The solved and unsolved issues," *J. Audio Eng. Soc. 56*, 2008.

[66] D. B. Roemer and P. Johansen, "Design of a high efficiency valve for use in a digital displacement hydraulic pump," Master's thesis, Aalborg University, Denmark, 2011.

[67] D. B. Roemer, "Design and optimization of fast switching valves for large scale digital hydraulic motors," Ph.D. dissertation, Section of Fluid Power and Mechatronic Systems, Department of Energy Technology. Aalborg University, 2014.

[68] RSSB, "Rssb funds powertrain demonstrator," 2017, accessed: 11/13-2017. [Online]. Available: https://www.rssb.co.uk/industry-news/rssb-funds-powertrain-demonstrator

[69] S. H. Salter and M. Rea, "Hydraulics for wind," *Proc. of the European Wind Energy Conference, Hamburg, Germany*, 1984.

[70] ——, "Hydraulics for wind," *Proc. of the European Wind Energy Conference, Hamburg, Germany, pp. 534–541.*, 1984.

[71] S. H. Salter and W. H. S. Rampen, "Pump control method and poppet valve therefore," England Patent EP0 361 927 A1, 1994.

[72] ——, "Improved fluid-working machine," England Patent EP0 494 236 B1, 1995.

[73] R. G. Sanfelice, "Control of hybrid dynamical systems: An overview of recent advances," *Book chapter in "Hybrid Systems with Constraints"*, 2013.

[74] ——, "Feedback control of hybrid dynamical systems," *Encyclopedia of Systems and Control*, 2015.

[75] ——, "Hybrid dynamical systems, feedback control of," *Encyclopedia of Systems and Control*, 2015.

[76] M. Sasaki, A. Yuge, T. Hayashi, H. Nishino, M. Uchida, and T. Noguchi, "Large capacity hydrostatic transmission with variable displacement," *Proc. of the 9th International Fluid Power Conference, 9, Aachen, Germany*, 2014.

[77] P. Silva, A. Giuffrida, N. Fergnani, E. Macchi, M. Cantù, R. Suffredini, M. Schiavetti, and G. Gigliucci, "Performance prediction of a multi-mw wind turbine adopting an advanced hydrostatic transmission," *Elsevier Energy, Vol 64*, 2014.

[78] M. Sniegucki, "Optimal cylinder commutation in digital hydraulc pumps and motors for pulsation minimization," Ph.D. dissertation, Technical University Damstadt, 2016.

[79] M. Sniegucki, M. Gottfried, and U. Klingauf, "Optimal control of digital hydraulic drives using mixed-integer quadratic programming," *9th IFAC symposium on nonlinear control systems*, 2013.

[80] X. Song, "Modeling and active vehicle suspension system with application of digital displacement pump motor," *Proc. of the ASME 2008 International Design Engineering Techical Conferences & Computers and Information in Engineering Conference, New York, USA*, 2008.

[81] J. Tammisto, M. Huova, M. Heikkilä, M. Linjama, and K. Huhtala, "Measured characteristics of an in-line pump with independently controlled pistons," *Proc. of The 7th International Fluid Power Conference, Aachen, Germany*, 2010.

[82] J. Taylor, W. Rampen, D. Abrhams, and A. Latham, "Demonstration of a digital displacement® hydrulic hybrid bus... a globally affordable way of saving fuel," *Proc. of the Annual JSAE Congress, Pacifico Yokohama, Japan*, 2015.

[83] J. Taylor, W. Rampen, A. Robertson, and N. Caldwell, "Digital displacement hydraulic hybrid - parallel hybrid drives for commercial vehicles," *Proc. of the Society of Automotive Engineers, Yokohama, Japan*, 2011.

[84] A. R. Teel, R. G. Sanfelice, and R. Goebel, "Hybrid control systems," *Encyclopedia of Complexity and Systems Science*, 2009.

[85] K. E. Thomsen, O. G. Dahlhaug, M. O. K. Niss, and S. K. Haugset, "Technological advances in hydraulic drive trains for wind turbines," *Elsevier Energy Procedia*, 2012.

[86] H. Tian, P. Y. Li, and J. D. V. de Ven, "Using an angle domain repetitive control to achieve variable valve timing for a digital displacement hydraulic motor," *Proc. of the ninth workshop on digital fluid power, Aalborg, Denmark*, 2017.

[87] M. Umaya, T. Noguchi, M. Uchida, M. Shibata, Y. Kawai, and R. Notomi, "Wind power generation -development status of offshore wind turbines-," *Mitsubishi Heavy Industries Technical Review Vol. 50 No. 3*, 2013.

[88] J. P. Uusitalo, "A novel digital hydraulic valve package: a fast and small multiphysics design," *Tampere University of Technology*, 2010.

[89] L. Wadsley, "Optimal system solutions enabled by digital pumps," *Proc. of the International Exposition for Power Transmission, Las Vegas, USA*, 2011.

[90] C. Williamson, "Danfoss power solutions," in *Digital Displacement® Technology - Danfoss Power Solutions*, 2017.

[91] WindPower, "World's largest floating turbine installed at fukushima," Accessed 11/13-2017 2015. [Online]. Available: https://www.windpoweroffshore.com/article/1358221/worlds-largest-floating-turbine-installed-fukushima

[92] C. Yigen, "Control of a digital displacement pump," Master's thesis, Aalborg University, 2012.

Part II

Papers

Paper A

Challenges with Respect to Control of Digital Displacement Hydraulic Units

Niels H. Pedersen, Per Johansen and Torben O. Andersen

The paper has been published in
Modeling, Identication and Control, Vol. 39, No. 2, 2018,
doi:10.4173/mic.2018.2.4.

The layout has been revised.

Modeling, Identification and Control, Vol. 39, No. 2, 2018, pp. 91–105, ISSN 1890–1328

Challenges with Respect to Control of Digital Displacement Hydraulic Units

N. H. Pedersen, P. Johansen, T. O. Andersen

Fluid Power and Mechatronic Systems, Department of Energy Technology, Aalborg University, Pontoppidanstraede 111, 9220 Aalborg, Denmark. E-mail: nhp@et.aau.dk, pjo@et.aau.dk, toa@et.aau.dk

Abstract

This paper investigates the many complications arising when controlling a digital displacement hydraulic machine with non-smooth dynamical behavior. The digital hydraulic machine has a modular construction with numerous independently controlled pressure chambers. For proper control of dynamical systems, a model representation of the systems fundamental dynamics is required for transient analysis and controller design. Since the input is binary (active or inactive) and it may only be updated discretely, the machine comprises both continuous and discrete dynamics and therefore belongs to the class of hybrid dynamical systems. The study shows that the dynamical system behavior and control complexity are greatly dependent on the configuration of the machine, the operation strategy, and in which application it is used. Although the system has non-smooth dynamics, the findings show that simple continuous and discrete approximations may be applicable for control development in certain situations, whereas more advanced hybrid control theory is necessary to cover a broader range of situations.

Keywords: Digital Displacement Units, Fluid Power, Control, Non-smooth System, Hybrid Systems

1 Introduction

Throughout the past decade, there has been an increasing interest in research and development of energy efficient fluid power systems for both conventional cylinder drives Schmidt et al. (2015); Jarf et al. (2016) and power take-off systems Hansen and Pedersen (2016); Hansen et al. (2014); Payne et al. (2007, 2005); Pedersen et al. (2016a); Rampen (2006); Salter et al. (2002). A promising technology is the so called digital displacement machine (DDM), which besides providing great energy efficiency also yields superb scalability. For successful deployment of the technology, proper control of the machine is considered a key challenge to be solved. However, this is a complicated task due to the non-smooth dynamical behavior.

For most computer controlled systems, either continuous or discrete approximation models are fairly accurate in describing the system macro dynamics. Either linear or non-linear control theory is then applied on these models to ensure stability and obtain the desired performance. However, control of DDM's is different in various ways, since the triggering of a control update is angle dependent and not time dependent. Additionally, the dynamics are highly influenced by the configuration of the machine and how it is operated, as well as in which application it is used. Since control of the digital displacement technology is a relatively unexplored field, an important first step is to identify the control challenges related to the non-smooth machine behavior. This paper provides an overview with respect to development of model based dynamical analysis and feedback control design methods for these machines. The investigation is based on a single module of a DDM with 5 cylinders as illustrated in Fig. 1. It is seen that the machine comprises numerous cylinder pressure chambers being radially distributed around an eccentric shaft. The flow to and from the

doi:10.4173/mic.2018.2.4

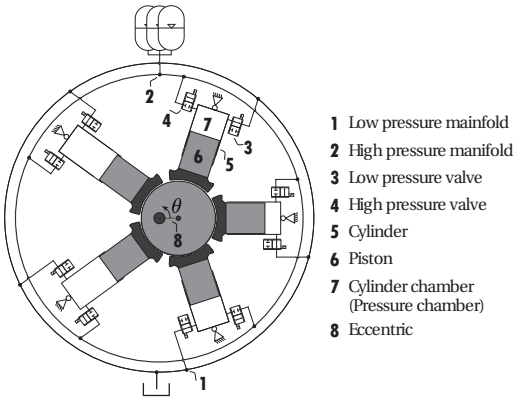

Figure 1: Illustration of the radial piston type digital displacement machine with 5 cylinders.

pressure chambers is controlled by electro-magnetically actuated on/off valves connecting each pressure chamber to the high and low pressure manifold. A more detailed description of the digital displacement technology may be found in several publications Ehsan et al. (1997); Payne et al. (2005); Rampen (2010); Roemer (2014); Noergaard (2017); Johansen (2014); Johansen et al. (2015b).

Published state of the art control strategies for digital displacement units is mostly limited to neglecting the transient behavior of the machine and utilizing pulse density modulation or pulse width modulation techniques to determine the actuation sequence for the pressure chambers Johansen et al. (2015a); Sniegucki et al. (2013). Another method where the dynamics has been neglected is through determination of the actuation sequence of the individual chambers as function of the displacement reference and shaft angle through offline optimization Armstrong and Yuan (2006); Sniegucki et al. (2013); Song (2008); Heikkila and Linjama (2013). However, none of these methods includes the machine dynamics which may introduce transient problems with respect to stability and performance. Dynamical models applicable for system analysis and controller design has been developed and governs both continuous, discrete and hybrid representations Johansen et al. (2017); Pedersen et al. (2016b, 2017a,b,c, 2018c); Sniegucki et al. (2013). However, the discrete and continuous models are often only valid in limited situations, while the hybrid models are often quite complex with respect to development of stabilizing feedback control laws. This paper provides a clarification of the related control challenges in a broad range of machine operations, machine designs and possible target applications. A discussion of the applicable control models and methods, as well as their limitations is made. The findings of the paper should hence serve as a tool for determining suitable control strategies and dynamical control oriented models when utilizing digital displacement machines.

2 Simplified model analysis

Instead of deriving a complex model for investigation of the control challenges, a relatively simple model with idealized behavior is used. The model maintains all the system wide control challenges and includes the fundamental dynamics of the machine. Although only system wide control is considered in this paper, valve control related problems are important for proper machine operation. The non-linear features during the switching event has been studied in Bender et al. (2018b); Roemer et al. (2015a, 2014, 2013, 2015b) and the repetitive nature of the machine has lead to several valve timing control strategies Bender et al. (2018a); Brendi et al. (2017); Breidi (2016); Merrill (2012). The derivation of the mathematical model of the macro dynamics is based on the illustration of a single pressure chamber shown in Fig. 2.

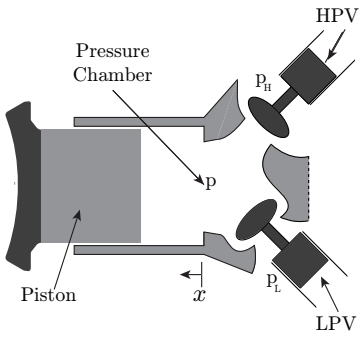

Figure 2: Illustration of the individual pressure chamber and the configuration of the corresponding valves.

It is seen that a normally closed high pressure valve (HPV) and a normally open low pressure valve (LVP) is used, such that each pressure chamber is normally in an idling mode at low pressure. The piston displacement, x, is kinematically described as function of the shaft angle given by

$$x_{\mathrm{i}}\left(\theta_{\mathrm{i}}\right) = r_{\mathrm{e}}\ \left(1 - \cos(\theta_{\mathrm{i}})\right) \tag{1}$$

where r_{e} is the eccentric radius, such that the piston stroke length is $\bar{x} = 2\, r_{\mathrm{e}}$. The local cylinder angle is

given by

$$\theta_\mathrm{i} = \theta + \frac{2\,\pi}{N_\mathrm{c}}\,i \qquad i \in \{0,\ldots,N_\mathrm{c}-1\} \tag{2}$$

where N_c is the number of cylinders. The cylinder chamber volume, V, is then given as

$$\begin{aligned} V_\mathrm{i}\left(\theta_\mathrm{i}\right) &= \frac{V_\mathrm{d}}{2}\,\left(1-\cos(\theta_\mathrm{i})\right)+V_0 \\ \dot{V}_\mathrm{i}\left(\theta\right) &= \frac{V_\mathrm{d}}{2}\,\sin(\theta_\mathrm{i})\,\dot{\theta} \end{aligned} \tag{3}$$

where V_0 is the minimum chamber volume and $V_\mathrm{d} = 2\,r_\mathrm{e}\,A_\mathrm{p}$ is the displacement volume, with A_p being the piston area. The pressure dynamics in one displacement chamber is governed by the continuity equation and is given to be

$$\dot{p}_\mathrm{i} = \frac{\beta_\mathrm{e}}{V_\mathrm{i}}\,\left(Q_\mathrm{H,i} - Q_\mathrm{L,i} - \dot{V}_\mathrm{i}\right) \tag{4}$$

Where Q_H and Q_L are the flows through the high and low pressure valve respectively and β_e is the effective bulk modulus. The oil-flows through the valves may be described by the orifice equation given by

$$\begin{aligned} Q_\mathrm{L,i} &= \frac{\bar{x}_\mathrm{L}}{k_\mathrm{f}}\,\sqrt{|p_\mathrm{i}-p_\mathrm{L}|}\,\mathrm{sign}\left(p_\mathrm{i}-p_\mathrm{L}\right) \\ Q_\mathrm{H,i} &= \frac{\bar{x}_\mathrm{H}}{k_\mathrm{f}}\,\sqrt{|p_\mathrm{H}-p_\mathrm{i}|}\,\mathrm{sign}\left(p_\mathrm{H}-p_\mathrm{i}\right) \end{aligned} \tag{5}$$

where k_f is the valve flow coefficient and $\bar{x}_\mathrm{L}$ and $\bar{x}_\mathrm{H}$ are normalized valve plunger positions. The torque from each pressure chamber is described by

$$\tau_\mathrm{i} = \frac{d\,V_\mathrm{i}\left(\theta_\mathrm{i}\right)}{d\theta}\,p_\mathrm{i} = \frac{V_\mathrm{d}}{2}\,\sin(\theta_\mathrm{i})\,p_\mathrm{i} \tag{6}$$

The dynamical behavior of a single pressure chamber is investigated by considering the pressure trajectories as function of the shaft angle in a polar phase plot shown in Fig. 3. In the simulation, the pressure is initially equal to the high pressure, $p = p_\mathrm{H}$, during the down-stroke, $\theta = [0;\pi]$ and the initially open HPV is closed $\bar{x}_\mathrm{H} : 1 \to 0$. This results in a depressurization and when $p < p_\mathrm{L}$ the LPV is passively opened $\bar{x}_\mathrm{L} : 0 \to 1$. During the upstroke, $\theta = [\pi;2\pi]$, the pressure is initially equal to the low pressure $p = p_\mathrm{L}$ and the initially open LPV is closed $\bar{x}_\mathrm{L} : 1 \to 0$. This results in a pressurization and when $p > p_\mathrm{H}$ the HPV is passively opened $\bar{x}_\mathrm{H} : 0 \to 1$. ϕ_mL is the latest angle that the LPV should be closed in order to obtain passive opening of the HPV at top dead center (TDC). ϕ_mH is the latest angle that the HPV should be closed during motoring for the LPV to be passively opened at bottom dead center (BDC). Similarly, ϕ_pL is the earliest angle that the pumping stroke may be initiated

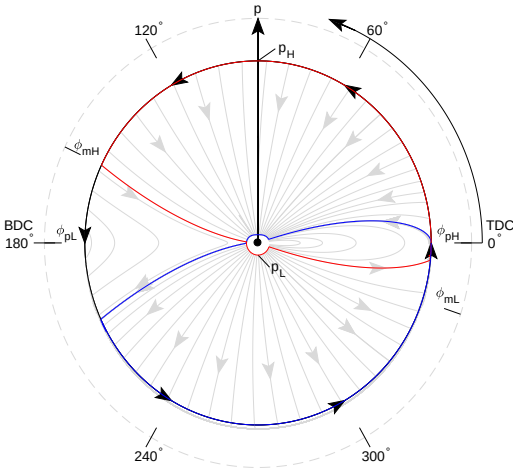

Figure 3: Phase portrait of the pressure dynamics as function of the angle. Red trajectory illustrates a full motoring stroke and blue trajectory illustrates a full pumping stroke.

and ϕ_pH is the angle where the HPV is closed to end the pumping stroke.

It is seen that the pressurization and depressurization are very fast as function of the angle except at BDC and TDC. Since the pressure is approximately constant when the HPV is open, the flow throughput may be simplified to be $Q_\mathrm{H} \approx \dot{V}_\mathrm{c}$, seen from (4), when considering the macro dynamics of the system. From the above analysis, the flow and torque as functions of the displacement volume are given by

$$\mathcal{D}(\theta) = \frac{V_\mathrm{d}}{2}\,\sin\left(\theta\right)\,\bar{x}_\mathrm{H} \qquad Q_\mathrm{H} = \mathcal{D}\,\dot{\theta} \qquad \tau = \mathcal{D}\;p \tag{7}$$

where $\bar{x}_\mathrm{H} = \{0,1\}$ depending on whether the chamber is active or inactive. The displacement throughput is used in the following analysis to examine the operation principle and control challenges related to the digital displacement machine. The control challenges for full- and partial-stroke operation are vastly different, since the system behavior is changed based on the chosen operation strategy. Therefore, the control challenges for the two operation strategies are investigated separately.

3 Control Challenges - Full stroke

Considering a full stroke operated DDM, the inputs may be considered to be $u = \{1,0,-1\}$ corresponding to motoring, idling and pumping respectively. For every chamber the decision to either motor or idle is done

once every revolution at ϕ_{mL}, while the decision to either pump or idle is done once every revolution at ϕ_{pL}. This angle dependent sampling yields an asynchronous sampling scheme for varying shaft speeds due to the relation

$$d\theta = \omega(t)dt \leftrightarrow dt = \frac{1}{\omega(\theta)}d\theta \tag{8}$$

An illustration of the sampling scheme in the position domain and time domain for an arbitrary variable speed DDM is illustrated in Fig. 4.

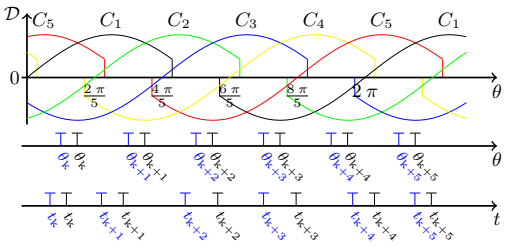

Figure 4: Displacement output response and control decision scheme of a full stroke operated DDM using both pumping and motoring strokes. Black samples are for motoring and blue samples are for pumping.

It is seen how a varying speed machine results in an asynchronous sampling scheme in the time domain, while the sampling scheme is synchronous in the angle domain if the machine is to only operate as a pump or motor. However, if the machine is to both motor and pump the sampling scheme is only periodic synchronous in the angle domain. Additionally, the inputs can only be chosen from $u_{\mathrm{m}} = \{1, 0\}$ for motoring samples and $u_{\mathrm{p}} = \{0, -1\}$ for pumping samples, similar to a pulse density modulation technique used in electrical circuit control. Furthermore, the impulse response is seen to be different, since the last part of the motoring stroke is not used, while the first part of a pumping stroke is not used. Since a full stroke lasts for approximately half of a revolution, it takes half of a revolution to activate all the pressure chambers. Hence, the response angle from zero to maximum displacement is also half of a revolution. As a result, both the control input frequency and response time is proportional to the speed of the machine, while the displacement discretization resolution is proportional to the number of cylinders.

3.1 Four quadrant operation

An additional complication is introduced if the machine is to operate in both directions of motion, which may be illustrated by a steep change in the rotation speed between positive and negative rotation as shown in Fig. 5.

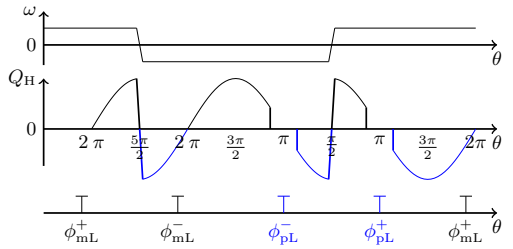

Figure 5: Illustration of response and sampling scheme with motion in both directions.

It is seen that a motoring decision is taken at ϕ^{+}_{mL} ahead of TDC, but as the direction of motion is changed, the stroke becomes a pumping stroke. As a result, the subsequent decision is also for motoring, but since the direction of motion is reverse, the sampling angle ahead of TDC is now at $\phi^{-}_{\mathrm{mL}} = 2\,\pi - \phi^{+}_{\mathrm{mL}}$. The same is illustrated for a change of direction during a pumping stroke, which similarly results in two pumping samples subsequently. It is seen that the sampling scheme for a DDM operating in both directions is asynchronous in both the time and position domain and the position domain is further not monotonically increasing.

4 Control Challenges - Partial stroke

The challenges with respect to control of a partial-stroke operated machine is very different than those identified for full-stroke operation. A partial motoring stroke is simply made by closing the HPV earlier and a partial pumping stroke by closing the LPV later as illustrated in Fig. 6.

It is seen that the impulse response of a partial stroke operated DD unit behaves different than that of a conventional dynamical system, since the input scales the width of the response rather than the amplitude. The input is the angle ϕ_{mH} for motoring and ϕ_{pL} for pumping, which controls the ratio where the given pressure chamber is active. The state changing input angle may be linearly normalized by an input variable change, such that the input is a displacement fraction $\eta = [0; 1]$. The input transformation is done by considering the committed displacement fraction for a motoring stroke

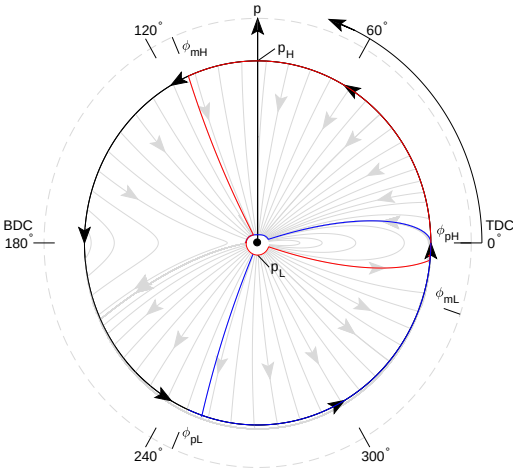

Figure 6: Phase portrait of the pressure dynamics as function of the angle. Red trajectory illustrates a 70% partial motoring stroke and blue trajectory illustrates a 70 % partial pumping stroke.

by use of (3) and yields

$$\eta_{\mathrm{m}} = \frac{V(\phi_{\mathrm{mH}})}{V(\pi)} = \frac{\frac{V_{\mathrm{d}}}{2}\,(1-\cos(\phi_{\mathrm{mH}}))}{\frac{V_{\mathrm{d}}}{2}\,(1-\cos(\pi))} = \frac{(1-\cos(\phi_{\mathrm{mH}}))}{2} \tag{9}$$

The resulting input transformation for motoring and pumping is then given by

$$\phi_{\mathrm{mH}}(\eta_{\mathrm{m}}) = \operatorname{acos}(1-2\,\eta_{\mathrm{m}}) \qquad \eta \in [0,\ \hat{\eta}_{\mathrm{m}}] \tag{10}$$

$$\phi_{\mathrm{pL}}(\eta_{\mathrm{p}}) = 2\,\pi - \operatorname{acos}(1-2\,\eta_{\mathrm{p}}) \qquad \eta \in [0,\ \hat{\eta}_{\mathrm{p}}] \tag{11}$$

where $\hat{\eta}_{\mathrm{m}}$ and $\hat{\eta}_{\mathrm{p}}$ are the maximum possible displacement fractions (corresponding to a full stroke) for motoring and pumping respectively. How the impulse response of the DD unit depends on the input is illustrated in Fig. 7 for a motoring stroke, where $\eta_{\mathrm{m}} = 0.7$ corresponding to a displacement of 70 % of the maximum displacement. It is seen that the state change of a chamber from active to inactive may only be given once for each revolution (considering motoring mode only) with conventional partial stroke. Therefore, the decision frequency is still proportional to the speed of the machine, but the response may be smoothened compared to full stroke operation. The state changing angle may however be updated continuously until the state change is carried out at the given angle. Considering, the input to be limited to only update at ϕ_{mL}, when the stroke is initiated, the system becomes a sample-and-hold system similar to that for

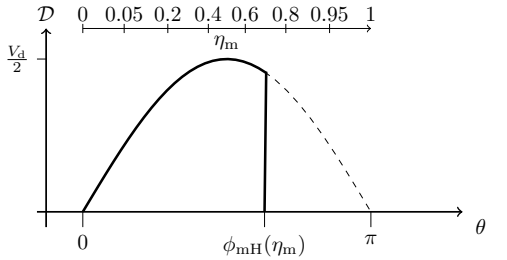

Figure 7: Impulse response as function of the input, $\eta_{\mathrm{m}} = 0.7$ in conventional partial stroke operation.

full-stroke. However, the impulse response is now time-varying, where the number of subsequent samples being made during the length of the impulse response varies as function of the input. This is illustrated in Fig. 8, where it is shown that 50% displacement during one revolution may be obtained with vastly different activation patterns.

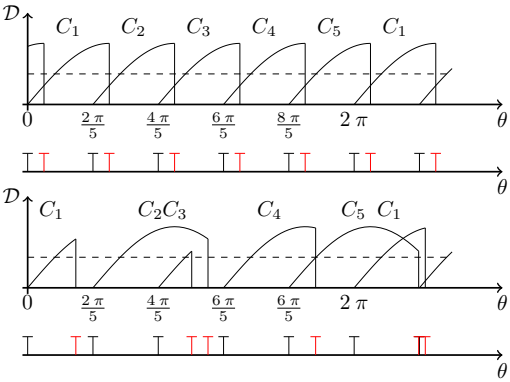

Figure 8: Flow/torque output response and control decision scheme of a partial stroke operated DDM, using only motoring strokes.

The top shown activation pattern corresponds to the output of a pulse width modulation strategy, while the bottom shown pattern is one arbitrary pattern of infinitely many, yielding an average of 50 % displacement during a full revolution. Since the flow is highest at the mid-point between TDC and BDC, the most severe flow spikes are also expected to occur if the valves are switched here. The flow level also has an impact on the energy cost when switching, which however is minor since the pressure across the valve is low when switching.

4.1 Sequential partial stroke

If the valves are designed to be able to open against high pressure difference, the sequential partial stroke method may be used to allow for multiple state changes during a revolution as illustrated in Fig. 9.

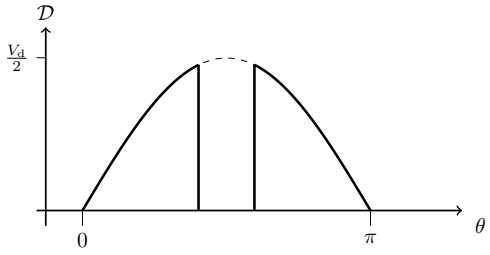

Figure 9: Impulse response as function of the input, $\eta_m = 0.7$, with sequential partial stroke.

It is seen that a 70 % stroke has been split into two sections, but in theory the displacement may be split into many more parts. With sequential partial stroke it is also possible to utilize the last part of the motoring stroke and first part of a pumping stroke, since the valves may be actively opened and closed independent of the angle. With this strategy, the state changing input may be updated continuously and is only constrained by the time it takes to open and close the valves. Therefore, the response may become even more smooth with this strategy. However, opening the HPV against high pressure difference (against the solution trajectories shown in Fig. 6) requires a substantially amount of energy and larger valves with higher actuation power is necessary Noergaard (2017). Even though the input may be updated continuously it is still binary, such that the output is in discrete levels based on the shaft angle as shown in Fig. 10. Only

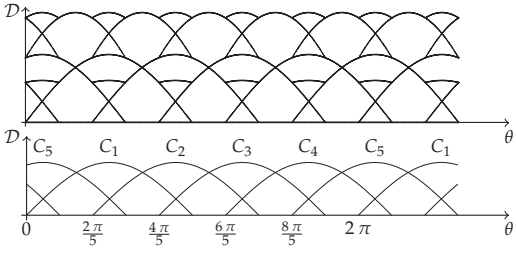

Figure 10: Illustration of the displacement combinations as function of the shaft angle with 5 cylinders.

motoring combinations are illustrated, but the number of combinations may be increased by including the possibility to pump. This does however mean that several cylinders will work against each other to lower the combined throughput. Contrary to conventional discrete input systems, it is seen that the discrete levels are changing as function of the angle.

4.2 Discussion of operation methods

The investigation clearly identifies that the dynamical behavior and control complications of the digital displacement machine is greatly influenced by the chosen operation strategy. A summarization of the dynamical behavior and control challenges is provided in Tab. 1. To give an overview of when to use which operation strategy, based on the mentioned advantages and disadvantages the following may be summarized:

- **Full stroke:** Is considered the favorable choice for high-speed machine operation, where energy efficiency is important. Also it is considered the most simple strategy, since state changes are done at fixed angles.
- **Partial stroke:** Is considered the favorable choice for low-speed machine operation, where both tracking performance and energy efficiency is important.
- **Sequential partial stroke:** Is considered the favorable choice for very low-speed machine operation, where control tracking performance is important and energy efficiency is of less importance.

Even though the advantages and disadvantages of each method are speed dependent, it may also be beneficial to use a full stroke strategy at low speed if tracking performance is not very important, but simplicity and energy efficiency is. Similar, it may be beneficial to use a partial stroke strategy at high speed, if tracking performance is very important, but simplicity and energy efficiency is not.

Based on the above analysis it may be favorable to utilize a combination of full-stroke and partial-stroke operation if the machine is to operate in a wide range of speeds. However, a combination of full and partial stroke operation is simply a partial stroke operation, since a full stroke is also a possible choice when utilizing a partial stroke strategy. Using the sequential partial stroke strategy, where several state changes may be made during each stroke also covers the conventional partial stroke strategy, since a possible choice is to only do one state change or none at all (full stroke). This does however not mean that it is advantageous to use the sequential partial stroke independent of the operation speed and application, since the strategy requires

Machine features

Pressure and mechanical dynamics	Non linear continuous differential equations	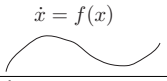
Control input type	Binary (active or inactive)	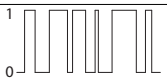

Operation strategy features

	Full stroke	**Partial Stroke**	**Sequential Partial stroke**	
Valve type and requirements	Only capable of opening against low pressure difference	Only capable of opening against low pressure difference	Capable of opening against high pressure difference	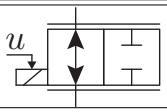
Control update rate	Proportional to the shaft speed and once every revolution at a fixed angle for both pumping and motoring	Proportional to the shaft speed and once every revolution at a variable angle for both pumping and motoring	Continuous, but constrained by the actuation time	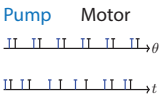
Displacement resolution	Proportional to the number of cylinders over one revolution and non-existent instantaneously	Continuous over one revolution and non-existent instantaneously	Continuous over one revolution, but proportional to the number of cylinders instantaneously with discrete levels being dependent on the angle	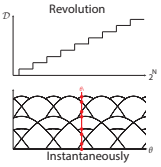
Chamber impulse response time	Proportional to the shaft speed (half of a revolution)	Scaled by the input, up to half of a revolution. The impulse response time is hence scaled by the input and shaft speed.	The time between each actuation decision	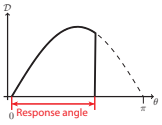
Machine response time (0 to max displacement)	Proportional to the shaft speed (half of a revolution)	Proportional to the shaft speed (up to half of a revolution)	Instantaneously (limited by the actuation time)	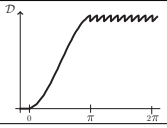
Pumping vs motoring	Impulse response is different (first part of pumping is not used and last part of motoring is not used)	Impulse response is different (first part of pumping is not used and last part of motoring is not used)	Similarly	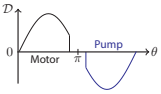
Change of rotation direction	Pumping becomes motoring and vice versa. Angle of control decision changes.	Pumping becomes motoring and vice versa. Angle of control decision changes.	Pumping becomes motoring and vice versa	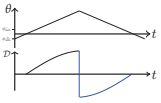
Energy cost and pressure spikes	Very low due to no pressure difference across the valve and no flow at switching	Dependent on the angle where the chamber is deactivated. Largest at mid-point between BDC and TDC	Dependent on the angle where the chamber is deactivated. Largest at mid-point between BDC and TDC.	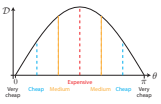

Table 1: Summarization of the dynamical behavior and control challenges of digital displacement units.

large active valves capable of opening against high pressure and the control complexity may be severely increased if the optimal control choice is e.g. only full strokes.

5 Control model development

For successful deployment of the digital displacement machine in a wide range of application it is beneficial to be able to analyze and design feedback controllers independently of operation. This is considered a complex task, especially since the dynamics is changing significantly depending on operation. Instead of developing a very complex control oriented model capable of handling every situation, it is considered beneficial to develop control oriented models for specific situations individually. In certain situations, simple dynamical approximation models may be sufficient for describing the systems macro dynamics.

5.1 Continuous approximation

Even though the non-smooth dynamical system is discretely controlled, a continuous approximation may be applicable in certain situations and results in a significantly simpler model for analysis and control design Pedersen et al. (2018a). The continuous approximation is illustrated for a full stroke operated pulse-density modulated (PDM) machine and a partial stroke pulse-width modulated (PWM) machine, where the input corresponds to a duty cycle. The step response for various duty cycles (normalized displacement fraction references), $\bar{\mathcal{D}}^* = \{0.1\ 0.2\ 0.4\ 0.6\ 0.8\ 1\}$, is shown in Fig. 11. Both responses for a machine with 5 cylinders and one with 20 cylinders is shown to illustrate the applicability of the method. It is seen that for a high number of pressure chambers, the response resembles a continuous response with ripples in the position domain. However, for low displacement fractions, the continuous approximation is seen to be quite poor for a full stroke PDM strategy, while it remains reasonably accurate with a partial stroke PWM strategy. The response may be fitted to a continuous transfer function by use of a spatial domain Laplace transformation defined as

$$F(\bar{s}) = \mathcal{L}\{f(\theta)\} = \int_0^\infty e^{-\bar{s}\,\theta}\, f(\theta) d\theta \tag{12}$$

Fitting the response dynamics to a second order system results in the transfer function given by

$$G(\bar{s}) = \frac{\mathcal{D}}{\mathcal{D}^*} = K \frac{\omega_\mathrm{n}^2}{\bar{s}^2 + 2\,\zeta\,\omega_\mathrm{n}\,\bar{s} + \omega_\mathrm{n}^2}\, e^{-\bar{s}\,\theta_\mathrm{d}} \tag{13}$$

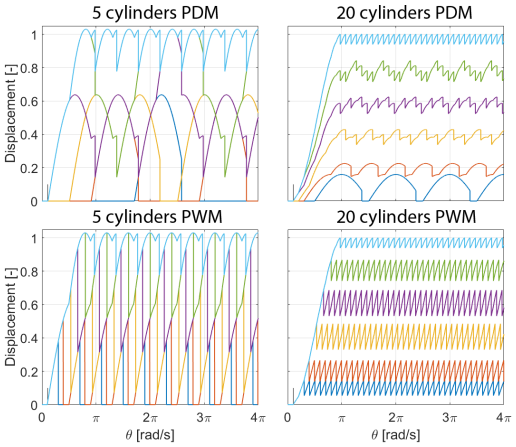

Figure 11: Step response for various displacements using delta-sigma modulation and pulse-density modulation.

where θ_d is the delay angle due to the decision being made ahead at ϕ_mL ahead of TDC, where the active motoring stroke starts. Converting the transfer function to the time domain by (8) yields a time-invariant system dependent on the machine speed. Therefore, if linear control is to be applied, a linearization point for the shaft speed must be chosen. In the time domain the bandwidth of the system is proportional to the shaft speed and to ensure stability in the case of linear control, the speed should be greater than the linearization speed. For high speed operation the dynamics of the machine is possibly significantly faster than the dynamics of the high pressure line and mechanical system it is connected to and may therefore possibly be neglected during control design. This is coherent with the non-smooth ripples in the response not being seen in the mechanical response for high mass inertia systems. It should however be clear that the method is very inaccurate for a low number of cylinders and for full stroke operation also at low displacements, where this method should not be applied. It is also important to consider that it is a discrete sampled system, so a continuous approximation is only valid up to a certain frequency where the sampling effect becomes significant.

5.2 Discrete approximation

To capture the discrete control effect of a full stroke operated digital displacement machine, a discrete approximation of the machine dynamics may be applied in several situations Johansen et al. (2017); Pedersen

et al. (2017a,b, 2018d). The displacement throughput between samples is given by the change in chamber volume divided by the constant sampling angle given as

$$\Delta\mathcal{D}[k] = \frac{\Delta V(\theta[k])}{\theta_s} = \frac{(V(\theta[k+1]) - V(\theta[k]))\ N}{2\,\pi} \tag{14}$$

where θ_s is the sampling angle and N is the number of cylinders. The discrete approximation of the displacement response is shown in Fig. 12 for a DDM with 15 cylinders.

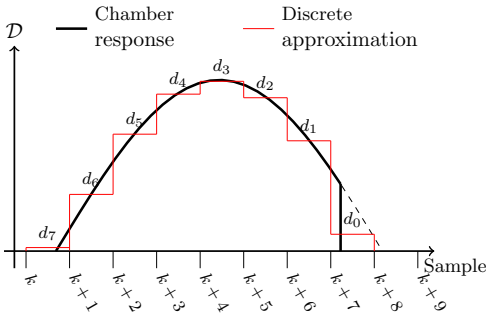

Figure 12: Discretization of displacement response for a motoring stroke.

The discrete response is seen to be fairly accurate for a high number of cylinders. The initial delay is again due to the decision being taking at ϕ_{mL} ahead of TDC. The discrete transfer function becomes that given by

$$G(z) = \frac{\mathcal{D}}{u} = \frac{d_7\,z^7 + d_6\,z^6 + \cdots + d_1\,z + d_0}{z^7} \tag{15}$$

where $u = \{0, 1\}$ depending on whether an active or inactive stroke is taken. Utilizing a pulse density modulator introduces a high non-linearity to the control system due to the quantizer given by

$$u[k] = \begin{cases} 1 & if \quad \bar{\mathcal{D}}^*[k] \geq 0.5 \\ 0 & if \quad \bar{\mathcal{D}}^*[k] < 0.5 \end{cases} \tag{16}$$

where $\bar{\mathcal{D}}^*[k]$ is the displacement fraction reference. Since the flow and torque are functions of the speed and pressure respectively given by (7), the output transfer function is non-linear. Additionally, for a variable speed machine the sampling scheme is asynchronous, why a transformation to the position domain by (17) is necessary to obtain a synchronous sampled system.

$$\frac{dx}{d\theta} = \frac{1}{\omega(\theta)}\,\frac{dx}{dt} \tag{17}$$

However, this transformation is seen to yield another non-linearity due to the speed being varying. Since non-linear discrete control is often quite complex, simpler linear approximations are often applied, which however limit the range of applicability. By linearizing around a steady-state speed, the operation speed should be greater than the linearization speed to ensure stability. The common method of describing a quantizer linearly is to simply consider the quantizer as an additive noise input, $u[k] = \bar{\mathcal{D}}^*[k] + n[k]$. This corresponds to a duty-cycle ratio approximation, where $n[k]$ is the noise input with intensity $I \in [0; 0.5]$. By omitting the noise term, the resulting response is shown in Fig. 13 for an input of $\bar{\mathcal{D}}^*[k] = 1/3$. The discretization is not shown for simplicity of illustration.

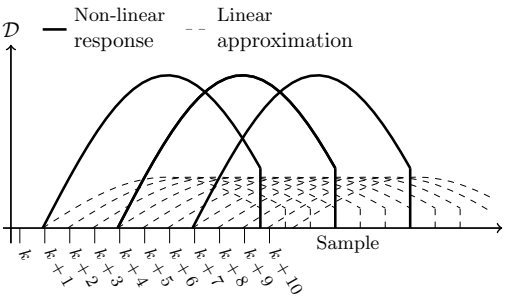

Figure 13: Discretization of displacement response.

It is seen that the linear approximation results in an angle average approximation, which is significantly more smooth than the non-linear physical response. Since the linear discrete approximation is poor at low displacement, it is not very accurate if the machine should both pump and motor. Furthermore, the pumping and motoring impulse responses are different, and if the method should both allow for pumping and motoring, synchronous sampling is required, which introduces additional delay to the system. The linear method hence includes the sampling effect and to some extent the ripples in the response, but the method range of validity is limited to machines with a high number of cylinders and high displacements, similar to the continuous approximation. Additionally, the direction of motion must not change since a monotonically increase in the sampling domain (angle or time) is required when applying discrete control methods.

5.2.1 Partial stroke strategy

It has been identified that partial stroke and sequential partial stroke methods are great for low speed operation, where tracking performance is quite poor for a full stroke strategy. However, for a partial stroke op-

eration, the energy cost of switching and the resulting pressure spikes are greatly influenced by the angle where the active stroke is stopped. With respect to control, the optimal solution may include trajectory tracking, energy efficiency, pressure spikes and frequency content, which is hardly achieved with a static control law. Therefore, model predictive control (MPC) is considered to have a high potential for control of a partial stroke operated DDM. MPC does however require a discrete model representation of the system dynamics Sniegucki et al. (2013); Pedersen et al. (2018c). For partial stroke operation, only a part of the full stroke is used, which introduces additional complications seen from a partial stroke discrete approximation shown in Fig. 14.

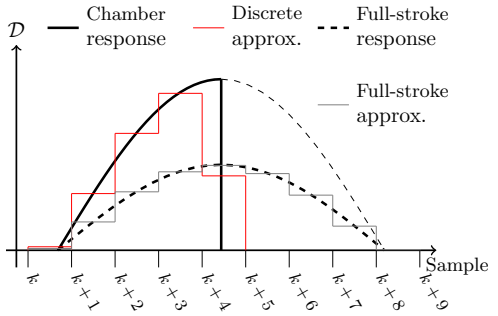

Figure 14: Discretization of displacement response, where $\eta = 0.5$ corresponding to half of a stroke. A full stroke $\eta = 1$, with $u = 0.5$ yields the angle average committed displacement as if $\eta = 0.5$ and $u = 1$.

In this partial stroke example, the displacement is seen to be committed over less samples, such that the transfer function order is reduced to

$$G(z) = \frac{\mathcal{D}}{u} = \frac{d_4\, z^4 + d_3\, z^3 + \cdots + d_1\, z + d_0}{z^4} \qquad (18)$$

Partial stroke operation hence results in an input dependent time-variant system, where the input to the transfer function is unity. This model is only obtainable if the stroke ratio is determined at sample k, where the stroke is initiated. If the stroke ratio may be updated continuously until the pressure chamber is deactivated, the impulse response and hence the discrete model is unknown when the stroke is initiated by closing the LPV at ϕ_{mH}. It is possible to apply model predictive control to such system, but it does not fulfill the requirements of classical MPC, where the input scales the magnitude of the response and not the model it self. To enable classical linear MPC control, an angle average approximation may me made, since a 50 % stroke, $\eta = 0.5$ with unity input, $u = 1$, has the same integrated displacement as a full stroke, $\eta = 1$, with input $u = 0.5$. This angle average approximation is also shown in Fig. 14 and is seen to smoothen the response and be decreasingly accurate for lower displacement fractions. However, the angle average approximation is quite conservative with respect to stability, since the slowest response with the largest phase angle is a full stroke (highest order model), but the gain is seen to be lowered simultaneously. It should be evident, that for a fixed sampling angle, the time between samples is inverse proportional to the machine speed and to solve the optimization problem in real time constrains the maximum speed.

Similarly to partial stroke operation, MPC has a high potential for sequential partial stroke operation, since energy efficiency and pressure ripples become increasingly important with an increased number of switchings. MPC for a sequential partial stroke operated DDM is very similar to conventional MPC control of continuous dynamical systems, since the input may be updated at every sample Pedersen et al. (2018e). However, the input is limited to be a discrete set of displacements, which requires optimization algorithms capable of handling such problem. The methods enable both motoring and pumping strokes, since the optimal combination of all combinations of active and inactive pressure chambers is considered. The method does however not allow for operation in both directions, since the sampling domain must increase monotonically.

5.3 Hybrid dynamical system

Since the non-smooth dynamics of the digital displacement machine is of hybrid nature, hybrid system theory is able to describe both the continuous and discrete dynamics of the system Pedersen et al. (2017c, 2018b); Sniegucki et al. (2013). Neither continuous nor discrete approximations are able to describe the machine dynamics if the machine is to operate in both directions. Therefore, hybrid dynamical system theory is necessary to capture the dynamics, especially since stability is of high concern at low speeds where the control update rate is low in full and partial stroke operation. Furthermore, the approximation methods have shown poor accuracy for a low number of cylinders, low displacements and low speeds, where hybrid theory might be necessary to ensure stability and obtain the desired transient behavior. Several hybrid formulations exist, which are able to describe the dynamical behavior (e.g. hybrid automaton, impulsive system, switched system), where each has their own advantages and disadvantages. Although, hybrid dynamical sys-

tem models are very intuitive, hybrid control theory is quite complex even for simple systems. Since a discrete event occurs every time a valve is opened or closed (or every time the pressure chamber is activated or deactivated) for every cylinder, the hybrid dynamical model of the digital displacement machine is not considered a simple system. Control theory for hybrid systems is an undergoing research topic, but stabilizing feedback control theory does exist, e.g. control Lyapunov function theory Teel et al. (2015); Goebel et al. (2009); Brogliato (2016).

6 Control challenges related to application and design

The control challenges when operating a system comprising digital displacement machines is highly dependent on the application where it is used. Furthermore, due to the modular construction of the machine, the control challenges are also greatly dependent on how the machine is designed and how it is connected to the individual target application.

6.1 Fluid Power Transmission

One application with very high potential for use of DDM's is a transmission system for converting low speed high torque power into high speed low torque power or vice versa. An illustration of a digital fluid power transmission is shown in Fig. 15. A ring cam design is used to increase the number of strokes per revolution of the slow rotating machine.

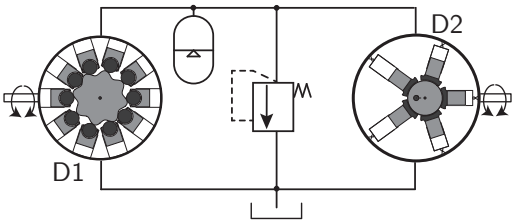

Figure 15: Illustration of a fluid power transmission system comprising two digital displacement machines.

Having multiple digital displacement machines which dynamics are directly influencing each other, the control challenges are further complicated. The high speed machine is seen to have 5 cylinders and the low speed machine to have 10 cylinders and 8 cam ring lobes for a total of 80 strokes per revolution. This means that for two digital displacement machines, where one is solely pumping and the other is solely motoring in a full stroke mode, the combined control input scheme is only periodic synchronous in the position domain even for fixed speed as illustrated in Fig. 16.

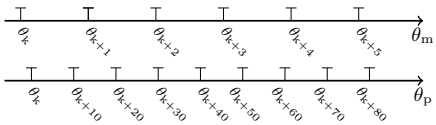

Figure 16: Input decision scheme for a digital hydraulic transmission with a high and a low speed digital displacement machine.

It is seen that if the number of strokes per revolution of the two machines are vastly different, a large amount of information is required to describe the combined sampling scheme in one revolution. Several drive trains need to operate in four quadrants, where each machine can both pump and motor and rotate in both directions (vehicle transmission etc.). Based on the identified control complications, it is clear that the control challenges of such system become significantly more complex and increasingly complicated if it is to utilize partial stroke operation also.

6.2 Direct cylinder drive

Another application where digital displacement machines has a large potential is in direct cylinder drives for large inertia systems, since they may potentially increase the energy efficiency significantly. A conceptional illustration of a multiple direct hydraulic cylinder drive is shown in Fig. 17.

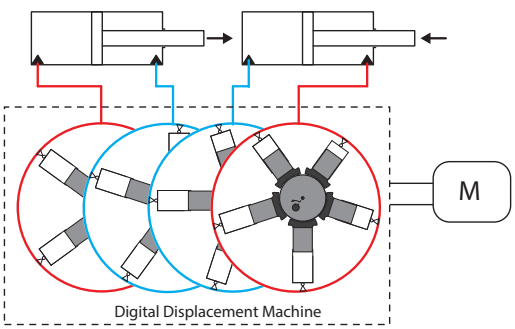

Figure 17: Conceptional drawing of a multiple cylinder digital displacement direct cylinder drive.

It is seen that one digital displacement machine is being powered by a motor and is used to control several hydraulic cylinders independently. In the illustrated concept, each module of the DDM is connected

to either the rod or piston side of a cylinder for separate metering control. Development of a dynamic model allowing for analysis and control of such system is complicated, since the dynamics of the whole system is coupled through the mechanical shaft. Since the input for each main cylinder chamber may only be updated every fourth sample, the sampling scheme is again asynchronous. In theory, the connections between the chambers of the digital hydraulic machine and the main cylinder chamber could be reconfigured in many different combinations (e.g. connecting additional chambers to a main cylinder with a high load), which would change the dynamical behavior.

6.3 Alternative machine design concepts

An alternative concept is to utilize multiple independent inlets/outlets for each pressure chamber, requiring additional high pressure valves. The concept is similar to the digital hydraulic power management system (DHPMS) developed by Heikkila and Linjama (2013). This concept directly increases the control update rate for each input to the main cylinder chambers and thereby possibly improves the control performance. The multiple inlet/outlet digital hydraulic cylinder drive concept is illustrated in Fig. 18.

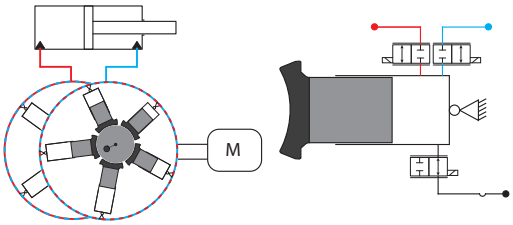

Figure 18: Conceptional drawing of a digital hydraulic direct cylinder drive with multiple inlets/outlets.

Even though the control update rate is doubled, the effective update rate is not, since multiple high pressure valves should not be opened simultaneously. This would result in a short circuit where the pressure is not controllable due to the differential cylinder and will thus lead to unwanted dynamical problems. With this concept the control input consists of multiple decisions, being pump to rod or piston or idle during up-stroke and motor to either piston or rod side or idle during down-stroke. Taking multiple decision is considered to further increase the control complexity, where classical discrete and continuous methods are not applicable.

With respect to control tracking performance, a high number of small cylinder chambers is beneficial, but it is much more costly than using a few larger cylinders. An alternative design that may be beneficial is to utilize multiple sized cylinders. Using such design with a full stroke operation strategy, the displacement discretization resolution is significantly improved without a huge increase in production cost. An illustration of a DDM with variable sized displacement chambers and its corresponding sampling scheme and impulse responses for motoring strokes is shown in Fig. 19.

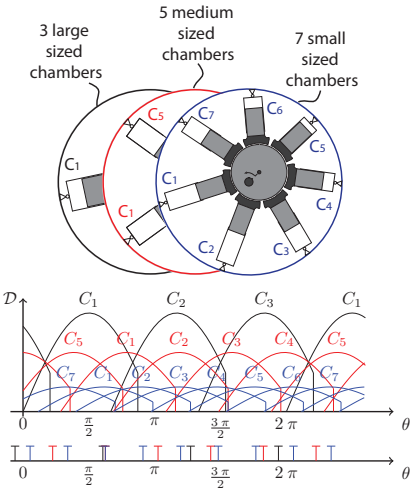

Figure 19: Illustration of a DDM with variable sized displacement chambers.

It is seen that the control update scheme is only periodic synchronous in the angle domain, while the impulse response is time varying dependent on the size of the chamber. As a result, this alternative concept introduces further complications with respect to model based dynamical analysis and control. Combining the different concepts: e.g. a multiple digital hydraulic direct cylinder drive with multiple sized displacement chambers and multiple inlets/outlets makes the dynamical control challenges tremendous, especially if it is to operate in all four quadrants and using both partial and full stroke methods.

To summarize the outcome of the investigation, it is identified that the control challenges and complexity is highly dependent on the machine configuration, operation strategy and the application it is used in. For the more complex systems, hybrid dynamical theory is considered necessary, but the development of stabilizing feedback control laws is very challenging and

remains an undergoing research topic.

7 Conclusion

This paper identifies many of the challenges related to model based feedback control of digital displacement machines. It is found that the challenges are highly dependent on the chosen operation strategy of the machine, as well as how the machine is configured and in which application it is used. Since the continuous dynamics of each pressure chamber is activated or deactivated discretely, the system dynamics belongs to the class of hybrid systems. Since control of hybrid dynamical systems is quite complex and remains an active research field, simpler continuous and discrete approximations have been investigated and deemed valid in certain situations. However, to be able to perform proper feedback stabilizing control and obtain the desired transient performance in a broad range of situations, more advanced control theory is required, e.g. hybrid control. The paper hence provides an overview of the many unsolved problems related to control of digital displacement machines, which is considered a key elements for successful deployment of the technology in a broad range of hydraulic applications.

Acknowledgments

This research was funded by the Danish Council for Strategic Research through the HyDrive project at Aalborg University, at the Department of Energy Technology (case no. 1305-00038B). The work is made in cooperation with the research council of Norway, SFI offshore mechatronics, project number 237896/O30.

References

Armstrong, B. S. R. and Yuan, Q. Multi-level control of hydraulic gerotor motors and pumps. *Proceedings of the american control conference, Minnesota, USA*, 2006. doi:10.1109/ACC.2006.1657450.

Bender, N. C., Pedersen, H. C., and Andersen, T. O. Multiagent evolution algorithm for control of a repetitive non-linear dynamic system. *Submitted to the ASME/BATH Symposium on Fluid Power and Motion Control, Bath, UK*, 2018a.

Bender, N. C., Pedersen, H. C., Winkler, B., and Plckinger, A. Modeling transient flow phenomena in hydraulic seat valve with annular flow geometry. *Submitted to the International Journal Fluid Power*, 2018b.

Breidi, F. E. *Investigation of digital pump/motor control strategies*. Ph.D. thesis, Purdue University, West Lafayette, 2016. URL http://docs.lib.purdue.edu/open_access_dissertations/752.

Brendi, F., Garrity, J., and Lumkes, J. Investigation of a real-time pressure based valve timing correction algorithm. *Proceedings of the ASME/BATH Symposium on Fluid Power and Motion Control*, 2017. doi:10.1115/FPMC2017-4342.

Brogliato, B. *Nonsmooth Mechanics - Models, Dynamics and Control (third edition)*. Springer, ISBN: 978-1-4471-0557-2, 2016.

Ehsan, M., Rampen, W., and Salter, S. Modeling of digital-displacement pump-motors and their application as hydraulic drives for nonuniform loads. *ASME. J. Dyn. Sys., Meas., Control.*, 1997. doi:10.1115/1.482444.

Goebel, R., Sanfelice, R. G., and Teel, A. R. Hybrid dynamical systems. *IEEE Control Systems Magazine, Vol. 29, Iss. 2, pp. 28-93*, 2009. doi:10.1109/MCS.2008.931718.

Hansen, A. H. and Pedersen, H. C. Optimal configuration of a discrete fluid power force system utilised in the PTO for WECs. *Ocean Engineering*, 2016. doi:10.1016/j.oceaneng.2016.03.032.

Hansen, R. H., Andersen, T. O., Pedersen, H. C., and Hansen, A. H. Control of a 420 kN Discrete Displacement Cylinder Drive for the Wavestar Wave Energy Converter. In *ASME/BATH 2014 Symposium on Fluid Power and Motion Control*. 2014. doi:10.1115/FPMC2014-7833.

Heikkila, M. and Linjama, M. Displacement control of a mobile crane using digital hydraulic power management system. *Mechatronics Volume 23, Issue 4, Pages 452-461*, 2013. doi:10.1016/j.mechatronics.2013.03.009.

Jarf, A., Minav, T., and Pietola, M. Nonsymmetrical flow compensation using hydraulic accumulator in direct driven differential cylinder application. *Proceedings of the 9th FPNI Ph.D. Symposium on Fluid Power, Florianpolis, Brazil*, 2016. doi:10.1115/FPNI2016-1516.

Johansen, P. *Tribodynamic Modeling of Digital Fluid Power Motors*. Ph.D. thesis, Energy Technology, Aalborg University, Denmark, 2014.

Johansen, P., Roemer, D. B., Andersen, T. O., and Pedersen, H. C. Delta-sigma modulated displacement of a digital fluid power pump. *The 7th workshop on digital fluid power, Linz, Austria*, 2015a.

Johansen, P., Roemer, D. B., Andersen, T. O., and Pedersen, H. C. On the Influence of Piston and Cylinder Density in Tribodynamics of a Radial Piston Digital Fluid Power Displacement Motor. In *ASME/BATH 2015 Symposium on Fluid Power and Motion Control*. 2015b. doi:10.1115/FPMC2015-9608.

Johansen, P., Roemer, D. B., Pedersen, H. C., and Andersen, T. O. Discrete linear time invariant analysis of digital fluid power pump flow control. *Journal of Dynamic Systems, Measurement and Control, Transactions of the ASME, Vol. 139*, 2017. doi:10.1115/1.4036554.

Merrill, K. J. *Modeling and analysis of active valve control of a digital pump-motor*. Ph.D. thesis, Purdue University, West Lafayette, 2012. URL https://docs.lib.purdue.edu/dissertations/AAI3544301.

Noergaard, C. *Design, Optimization and Testing of Valves for Digital Displacement Machines*. Ph.D. thesis, Department of Energy Technology, Aalborg University, Denmark, 2017. doi:10.5278/vbn.phd.eng.00013.

Payne, G. S., Kiprakis, A. E., Ehsan, M., Rampen, W., Chick, J. P., and Wallace, A. R. Efficiency and dynamic performance of digital displacement hydraulic transmission in tidal current energy converters. *Journal of Power and Energy, Proc. IMechE, Vol. 221, Part A, pp. 207-218.*, 2007. doi:10.1243/09576509JPE298.

Payne, G. S., Stein, U. P. P., Ehsan, M., Caldwell, N. J., and Rampen, W. H. S. Potential of digital displacement hydraulics for wave energy conversion. *In Proc. of the 6th European Wave and TIdal Energy Conference, Glasgow UK.*, 2005.

Pedersen, H. C., Hansen, R. H., Hansen, A. H., Andersen, T. O., and Bech, M. M. Design of full scale wave simulator for testing power take off systems for wave energy converters. *International Journal of Marine Energy, Vol. 13, pp. 130-156*, 2016a. doi:10.1016/j.ijome.2016.01.005.

Pedersen, N. H., Johansen, P., and Andersen, T. O. Lqr feedback control development for wind turbines featuring a digital fluid power transmission system. *Proceedings of the 9th FPNI Ph.D. Symposium on Fluid Power. American Society of Mechanical Engineers*, 2016b. doi:10.1115/FPNI2016-1537.

Pedersen, N. H., Johansen, P., and Andersen, T. O. Event-driven control of a speed varying digital displacement machine. *Proceedings of the 2017 Bath/ASME Symposium on Fluid Power and Motion Control*, 2017a. doi:10.1115/FPMC2017-4260.

Pedersen, N. H., Johansen, P., and Andersen, T. O. Optimal control of a wind turbine with digital fluid power transmission. *Nonlinear Dyn. 91: 591*, 2017b. doi:10.1007/s11071-017-3896-0.

Pedersen, N. H., Johansen, P., and Andersen, T. O. Feedback control of multi-level pulse-density modulated digital displacement transmission. *Submitted to IEEE/ASME Transaction on Mecatronics*, 2018a.

Pedersen, N. H., Johansen, P., and Andersen, T. O. Four quadrant hybrid control oriented dynamical system model of digital displacement units. *Submitted to the 2018 Bath/ASME Symposium on Fluid Power and Motion Control*, 2018b.

Pedersen, N. H., Johansen, P., and Andersen, T. O. Model predictive control and discrete analysis of partial stroke operated digital displacement machine. *Submitted to the Global Fluid Power Society PhD Symposium*, 2018c.

Pedersen, N. H., Johansen, P., Andersen, T. O., and Scheidl, R. Non-linear hybrid control oriented modelling of a digital displacement machine. *The Ninth Workshop on Digital Fluid Power, September 7-8, Aalborg, Denmark*, 2017c.

Pedersen, N. H., Johansen, P., Andersen, T. O., and Scheidl, R. Discrete optimal control and potential analysis of a digital direct hydraulic cylinder drive. *Submitted to Elsevier Journal of Mechatronics*, 2018d.

Pedersen, N. H., Johansen, P., Hansen, A. H., and Andersen, T. O. Model predictive control of low-speed partial stroke operated digital displacement pump unit. *Submitted to Journal of Model, Identification and Control*, 2018e.

Rampen, W. Gearless transmissions for large wind turbines the history and future of hydraulic drives. *Bremen*, 2006.

Rampen, W. The development of digital displacement technology. *In Proceedings of Bath/ASME FPMC Symposium*, 2010.

Roemer, D. B. *Design and Optimization of Fast Switching Valves for Large Scale Digital Hydraulic Motors*. Ph.D. thesis, Department of Energy Technology, Aalborg University, 2014. Department of Energy Technology, Aalborg University.

Roemer, D. B., Johansen, P., Pedersen, H. C., and Andersen, T. O. Design and modelling of fast switching efficient seat valves for digital displacement pumps. *Transactions of the Canadian Society for Mechanical Engineering*, 2013. 37(1):71–88. doi:10.1139/tcsme-2013-0005.

Roemer, D. B., Johansen, P., Pedersen, H. C., and Andersen, T. O. Oil Stiction in Fast Switching Annular Seat Valves for Digital Displacement Fluid Power Machines. In *Proceedings of the 12th Biennial Conference on Engineering Systems Design and Analysis*. 2014. doi:10.1115/ESDA2014-20443.

Roemer, D. B., Johansen, P., Pedersen, H. C., and Andersen, T. O. Fluid Stiction Modeling for Quickly Separating Plates Considering the Liquid Tensile Strength. *Journal of Fluids Engineering*, 2015a. doi:10.1115/1.4029683.

Roemer, D. B., Johansen, P., Schmidt, L., and Andersen, T. O. Modeling of Movement-Induced and Flow-Induced Fluid Forces in Fast Switching Valves. In *Inter. Conf. Fluid Power and Mechatronics*. 2015b. doi:10.1109/FPM.2015.7337257.

Salter, S. H., Taylor, J. R. M., and Caldwell, N. J. Power conversion mechanisms for wave energy. *Journal of Engineering for the Maritime Environment, pp. 1-27*, 2002. doi:10.1243/147509002320382103.

Schmidt, L., Roemer, D. B., Pedersen, H. C., and Andersen, T. O. Speed-variable switched differential pump system for direct operation of hydraulic cylinders. *Proceedings of ASME/BATH 2015 Symposium on Fluid Power and Motion Control, American Society of Mechanical Engineers*, 2015. doi:10.1115/FPMC2015-9575.

Sniegucki, M., Gottfried, M., and Klingauf, U. Optimal control of digital hydraulic drives using mixed-integer quadratic programming. *Proceedings of the 9th IFAC Symposium on Nonlinear Control Systems*, 2013. doi:10.3182/20130904-3-FR-2041.00013.

Song, X. Modeling and active vehicle suspension system with application of digital displacement pump motor. *Proceedings of the ASME 2008 International Design Engineering Techical Conferences & Computers and Information in Engineering Conference, New York, USA*, 2008. doi:10.1115/DETC2008-49035.

Teel, A. R., Sanfelice, R. G., and Goebel, R. Feedback control of hybrid dynamical systems. *Encyclopedia of Systems and Control*, 2015. doi:10.1007/978-1-4471-5102-9_271-2.

Paper B

Analysis of the Non-Smooth Dynamical Effects and Suitable Operation and Control Strategies for Digital Displacement Units

Niels H. Pedersen, Per Johansen and Torben O. Andersen

The paper has been submitted for The Tenth Workshop on Digital Fluid Power, February 28 - March 1, 2019, Linz, Austria

The layout has been revised.

Analysis of the Non-Smooth Dynamical Effects and Suitable Operation and Control Strategies for Digital Displacement Units

Niels H. Pedersen, Per Johansen, Torben O. Andersen
Department of Energy Technology, Aalborg University
Pontoppidanstraede 111, 9220 Aalborg East, Denmark
E-mail: nhp@et.aau.dk, pjo@et.aau.dk, toa@et.aau.dk

ABSTRACT

Newly emerging digital hydraulic pump-motor units enable high efficient operation and thereby span widely with respect to potentially application use. The digital displacement machine (DDM) provides four-quadrant operation at lower losses compared to conventional fluid power machines, due to the possibility of activating/deactivating individual pressure chambers. However, its non-smooth digital effects introduces pressure oscillations and complicates the control system development. This possibly explains why most state-of-the-art control strategies neglects the transient machine behavior when synthesizing controllers for the actuated plant. Since the dynamical behavior and control performance is greatly dependent on the chosen operation strategy and rotational speed of the machine, this paper identifies how the suitable operation and control strategy changes as function of the rotational speed. The paper shows that the DDM dynamics should only be neglected for a machine with a relatively high number of cylinders, relatively high displacement operation and if the rotational speed of the DDM is significantly faster than the plant dynamics.

KEYWORDS: Fluid Power, Digital Displacement, Hybrid system, Control model, Event-driven

1 INTRODUCTION

Energy efficient fluid power systems have received increasing research interest in the past decade both in academia and industry. Application utilization spans from cylinder drives [1, 2], to transmissions and power take-off systems [3, 4, 5, 6, 7, 8, 9]. In this paper, the digital displacement technology is considered which has great potential for use in all of the above mentioned applications. The machine uses the radial piston type design, where cylinders are radially located on a eccentric shaft, resulting in a reciprocating piston motion. The use of digital control valves located between each pressure chamber and high and low pressure manifold enables each chamber to be controlled individually. Thereby, the efficiency may be improved significantly, especially at part load operation. Additionally, the technology provides great redundancy and scalability due to its modular design. However, several challenges remains for the technology to be deployed on the market, which explains the large work focusing on design and performance optimization of the

machine [6, 10, 11, 12, 13, 14, 15, 16]. For the technology to be competitive to existing solutions, proper displacement control is considered of major importance, but is complicated by the non-smooth digital effects. Most state-of-the-art control strategies for the digital displacement machine neglects the transient machine behavior, and determines the cylinder chamber activation sequence based on either offline optimization or estimation techniques in a look-ahead angle [17, 18, 19, 20, 21, 22]. However, since the activation of the pressure chamber is conducted as function of the shaft angle and not time, the response time of the DDM is proportional to the rotational shaft speed. This paper investigates the dynamics of the digital displacement machine (DDM) as function of machine speed and operation strategy and shows that the dynamics should not always be neglected if proper operation and stability are to be guaranteed. Furthermore, the paper shows that the suitable operation and control strategy changes as function of machine speed and proposals on suitable strategies are provided accordingly. To simplify the dynamical analysis, the investigation is based on a relatively simple mathematical model, which only captures the fundamental dynamics of the DDM.

2 MATHEMATICAL MODEL

The relatively simple mathematical model is established based on the illustration of the DDM and a single pressure chamber shown in Fig. 1.

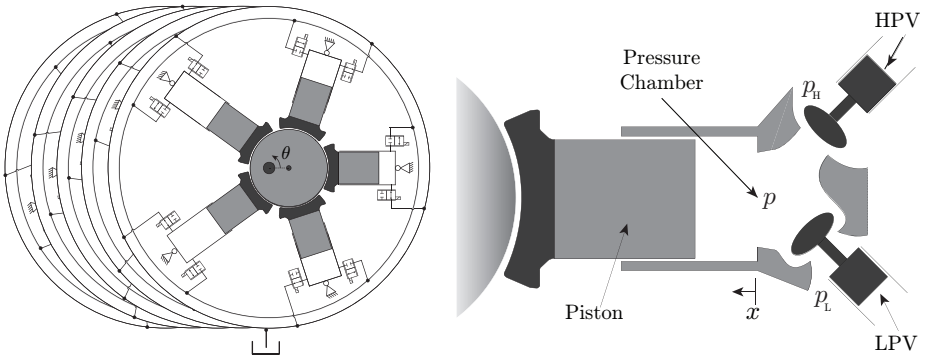

Figure 1: Illustration of the radial piston type digital displacement machine (25 cylinder machine) and definition of variables used for the mathematical model [23, 26].

The piston displacement for the i'th cylinder, x_{i}, is described as function of the shaft angle by

$$x_i = r_{\mathrm{e}}\,(1-\cos(\theta_i)) \qquad \theta_{\mathrm{i}} = \theta + \frac{2\,\pi}{N_{\mathrm{c}}}\,(i-1) \qquad i \in \{1,\ldots,N_{\mathrm{c}}\} \tag{1}$$

where r_{e} is the eccentric shaft radius and N_{c} is the number of cylinders. The displacement volume is thus given as $V_{\mathrm{d}} = 2\,r_{\mathrm{e}}\,A_{\mathrm{p}}$, where A_{p} is the piston area. The chamber volume for the i'th cylinder, V_{i}, and its time derivative are then given by

$$V_i = \frac{V_{\mathrm{d}}}{2}\,(1-\cos(\theta_i)) + V_0 \qquad \dot{V}_i = \frac{V_{\mathrm{d}}}{2}\,\sin(\theta_i)\,\dot{\theta} \tag{2}$$

where A_p is the piston area and V_0 is the minimum chamber volume. The continuity equation is used to describe the pressure build-up for the i'th cylinder given by

$$\dot{p}_i = \frac{\beta_\mathrm{e}(p_\mathrm{i})}{V_\mathrm{i}} \left(Q_{\mathrm{H},i} - Q_{\mathrm{L},i} - \dot{V}_i\right) \tag{3}$$

where β_e is the pressure dependent effective bulk modulus. Q_L and Q_H are the flows through the low and high pressure valve respectively. The orifice equation is used to describe the flows through the valves and are given to be

$$Q_{\mathrm{L},i} = \frac{x_\mathrm{L,i}}{k_\mathrm{f}} \sqrt{|p_i - p_\mathrm{L}|}\,\mathrm{sign}\,(p_i - p_\mathrm{L}) \qquad Q_{\mathrm{H},i} = \frac{x_\mathrm{H,i}}{k_\mathrm{f}} \sqrt{|p_\mathrm{H} - p_i|}\,\mathrm{sign}\,(p_\mathrm{H} - p_i) \tag{4}$$

where $x_\mathrm{L} \in [0,1]$ and $x_\mathrm{H} \in [0,1]$ are normalized valve plunger positions, while k_f is the valve flow coefficient. When considering the fundamental machine dynamics it is deemed sufficient to model the valves as a simple first order system given as

$$\dot{x}_\mathrm{H,i} = \frac{1}{\tau_\mathrm{v}} (u_\mathrm{H,i} - x_\mathrm{H,i}) \qquad \dot{x}_\mathrm{L,i} = \frac{1}{\tau_\mathrm{v}} (u_\mathrm{L,i} - x_\mathrm{L,i}) \tag{5}$$

where u_H and u_L are the inputs to the high and low pressure valve respectively, while t_v is the valve time constant. The torque contribution from the i'th pressure chamber is derived to be given by

$$\tau_i = \frac{d\,V_i(\theta_i)}{d\theta}\, p_i = \frac{V_\mathrm{d}}{2} \sin(\theta_i)\, p_i \tag{6}$$

The dynamical behavior of the pressure build-up in a pressure chamber is investigated by simulation the pressure trajectories in a polar plot as presented in [23]. The pressure trajectories for a pumping and motoring stroke is shown in Fig. 2a for a full-stroke response and in Fig. 2b for a partial-stroke response.

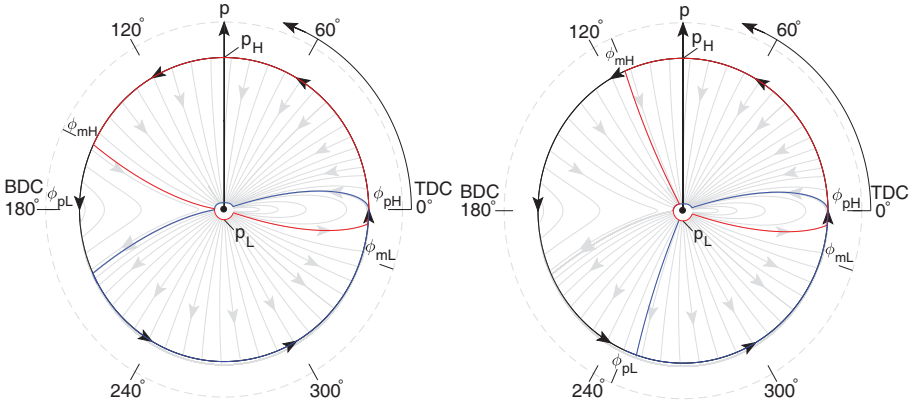

(a) Full stroke operation phase plot.

(b) Partial stroke operation phase plot.

Figure 2: Polar phase plot of the pressure trajectories of a single pressure chamber. Red trajectory indicates a motoring stroke and blue trajectory indicates a pumping stroke [23, 26].

An active stroke is initiated by closing the low pressure valve (LPV) at ϕ_mL and ϕ_pL for motoring and pumping respectively. As the pressure exceeds the high pressure due

to compression, the high pressure valve (HPV) is passively opened. The pressure level remains high until the active stroke is ended by closing the HPV at ϕ_{mH} and ϕ_{pH} for motoring and pumping respectively. It is seen that the last part of the motoring stroke and the first part of the pumping stroke in full-stroke operation is not utilized. This is done such that passive valve opening of the LPV due to the generated suction force may be utilized to reduce the energy losses.

It is seen that the pressure dynamics with respect to the angle is relatively fast, why it is considered valid to neglect the transient pressure build-up. As a result, the flow and torque throughput may either be active or inactive depending on the binary input, $\bar{u} \in \{0,1\}$, given by

$$\mathcal{D}_i = \frac{V_{\mathrm{d}}}{2} \sin(\theta_i)\, \bar{u}_i \qquad Q_{\mathrm{H},i} = \mathcal{D}_i\, \dot{\theta}_i \qquad \tau_i = \mathcal{D}_i\, p_i \tag{7}$$

where $\mathcal{D}_{\mathrm{i}}$ is the displacement throughput of the i'th pressure chamber. An illustration of the piston position, chamber pressure, valve plunger positions and displacement throughput is shown in Fig. 3 for full stroke operation.

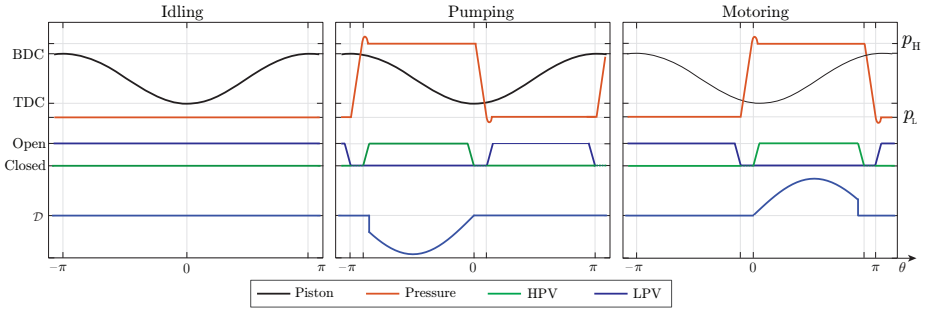

Figure 3: Illustration of the machine response in full stroke operation.

It is seen that the displacement response may be simplified to be a fraction of a sine wave, when neglecting the pressure dynamics. In the remainder of this paper, this simplification is used to describe the input-output relation of the DDM, whereby the complexity of dynamical analysis is significantly reduced.

The different operation strategies considered in this study are shown in Fig. 4 together with a comparison of the important characteristics. Since every operation strategy has its associated advantages and disadvantages, they should be applied accordingly to obtain the best possible performance. The dynamical behavior of the operation strategies are also vastly different, such that the suitable control strategy for each operation strategy is different and should be applied accordingly. This paper investigates the non-smooth dynamical effect of the different operation strategies and provides proposals on suitable control strategies for each operation strategy.

3 THE NON-SMOOTH DYNAMICAL EFFECT OF THE DDM

Most state-of-the-art control strategies for digital displacement units neglects the dynamical behavior of the DDM when designing the control system for the actuated plant. This paper investigates under which operation conditions it is sufficient to neglect the DDM dynamics and how the operation conditions affects the dynamical behavior. This is done

Figure 4: Operation strategies for the digital displacement machine [26].

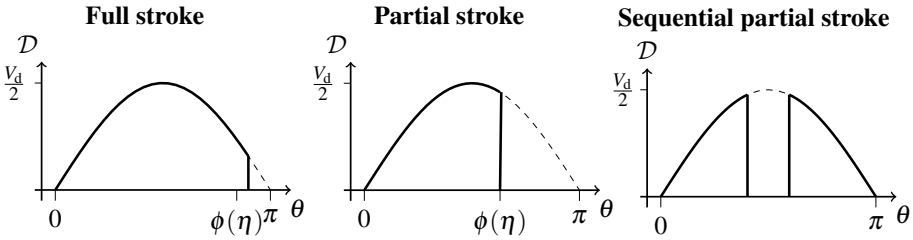

- Most simple and energy efficient strategy, due to switching at low flow and pressure levels for only a fraction of cylinders
- Small and fast valves incapable of opening against high pressure
- Control update rate is proportional to the machine speed.
- Displacement is quantized by the number of cylinders per revolution and not changeable instantaneously

- Medium energy efficient strategy, due to switching at higher flow rates, but low pressure difference for every cylinder
- Small and fast valves incapable of opening against high pressure
- Control update rate is proportional to the machine speed
- Displacement is continuously controlled per revolution and not changeable instantaneously

- Least energy efficient strategy, due to occasionally opening against high pressure difference multiple times every stroke
- Larger and slow valves capable of opening against high pressure
- Control update rate is speed independent and only constrained by valve switching time
- Displacement is instantaneously quantized by the number of cylinders and continuous per revolution

by comparing the response of a continuous first order plant actuated by the DDM to the response of an ideal infinitely fast actuator (corresponding to neglecting the DDM dynamics). The comparison is illustrated in Fig. 5 where a full-stroke delta-sigma modulation strategy is considered [24, 25]. η is the constant displacement fraction input, $\bar{\eta}$ is the binary input sequence determine whether the current cylinder chamber should be active or inactive. y_c is the total output displacement of all pressure chambers and y_p is the plant response. The plant is scaled with the constant $\pi/(\eta_m N_c)$ to obtain unity dc-gain and enable comparison to the ideal actuated plant. The constant $\eta_m \approx 0.96$ is the maximum full stroke displacement fraction. The plant eigen-frequency, ω_n, represents the plant inertness and is expected to have a large influence on the severity of pulsations in the plant response due to its filtering property. The difference between the plant response with and without the DDM, Δy, gives a measure of the digital effect introduced by the DDM. Simulation results for investigation of the DDM dynamical and non-smooth effect is shown in Fig. 6 for both a full-stroke pulse density modulated (PDM) and a partial-stroke pulse width modulated (PWM) digital displacement machine. A 5 cylinder DDM with a displacement fraction input of $\eta = 0.5$ is considered for simplicity of illustration.

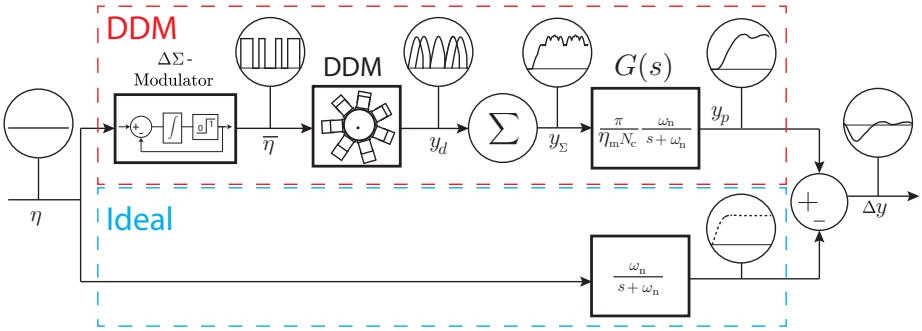

Figure 5: Strategy for investigation of the digital effect of the DDM. A full-stroke delta-sigma modulation strategy is considered [26].

It is seen that every second cylinder is activated for the full stroke period with the PDM strategy and every cylinder is activated for half of the stroke period with the PWM strategy. The red line indicates the angle delay, θ_{d}, in the response from the actuation decision is made until the first committed output. The dashed line shown for the plant response, y_{p}, is the ideal actuated response and thus has no delay. The important dynamical characteristics of the DDM may be divided into three parts; time-delay, response time and steady state energy of the oscillations. The time-delay is known to introduce phase-lag to a closed loop control system and is therefore of high importance with respect to ensuring stability. The DDM response angle, ϕ, from zero to maximum displacement is equal to the angle where the active stroke part is ended and is determined by the displacement fraction as

$$\begin{aligned} \eta &= \frac{V(\phi)}{V(\pi)} = \frac{\frac{V_{\mathrm{d}}}{2}\,(1-\cos(\phi))}{\frac{V_{\mathrm{d}}}{2}\,(1-\cos(\pi))} = \frac{(1-\cos(\phi))}{2} \\ \phi(\eta) &= \operatorname{acos}(1-2\,\eta) \qquad\qquad \eta \in [0,\, \eta_{\mathrm{m}}] \end{aligned} \tag{8}$$

Therefore, the DDM response time is inversely proportional to the machine speed, ω given by

$$T_{\mathrm{r}} = \frac{\phi(\eta)}{\omega} \tag{9}$$

where $\eta = \eta_{\mathrm{m}}$ for a full stroke operated machine. The energy in the steady state part of the difference signal, Δy, is a measure of the severity of the oscillation caused by the DDM. This measure is calculated by the squared average energy in the steady-state response of the difference signal and is evaluated for 10 full revolutions indicated by the blue line in Fig. 6 and is given by

$$E = \frac{1}{20\,\pi} \int_{\theta_0}^{\theta_0+20\,\pi} \Delta_{\mathrm{y}}(\theta)^2 d\theta \tag{10}$$

where θ_0 is the initial angle during steady state operation. Since the steady state energy is dependent on four variables; displacement fraction, number of cylinders, machine speed

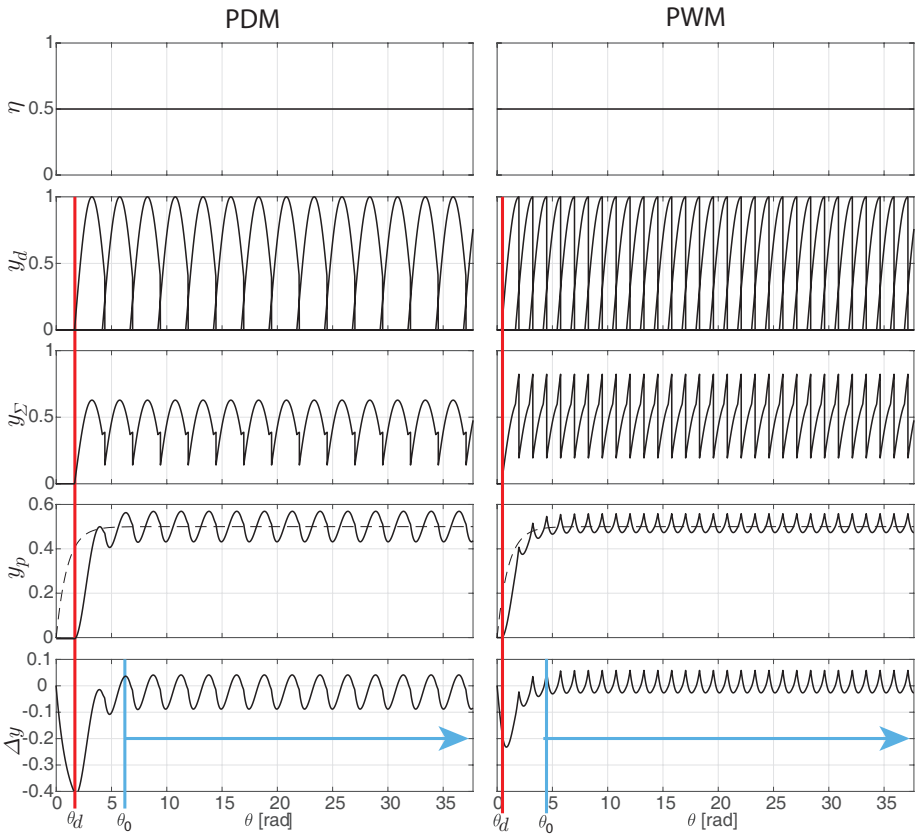

Figure 6: Simulation results for analysis of the digital effect. Red line indicates the DDM response delay and the blue line indicates the initial steady state angle [26].

and plant eigen-frequency, a relative eigen-frequency, ω_r, is introduced and given by

$$\omega_\mathrm{r} = \frac{\omega_\mathrm{n}}{\omega} \tag{11}$$

The relative frequency hence reduces the number of variables by one and exploits that the response in the angle domain is identical for a constant ω_r. Results for the time-delay and steady state energy is shown in Fig. 7 for a PDM operated DDM and in Fig. 8 for a PWM operated DDM. The response time is not shown, since it may be directly calculated from (9) and is only dependent on the machine speed for a PDM strategy. It is seen that the energy in the steady state response is decreasing for a higher number of cylinders and a lower relative frequency. Additionally, the energy is approximately reflected around $\eta = 0.5$, since actuating a single cylinder yields the same oscillation amplitude as deactivating a single cylinder in full-stroke. However, the relative oscillation energy with respect to the input, E/η, is much larger for low displacements, since the energy in the input signal is significantly lower. For PDM operation, the time delay is seen to be decreasing for a higher number of cylinders and a higher machine speed. For PWM operation the time-delay is always the minimum delay since all cylinders are activated, while the minimum time-delay for PDM operation occurs when the current cylinder is

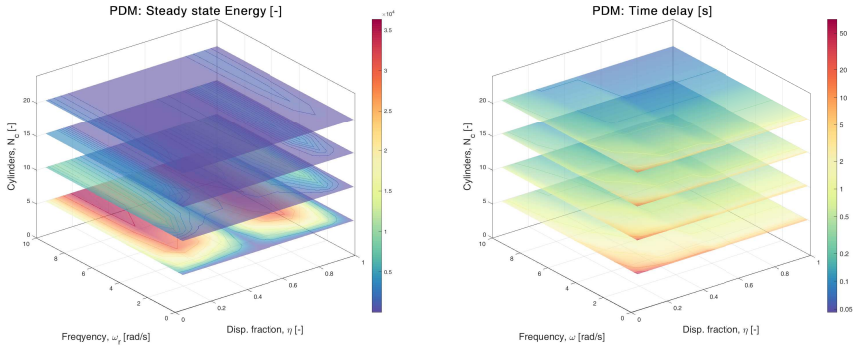

(a) Steady state energy. (b) Time delay.

Figure 7: Pulse Density Modulation.

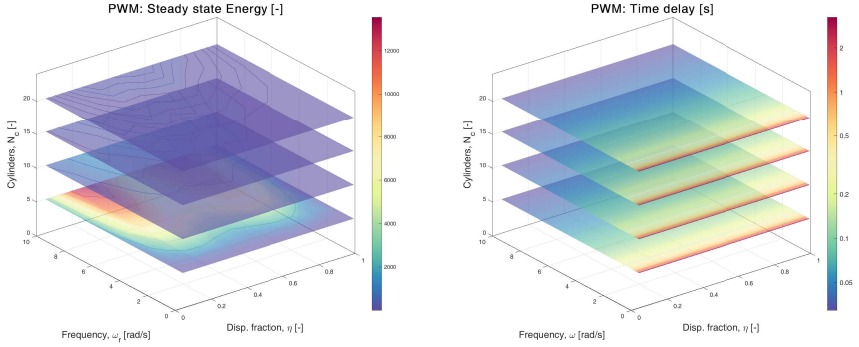

(a) Steady state energy [26]. (b) Time delay.

Figure 8: Pulse Width Modulation [26].

activated.

It is clear that the dynamics of the DDM can only be neglected in the control design process if the number of cylinders is relatively high, the relative frequency, ω_r, is relatively low and the displacement fraction is relatively high. To avoid unmodeled phase when omitting the DDM dynamics it is required that $\omega > 10\,\omega_n$. However, providing specific numbers about when it is considered sufficient to neglect the DDM dynamics is not done in this paper, since it is difficult to give a conclusive answer. A further investigation of the introduced phase-lag as function of displacement for a PDM operated machine is made. The discrete $\Delta\Sigma$-modulator has the form given by

$$\bar{\eta}(k) = \begin{cases} 1 & \text{for} \quad \sum_{k=0}^{n} \eta(k) - \bar{\eta}(k) \geq \frac{1}{2} \\ 0 & \text{for} \quad \sum_{k=0}^{n} \eta(k) - \bar{\eta}(k) < \frac{1}{2} \end{cases} \tag{12}$$

The discrete integrated displacement fraction error, which is the input to the quantizer always has a value of $q(k) \in \left[-\frac{1}{2}, \frac{3}{2}\right[$. The maximum delay in the output occurs if the integrator is on its boundary values, where the number of samples needed before the next cylinder is activated is given by $n_d = \text{floor}(1/\eta)$. The time-delay in the output is then

calculated to be given by

$$T_\mathrm{d} = \frac{\theta_\mathrm{d}}{\omega} \qquad \theta_\mathrm{d} = \frac{2\,\pi}{N_\mathrm{c}}\,n_\mathrm{d} \qquad \rightarrow \qquad T_\mathrm{d} = \frac{2\,\pi}{\omega\,N_\mathrm{c}}\,n_\mathrm{d} \tag{13}$$

Since the activation of the pressure chambers with continuous dynamics is done at discrete angles, the system is essentially a hybrid dynamical system. To simplify the analysis a frequency response of the DDM, where the delay-time is included is conducted based on a discrete approximation. The discrete approximation of the machine dynamics is done by utilization of the method presented in [27].

3.1 Frequency response based on DLTI model

Considering a motoring stroke, the decision to motor or idle is taken at ϕ_mL, where the LPV is either closed to activate the chamber or held open to idle the chamber. The discrete displacement fraction between samples is then calculated by

$$\begin{aligned} \Delta\mathcal{D}[k] &= \frac{\Delta V[k]}{\theta_\mathrm{s}} = \frac{\left(V\left(\theta[k+1]\right) - V\left(\theta[k]\right)\right) N_\mathrm{c}}{2\,\pi} \\ \theta[k] &= \phi_\mathrm{mL} + \theta_\mathrm{s}\,(k-1) \qquad\qquad k \in \{1,\ldots,N_\mathrm{c}\} \end{aligned} \tag{14}$$

where $\theta_\mathrm{s} = 2\,\pi/N_\mathrm{c}$ is the constant sampling angle. The discrete approximation of the displacement throughput is done by use of (15) and results in the impulse response shown in Fig. 9 for a 25 cylinders machine.

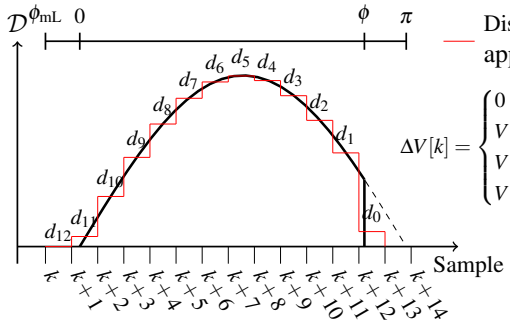

Discrete approximation — Chamber response

$$\Delta V[k] = \begin{cases} 0 & \theta[k],\theta[k+1] \notin [0\,;\phi] \\ V(\theta[k+1]) - V(\theta[k]) & \theta[k],\theta[k+1] \in [0\,;\phi] \\ V(\theta[k+1]) - V(0) & \theta[k] < 0 < \theta[k+1] \\ V(\phi_\mathrm{mH}) - V(\theta[k]) & \theta[k] < \phi < \theta[k+1] \end{cases} \tag{15}$$

Figure 9: Discrete approximation of displacement throughput of the digital displacement machine.

It is seen that $p = 12$ samples is needed to describe the full stroke. The shown displacement fractions are evaluated accordingly to $d_\mathrm{k} = \Delta\mathcal{D}[p-k]$ and results in the discrete transfer function given by

$$G(z) = \frac{\mathcal{D}(z)}{u(z)} = \frac{d_\mathrm{p}\,z^p + d_\mathrm{p\text{-}1}\,z^{p-1} + \cdots + d_1\,z + d_0}{z^p} \tag{16}$$

A frequency response plot is made of the discrete transfer function, where the machine operates at three different rotational speeds $\omega \in \{1,\,10,\,100\}$ rad/s. The frequency response is shown in Fig. 10, where the time-delay as function of displacement fraction

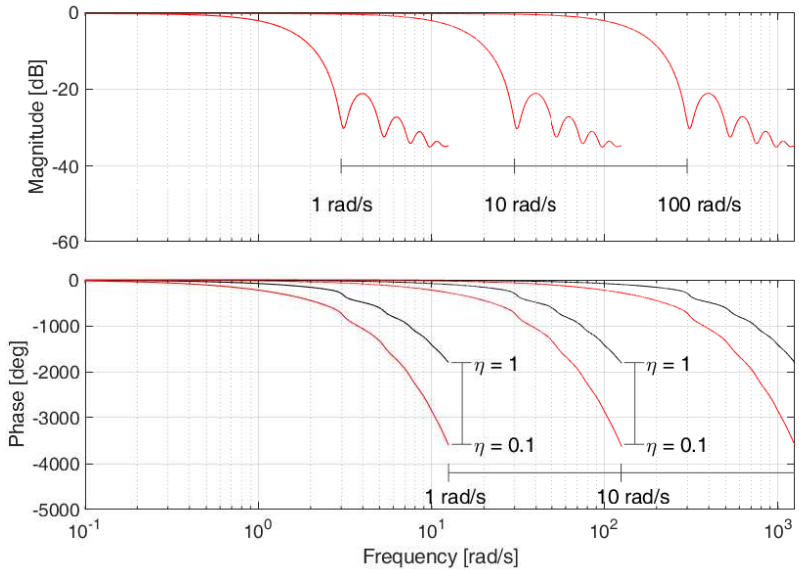

Figure 10: Frequency response of the DDM for varying rotational speed and displacement fractions in full-stroke operation.

input is shown. It is seen that the bandwidth of the DDM is directly proportional to the rotational speed and that the time-delay due to full stroke operation may cause stability problems for the closed-loop system if it is neglected during control design. As the displacement fraction goes towards zero, the time-delay goes towards infinity. However, if the desired displacement fraction is very low, it follows that the system is close to being at an equilibrium point and thus the very large time-delay might not be of major concern. Therefore, the included time-delay in the control model should not be a worst-case scenario, but should neither be completely omitted with respect to stability analysis.

By varying the closing angle by the displacement fraction, $\phi(\eta)$, the frequency response of a partial stroke operated DDM is generated and is shown in Fig. 11. It should be noticed that the frequency response has been generated in the angle domain, so the frequency should be interpreted as radians per radians of shaft angle. It is seen that the frequency response varies significantly with displacement fraction input. Since the number of samples that the displacement is committed over varies with the displacement fraction, the model order varies for partial stroke operation. With respect to control development a varying model structure depending on the input may be considered. Alternatively, it is seen that the highest phase-lag is introduced for a full stroke, such that a conservative approximation would be to linearize for $\eta = \eta_{\mathrm{m}}$ [28].

4 OPTIMAL OPERATION AND CONTROL STRATEGY

Since the displacement of the DDM is committed as function of the shaft angle, the rotational speed has a large influence on the performance of the different operation strategies. The following section shows that the suitable choice of operation strategy and control

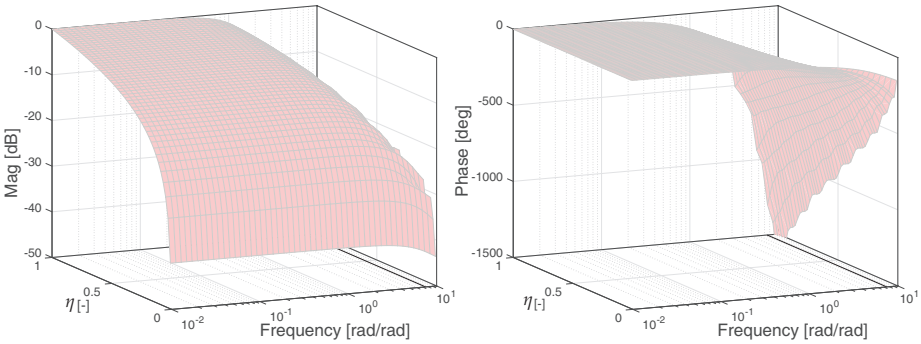

Figure 11: Frequency response of the DDM for varying displacement fractions in partial-stroke operation [28].

strategy varies with the speed of the machine. The control performance of the three operation strategies (full, partial and sequential partial) stroke is compared through simulation of the simplified model with sinusoidal displacement outputs. To provide a more clear view of the results, the number of cylinders has been reduced to 10. In this simulation study only reference tracking performance of a displacement fraction input is considered. For the full-stroke mode, the delta-sigma PDM strategy is used and for partial stroke the PWM strategy is used. To simplify the problem of determine the actuation sequence for the sequential partial-stroke operation, the full stroke is divided into 5 sections such that a cylinder activation/deactivation is made simultaneously for all cylinders. This is a rough simplification, since the cylinders in reality could be switched at any angle for an improved tracking performance. An illustration of the division of the full stroke into sequences, where the cylinders may be activated/deactivated, is shown in Fig. 12. The resulting displacement fraction output as function of combination of active/inactive pressure chambers is shown in Fig. 13.

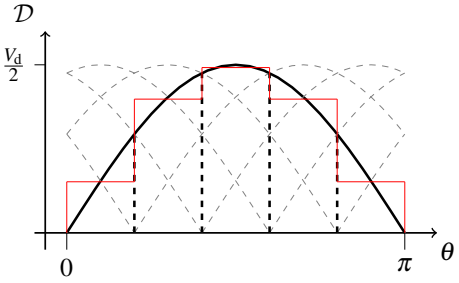

Figure 12: Operation strategies for the digital displacement machine.

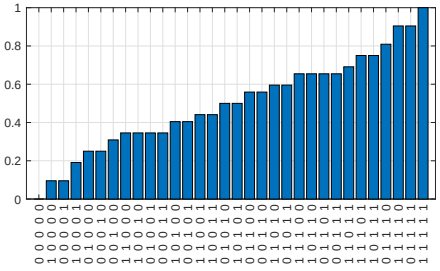

Figure 13: Displacement fractions outputs as function of the combinations

The red line on the left figure shows the discrete displacement between samples, which combinations are used to generate the displacement fraction combinations shown in the right figure. A displacement fraction of 1 is thus obtained by activating all 5 cylinders in the motoring stroke part. The combination that yields the lowest displacement error is thus used at the current activation decision. An integrator is furthermore introduced to account for the displacement error over time, similar to the discrete integrator in the PDM

strategy. No outer control loop is considered, since the objective is solely to compare the different operation strategies.

Since sequential partial stroke requires larger valves capable of generating a higher force to open against high pressure differences, the switching time is slower than for the fast valves which may be used for full and partial stroke operation. Switching time of valves for the full and partial stroke operation has been reported to be below $T_s < 5\,\text{ms}$ [29, 30], while the switching time of commercially available valves applicable for sequential partial stroke is in the range of $T_s \in [20-25]$ ms [31]. If it is considered that the switching time for opening and closing must at maximum occupy 10 % of an activation and it should be possible to at least divide the full stroke into two sections, the maximum rotational speed of the DDM becomes

$$\omega \leq \frac{2\,\pi}{2 \cdot T_s \cdot 10} \approx 21\,\text{rad/s} \tag{17}$$

It is evident that the switching time of the valves sets a direct requirement to the maximum possible speed when utilizing sequential partial stroke. Since this simulation study considers infinite fast switchings, the problem with respect to maximum speed of the DDM in partial stroke has not been taken into account. The simulated displacement outputs of the three different operation and corresponding control strategies are shown in Fig. 14. The plant responses of the first order system actuated by the DDM are shown in Fig. 5.

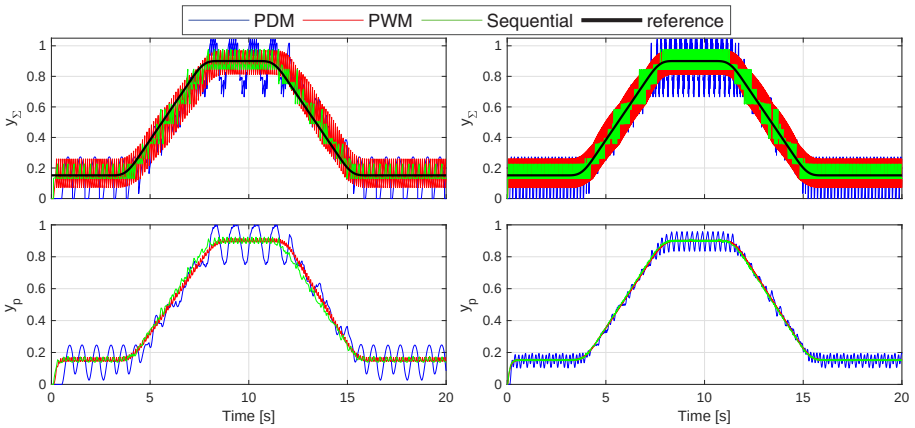

(a) $\omega = 5\,\text{rad/s}$ (b) $\omega = 20\,\text{rad/s}$

Figure 14: Response of digital displacement machine and first order plant for a PDM, PWM and sequential partial stroke strategy, $\omega_n = 10\,\text{rad/s}$.

It is seen that the full-stroke PDM strategy performs poorly at low speed, which is due the control update rate being proportional to the machine speed and the many time-delays introduced due to only fully activating a fraction of cylinders. In general the sequential partial stroke yields the best tracking performance, but one has to bear in mind that instantaneous switching is considered. Improved performance may likely be obtained by allowing valve switching at any angle for partial and sequential partial stroke operation. For the rotational speed of 20 rad/s the machine dynamics is 10 times higher than the plant dynamics $\omega_n = 10\,\text{rad/s}$, in which case the dynamics of the machine may be neglected when considering a frequency response and neglecting the time-delays due to the

binary input. However, it is seen that the plant response has noticeable fluctuations and simply neglecting the DDM dynamics may cause poorer tracking performance and might even stability problems.

One newly proposed and mention-worth control strategy is the co-called "creep mode" operation [31], which is significantly different compared to the conventional operation strategies. The strategy relies on closing all valves (both the HPV and LVP), where after the system finds a force equilibrium due to the friction and load force. Then movement in the clockwise direction may be obtained by opening a single HPV that pressurizes a chamber that yields positive torque or by opening a single LPV that de-pressurizes a chamber that yields negative torque. Shaft movement thus occurs until a new equilibrium is reached, where after the valve is closed to lock the shaft in the new position. The strategy may afterwards be continued to obtain small shaft movements in the desired direction. The strategy yields the lowest possible step movement in the shaft position and is thus very good for precise shaft position control. However, due to the many valve actuations at high pressure difference, the strategy is not very energy efficient.

Based on the presented investigation and results regarding the different operation strategies, a summarization is made and is used to suggest suitable control strategies.

- **Full stroke:** Is the favorable choice for high-speed machine operation, where energy efficiency is important. Furthermore, it is considered the simplest strategy since valve switchings are done at fixed angles. Due to the high speed, the control update rate is fast and a static feedback control law with a pulse-density modulator is desired. In case of a relative slow dynamical plant, relatively high number of cylinders and operation at relatively high displacement the DDM dynamics may be omitted in the control design. Alternatively, continuous, discrete or hybrid dynamical approximation may be used to describe the DDM dynamics [32, 27, 33, 25, 34, 35].

- **Partial stroke:** Is the favorable choice for low/medium speed machine operation, where both tracking performance and energy efficiency are important. Since multiple objectives are important and the time between samples are significantly higher due to the lower machine speed, a model-predictive control strategy is considered favorable. Both discrete linear time invariant (DLTI) and time variant (DLTV), as well as hybrid mixed logical dynamical programming model predictive strategies has been suggested [28, 36]. Additional, objectives like frequency content of output is also possible to optimize with respect to if desired.

- **Sequential partial stroke:** Is the favorable choice for very low speed operation, where control tracking performance is important and energy efficiency is of less importance. In sequential partial stroke, there are an infinite number of switching combinations that yields similar output, but the energy losses may be very different. Since valve opening against high pressure is conducted, the energy losses may be very high if not considered. Therefore, a model predictive control strategy is also deemed the suitable strategy for this operation. However, only a simple strategy where the stroke is divided into fixed sections has been published, leaving potential for further improvements [37].

- **Creep mode:** Is the favorable choice for very accurate DDM shaft position control in the vicinity of standstill. So far only a single paper has been published on the subject [31], which activates cylinders sequentially or in parallel. For smoother

operation, further research could include overlapping the actuation of cylinders and model predictive strategies taking into account the many activation combinations.

Since the suitable operation strategy and control strategy changes as function of the rotational frequency, switching of strategies occur if the machine is operated in a broad speed range. Therefore, it is proposed to investigate the use of supervisory control, which is also a class of hybrid dynamical systems due to the switching event behavior. A proposal on a supervisor for control of a DDM is illustrated in Fig. 15.

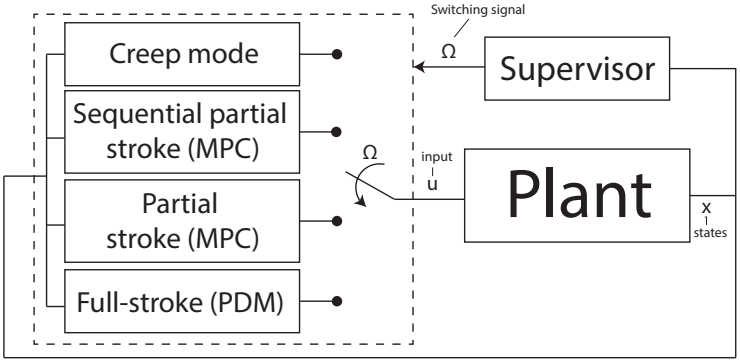

Figure 15: Supervisory control strategy for control of digital displacement machine at various rotation frequencies.

It is seen that the operation strategy and control law is switched by the switching signal, Ω, which in this case is the measured shaft speed. However, the influence of the switching event on stability for such complex problem is expected to be very complicated. However, supervisory control theory does exist and is still undergoing a rapid development [38]. It is evident, that many control related challenges remain for the DDM to be operated and controlled optimally, where this paper only discusses and proposes in which direction to pursue with respect to control development.

5 CONCLUSION

The paper shows that the dynamics of digital displacement machine (DDM) should not always be neglected to ensure proper control performance and stability. Since the response time of the DDM in full and partial stroke operation is proportional to the rotational shaft speed, the non-smooth dynamical effects are substantial for low speed operation. Especially, if the actuated plant dynamics is relatively fast compared to the DDM dynamics and that the number of cylinders and displacement fraction are relatively low. The four operation strategies; full stroke, partial stroke, sequential partial stroke and creep mode are compared. The energy efficiency is highest in the given order, while the energy efficiency is highest in the reverse given order. To avoid poor control performance at low speed, it is deemed favorable to alter the operation strategy in the reverse given order with respect to the rotational shaft speed. In partial and sequential partial stroke operation there is an infite number of combination that yields the same displacement output over a revolution, but the energy efficiency and induced pressure pulsations may be very different as function of the valve switching angle. Therefore, it is deemed favorable to apply a model-predictive control strategy for these operation modes, where the low control

update rate ensures online solving capability. At higher speed in full-stroke operation, a static pulse-density-modulation based control law is assessed to be favorable. If the machine is to operate at both low and high speed in varying operation modes, an illustrative supervisory control strategy is proposed to ensure proper operation and stability in the vicinity of the switching event.

6 ACKNOWLEDGMENT

This research was funded by the Danish Council for Strategic Research through the Hy-Drive project at Aalborg University, at the Department of Energy Technology (case no. 1305-00038B).

References

[1] L. Schmidt, D. B. Roemer, H. C. Pedersen, and T. O. Andersen, "Speed-variable switched differential pump system for direct operation of hydraulic cylinders," *Proceedings of ASME/BATH 2015 Symposium on Fluid Power and Motion Control, American Society of Mechanical Engineers*, 2015.

[2] A. Jarf, T. Minav, and M. Pietola, "Nonsymmetrical flow compensation using hydraulic accumulator in direct driven differential cylinder application," *Proceedings of the 9th FPNI Ph.D. Symposium on Fluid Power, Florianpolis, Brazil*, 2016.

[3] A. H. Hansen and H. C. Pedersen, "Optimal configuration of discrete fluid power force system utilised in the pto for wecs.," *Ocean Engineering, Vol. 117, OE3694, pp. 88-98*, 2016.

[4] R. H. Hansen, T. O. Andersen, H. C. Pedersen, and A. H. Hansen, "Control of a 420 kN Discrete Displacement Cylinder Drive for the Wavestar Wave Energy Converter," in *ASME/BATH 2014 Symposium on Fluid Power and Motion Control*, 2014.

[5] G. S. Payne, A. E. Kiprakis, M. Ehsan, W. Rampen, J. P. Chick, and A. R. Wallace, "Efficiency and dynamic performance of digital displacement hydraulic transmission in tidal current energy converters," *Journal of Power and Energy, Proc. IMechE, Vol. 221, Part A, pp. 207-218.*, 2007.

[6] G. S. Payne, U. P. P. Stein, M. Ehsan, N. J. Caldwell, and W. H. S. Rampen, "Potential of digital displacement hydraulics for wave energy conversion," *In Proc. of the 6th European Wave and TIdal Energy Conference, Glasgow UK.*, 2005.

[7] H. C. Pedersen, R. H. Hansen, A. H. Hansen, T. O. Andersen, and M. M. Bech, "Design of full scale wave simulator for testing power take off systems for wave energy converters.," *International Journal of Marine Energy, Vol. 13, pp. 130-156*, 2016.

[8] W. Rampen, "Gearless transmissions for large wind turbines the history and future of hydraulic drives.," *Bremen*, 2006.

[9] S. H. Salter, J. R. M. Taylor, and N. J. Caldwell, "Power conversion mechanisms for wave energy," *Proc. of the Institution of Mechanical Engineers, Part M - Journal of Engineering for the Maritime Environment, pp. 1-27*, 2002.

[10] W. R. M. Ehsan and S. Salter, "Modeling of digital-displacement pump-motors and their application as hydraulic drives for nonuniform loads," *ASME, Journal of dynamic system measurement and control, Vol. 122, pp. 210-215*, March 2000.

[11] W. Rampen, "The development of digital displacement technology," *In Proceedings of Bath/ASME FPMC Symposium*, 2010.

[12] P. Johansen, *Tribodynamic Modeling of Digital Fluid Power Motors*. PhD thesis, Department of Energy Technology, Aalborg University, 2014.

[13] D. B. Roemer, *Design and Optimization of Fast Switching Valves for Large Scale Digital Hydraulic Motors*. PhD thesis, 2014. Department of Energy Technology, Aalborg University.

[14] G. Wilfong, M. Batdorff, and J. Lumkes, "Design and dynamic analysis of high speed on/off poppet valves for digital pump/motors," *In Proceedings of the 6th FPNI-PhD Symposium*, 2010.

[15] G. Wilfong, M. Holland, and J. Lumkes, "Design and analysis of pilot operated high speed on/off valves for digital pump/motors," *In Proceedings of the 52nd National Conference on Fluid Power*, 2011.

[16] K. Merrill, M. Holland, and J. Lumkes, "Analysis of digital pump/motor operating strategies," *Proceedings of the 52nd National Conference on Fluid Power*, 2011.

[17] M. Ehsan, W. Rampen, and S. Salter, "Modeling of digital-displacement pumpmotors and their application as hydraulic drives for nonuniform loads," *Journal of Dynamic Systems, Measurement and Control, vol. 122, no. 1, pp. 210215*, 2000.

[18] M. Heikkil and M. Linjama, "Displacement control of a mobile crane using a digital hydraulic power management system," *Mechatronics, Volume 23, Issue 4*, 2013.

[19] B. S. R. Armstrong and Q. Yuan, "Multi-level control of hydraulic gerotor motors and pumps," *Proc. of the american control conference, Minnesota, USA*, 2006.

[20] X. Song, "Modeling and active vehicle suspension system with application of digital displacement pump motor," *Proc. of the ASME 2008 International Design Engineering Techical Conferences & Computers and Information in Engineering Conference, New York, USA*, 2008.

[21] S. Nordaas, M. K. Ebbesen, and T. O. Andersen, "Feasibility study of a digital hydraulic winch drive system," *Proc. of the Ninth Workshop on Digital Fluid Power, Aalborg, Denmark*, 2017.

[22] S. Nordaas, M. K. Ebbesen, and T. O. Andersen, "The potential of a digital hydrulic winch drive system," *Proc. of the Ninth Workshop on Digital Fluid Power, Aalborg, Denmark*, 2017.

[23] N. H. Pedersen, P. Johansen, and T. O. Andersen, "Challenges with respect to control of digital displacement hydraulic units," *Modeling, Identification and Control*, 2018.

[24] P. Johansen, D. B. Roemer, T. O. Andersen, and H. C. Pedersen, "Delta-sigma modulated displacement of a digital fluid power pump," *Proc. of the 7th workshop on digital fluid power, Linz, Austria*, 2015.

[25] N. H. Pedersen, P. Johansen, and T. O. Andersen, "Optimal control of a wind turbine with digital fluid power transmission," *Nonlinear Dynamics*, 2018.

[26] N. H. Pedersen, *Development of Control Strategies for Digital Displacement Units*. PhD thesis, Aalborg University, 2018.

[27] P. Johansen, D. B. Roemer, T. O. Andersen, and H. C. Pedersen, "Discrete linear time invariant analysis of digital fluid power pump flow control," *Journal of Dynamic Systems, Measurement and Control*, 2017.

[28] N. H. Pedersen, P. Johansen, and T. O. Andersen, "Model predictive control and discrete analysis of partial stroke operated digital displacement unit," *In Proc. of the Global Fluid Power Society PhD Symposium (GFPS), Samara, Russia*, 2018.

[29] D. B. Roemer, *Design and Optimization of Fast Switching Valves for Large Scale Digital Hydraulic Motors*. PhD thesis, Section of Fluid Power and Mechatronic Systems, Department of Energy Technology. Aalborg University, 2014.

[30] C. Noergaard, *Design, Optimization and Testing of Valves for Digital Displacement Machines*. PhD thesis, Department of Energy Technology. Aalborg University, 2017.

[31] H. B. Larsen, M. Kjelland, A. Holland, and P. N. Lindholdt, "Digital hydraulic winch drives," *In Proc. of the BATH/ASME Symposium on Fluid Power and Motion Control*, 2018.

[32] N. H. Pedersen, P. Johansen, and T. O. Andersen, "Feedback control of pulse-density modulated digital displacement transmission using a continuous approximation," *Submitted to IEEE/ASME Transactions on Mechatronics*, 2018.

[33] N. H. Pedersen, P. Johansen, and T. O. Andersen, "Event-driven control of a speed varying digital displacement machine," *Proceedings of ASME/BATH FPMC Symposium on Fluid Power and Motion Control, Sarasota, Florida, USA*, 2017.

[34] N. H. Pedersen, P. Johansen, and T. O. Andersen, "Non-linear hybrid control oriented modelling of a digital displacement machine," *Proc. of 9th Workshop on Digital Fluid Power, Aalborg, Denmark*, 2017.

[35] N. H. Pedersen, P. Johansen, and T. O. Andersen, "Four qudrant hybrid control oriented dynamical system model of digital displacement units," *Proc. of the Bath/ASME Symposium on Fluid Power and Motion Control, Bath, UK*, 2018.

[36] K. U. Snieguckі M, Gottfried M, "Optimal control of digital hydraulic drives using mixed-integer quadratic programming," September 2013. 9th IFAC Symposium on Nonlinear Control System, Toulouse.

[37] N. H. Pedersen, P. Johansen, and T. O. Andersen, "Model predictive control of low-speed partial stroke operated digital displacement pump unit," *Modeling, Identication and Control, Vol 39, No. 3*, 2018.

[38] W. M. Wonham and K. Cai, *Supervisory Control of Discrete-Event Systems*. Springer, 2019.

Paper C

Feedback Control of Pulse-Density Modulated Digital Displacement Transmission using a Continuous Approximation

Niels H. Pedersen, Per Johansen and Torben O. Andersen

The paper has been submitted for publication in
IEEE/ASME Transactions on Mechatronics, 2018. Status: Under 3rd revision.

The layout has been revised.

Feedback Control of Pulse-Density Modulated Digital Displacement Transmission using a Continuous Approximation

Niels Henrik Pedersen, Per Johansen and Torben Ole Andersen
nhp@et.aau.dk, pjo@et.aau.dk and toa@et.aau.dk
Department of Energy Technology, Aalborg University, Denmark

***Abstract*—Feedback control of digital displacement machines is complicated due to the non-smooth digital behavior. Full stroke operated digital displacement machines are characterized by delivering a discrete volumetric output based on the ratio of activated cylinder chambers. The binary input decision (active or inactive) is made discretely with an update rate proportional to the speed of the machine. For a digital fluid power transmission with two digital displacement machines with varying and different speeds and which dynamics greatly influence each other through the pressurized fluid line, the control task is further complicated. To overcome this problem, this paper presents a continuous approximation of a pulse-density modulated digital displacement machine, which allows for dynamic analysis and control design. The paper shows that linear feedback control theory is adequately to show stability if the number of cylinders, displacement throughput and rotational speed of the machine is sufficiently high. Additionally, the excitation frequencies must be sufficiently low to not excite the discrete behavior. An optimal state feedback controller is synthesized and tested in a non-linear simulation model, which represent the physical digital hydraulic transmission. Simulation results shows great tracking performance similar to a transmission with ideal fluid power machines, but with noticeable fluctuations due to the digital machine characteristics.**

***Index Terms*—Control, Digital Displacement, Fluid Power, Hydrostatic Transmission.**

I. Introduction

THE use of digital fluid power as drive trains has a great potential, due to inherent features such as being mechanically decoupled, great power to weight ratio, robust, as well as having a high energy efficiency and redundancy compared to conventional fluid power [1]. Digital displacement machines are therefore receiving an increasing interest for use as the key component in future fluid power transmissions. Design and performance optimization of these machines are hence the topics of numerous research papers [2], [3], [4], [5], [6], [7], [8], [9].

Control of the digital displacement machines is an important task with respect to performance optimization and several papers regarding control development has been published. The control strategies are however often limited to comprise a single machine operating at a fixed speed and under simplified operation conditions, often in an open loop configuration [3], [10], [11], [12]. A mixed logical dynamic programming feedback control structure is presented by Sniegucki et. al. [13], which yields promising tracking performance and torque fluctuations despite being limited to offline optimization. Johansen et. al [14] proposes a feedback control structure for a full stroke Pulse-Density Modulated (PDM) digital displacement machine and presents a discrete linear approximation of the dynamics of a fixed speed machine [15].

Discrete feedback control of a digital fluid power transmission with a single PDM full stroke operated digital displacement machine has been studied by Pedersen et. al. [16], [17]. The same author extends the control strategy to be applicable for speed varying machines by utilizing discrete control in the spatial domain, resulting in a fixed angle update rate [18]. With both the pump and motor being of type digital displacement, this is no longer possible since the sampling rate of the two machines are asynchronous relative to each other. Multi-rate control strategies seem unsuitable to solve this problem, since the sampling schemes cannot be superpositioned and the number of states becomes enormous for vastly different speeds with a high number of cylinders. To overcome this problem Pedersen et. al. [19] presents a hybrid model of a digital fluid power transmission which describes the non-linear and discrete behavior intuitively and allowing the design of feedback controllers. However, the design of globally asymptotically stabilizing controllers for relatively complex hybrid dynamical systems is a complicated task. This provides an incentive to simplify the control task by approximating the digital machine dynamics and thereby enabling control design for a digital fluid power transmission.

This paper presents a novel continuous linear model approximation of the digital displacement machine dynamics in the spatial domain and shows how the response time is proportional to the speed of the machine in the time-domain. An analysis is conducted where it is shown that the relatively simple continuous approximation model is sufficient in describing the machine dynamics if the number of cylinders and displacement throughput is sufficiently high, while the excitation frequencies are sufficiently low. The proposed continuous approximation is the first control model to be applicable for dynamical analysis and model based feedback control design of a fluid power transmission comprising two digital displacement machines. To demonstrate the control strategy, a deterministic optimal controller is designed and tested in a non-linear simulation

The presented reasearch has been supported by the Danish Council for Strategic Research through the HyDrive project at Aalborg University, at the Department of Energy Technology (case no. 1305-00038B).

model representing the physical digital hydraulic transmission system.

II. System Description

This paper concerns a digital fluid power transmission comprising a low speed / high torque digital displacement machine (DDM) and a high speed / low torque DDM. This type of transmission has the potential of being the future drive train for wind turbines, vehicles and gear drives. In this paper, a large scale 5 MW transmission is considered, where the low speed pump is driven by an external force (e.g. wind turbine rotor) and the high speed motor is connected to an electrical generator. An illustration of a digital fluid power transmission is shown in Fig. 1.

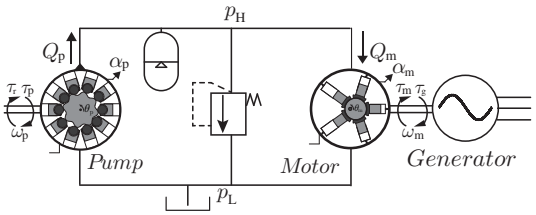

Fig. 1: Illustration of the Digital Fluid Power transmission system.

The input torque, τ_r, is seen to drive the pump, which generates a high-pressure fluid flow, Q_p, to the common high pressure line with pressure, p_H. The motor intakes a flow, Q_m, and generates a torque, τ_m, driving the generator. The system has the pump and motor displacements α_p and α_m respectively, as well as the generator torque, τ_g, as control inputs. Considering a conventional fluid power transmission, the system dynamics may be described by the three governing differential equations [20], [21]:

$$\begin{aligned}
\dot{\omega}_p &= -\frac{d_p}{J_p}\,\omega_p - \frac{1}{J_p}\,\tilde{V}_p\,\Delta p\,\alpha_p + \frac{1}{J_p}\,\tau_r \\
\dot{\Delta p} &= -\frac{\beta_e}{V_L}\,k_l\,\Delta p + \frac{\beta_e}{V_L}\,\tilde{V}_p\,\omega_p\,\alpha_p - \frac{\beta_e}{V_L}\,\tilde{V}_m\,\omega_m\,\alpha_m \\
\dot{\omega}_m &= -\frac{d_m}{J_m}\,\omega_m + \frac{1}{J_m}\,\tilde{V}_m\,\Delta p\,\alpha_m - \frac{1}{J_m}\,\tau_g
\end{aligned} \tag{1}$$

where J_p and J_m are the moments of inertia, d_p and d_m are the viscous damping coefficients, $\tilde{V}_p$ and $\tilde{V}_m$ are the volumetric displacements for the pump and motor respectively. β_e is the effective bulk modulus, V_L is the volume in the high pressure line and k_l is the fluid leakage coefficient between the high and low pressure line. For simplicity, the hydraulic accumulator shown in Fig. 1 has been omitted since it does not influence the presented control method. It does however provide some buffering capacity, which gives short term energy storage and aid in the reduction of pressure pulsations and should hence be considered in a physical setup.

The parameter values and a description of them for the 5 MW transmission is given in Tab. I. With respect to control of such system with three inputs and three outputs, a Multiple Input Multiple Output (MIMO) control strategy seems suitable. However, the digital displacement machine dynamics is non-smooth (continuous with binary inputs being updated at discrete shaft angles), the dynamics belongs to the class of hybrid dynamical systems, having both discrete and continuous dynamics. Since control of hybrid systems are challenging, simpler discrete and continuous approximations are sought, which may often be sufficient in a limited number of situations. However, discrete approximations seem unsuitable in describing the combined dynamics of the digital transmission, due to the asynchronous and vastly different sampling schemes of the two digital machines. Also decoupling the two machine dynamics by considering a constant pressure (like a converter DC-link) seems like a poor solution due to the severe input-output couplings illustrated by the relative gain array (RGA-values) shown in Fig. 2 of the system in (1). For linear analysis, linearization around steady state values are required and chosen as $\begin{bmatrix}\bar{\omega}_p & \bar{\omega}_m & \bar{\Delta p} & \bar{\alpha}_p & \bar{\alpha}_m\end{bmatrix} = \begin{bmatrix}1.27 & 157 & 350e5 & -/1 & 1/-\end{bmatrix}$. The displacement fraction inputs are varied between minimum and maximum for one of the inputs and held constant at maximum for the other. The RGA matrix is determined by (2), where the transfer function for the system (1) is found in (18) [22].

$$\mathrm{RGA}(\mathbf{G}_p) = \mathbf{G}_p \times \left(\mathbf{G}_p^{-1}\right)^T = \begin{bmatrix}\lambda_{11} & \lambda_{12} & \lambda_{13} \\ \lambda_{21} & \lambda_{22} & \lambda_{23} \\ \lambda_{31} & \lambda_{32} & \lambda_{33}\end{bmatrix} \tag{2}$$

It is seen that the dynamics is severely coupled in the majority of frequencies with RGA-values up to 10. Choosing a low pressure linearization point, where the transmission may also operate, is found to further increase the RGA-values up to above 20 at certain frequencies. This indicates a highly input-output coupled system and as a result, a decoupling strategy seems insufficient in describing the system dynamics. Therefore, a dynamical model of the complete system comprising DDMs is desired to proper analyze stability and synthesize controllers. To aid in solving this problem, this paper proposes a continuous approximation of a pulse-density modulated digital displacement machine which enables dynamical analysis and MIMO control of the fluid power transmission system. To develop such model, a description and a mathematical model of the DDM is made.

TABLE I: Parameters of the 5 MW transmission

Parameter	Symbol	Value	Unit
Pump damping coefficient	d_p	50000	Nm s/rad
Motor damping coefficient	d_m	10	Nm s/rad
Pump moment of inertia	J_p	387e5	kg m^2
Motor moment of inertia	J_m	534	kg m^2
Pump volumetric displacement	$\tilde{V}_p$	127	L/rad
Motor volumetric displacement	$\tilde{V}_m$	1	L/rad
Effective bulk modulus	β_e	16000	bar
High pressure line volume	V_L	87.5	L
Fluid leakage coefficient	k_l	1	cm^3/(bar s)

III. Digital Displacement Machine model

The digital displacement pump is a multi-lobe ring cam type, which gives a compact machine with a large displace-

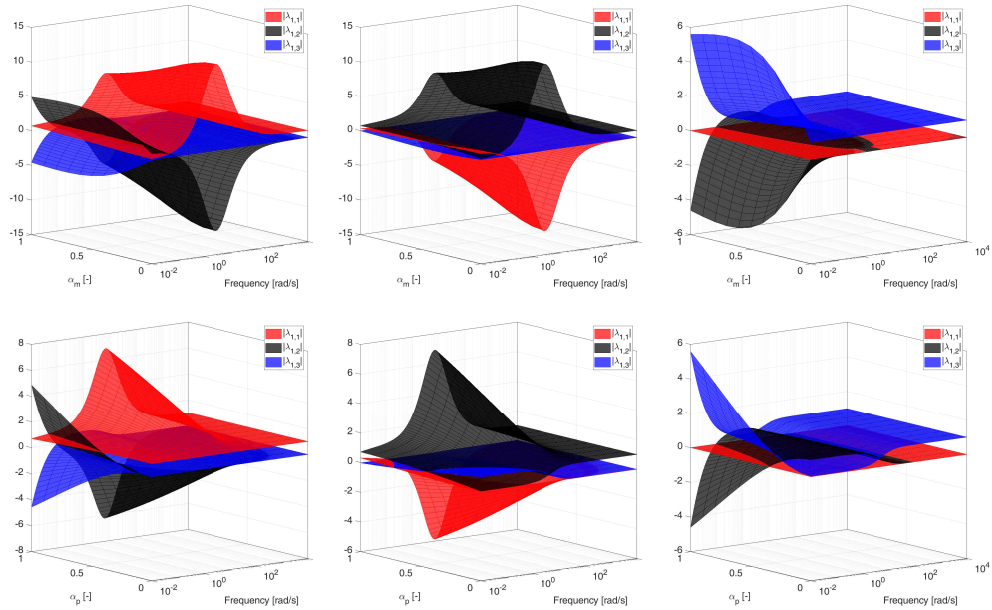

Fig. 2: Relative gain array analysis of the fluid power transmission system. The coupling between each input and output is shown at varying displacements and frequencies. The three top plots is for varying motor displacements and the bottom plot is for varying pump displacements.

ment volume at a low speed, while the digital displacement motor is of eccentric single-lobe type as illustrated in Fig. 1. The machine size with respect to number of cylinders is provided in Tab. II.

TABLE II: Motor and pump design parameters

Parameter	Symbol	Value	Unit
Pump cylinders pr. module	N_{pc}	25	-
Pump lobes pr. module	N_{pl}	16	-
Pump modules	N_{pm}	4	-
Motor cylinders pr. module	N_{mc}	7	-
Motor modules	N_{mm}	6	-

In total there is $N_{\mathrm{p}} = N_{\mathrm{pc}} N_{\mathrm{pm}} = 100$ radially distributed cylinders in the pump that each goes through $N_{\mathrm{pl}} = 16$ reciprocating piston strokes for each pump revolution and there is $N_{\mathrm{m}} = N_{\mathrm{mc}} N_{\mathrm{mm}} = 42$ radially distributed cylinders in the motor going through one reciprocating stroke for each motor revolution. In this paper, both the motor and pump are using a full stroke operation strategy, where each cylinder in the pump is either pumping or idling for a full stroke and each motor cylinder is either motoring or idling for a full stroke [16], [17], [18], [19]. Each cylinder pressure chamber is actuated by two fast switching and leakage free on/off poppet valves. A High Pressure Valve (HPV) and Low Pressure Valve (LPV) is controlling the flow to and from the high and low pressure line respectively, as illustrated in Fig. 3. The same governing equations may be used to describe

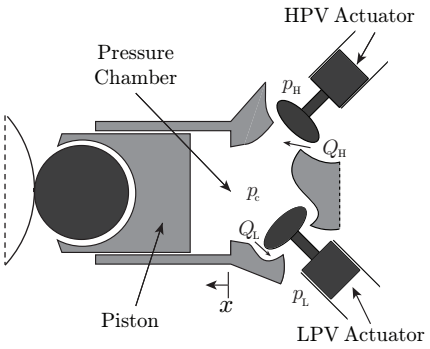

Fig. 3: Sketch of a single pressure chamber.

both the motor and pump dynamics. The only difference is that the piston stroke rate for the pump design is N_{pl} times faster than the pump speed. Therefore, the governing equations are presented for both machines simultaneously, where a more comprehensive description of the model is found in [16], [17], [18]. The piston displacement, x, as function of the shaft angle is described by

$$x_i = r_{\mathrm{s}} \left(1 - \cos(\theta_i)\right) \quad \theta_i = \theta + \frac{2\pi}{N}(i-1) \quad i \in \{1,..,N\} \quad (3)$$

where N is the number of cylinders and r_s is half the stroke length. Since the same equations are used to describe all the pressure chambers, the indexing has been omitted in the following. The cylinder chamber volume, V_c, is then given as

$$V_c = \frac{V_d}{2}\left(1-\cos(\theta)\right)+V_0 \quad \dot{V}_c = \frac{V_d}{2}\dot{\theta}\sin(\theta) \tag{4}$$

V_0 is the minimum chamber volume and $V_d = 2r_s A_p$, where A_p is the piston area. The pressure dynamics in one displacement chamber is given by

$$\dot{p}_c = \frac{\beta_e(p_c)}{V_c}\left(Q_H - Q_L - \dot{V}_c\right) \tag{5}$$

The bulk-modulus pressure dependency is modeled in accordance with [23]. Q_H and Q_L are the flows through the high and low-pressure valve respectively. The flows through these valves are described by the orifice equation and are given by

$$\begin{aligned} Q_L &= \frac{x_L}{k_f}\sqrt{|p_c - p_L|}\,\mathrm{sign}\left(p_c - p_L\right) \\ Q_H &= \frac{x_H}{k_f}\sqrt{|p_H - p_c|}\,\mathrm{sign}\left(p_H - p_c\right) \end{aligned} \tag{6}$$

Where k_f is the valve flow coefficient. x_L and x_H are the normalized valve position of the low- and high-pressure valve respectively. The valve dynamics is simplified to be described as a constant acceleration and thus independent of valve design as shown in Fig. 4 for opening of the valves.

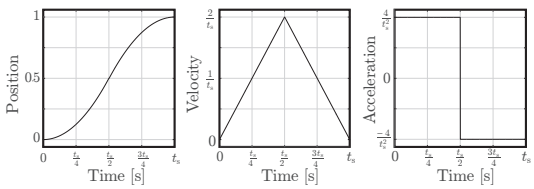

Fig. 4: Position, velocity and acceleration responses for the on/off valve.

Where, t_s, is the valve opening/closing time. This is seen to yield a smooth position response, similar to what may be expected if a more detailed model of the valve dynamics and forces is used. Despite the simplicity of the valve model, the fundamental characteristics with respect to machine control is captured. For closing of the valves, the negative of the acceleration profile shown in Fig. 4 is used. The torque contribution is given by

$$\tau_c = \frac{dV_c(\theta)}{d\theta}p_c = \frac{V_d}{2}\sin(\theta)\,p_c \tag{7}$$

It should be noted that for the pump, a local angle with rate of change being the number of lobes times faster than the pump speed is used. Simulation results of the non-linear model representing the physical system are shown in Fig. 5 for both the motor and pump. The negative of the pump flow and torque is shown, such that they are positive. Variables indexed by p is for the pump and variables indexed by m is for the motor, e.g. $x_{L,p}$, is the low pressure valve position for the pump and, $Q_{H,m}$, is the flow through the HPV for the motor. A pumping stroke is committed by closing the LPV at, $\theta_{L,p}$, shortly ahead of Bottom Dead Center (BDC). This yields a chamber pressurization during upstroke and results in a passive opening of the HPV as the chamber pressure exceeds the high pressure. The HPV is afterwards closed at, $\theta_{H,p}$, near ahead of Top Dead Center (TDC) to end the pumping stroke. Due to depressurization as the chamber volume decreases, a passive opening of the LPV is achieved as the pressure falls below the low pressure. Similarly, a motor stroke is committed by closing the LPV at, $\theta_{L,m}$, near ahead of TDC, which result in a chamber pressurization and a passive opening the HPV at TDC. The HPV is closed at, $\theta_{H,m}$ ahead of BDC to end the motoring stroke and yield a passive opening of the LPV.

It is seen that the pump and motor responses are roughly a reflected version of each other with respect to the angle. However, the first part of the pumping stroke is not used (no torque and flow are generated), since passive HPV opening due to compression is utilized. Similarly, the last part of the motoring stroke is not used, since passive LPV opening due to suction is utilized. Therefore, a small amount, ($\approx 5\%$), of the full stroke is not used with a full stroke operation strategy.

The total machine torque and flow is the sum of individual contributions given by

$$Q = \sum_{j=1}^{N} Q_{H,j} \qquad \tau = \sum_{j=1}^{N} \tau_{c,j} \tag{8}$$

The modeling parameter values are those given in Tab. III.

TABLE III: Parameters of the chamber model

Parameter	Symbol	Value	Unit
Pump stroke radius	$r_{s,p}$	46	mm
Motor stroke radius	$r_{s,m}$	31.25	mm
Pump displacement volume	$V_{d,p}$	499	cm^3
Motor displacement volume	$V_{d,m}$	151	cm^3
Pump flow coefficient	$k_{f,p}$	5e4	$\sqrt{Pa}\,s/m^3$
Motor flow coefficient	$k_{f,m}$	5e4	$\sqrt{Pa}\,s/m^3$
Pump valve actuation time	$t_{s,p}$	2	ms
Motor valve actuation time	$t_{s,m}$	2	ms
Pump LPV closing angle	$\theta_{L,p}$	3.12	rad
Motor LPV closing angle	$\theta_{L,m}$	5.82	rad
Pump HPV closing angle	$\theta_{H,p}$	5.71	rad
Motor HPV closing angle	$\theta_{H,m}$	2.57	rad
Low pressure	p_L	1	bar

IV. Control Strategy

For control of the full transmission, there are three inputs being the pump displacement, α_p, the motor displacement, α_m, and the generator torque, τ_g. This provides the possibility of controlling up to three outputs. Since the fluid power transmission is to work as a variable hydraulic gear, it is chosen to control the pump speed, ω_p, high pressure, p_H, and motor speed, ω_m. To illustrate the idea behind the control structure, control of a single digital displacement machine is considered as illustrated in Fig. 6. The controller output is a continuous displacement fraction reference, $\alpha^* = [0,1]$, which is converted to a Pulse-Density Modulated (PDM) actuation signal, $\bar{\alpha}$ by a first order delta-sigma modulator [16], [17], [18]. The discrete modulator is evaluated for every cylinder as function of the shaft angle, with the sampling angle

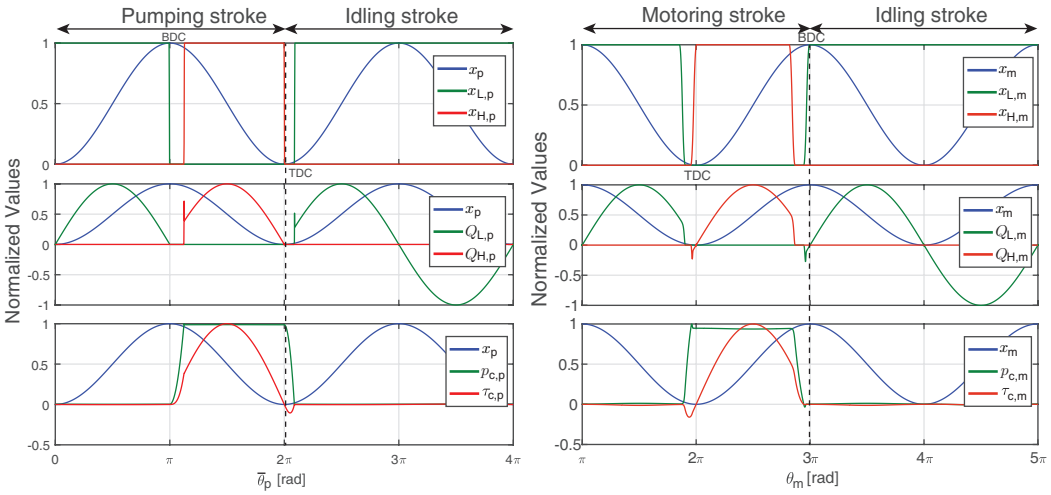

(a) Pumping and idling mode.

(b) Motoring and idling mode.

Fig. 5: Responses of a single digital displacement chamber. $p_H = 350\,\text{bar}$, $\omega_p = 10\,\text{rpm}$ and $\omega_m = 1500\,\text{rpm}$.

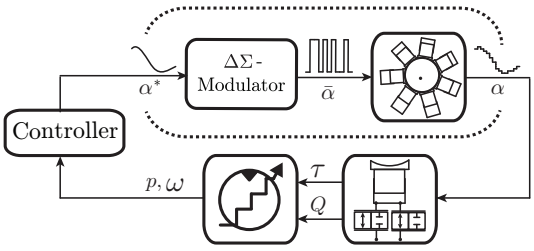

Fig. 6: Illustration of the control strategy.

$\theta_s = 2\pi/N$. A PDM value of 1 corresponds to an active stroke (pumping or motoring based on the machine) and a PDM value of 0 corresponds to an inactive stroke (idling).

V. Continuous DDM Approximation

A continuous approximation of the output displacement fraction, may be calculated from the flow Q and torque τ as

$$\alpha_Q = \frac{Q}{\tilde{V}\,\omega} \qquad \alpha_\tau = \frac{\tau}{\tilde{V}\,\Delta p} \tag{9}$$

where $\tilde{V}$ is the total machine displacement which values are found in Tab. I and are given by $\tilde{V}_p = V_{d,p}\,N_p\,N_{pl}/(2\,\pi)$ and $\tilde{V}_m = V_{d,m}\,N_m/(2\,\pi)$ for the pump and motor respectively. Ideally, $\alpha^* = \alpha_Q = \alpha_\tau$, in which case the presented equations in (1) describes the hydraulic transmission system. However, the digital machine is known to have dynamics and have fluctuations in its response due to the digital behavior. To investigate the actual response, α_Q and α_τ have been simulated using the non-linear model presented in Sec. III with the delta-sigma modulator implemented. A digital displacement motor operating at three different speeds, $\omega_m = \{1000, 1250, 1500\}$ rpm and with displacement fractions references of $\alpha_m^* = \{0.3, 0.6, 1\}$ have been studied. The step responses for α_Q (Black) and α_τ (red) are shown in Fig. 7.

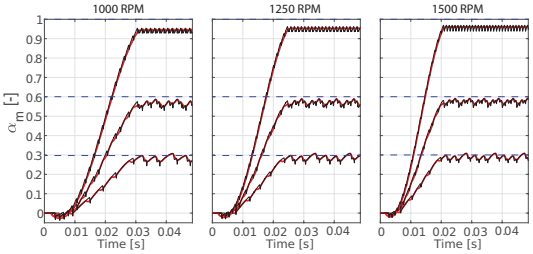

Fig. 7: Displacement fraction step responses for a digital displacement motor. Red is for the torque and black is for the flow.

A static DC-gain slightly less than one is observed. This is due to the minor amount ($\approx 5\,\%$) of the active full stroke not being used as identified in Fig. 5. As expected, the output has a ripple for every time a cylinder is activated, but a smooth averaging approximation is able to describe the fundamental dynamics.

Since the response time is proportional to the speed of the machine, the dynamical response approximation is carried out in the spatial domain as shown in Fig. 8. All three responses in Fig. 7 with $\alpha_m^* = 1$ have been plotted on top of each other as function of the angle, θ_m. It is seen that the responses are very similar in the angle domain, with an initial angle delay and that the response angle is approximately half a revolution. $\theta_{DSM} = 2\,\pi/N_m$ is the single sample delay due to the delta-sigma modulator. The remaining angle delay is due to the

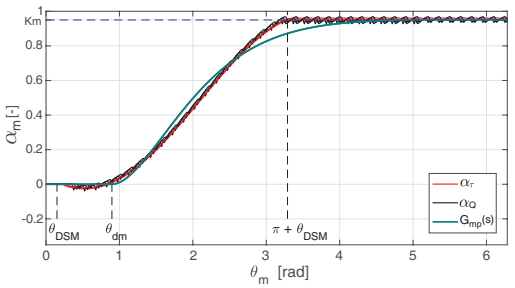

Fig. 8: Step responses of Digital Displacement motor in spatial domain. Black = α_Q and red = α_τ, green = approximated.

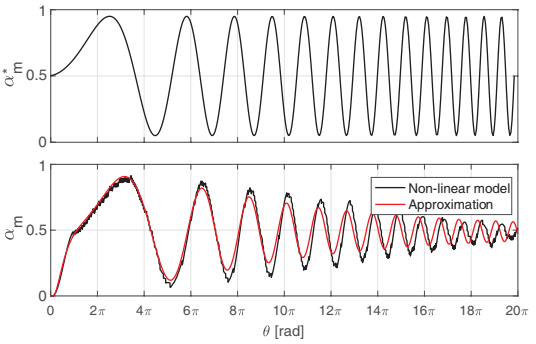

Fig. 9: Comparison of non-linear and continuous approximation model of the digital displacement motor.

angle between closing the LPV and the initial output (flow and torque) being generated as seen in Fig. 5b. A second order system (green) has been used to approximate the response and it is seen to match the dynamics fairly well. However, discrepancies are observed since the response is not truly of a second order system. The machine response is seen to have an almost constant slope in the transient period and a steady state response containing ripples due to the non-smooth machine behavior. Although the continuous approximation is not a perfect fit, it is considered sufficient for describing the systems fundamental dynamics. The transfer function is obtained by use of a spatial domain Laplace transformation defined as

$$F(\bar{s}) = \mathscr{L}\{f(\theta)\} = \int_0^\infty e^{-\bar{s}\theta} f(\theta) d\theta \tag{10}$$

The second order spatial transfer function of the digital displacement machine dynamics is then given by

$$G_{mp}(\bar{s}) = \frac{\alpha_m}{\alpha^*_m} = K_m \frac{\omega^2_{nm}}{\bar{s}^2 + 2\,\zeta_m\,\omega_{nm}\,\bar{s} + \omega^2_{nm}} e^{-\bar{s}\theta_{dm}} \tag{11}$$

where, ω_{nm}, is the approximated eigenfrequency in the angle domain, ζ_m, is the approximated damping coefficient and K_m is the static DC-gain. The accuracy of the approximation is investigated by applying a variable frequency input and comparing the approximated response with the non-linear model response representing the physical system. The results are shown in Fig. 9. It is seen that the phase is captured well at relatively low frequencies, but drift a bit at higher frequencies where the approximated response lead the non-linear response. Additionally, the gain of the approximated response is seen to be a bit lower than the physical response at low frequencies, but larger at higher frequencies. These derivation are expected, since the system does not behave like an ordinary second order system. The derivation characteristics is likely due to the approximated response being faster in the initially transient period and has a lower gain near settling seen in Fig. 8.

To further examine the dynamics of the approximation, a frequency response comparison has been made. Since the non-smooth system does not behave like an ordinary linear system, the gain and phase may depend on the amplitude and offset of the input. Additionally, the non-linear system response contains fluctuations, which complicates the identification of a static DC-gain. Therefore, a method has been developed which identifies a gain and a phase-band, where the non-linear system response will be within. The method for obtaining the gain band is illustrated in Fig. 10.

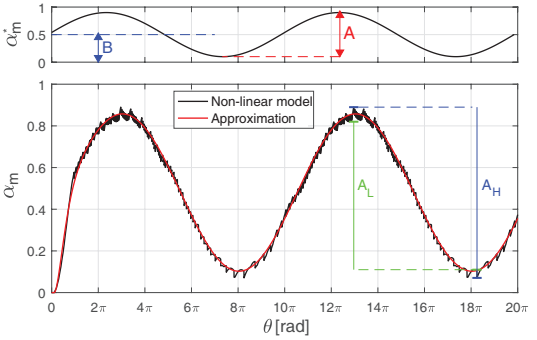

Fig. 10: Illustration of the evaluation method for obtaining the frequency response.

The input being a sine wave is given as $\alpha^*_m = 0.5\sin(\omega_i\,\theta)\,A + B$ and has the offset B, the gain A and the input frequency ω_i. The maximum and minimum response values are identified as shown with a thick blue line, where the difference, A_H, corresponds to the maximum gain. Within an angle of $\pm 2\%$ of the angle where the maximum value occurs, a minimum value is identified and shown with a thick green line. Similarly, the maximum value within $\pm 2\%$ of the angle where the minimum value occurs is identified and is shown with a thick green line. The difference between the thick green values illustrates a minimum gain. By varying the input offset and gain in a wide range and examining 10 of the periodic responses, the maximum and minimum gain has been identified at varying frequencies. Likewise, the maximum and minimum phase-angle has been identified. The resulting frequency response for the non-smooth digital displacement machine is shown in Fig. 11 and compared to the linear

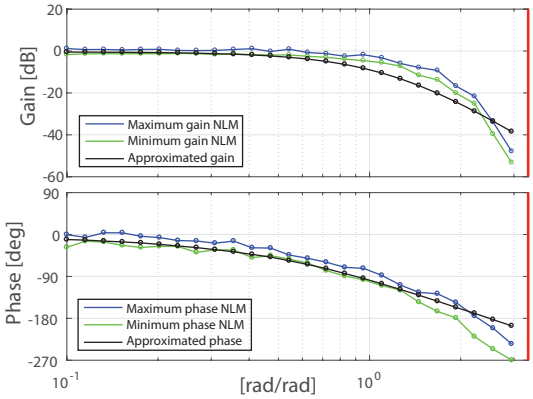

Fig. 11: Frequency response comparison of the non-linear and the approximated linear model for the digital displacement motor.

approximated response. Since the frequency response is made in the spatial domain, the frequency axis should be interpreted as radians of the input relative to the radians of the shaft angle. Since the modulator comprises a discrete sampler updating with an angle of $\theta_s = 2\pi/N$, the continuous approximation is only valid up to a certain frequency (Nyquist-frequency) $f_N = 1/2\ N/(2\pi)$ illustrated with a red line. As a result, the presented method is only valid if the system is not excited with high frequencies, which is complied in the presented example for a large scale transmission system. It should be evident that the maximum and minimum gain values are very conservative, since they are obtained by using peak values in the response. The phase of the approximation is seen to be within the shown frequency band for the majority of frequencies. The approximated gain is seen to be captured well at low frequencies, but crosses the minimum and maximum gains at higher frequencies. This phenomenon is also seen in Fig. 9, where the gain of the approximation is lower at relatively low frequencies, but higher at relatively high frequencies. Also the phase of the approximated response is seen to increasingly lead compared to the non-linear response at higher frequencies close to the Nyquist frequency. It is not considered possible to improve the linear approximation, since reduction in the gain deviation leads to an increase in the phase deviation and vice versa. However, the fundamental dynamics is considered to be captured for the majority of frequencies and deemed sufficient with respect to control and stability analysis as long as the excitation frequencies are below the Nyquist frequency.

The applicability of the presented continuous approximation method is investigated further by calculating the RMS-error between the non-linear and the approximated 2nd order system response by use of (12) for varying number of cylinders (strokes per revolution) and displacement step inputs. The RMS-error is calculated by

$$e_{\text{rms}} = \sqrt{\int_0^{10\pi/\omega} \left(\alpha(t) - \alpha_{\text{m}}(t)\right)^2 dt} \tag{12}$$

where $\alpha = \alpha_{\text{Q}} \approx \alpha_\tau$ is the displacement fraction from the non-linear model and α_{m} is the approximated displacement response. Five full revolutions are simulated, since it ensures at least a few chamber actuations for the smallest displacement fractions. The RMS-error as function of number of cylinders (strokes per revolution) and displacement fraction is shown in Fig. 12 for the digital displacement motor.

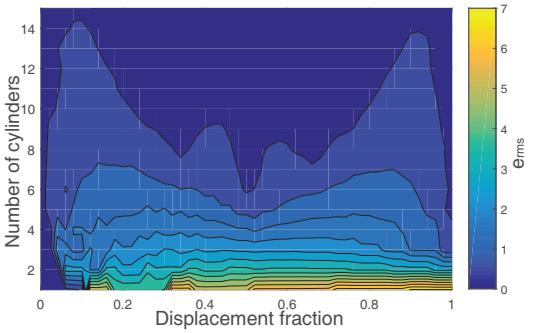

Fig. 12: RMS-error between non-linear physical model response and approximated second order system model response as function of strokes per revolution and displacement fraction.

It is seen that the approximation becomes increasingly accurate for a higher number of cylinders, which is expected since the displacement resolution is proportional to the number of cylinders. The displacement fraction is seen to only have minor influence on the error. However, since the signal values are higher at larger displacement, the relative error with respect to the input size is increasingly lowered at higher displacements. The approximation method is hence considered too simple for describing the machine dynamics for a low number of cylinders, especially if it is operated at low displacements. Since the machine response (flow and torque) contains ripples that are omitted with the continuous approximation method, it may introduce considerable pressure and velocity pulsations if the system inertness is relatively low. As a consequence, one should be careful when applying the presented method in systems with relatively large fluid and mechanical stiffness.

To obtain a transfer function representation in the time domain, the derived spatial domain transfer function is converted by the relation:

$$\frac{d\alpha_m}{d\theta_{\text{m}}} \underbrace{\frac{d\theta_{\text{m}}}{dt}}_{\omega_{\text{m}}} = \frac{d\alpha_m}{dt} \tag{13}$$

Using this relation yields the time transfer function given by

$$G_{\text{mt}}(s) = \frac{\alpha_{\text{m}}}{\alpha_{\text{m}}^*} = K_{\text{m}} \frac{\omega_{\text{nm}}^2\, \omega_{\text{m}}^2}{s^2 + 2\,\zeta_{\text{m}}\,\omega_{\text{nm}}\,\omega_{\text{m}}\,s + \omega_{\text{nm}}^2\,\omega_{\text{m}}^2}\, e^{-s\,\frac{\theta_{\text{dm}}}{\omega_{\text{m}}}} \tag{14}$$

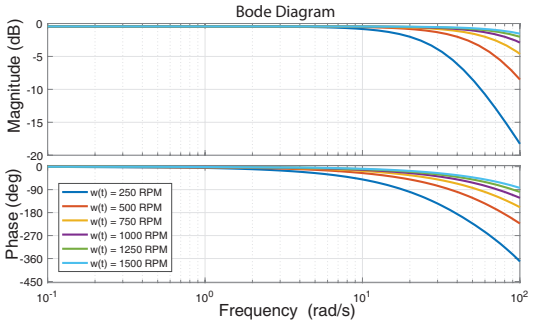

Fig. 13: Frequency response of the digital displacement motor.

It is evident that the linear approximation in the spatial domain is non-linear in the time domain, since the eigenfrequency in the time domain is proportional to the speed of the machine. A frequency response of the transfer function $G_{\mathrm{mt}}(s)$ is shown in Fig. 13 for varying motor speeds to investigate the influence of the digital machine dynamics on the full transmission dynamics. It is seen that the response may be considered as a static DC-gain of K_{m} up to a frequency of $\omega_{\mathrm{cm}} = 0.1\,\omega_{\mathrm{hm}}\,\omega_{\mathrm{m}}$, since the phase-shift due to delay is neglectable at lower frequencies. The phase-shift of the plant is given as

$$\angle G_{\mathrm{mt}}(j\,\omega_{\mathrm{l}}) = \operatorname{atan}\left(\frac{2\,\zeta\,\omega_{\mathrm{nm}}\,\omega_{\mathrm{m}}\,\omega_{\mathrm{l}}}{\omega_{\mathrm{nm}}^2\,\omega_{\mathrm{m}}^2 - \omega_{\mathrm{l}}^2}\right) + \omega_{\mathrm{l}}\,\frac{\theta_{\mathrm{dm}}}{\omega_{\mathrm{m}}} \tag{15}$$

To ensure a stable closed loop system when applying linear control theory the phase-shift puts strict requirements on the minimum speed of the machine.

The same procedure is carried out for the pump where the step responses for $\omega_{\mathrm{p}} = \{0.75, 1, 1.25\}$ are shown in Fig. 14.

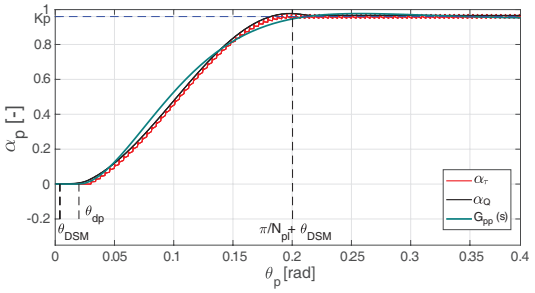

Fig. 14: Step responses of Digital Displacement pump in spatial domain.

The response is seen to be similar to the motor response, it should however be noted that the response angle is now π/N_{pl}, due to the ring-cam design. The approximated second order time transfer function is given by

$$G_{\mathrm{pt}}(s) = \frac{\alpha_{\mathrm{p}}}{\alpha_{\mathrm{p}}^*} = K_{\mathrm{p}}\,\frac{\omega_{\mathrm{np}}^2\,\omega_{\mathrm{p}}^2}{s^2 + 2\,\zeta_{\mathrm{p}}\,\omega_{\mathrm{np}}\,\omega_{\mathrm{p}}\,s + \omega_{\mathrm{np}}^2\,\omega_{\mathrm{p}}^2}\,e^{-s\,\frac{\theta_{\mathrm{dp}}}{\omega_{\mathrm{p}}}} \tag{16}$$

The estimated values of the continuous transfer function approximations are given in Tab. IV.

TABLE IV: Transfer function approximation values

Parameter	Symbol	Value	Unit
Static pump gain	K_{p}	0.96	-
Static motor gain	K_{m}	0.95	-
Pump eigenfrequency	ω_{np}	20	rad/s
Motor eigenfrequency	ω_{nm}	1.43	rad/s
Pump damping coefficient	ζ_{p}	0.75	-
Motor damping coefficient	ζ_{m}	0.9	-
Pump angle delay	θ_{dp}	0.02	rad
Motor angle delay	θ_{dm}	0.9	rad

This papers main contribution is the continuous linear angle invariant model approximation of the digital displacement machine dynamics, which enables model based feedback control of a digital hydraulic transmission. The fact that the eigenfrequency of the system is proportional to the speed of the machine in the time domain yields a non-linear model. Additionally, the equations describing the transmission system given in (1) are also non-linear. Since the full transmission system has a great number of non-linearities where system states are multiplied, one may choose to pursuit non-linear control strategies for such system. However, in this paper it is chosen to illustrate that linear control theory is sufficient for ensuring stability if the speed of the digital displacement machines is lower bounded by the linearization point.

Linear control strategies that are similar to the one proposed in this paper has previously been successfully applied on conventional fluid power drive trains for wind turbines [20], [21].

VI. Linear Transmission System Representation

A linear representation of the presented transmission system equations in (1) is obtained through linearization by a first order Taylor approximation around a steady state operation point. The linear system representation becomes

$$\underbrace{\begin{bmatrix}\dot{\omega}_{\mathrm{p}}\\ \dot{\Delta p}\\ \dot{\omega}_{\mathrm{m}}\end{bmatrix}}_{\dot{\mathbf{x}}} = \underbrace{\begin{bmatrix} -\frac{d_{\mathrm{p}}}{J_{\mathrm{p}}} & -\frac{1}{J_{\mathrm{p}}}\,\bar{V}_{\mathrm{p}}\,\bar{\alpha}_{\mathrm{p}} & 0\\ \frac{\beta}{V_{\mathrm{L}}}\,\bar{V}_{\mathrm{p}}\,\bar{\alpha}_{\mathrm{p}} & -\frac{\beta}{V_{\mathrm{L}}}\,k_{\mathrm{l}} & -\frac{\beta}{V_{\mathrm{L}}}\,\bar{V}_{\mathrm{m}}\,\bar{\alpha}_{\mathrm{m}}\\ 0 & \frac{1}{J_{\mathrm{m}}}\,\bar{V}_{\mathrm{m}}\,\bar{\alpha}_{\mathrm{m}} & -\frac{d_{\mathrm{m}}}{J_{\mathrm{m}}}\end{bmatrix}}_{\mathbf{A}}\underbrace{\begin{bmatrix}\omega_{\mathrm{p}}\\ \Delta p\\ \omega_{\mathrm{m}}\end{bmatrix}}_{\mathbf{x}}$$
$$+\underbrace{\begin{bmatrix}\frac{1}{J_{\mathrm{p}}}\,\bar{V}_{\mathrm{p}}\,\Delta p & 0 & 0\\ \frac{\beta}{V_{\mathrm{L}}}\,\bar{V}_{\mathrm{p}}\,\bar{\omega}_{\mathrm{p}} & \frac{\beta}{V_{\mathrm{L}}}\,\bar{V}_{\mathrm{m}}\,\bar{\omega}_{\mathrm{m}} & 0\\ 0 & \frac{1}{J_{\mathrm{m}}}\,\bar{V}_{\mathrm{m}}\,\Delta p & -\frac{1}{J_{\mathrm{m}}}\end{bmatrix}}_{\mathbf{B}}\underbrace{\begin{bmatrix}\alpha_{\mathrm{p}}\\ \alpha_{\mathrm{m}}\\ \tau_{\mathrm{g}}\end{bmatrix}}_{\mathbf{u}} \tag{17}$$
$$\mathbf{y} = \underbrace{\begin{bmatrix}1 & 0 & 0\\ 0 & 1 & 0\\ 0 & 0 & 1\end{bmatrix}}_{\mathbf{C}}\underbrace{\begin{bmatrix}\omega_{\mathrm{p}}\\ \Delta p\\ \omega_{\mathrm{m}}\end{bmatrix}}_{\mathbf{x}}$$

Where variables denoted with a bar indicates a linearization point. Including the digital pump and motor dynamics results

in the linear system transfer function given as

$$\mathbf{G}(s) = \underbrace{\mathbf{C}\,(s\mathbf{I}-\mathbf{A})^{-1}\,\mathbf{B}}_{\mathbf{G}_\mathrm{p}(s)} \begin{bmatrix} G_{\mathrm{pt(s)}} & 0 & 0 \\ 0 & G_{\mathrm{mt(s)}} & 0 \\ 0 & 0 & 1 \end{bmatrix} \tag{18}$$

Due to the many non-linearities, the system couplings and frequency response is strongly dependent on the operation point and thus the choice of linearization point puts constraints to the stable operation region. The choice of linearization points are those provided in Tab. V.

TABLE V: Choice of linearization points

Parameter	Operation range	Linearization value	Unit
ω_p	$[6, 12]$	6	rpm
ω_m	$[800, 1500]$	800	rpm
Δp	$[250, 350]$	300	bar
α_p	$[0, 1]$	0.5	-
α_m	$[0, 1]$	0.5	-

The pump and motor speed linearization points are chosen conservatively to the lowest values, yielding the lowest system eigenfrequency. The remaining values are chosen at the mid-point to ensure operation in the vicinity of the linearization point. To investigate the difference in system response with and without the dynamics from the digital machines, a plot of the singular values is shown in Fig. 15.

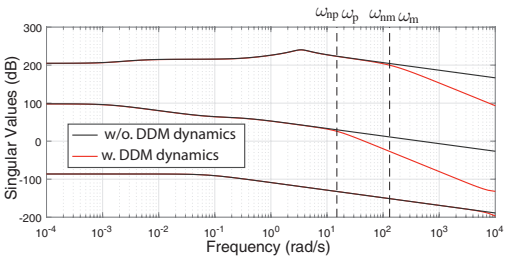

Fig. 15: Singular values of the system with and without pump and motor dynamics.

It is seen that the gains are identical up to a frequency of $\omega_{\mathrm{nm}}\,\omega_\mathrm{m}$ in the direction of the maximum singular values and up to a frequency of $\omega_{\mathrm{np}}\,\omega_\mathrm{p}$ in the orthogonal direction. Considering the pump and motor displacement responses as inner control loops, the dynamics of the machines may be considered as a static gain if the digital machine dynamics is at least 10 times faster than the transmission dynamics. Therefore, the following requirement is specified regarding the bandwidth of the closed loop system when neglecting the digital machine dynamics: $\omega_\mathrm{cl} < 0.1\,\omega_{\mathrm{np}}\,\bar{\omega}_\mathrm{p}$, where $\bar{\omega}_\mathrm{p}$ is the minimum pump velocity. This is a conservative design requirement, since the motor is ideal up to a frequency of $0.1\,\omega_{\mathrm{nm}}\,\bar{\omega}_\mathrm{m}$, which may weaken the constraints regarding the response time of the motor speed and pressure. Alternatively, the digital machine dynamics could be included in the controller design, which in the case of state-feedback control requires an observer to estimate the digital machine states. This is however not investigated further in this paper.

VII. Controller Synthesis

Either state-space control or a decoupling strategy is a logical choice when utilizing feedback control of a MIMO-system with three inputs and outputs. In this case, the transmission dynamics has a complex-conjugated pole, why it is not possible to fully input-output decouple the system. Therefore, a deterministic optimal controller is chosen which simplifies the problem of obtaining great closed-loop tracking performance when comparing to a classical pole placement design technique. To obtain unity DC-gain, integral action is implemented on the form given by

$$\mathbf{x}_\mathrm{int} = \int_0^t \mathbf{y}_\mathrm{ref}(\tau) - \mathbf{y}(\tau) d\tau \tag{19}$$

Extending the state-space model of the system with the integral states yields

$$\begin{aligned} \underbrace{\begin{bmatrix} \dot{\mathbf{x}} \\ \dot{\mathbf{x}}_\mathrm{int} \end{bmatrix}}_{\dot{\mathbf{x}}_\mathrm{a}} &= \underbrace{\begin{bmatrix} \mathbf{A} & \mathbf{0} \\ -\mathbf{C} & \mathbf{0} \end{bmatrix}}_{\mathbf{A}_\mathrm{a}} \underbrace{\begin{bmatrix} \mathbf{x} \\ \mathbf{x}_\mathrm{int} \end{bmatrix}}_{\mathbf{x}_\mathrm{a}} + \underbrace{\begin{bmatrix} \bar{\mathbf{B}} \\ \mathbf{0} \end{bmatrix}}_{\mathbf{B}_\mathrm{a}} \mathbf{u} + \underbrace{\begin{bmatrix} \mathbf{0} \\ \mathbf{1} \end{bmatrix}}_{\mathbf{B}_y} \mathbf{y}_\mathrm{ref} \\ \mathbf{y} &= \underbrace{\begin{bmatrix} \mathbf{C} & \mathbf{0} \end{bmatrix}}_{\mathbf{C}_\mathrm{a}} \mathbf{x}_\mathrm{a} \end{aligned} \tag{20}$$

Where $\bar{\mathbf{B}} = \mathrm{diag}(\begin{bmatrix} K_\mathrm{p} & K_\mathrm{m} & 1 \end{bmatrix})\,\mathbf{B}$ accounts for the static dc-gain of the digital machines. It should be noted that the transmission states are normalized by the maximum values given in Tab. V to ease the design process.

The continuous LQR control problem is to minimize the quadratic cost function given in (21) by applying the optimal control input, $\mathbf{u}$ [22].

$$J = \int_0^\infty \left(\mathbf{x}_\mathrm{a}^T\,\mathbf{Q}\,\mathbf{x}_\mathrm{a} + \mathbf{u}^T\,\mathbf{R}\,\mathbf{u}\right) \tag{21}$$

Where $\mathbf{R} = \mathbf{R}^T \geq \mathbf{0}$ weighs the importance of minimizing the control effort and $\mathbf{Q} = \mathbf{Q}^T \geq \mathbf{0}$ weighs the importance of driving the states to zero. The feedback control law is given as

$$u = -\underbrace{\begin{bmatrix} \mathbf{K} & \mathbf{K}_\mathrm{int} \end{bmatrix}}_{\mathbf{K}_\mathrm{a}} \underbrace{\begin{bmatrix} \mathbf{x} \\ \mathbf{x}_\mathrm{int} \end{bmatrix}}_{\mathbf{x}_\mathrm{a}} \tag{22}$$

The optimal solution for the feedback controller gain vector is given as

$$\mathbf{K}_\mathrm{a} = \mathbf{R}^{-1}\,\mathbf{B}_\mathrm{a}^T\,\mathbf{S} \tag{23}$$

The positive-semi-definite matrix $\mathbf{S} = \mathbf{S}^T \geq \mathbf{0}$ is the unique solution to the Ricatti equation given as

$$\mathbf{0} = \mathbf{A}_\mathrm{a}^T\,\mathbf{S} + \mathbf{S}\,\mathbf{A}_\mathrm{a} - \mathbf{S}\,\mathbf{B}_\mathrm{a}\,\mathbf{R}^{-1}\,\mathbf{B}_\mathrm{a}^T\,\mathbf{S} + \mathbf{Q} \tag{24}$$

The integral state is weighted with high importance to minimize the reference tracking error and is chosen as $\mathbf{Q} = \mathrm{diag}\left\{\begin{bmatrix} 0 & \cdots & 0 & 1 & 0.5 & 1 \end{bmatrix}\right\}$ relative to the input weighting $\mathbf{R} = \mathrm{diag}\begin{bmatrix} 1 & 1 & 1 \end{bmatrix}$. These values are found through trial-and-error with the objective of yielding a relative fast response, while fulfilling the requirement to the maximum eigenfrequency, ω_cl. Alternatively, a Linear Matrix Inequality

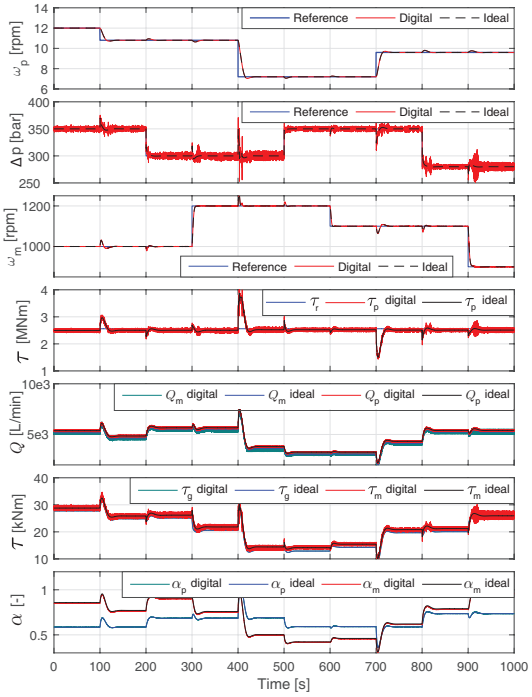

Fig. 16: Simulation results of Digital Fluid Power Transmission with digital displacement machines.

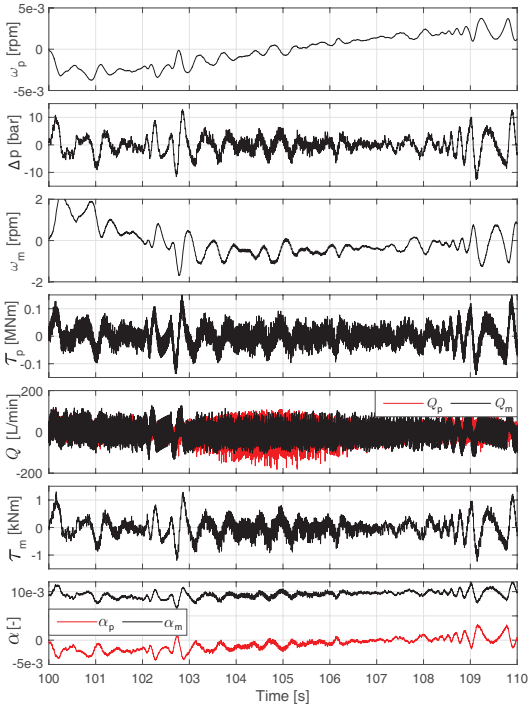

Fig. 17: Difference signal between ideal and digital response.

approach may be used, which allows for specifying constraints on the closed-loop pole location at the cost of being more complex.

VIII. Results

The designed controller is tested by simulation in the non-linear model representing the physical transmission system. To examine the influence of the digital displacement machines, the simulation is made with and without the digital displacement machines. The simulation without illustrates the ideal system given by the equations in (1) (ideal pump and motor). Reference tracking performance is tested by stepping in the three references within the specified operation region at a constant input load. The simulation results are shown in Fig. 16. It is seen, that the response of the ideal system and the actual system are similar and follows the reference with a response time fulfilling the design requirements. If a faster response time is desired, the minimum speed of the digital machines must proportionally be increased to ensure stability. Alternatively, the digital machine dynamics could be included in the design process where an observer may be used to estimate the machine states as mentioned.

To provide a deeper insight on the effect of using digital displacement machines relative to conventional fluid power pump-motors, the difference signal between the digital response and the ideal response is shown in Fig. 17 in a small time window. The maximum difference between the ideal and the digital response with respect to tracking of the pump and motor speed is less than 0.2 %. However, the pressure difference is up to 10 bar, but tracking of the pressure is less important since it only affect the energy efficiency and not the gearing ratio. It is evident, that the difference between the two responses is caused by fluctuations in the flow and torques due to the digital displacement machine. These fluctuations are however inevitable when using such non-smooth system with a full stroke operation strategy. The fluctuations could however be reduced by use of a hydraulic accumulator placed in the high pressure line. The introduction of a hydraulic accumulator does not change the presented control strategy, but requires a re-tuning of the controller to include the accumulators dynamical effect. A further and interesting study is to examine the performance of the digital fluid power transmission in a more realistic setup, e.g. a wind turbine transmission with accumulators and pipelines. The presented control strategy is expected to work equally well on a more realistic system, since the dynamics of the digital machines is so much faster than the large scale transmission dynamics. However, even though the fluctuations may be reduced, the performance with respect to tracking and fluctuations are not expected to be equally well compared to a conventional hydrostatic transmission.

IX. Conclusion

To enhance the use of energy efficient digital displacement machines in fluid power transmission systems, control strategies and design methods are demanded. This paper presents a pulse-density modulation control strategy and shows that a continuous approximation of the digital machines is sufficient in describing the fundamental dynamics if the number of cylinders and displacement fractions are sufficiently high. Additionally, the excitation frequencies should be less than the Nyquist frequency to not excite the discrete behavior. It is further shown that linear control theory is adequate if the rotational speeds of the digital machines are lower bounded by their linearization points. A dynamical analysis shows that if the speed of the digital machines are sufficiently high relative to the dynamics of the mechanical system and pressure line, it may be neglected during control design. Alternatively, the continuous approximation of the digital machines may be used for control design in conjunction with an estimator. Using an optimal linear deterministic MIMO control strategy, simulation results show similar tracking performance to that obtained when considering ideal fluid power machines. Fluctuations in the response is however observed, which is unavoidable due to the non-smooth digital machines. Hydraulic accumulators may however be implemented to reduce these fluctuations and thereby reduce stresses, which however requires retuning of the controller.

References

[1] M. Linjama, "Digital fluid power state of the art," *The Twelfth Scandinavian International Conference on Fluid Power, May 18-20, Tampere, Finland*, 2011.

[2] G. S. Payne, U. P. P. Stein, M. Ehsan, N. J. Caldwell, and W. H. S. Rampen, "Potential of digital displacement hydraulics for wave energy conversion," *In Proc. of the 6th European Wave and TIdal Energy Conference, Glasgow UK.*, 2005.

[3] W. R. M. Ehsan and S. Salter, "Modeling of digital-displacement pump-motors and their application as hydraulic drives for nonuniform loads," *ASME, Journal of dynamic system measurement and control, Vol. 122, pp. 210-215*, March 2000.

[4] W. Rampen, "The development of digital displacement technology," *In Proceedings of Bath/ASME FPMC Symposium*, 2010.

[5] P. Johansen, *Tribodynamic Modeling of Digital Fluid Power Motors*. PhD thesis, Department of Energy Technology, Aalborg University, 2014.

[6] D. B. Roemer, *Design and Optimization of Fast Switching Valves for Large Scale Digital Hydraulic Motors*. PhD thesis, 2014. Department of Energy Technology, Aalborg University.

[7] G. Wilfong, M. Batdorff, and J. Lumkes, "Design and dynamic analysis of high speed on/off poppet valves for digital pump/motors," *In Proceedings of the 6th FPNI-PhD Symposium*, 2010.

[8] G. Wilfong, M. Holland, and J. Lumkes, "Design and analysis of pilot operated high speed on/off valves for digital pump/motors," *In Proceedings of the 52nd National Conference on Fluid Power*, 2011.

[9] K. Merrill, M. Holland, and J. Lumkes, "Analysis of digital pump/motor operating strategies," *Proceedings of the 52nd National Conference on Fluid Power*, 2011.

[10] M. Heikkila and M. Linjama, "Displacement control of a mobile crane using digital hydraulic power management system," *Mechatronics 23(4), pp. 452 - 461*, 2013.

[11] X. Song, "Modeling an active vehicle suspension system with application of digital displacement pump motor," *Proceedings of the ASME 2008 International Design Engineering Techical Conference/Computers and Information in Enegineering Conference, Brooklyn - New York, Vol. 5, pp. 749-753*, 2008.

[12] B. S. R. Armstrong and Q. Yuan, "Multi-level control of hydraulic gerotor motor and pumps," *Proceedings of the 2006 American Control Conference, Minneapolis, Minnesota, USA*, June 2006. Proceedings of the 2006 American Control Conference Minneapolis, Minnesota.

[13] K. U. Sniegucki M, Gottfried M, "Optimal control of digital hydraulic drives using mixed-integer quadratic programming," September 2013. 9th IFAC Symposium on Nonlinear Control System, Toulouse.

[14] P. Johansen, D. B. Roemer, H. C. Pedersen, and T. O. Andersen, "Delta-sigma modulated displacement of a digital fluid power pump," *Proceedings of the 7th Workshop on Digital Fluid Power. LCM GmbH, 2015. s. 1-9*, February 2015 2015. The Seventh Workshop on Digital Fluid Power, Linz, Austria.

[15] P. Johansen, D. B. Roemer, H. C. Pedersen, and T. O. Andersen, "Discrete linear time invariant analysis of digital fluid power pump flow control," *Journal of Dynamic Systems, Measurement and Control, Transactions of the ASME, Vol. 139, Nr. 10, 101007*, 2017.

[16] N. H. Pedersen, P. Johansen, and T. O. Andersen, "Lqr-feedback control development for wind turbines featuring a digital fluid power transmission system," *9th FPNI PhD symposium on fluid power, Florianpolis, Brazil*, 2017.

[17] N. H. Pedersen, P. Johansen, and T. O. Andersen, "Optimal control of a wind turbine with digital fluid power transmission," 2016.

[18] N. H. Pedersen, P. Johansen, and T. O. Andersen, "Event-driven control of a speed varying digital displacement machine," *Proceedings of ASME/BATH FPMC Symposium on Fluid Power and Motion Control, Sarasota, Florida, USA*, 2017.

[19] N. H. Pedersen, P. Johansen, T. O. Andersen, and R. Scheidl, "Non-linear hybrid control oriented modelling of a digital displacement machine," *9th Workshop on Digital Fluid Power*, 2017.

[20] B. Dolan and H. Aschemann, "Control of a wind turbine with a hydrostatic transmission - an extended linearisation approach," *17th International Conference on Methods and Models in Automation and Robotics*, 2012.

[21] A. J. Laguna, N. F. Diepeveen, and J. W. van Wingerden, "Analysis of dynamics of fluid power drive-trains for variable speed wind turbines: parameter study," *IET Renewable Power Generation Vol. 8, Iss. 4*, 2014.

[22] S. Skogestad and I. Postlethwaite, *Multivariable Feedback Control - Analysis and Design 2nd edition*. Wiley, 2005.

[23] T. O. Andersen and M. R. Hansen, "Fluid power systems - modelling and analysis," *Institute of Energy Technology, Aalborg University, Denmark. 2nd Edition*, 2003.

Paper D

LQR Feedback Control Development for Wind Turbines Featuring a Digital Fluid Power Transmission System

Niels H. Pedersen, Per Johansen and Torben O. Andersen

The paper has been published in
Proceedings of the 9th Fluid Power Net International Ph.D. Symp. on Fluid Power,
ISBN:978-0-7918-5047-3, doi:10.1115/FPNI2016-1537.

The layout has been revised.

Proceedings of the FPNI Ph.D Symposium on Fluid Power
FPNI 2016
October 26-28, 2016, Florianpolis, Brazil

FPNI2016-1537

LQR FEEDBACK CONTROL DEVELOPMENT FOR WIND TURBINES FEATURING A DIGITAL FLUID POWER TRANSMISSION SYSTEM

Niels H. Pedersen
Fluid Power and Mechatronic Systems
Department of Energy Technology
Aalborg University
9220 Aalborg East, Denmark
Email: nhp@et.aau.dk

Per Johansen
Torben O. Andersen
Fluid Power and Mechatronic Systems
Department of Energy Technology
Aalborg University
9220 Aalborg East, Denmark
Email: pjo@et.aau.dk; toa@et.aau.dk

ABSTRACT

Research within digital fluid power (DFP) transmissions is receiving an increased attention as an alternative to conventional transmission technologies. The use of DFP displacement machines entails a need for applicable control algorithms. However, the design and analysis of controllers for such digital systems are complicated by its non-smooth behavior. In this paper a control design approach for a digital displacement machine® is proposed and a performance analysis of a wind turbine using a DFP transmission is presented. The performance evaluation is based on a dynamic model of the transmission with a DFP motor, which has been combined with the NREL 5-MW reference wind turbine model. A classical variable speed control strategy for wind speeds below rated is proposed for the turbine, where the pump displacement is fixed and the digital motor displacement is varied for pressure control. The digital motor control strategy consists of a full stroke operation strategy, where a Delta-Sigma pulse density modulator is used to determine the chamber activation sequence. In the LQR-control design approach, the discrete behavior of the motor and Delta-Sigma modulator is described by a discrete linear time invariant model. Using full-field flow wind profiles as input, the design approach and control performance is verified by simulation in the dynamic model of the wind turbine featuring the DFP transmission. Additionally, the performance is compared to that of the conventional NREL reference turbine, transmission and controller.

INTRODUCTION

Conventional power transmission systems for variable-speed variable-pitch wind turbines consist of a generator connected to the turbine rotor shaft through a gearbox. Replacing the gearbox with a hydrostatic transmission allows for continuous variable transmission being mechanical decoupled. This further allows for an optional use of a synchronous generator, whereby the power converter may be omitted. A hydrostatic transmission thereby benefit by the possibility of an increased reliability, since the gearbox and power converter being two major contributers to the turbine downtime is replaced [1]. A hydrostatic transmission for a wind turbine is not a new concept, but has so far been considered infeasible due to poor efficiencies of the hydraulic pumps and motors, especially at part load operation. Recent research within digital fluid power (DFP) technologies has lead to a successfully increase in the energy efficiencies of hydraulic fluid power machines [2, 3]. The DFP displacement technology is characterized by the use of numerous displacement chambers enabled or disabled, based on the desired displacement, by actively controlled electrical valves. A detailed description of the DFP displacement technology and possible applications is found in [4–6].

To the best of author's knowledge, no papers regarding control of a wind turbine transmission using digital displacement machines® has been published. A relatively high number of patents has been published on the subject by Mitsubishi Heavy Industries Ltd [7–10] et. al. However, no scientific results of

the various control strategies is provided and none of them utilizes model based feedback control theory. A control strategy for a tidal current generator with a similar DFP transmission has been developed, where the digital pump displacement is varied to maximize the energy capture and the digital motor displacement is varied to yield a uniform power output, with the aid of an hydraulic accumulator [6]. Additionally, several papers regarding flow, pressure, speed and torque control of digital displacement machines® has been published, where the machines are running at simplified load conditions at a fixed speed [4, 11–13]. Also none of these presented control strategies utilize model based feedback control design.

In this paper, a control strategy for a variable speed variable pitch wind turbine featuring a digital fluid power transmission is presented. In the proposed control strategy, the turbine rotor speed is controlled by varying the motor displacement in a full stroke operation. Due to the discrete behavior of the motor, the cylinder chamber actuation sequence is determined by a Delta-Sigma modulator as proposed in [14]. The dynamic behavior of the DFP motor is described by a discrete linear time invariant model based on [15], allowing for use of closed loop control design. A discrete linear feedback control strategy is used, where control tuning is done by use of Linear Quadratic Regulator (LQR) control.

Digital fluid power transmission

This study takes basis in the National Renewable Energy Laboratory (NREL) 5 MW wind turbine, since its data and model is readily available [16]. The wind turbine model serves as a tool for system analysis and performance evaluation of the digital fluid power transmission and corresponding control system. A schematic of the wind turbine with a continuous variable digital fluid power transmission is illustrated in Fig. 1.

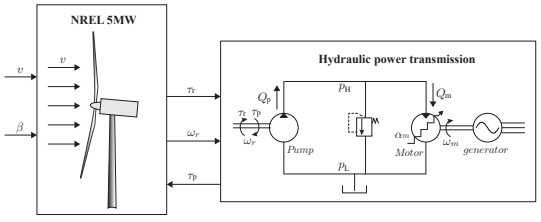

FIGURE 1. ILLUSTRATION OF THE DIGITAL FLUID POWER TRANSMISSION FOR THE NREL 5 MW TURBINE.

The wind turbine has the wind speed v, the turbine pitch angle, β, and the reactive pump torque, τ_{p}, as inputs. The torque from the low speed rotor shaft of the wind turbine, τ_{r}, drives the hydraulic pump, which output a pressurized fluid flow, Q_{p}. The fluid flow, Q_{m}, is further used to drive the hydraulic motor, with displacement input α_{m}, being connected to a high speed synchronous generator. In this study a conventional fixed displacement pump and a variable digital displacement motor is used. However, both the pump and the motor may be of type digital displacement, allowing for more advanced control possibilities. This simplification has been made since this paper investigates the use of closed loop model based control design for such system and the model and control method may easily be expanded to include a digital pump. Optionally, a hydraulic accumulator may be placed in the high pressure line to reduce pressure pulsations and yield a short term energy storage, but this is not investigated further in this paper.

Mathematical modeling

Turbulent Wind Model

Wind speed is known to be stochastic of nature and vary both globally and locally. The wind may be modeled by two components, being the mean wind speed and the turbulence wind speed as $v(t) = \bar{v} + \Delta v(t)$. The mean wind, $\bar{v}$, is a slowly variable component, while the turbulence wind speed, $\Delta v(t)$, is a rapidly varying component. In this paper, the IEC 61400-1 Kaimal turbulence spectrum and normal turbulence model is used for generation of wind profiles. The turbulence intensity is site specific, but has in this study been specified to be low (12 %). The 3D wind speed time series data is generated by the NREL code - TurbSim and given as input to the wind turbine model.

Wind Turbine Model

To describe the aerodynamics and elastic characteristics of the NREL 5 MW wind turbine, the open source code FAST (Fatigue, Aerodynamics, Structures and Turbulence program) is used, which model is based on the Blade Element Momentum method. The wind turbine model has been combined with the DFP transmission model through a Matlab/Simulink interface.

For transmission control design purpose, a simplified static model is used to describe the aerodynamic rotor power P_{r} and torque, τ_{r}, which are given in Eqn. (1) and Eqn. (2) respectively.

$$P_{\mathrm{r}} = \frac{1}{2} A_{\mathrm{r}} \rho_{\mathrm{air}} C_{\mathrm{p}}(\lambda, \beta)\, v^3 \tag{1}$$

$$\tau_{\mathrm{r}} = \frac{1}{2} A_{\mathrm{r}} R_{\mathrm{r}} \rho_{\mathrm{air}} C_{\mathrm{q}}(\lambda, \beta)\, v^2 \tag{2}$$

Where A_{r} is the rotor swept area, R_{r} is the blade radius, ρ_{air} is the air density and v is the wind speed perpendicular to the rotor blades. The power and torque coefficients $C_{\mathrm{p}}(\lambda, \beta)$ and $C_{\mathrm{q}}(\lambda, \beta)$ are dependent on the tip speed ratio, λ, and the blade pitching angle, β. The tip-speed ratio describing the relationship between the speed of the blade tip and the wind speed is defined as $\lambda = \frac{\omega_r R_r}{v}$. Where ω_r is the rotational speed of the rotor. The power

and torque coefficients are nonlinear turbine specific functions and are used for optimal control of the wind turbine described later. The dynamics of the turbine rotor may be approximated by the first order differential equation given in Eqn. (3).

$$\dot{\omega}_\mathrm{r} = \frac{1}{J_\mathrm{r}} \left(\tau_\mathrm{r} - d_\mathrm{r}\, \omega_\mathrm{r} - \underbrace{\frac{\bar{V}_\mathrm{p}\, \Delta p}{\eta_\mathrm{p}}}_{\tau_\mathrm{p}} \right) \tag{3}$$

Where J_r is the moment of inertia of the entire rotor including hub, blades and rotor shaft. d_r is the viscous damping coefficient, $\Delta p = p_\mathrm{H} - p_\mathrm{L}$ is the pressure difference between the high and low pressure side and η_p is the efficiency coefficient of the rotor taking the static friction into account. $\bar{V}_\mathrm{p}$ is the volumetric pump displacement per radians. The main specifications of the NREL 5 MW wind turbine is shown in Tab. 1 and the parameter values for the variables used for modeling of the DFP transmission is found in Tab. 2.

TABLE 1. MAIN PARAMETERS OF THE NREL 5 MW [16]

Parameter	Symbol	Value	Unit
Cut-in wind speed	v_in	4	m/s
Rated wind speed	v_r	11.4	m/s
Cut-out wind speed	v_out	25	m/s
Blade radius	R_r	63	m
Tower height	h_t	90	m
Rated rotor speed	ω_nom	12.13	rpm
Rotor and shaft inertia	J_r	3.87e7	kg $\cdot$m^2
Optimal tip speed ratio	λ^*	7.55	-
Maximum power coefficient	C_p^*	0.485	-

Hydrostatic Transmission Model

The low pressure, p_L, is controlled by an external boost pump and is for simplicity considered constant. The pressure difference dynamics is described by Eqn. (4).

$$\dot{\Delta}_\mathrm{p} = C_\mathrm{H} \left(\underbrace{\bar{V}_\mathrm{p}\, \omega_\mathrm{r}}_{Q_\mathrm{p}} - Q_\mathrm{m} \right) - C_\mathrm{l}\, \Delta_\mathrm{p} \tag{4}$$

Where $C_\mathrm{H} = \frac{\beta_\mathrm{e}}{V_\mathrm{H}}$ and $C_\mathrm{l} = \frac{\beta_\mathrm{e}}{V_\mathrm{H}}\, k_\mathrm{l}$. β_e is the effective oil bulk modulus, V_H is the volume of the high pressure line and k_l is the combined pump and motor leakage coefficient.

Digital Displacement Motor

To give an expression for the motor flow intake, a deeper insight in the working principle of the digital displacement motor (DDM) is presented. A sketch of the DDM is shown in Fig. 2.

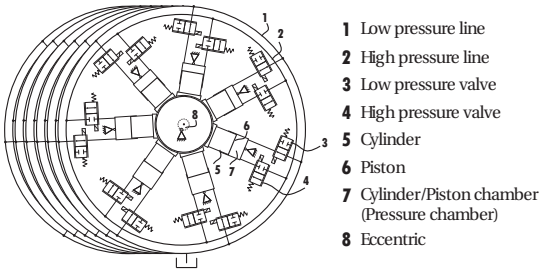

FIGURE 2. SKETCH OF THE DIGITAL DISPLACEMENT MOTOR [13].

The machine design consist of seven piston chambers in a slice connected to an eccentric, resulting in a reciprocating piston movement. Six of these slices are utilized, such that there is a total of $N = 42$ pressure chambers. This design is based on previous work with a 5 MW digital displacement motor [17]. An electrical controlled digital valve is placed between both the high and the low pressure line and the pressure chamber. Proper control of the valves yields a motoring stroke, where the pressurized fluid flow drives the piston and thereby the motor shaft. In this paper a full stroke operation is used where a cylinder is either motoring or idling for a full revolution. Idling operation is performed by maintaining the low pressure valve open and the high pressure valve closed for a full revolution. The utilization of pumping mode is not considered in the present work, since the displacement fraction reference is always positive during normal operation.

The modeling of the pressure chambers takes basis in the schematic shown in Fig. 3 and is based on previous work with a similar machine [18]. The piston displacement, x_p, is described as a function of the angular position given in Eqn. (5).

$$x_\mathrm{p}(\theta) = r_\mathrm{e}\, (1 - \cos\theta) \tag{5}$$

Where r_e is the eccentric radius. Using this expression, the chamber volume as a function of the angular position, θ, becomes that in Eqn. (6).

$$V_\mathrm{c}(\theta) = \frac{V_\mathrm{d}}{2}\, (1 - \cos\theta) + V_0 \qquad \dot{V}_\mathrm{c}(\theta) = \frac{V_\mathrm{d}}{2}\, \dot{\theta}\, \sin\theta \tag{6}$$

V_0 is the minimum chamber volume and $V_\mathrm{d} = V_0 = 2\, r_\mathrm{e}\, A_\mathrm{p}$ is the displacement volume, where A_p is the piston area. The motor ro-

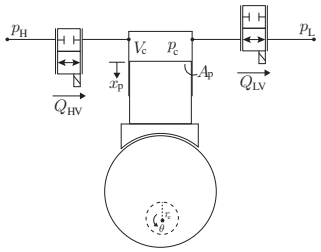

FIGURE 3. SKETCH OF A SINGLE PRESSURE CHAMBER WITH VARIABLES USED FOR MODELING.

tational speed $\omega_m = \dot{\theta}$ is considered constant as a simplification, since it is expected that the generator may be excited to yield an approximately constant rotation speed.

The pressure dynamics in a pressure chamber is described by Eqn. (7).

$$\dot{p}_c = \frac{\beta_e}{V_c}\left(Q_{HV} - Q_{LV} - \dot{V}_c\right) \tag{7}$$

The flow through the high and low pressure valves are described by the orifice equation given in Eqn. (8).

$$\begin{aligned} Q_{LV} &= \frac{\bar{x}_L}{k_f}\sqrt{|p_c - p_L|}\,\mathrm{sign}\,(p_c - p_L) \\ Q_{HV} &= \frac{\bar{x}_H}{k_f}\sqrt{|p_H - p_c|}\,\mathrm{sign}\,(p_H - p_c) \end{aligned} \tag{8}$$

k_f is the flow coefficient of the valves, $\bar{x}_L$ and $\bar{x}_H$ is the normalized valve position of the low and high pressure valve respectively. The valve dynamics are simplified to be described by a constant acceleration given by Eqn. (9) for opening of the valve.

$$a_{v+} = \begin{cases} 4/t_s^2 & for\ \ 0 \le t \le t_s/2 \\ -4/t_s^2 & for\ \ t_s/2 \le t \le t_s \end{cases} \tag{9}$$

t_s is the valve opening/closing time. This function yields a smooth valve position with a maximum velocity at the mid point. For closing of the valve the acceleration is given by $a_{v\text{-}} = -a_{v+}$. For a full stroke operation both valves are actively closed at a rotation angle of $\theta_{H\text{-}cl}$ and $\theta_{L\text{-}cl}$ for the high and low pressure valve respectively (HPV and LPV). Passive opening of the valves is utilized such that the high pressure valve is opened when $p_c > p_H$ and the low pressure valve is opened when $p_c < p_L$.

Simulation results for a single pressure chamber is shown in Fig. 4 for one motoring stroke and one idling stroke. In the

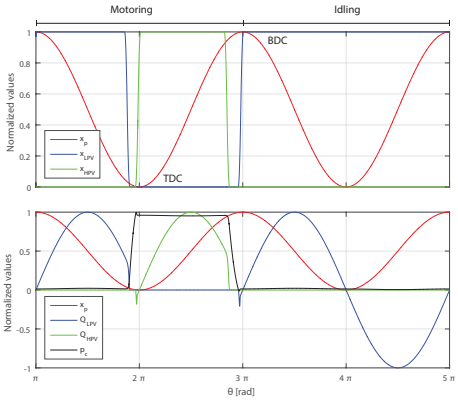

FIGURE 4. SIMULATION OF A SINGLE PRESSURE CHAMBER DYNAMICS.

motoring stroke, it is seen that the pressure rises fast when the LPV is closed since the piston position is decreasing, resulting in a fluid compression. At some point near top dead center (TDC) the chamber pressure exceeds the high pressure, $p_c > p_H$ and the HPV is passively opened due to pressure force. As evident, a back flow into the high pressure line occurs momentarily, since the chamber pressure is greater than the high pressure. During intake the HPV is held open and high pressure fluid is entering the cylinder chamber and thereby drives the piston and motor shaft. Near bottom dead center (BDC) the HPV is closed and at some point the chamber pressure decreases below the low pressure, $p_c < p_L$, resulting in a passive opening of the LPV due to suction. As a result, a minor part of the motoring stroke is not usable for supplying fluid flow to the motor.

Since the valve dynamics are very fast compared to the turbine dynamics, the pressure chamber equations has been solved for various difference pressures and implemented as a look-up table to reduce solving time significantly. The fluid flow into the motor from the high pressure line is the sum of each individual flow into a pressure chamber and is described by Eqn. (10).

$$Q_m = \sum_{i=1}^{N} Q_{HV}(i) \tag{10}$$

Wind Turbine Operation and Control Objectives

The control objective of a variable-speed variable-pitch wind turbine is to maximize the energy capture while avoiding excessive mechanical structural loads. The overall control objective is divided into 4 distinct operation regions shown on the power curve in Fig. 5. Region I is where the wind speed is below the cut-in wind speed, v_{in}, and power production is infeasible. In

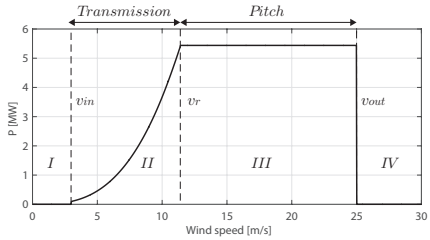

FIGURE 5. POWER CURVE FOR THE NREL WIND TURBINE.

region II maximum power tracking is performed by maintaining the optimal tip-speed ratio. In region III the turbine is operated at rated speed mainly controlled by the pitch system. In region IV above the cut-out wind speed, v_{out}, the turbine is shut down for safety reasons. Since this paper is about transmission control the focus will be on maximum power tracking control in region II below rated wind speeds.

Region II Control

The maximum power tracking control in region II is a compromise between maintaining the optimal tip-speed ratio and avoiding excessive fluctuations in the reactive pump torque. The commonly used $K\,\omega^2$ control law is used since it only requires measurement of the rotor speed having slow dynamics. This way the high turbulence wind disturbance is filtered away at the cost of less accurate tracking of the optimal tip-speed ratio. The $K\,\omega^2$ law is derived based on the aerodynamic rotor torque equation given in Eqn. (2). By use of the static relation $C_{\text{p}}(\lambda,\beta) = \lambda\, C_{\text{q}}(\lambda,\beta)$, the torque equation may be rewritten into that in Eqn. (11).

$$\begin{aligned} \tau_{\text{r}} &= \frac{1}{2} A_{\text{r}} R_{\text{r}} \rho_{\text{air}} \frac{C_{\text{p}}(\lambda,\beta)}{\lambda} \left(\frac{R_{\text{r}}\,\omega_{\text{r}}}{\lambda}\right)^2 \\ \tau_{\text{r}}^* &= \underbrace{\frac{1}{2} A_{\text{r}} R_{\text{r}}^3 \rho_{\text{air}} \frac{C_{\text{p}}^*}{\lambda^{*3}}}_{K_2}\, \omega_{\text{r}}^2 \end{aligned} \tag{11}$$

τ_{r}^* is the aerodynamic torque reference, C_{p}^* is the maximum power coefficient and λ^* is the optimal tip speed ratio.

Wind Turbine Control Structure

To control the rotor speed by the aerodynamic torque requires accurate tracking of the torque reference. Since the pressure is more easily and precise measured than the torque, the torque reference τ_{r}^* is converted into a pressure reference Δ_{p}^* through use of Eqn. (12).

$$\Delta_{\text{p}}^* = (\tau_{\text{r}}^* - d_{\text{r}}\,\omega_{\text{r}})\,\frac{\eta_{\text{p}}}{\bar{V}_{\text{p}}} \tag{12}$$

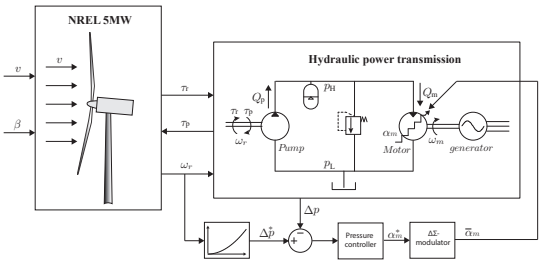

FIGURE 6. CONTROL STRUCTURE FOR HYDROSTATIC WIND TURBINE TRANSMISSION.

The closed loop control structure for variable speed control is shown in Fig. 6. Similar control structures has successfully been used for control of a conventional hydrostatic transmission for a wind turbine, see [19, 20]. The control structure only requires measurement of the rotor speed ω_{r} and the pressure difference Δp. The pressure controller outputs a displacement fraction reference α_{m}^* for the digital motor between 0 and 1. The displacement fraction reference is converted into a binary sequence by a Delta-Sigma modulator, determine whether the next cylinder chamber should use a motoring or an idling stroke.

Linear Model Representation

In this study it is attempted to use linear state feedback control. Since the motor operation is discrete by nature, a discrete linear time invariant (DLTI) model of the system dynamics is derived. First a discrete linear representation of the Delta-Sigma modulator and digital motor is presented. Following this, the establishment of a discrete state space model of the complete system is provided.

Delta-Sigma Modulator

The Delta-Sigma modulator (DSM) outputs the pressure chamber actuation sequence based on the displacement reference α_{m}^*. The actuation sequence is binary where 1 and 0 represents an active (motoring) and an inactive (idling) chamber respectively. In this study, a first order DSM is utilized and a block diagram representation of it is shown in Fig. 7, [21]. The modulator outputs the binary actuation sequence, $\bar{\alpha}_{\text{m}}$, which time average approximates the input displacement fraction reference α_{m}^*. The first order DSM consist of a discrete time integrator and a 1 bit quantizer. The non-linearity introduced by the quantizer may be linear represented by an additive noise input n as shown in Fig. 8. From the block diagram, a discrete linear transfer function of the modulator may be written to be that in Eqn. (13).

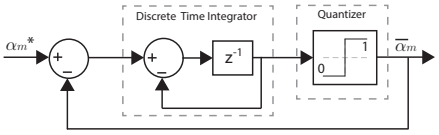

FIGURE 7. FIRST ORDER DELTA-SIGMA MODULATOR BLOCK DIAGRAM.

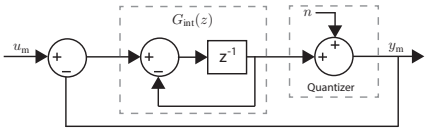

FIGURE 8. LINEAR REPRESENTATION OF THE FIRST ORDER DELTA-SIGMA MODULATOR.

$$\begin{aligned} Y_m(z) &= \underbrace{\frac{1}{z}}_{\mathrm{STF}(z)} U_m(z) + \underbrace{\frac{z-1}{z}}_{\mathrm{NTS}(z)} N(z) \\ y_m(k) &= u_m(k-1) + n(k) - n(k-1) \end{aligned} \tag{13}$$

The linear modulator transfer function consist of two parts being a signal and a noise transfer function, STF(z) and NTF(z) respectively. The output is seen to consist of a single sample delayed input signal and a discrete differentiated noise signal.

Digital Fluid Power Motor

The discrete linear motor model is derived by establishing a relation between the displacement reference and the motor flow intake, as a convolution sum of flows between each sample. Since a decision to either active or deactivate the next cylinder chamber has to be done for all cylinders during one revolution, the sampling time is dependent on the motor rotational speed and the number of cylinders given by $T_s = \frac{2\pi}{\omega_m N}$. Each flow intake between two samples may then be described by Eqn. (14).

$$Q_{HV}[k] \approx \frac{V_d}{T_s}\left(\bar{V}_c(\theta[k+1]) - \bar{V}_c(\theta[k])\right) = \frac{V_d}{T_s}\Delta\bar{V}_c[k] \tag{14}$$

Where $\bar{V}_c(\theta)$ is the normalized chamber volume. The derivation of the discrete linear model is based on the illustration shown in Fig. 9.

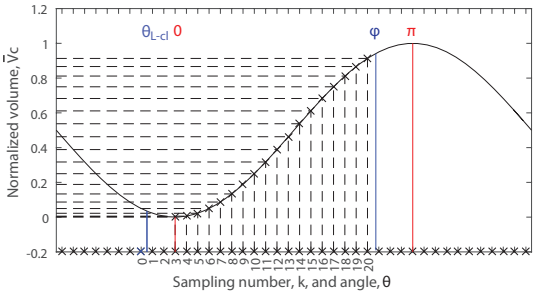

FIGURE 9. ILLUSTRATION USED FOR ESTABLISHING THE DISCRETE LINEAR MOTOR MODEL.

The LPV closing angle is located between sampling instance $k = 0$ and $k = 1$, where $k = 0$ is the sampling instance where the chamber activation decision is made. With $N = 42$ cylinder chambers a full motoring stroke will ideally last for 21 samples between $\theta = 0$ and $\theta = \pi$. Three sampling delays are introduced due to valve dynamics, why the motoring stroke starts at sampling instance $k = 3$. Again due to valve dynamics and the fact that the LPV has to be passively opened at $\theta = \pi$, the motoring stroke ends at an angle ϕ, ahead of this angle.

A convolution sum representation of the motor displacement, α_m, as a function of the displacement reference input, $\bar{\alpha}_m$, is obtained by use of Eqn. (15). Also the relation between the motor displacement and the motor flow is provided.

$$\alpha_m[k] = \sum_{m=0}^{k} \Delta\bar{V}_c[k-m]\,\bar{\alpha}_m[m] \qquad Q_m[k] = \underbrace{\frac{V_d}{T_s}}_{k_q}\alpha_m[k] \tag{15}$$

Where the displacement fractions are calculated by Eqn. (16).

$$\Delta\bar{V}_c[k] = \begin{cases} 0 & \theta[k], \theta[k+1] \notin [0\,;\phi] \\ \bar{V}_c(\theta[k+1]) - \bar{V}_c(\theta[k]) & \theta[k], \theta(k+1) \in [0\,;\phi] \\ \bar{V}_c(\theta[k+1]) - \bar{V}_c(0) & \theta[k] < 0 < \theta[k+1] \\ \bar{V}_c(\phi) - \bar{V}_c(\theta[k]) & \theta[k] < \phi < \theta[k+1] \end{cases} \tag{16}$$

It may be identified that the displacement is 0 outside the interval $\theta = [0\,;\phi]$ and the displacement fractions are 0 outside the interval $k = [3\,;20]$. For a more detailed description of the method, see [15].

The discrete model of the digital fluid power motor is verified by an impulse response simulation, where the results are shown in Fig. 10. $Q_{\text{non-linear}}$ is the motor flow intake response

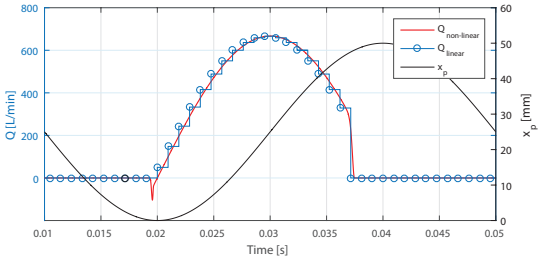

FIGURE 10. COMPARISON OF THE DIGITAL MOTOR FLOW DESCRIBED BY THE DISCRETE LINEAR MODEL AND THE NON-LINEAR MODEL.

obtained by simulation of the non-linear model of the motor with valve dynamics and Q_{linear} is the flow intake approximated by the DLTI model of the motor. It is seen that the DLTI model has a high accuracy except at the end points of the motoring stroke, where it is not able to predict the back-flow and the dynamics due to valve actuation. The errors are however minor and the motor model is thus verified.

The main modeling parameters for the transmission are provided in Tab. 2.

TABLE 2. PARAMETERS OF THE HYDROSTATIC TRANSMISSION

Parameter	symbol	value	Unit
Pump mechanical efficiency	η_p	0.95	-
Fixed pump displacement	$\bar{V}_\text{p}$	121.88	L/rad
Pipeline volume	V_H	78.5	L
Effective bulk modulus	β_e	16000	bar
Transmission leakage coefficient	k_l	0.1	L/bar
Synchronous motor speed	ω_m	1500	rpm
Motor piston area	A_p	79	cm^2
Motor eccentric radius	r_m	37.5	mm
Chamber flow coefficient	k_f	$0.5 \cdot 10^5$	$\sqrt{pa}\,s/\text{m}^3$
Valve actuation time	t_s	1	ms
HPV closing angle	$\theta_\text{H-cl}$	148.2	deg
LPV closing angle	$\theta_\text{L-cl}$	334.7	deg

State Space Representation

The state space representation of the turbine and pressure dynamics becomes that in Eqn. (17) by combining Eqn. (3) and Eqn. (4). The plant model has been normalized such that $-1 \leq \omega_\text{r} \leq 1$ and $-1 \leq \Delta p \leq 1$, to ease the controller design in the following sections, but the notation of this has been left out.

$$\begin{aligned}\underbrace{\begin{bmatrix}\dot{\omega}_\text{r}\\ \dot{\Delta}_\text{p}\end{bmatrix}}_{\dot{\mathbf{x}}} &= \underbrace{\begin{bmatrix}-\frac{d_\text{r}}{J_\text{r}} & -\frac{\bar{V}_\text{p}}{J_\text{r}\eta_\text{p}}\\ C_\text{H}\bar{V}_\text{p} & -C_\text{p}\end{bmatrix}}_{\mathbf{A}}\underbrace{\begin{bmatrix}\omega_\text{r}\\ \Delta_\text{p}\end{bmatrix}}_{\mathbf{x}} + \underbrace{\begin{bmatrix}0\\ -C_\text{H}\end{bmatrix}}_{\mathbf{B}}\underbrace{Q_\text{m}}_{u} + \underbrace{\begin{bmatrix}\frac{1}{J_\text{r}}\\ 0\end{bmatrix}}_{\mathbf{E}}\tau_\text{r}\\ \mathbf{y} &= \underbrace{\begin{bmatrix}1&0\\0&1\end{bmatrix}}_{\mathbf{C}}\mathbf{x}\end{aligned} \tag{17}$$

Since the motor control is performed discretely, a discrete representation of the continuous state model is necessary. The discrete state representation of Eqn. (17) becomes that in Eqn. (18).

$$\begin{aligned}\mathbf{x}(k+1) &= \mathbf{A}_\text{p}\,\mathbf{x}(k) + \mathbf{B}_\text{p}\,u(k) + \mathbf{E}_\text{p}\,\tau_\text{r}(k)\\ \mathbf{y}(k) &= \mathbf{C}_\text{p}\,\mathbf{x}(k)\end{aligned} \tag{18}$$

The discrete modulator transfer function derived in Eqn. (13) is rewritten into state space form resulting in Eqn. (19).

$$\begin{aligned}x_\text{m}(k+1) &= \underbrace{[0]}_{\mathbf{A}_\text{m}}x_\text{m}(k) + \underbrace{[1]}_{\mathbf{B}_\text{m}}u_\text{m}(k) - \underbrace{[1]}_{\mathbf{E}_\text{m}}n(k)\\ y_\text{m}(k) &= \underbrace{[1]}_{\mathbf{C}_\text{m}}x_\text{m}(k) + \underbrace{[1]}_{\mathbf{V}_\text{m}}n(k)\end{aligned} \tag{19}$$

The discrete difference equation model derived in Eqn. (15) is rewritten into state space form resulting in Eqn. (20).

$$\begin{aligned}&\underbrace{\begin{bmatrix}u_\text{d}(k)\\ u_\text{d}(k-1)\\ u_\text{d}(k-2)\\ \vdots\\ u_\text{d}(k-p+1)\end{bmatrix}}_{\mathbf{x}_\text{d}(k+1)} = \underbrace{\begin{bmatrix}0&0&\cdots&0&0\\ 1&0&\cdots&0&0\\ 0&1&\cdots&0&0\\ \vdots&\vdots&\ddots&\vdots&\vdots\\ 0&0&\cdots&1&0\end{bmatrix}}_{\mathbf{A}_\text{d}}\underbrace{\begin{bmatrix}u_\text{d}(k-1)\\ u_\text{d}(k-2)\\ u_\text{d}(k-3)\\ \vdots\\ u_\text{d}(k-p)\end{bmatrix}}_{\mathbf{x}_\text{d}(k)} + \underbrace{\begin{bmatrix}1\\0\\0\\ \vdots\\0\end{bmatrix}}_{\mathbf{B}_\text{d}}u_\text{d}(k)\\ &y_\text{d}(k) = \underbrace{k_\text{q}\,\left[\Delta\bar{V}_\text{c}[1]\;\Delta\bar{V}_\text{c}[2]\;\Delta\bar{V}_\text{c}[3]\;\cdots\;\Delta\bar{V}_\text{c}[p]\right]}_{\mathbf{C}_\text{d}}x_\text{d}(k)\\ &+\underbrace{k_\text{q}\,\left[\Delta\bar{V}_\text{c}[0]\right]}_{\mathbf{D}_\text{m}}u_\text{d}(k)\end{aligned} \tag{20}$$

Where $p = 20$ is the last sampling instance with a displacement fraction $\Delta\bar{V}_\text{c} \neq 0$.

In this paper, the feedback control gain vector is determined by use of Linear Quadratic Regulator (LQR) optimal control. The wind speed and quantization disturbance input on the control

system is thereby neglected from the model. Alternatively, LQG, is a solid choice for design of the feedback controller, since an observer is used to estimate the disturbances and the controller may hence compensate for them.

The complete discrete state space model is obtained by combining Eqn. (18), Eqn. (19) and Eqn. (20) resulting in Eqn. (21). Here the disturbance inputs due to the aerodynamic rotor torque and the quantization error has been omitted.

$$\underbrace{\begin{bmatrix}\mathbf{x}(k+1)\\ \mathbf{x}_\mathrm{d}(k+1)\\ x_\mathrm{m}(k+1)\end{bmatrix}}_{\mathbf{x}_\mathrm{t}(k+1)} = \underbrace{\begin{bmatrix}\mathbf{A}_\mathrm{p} & \mathbf{B}_\mathrm{p}\,\mathbf{C}_\mathrm{d} & \mathbf{0}\\ \mathbf{0} & \mathbf{A}_\mathrm{d} & \mathbf{B}_\mathrm{d}\,\mathbf{C}_\mathrm{m}\\ \mathbf{0} & \mathbf{0} & \mathbf{A}_\mathrm{m}\end{bmatrix}}_{\mathbf{A}_\mathrm{t}} \underbrace{\begin{bmatrix}\mathbf{x}(k)\\ \mathbf{x}_\mathrm{d}(k)\\ x_\mathrm{m}(k)\end{bmatrix}}_{\mathbf{x}_\mathrm{t}(k)} + \underbrace{\begin{bmatrix}\mathbf{0}\\ \mathbf{0}\\ \mathbf{B}_\mathrm{m}\end{bmatrix}}_{\mathbf{B}_\mathrm{t}} u_\mathrm{m}(k)$$
$$\mathbf{y}(k) = \underbrace{\begin{bmatrix}\mathbf{C}_\mathrm{p} & \mathbf{0} & \mathbf{0}\end{bmatrix}}_{C_\mathrm{t}} \mathbf{x}_\mathrm{t} \tag{21}$$

Control Feedback and Integral State Introduction

To apply linear control theory a linearization of the $K\,\omega^2$ law given in Eqn. (11) is required. The linear expression for the pressure reference given in Eqn. (12) becomes that in Eqn. (22).

$$\begin{aligned}\Delta_\mathrm{p}^* &= \left(\frac{d\,\tau_\mathrm{r}^*(\omega_\mathrm{r})}{d\,\omega_\mathrm{r}}|_{\omega_\mathrm{r}=\omega_0}\,\omega_\mathrm{r} - d_\mathrm{r}\,\omega_\mathrm{r}\right)\frac{\eta_\mathrm{p}}{\bar{V}_\mathrm{p}}\\ \Delta_\mathrm{p}^* &= \underbrace{\left(2\,K_2\,\omega_0 - d_\mathrm{r}\right)\frac{\eta_\mathrm{p}}{\bar{V}_\mathrm{p}}}_{K_{\omega r}}\,\omega_\mathrm{r}\end{aligned} \tag{22}$$

Where ω_0 is taken at some mean wind speed, $\bar{v}$, given by $\omega_0 = \frac{\lambda^*\,\bar{v}}{R_\mathrm{r}}$. To achieve unity dc-gain the system is appended with an integral state acting on the pressure error. The integral state vector is derived to be that in Eqn. (23).

$$\begin{aligned}\dot{x}_\mathrm{int} &= \Delta p^* - \Delta p = K_{\omega r}\,\omega_\mathrm{r} - \Delta p\\ \dot{x}_\mathrm{int} &= \frac{x_\mathrm{int}(k+1) - x_\mathrm{int}(k)}{T_\mathrm{s}}\\ x_\mathrm{int}(k+1) &= \underbrace{\begin{bmatrix}K_{\omega r}\,T_\mathrm{s} & -T_\mathrm{s}\end{bmatrix}}_{\mathbf{K}_\mathrm{y}}\underbrace{\begin{bmatrix}\omega_\mathrm{r}(k)\\ \Delta p(k)\end{bmatrix}}_{\mathbf{y}(k)} + x_\mathrm{int}(k)\end{aligned} \tag{23}$$

The extended state space representation with integral state hence becomes that given in Eqn. (24).

$$\underbrace{\begin{bmatrix}\mathbf{x}_\mathrm{t}(k+1)\\ x_\mathrm{int}(k+1)\end{bmatrix}}_{\mathbf{x}_\mathrm{s}(k+1)} = \underbrace{\begin{bmatrix}\mathbf{A}_\mathrm{t} & \mathbf{0}\\ \mathbf{K}_\mathrm{y}\,\mathbf{C}_\mathrm{t} & 1\end{bmatrix}}_{\mathbf{A}_\mathrm{s}}\underbrace{\begin{bmatrix}\mathbf{x}_\mathrm{t}(k)\\ x_\mathrm{int}(k)\end{bmatrix}}_{\mathbf{x}_\mathrm{s}(k)} + \underbrace{\begin{bmatrix}\mathbf{B}_\mathrm{t}\\ \mathbf{0}\end{bmatrix}}_{\mathbf{B}_\mathrm{s}} u_\mathrm{m}(k)$$
$$\mathbf{y}(k) = \underbrace{\begin{bmatrix}\mathbf{C}_\mathrm{t} & \mathbf{0}\end{bmatrix}}_{\mathbf{C}_\mathrm{s}}\mathbf{x}_\mathrm{s}(k) \tag{24}$$

Optimal State Feedback Controller

Due to the high number of states it is difficult to obtain the desired closed loop performance, by using classical pole placement techniques. Therefore, the controller design and tuning is based on Linear Quadratic Regulator, LQR, optimal control. The LQR control problem is to find the optimal control input, $u_\mathrm{m}(k)$, which minimizes Eqn. (25)

$$J = \sum_{k=1}^{\infty}\left(\mathbf{x}_\mathrm{s}(k)^T\,\mathbf{Q}\,\mathbf{x}_\mathrm{s}(k) + u_\mathrm{m}(k)^T\,\mathbf{R}\,u_\mathrm{m}(k)\right) \tag{25}$$

Where $\mathbf{Q} = \mathbf{Q}^T \geq \mathbf{0}$ and $\mathbf{R} = \mathbf{R}^T \geq \mathbf{0}$ are weighting matrices for the states and input respectively. $\mathbf{Q}$ describes the relative importance with respect to $\mathbf{R}$ of driving each state to zero and $\mathbf{R}$ the importance of the control effort to do so. The optimal solution for the control law $u_\mathrm{m}(k) = -\mathbf{K}_\mathrm{s}\,\mathbf{x}_\mathrm{s}(k)$ is given in Eqn. (26)

$$\mathbf{K}_\mathrm{s} = \left(\mathbf{B}_\mathrm{s}^T\,\mathbf{S}\,\mathbf{B}_\mathrm{s} + \mathbf{R}\right)^{-1}\left(\mathbf{B}_\mathrm{s}^T\,\mathbf{S}\,\mathbf{A}_\mathrm{s}\right) \tag{26}$$

Where $\mathbf{K}_\mathrm{s} = \begin{bmatrix}\mathbf{K} & K_\mathrm{int}\end{bmatrix}$ and $\mathbf{S} = \mathbf{S}^T \geq \mathbf{0}$ is the solution to the algebraic Ricatti equation given in Eqn. (27).

$$\begin{aligned}\mathbf{0} &= \mathbf{A}_\mathrm{s}^T\,\mathbf{S}\mathbf{A}_\mathrm{s} - \mathbf{S} + \mathbf{Q}\\ &\quad - \left(\mathbf{A}_\mathrm{s}^T\,\mathbf{S}\,\mathbf{B}_\mathrm{s}\right)\left(\mathbf{B}_\mathrm{s}^T\,\mathbf{S}\,\mathbf{B}_\mathrm{s} + \mathbf{R}\right)^{-1}\left(\mathbf{B}_\mathrm{s}^T\,\mathbf{S}\,\mathbf{A}_\mathrm{s}\right)\end{aligned} \tag{27}$$

The input weighting matrix is chosen as $\mathbf{R} = 1$ and the state weighting matrix is determined relative to this value. Since it is a servo control problem with the reference tracking being the main objective, the integral state is weighted high, resulting in $\mathbf{Q} = \mathrm{diag}\left\{\begin{bmatrix}0 & 0 & \cdots & 0 & 10\end{bmatrix}\right\}$.

Simulation Results

The presented controller is validated by numerical simulation in Matlab/Simulink. For performance evaluation with respect to pressure tracking and aerodynamic torque fluctuations, a wind profile has been generated with a mean wind speed of $\bar{v} = 8\,\mathrm{m/s}$. The obtained results for the Digital Fluid Power Transmission (DFPT) are compared with results for the conventional NREL transmission, where the NREL reference PI-controller is used [16]. The NREL PI-controller is a classical Proportional-Integral controller, controlling the generator speed and thus the rotor speed of the conventional transmission system. The simulation results are shown in Fig. 11. The wind speed is seen to be exclusively in region II below rated wind speed. Comparing the reference transmission and PI-controller with the DFPT and controller, it is seen that the responses are very similar with respect to both rotor speed and torque. It is identified that the minor offset between the responses are due to the optimal coefficient for

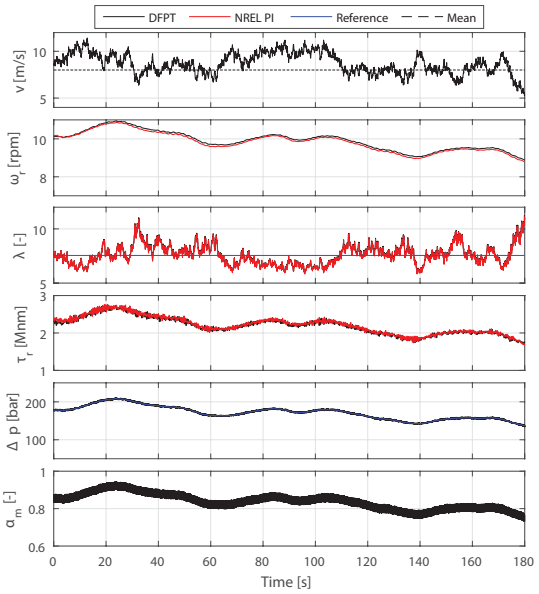

FIGURE 11. SIMULATION RESULTS FOR NREL 5 MW TURBINE WITH TURBULENT WIND PROFILE, $\bar{v} = 8\,m/s$.

region II control in the reference PI-controller is not entirely accurate. The pressure reference tracking accuracy is considered very good, which is more clearly seen on the zoomed-view in Fig. 12, but has minor ripples around the reference. The motor displacement fraction is seen to be highly oscillating, which is also expected due to the binary motor states.

A zoomed view of the difference pressure, motor flow and control signals are shown in Fig. 12. It is seen that a displacement fraction of $\alpha_m = [0.83\,;\,0.87]$ is obtained by activating approximately 5 out of every 6 cylinders. The results of this is seen in the step-wise behavior of the displacement fraction, since the last 20 decisions are used as state feedbacks. The periodic behavior is further transfered to the motor flow followed by the pressure response. The sudden small spikes in the motor flow is due to the back flow identified in Fig. 10, but is not excited much in the pressure response. The pressure tracking performance is considered great, since the error is at maximum $\pm\,2\,bar$ corresponding to $\approx 1\,\%$ of the reference value. Each individual pressure oscillations is found to have an amplitude of less than $2\,bar$, corresponding to the activation of one additional pressure chamber. However, the induced fluctuation in the pressure is directly transfered to the reactive pump torque having a large influence on the system reliability. It is therefore assessed that a hydraulic

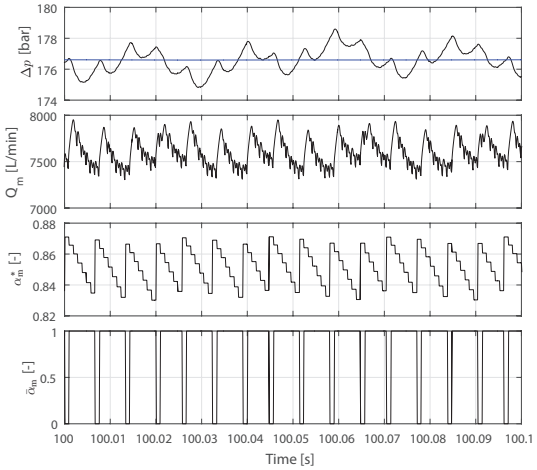

FIGURE 12. ZOOMED VIEW OF SIMULATION RESULTS FOR NREL 5 MW TURBINE WITH TURBULENT WIND PROFILE, $\bar{V} = 8\,M/S$.

accumulator is necessary in order to reduce the fast dynamic reactive torque ripples to an acceptable level. However, the implementation of an accumulator has a large impact on the system dynamics, why an extended model of the hydraulic transmission has to be formulated and used for retuning of the controller. The method used for describing the dynamics of the discrete motor, as well as the control structure and controller design method is still valid.

Conclusion

The focus of this study has been to develop model based feedback control for a variable speed turbine with a digital fluid power transmission. The study took basis in the NREL 5-MW turbine, where its model was combined with a dynamic model of the digital fluid power transmission.

The paper presented a control structure for wind speeds below rated, where the rotor speed is controlled by the reactive pump torque, through control of the pressure difference. The pressure difference is further controlled by varying the digital motor displacement fraction. A full stroke digital motor operation was used, where a Delta-Sigma modulator determined the cylinder chamber actuation sequence. A discrete state model of the system was established and closed loop state feedback control was utilized. The control design and tuning was done by the LQR-method, with the objective of accurate pressure tracking.

The simulation results showed great pressure tracking performance and the work therefore supports the hypothesis of

utilizing model based control for such system with digital hydraulics. The results did however also reveal a high amount of fluctuations in the pressure/torque response. These fluctuations are a direct results of the discrete operation of the digital motor and it would be required to reduce these significantly by use of a hydraulic accumulator to make the presented work feasible.

Further work will include the implementation of hydraulic accumulators, which would also allow for short term energy storage, yielding a possibility of an increased energy extraction. It is further expected that LQG-control may improve the performance due to the improved disturbance rejection. Also more advanced control strategies extended to work for all operation regions and the use of a variable digital displacement pump is of interest.

ACKNOWLEDGMENT

This research was funded by the Danish Council for Strategic Research through the HyDrive project at Aalborg University, at the Department of Energy Technology (case no. 1305-00038B).

REFERENCES

[1] Wilkinson, M., 2011. "Measuring wind turbine reliability - results of the reliawind project". Scientific Track Proceedings, European Wind Energy Conference 2011, Brussels.

[2] Rampen, W. "Gearless transmissions of large wind turbines - the history and future of hydraulic drives". Artemis IP Ltd., Scotland.

[3] P. Silva, A. Giuffrida, E. M. G. G., December 2013. "Performance prediction of a multi-mw wind turbine adopting an advanced hydrostatic transmission". *Energy, Vol. 64, pp. 450 - 461*.

[4] M. Ehsan, W. R., and Salter, S., March 2000. "Modeling of digital-displacement pump-motors and their application as hydraulic drives for nonuniform loads". *ASME, Journal of dynamic system measurement and control, Vol. 122, pp. 210-215*.

[5] Taylor, S. S. J., and Caldwell, N., 2002. "Power conversion mechanisms for wave energy". *Proceedings of the Institution of Mechanical Engineers, Part M: Journal of Engineering for the Maritime Environment*.

[6] S. Payne, A. K., and Rampen, E., 2007. "Efficiency and dynamic performance of digital displacement hydraulic transmission in tidal current energy converters". *Journal of Power and Energy, Proc. IMechE, Vol. 221, Part A, pp. 207-218*.

[7] Mitsubishi Heavy Industries, L., 2013. Wind turbine generator and tidal current generator and operation method thereof, Patent: US20120104752 A1, 2012.

[8] Mitsubishi Heavy Industries, L., 2013. Power generating apparatus of renewable energy type and operation method thereof, Patent: US20130214537.

[9] Mitsubishi Heavy Industries, L., 2013. Power generating apparatus of renewable energy type and method of operating the same, Patent: US 20130307493 A1.

[10] Mitsubishi Heavy Industries, L., 2015. Hydraulic transmission, power generating apparatus of renewable energy type, and operation method thereof, Patent: EP 2899432 A2.

[11] M. Heikkila, M. L., 2013. "Displacement control of a mobile crane using digital hydraulic power management system". *Mechatronics 23, pp. 452 461*.

[12] B. S. R. Armstrong, Q. Y., June 2006. "Multi-level control of hydraulic gerotor motor and pumps". Proceedings of the 2006 American Control Conference Minneapolis, Minnesota.

[13] M. Suiegucki, M. G., and Klingauf, U., September 2013. "Optimal control of digital hydraulic drives using mixed-integer quadratic programming". 9th IFAC Symposium on Nonlinear Control Systems.

[14] P. Johansen, D. B. Roemer, H. C. P., and Andersen, T. O. "Delta-sigma modulated displacement of a digital fluid power pump". The Seventh Workshop on Digital Fluid Power, Linz, Austria.

[15] P. Johansen, D. B. Roemer, H. C. P., and Andersen, T. O., 2016. "Discrete linear time invariant analysis of digital fluid power pump flow control". *Journal of dynamic system measurement and control, ASME, accepted for publication*.

[16] J. M. Jonkman, S. Butterfield, W. M., and Scott, G., 2009. Definition of a 5-mw reference wind turbine for offshore system development.

[17] Johansen, P., 2014. "Tribodynamic modeling of digital fluid power motors". PhD thesis. Department of Energy Technology, Aalborg University.

[18] Roemer, D. B., 2014. "Design and optimization of fast switching valves for large scale digital hydraulic motors". PhD thesis. Department of Energy Technology, Aalborg University.

[19] A. J. Laguna, N. F. B. D., and van Wingerden, J. W., 2013. "Analysis of dynamics of fluid power drive-trains for variable speed wind turbines: parameter study". European Wind Energy Association.

[20] Wang, F., and Stelson, K. A. "Midsize wind turbines with hydraulic transmissions". Center for Compact and Efficient Fluid Power Department of Mechanical Engineering University of Minnesota, Minneapolis.

[21] Reiss, J. D., January/Februar 2008. "Understanding sigma-delta modulation: The solved and unsolved issues". *Journal Audio Engineering Society, Vol. 56, No. 1/2*.

Paper E

Optimal Control of a Wind Turbine with Digital Fluid Power Transmission

Niels H. Pedersen, Per Johansen and Torben O. Andersen

The paper has been published in
Nonlinear Dynamics, January 2018, Vol. 91, Iss. 1, pp. 591-607,
doi:10.1007/s11071-017-3896-0.

The layout has been revised.

Nonlinear Dyn
DOI 10.1007/s11071-017-3896-0

ORIGINAL PAPER

Optimal control of a wind turbine with digital fluid power transmission

Niels H. Pedersen · **Per Johansen** · **Torben O. Andersen**

Received: 1 September 2016 / Accepted: 21 October 2017

Abstract Digital fluid power (DFP) technology may lead to a paradigm shift in large-scale transmission systems in, e.g., wind and wave energy. Therefore, the development of applicable control algorithms is of major importance, but is complicated by the non-smooth behavior of the DFP displacement machines. The power throughput of a full stroke operated digital displacement machine is quantized by the number of pressure chambers. The dynamics of each pressure chamber may be described by highly nonlinear continuous differential equations, whereas the input is discretely updated and binary (active or inactive). This paper contributes with a feedback control strategy for a digital displacement machine, where the binary inputs are handled by a pulse density modulator. The paper presents a linearization method of handling the many nonlinearities and thereby enabling the use of Discrete Linear Time Invariant (DLTI) control theory. The control strategy is validated for control of a digital fluid power wind turbine transmission, where both a deterministic and a stochastic optimal controllers are synthesized. The study is based on the NREL 5-MW reference wind turbine, where its model is combined with a nonlinear model of the DFP transmission and full-field flow wind profiles are used for a realistic performance evaluation scenario. By simulation, it is found that the performance of the optimal controllers using the DFP transmission is similar to that of the NREL controller using a conventional transmission.

Keywords Optimal control · Wind turbine · Digital displacement · Fluid power · Hydrostatic transmission

1 Introduction

In recent years, the development of energy efficient fluid power systems is receiving an increasing interest, both with regard to conventional cylinder drives [18,48] and power take-off systems [32–34,36,45]. In this context, digital fluid power is a promising technology, due to high efficiency and superb scalability. Digital fluid power technology is characterized by the use of electrical actuated on/off valves. In order to enable this technology further, design optimization of these on/off valves is receiving a large amount of attention [40,41,43,47,55–59]. The use of digital valves entail challenges with respect to non-smooth dynamical behavior, which increases pressure oscillations [7–9] and complicates model-based feedback control development.

A research area within digital fluid power is the digital displacement technology®, which has a large potential in wind and wave energy transmission systems, since it benefits of being continuous variable and mechanical decoupled. The technology has, however, also been applied in various other fields, e.g. vehicle drive trains, suspensions and excavators [2,10,50,53].

N. H. Pedersen ( ) · P. Johansen · T. O. Andersen
Fluid Power and Mechatronic Systems, Department of Energy Technology, Aalborg University, Aalborg, Denmark
e-mail: nhp@et.aau.dk

Published online: 02 November 2017

Digital displacement machines are characterized by having a modular construction with numerous displacement chambers controlled by electrical actuated on/off valves. A comprehensive description of the digital displacement technology and development history is documented in several publications [22,33,37].

A significant amount of research has been conducted in the field of dynamic behavior and control of electro-hydraulic servo systems [6,46,60]. However, the non-smooth behavior of the digital displacement machine complicates dynamic system analysis and control development. So far control of digital displacement machines is mostly limited to small-scale applications in an open-loop configuration and often at simplified load conditions with fixed speed operation. Ehsan et al. [22] present a full stroke pressure and flow valve timing control method, where the chamber actuation decision is based on a displacement volume estimation. A look-ahead angle accounting for the response delay is included to improve the method. Using a similar control strategy, the displacement volume estimation method has been extended to include the oil compressibility by Heikkilä and Linjama [10]. Xubin [50] presents a five-level flow control strategy including both full and partial stroke operation, where the valve activation sequence is preprogrammed based on the flow requirement. Armstrong and Yuan [1] describes a multi-level control strategy for speed control of a digital fluid power motor. The outer control level consists of a velocity PI-controller, while the inner control level identifies the optimal cylinder actuation sequence, based on an estimate of the motor torque output using all the possible combination of active/inactive chambers. Johansen et al. [13] uses a full stroke delta-sigma modulation control strategy in a closed-loop configuration. The author also presents a flow control strategy using a discrete linear time invariant model-based design approach [14]. Sniegucki et al. [49] presents a torque control strategy using full stroke. The controller synthesis features a mixed logical dynamic system representation, which is used to setup a constrained optimization problem. Despite yielding improved steady-state accuracy and reduced torque ripples compared to pulse density modulation strategies, the method only allows for offline optimization.

The literature concerning digital fluid power transmissions for wind turbines is very limited and is mostly comprised by patents from Mitsubishi Heavy Industries Ltd. [25–30]. The documented control strategies are open-loop and based on estimation techniques, from where system stability and disturbance rejection ability is unknown.

In this work, a feedback control strategy for a wind turbine with a digital fluid power transmission is presented, since the digital displacement machines have a high potential for use in large-scale transmission systems. A delta-sigma pulse density modulator is used to determine the actuation sequence of the full stroke operated pressure chambers of the digital displacement motor. The discrete operation of the digital motor complicates a dynamic analysis of the system and the use of feedback control. Additionally, highly nonlinear effects are introduced by the stochastic wind speed and turbine characteristics, as well as the digital motor and pulse density modulator. Therefore, a linear approximation of the system equations is made, allowing for use of linear optimal feedback control.

2 System description

2.1 Turbine and transmission system

The digital fluid power transmission system for the wind turbine comprises a conventional fixed displacement pump, a high- and low-pressure line and a variable digital displacement motor as illustrated in Fig. 1.

The wind turbine model has the wind speed, v, and the blade pitching angle, β, as inputs and output the aerodynamic rotor torque, τ_r, driving a fixed displacement pump. The hydraulic pump outputs a pressurized fluid flow, Q_p, and the digital motor flow intake, Q_m, is controlled by the motor displacement fraction, α_m. The high-pressure motor fluid flow is further converted into a shaft rotation of the generator.

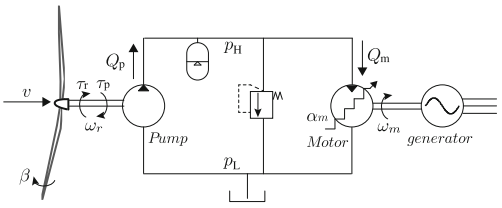

Fig. 1 Illustration of the digital fluid power transmission for a wind turbine

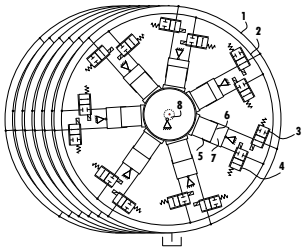

Fig. 2 Schematic of the digital displacement motor with 42 pressure chambers. The sketch is based on work by [49]

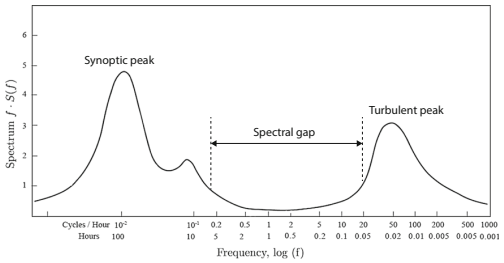

Fig. 3 Van der Hoven power spectrum of horizontal wind speeds [11]

With application control of a digital displacement unit being the main objective of this study, several simplifications to the system have been made. The hydraulic accumulator in the high-pressure line and the external boost system controlling the low pressure is omitted. Furthermore, it is assumed that the motor speed is constant since an ideal synchronous generator is considered. A digital displacement pump could be used for more advanced control strategies than the one presented, but is for simplicity not considered in this study.

2.2 Digital displacement motor

The digital displacement motor is a radial piston type, where the design under consideration consists of 6 modules with 7 cylinders in each module. An actively controlled high- and low-pressure digital valve (HPV and LPV) controls the flow throughput between the cylinder chamber and the high- and low-pressure line, respectively. A reciprocating piston motion is generated by the pressurized fluid flow and takes place since each piston is connected to a common eccentric shaft. A simplified illustration of the digital displacement motor is shown in Fig. 2.

In a full stroke operation, each displacement chamber is either using an idling (Inactive) or a motoring (Active) stroke during a shaft revolution. In an idling stroke, the HPV is kept closed and the LPV is kept open during the full revolution, resulting in a low chamber pressure and thus no work. During a motoring stroke, the low-pressure valve is closed and the high-pressure valve is opened during the intake part of the stroke, where high-pressure fluid flow enters the pressure chamber and drives the motor shaft. The displacement fraction input, α_{m}, is hence the fraction of activated cylinders and thus determines the amount of pressurized fluid flow used to drive the motor shaft. A pumping stroke is not considered in this work, since the motor displacement reference is positive during normal operation.

3 Mathematical modeling

The system model comprises a turbulent wind model, a simplified model of the turbine main dynamics and aerodynamic efficiency, as well as a model of the hydrostatic transmission, including the digital fluid power motor.

3.1 Turbulent wind model

Full-field flow time-series data of the wind speed are given as input to the turbine model. The data are generated by use of the open-source software TurbSim by NREL [15,16], where the IEC 61400-1 normal turbulence model and Kaimal turbulence spectrum are utilized. A low turbulence intensity of 12 % is arbitrary chosen since offshore operation at no specific site is considered.

To include the stochastic wind disturbance effect in the control design, a nonlinear model of the turbulence wind speed is presented. The wind speed may be divided into two distinct components given as

$$v(t) = \bar{v} + \Delta v(t) \tag{1}$$

where $\bar{v}$ is the slowly varying mean wind speed and $\Delta v(t)$ is the rapidly varying turbulent component being a stochastic process. These two distinct components may also be viewed on the Van der Hoven power spectrum shown in Fig. 3.

For time-series data of the wind speed of less than 10 minutes, the synoptic peak corresponding to the macro-meteorology mean wind speed may be treated as constant. The analytical Kaimal power spectrum model is used to describe the turbulent part and is given by Eq. (2). The model is provided in accordance with the IEC 61400-1 standard [3], and is a modification of the spectrum originally presented by Kaimal et al. [19].

$$\mathcal{S}(f) = \frac{4\,\sigma_{\mathrm{u}}^2\,\frac{L_{\mathrm{u}}}{\bar{v}}}{\left(1+6\,\frac{L_{\mathrm{u}}}{\bar{v}}\,f\right)^{5/3}} \tag{2}$$

where σ_{u} and L_{u} are the standard deviation and scale parameter, respectively, and are specified in IEC 61400-1 [3] as functions of the turbulence intensity. For a 12 % turbulence intensity $\sigma_{\mathrm{u}} = 1.94$ and $L_{\mathrm{u}} = 340.2$. In this study, a mean wind speed of $\bar{v} = 8$ m/s has been chosen since it corresponds to approximately the midpoint of operation region II, where the transmission is used to control the extracted wind energy (An elaboration of this is documented in Sect. 4).

3.2 Wind turbine model

The wind turbine considered in this study is the National Renewable Energy Laboratory (NREL) 5-MW reference turbine. Its model is combined with the dynamical model of the digital fluid power transmission through the use of a MATLAB/Simulink interface. The dynamics and aero-elastic effects of the wind turbine are simulated by use of the open-source program FAST (Fatigue, Aerodynamics, Structures and Turbulence program) [17], which model is based on the blade element momentum theory. For control purpose, a simplified nonlinear model is derived for the main turbine dynamics. Additionally, a static description of the aerodynamic power P_{r} and torque τ_{r} is used and is given by Eqs. (3) and (4), respectively.

$$P_{\mathrm{r}} = \frac{1}{2}\,A_{\mathrm{r}}\,\rho_{\mathrm{air}}\,C_{\mathrm{p}}\,(\lambda,\beta)\;v^3 \tag{3}$$

$$\tau_{\mathrm{r}} = \frac{1}{2}\,A_{\mathrm{r}}\,R_{\mathrm{r}}\,\rho_{\mathrm{air}}\,C_{\mathrm{q}}\,(\lambda,\beta)\;v^2 \tag{4}$$

where A_{r} and R_{r} describe the rotor swept area and radius, respectively, and ρ_{air} is the air density. $C_{\mathrm{p}}\,(\lambda,\beta)$ and $C_{\mathrm{q}}\,(\lambda,\beta)$ are the turbine specific power and torque coefficient, which are nonlinear functions with respect to the tip-speed ratio, λ, and blade pitch angle, β. The tip-speed ratio is defined in Eq. (5) and describes the ratio between the tip-speed of the blades and the wind speed.

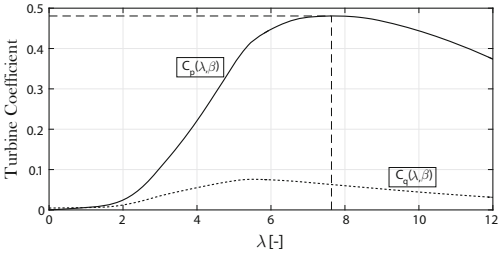

Fig. 4 Power and torque coefficient as a function of tip-speed ratio at the maximum power pitching angle for the NREL 5 MW turbine

$$\lambda = \frac{\omega_r\,R_r}{v} \tag{5}$$

The nonlinear turbine coefficients C_{p} and C_{q} are used actively for optimal power control of the turbine. A plot of the turbine coefficients as a function of the tip-speed ratio at the maximum power pitch angle is shown in Fig. 4.

The maximum power coefficient is identified to be $C_{\mathrm{p}}^* = 0.485$ and occurs at a tip-speed ratio of $\lambda^* = 7.55$. This information is used in the control structure described later in Sect. 4 to maximize the power capture below rated wind speed.

A simplified model of the turbine dynamics is derived to be that given by

$$\dot{\omega}_{\mathrm{r}} = \frac{1}{J_{\mathrm{r}}}\left(\tau_{\mathrm{r}} - d_{\mathrm{r}}\,\omega_{\mathrm{r}} - \underbrace{\frac{\bar{V}_{\mathrm{p}}\,\Delta p}{\eta_{\mathrm{p}}}}_{\tau_{\mathrm{p}}}\right) \tag{6}$$

where J_{r} describes the combined mass moment of inertia of the turbine rotor consisting of the blades, shaft and hub. d_{r} is the viscous friction coefficient of the rotor shaft, $\bar{V}_{\mathrm{p}}$ is the pump displacement volume per radians and η_{p} is the mechanical efficiency coefficient, which includes the static friction of the shaft.

Table 1 Parameters of the NREL 5 MW

Parameter	Symbol	Value	Unit
Cut-in wind speed	v_{in}	4	m/s
Rated wind speed	v_{r}	11.4	m/s
Cut-out wind speed	v_{out}	25	m/s
Air density	ρ_{air}	1.225	kg/m^3
Blade radius	R_{r}	63	m
Rotor swept area	A_{r}	12469	m^2
Tower height	h_{t}	90	m
Rated rotor speed	$\omega_{\text{r-nom}}$	12.13	rpm
Rotor and shaft inertia	J_{r}	3.87e7	kg m^2
Viscous friction	d_{r}	50e3	N m s /rad
Optimal tip-speed ratio	λ^*	7.55	–
Maximum power coefficient	C_{p}^*	0.485	–

The main parameters of the NREL 5-MW wind turbine are provided in Table 1.

3.3 Hydrostatic transmission model

The low-pressure line is simplified to be constant, since it may be externally controlled by a boost pump circuit. Defining the pressure difference as $\Delta p = p_{\text{H}} - p_{\text{L}}$, its dynamics is described by

$$\dot{\Delta}_{\text{p}} = \frac{\beta_{\text{e}}}{V_{\text{H}}} \left(\underbrace{\bar{V}_{\text{p}}\, \omega_{\text{r}}}_{Q_{\text{p}}} - Q_{\text{m}} - k_{\text{l}}\, \Delta_{\text{p}} \right) \tag{7}$$

where β_{e} is the effective oil bulk modulus, V_{H} is the volume of the high-pressure line and k_{l} is the leakage coefficient between the high- and low-pressure lines.

3.4 Digital displacement motor

The utilized mathematical model of the digital machine is inspired by Roemer [39] and is based on the schematic of a single cylinder chamber shown in Fig. 5.

V_c is the chamber volume and A_{p} is the piston area. The piston displacement x_{p} as a function of the shaft rotation angle θ is described by Eq. (8), where r_{e} is the eccentric radius.

$$x_{\text{p}}(\theta) = r_{\text{e}}\ (1 - \cos\theta) \tag{8}$$

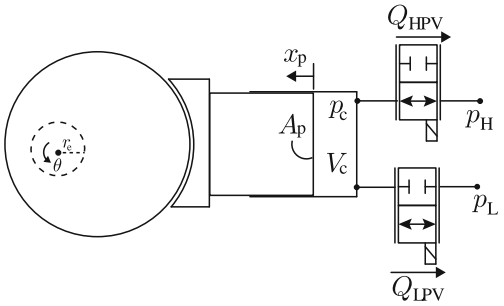

Fig. 5 Schematic of a single pressure chamber with definition of model variables

With the piston displacement volume described by $V_{\text{d}} = 2\, r_{\text{e}}\, A_{\text{p}}$, the chamber volume and its time derivative is given as

$$V_{\text{c}}(\theta) = \frac{V_{\text{d}}}{2}\ (1 - \cos\theta) + V_0 \quad \dot{V}_{\text{c}}(\theta) = \frac{V_{\text{d}}}{2}\ \dot{\theta}\ \sin\theta \tag{9}$$

where V_0 is the minimum chamber volume. Applying the continuity equation to the pressure chamber, its pressure p_{c} is described by

$$\dot{p}_{\text{c}} = \frac{\beta_{\text{e}}}{V_{\text{c}}} \left(Q_{\text{HPV}} - Q_{\text{LPV}} - \dot{V}_{\text{c}} \right) \tag{10}$$

By use of the orifice equation, the flow through the high- and low-pressure valves (Q_{HPV} and Q_{LPV}) are expressed as

Table 2 Parameters of the hydrostatic transmission

Parameter	Symbol	Value	Unit
Pump mechanical efficiency	η_p	0.95	–
Fixed pump displacement	$\bar{V}_\mathrm{p}$	121.88	L/rad
Pipeline length	l_p	10	m
Pipeline internal diameter	d_p	100	mm
Transmission line volume	V_H	78.54	L
Effective bulk modulus	β_e	16000	bar
Transmission leakage coefficient	k_l	0.1	L/bar
Low pressure	p_L	5	bar
Synchronous motor speed	ω_m	1500	rpm
Motor piston area	A_p	79	cm^2
Motor eccentric radius	r_e	37.5	mm
Motor displacement volume	V_d	498.57	cm^3
Chamber flow coefficient	k_f	$0.5 \cdot 10^5$	$\sqrt{pa}\, s/\mathrm{m}^3$
Valve actuation time	t_s	1	ms
HPV closing angle	$\theta_\mathrm{H\text{-}cl}$	148.2	deg
LPV closing angle	$\theta_\mathrm{L\text{-}cl}$	334.7	deg
Nominal pressure	Δp_nom	350	bar
Nominal rotor torque	$\tau_\mathrm{r\text{-}nom}$	4.25	MN m

$$
\begin{aligned}
Q_\mathrm{HPV} &= \frac{\bar{x}_\mathrm{H}}{k_\mathrm{f}} \sqrt{|p_\mathrm{H} - p_\mathrm{c}|}\, \mathrm{sign}\,(p_\mathrm{H} - p_\mathrm{c}) \\
Q_\mathrm{LPV} &= \frac{\bar{x}_\mathrm{L}}{k_\mathrm{f}} \sqrt{|p_\mathrm{c} - p_\mathrm{L}|}\, \mathrm{sign}\,(p_\mathrm{c} - p_\mathrm{L})
\end{aligned}
\tag{11}
$$

where $\bar{x}_\mathrm{H}$ and $\bar{x}_\mathrm{L}$ are normalized valve plunger positions of the high- and low-pressure valve, respectively, and k_f is the valve flow coefficient. The valve dynamics is simplified to be described as a constant plunger acceleration given in Eq. (12) for valve opening. The constant acceleration approximation omits the dynamic description of the actuation and fluid forces, as well as the stiction effects [31,42,44], which entail impractical and long simulation durations.

$$
a_{\mathrm{v}+} = \begin{cases} 4/t_\mathrm{s}^2 & for \quad 0 \le t \le t_\mathrm{s}/2 \\ -4/t_\mathrm{s}^2 & for \quad t_\mathrm{s}/2 \le t \le t_\mathrm{s} \end{cases}
\tag{12}
$$

where t_s is the valve opening/closing time. The constant acceleration results in a smooth plunger position with a maximum velocity at the midpoint between fully closed and open. The valve closing is similar described as $a_{\mathrm{v}-} = -a_{\mathrm{v}+}$.

The motor flow intake Q_m is the sum of flows through each individual high-pressure valve given by

$$
Q_\mathrm{m} = \sum_{i=1}^{N} Q_\mathrm{HPV}(i)
\tag{13}
$$

where $N = 42$ is the number of pressure chambers. The parameter values used in the mathematical model of the hydrostatic transmission are provided in Table 2.

3.5 DDM operation strategy and simulation results

The digital valves are controlled by actively closing them at an angle of $\theta_\mathrm{H\text{-}cl}$ and $\theta_\mathrm{L\text{-}cl}$ for the high- and low-pressure valve, respectively. Passive valve opening is utilized where the high-pressure valve is opened due to pressure force when $p_\mathrm{c} > p_\mathrm{H}$ and the low-pressure valve is opened due to suction when $p_\mathrm{c} < p_\mathrm{L}$. Simulation results of a pressure chamber for a motoring and an idling stroke are shown in Fig. 6 For the idling stroke, the high-pressure valve is kept closed and the low pressure valve is kept open during a full revolution, resulting in no chamber pressurization. For the

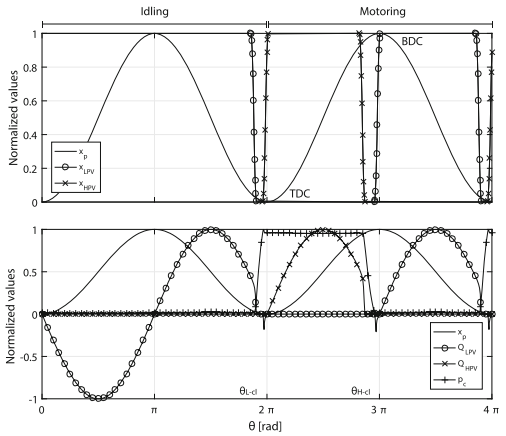

Fig. 6 Simulation results for a single pressure chamber

motoring stroke, the low-pressure valve is closed at $\theta_{\text{L-cl}}$ near top dead center (TDC), resulting in a pressure build up, followed by a passive opening of the high-pressure valve. A backflow into the high-pressure line is created momentarily due to the chamber pressure exceeding the high pressure. During the intake stroke part, high-pressure oil is entering the pressure chamber and thereby driving the piston and eccentric. Near bottom dead center (BDC) at $\theta_{\text{H-cl}}$, the high-pressure valve is actively closed causing a de-pressurization due to piston extension. This further results in a passive opening of the low-pressure valve due to suction.

Since the pressure chamber dynamics is very fast compared to that of the wind turbine, the pressure chamber model has been solved for various high pressures and the results has been implemented in a look-up table for a significantly reduction is simulation time.

4 Wind turbine operation and control objectives

The conventional operation strategy for a variable-speed variable-pitch wind turbine is divided into four regions dependent on the wind speed. In this paper, the turbine control has been limited to region II between cut-in wind speed, v_{in}, and rated wind speed, v_{r}, since the turbine is solely controlled by the transmission system in this region. Therefore, the pitching system and control of it is not investigated in the presented work.

4.1 Region II control

In the outer turbine control level, the popular $k\,\omega^2$ control law is used, which yield a good compromise between maximum power capture and rotor torque fluctuations. It is found in Fig. 4 that the maximum power capture is obtained by maintaining the optimal tip-speed ratio, λ^*, yielding the maximum power coefficient C_{p}^*. Combining this information with the static rotor torque equation in Eq. (4) and the fact that $C_{\text{p}}(\lambda,\beta) = \lambda\, C_{\text{q}}(\lambda,\beta)$, the $k\,\omega^2$ control law is derived to be that given by

$$\begin{aligned} \tau_{\text{r}} &= \frac{1}{2}\, A_{\text{r}}\, R_{\text{r}}\, \rho_{\text{air}}\, \frac{C_{\text{p}}(\lambda,\beta)}{\lambda} \left(\frac{R_{\text{r}}\,\omega_{\text{r}}}{\lambda}\right)^2 \\ \tau_{\text{r}}^* &= \underbrace{\frac{1}{2}\, A_{\text{r}}\, R_{\text{r}}^3\, \rho_{\text{air}}\, \frac{C_{\text{p}}^*}{\lambda^{*3}}}_{K_2}\, \omega_{\text{r}}^2 \end{aligned} \tag{14}$$

The rotor torque reference τ_{r}^* is thus only a function of the rotor speed ω_{r}, why the high-frequency wind speed fluctuations are filtered away in the control law, at the cost of a minor reduction in optimal tip-speed ratio tracking. Since the rotor torque in this study is controlled by the DFP transmission, the rotor torque reference is converted into a difference pressure reference by static use of Eq. (6) resulting in

$$\Delta_{\text{p}}^* = \left(\tau_{\text{r}}^* - d_{\text{r}}\,\omega_{\text{r}}\right)\, \frac{\eta_{\text{p}}}{\bar{V}_{\text{p}}} \tag{15}$$

4.2 Wind turbine control structure

The proposed control structure takes basis in the objective of accurately controlling the difference pressure, Δ_{p}, by the motor displacement fraction, α_{m}, using a full stroke operation strategy and state feedback. The proposed feedback control strategy is shown in Fig. 7 and is similar to that applied for a conventional fluid power wind turbine transmission by various authors [5,21,54].

A pressure controller is seen to act on the pressure reference, Δ_{p}^*, based on the measured states, Δ_{p} and ω_{r} and output a motor displacement fraction reference α_{m}^* being between 0 and 1. The displacement reference is converted into a pressure chamber activation sequence by a delta-sigma pulse density modulator, determine whether the current cylinder chamber should use a

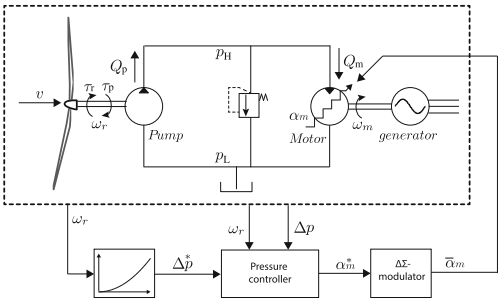

Fig. 7 Control structure for hydrostatic wind turbine transmission

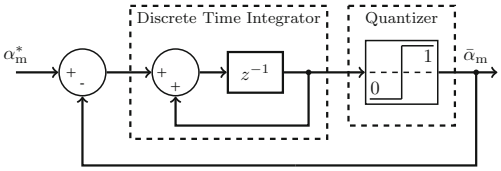

Fig. 8 First-order delta sigma Modulation block diagram

motoring or an idling stroke as proposed by Johansen et al. [13]. The chamber activation sequence $\bar{\alpha}_m$ is thus a binary signal, which time average output is equal to the displacement fraction reference.

The decision to either use a motoring (Active) or an idling (Inactive) stroke is performed once every revolution for each cylinder. As a consequence, the system nature implies use of discrete control. The discrete sampling time, T_s, is therefore dependent on the motor rotation speed and the number of cylinders given as

$$T_s = \frac{2\pi}{\omega_m N} \tag{16}$$

where $\omega_m = \dot{\theta}$ is the motor rotational speed, such that $T_s = 0.952$ ms for $\omega_r = 1500$ rpm. This corresponds to a decision for every $\theta_s = 2\pi/N = 8.6°$ of shaft angle rotation.

4.3 Delta-sigma modulator

A discrete first-order DSM is utilized in this study, but theoretically any 1 bit analog-to-digital converter may be used. A block diagram representation of the discrete first-order DSM is shown in Fig. 8.

The modulator consists of a discrete time integrator and a quantizer in a feedback structure. The integrator is hence acting on the displacement fraction error and thereby yielding a time average approximation of the input. As a result, the quantizer of the modulator introduces an additional high nonlinearity to the control system.

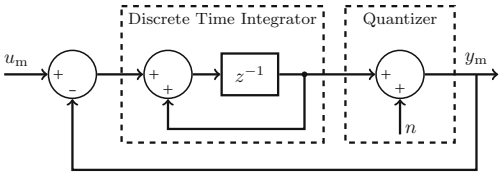

Fig. 9 Linear representation of delta sigma Modulator

5 Linear model approximation

It is evident that the system comprises a number of severe nonlinearities and stochastic disturbance effects. Stochastic optimal control of nonlinear systems is a mature field with numerous applications [12,24,51]. Both continuous and discrete stochastic linear optimal control has been successfully applied for control of variable-speed wind turbines [20,23,35]. On this basis, linear optimal control is the strategy of choice in present study. However, the use of optimal linear control of digital displacement machines is a new field and is unconventional since most of the states are binary, which becomes evident in the following section. In consequence, a linear approximation of the system nonlinearities is derived and used to set up a state model describing the system dynamics.

5.1 Delta-sigma modulator

The modulator may be considered linearly by assuming the quantizer as an additive noise input n as illustrated in Fig. 9.

The noise input is hence a time varying value between $\pm$ 0.5 describing the discretization error. A linear transfer function representation of the modulator is derived to be that given as

$$\begin{aligned} Y_m(z) &= \frac{1}{z} U_m(z) + \frac{z-1}{z} N(z) \\ y_m(k) &= u_m(k-1) + n(k) - n(k-1) \end{aligned} \tag{17}$$

The output of the linear representation of the first-order DSM is hence a single sampled delayed input together with the noise input discrete differentiated.

The quantization error noise $n(k)$ may be described as a white noise source with intensity Q_m in accordance with Reiss et al. [38]. For a one bit quantizer, the discretization step size is $q = 1$, resulting in the quantization error span $-\frac{q}{2} \leq e_\mathrm{q} \leq -\frac{q}{2}$. The noise error may be assumed to be statistically described by a uniform distribution function with mean error $\bar{e}_\mathrm{q} = 0$. The noise power is then identified by investigating the quantizer error variance determined by

$$\sigma_\mathrm{e}^2 = E\{\left(e_\mathrm{q} - \bar{e}_\mathrm{q}\right)^2\} = \frac{1}{q}\int_{-q/2}^{q/2} e_\mathrm{q}^2 de_\mathrm{q} = \frac{q^2}{12} \tag{18}$$

Since the quantizer disturbance is to be described with a white noise input, the power spectral density of it is also uniformly distributed across the frequency range of the Nyquist band. The power spectral density function of the quantization noise then becomes

$$\Phi_\mathrm{e}(f) = \frac{\sigma_\mathrm{e}^2}{f_\mathrm{s}} = Q_\mathrm{d} \tag{19}$$

where $f_\mathrm{s} = 1050\,\mathrm{Hz}$ is the sampling frequency. The error noise filter is therefore given by $n(k) = \sqrt{Q_\mathrm{d}}\, w_2(k)$, where $w_2(k)$ is a white noise input having unity intensity. Inserting this expression into the linear discrete modulator model given in Eq. (17) yields

$$y_\mathrm{m}(k) = u_\mathrm{m}(k-1) + \sqrt{Q_\mathrm{d}}\, w_2(k) - \sqrt{Q_\mathrm{d}}\, w_2(k-1) \tag{20}$$

In conventional stochastic optimal control, it is assumed that the disturbance is Gaussian white noise having a normal distribution. Despite the modulator noise having a uniform distribution function, the estimator to be designed is still the optimal linear one [4].

5.2 Digital fluid power motor

The non-smooth behavior of the digital fluid power flow dynamics complicates the construction of a linear approximation by the conventional first-order Taylor series expansion method. Alternatively, in this study an approach based on a direct discrete linear approximation of the continuous non-smooth motor dynamics is used to overcome this difficulty. The model is derived by approximating each motor flow between samples by

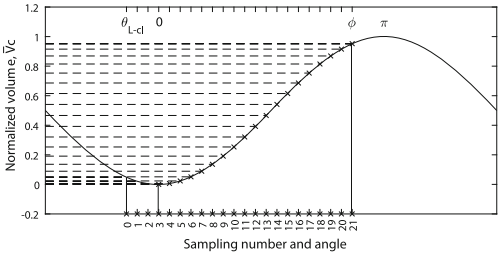

Fig. 10 Illustration of motor displacement fraction output as a function of sampling number

Eq. (21) and thereby neglecting the transient pressure dependency.

$$\begin{aligned} Q_\mathrm{HPV} &\approx \frac{dV_\mathrm{c}(\theta(t))}{dt} \\ Q_\mathrm{HPV}[k] &\approx \frac{V_\mathrm{d}}{T_\mathrm{s}}\left(\bar{V}_\mathrm{c}(\theta[k+1]) - \bar{V}_\mathrm{c}(\theta[k])\right) = \frac{V_\mathrm{d}}{T_\mathrm{s}}\,\Delta\bar{V}_\mathrm{c}[k] \end{aligned} \tag{21}$$

where $\bar{V}_\mathrm{c}$ is the normalized displacement volume. The discrete motor model is derived based on Fig. 10, showing the normalized displacement volume as a function of sampling number and shaft angle.

With 42 pressure chambers, a full motoring stroke ideally last for 21 samples between $0 \leq \theta \leq \pi$. Due to valve actuation dynamics, $\theta_\mathrm{L\text{-}CL}$ is located ahead of this and two delay samples are introduced such that motoring starts just before sample $k = 3$. Sample $k = 0$ is the chamber activation decision sample and thus lies at $\theta_\mathrm{L\text{-}CL}$.

Since the HPV must be closed in time for the LPV to be fully open at $\theta = \pi$, it is not possible to utilize a full motoring stroke. ϕ indicates the angle where the high-pressure valve is half way closed, which is the midpoint angle between $\theta_\mathrm{H\text{-}CL}$ and the angle where the valve becomes fully closed. ϕ should hence correspond to the best discrete estimate of when motoring stops.

The motor displacement fraction, α_m, is described by a sum of displacement fractions between samples during motoring based on the convolution sum method presented by Johansen et al. [14] and is given in Eq. (22). Also, an expression for the approximated motor flow is provided.

$$\alpha_\mathrm{m}[k] = \sum_{m=0}^{k} \Delta\bar{V}_\mathrm{c}[k-m]\,\bar{\alpha}_\mathrm{m}[m]$$

$$Q_{\mathrm{m}}[k] = \underbrace{\frac{V_{\mathrm{d}}}{T_{\mathrm{s}}}}_{k_{\mathrm{q}}} \alpha_{\mathrm{m}}[k] \tag{22}$$

where the displacement fractions are calculated by Eq. (23), which may be validated from Fig. 10.

$$\Delta\bar{V}_{\mathrm{c}}[k] = \begin{cases} 0 & \theta[k], \theta[k+1] \notin [0\,;\phi] \\ \bar{V}_{\mathrm{c}}(\theta[k+1]) - \bar{V}_{\mathrm{c}}(\theta[k]) & \theta[k], \theta[k+1] \in [0\,;\phi] \\ \bar{V}_{\mathrm{c}}(\theta[k+1]) - \bar{V}_{\mathrm{c}}(0) & \theta[k] < 0 < \theta[k+1] \\ \bar{V}_{\mathrm{c}}(\phi) - \bar{V}_{\mathrm{c}}(\theta[k]) & \theta[k] < \phi < \theta[k+1] \end{cases} \tag{23}$$

It is seen that the displacement fraction is 0 outside the interval $\theta = [0\,;\phi]$, resulting in it being 0 outside the sampling interval $k = [2\,;20]$.

A comparison of the digital motor flow described by the discrete linear approximation model and the nonlinear dynamic model is shown in Fig. 11.

The discrete linear model approximation is seen to have a great accuracy, with the exception that it does not include valve and pressure dynamics, why the backflow is not seen. Due to the fairly high accuracy in the majority of the motor stroke, the linear approximation is considered validated and used to describe the digital motor flow when designing controllers.

5.3 Turbulent wind model

The turbulence wind speed is modeled as a linear filter with white noise input given by $v(t) = H_{\mathrm{v}}(t)\, w_1(t)$, where the white noise has intensity Π_{v}. The power spectrum of the output $v(t)$ of the linear model is given by Eq. (24).

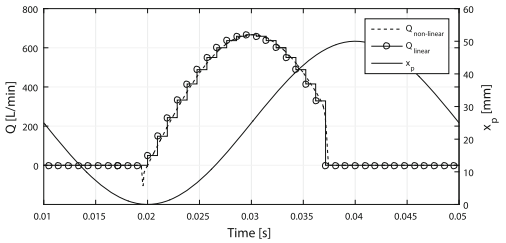

Fig. 11 Comparison of the linear and nonlinear model of the digital motor flow

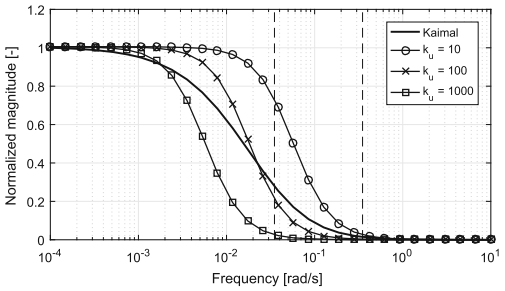

Fig. 12 Normalized magnitude of the Kaimal spectrum and approximations. (Dashed lines indicates desired frequency band)

$$\Phi_{\mathrm{v}}(\omega) = H_{\mathrm{v}}(j\,\omega)\, \Pi_{\mathrm{v}}\, H_{\mathrm{v}}(-j\,\omega) \tag{24}$$

A linear approximation of the power spectrum is thus necessary and is derived to be that in Eq. (25), based on the approach described by Vepa [52].

$$\Phi_{\mathrm{v}}(\omega) = \frac{4\,\sigma_{\mathrm{u}}^2\,\frac{L_{\mathrm{u}}}{\bar{v}}}{\left(1 + 6\,\frac{L_{\mathrm{u}}}{2\,\pi\,\bar{v}}\,\omega\right)^{5/3}} \approx \frac{4\,\sigma_{\mathrm{u}}^2\,\frac{L_{\mathrm{u}}}{\bar{v}}}{\left(1 + k_{\mathrm{u}}\left(\frac{\omega}{\omega_{\mathrm{c}}}\right)^2\right)} \tag{25}$$

where $\omega_{\mathrm{c}} = 2\pi\,\bar{v}/L_{\mathrm{u}}$ and k_{u} is a frequency factor specifying at which frequency the approximation is most accurate. From the Van der Hoven frequency spectrum of the wind shown in Fig. 3, it is identified that the turbulent peak has a frequency band between 20 and 200 cycles/hour, corresponding to $0.035 \leq \omega \leq 0.35$ rad/s. The optimal frequency factor is determined from the semi-logarithmic plot of the normalized power spectrum function shown in Fig. 12.

A reasonable approximation for the desired frequency band is found for $k_{\mathrm{u}} = 100$. By using Eq. (24) and Eq. (25), it is derived that the state representation of the linear filter is given by Eq. (26) when the white noise input has unity intensity.

$$\dot{v} = \underbrace{-\frac{\omega_{\mathrm{c}}}{\sqrt{k_{\mathrm{u}}}}}_{a_v}\, v + \underbrace{2\,\omega_{\mathrm{c}}\,\sigma_{\mathrm{u}}\sqrt{\frac{L_{\mathrm{u}}}{k_{\mathrm{u}}\,\bar{v}}}}_{b_v}\, w_1 \tag{26}$$

5.4 Aerodynamic rotor torque

A linear approximation by first-order Taylor expansion of the aerodynamic rotor torque is derived to be that given as

$$\begin{aligned}
\delta\tau_\mathrm{r} &= \underbrace{\left(\frac{d\tau_\mathrm{r}}{dv}\left(\frac{1}{2}\,A_\mathrm{r}\,R_\mathrm{r}\,\rho_\mathrm{air}\,C_\mathrm{q}\,(\lambda,\beta)\;v^2\right)|_{v=\bar{v},\lambda=\lambda^*,\beta=0}\right)}_{k_{\tau v}}\,\delta v \\
k_{\tau v} &= A_\mathrm{r}\,R_\mathrm{r}\,\rho_\mathrm{air}\,C_\mathrm{q}(\lambda^*,0)\,\bar{v} \\
\delta\tau_\mathrm{r} &= k_{\tau v}\,\delta v \longrightarrow \delta v = k_{\tau v}^{-1}\,\delta\tau_\mathrm{r}
\end{aligned} \tag{27}$$

By combining Eqs. (26) and (27), the linear model of the rotor torque described as filtered white noise is given as

$$\dot{\tau}_\mathrm{r} = -a_v\,\tau_\mathrm{r} + k_{\tau v}\,b_v\,w_1 \tag{28}$$

6 State model representation

To allow for discrete optimal control, a discrete state representation of the system dynamical equations is required. Therefore, the continuous transmission and turbine model is initially discretized and afterward combined with the discrete motor and modulator models.

6.1 State-space representation

The linear continuous state-space representation of the turbine and transmission dynamics is given in Eq. (29) and is obtained by combining Eqs. (6), (7) and (28).

$$\begin{aligned}
\underbrace{\begin{bmatrix}\dot{\omega}_\mathrm{r}\\ \dot{\Delta}_\mathrm{p}\\ \dot{\tau}_\mathrm{r}\end{bmatrix}}_{\dot{\mathbf{x}}(t)} &= \underbrace{\begin{bmatrix} -\frac{d_\mathrm{r}}{J_\mathrm{r}} & -\frac{\bar{V}_\mathrm{p}}{J_\mathrm{r}\eta_\mathrm{p}} & \frac{1}{J_\mathrm{r}} \\ \frac{\beta_\mathrm{e}}{V_\mathrm{H}}\,\bar{V}_\mathrm{p} & -\frac{\beta_\mathrm{e}}{V_\mathrm{H}}\,k_\mathrm{l} & 0 \\ 0 & 0 & -a_v \end{bmatrix}}_{\mathbf{A}} \underbrace{\begin{bmatrix}\omega_\mathrm{r}\\ \Delta_\mathrm{p}\\ \tau_\mathrm{r}\end{bmatrix}}_{\mathbf{x}(t)} + \underbrace{\begin{bmatrix}0\\ -\frac{\beta_\mathrm{e}}{V_\mathrm{H}}\\ 0\end{bmatrix}}_{\mathbf{B}} \underbrace{Q_\mathrm{m}}_{u(t)} + \underbrace{\begin{bmatrix}0\\ 0\\ k_{\tau v}\,b_v\end{bmatrix}}_{\mathbf{G}} w_1(t) \\
\mathbf{y}(t) &= \underbrace{\begin{bmatrix}1&0&0\\ 0&1&0\end{bmatrix}}_{\mathbf{C}}\,\mathbf{x}(t)
\end{aligned} \tag{29}$$

To ease the controller design in the following section, the plant has been normalized by the diagonal matrix $\mathbf{H} = \mathrm{diag}\left\{\left[\omega_\text{r-nom}\;\Delta p_\text{nom}\;\tau_\text{r-nom}\right]\right\}$ containing the nominal/rated state values.

A discretization of the continuous model is performed to allow for discrete control. In the discretization approach, a zero-order hold input to the continuous plant is assumed, although the motor flow truly is time varying between samples. This approximation is, however, justified by the relative high number of cylinders. The discrete state-space representation of the transmission and turbine model is given by

$$\begin{aligned}
\mathbf{x}(k+1) &= \mathbf{A}_\mathrm{p}\,\mathbf{x}(k) + \mathbf{B}_\mathrm{p}\,u(k) + \mathbf{G}_\mathrm{p}\,w_1(k) \\
\mathbf{y}(k) &= \mathbf{C}_\mathrm{p}\,\mathbf{x}(k) \\
\mathbf{A}_\mathrm{p} &= e^{\mathbf{A}\,T} \quad \mathbf{B}_\mathrm{p} = \mathbf{A}^{-1}\left(e^{\mathbf{A}\,T} - \mathbf{I}\right)\mathbf{B} \\
\mathbf{C}_\mathrm{p} &= \mathbf{C} \quad \mathbf{G}_\mathrm{p} = \mathbf{A}^{-1}\left(\mathbf{A}_\mathrm{p} - \mathbf{I}\right)\mathbf{G}
\end{aligned} \tag{30}$$

The discrete convolution sum model of the digital motor derived in Eq. (22) is rewritten into state space form resulting in

$$\begin{aligned}
\underbrace{\begin{bmatrix} u_\mathrm{d}(k) \\ u_\mathrm{d}(k-1) \\ u_\mathrm{d}(k-2) \\ \vdots \\ u_\mathrm{d}(k-p+1) \end{bmatrix}}_{\mathbf{x}_\mathrm{d}(k+1)} &= \underbrace{\begin{bmatrix} 0 & 0 & \cdots & 0 & 0 \\ 1 & 0 & \cdots & 0 & 0 \\ 0 & 1 & \cdots & 0 & 0 \\ \vdots & \vdots & \ddots & \vdots & \vdots \\ 0 & 0 & \cdots & 1 & 0 \end{bmatrix}}_{\mathbf{A}_\mathrm{d}} \underbrace{\begin{bmatrix} u_\mathrm{d}(k-1) \\ u_\mathrm{d}(k-2) \\ u_\mathrm{d}(k-3) \\ \vdots \\ u_\mathrm{d}(k-p) \end{bmatrix}}_{\mathbf{x}_\mathrm{d}(k)} + \underbrace{\begin{bmatrix}1\\0\\0\\ \vdots \\ 0\end{bmatrix}}_{\mathbf{B}_\mathrm{d}} u_\mathrm{d}(k) \\
y_\mathrm{d}(k) &= \underbrace{k_\mathrm{q}\left[\Delta\bar{V}_\mathrm{c}[1]\;\Delta\bar{V}_\mathrm{c}[2]\;\Delta\bar{V}_\mathrm{c}[3]\;\cdots\;\Delta\bar{V}_\mathrm{c}[p]\right]}_{\mathbf{C}_\mathrm{d}}\,x_\mathrm{d}(k) \\
&+ \underbrace{k_\mathrm{q}\left[\Delta\bar{V}_\mathrm{c}[0]\right]}_{\mathbf{D}_\mathrm{m}}\,u_\mathrm{d}(k)
\end{aligned} \tag{31}$$

$p = 20$ indicates the last sampling instance with a displacement fraction $\Delta\bar{V}_\mathrm{c} \neq 0$. Also it should be noticed that $\Delta\bar{V}_\mathrm{c}[0] = \mathbf{D}_\mathrm{m} = 0$, why no direct input/output coupling is present.

By use of the discrete modulator representation in Eq. (20), the discrete modulator state model becomes

$$\begin{aligned}
x_\mathrm{m}(k+1) &= \underbrace{[0]}_{A_\mathrm{m}}\,x_\mathrm{m}(k) + \underbrace{[1]}_{B_\mathrm{m}}\,u_\mathrm{m}(k) - \underbrace{\left[\sqrt{Q_\mathrm{d}}\right]}_{G_\mathrm{m}}\,w_2(k) \\
y_\mathrm{m}(k) &= \underbrace{[1]}_{C_\mathrm{m}}\,x_\mathrm{m}(k) + \underbrace{\left[\sqrt{Q_\mathrm{d}}\right]}_{V_\mathrm{m}}\,w_2(k)
\end{aligned} \tag{32}$$

Combining the above discrete state-space representations of the various sub-systems given in Eqs. (30), (31) and (32) results in the complete discrete linear state model given by

$$\underbrace{\begin{bmatrix}\mathbf{x}(k+1)\\ \mathbf{x}_\mathrm{d}(k+1)\\ x_\mathrm{m}(k+1)\end{bmatrix}}_{\mathbf{x}_\mathrm{t}(k+1)} = \underbrace{\begin{bmatrix}\mathbf{A}_\mathrm{p} & \mathbf{B}_\mathrm{p}\,\mathbf{C}_\mathrm{d} & \mathbf{0}\\ \mathbf{0} & \mathbf{A}_\mathrm{d} & \mathbf{B}_\mathrm{d}\,\mathbf{C}_\mathrm{m}\\ \mathbf{0} & \mathbf{0} & A_\mathrm{m}\end{bmatrix}}_{\mathbf{A}_\mathrm{t}} \times \underbrace{\begin{bmatrix}\mathbf{x}(k)\\ \mathbf{x}_\mathrm{d}(k)\\ x_\mathrm{m}(k)\end{bmatrix}}_{\mathbf{x}_\mathrm{t}(k)} + \underbrace{\begin{bmatrix}\mathbf{0}\\ \mathbf{0}\\ B_\mathrm{m}\end{bmatrix}}_{\mathbf{B}_\mathrm{t}} u_\mathrm{m}(k) + \underbrace{\begin{bmatrix}\mathbf{G}_\mathrm{p} & \mathbf{0}\\ \mathbf{0} & \mathbf{B}_\mathrm{d}\,V_\mathrm{m}\\ \mathbf{0} & -G_\mathrm{m}\end{bmatrix}}_{\mathbf{G}_\mathrm{t}} \underbrace{\begin{bmatrix}w_1(k)\\ w_2(k)\end{bmatrix}}_{\mathbf{w}(k)} \quad \mathbf{y}_\mathrm{t}(k) = \underbrace{\begin{bmatrix}\mathbf{C}_\mathrm{p} & \mathbf{0}\,\mathbf{0}\\ \mathbf{0} & \mathbf{I}\,\mathbf{0}\end{bmatrix}}_{C_\mathrm{t}} \mathbf{x}_\mathrm{t}(k) \tag{33}$$

A full-state observer is to be designed for the stochastic controller, why as much information as possible is provided to the observer. Therefore, all the states except the two states driven by white noise are chosen as outputs.

6.2 Control feedback and integral state

Since linear control theory is to be used, a linearization of the $K\,\omega^2$ law given in Eq. (14) is necessary. A linear expression of the pressure reference given in Eq. (15) is derived to be that in Eq. (34).

$$\begin{aligned}\Delta_\mathrm{p}^* &= \left(\frac{d\tau_\mathrm{r}^*(\omega_\mathrm{r})}{d\omega_\mathrm{r}}|_{\omega_\mathrm{r}=\omega_0}\,\omega_\mathrm{r} - d_\mathrm{r}\,\omega_\mathrm{r}\right)\frac{\eta_\mathrm{p}}{\bar{V}_\mathrm{p}}\\ \Delta_\mathrm{p}^* &= \underbrace{(2\,K_2\,\omega_0 - d_\mathrm{r})\,\frac{\eta_\mathrm{p}}{\bar{V}_\mathrm{p}}}_{K_{\omega r}}\,\omega_\mathrm{r}\end{aligned} \tag{34}$$

where the rotor speed linearization point is determined as $\omega_0 = \frac{\lambda^*\,\bar{v}}{R_\mathrm{r}}$.

An integral state acting on the pressure error is introduced such that the closed-loop system achieves unity dc-gain. The expression for the integral state is derived to be that given by

$$\begin{aligned}\dot{x}_\mathrm{int} &= \Delta p^* - \Delta p = K_{\omega r}\,\omega_\mathrm{r} - \Delta p\\ \dot{x}_\mathrm{int} &= \frac{x_\mathrm{int}(k+1) - x_\mathrm{int}(k)}{T_\mathrm{s}}\\ x_\mathrm{int}(k+1) &= \underbrace{\begin{bmatrix}K_{\omega r} & T_\mathrm{s} & -T_\mathrm{s}\end{bmatrix}}_{\mathbf{K}_\mathrm{y}} \underbrace{\begin{bmatrix}\omega_\mathrm{r}(k)\\ \Delta p(k)\end{bmatrix}}_{\mathbf{y}(k)} + x_\mathrm{int}(k)\end{aligned} \tag{35}$$

$$x_\mathrm{int}(k+1) = \underbrace{\mathbf{K}_\mathrm{y}\,\begin{bmatrix}\mathbf{C}_\mathrm{p} & \mathbf{0}\,\mathbf{0}\end{bmatrix}}_{\mathbf{C}_\mathrm{y}}\,\mathbf{x}_\mathrm{t}(k) + x_\mathrm{int}(k)$$

The complete state model appended with an integral state becomes that given in Eq. (36), by combining Eqs. (33) and (35).

$$\underbrace{\begin{bmatrix}\mathbf{x}_\mathrm{t}(k+1)\\ x_\mathrm{int}(k+1)\end{bmatrix}}_{\mathbf{x}_\mathrm{s}(k+1)} = \underbrace{\begin{bmatrix}\mathbf{A}_\mathrm{t} & \mathbf{0}\\ \mathbf{C}_\mathrm{y} & 1\end{bmatrix}}_{\mathbf{A}_\mathrm{s}} \underbrace{\begin{bmatrix}\mathbf{x}_\mathrm{t}(k)\\ x_\mathrm{int}(k)\end{bmatrix}}_{\mathbf{x}_\mathrm{s}(k)} + \underbrace{\begin{bmatrix}\mathbf{B}_\mathrm{t}\\ \mathbf{0}\end{bmatrix}}_{\mathbf{B}_\mathrm{s}} u_\mathrm{m}(k) + \underbrace{\begin{bmatrix}\mathbf{G}_\mathrm{t}\\ \mathbf{0}\end{bmatrix}}_{\mathbf{G}_\mathrm{s}} \mathbf{w}(k) \quad \mathbf{y}_\mathrm{t}(k) = \underbrace{\begin{bmatrix}\mathbf{C}_\mathrm{t} & \mathbf{0}\end{bmatrix}}_{\mathbf{C}_\mathrm{s}} \mathbf{x}_\mathrm{s}(k) + \mathbf{v}(k) \tag{36}$$

$\mathbf{v}(k)$ is a measurement noise vector describing potential sensor noise disturbances.

7 Controller synthesis

A deterministic and a stochastic optimal controller are designed, where the deterministic is a Linear Quadratic Regulator (LQR) and the stochastic is a Linear Quadratic Gaussian (LQG) controller. The LQG-control problem consists of two subproblems being the LQR-control problem and the LQE-estimator problem.

7.1 LQR optimal control design

Since the LQR-control problem is also a part of the LQG-control design, only the LQG-design is documented. For the LQR-controller the same design procedure is applied, but where the two disturbance states are truncated.

The LQR-control problem is to minimize the quadratic cost function given in Eq. (37) by providing the optimal control input $u_\mathrm{m}(k)$.

$$\mathcal{J} = \sum_{k=1}^{\infty}\left(\mathbf{x}_\mathrm{s}(k)^T\,\mathbf{Q}\,\mathbf{x}_\mathrm{s}(k) + u_\mathrm{m}(k)^T\,\mathbf{R}\,u_\mathrm{m}(k)\right) \tag{37}$$

where $\mathbf{R} = \mathbf{R}^T \geq \mathbf{0}$ and $\mathbf{Q} = \mathbf{Q}^T \geq \mathbf{0}$ are positive definite weighting matrices. The input weighting matrix $\mathbf{R}$ specifies the importance of minimizing the control effort, and the state weighting matrix $\mathbf{Q}$ specifies the importance of driving the states to zero. The feedback

control law $u_{\mathrm{m}}(k) = -\mathbf{K}\,\hat{\mathbf{x}}_{\mathrm{t}}(k) + K_{\mathrm{int}}\,x_{\mathrm{int}}$ has the optimal solution of the feedback gain vector given as

$$\mathbf{K}_{\mathrm{s}} = \left(\mathbf{B}_{\mathrm{s}}^{T}\,\mathbf{S}\,\mathbf{B}_{\mathrm{s}} + \mathbf{R}\right)^{-1}\,\left(\mathbf{B}_{\mathrm{s}}^{T}\,\mathbf{S}\,\mathbf{A}_{\mathrm{s}}\right) \tag{38}$$

where $\mathbf{K}_{\mathrm{s}} = \left[\mathbf{K}\ K_{\mathrm{int}}\right]$ is the feedback gain vector. $\mathbf{S} = \mathbf{S}^{T} \geq \mathbf{0}$ is the unique positive-semi-definite solution to the Ricatti equation given by

$$\begin{aligned}\mathbf{0} &= \mathbf{A}_{\mathrm{s}}^{T}\,\mathbf{S}\mathbf{A}_{\mathrm{s}} - \mathbf{S} + \mathbf{Q} \\ &\quad - \left(\mathbf{A}_{\mathrm{s}}^{T}\,\mathbf{S}\,\mathbf{B}_{\mathrm{s}}\right)\,\left(\mathbf{B}_{\mathrm{s}}^{T}\,\mathbf{S}\,\mathbf{B}_{\mathrm{s}} + \mathbf{R}\right)^{-1}\,\left(\mathbf{B}_{\mathrm{s}}^{T}\,\mathbf{S}\,\mathbf{A}_{\mathrm{s}}\right)\end{aligned} \tag{39}$$

The state weighting matrix has been specified relative to an input weighting matrix chosen as $\mathbf{R} = 1$. With the objective of minimizing the reference tracking error, the integral state is weighted high, resulting in $\mathbf{Q} = \mathrm{diag}\left\{\left[0\ 0\ \cdots\ 0\ 10\right]\right\}$. For both the LQG and LQR-controllers, a weighting of 10 on the integral state and 0 for all other states is chosen. As a result, the control problem has been reduced significantly from being rather complicated to tuning of a single parameter, being the weighting of the integral state.

7.2 LQE optimal state estimation

The optimal state estimation is done by use of a discrete Kalman filter having the state equation given by.

$$\begin{aligned}\hat{\mathbf{x}}_{\mathrm{t}}(k+1) &= \mathbf{A}_{\mathrm{t}}\,\hat{\mathbf{x}}_{\mathrm{t}}(k) + \mathbf{B}_{\mathrm{t}}\,u_{\mathrm{m}}(k) + \mathbf{L}\,\left(\mathbf{y}_{\mathrm{t}}(k) - \hat{\mathbf{y}}(k)\right) \\ \hat{\mathbf{y}}(k) &= \mathbf{C}_{\mathrm{t}}\,\hat{\mathbf{x}}_{\mathrm{t}}(k)\end{aligned} \tag{40}$$

The optimal estimation problem is to determine the Kalman filter gain $\mathbf{L}$, which minimize the variance of the state estimation error expressed as

$$\mathcal{J} = E\left\{\left(\mathbf{x}_{\mathrm{t}}(k) - \hat{\mathbf{x}}_{\mathrm{t}}(k)\right)^{T}\,\left(\mathbf{x}_{\mathrm{t}}(k) - \hat{\mathbf{x}}_{\mathrm{t}}(k)\right)\right\} \tag{41}$$

The noise covariance matrices necessary for designing the LQG controller is provided in Eq. (42). It is assumed that there is no cross-correlation between the state noise $\mathbf{w}$ and the measurement noise $\mathbf{v}$.

$$E\left\{\mathbf{w}(k)\,\mathbf{w}(k)^{T}\right\} = \mathbf{W} \quad E\left\{\mathbf{v}(k)\,\mathbf{v}(k)^{T}\right\} = \mathbf{V} \tag{42}$$

The optimal solution to the Kalman filter may be derived to be that given by

$$\mathbf{L} = \mathbf{A}_{\mathrm{t}}\,\mathbf{P}\,\mathbf{C}_{\mathrm{t}}^{T}\,\left(\mathbf{C}_{\mathrm{t}}\,\mathbf{P}\,\mathbf{C}_{\mathrm{t}}^{T} + \mathbf{V}\right)^{-1} \tag{43}$$

where the matrix $\mathbf{P} = \mathbf{P}^{T} \geq \mathbf{0}$ is the unique positive-semi-definite solution to the steady-state Ricatti equation given by

$$\begin{aligned}\mathbf{0} &= \mathbf{A}_{\mathrm{t}}\,\mathbf{P}\,\mathbf{A}_{\mathrm{t}}^{T} - \mathbf{P} + \mathbf{G}_{\mathrm{t}}\mathbf{W}\,\mathbf{G}_{\mathrm{t}}^{T} \\ &\quad - \mathbf{A}_{\mathrm{t}}\,\mathbf{P}\,\mathbf{C}_{\mathrm{t}}^{T}\,\left(\mathbf{C}_{\mathrm{t}}\,\mathbf{P}\,\mathbf{C}_{\mathrm{t}}^{T} + \mathbf{V}\right)^{-1}\,\mathbf{C}_{\mathrm{t}}\,\mathbf{P}\,\mathbf{A}_{\mathrm{t}}^{T}\end{aligned} \tag{44}$$

A measurement noise of $e = 1\ \%$ has been assumed for both the pressure and rotor speed, while no measurement noise is present for the binary motor states. As a result, the measurement noise covariance matrix becomes $\mathbf{V} = \mathrm{diag}\left\{\left[e^2\ e^2\ 0\ \cdots\ 0\right]\right\}$.

The state covariance matrix is obtained by finding the power of the disturbance states. The power in the quantizer error state is found in Eq. (19) to be Q_{d}. The power in the aerodynamic torque state is identified from the discrete algebraic Lyapunov equation given by

$$\mathbf{A}_{\mathrm{p}}\,Q_{\tau}\,\mathbf{A}_{\mathrm{p}}^{T} - Q_{\tau} + \mathbf{G}_{\mathrm{p}}\,\Pi_{\tau}\,\mathbf{G}_{\mathrm{p}}^{T} = 0 \tag{45}$$

where $\Pi_{\tau} = 1$ is the white noise intensity. As a result the state noise covariance matrix becomes $\mathbf{W} = \mathrm{diag}\left\{\left[Q_{\tau}\ Q_{\mathrm{d}}\right]\right\}$.

A block diagram representation of the LQG closed-loop control system is shown in Fig. 13. In the LQR case, no estimator and noise inputs are present and the designed controller acts directly on the measured states.

8 Simulation results

The performance of the optimal controllers is investigated by simulation in the nonlinear dynamic model of the NREL 5-MW turbine including the DFP transmission and using the generated full-field flow wind profiles as input. Additionally, the performance of the optimal controllers is compared to that of the NREL PI-controller, with a conventional transmission system described in [17]. The simulation results are shown in Fig. 14 for a mean wind speed input of 8 m/s. It is seen that the output response using the three different controllers are quite similar. The results reveal that the

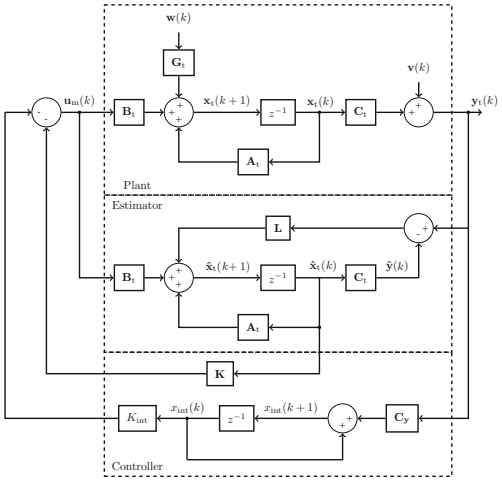

Fig. 13 Block diagram of the LQG-controller

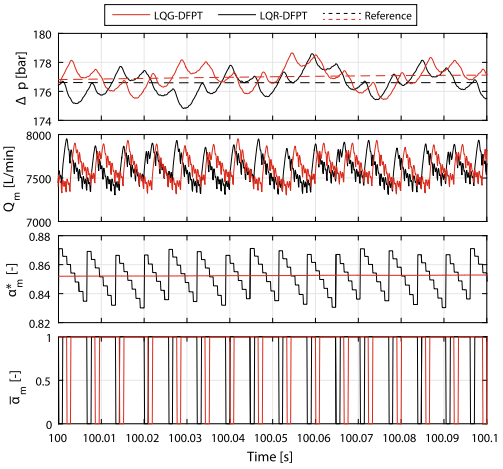

Fig. 15 Zoomed view of simulation results for NREL 5 MW turbine with turbulent wind profile, $\bar{v} = 8\,m/s$

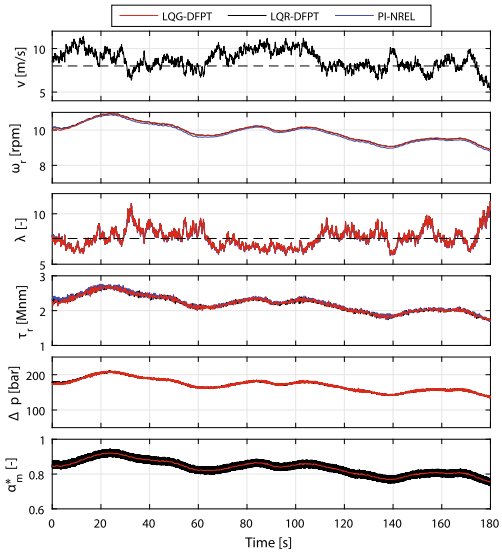

Fig. 14 Simulation results for NREL 5 MW turbine with turbulent wind profile, $\bar{v} = 8\,m/s$

rotor speed using the PI-controller has a minor offset with respect to the optimal controllers. This is caused by the gain used in the $K\,\omega^2$ control law which is not the precise optimal one in the NREL PI-controller. For a clearer view and to compare the pressure tracking performance of the two optimal controllers, a zoomed view of the pressure difference is shown in Fig. 15.

The simulation results shows that both controllers have a great pressure tracking performance with a maximum pressure error of $\approx$ 2 bar. No tracking performance improvement has thus been obtained by including the wind and quantization disturbances. The stepwise behavior of the LQR-control signal, α^*_{m}, is not seen for the LQG-controller, since the estimated states are not limited to being binary. The significantly smoother control signal is, however, quantized afterward, why it does not contribute to an improved transient performance. An improved disturbance rejection might have been obtained, but the shown simulation results are inconclusive with respect to this. It is expected that an improved disturbance rejection may be obtained with a LQG-controller if an integral state is not added to the system, but this has not been investigated. Both controllers have similar fluctuations in the pressure response with an amplitude in the range of $\pm$ 2 bar. The pressure fluctuations are a direct result of the large peak in the motor flow due to the activation of a single additional pressure chamber. It is therefore assessed that a significant increase in tracking performance and reduction in torque fluctuations are hardly achieved control wise. Instead a hydraulic accumulator and/or a partial stroke operation strategy is expected to improve the transient performance. It should be noted that a partial stroke operation entails several difficulties, since a time varying model is obtained with the presented approach (or a vague linear approximation at a displacement frac-

tion) and the valve closing angles has to be estimated for every actuation.

9 Conclusion

In this paper, a control strategy for a full stroke operated digital displacement machine is presented. In the proposed control strategy, a model-based design approach for feedback control of a digital transmission-based variable-speed wind turbine is developed. A linearization method of handling the combination of nonlinear continuous dynamics with discretely updated binary inputs is given and allows for use of linear control theory. A stochastic (LQG) and a deterministic (LQR) optimal controller have been synthesized, with the objective of accurate pressure reference tracking for optimal energy extraction. Simulation results reveal that both controllers are able to track the optimal rotor speed similar to a conventional transmission with corresponding controller. It is therefore rendered probably that it is possible to utilize linear model-based feedback control for such system with nonlinear continuous, discrete, binary and stochastic effects. The LQG-controller with disturbance compensation does not improve the tracking performance compared to the LQR-controller under the tested conditions. This indicates that the simpler LQR-controller with integral state is sufficient for accurate tracking performance. It is assessed that a significant improvement in tracking performance and torque fluctuation reduction is hardly achievable simply by control if a full stroke operation strategy is used without a hydraulic accumulator.

Acknowledgements This research was funded by the Danish Council for Strategic Research through the HyDrive project at Aalborg University, at the Department of Energy Technology (case no. 1305-00038B).

References

1. Armstrong, B.S.R., Yuan, Q.: Multi-level control of hydraulic gerotor motor and pumps. In: Proceedings of the 2006 American Control Conference, Minneapolis, Minnesota, USA (June 2006)
2. Chapple, P., Lindholdt, P.N., Larsen, H.B.: An approach to digital distributor valves in low speed pumps and motors. ASME/BATH 2014 Symposium on Fluid Power and Motion Control, Bath, United Kingdom (2014)
3. Commission, I.E.: International Standard, IEC 61400-1 3rd edition (2005)
4. Das, S., Pan, I.: Fractional Order Signal Processing: Introductory Concepts and Applications. Springer, Berlin. ISBN 978-3-642-23117-9 (2012)
5. Dolan, B., Aschemann, H.: Control of a wind turbine with a hydrostatic transmission an extended linearisation approach. In: 17th International Conference on Methods and Models in Automation and Robotics (2012)
6. Han, H.Y., Wang, J., Huang, Q.X.: Analysis of unsymmetrical valve controlling unsymmetrical cylinder stability in hydraulic leveler. Nonlinear Dyn. **70**, 1199–1203 (2012)
7. Hansen, A.H., Pedersen, H.C.: Energy cost of avoiding pressure oscillations in a discrete fluid power force system. In: Proceedings of the ASME/BATH 2015 Symposium on Fluid Power and Motion Control, FPMC, American Society of Mechanical Engineers, pp. 1–10 (2015)
8. Hansen, A.H., Pedersen, H.C.: Optimal configuration of discrete fluid power force system utilised in the pto for wecs. Ocean Eng. **117**(OE3694), 88–98 (2016)
9. Hansen, A.H., Pedersen, H.C.: Reducing pressure oscillations in discrete fluid power systems. Proc. Part I J. Syst. Control Eng. **230**(10), 1093–1105 (2016)
10. Heikkila, M., Linjama, M.: Displacement control of a mobile crane using digital hydraulic power management system. Mechatronics **23**(4), 452–461 (2013)
11. Hoven, V.D.: Power spectrum of horizontal wind speed in the frquency range from 0.0007 to 900 cycles per hour. J. Atmos. Sci. **14**, 160–164 (1957)
12. Jin, Y., Luo, X.: Stochastic optimal active control of a half-car nonlinear suspension under random road excitation. Nonlinear Dyn. **72**, 185–195 (2013)
13. Johansen, P., Roemer, D.B., Pedersen, H.C., Andersen, T.O.: Delta-sigma modulated displacement of a digital fluid power pump. In: Proceedings of the 7th Workshop on Digital Fluid Power. LCM GmbH. s. The Seventh Workshop on Digital Fluid Power, Linz, Austria, pp. 1–9. (2015)
14. Johansen, P., Roemer, D.B., Pedersen, H.C., Andersen, T.O.: Discrete linear time invariant analysis of digital fluid power pump flow control. J. Dyn. Syst. Measurement and Control Trans. ASME **139**(10), 101007 (2017)
15. Jonkman, B.J.: TurbSim Users Guide: Version 1.50, National Renewable Energy Laboratory, US Department of Energy (2009)
16. Jonkman, B.J.: Overview of the TurbSim Stochastic Inflow Turbulence Simulator, National Renewable Energy Laboratory. US, Department of Energy (2009)
17. Jonkman, J.M., Butterfield, S., Musial, W., Scott, G.: Definition of a 5-mw reference wind turbine for offshore system development (2009)
18. Jrf, A., Minav, T., Pietola, M.: Nonsymmetrical flow compensation using hydraulic accumulator in direct driven differential cylinder application. In: Proceedings of the 9th FPNI PhD Symposium on Fluid Power, Florianpolis, Brazil (2016)
19. Kaimal, J.C., Wyngaard, J.C., Izumi, Y., Cote, O.R.: Spectral characteristics of surface-layer turbulence. Q. J. R. Meteorol. Soc. **98**, 563–589 (1972)
20. Kalbat, A.: Linear quadratic gaussian (lqg) control of wind turbines. In: Proceddings of the 3rd International Conference on Electric Power and Energy Conversion Systems (2013)
21. Laguna, A.J., Diepeveen, N.F.B., van Wingerden, J.W.: Analysis of dynamics of fluid power drive-trains for variable

speed wind turbines: parameter study. IET Renew. Power Gener. **8**(4), 398–410 (2014)
22. M. Ehsan, W.R., Salter, S.: Modeling of digital-displacement pump-motors and their application as hydraulic drives for nonuniform loads. J. Dyn. Syst. Measurement and Control **122**, 210–215 (2000)
23. Mateescu, R., Pintea, A., Stefanoiu, D.: Discrete-time lqg control with disturbance rejection for variable speed wind turbines. In: Proceedings of the 1st International Confeference on System and Computer Science, Lille, France, pp. 1–6. (2012)
24. Ming, Z., Hong, N., Rupeng, Z.: Stochastic optimal control of flexible aircraft taxiing at constant or variable velocity. Nonlinear Dyn. **62**, 485–497 (2010)
25. Mitsubishi Heavy Industries, L.: Wind turbine generator and tidal current generator and operation method thereof, Patent: US 20120104752 A1, 2012 (2013)
26. Mitsubishi Heavy Industries, L.: Power generating apparatus of renewable energy type and operation method thereof, Patent: US 20130214537 (2013)
27. Mitsubishi Heavy Industries, L.: Power generating apparatus of renewable energy type and method of operating the same, Patent: US 20130307493 A1 (2013)
28. Mitsubishi Heavy Industries, L.: Energy extraction device, group of energy extraction devices and operating methods, Patent: US 20130221676 A1 (2013)
29. Mitsubishi Heavy Industries, L.: Hydraulic transmission, power generating apparatus of renewable energy type, and operation method thereof, Patent: EP 2899432 A2 (2015)
30. Mitsubishi Heavy Industries, L.: Hydraulic transmission comprising variable displacement pump or motor operable with discontinuous range of displacements, Patent: EP 2649348 A1 (2015)
31. Noergaard, C., Bech, M.M., Roemer, D.B., Schmidt, L.: Experimental validation of modelled fluid forces in fast switching hydraulic on/off valves. In: Proceedings of the 2015 International Conference on fluid power and Mechatronics (FPM), IEEE Press, pp. 68–73 (2015)
32. Payne, G.S., Kiprakis, A.E., Ehsan, M., Rampen, W., Chick, J.P., Wallace, A.R.: Efficiency and dynamic performance of digital displacement hydraulic transmission in tidal current energy converters. J. Power and Energy Proc. IMechE Part A **221**, 207–218 (2007)
33. Payne, G.S., Stein, U.P.P., Ehsan, M., Caldwell, N.J., Rampen, W.H.S.: Potential of digital displacement hydraulics for wave energy conversion. In: Proceedings of the 6th European Wave and TIdal Energy Conference, Glasgow UK. (2005)
34. Pedersen, H.C., Hansen, R.H., Hansen, A.H., Andersen, T.O., Bech, M.M.: Design of full scale wave simulator for testing power take off systems for wave energy converters. Int. J. Mar. Energy **13**, 130–156 (2016)
35. Pintea, A., Christov, N., Borne, P., Popescu, D., Badea, A.: Optimal control of variable speed wind turbines. In: The 19th Mediterranean Conference on Control and Automation, Corfu, Greece (2011)
36. Rampen, W.: Gearless transmissions for large wind turbines—the history and future of hydraulic drives. Artemis IP Ltd, Scotland Artemis IP Ltd., Scotland
37. Rampen, W.: The development of digital displacement technology. In: Proceedings of Bath/ASME FPMC Symposium (2010)
38. Reiss, J.D.: Understanding sigma-delta modulation: The solved and unsolved issues. J. Audio Eng. Soc. **56**(1/2), 49–64 (2008)
39. Roemer, D.B.: Design and optimization of fast switching valves for large scale digital hydraulic motors. PhD thesis, Department of Energy Technology, Aalborg University (2014)
40. Roemer, D.B., Johansen, P., Pedersen, H.C., Andersen, T.O.: Design method for fast switching seat valves for digital displacement machines. In: Proceedings of the 8th FPNI PhD Symposium on Fluid Power (2014)
41. Roemer, D.B., Johansen, P., Pedersen, H.C., Andersen, T.O.: Optimum design of seat region in valves suitable for digital displacement machines. Int. J. Mechatron. Autom. **4**(2), 116–126 (2014)
42. Roemer, D.B., Johansen, P., Pedersen, H.C., Andersen, T.O.: Fluid stiction modeling for quickly separating plates considering the liquid tensile strength. J. Fluids Eng. **137**(6), 061205 (2015)
43. Roemer, D.B., Johansen, P., Pedersen, H.C., Andersen, T.O.: Optimum design of moving coil actuator for fast-switching valves in digital hydraulic pumps and motors. IEEE ASME Trans. Mechatron. **20**(6), 2761–2770 (2015)
44. Roemer, D.B., Johansen, P., Schmidt, L., Andersen, T.O.: Modeling of movement-induced and flow induced fluid forces in fast switching valves. In: Proceedings of the 2015 International Conference on Fluid Power and Mechatronics (FPM). IEEE press, pp. 978–983 (2015)
45. Salter, S.H., Taylor, J.R.M., Caldwell, N.J.: Power conversion mechanisms for wave energy. Proc. Inst. Mech. Eng. Part M J. Eng. Marit. Environ. **216**(1), 1–27 (2002)
46. Scheidl, R., Manhartsgruber, B.: On the dynamic behavior of servo-hydraulic drives. Nonlinear Dyn. **17**, 247–268 (1998)
47. Scheidl, R., Manhartsgruber, B.: State of the art in hydraulic switching control—componets, systems, applications. In: Proceedings of the 9th Scandinavian International Conference on Fluid Power (2005)
48. Schmidt, L., Roemer, D.B., Pedersen, H.C., Andersen, T.O.: Speed-variable switched differential pump system for direct operation of hydraulic cylinders. In: Proceedings of ASME/BATH 2015 Symposium on Fluid Power and Motion Control, American Society of Mechanical Engineers (2015)
49. Sniegucki, M., Gottfried, M., Klingauf, U.: Optimal control of digital hydraulic drives using mixed-integer quadratic programming. In: 9th IFAC Symposium on Nonlinear Control Systems (2013)
50. Song, X.: Modeling an active vehicle suspension system with application of digital displacement pump motor. In: Proceedings of the ASME 2008 International Design Engineering Techical Conference/Computers and Information in Enegineering Conference, Brooklyn - New York, Vol. 5, pp. 749–753 (2008)
51. Tahavori, M., Leth, J., Kallese, C., Wisniewski, Rafael: Optimal control of nonlinear hydraulic networks in the presence of disturbance. Nonlinear Dyn. **75**, 539–548 (2013)
52. Vepa, R.: Dynamic Modeling, Simulation and Control of Energy Generation. Springer, Berlin. ISBN 978-1-4471-5400-6 (2013)

53. Wadsley, L.: Optimal system solutions enabled by digital pumps. International Exposition for Power Transmission, Las Vegas (2011)
54. Wang, F., Stelson, K.A.: Model predictive control for power optimization in a hydrostatic wind turbine. In: 13th Scandinavian International Conference on Fluid Power, Linkping, Sweden (2013)
55. Wilfong, G., Batdorff, M., Lumkes, J.: Design and dynamic analysis of high speed on/off poppet valves for digital pump/motors. In: Proceedings of the 6th FPNI-PhD Symposium (2010)
56. Wilfong, G., Holland, M., Lumkes, J.: Design and analysis of pilot operated high speed on/off valves for digital pump/motors. In: Proceedings of the 52nd National Conference on Fluid Power (2011)
57. Winkler, B.: Development of a fast low-cost switching valve for big flow rates. In: Proceedings of the 3rd FPNI PhD symposium on Fluid Power (2004)
58. Winkler, B., Ploeckinger, A., Scheidl, R.: Components for digital and swithcing hydraulics. In: Proceedings of 1st Workshop on Digital Fluid Power (2008)
59. Winkler, B., Scheidl, R.: Optimization of a fast switching valve for big flow rates. In: Proceedings of the Bath Workshop on Power Transmission and Motion Control (2006)
60. Zhu, Y., Jiang, W.L., Kong, X.D., Zheng, Z.: Study on nonlinear dynamics characteristics of electrohydraulic servo system. Nonlinear Dyn. **80**, 723–737 (2015)

Paper F

Event-Driven Control of a Speed Varying Digital Displacement Machine

Niels H. Pedersen, Per Johansen and Torben O. Andersen

The paper has been published in
Proceedings of the 2017 ASME/Bath Symposium on Fluid Power and Motion Control, Sarasota, USA, ISBN:978-0-7918-5833-2,
doi:10.1115/FPMC2017-4260.

The layout has been revised.

Proceedings of the 2017 Bath/ASME Symposium on Fluid Power and Motion Control
FPMC2017
October 16-19, 2017, Sarasota, FL, USA

FPMC2017-4260

EVENT-DRIVEN CONTROL OF A SPEED VARYING DIGITAL DISPLACEMENT MACHINE

Niels H. Pedersen
Fluid Power and Mechatronic Systems
Department of Energy Technology
Aalborg University
9220 Aalborg East, Denmark
Email: nhp@et.aau.dk

Per Johansen
Torben O. Andersen
Fluid Power and Mechatronic Systems
Department of Energy Technology
Aalborg University
9220 Aalborg East, Denmark
Email: pjo@et.aau.dk; toa@et.aau.dk

ABSTRACT

The design and analysis of feedback controllers for digital displacement machines requires a control oriented model. The displacement throughput of a full stroke operated machine is altered on a stroke-by-stroke basis at fixed rotation angles. In the case of a fixed speed operation, it may be treated as a Discrete Linear Time Invariant control problem with synchronous sampling rate. To make synchronous linear control theory applicable for a variable speed digital displacement machine, a method based on event-driven control is presented. Using this method, the time domain differential equations are converted into the spatial (position) domain to obtain a constant sampling rate and thus allowing for use of classical control theory. The method is applied to a down scaled digital fluid power motor, where the motor speed is controlled at varying references under varying pressure and load torque conditions. The controller synthesis is carried out as a discrete optimal deterministic problem with full state feedback. Based on a linear analysis of the feedback control system, stability is proven in a pre-specified operation region. Simulation of a non-linear evaluation model with the controller implemented shows great performance, both with respect to tracking and disturbance rejection.

INTRODUCTION

Due to the fast power level increase in wind and wave energy, focus has in the recent years been drawn towards improving large scale power transmission systems. One high potential solution is to utilize a digital fluid power transmission, which replaces the conventional mechanical gear box. One promising fluid power machine topology is the digital displacement machine, which is characterized by having a modular construction with numerous displacement chambers controlled by electrically actuated on/off valves. A detailed description of the digital displacement technology is not covered in this paper, but may be found in several other publications [1–6].

To enhance the use of Digital Fluid Power (DFP) machines in large scale transmission systems requires applicable control algorithms, which are complicated to develop due to the non-smooth behavior of the machines. So far only limited research within control of digital displacement machines has been conducted, which have mostly been limited to open-loop control at a fixed speed operation and under simplified load conditions. Ehsan et al. [2] presents a full stroke valve timing control method, where the actuation decision is determined by an estimation of the displacement volume. Heikkilä and Linjama [7] extended the method to include oil compressibility. A multi-level flow control strategy comprising both partial and full stroke operation is proposed by Xubin [8]. Here the valve activation decision is determined based on preprogrammed flow requirements. Armstrong and Yuan [9] presents a two level strategy for speed control, where the outer loop is a PI speed controller and the inner control loop identifies the optimal cylinder actuation sequence based on the torque requirement. Sniegucki et al. [10]

presents a mixed logical dynamic system representation used for synthesizing an optimal controller. Despite yielding great performance, the method is restricted to offline optimization due to the large computational effort. A full stroke delta-sigma modulated feedback control strategy is proposed by Johansen et al. [11]. The same author also presents a discrete linear time invariant (DLTI) control strategy [12], where the flow throughput is described as a convolution sum of impulse responses of each displacement chamber. Pedersen et al. [13] combined the method of using a delta-sigma modulator and describing the digital machine dynamics by a DLTI model for optimal control of a digital fluid power wind turbine transmission.

The contribution of this paper is an extension to the combined DLTI and delta-sigma modulation method, making it applicable to speed varying digital displacement machines. To overcome the problem with the sampling being position dependent instead of time dependent, event-driven control theory is utilized. Here the dynamics of the system is described in the spatial (position) domain, which results in a synchronous control system with a fixed update angle, allowing for classical linear control synthesis. The method has previously been successfully applied for control of DC-motors with variable speed and a very low resolution encoder [14–16]. The method is exemplified by speed control of a digital displacement motor under varying load and pressure conditions.

1 System description and model

In this paper, only the motor part of a digital fluid power transmission is considered to reduce the comprehensiveness of modeling and analysis. The performance of the control system to be designed is tested by simulation in a non-linear model of the system. The non-linear model of the digital motor displacement chambers is documented in the paper by Pedersen et. al. [13] for a 5 MW motor comprising of 42 cylinders. However, to reduce the complexity further, the motor has been downsized to include 15 cylinders.

The simplified system under consideration in this paper consist of a digital displacement motor connected to a high and a low fluid power pressure line as illustrated in Fig. 1. The motor flow, Q_m, and motor torque, τ_m, throughput of the machine may be altered by the displacement fraction input, $\alpha_\mathrm{m} \in [0, 1]$. In this paper the motor torque is altered for speed control with the presence of a disturbance torque τ_d. To test the linear controller under varying operation conditions, the pressure p_H is varied in a specified region by the flow Q_d. The proposed control strategy is also valid for pressure control of a speed varying digital machine, but this is not investigated in this paper.

For feedback control development, a dynamic model of the system is necessary. The pressure and speed of the system is described by the following differential equations

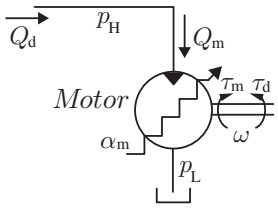

FIGURE 1. ILLUSTRATION OF THE SIMPLIFIED SYSTEM USED AS BASIS FOR CONTROL DEVELOPMENT AND TESTING.

$$\begin{aligned}\frac{d\omega}{dt} &= \frac{1}{J}\left(\tau_\mathrm{m}(t) - d_\mathrm{r}\,\omega(t) - \tau_\mathrm{d}(t)\right)\\ \frac{dp_\mathrm{H}}{dt} &= \frac{\beta_\mathrm{e}}{V_\mathrm{H}}\left(Q_\mathrm{m}(t) - Q_\mathrm{d}(t) - k_\mathrm{l}\,p_\mathrm{H}(t)\right)\end{aligned} \tag{1}$$

Here a simplified viscous friction term is used having the coefficient d_r. J is the shaft mass moment of inertia, β_e is the effective bulk modulus of the fluid, V_H is the volume in the high pressure line and k_l is the leakage coefficient. The parameter values used in the model are provided in the table below

TABLE 1. Parameters values used in the model

Parameter	symbol	value	Unit
Viscous friction	d_r	7.5	N s/rad
Inertia mass	J	120	kg m^2
Leakage coefficient	k_l	1e-12	Pa m^3/s
High pressure volume	V_H	4	m^3
Effective bulk modulus	β_e	16000	bar

1.1 Digital fluid power motor

The digital displacement motor is a radially piston type machine, with distributed cylinders placed around an eccentric shaft. The pressure level of each of the cylinder chambers are controlled by electrically actuated fast switching on/off valves as illustrated in Fig. 2. The motor has 5 cylinders in each module and 3 modules for a total of 15 cylinders. Each module is radially shifted with respect to each other, to yield a constant angle between each of the 15 cylinders. A comprehensive non-linear mathematical model of the digital displacement motor used for model validation, as well as controller evaluation and testing is documented in [13]. Therefore only a brief summarization of the governing equations is provided in this paper. The pistion

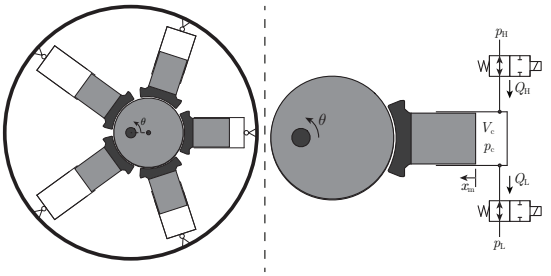

FIGURE 2. ILLUSTRATION OF THE RADIAL PISTON TYPE DIGITAL DISPLACEMENT MOTOR AND ONE PRESSURE CHAMBER.

displacement, x_m, as function of the shaft angle is described by

$$x_m(\theta) = r_e\,(1-\cos(\theta)) \tag{2}$$

Where r_e is the eccentric radius. The cylinder chamber volume, V_c is then given as

$$\begin{aligned} V_c(\theta) &= \frac{V_d}{2}\,(1-\cos(\theta)) + V_0 \\ \dot{V}_c(\theta) &= \frac{V_d}{2}\,\dot{\theta}\,\sin(\theta) \end{aligned} \tag{3}$$

Where V_0 is the minimum chamber volume and $V_d = 2\,r_e A_p$, with A_p being the piston area. The pressure dynamics in one displacement chamber is given by

$$\dot{p}_c = \frac{\beta_e}{V_c}\,\left(Q_H - Q_L - \dot{V}_c\right) \tag{4}$$

Where Q_H and Q_L are the flows through the high and low pressure valve respectively. The flow through these valves is described by the orifice equation and is given by

$$\begin{aligned} Q_L &= \frac{\bar{x}_L}{k_f}\,\sqrt{|p_c - p_L|}\,\mathrm{sign}\,(p_c - p_L) \\ Q_H &= \frac{\bar{x}_H}{k_f}\,\sqrt{|p_H - p_c|}\,\mathrm{sign}\,(p_H - p_c) \end{aligned} \tag{5}$$

Where $\bar{x}_H$ and $\bar{x}_L$ are the normalized valve position of the high and low pressure valve respectively and k_f is the valve flow coefficient. The valve dynamics is simplified to be described as a constant acceleration as shown in Fig. 3 for opening of the valves. Where t_s is the valve opening/closing time. This is seen

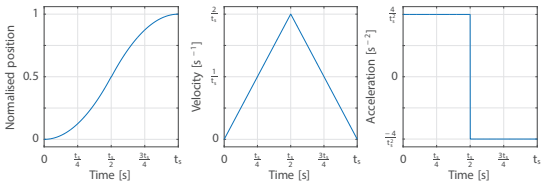

FIGURE 3. Position, velocity and acceleration responses for the on-off valve.

to yield a smooth position response, similar to what may be expected if a more detailed model of the valve dynamics and forces had been used. Despite the simplicity of the valve model, the important characteristics with respect to system wide control is captured. For closing of the valve the inverse function of the acceleration is used.

The torque contribution to the eccentric motor shaft is given by

$$\tau_c = \frac{dV_c(\theta)}{d\theta}\,p_c = \frac{V_d}{2}\,\sin(\theta)\,p_c \tag{6}$$

The parameters used to set up the non-linear simulation model of the digital displacement pump is provided in the table below.

TABLE 2. Parameters of the digital displacement motor

Parameter	symbol	value	Unit
Piston area	A_p	31	cm^2
Piston displacement	r_e	25	mm
Chamber flow coefficient	k_f	$0.5\cdot 10^5$	$\sqrt{pa}\,s/m^3$
Valve actuation time	t_s	3	ms
LPV closing angle	$\theta_{\text{L-cl}}$	333.7	deg
HPV closing angle	$\theta_{\text{H-cl}}$	147.2	deg
Low pressure	p_L	1	bar

Simulation results for one pressure chamber during a motoring and an idling stroke is shown in Fig. 4. Using a full stroke operation, the low pressure valve is closed shortly before TDC and the high pressure valve is closed shortly before BDC, at angles of $\theta_{\text{L-cl}}$ and $\theta_{\text{H-cl}}$ for the low and high pressure valve respectively. Passive opening of both valves are utilized such that the high pressure valve is opened when $p_c > p_H$ and the low pressure valve is opened when $p_c < p_L$.

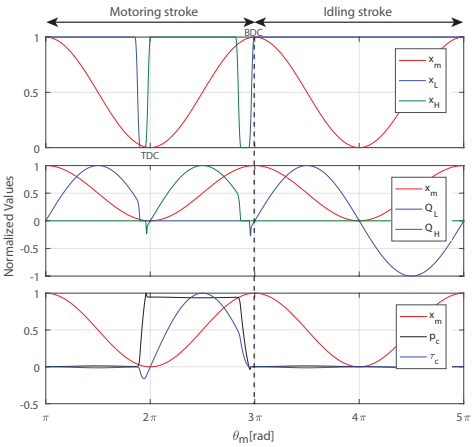

FIGURE 4. Simulation results of a motor pressure chamber during a pumping and an idling stroke. $\omega = 1500\,\text{rpm}$ and $p_H = 300\,\text{bar}$.

The total motor flow, Q_m from the high pressure line and the total torque output, τ_m are the sum of each individual contributions and is given by

$$Q_m = \sum_{j=1}^{N} Q_{H,j} \qquad \tau_m = \sum_{j=1}^{N} \tau_{c,j} \tag{7}$$

Where $N = 15$ is the number of cylinders.

2 Control strategy and model establishment

A full stroke operation strategy of the digital motor is utilized, where the operation mode of each pressure chamber is altered on a stroke by stroke basis once every revolution. Since the decision to activate (motoring) or deactivate (idling) a pressure chamber is done at a fixed rotation angle for every cylinder, the measure and control signal is updated with the rate of decisions. An illustration of the proposed control strategy is shown in Fig. 5.

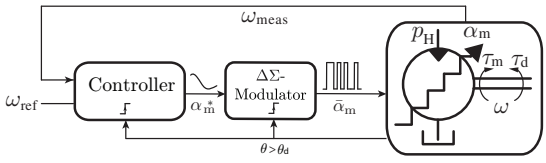

FIGURE 5. CONTROL STRATEGY FOR SPEED CONTROL OF THE DIGITAL FLUID POWER MOTOR.

ω_{ref} and ω_{meas} represent the reference and measured values of the motor speed respectively. The controller and modulator updates its value each time the threshold $\theta > \theta_d$ is meet. Where θ_d is the decision angle, where the corresponding cylinder is set to motoring or idling ($\theta_d = \theta_{L\text{-}cl}$). The controller is seen to output a displacement fraction reference α_m^*, which is converted to a binary actuation signal, $\bar{\alpha}_m$, by a Delta-Sigma Modulator. A binary value of 1 hence indicates the activation (Motoring) of the current cylinder and a binary value of 0 indicates a deactivation (Idling).

2.1 Delta-Sigma Modulator

In this study a discrete first order DSM is used for the binary quantization, but any 1 bit analog-to-digtal converter is applicable. A block diagram representation of the modulator is shown in Fig. 6.

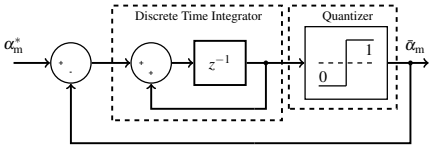

FIGURE 6. FIRST ORDER DELTA SIGMA MODULATION BLOCK DIAGRAM.

The modulator consists of a discrete integrator and a 1 bit quantizer in a feedback structure. The integrator is acting on the displacement error, such that the output is time averagely equal to the input.

2.2 Discrete Motor Approximation

Due to the digital nature of the machine operation, where the operation mode may only be altered at discrete motor angles, a discrete control oriented model of the digital machine is established. The sampling time, being the time between each actuation decision is given by

$$T_s = \frac{2\pi}{\omega N} \tag{8}$$

Since the rotational speed of the motor is varying, the sampling time is asynchronous and classical discrete control theory is not directly applicable. Therefore, the discrete model is established in the spatial domain where the constant sampling angle is given by $\theta_s = 2\pi/N$. The discrete model of the motor flow and torque is obtained by considering the instantaneous values for a single

chamber given as

$$Q_{\mathrm{H}} \approx \frac{dV_{\mathrm{c}}(\theta(t))}{dt} \qquad \tau_{\mathrm{c}} = \frac{dV_{\mathrm{c}}(\theta(t))}{d\theta(t)}\, p_{\mathrm{c}}(t) \tag{9}$$

A discrete approximation of the above continuous representations becomes those given in Eq. (10). In the approximation the valve and pressure dynamics has been omitted, such that it is assumed that $p_{\mathrm{c}} \approx p_{\mathrm{H}}$ during the complete motoring stroke.

$$\begin{aligned} Q_{\mathrm{H}}[k] &\approx \frac{V_{\mathrm{d}}}{T_{\mathrm{s}}}\left(\bar{V}_{\mathrm{c}}(\theta[k+1]) - \bar{V}_{\mathrm{c}}(\theta[k])\right) \\ &\approx \frac{V_{\mathrm{d}} N}{2\pi}\, \omega[k]\, \Delta\bar{V}_{\mathrm{c}}[k] \\ \tau_{\mathrm{c}}[k] &\approx \frac{V_{\mathrm{d}}}{\theta_{\mathrm{s}}}\left(\bar{V}_{\mathrm{c}}(\theta[k+1]) - \bar{V}_{\mathrm{c}}(\theta[k])\right) p_{\mathrm{c}}[k] \\ &\approx \frac{V_{\mathrm{d}} N}{2\pi}\, p_{\mathrm{H}}[k]\, \Delta\bar{V}_{\mathrm{c}}[k] \end{aligned} \tag{10}$$

Where $\bar{V}_{\mathrm{c}}$ is the normalized chamber volume. The displacement fraction values $\Delta\bar{V}_{\mathrm{c}}$ between samples is obtained by considering the normalized displacement volume function in Eq. (3) and is shown in Fig. 7.

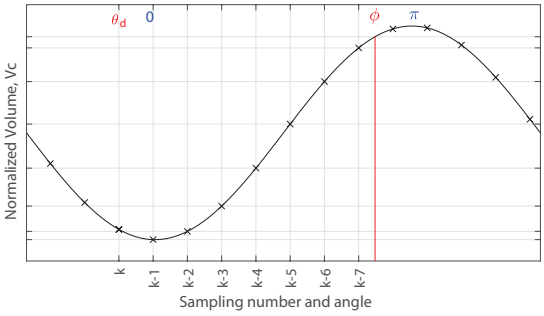

FIGURE 7. DERIVATION OF FRACTIONAL DISPLACEMENT OUTPUT AS FUNCTION OF SAMPLING NUMBER.

The active motoring stroke begins at $\theta = 0$, where a fluid intake starts. However, due to valve dynamics the operation mode decision angle is made ahead at θ_{d}. θ_{d} is hence the angle at which the low pressure valve is closed for an initiation of a motoring stroke. Again due to valve dynamics, the motoring stroke is ended before $\theta = \pi$, at ϕ.

It is seen that the active part of the motoring stroke ends after 7 samples, where the first sample is a delay sample. As a result, a 7'th order difference equation is able to describe the motor output dynamics.

Using Fig. 7 the displacement fractions are calculated as

$$\Delta\bar{V}_{\mathrm{c}}[k] = \begin{cases} 0 & \theta[k], \theta[k+1] \notin [0\,;\phi] \\ \bar{V}_{\mathrm{c}}(\theta[k+1]) - \bar{V}_{\mathrm{c}}(\theta[k]) & \theta[k], \theta(k+1) \in [0\,;\phi] \\ \bar{V}_{\mathrm{c}}(\theta[k+1]) - \bar{V}_{\mathrm{c}}(0) & \theta[k] < 0 < \theta[k+1] \\ \bar{V}_{\mathrm{c}}(\phi) - \bar{V}_{\mathrm{c}}(\theta[k]) & \theta[k] < \phi < \theta[k+1] \end{cases} \tag{11}$$

The discrete approximation of the total motor flow and torque is given in Eq. (12) as a convolution sum of impulse responses of the individual chamber contributions derived in Eq. (7).

$$\begin{aligned} \alpha_{\mathrm{m}}[k] &= \sum_{m=0}^{k} \Delta\bar{V}_{\mathrm{c}}[k-m]\, \bar{\alpha}_{\mathrm{m}}[m] \\ Q_{\mathrm{m}}[k] &= \underbrace{\frac{V_{\mathrm{d}} N}{2\pi}}_{k_{\mathrm{m}}}\, \omega[k]\, \alpha_{\mathrm{m}}[k] \qquad \tau_{\mathrm{m}}[k] = \underbrace{\frac{V_{\mathrm{d}} N}{2\pi}}_{k_{\mathrm{m}}}\, p_{\mathrm{H}}[k]\, \alpha_{\mathrm{m}}[k] \end{aligned} \tag{12}$$

Validation of the discrete approximation is carried out by a comparison between the non-linear and the discrete model with respect to flow and torque throughput. The result of this comparison is shown in Fig. 8.

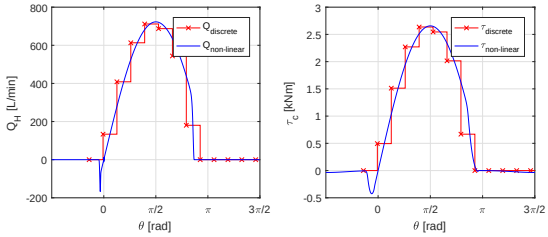

FIGURE 8. VALIDATION OF DISCRETE MOTOR FLOW AND TORQUE APPROXIMATION. $P_{\mathrm{H}} = 350\,\mathrm{BAR}$ AND $\omega = 1500\,\mathrm{RPM}$.

Is is seen that there is a great coherence between the discrete approximation and the non-linear model in the majority of the stroke. However, since the valve and pressure dynamics has been omitted, there is discrepancies at the beginning and end of the active motoring stroke part. A more precise approximation could have been obtained by manipulating the displacement fraction to be more accurate, which would include negative fractions in the

beginning of the stroke. However, the back flow and torque in the beginning are both pressure and speed dependent and thus complex to model. Since these discrepancies are relatively small compared to the complete output, the proposed approximation is accepted.

2.3 Event-driven control

It is evident that the developed motor and modulator models are described in the position domain, but the dynamics of the shaft and pressure is described in the time domain. To combine these models a transformation to the spatial domain is performed by use of the relation between the time and angle, being the rotational speed given by

$$\frac{d\theta(t)}{dt} = \omega(t) \rightarrow \frac{dt(\theta)}{d\theta} = \frac{1}{\omega(\theta)} \tag{13}$$

Here $t(\theta)$ denotes the time at which the shaft reaches the angle θ. The relation requires the conditions of $\omega(t) \neq 0$ and $t > 0$, which holds during normal operation in positive direction. Applying this transformation to the shaft and pressure dynamics results in

$$\begin{aligned} \frac{d\omega}{d\theta} &= \frac{1}{J\,\omega(\theta)}\left(\tau_\mathrm{m}(\theta) - d_\mathrm{r}\,\omega(\theta) - \tau_\mathrm{d}(\theta)\right) \\ \frac{dp_\mathrm{H}}{d\theta} &= \frac{\beta_\mathrm{e}}{V_\mathrm{H}\,\omega(\theta)}\left(Q_\mathrm{m}(\theta) - Q_\mathrm{d}(\theta) - k_\mathrm{l}\,p_\mathrm{H}(\theta)\right) \end{aligned} \tag{14}$$

It is clear that the linear model in the time domain is now a non-linear model in the position domain, which brings complications when using linear control theory.

2.4 Linear discrete state model

To enable the use of classical linear control theory a small signal model around a steady-state rotational speed is considered, resulting in the linear system given by Eq. (15). This method of linearization is identically to that used before for event-driven control [14–16] and benefits of maintaining the systems damping information.

$$\begin{aligned} \frac{d\Delta\omega}{d\theta} &= \frac{1}{J\,\omega_0}\left(\Delta\tau_\mathrm{m}(\theta) - d_\mathrm{r}\,\Delta\omega(\theta) - \Delta\tau_\mathrm{d}(\theta)\right) \\ \frac{d\Delta p_\mathrm{H}}{d\theta} &= \frac{\beta_\mathrm{e}}{V_\mathrm{H}\,\omega_0}\left(\Delta Q_\mathrm{m}(\theta) - \Delta Q_\mathrm{d}(\theta) - k_\mathrm{l}\,\Delta p(\theta)\right) \end{aligned} \tag{15}$$

Where ω_0 is the steady state linearization point for the speed. The continuous model is rewritten to state space form in Eq. (16), where the disturbance torque and flow has been omitted for the purpose of deterministic control design.

$$\underbrace{\begin{bmatrix} \frac{d\Delta\omega}{d\theta} \\ \frac{d\Delta p_\mathrm{H}}{d\theta} \end{bmatrix}}_{\dot{\mathbf{x}}_\mathrm{c}} = \underbrace{\begin{bmatrix} \frac{-d_\mathrm{r}}{J\,\omega_0} & 0 \\ 0 & -\frac{k_\mathrm{l}\,\beta_\mathrm{e}}{V_\mathrm{H}\,\omega_0} \end{bmatrix}}_{\mathbf{A}_\mathrm{c}} \underbrace{\begin{bmatrix} \Delta\omega \\ \Delta p_\mathrm{H} \end{bmatrix}}_{\mathbf{x}_\mathrm{c}} + \underbrace{\begin{bmatrix} \frac{1}{J\,\omega_0} & 0 \\ 0 & \frac{\beta_\mathrm{e}}{V_\mathrm{H}\,\omega_0} \end{bmatrix}}_{\mathbf{B}_\mathrm{c}} \underbrace{\begin{bmatrix} \Delta\tau_\mathrm{m} \\ \Delta Q_\mathrm{m} \end{bmatrix}}_{\mathbf{u}_\mathrm{c}}$$

$$\Delta\omega = \underbrace{\begin{bmatrix} 1 & 0 \end{bmatrix}}_{\mathbf{C}_\mathrm{c}} \mathbf{x}_\mathrm{c} \tag{16}$$

2.5 Linear Discrete model

The continuous model in Eq. (16) is discretized in the position domain with a sampling size of θ_s, to yield a discrete representation of the continuous state in the position domain given as

$$\begin{aligned} \mathbf{x}_\mathrm{p}(k+1) &= \mathbf{A}_\mathrm{p}\,\mathbf{x}_\mathrm{p}(k) + \mathbf{B}_\mathrm{p}\,\mathbf{u}_\mathrm{p}(k) \\ \omega(k+1) &= \mathbf{C}_\mathrm{p}\,\mathbf{x}_\mathrm{p}(k) \end{aligned} \tag{17}$$

The convolution sum model of the digital motor displacement derived in Eq. (12) is rewritten into state space form resulting in Eq. (18). The flow and torque outputs are seen to be functions of multiple states, why it is again chosen to linearize the model by considering small signal operation around a steady state velocity and pressure.

$$\underbrace{\begin{bmatrix} \bar{\alpha}_\mathrm{m}(k) \\ \bar{\alpha}_\mathrm{m}(k-1) \\ \bar{\alpha}_\mathrm{m}(k-2) \\ \vdots \\ \bar{\alpha}_\mathrm{m}(k-p+1) \end{bmatrix}}_{\mathbf{x}_\mathrm{d}(k+1)} = \underbrace{\begin{bmatrix} 0 & 0 & \cdots & 0 & 0 \\ 1 & 0 & \cdots & 0 & 0 \\ 0 & 1 & \cdots & 0 & 0 \\ \vdots & \vdots & \ddots & \vdots & \vdots \\ 0 & 0 & \cdots & 1 & 0 \end{bmatrix}}_{\mathbf{A}_\mathrm{d}} \underbrace{\begin{bmatrix} \bar{\alpha}_\mathrm{m}(k-1) \\ \bar{\alpha}_\mathrm{m}(k-2) \\ \bar{\alpha}_\mathrm{m}(k-3) \\ \vdots \\ \bar{\alpha}_\mathrm{m}(k-p) \end{bmatrix}}_{\mathbf{x}_\mathrm{d}(k)} + \underbrace{\begin{bmatrix} 1 \\ 0 \\ 0 \\ \vdots \\ 0 \end{bmatrix}}_{\mathbf{B}_\mathrm{d}} \bar{\alpha}_\mathrm{m}(k)$$

$$\begin{bmatrix} \tau_\mathrm{m}(k) \\ Q_\mathrm{m}(k) \end{bmatrix} = \underbrace{k_\mathrm{m} \begin{bmatrix} p_\text{H-0} \\ \omega_0 \end{bmatrix} \begin{bmatrix} \Delta\bar{V}_\mathrm{c}[1] & \Delta\bar{V}_\mathrm{c}[2] & \cdots & \Delta\bar{V}_\mathrm{c}[p] \end{bmatrix}}_{\mathbf{C}_\mathrm{d}} \mathbf{x}_\mathrm{m}(k) \tag{18}$$

Where $p = 7$ indicates the last sampling instance with a displacement fraction $\Delta\bar{V}_\mathrm{c} \neq 0$ and $p_\text{H-0}$ is the linearization point for the high pressure.

Considering the non-linear quantizer of the modulator as an additive noise input disturbance, the deterministic discrete modulator state model becomes that in

$$\begin{aligned} x_\mathrm{m}(k+1) &= \underbrace{\begin{bmatrix} 0 \end{bmatrix}}_{A_\mathrm{m}} x_\mathrm{m}(k) + \underbrace{\begin{bmatrix} 1 \end{bmatrix}}_{B_\mathrm{m}} \alpha^*_\mathrm{m}(k) \\ \bar{\alpha}_\mathrm{m}(k) &= \underbrace{\begin{bmatrix} 1 \end{bmatrix}}_{C_\mathrm{m}} x_\mathrm{m}(k) \end{aligned} \tag{19}$$

Combining the discrete state models of the plant motor and modulator results in

$$\underbrace{\begin{bmatrix}\mathbf{x}_\mathrm{p}(k+1)\\ \mathbf{x}_\mathrm{d}(k+1)\\ x_\mathrm{m}(k+1)\end{bmatrix}}_{\mathbf{x}_\mathrm{t}(k+1)} = \underbrace{\begin{bmatrix}\mathbf{A}_\mathrm{p} & \mathbf{B}_\mathrm{p}\mathbf{C}_\mathrm{d} & 0\\ \mathbf{0} & \mathbf{A}_\mathrm{d} & \mathbf{B}_\mathrm{d}\mathbf{C}_\mathrm{m}\\ 0 & 0 & A_\mathrm{m}\end{bmatrix}}_{\mathbf{A}_\mathrm{t}} \underbrace{\begin{bmatrix}\mathbf{x}_\mathrm{p}\\ \mathbf{x}_\mathrm{d}(k)\\ x_\mathrm{m}(k)\end{bmatrix}}_{\mathbf{x}_\mathrm{t}(k)} + \underbrace{\begin{bmatrix}\mathbf{0}\\ \mathbf{0}\\ B_\mathrm{m}\end{bmatrix}}_{\mathbf{B}_\mathrm{t}} \alpha_\mathrm{m}^*(k)$$

$$\omega(k) = \underbrace{\begin{bmatrix}\mathbf{C}_\mathrm{p} & 0 & 0\end{bmatrix}}_{C_\mathrm{t}} \mathbf{x}_\mathrm{t}(k) \tag{20}$$

The above representation is hence a Discrete Linear Time Invariant state model of the system from modulator input to velocity output. Despite the representation is given in the position domain and the the system has a relatively high number of states, linear control theory may be applied and a relatively simple control problem is obtained.

2.6 Control synthesis

The complete state model is appended with an integral state to yield unity DC-gain and compensate for the plant disturbances. The integral state is given as

$$\begin{aligned} x_\mathrm{int}(k+1) &= x_\mathrm{int}(k) + e(k)\\ x_\mathrm{int}(k+1) &= x_\mathrm{int}(k) + (\omega_\mathrm{ref}(k) - \omega(k)) \end{aligned} \tag{21}$$

Where ω_ref is the motor speed reference and x_int is the integral state. The appended state model becomes that given by

$$\underbrace{\begin{bmatrix}\mathbf{x}_\mathrm{t}(k+1)\\ x_\mathrm{int}(k+1)\end{bmatrix}}_{\mathbf{x}(k+1)} = \underbrace{\begin{bmatrix}\mathbf{A}_\mathrm{t} & \mathbf{0}\\ -\mathbf{C}_\mathrm{t} & 1\end{bmatrix}}_{\mathbf{A}} \underbrace{\begin{bmatrix}\mathbf{x}_\mathrm{t}(k)\\ x_\mathrm{int}(k)\end{bmatrix}}_{\mathbf{x}(k)} + \underbrace{\begin{bmatrix}\mathbf{B}_\mathrm{t}\\ 0\end{bmatrix}}_{\mathbf{B}} \underbrace{\alpha_\mathrm{m}^*(k)}_{u(k)} + \underbrace{\begin{bmatrix}\mathbf{0}\\ 1\end{bmatrix}}_{\mathbf{B}_\omega} \omega_\mathrm{ref}(k)$$

$$\underbrace{\omega(k)}_{y(k)} = \underbrace{\begin{bmatrix}\mathbf{C}_\mathrm{t} & \mathbf{0}\end{bmatrix}}_{\mathbf{C}} \mathbf{x}(k) \tag{22}$$

As a consequence of the large number of states it is difficult to utilize manual pole placement techniques to obtain the desired closed-loop characteristics. Therefore, a deterministic optimal Linear Quadratic Regulator (LQR) control method is proposed.

The discrete LQR control problem is to minimize the quadratic cost function given in Eq. (23) by applying the optimal control input $u(k)$.

$$J = \sum_{k=1}^{\infty} \left(\mathbf{x}(k)^T \mathbf{Q}\, \mathbf{x}(k) + u(k)^T \mathbf{R}\, u(k)\right) \tag{23}$$

The input weighting matrix $\mathbf{R} = \mathbf{R}^T \geq \mathbf{0}$ specifies the importance of minimizing the control effort. Similarly, the state weighting matrix $\mathbf{Q} = \mathbf{Q}^T \geq \mathbf{0}$ specifies the importance of driving the states to zero. The full state feedback control law is given by

$$u(k) = -\underbrace{\begin{bmatrix}\mathbf{K} & K_\mathrm{int}\end{bmatrix}}_{\mathbf{K}_\mathrm{a}} \underbrace{\begin{bmatrix}\mathbf{x}_\mathrm{t}(k)\\ x_\mathrm{int}(k)\end{bmatrix}}_{\mathbf{x}(t)} \tag{24}$$

The optimal solution for the feedback controller gain vector is given as

$$\mathbf{K}_\mathrm{a} = \left(\mathbf{B}^T \mathbf{S}\, \mathbf{B} + \mathbf{R}\right)^{-1} \left(\mathbf{B}^T \mathbf{S}\, \mathbf{A}\right) \tag{25}$$

Where $\mathbf{S} = \mathbf{S}^T \geq \mathbf{0}$ is the positive-semi-definite unique solution to the Ricatti equation given by

$$\begin{aligned} \mathbf{0} &= \mathbf{A}^T \mathbf{S}\mathbf{A} - \mathbf{S} + \mathbf{Q}\\ &\quad - \left(\mathbf{A}^T \mathbf{S}\, \mathbf{B}\right) \left(\mathbf{B}^T \mathbf{S}\, \mathbf{B} + \mathbf{R}\right)^{-1} \left(\mathbf{B}^T \mathbf{S}\, \mathbf{A}\right) \end{aligned} \tag{26}$$

The state weighting is determined relative to the input weighting matrix chosen as $\mathbf{R} = 1$. Since the control objective is to minimize the reference tracking error, the integral state is weighted with high importance, resulting in
$\mathbf{Q} = \mathrm{diag}\left\{\begin{bmatrix}0 & 0 & \cdots & 0 & 0.01\end{bmatrix}\right\}$. The weighting are made such that the actuation signal barely goes into saturation if the command signal is stepped with a high amplitude. However, anti-windup of the integral state has been added with a feedback gain of 1, such that saturation does not influence the control performance.

2.7 Stability considerations

Inserting the control law in Eq. (24) into the system state representation in Eq. (22), yields the closed loop compensated system with the state equation given by

$$\mathbf{x}(k+1) = \underbrace{\left(\mathbf{A} - \mathbf{B}\, \mathbf{K}_\mathrm{a}\right)}_{\mathbf{A}_{cl}} \mathbf{x}(k) + \mathbf{B}_\omega\, \omega^* \tag{27}$$

The eigenvalues of the closed loop system matrix $\mathbf{A}_\mathrm{cl}$ determines the dynamic characteristics of the compensated system. Since the state equations has been linearized around a steady state point for of the pressure and speed, the operation point may have a significant influence on the closed loop dynamics. Therefore, the variation of closed loop pole location has been investigated to ensure stability within a specified operation region. In this study the operation interval of the pressure and speed has been

specified to those in Eq. (28) and the linearization points are chosen as the midpoint value.

$$\begin{aligned} \omega &\in \begin{bmatrix} 1200 & 1800 \end{bmatrix} \text{ rpm} \\ p_{\mathrm{H}} &\in \begin{bmatrix} 250 & 350 \end{bmatrix} \text{ bar} \\ \omega_0 &= 1500\,\text{rpm} \qquad p_{\mathrm{H0}} = 300\,\text{bar} \end{aligned} \tag{28}$$

These values are considered realistic for a high speed motor in a large scale fluid power transmission system, where the motor is driving a grid connected generator. The resulting pole locations when operated at the linearization point is shown in Fig. 9, together with the location of the worst case operation points in the chosen operation region.

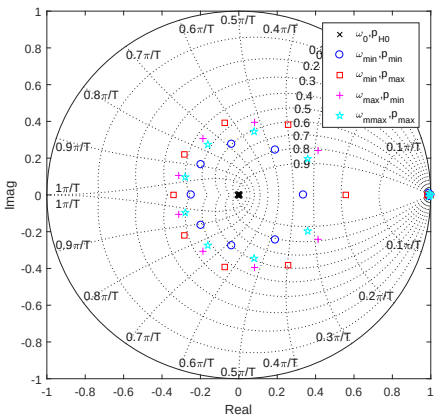

FIGURE 9. CLOSED LOOP POLE LOCATION AT VARYING OPERATION POINTS.

It is evident, that the pole locations are significantly shifted based on the given operation point, such that the dynamic performance of the system is changed accordingly. It is however observed, that the controller is stable within the specified operation region, although it has been identified that the controller becomes unstable for very low velocities of approximately $\omega < 100\,\text{rpm}$. This is also intuitive, since the time between samples are proportional to the operation speed and an increased sample time adds phase lag to the control system. Therefore, if the operation region has to be expanded to work in the unstable region it is necessary to utilize gain-scheduling techniques if the same control strategy is to be utilized. The impact of chosen linearization point has been examined as well and it is found that the choice of high pressure linearization point have a very low impact and only shift the closed-loop poles marginally. However, when choosing $\omega_0 = 1000\,\text{rpm}$, the unstable region is reduced to velocities of approximately $\omega < 45\text{rpm}$. Unfortunately, by doing this the poles for high speed operation $\omega = 1800\,\text{rpm}$ is shifted towards the vicinity of the unit circle resulting in a reduced performance with respect to overshoot.

3 Simulation results

The performance of the compensated system has been investigated through simulation in the non-linear system model. Two performance test cases has been made, one where the speed reference is stepped with varying amplitude in fixed intervals at constant load torque and one where the load torque is stepped with varying amplitude in fixed intervals at a constant speed reference. In the simulation, the flow Q_{d} is simply a first order filtered version of the motor flow with a time constant of 1. This way the pressure is kept within the desired operation region and it is ensured that it is always possible to deliver the desired torque to maintain the speed reference. The simulation results are shown in Fig. 10.

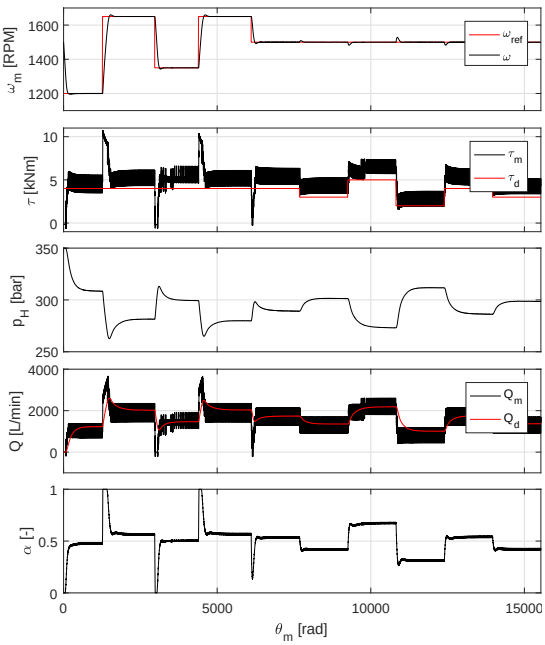

FIGURE 10. PERFORMANCE SIMULATION OF THE DESIGNED CONTROLLER.

It should be noted that the results are plotted as a function of the shaft position and not the time to maintain a synchronous control update rate. It is seen that the tracking performance is great when the speed reference is stepped. A minor overshoot is seen together with a short saturation in the actuation signal. This saturation could be avoided by reducing the weighting of the integral state when designing the controller at the cost of a slower response time. The disturbance rejection is also seen to be satisfactory with a maximum derivation of $\approx 2\,\%$ at a step of $\approx 33\,\%$ of the maximum torque. The motor torque and flow are seen to have severe ripples, which is inevitable due to the output is discretized by the relative low number of cylinders. A reduction in ripples could be obtained by implementation of an accumulator or by using partial stroke operation. This would however required a re-design of the control system, but the event-triggered control method would still be applicable.

4 Conclusion

To enable control development for a variable speed digital displacement fluid power machine, having an asynchronous sampling rate in the time domain, the method of event-driven control has been proposed. By transforming the continuous dynamic equations from the time domain to the position domain, a synchronous sampling system is obtained where traditional analysis and control design methods may be applied. The method has been applied for speed control of a digital displacement fluid power motor operating at varying pressure and load torque. Using linear deterministic optimal control, stability was shown in a specified operation region, although the closed loop pole locations are varying significantly with operation conditions. The designed controller showed great performance, both with respect to reference tracking and disturbance rejection. The performance is however limited by the digital nature of the machine, since outputs are divided into discrete levels when utilizing full stroke operation.

ACKNOWLEDGMENT

This research was funded by the Danish Council for Strategic Research through the HyDrive project at Aalborg University, at the Department of Energy Technology (case no. 1305-00038B).

REFERENCES

[1] Payne, G. S., Stein, U. P. P., Ehsan, M., Caldwell, N. J., and Rampen, W. H. S., 2005. "Potential of digital displacement hydraulics for wave energy conversion". *In Proc. of the 6th European Wave and Tidal Energy Conference, Glasgow UK*.

[2] M. Ehsan, W. R., and Salter, S., March 2000. "Modeling of digital-displacement pump-motors and their application as hydraulic drives for nonuniform loads". *ASME, Journal of dynamic system measurement and control, Vol. 122, pp. 210-215*.

[3] Rampen, W., 2010. "The development of digital displacement technology". *In Proceedings of Bath/ASME FPMC Symposium*.

[4] Wilfong, G., Batdorff, M., and Lumkes, J., 2010. "Design and dynamic analysis of high speed on/off poppet valves for digital pump/motors". *In Proceedings of the 6th FPNI-PhD Symposium*.

[5] Wilfong, G., Holland, M., and Lumkes, J., 2011. "Design and analysis of pilot operated high speed on/off valves for digital pump/motors". *In Proceedings of the 52nd National Conference on Fluid Power*.

[6] Merrill, K., Holland, M., and Lumkes, J., 2011. "Analysis of digital pump/motor operating strategies". *Proceedings of the 52nd National Conference on Fluid Power*.

[7] Heikkila, M., and Linjama, M., 2013. "Displacement control of a mobile crane using digital hydraulic power management system". *Mechatronics 23(4), pp. 452 - 461*.

[8] Song, X., 2008. "Modeling an active vehicle suspension system with application of digital displacement pump motor". *Proceedings of the ASME 2008 International Design Engineering Techical Conference/Computers and Information in Enegineering Conference, Brooklyn - New York, Vol. 5, pp. 749-753*.

[9] Armstrong, B. S. R., and Yuan, Q., June 2006. "Multi-level control of hydraulic gerotor motor and pumps". *Proceedings of the 2006 American Control Conference, Minneapolis, Minnesota, USA*. Proceedings of the 2006 American Control Conference Minneapolis, Minnesota.

[10] Sniegucki, M., Gottfried, M., and Klingauf, U., 2013. "Optimal control of digital hydraulic drives using mixed-integer quadratic programming". *In 9th IFAC Symposium on Nonlinear Control Systems*.

[11] Johansen, P., Roemer, D. B., Pedersen, H. C., and Andersen, T. O., 2015. "Delta-sigma modulated displacement of a digital fluid power pump". *In Proceedings of the 7th Workshop on Digital Fluid Power*, February 2015. The Seventh Workshop on Digital Fluid Power, Linz, Austria.

[12] Johansen, P., Roemer, D. B., Pedersen, H. C., and Andersen, T. O., 2016. "Discrete linear time invariant analysis of digital fluid power pump flow control". *Journal of dynamic system measurement and control, ASME, accepted for publication*.

[13] Pedersen, N. H., Johansen, P., and Andersen, T. O., 2016. "LQR feedback control development for wind turbines featuring a digital fluid power transmission system".

[14] Sandee, J. H., Heemels, W. P. M. H., and Hulsenboom, S. B. F. "Analysis and experimental validation of a sensor-

based event-driven controller".
[15] Sandee, J. H., Heemels, W. P. M. H., and Hulsenboom, S. B. F., 2007. "Analysis and experimental validation of a sensor-based event-driven controller". *Proceedings of the 2007 American Control Conference*.
[16] Hellems, W. P. M. H., Gorter, R. J. A., van Zijl, A., vand den Bosch, P. B. J., Weiland, S., Hendrix, W. H. A., and vonder, M. R., 1999. "Asynchronous measurement and control: a case study on motor synchronization". *Control Engineering Practice 7, 1467-1482*.

Paper G

Model Predictive Control and Discrete Analysis of Partial Stroke Operated Digital Displacement Machine

Niels H. Pedersen, Per Johansen and Torben O. Andersen

The paper has been published in
Proceedings of the 2018 Global Fluid Power Society PhD Symposium, Samara, Russia, ISBN: 978-1-5386-4785-1, doi:10.1109/GFPS.2018.8472366.

The layout has been revised.

Model Predictive Control and Discrete Analysis of Partial Stroke Operated Digital Displacement Unit

Niels Henrik Pedersen
Department of Energy Technology
Aalborg University
9220 Aalborg East, Denmark
Email: nhp@et.aau.dk

Per Johansen
Department of Energy Technology
Aalborg University
9220 Aalborg East, Denmark
Email: pjo@et.aau.dk

Torben Ole Andersen
Department of Energy Technology
Aalborg University
9220 Aalborg East, Denmark
Email: toa@et.aau.dk

***Abstract*— Successful deployment of the digital displacement machine (DDM) as the solution for future fluid power pump and motor units, demands control strategies and dynamical analysis methods for the technology. For a relatively low speed operated DDM with a relatively low number of cylinders, a partial stroke operation strategy is considered a favorable choice in the attempt of obtaining a smooth response and accurate tracking control. In partial stroke operation, the energy efficiency and severity of flow and pressure spikes are highly dependent on the flow and pressure levels when the on-off valves are opened and closed. A promising control strategy is therefore model predictive control (MPC), enabling the control objective to be a trade-off between tracking performance and energy efficiency. This paper presents a MPC strategy for a partial stroke operated digital displacement motor, controlling the pressure in a simplified load system. Since the discrete MPC model is based on discrete approximations of the non-smooth machine dynamics, an analysis study is made on the applicability of the approximation. The control strategy is validated by simulation in a non-linear model and tested under different importance weights of set-point tracking relative to energy efficiency.**

***Index Terms*—Digital Displacement machines, Fluid Power, Model Predictive Control**

I. Introduction

The digital displacement machine (DDM) is a promising technology as the solution for the future fluid power pump and motor units, since the efficiency may be significantly increased with respect to conventional fluid power machines [1], [2]. The DDM has a modular design with several individual pressure chambers, where each chamber has two electro-magnetically actuated on/off valves controlling the flow to and from the high and low pressure manifold. This way the displacement throughput may be lowered effectively for partial load operation, since the individual pressure chambers may be held inactive at a low pressure. A detailed description of the digital displacement (DD) technology is published in several papers [3]–[5]. The simplest and most energy efficient operation strategy is full-stroke, where the displacement throughput is determined by the ratio of active pressure chambers, such that each chamber may either commit its full displacement or none. Since the control update rate in full stroke operation is done at fixed shaft angles, the control performance suffers at low speed. Additionally, full stroke operation yields a discrete output based on the ratio of activated pressure chambers. As a result, it is considered beneficial to utilize a partial-stroke strategy for low speed operation, where a fraction of the full-stroke may be committed for each pressure chamber. The displacement fraction of a partial stroke operated DD unit is determined by the angle where the pressure chamber is deactivated through switching the valve states. However, the energy efficiency and severity of pressure and flow spikes depends on the deactivation angle. It is most costly to switch the valve states at high flow rates occurring at the midpoint in a stroke, where also the largest pressure spikes are obtained as a result. Optimal control performance is therefore considered a trade-off between reference tracking and energy efficiency.

Several research studies on partial stroke operation have been conducted, but they do in general neglect transient behavior and energy efficiency. Ehsan et. al. [3] presents a control algorithm based on a volume estimation needed to attain the pressure reference in a look-ahead angle. A similar strategy is proposed by Heikkilä and Linjama [6], where the oil compressibility is included to improve the method. Despite that these methods show great practical applicability, they do not enable dynamic model based feedback control and further do not allow to optimize the energy efficiency.

To enable model based feedback control design and include energy efficiency as a performance objective, this paper proposes a model predictive control (MPC) strategy for a partial stroke operated DD motor, where the cost function includes the energy efficiency. The discretization method used for describing the DDM dynamics is based on previous studies [7], which has been successfully applied for full stroke control of a digital fluid power transmission for a wind turbine [8], [9]. In this article the partial stroke MPC strategy is exemplified for pressure control of a simplified load transmission system and tested in a non-linear simulation model representing the physical behavior of the DDM. Even though the transmission test system is simple, the control method of the DDM is still considered to be applicable for more advanced hydraulic systems.

II. System description and model

To evaluate the control performance a non-linear mathematical model describing the digital displacement machine

978-1-5386-4785-1/18/$31.00

dynamics is presented. In this paper, a motor operation is considered, but the presented model and control strategy is also valid for pump operation. The model is based on the illustration of the machine shown in Fig. 1.

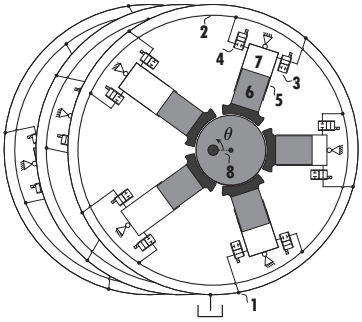

Fig. 1. Illustration of the radial piston digital displacement motor with 15 pressure chambers. With inspiration from [10].

It is seen that the DDM consists of three modules with five cylinders in each for a total of 15 radially distributed cylinders. Electro-magnetic actuated on-off valves is seen to control the flows to and from the high (HPV) and low (LPV) pressure manifold respectively. How these valves are opened and closed hence regulates the pressure level in the cylinder chamber.

The proposed control strategy is to be tested in a non-linear simulation model representing the physical system, why the governing equations describing the system dynamics are presented. The model is inspired by the work in [11], where a similar machine is modeled. The piston stroke length, x, as function of the shaft angle is given by

$$x_i = r_\mathrm{e}\ (1-\cos(\theta_i)) \quad \theta_i = \theta + \frac{2\,\pi}{N_\mathrm{c}}\ (i-1) \quad i \in \{1,..,N_\mathrm{c}\} \tag{1}$$

where r_e is the eccentric radius being equal to half the stroke length and $N_\mathrm{c} = 15$ is the number of cylinders. The cylinder chamber volume, V is then described by

$$\begin{aligned} V_i &= \frac{V_\mathrm{d}}{2}\ (1-\cos(\theta_i)) + V_0 \\ \dot{V}_i &= \frac{V_\mathrm{d}}{2}\,\dot{\theta}\ \sin(\theta_i) \end{aligned} \tag{2}$$

The chamber volume is given as $V_\mathrm{d} = V_0 = 2\,r_\mathrm{e}\,A_\mathrm{p}$, where A_p is the piston area. The pressure dynamics is described by the continuity equation and is given by

$$\dot{p}_i = \frac{\beta_\mathrm{e}(p_\mathrm{i})}{V_i}\ \left(Q_{\mathrm{H},i} - Q_{\mathrm{L},i} - \dot{V}_i\right) \tag{3}$$

where Q_H and Q_L are the flows through the high and low pressure valve respectively and β_e is the effective oil bulk modulus, which pressure dependency is modeled in accordance with [12]. The valve flows are described by a modified orifice equation yielding

$$\begin{aligned} Q_{\mathrm{L},i} &= \frac{\bar{x}_\mathrm{L}}{k_\mathrm{f}}\ \sqrt{|p_i - p_\mathrm{L}|}\ \mathrm{sign}\,(p_i - p_\mathrm{L}) \\ Q_{\mathrm{H},i} &= \frac{\bar{x}_\mathrm{H}}{k_\mathrm{f}}\ \sqrt{|p_\mathrm{H} - p_i|}\ \mathrm{sign}\,(p_\mathrm{H} - p_i) \end{aligned} \tag{4}$$

where k_f is the valve flow coefficient and $\bar{x}_\mathrm{L}$ and $\bar{x}_\mathrm{H}$ are normalized valve plunger positions. The plunger dynamics is modeled as a constant acceleration term given by

$$a_{\mathrm{v}+} = \begin{cases} 4/t_\mathrm{s}^2 & for\ \ 0 \le t \le t_\mathrm{s}/2 \\ -4/t_\mathrm{s}^2 & for\ \ t_\mathrm{s}/2 \le t \le t_\mathrm{s} \end{cases} \tag{5}$$

where t_s is the plunger opening/closing time. This results in a position response that is smooth and similar to what may be expected if a more detailed valve model with forces had been utilized. For a more detailed model see e.g. [11], [13], [14]. Despite the relatively simple valve model, the important characteristics with respect to machine level control is included.

A. Valve timing and control

The valve actuation is described by considering the hybrid automaton shown in Fig. 2. The system input is hence the actuation signal to the valves, $u = \begin{bmatrix} u_\mathrm{H} & u_\mathrm{L} \end{bmatrix}^T$ for the high and low pressure valve respectively.

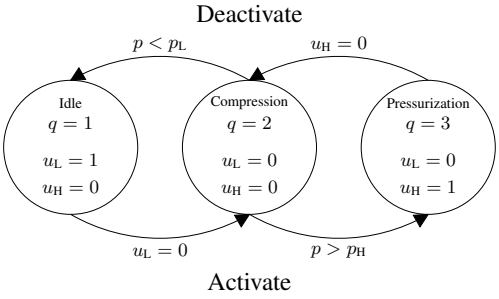

Fig. 2. Hybrid Automaton representation of valve control of the digital displacement machine.

An active valve closing and passive valve opening is used, where the closing of the low pressure valve (LPV) is done closely before top dead center (TDC) for motoring operation. With both valves closed as the chamber volume decreases, the chamber pressure increases and exceeds the high pressure at TDC, which then passively opens the high pressure valve (HPV) due to the pressure force. The HPV is similarly closed at an angle that yields the desired displacement during the motoring stroke. Again, with both valves closed as the chamber volume increases, the LPV is passively opened due to suction shortly after. Simulation results of the non-linear model is shown in Fig. 3, where a full motor stroke is committed. A full stroke is seen to end ahead of BDC to allow for

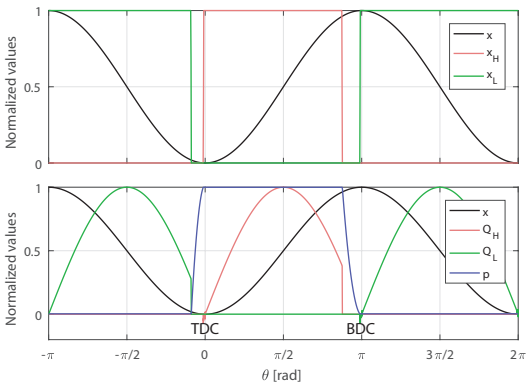

Fig. 3. Simulation results of the non-linear model using a full stroke. $p_{\mathrm{H}} = 300$ bar and $\dot{\theta} = 100$ rpm.

passive opening of the LPV ahead of BDC, why the maximum theoretically displacement is not fully utilized. It is seen that the flow characteristic is approximately a sine wave and the angle where the HPV is closed determines the fraction of the sine wave that yields an output.

The total flow to the high pressure line is the sum of flows from the individual chambers through the high pressure valves and is determined by

$$Q_{\mathrm{m}} = \sum_{i=1}^{N_{\mathrm{c}}} Q_{\mathrm{H,i}} \tag{6}$$

The parameters used to set up the non-linear simulation model of the DD motor is provided in Tab. II-A.

TABLE I
PARAMETERS OF THE DIGITAL DISPLACEMENT MOTOR

Parameter	symbol	value	Unit
Piston area	A_{p}	31	cm^2
Piston displacement	r_{e}	25	mm
Chamber flow coefficient	k_{f}	$0.5 \cdot 10^5$	$\sqrt{Pa}\ s/\mathrm{m}^3$
Valve actuation time	t_{s}	3	ms
LPV closing angle	$\theta_{\mathrm{L\text{-}cl}}$	-16.5	deg
Low pressure	p_{L}	1	bar
Maximum bulk modulus	β_{e}	16000	bar

III. DLTI MODEL AND ANALYSIS

The flow throughput of the DDM may be approximated discretely by considering the impulse response of a single pressure chamber, which results in a Discrete Linear Time Invariant (DLTI) model. It is identified in Fig. 3 that the chamber pressure is equal to the high pressure and thus approximately constant in the active part of the motoring stroke, why $Q_{\mathrm{H}} \approx \dot{V}$ is a valid assumption of the flow characteristic. This approximation yields the following relation between displacement and flow

$$Q_{\mathrm{H}} \approx \frac{dV(\theta(t))}{dt} = \frac{dV(\theta(t))}{d\theta}\,\dot{\theta} \tag{7}$$

$$\mathcal{D}_{\mathrm{c}} = \frac{dV(\theta(t))}{d\theta} = \frac{V_{\mathrm{d}}}{2}\sin(\theta) \tag{8}$$

where $\mathcal{D}_{\mathrm{c}}$ is the oil displacement volume. The impulse response of a partial stroke operated DD unit behaves different than that of a conventional dynamical system. This is due to the input being a state changing angle, ϕ, that scales the width of the response, rather than a conventional system which input scales the magnitude of the response. To normalize the input, an input variable change is made, such that the input is a displacement fraction $\eta \in [0\,;1]$. The input transformation is done by the relation given by

$$\eta = \frac{V(\phi(\eta))}{V(\pi))} \quad \rightarrow \quad \phi(\eta) = \mathrm{acos}(1-2\,\eta) \quad \eta \in [0\,;1] \tag{9}$$

The new normalized input hence describes the percentage of the maximum displacement. How the impulse response of the DD unit depends on the input is illustrated in Fig. 4.

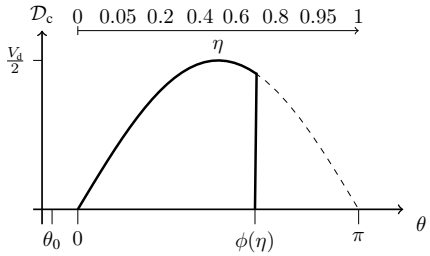

Fig. 4. Impulse response as function of the input, $\eta = 0.7$.

How the input changes the system dynamics becomes evident when performing discretization of the response. This is done by considering the flow throughput between samples, which relates to the displacement fraction between samples given by

$$\begin{aligned} Q_{\mathrm{H}}[k] &\approx \frac{V_{\mathrm{d}}}{\theta_{\mathrm{s}}}\left(\bar{V}(\theta[k+1]) - \bar{V}(\theta[k])\right)\,\dot{\theta} \\ &\approx \frac{V_{\mathrm{d}}\,N}{2\,\pi}\,\dot{\theta}\,\Delta\bar{V}[k] \end{aligned} \tag{10}$$

where $\bar{V}$ is the normalized chamber volume. In MPC control, the prediction horizon and sampling time are two key parameters. Since the energy cost of a state change is directly influenced by the angle ϕ, it is considered beneficial to have a prediction horizon equal to half of a revolution (corresponding to a full stroke). Furthermore, to reduce the input delay it is beneficial to have a sample each time a motoring decision

is made (the angle where the LPV is closed). Therefore, the angle where a sample occurs is given by

$$\theta[k] = \theta_0 + \frac{2\,\pi}{N_\mathrm{c}}\,k \qquad k \in \{0, \ldots, N_\mathrm{c} - 1\} \tag{11}$$

where θ_0 is the local angle where the LPV is closed.

Considering the impulse response shown in Fig. 4, a discretization with the sampling angle, θ_s, results in the displacement fraction as function of sample number determined by

$$\Delta\bar{V}[k] = \begin{cases} 0 & \theta[k], \theta[k+1] \notin [0\,;\phi] \\ \bar{V}(\theta[k+1]) - \bar{V}(\theta[k]) & \theta[k], \theta(k+1) \in [0\,;\phi] \\ \bar{V}(\theta[k+1]) - \bar{V}(0) & \theta[k] < 0 < \theta[k+1] \\ \bar{V}(\phi) - \bar{V}(\theta[k]) & \theta[k] < \phi < \theta[k+1] \end{cases} \tag{12}$$

The motor flow response may then be written as a convolution sum given by

$$Q_\mathrm{m}[k] = \underbrace{\frac{V_\mathrm{d}\,N_\mathrm{c}}{2\,\pi}}_{k_\mathrm{m}}\,\dot{\theta}\,\alpha[k] \quad \alpha[k] = \sum_{m=0}^{k} \Delta\bar{V}[k-m]\,u[m] \tag{13}$$

For the full stroke shown in Fig. 3, the maximum displacement is $\hat{\eta} = 0.96$, which yields the discrete impulse response shown in Fig. 13.

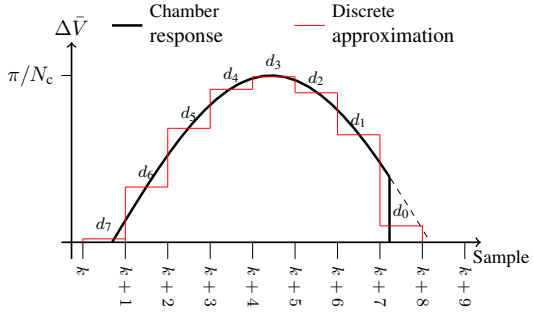

Fig. 5. Discretization of displacement response, where $\eta = 0.96$ corresponding to the maximum displacement.

It is seen that the resolution of the discrete approximation is determined by the number of cylinders, but the discrete model is fairly accurate since the displacement between samples in the model is equal to that of the physical machine.

A control challenge when using DLTI-control of this system is that the system order depends on the input η. For the full stroke shown in Fig. 5 the convolution model may be written as a discrete transfer function given by

$$G(z) = \frac{\alpha}{u} = \frac{d_7\,z^7 + d_6\,z^6 + \cdots + d_1\,z + d_0}{z^7} \tag{14}$$

where $d_\mathrm{k} = \bar{\Delta}V[7-k]$ is the displacement fraction between samples. Having a displacement fraction input of $\eta = 0.5$ yields the impulse response shown in Fig. 6.

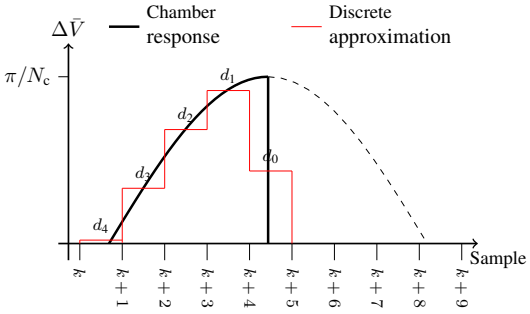

Fig. 6. Discretization of displacement response, where $\eta = 0.5$ corresponding to half of a stroke.

In this partial stroke example, the displacement is committed over less samples, such that the transfer function order is reduced to

$$G(z) = \frac{\alpha}{u} = \frac{d_4\,z^4 + d_3\,z^3 + \cdots + d_1\,z + d_0}{z^4} \tag{15}$$

The system is thus seen to be time invariant depending on the input, η. However, the magnitude of the response is constant for all inputs, meaning that the discrete model input is always unity, $u = 1$. Since this input is constant, it is not possible to apply time-variant MPC, which search for the optimum input, u, that minimizes a cost function. To overcome this problem a conservative angle averaging approximation is proposed, which results in a time-invariant model applicable for MPC.

A. Angle averaging approach

The control challenge imposed by having an input that scales the width of the response instead of the amplitude of the response is in this article solved conservatively by an angle averaging approach. This approach exploits that the full stroke DLTI-model where $\eta = 1$ and with input $u \in [0\,;1]$, yields the same integrated output as a partial stroke model with $\eta \in [0\,;1]$ and the input $u = 1$ over a half of a shaft revolution. This is illustrated in Fig. 7.

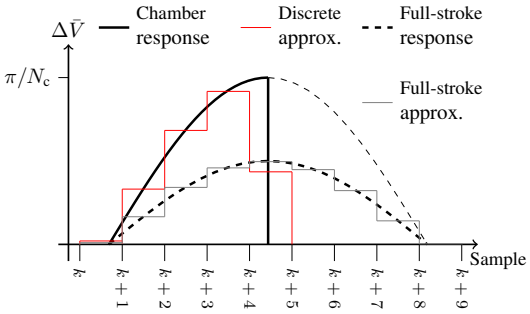

Fig. 7. Illustration how a full stroke $\eta = 1$, with $u = 0.5$ yields the angle average committed displacement as if $\eta = 0.5$ and $u = 1$.

The sum of displacements of a partial stroke with $\eta = 0.5$ is seen to be the same as a full stroke multiplied by 0.5 and as a result the two model approaches are angle averaging equal for every half of a revolution. However, the full stroke approximation method is seen to introduce the maximum amount of phase to the impulse response, since additional samples are introduced. This is a result of the longer time the displacement commitment takes with the approximation. This approach corresponds to choosing a linearization point of $\eta = 1$ when developing a DLTI model, which corresponds to a worst-case scenario with respect to the phase as shown by the frequency response as function of the displacement fraction in Fig. 8.

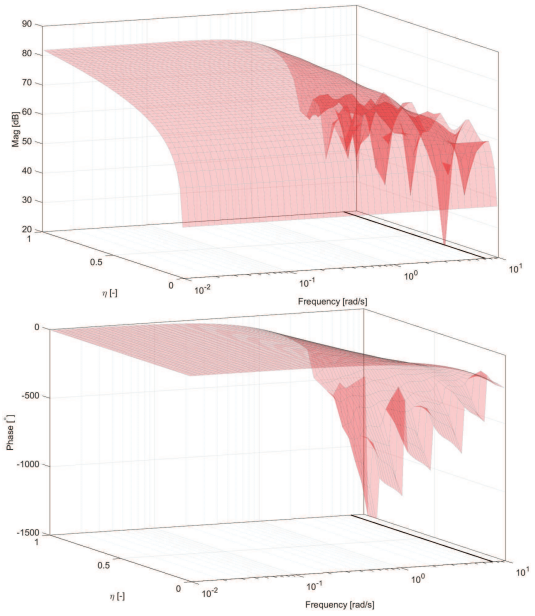

Fig. 8. Frequency response of the DLTI model as function of the displacement fraction η. The thick black line indicates the Nyquist frequency.

It is seen how extra phase is added to the system in discrete steps every time the order is increased and that the maximum phase is for a full stroke as expected. The reduced gain at lower displacement does not raise concerns with respect to control, since it may be compensated for by the controller gain.

B. Discrete load model

A simplified load system is constructed for the purpose of illustrating the applicability of the control strategy. The simplified load system is shown in Fig. 9. A fixed-speed fixed-displacement pump is considered, supplying a pressurized fluid flow, Q_p to the high pressure line. The fixed speed DD motor intakes the flow, Q_m, and is used to control high pressure by the displacement fraction, η. Defining the pressure

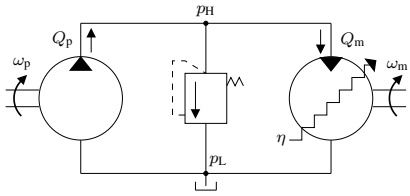

Fig. 9. The simplified load system used for illustration of MPC structure.

difference as $\Delta_\mathrm{p} = p_\mathrm{H} - p_\mathrm{L}$, where the low pressure is considered constant, the pressure dynamics of the transmission is described by

$$\begin{aligned} \Delta\dot{p} &= \frac{\beta_\mathrm{e}}{V_\mathrm{H}} \left(\underbrace{V_\mathrm{p}\,\omega_\mathrm{p}}_{Q_\mathrm{p}} - Q_\mathrm{m} - k_\mathrm{l}\,\Delta_\mathrm{p} \right) \\ \underbrace{\Delta\dot{p}}_{\dot{x}_\mathrm{p}} &= \underbrace{-\frac{\beta_\mathrm{e}}{V_\mathrm{H}}\,k_\mathrm{l}}_{A_\mathrm{c}}\,\underbrace{\Delta p}_{x_\mathrm{p}} - \underbrace{\frac{\beta_\mathrm{e}}{V_\mathrm{H}}}_{B_\mathrm{c}}\,\underbrace{Q_\mathrm{m}}_{u_\mathrm{p}} + \underbrace{\frac{\beta_\mathrm{e}}{V_\mathrm{H}}}_{B_\mathrm{cq}}\,\underbrace{Q_\mathrm{p}}_{u_\mathrm{q}} \end{aligned} \tag{16}$$

A constant bulk-modulus is used since the pressure is controlled such that it is sufficiently high to consider the fluid stiffness constant. The parameters of the load transmission is provided in Tab. III-B.

TABLE II
PARAMETERS OF THE LOAD TRANSMISSION

Parameter	symbol	value	Unit
Effective Bulk modulus	β_e	16000	bar
High pressure volume	V_H	50	l
Leakage coefficient	k_l	6e-3	l/(min · bar)
Pump flow	Q_p	78	l/min

A discretization of the load plant yields the discrete state model given by Eq. (17), where the sampling time is given by $T_\mathrm{s} = 2\,\pi/(N_\mathrm{c}\,\dot{\theta})$.

$$\begin{aligned} x_\mathrm{p}(k+1) &= A_\mathrm{p}\,x_\mathrm{p}(k) + B_\mathrm{p}\,u_\mathrm{p}(k) + B_\mathrm{q}\,u_\mathrm{q}(k) \\ y(k) &= C_\mathrm{p}\,x_\mathrm{p}(k) \end{aligned} \tag{17}$$

The discrete transfer function in Eq. (14) or the convolution model representation in Eq. (13) of the motor flow, where $\eta = 1$ may be rewritten into a state-space formulation resulting in

$$\begin{aligned} \underbrace{\begin{bmatrix} x_\mathrm{m}(k) \\ x_\mathrm{m}(k-1) \\ x_\mathrm{m}(k-2) \\ \vdots \\ x_\mathrm{m}(k-p+1) \end{bmatrix}}_{\mathbf{x}_\mathrm{m}(k+1)} &= \underbrace{\begin{bmatrix} 0 & 0 & \cdots & 0 & 0 \\ 1 & 0 & \cdots & 0 & 0 \\ 0 & 1 & \cdots & 0 & 0 \\ \vdots & \vdots & \ddots & \vdots & \vdots \\ 0 & 0 & \cdots & 1 & 0 \end{bmatrix}}_{\mathbf{A}_\mathrm{m}} \underbrace{\begin{bmatrix} x_\mathrm{m}(k-1) \\ x_\mathrm{m}(k-2) \\ x_\mathrm{m}(k-3) \\ \vdots \\ x_\mathrm{m}(k-p) \end{bmatrix}}_{\mathbf{x}_\mathrm{m}(k)} + \underbrace{\begin{bmatrix} 1 \\ 0 \\ 0 \\ \vdots \\ 0 \end{bmatrix}}_{\mathbf{B}_\mathrm{m}} u(k) \\ u_\mathrm{p}(k) &= \underbrace{k_\mathrm{m}\,\dot{\theta}\,\begin{bmatrix} \Delta\bar{V}_\mathrm{c}[1] & \cdots & \Delta\bar{V}_\mathrm{c}[p] \end{bmatrix}}_{\mathbf{C}_\mathrm{m}} \mathbf{x}_\mathrm{m}(k) + \underbrace{k_\mathrm{m}\,\dot{\theta}\,\begin{bmatrix} \Delta\bar{V}_\mathrm{c}[0] \end{bmatrix}}_{D_\mathrm{m}} u(k) \end{aligned} \tag{18}$$

Combining the discrete load model and the motor flow model results in the discrete state representation of the complete system given by

$$\underbrace{\begin{bmatrix} x_\mathrm{p}(k+1) \\ \mathbf{x}_\mathrm{m}(k+1) \end{bmatrix}}_{x(k+1)} = \underbrace{\begin{bmatrix} A_\mathrm{p} & B_\mathrm{p}\,\mathbf{C}_\mathrm{m} \\ \mathbf{0} & \mathbf{A}_\mathrm{m} \end{bmatrix}}_{A} \underbrace{\begin{bmatrix} x_\mathrm{p} \\ \mathbf{x}_\mathrm{m}(k) \end{bmatrix}}_{x(k)} + \underbrace{\begin{bmatrix} B_\mathrm{p}\,D_\mathrm{m} \\ \mathbf{B}_\mathrm{m} \end{bmatrix}}_{B} u(k) + \underbrace{\begin{bmatrix} B_\mathrm{q} \\ 0 \end{bmatrix}}_{\bar{B}q} u_\mathrm{q}(k)$$
$$y(k) = \underbrace{\begin{bmatrix} C_\mathrm{p} & 0 \end{bmatrix}}_{C} x(k) \tag{19}$$

This model is used to set-up a model predictive optimization problem for control of the pressure.

IV. MODEL PREDICTIVE CONTROL

This paper presents a pressure control method, but the presented MPC control strategy could be applied for flow, torque or speed control as well. In this paper a fixed speed machine is considered. However, applying the strategy for a varying speed DDM is possible but requires transformation of the load dynamics into the position domain by the method presented in [15]. The optimization problem is to identify the optimal displacement fraction input, η^*, based on a combination of reference tracking accuracy and energy cost given by

$$u^* = \eta^* = \underset{\eta^* \in [\bar{\eta},\, \hat{\eta}]}{\operatorname{argmin}} \left\{ J_1^T\, J_1 + W_1\, J_2^T\, J_2 \right\} \tag{20}$$

$$J_1 = \sum_{k=1}^{p} \left(y[k] - y_\mathrm{ref}[k] \right) \tag{21}$$

$$J_2 = \frac{1}{p_\mathrm{e}} \sum_{k=1}^{p_\mathrm{e}} V'(\phi(\eta[i])) \tag{22}$$

where η^* is a vector containing the optimal inputs in the prediction horizon, p, while $\bar{\eta} = 0.96$ and $\underline{\eta} = 0$ are the maximum and minimum displacement fractions. J_1 is the cost function for the reference tracking, J_2 is the cost function for the energy cost and W_1 is a weight parameter between the two cost functions. The tracking error cost function J_1 is seen to be the sum of errors in the prediction horizon and J_2 is a normalized term specifying the flow level when switching. $p_\mathrm{e} \in [1\,;p]$ specifies the number of inputs considered in the energy cost function. Alternatively, a weighting function could be introduced to increase the importance of the first sample/samples in the prediction horizon, which similarly could be made for the reference tracking cost function. The function V' takes into account it is costlier to switch at high flow, where larger losses and pressure spikes occur and is given as

$$V'(\theta) = c + \max(\sin(\theta), 0) \tag{23}$$

An illustration of the model predictive control strategy for estimating the individual chamber displacement fractions and for evaluation of the energy cost function is shown in Fig. 10 The current sample is seen to be for cylinder 5, where the displacement fraction is $\eta = 0.49$. The displacement fractions for the previously cylinders in the prediction horizon is already fixed, while the MPC algorithm estimates the optimal displacement fraction for the subsequent cylinders in the prediction horizon.

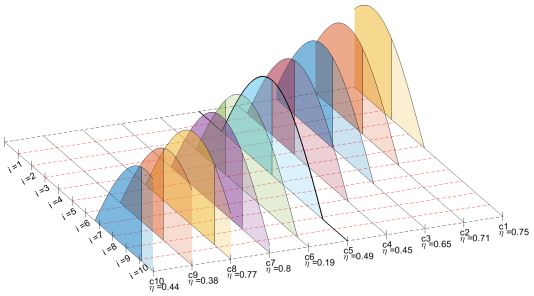

Fig. 10. Illustration of the flow profiles of the digital displacement machine within the prediction horizon.

The derivation for determine the output in the prediction horizon is done by considering the DLTI state equation in Eq. (19) and rewrite it as

$$\begin{aligned} x(k+1) &= A\,x(k) + B\,u(k) + \bar{B}_\mathrm{q}\,u_\mathrm{q}(k) \\ y(k) &= C\,x(k) \end{aligned} \tag{24}$$

Due to the DLTI approximation and since the pump flow is a disturbance to the linear control system, integral action is added to obtain offset-free reference tracking. The integral state is added by modifying the state equation to a state difference equation in accordance with [16], resulting in

$$\begin{aligned} \Delta x(k+1) &= A\,\Delta x(k) + B\,\Delta u(k) + \bar{B}_\mathrm{q} \cancelto{0}{\Delta u_\mathrm{q}(k)} \\ \Delta y(k+1) &= C\,\Delta x(k+1) \end{aligned} \tag{25}$$

where $\Delta x(k) = x(k) - x(k-1)$, $\Delta u(k) = u(k) - u(k-1)$ and $\Delta y(k) = y(k) - y(k-1)$. Combining the state and output expression yields the desired recursive output state given by

$$\begin{aligned} \Delta y(k+1) &= C\,\Delta x(k+1) \\ y(k+1) - y(k) &= C\,\left(A\,\Delta x(k) + B\,\Delta u(k)\right) + D\,\Delta u(k) \\ y(k+1) &= C\,A\,\Delta x(k) + C\,B\,\Delta u(k) + y(k) \end{aligned} \tag{26}$$

The resulting output formulation is seen to act as a discrete integral state. The resulting state formulation of the system then becomes

$$\underbrace{\begin{bmatrix} \Delta x(k+1) \\ y(k+1) \end{bmatrix}}_{\bar{x}(k+1)} = \underbrace{\begin{bmatrix} A & 0 \\ C\,A & I \end{bmatrix}}_{\bar{A}} \underbrace{\begin{bmatrix} \Delta x(k) \\ y(k) \end{bmatrix}}_{\bar{x}(k)} + \underbrace{\begin{bmatrix} B \\ C\,B \end{bmatrix}}_{\bar{B}} \Delta u(k)$$
$$y(k) = \underbrace{\begin{bmatrix} 0 & I \end{bmatrix}}_{\bar{C}} \bar{x}(k) \tag{27}$$

By recursive evaluation, the presented state model is used to predict the future state development in the prediction horizon. The recursive state estimation is given by

$$\underbrace{\begin{bmatrix}\bar{x}(k+1)\\ \bar{x}(k+2)\\ \bar{x}(k+3)\\ \vdots\\ \bar{x}(k+p)\end{bmatrix}}_{\underline{\mathrm{x}}} = \underbrace{\begin{bmatrix}\bar{B} & 0 & 0 & \dots & 0\\ \bar{A}\,\bar{B} & \bar{B} & 0 & \dots & 0\\ \bar{A}^2\,\bar{B} & \bar{A}\,\bar{B} & \bar{B} & \dots & 0\\ \vdots & \ddots & & \ddots & \vdots\\ \bar{A}^{p-1}\,\bar{B} & \bar{A}^{p-2}\,\bar{B} & \bar{A}^{p-3}\,\bar{B} & \dots & \bar{B}\end{bmatrix}}_{\underline{\mathrm{A}}} \underbrace{\begin{bmatrix}\Delta u(k)\\ \Delta u(k+1)\\ \Delta u(k+2)\\ \vdots\\ \Delta u(k+p-1)\end{bmatrix}}_{\Delta\underline{\mathrm{u}}} + \underbrace{\begin{bmatrix}\bar{A}\\ \bar{A}^2\\ \bar{A}^3\\ \vdots\\ \bar{A}^p\end{bmatrix}}_{\underline{\mathrm{B}}} \bar{x}(k)$$

$$\underline{\mathrm{y}} = \underbrace{\begin{bmatrix}\bar{C} & 0 & 0\dots & 0\\ 0 & \bar{C} & 0\dots & 0\\ 0 & 0 & \bar{C}\dots & 0\\ \vdots & \vdots & \vdots\ddots & \vdots\\ 0 & 0 & 0\dots & \bar{C}\end{bmatrix}}_{\underline{\mathrm{C}}} \underline{\mathrm{x}} \tag{28}$$

The resulting output estimation may thus be written on a simplified form as

$$\underline{\mathrm{y}} = \underbrace{\underline{\mathrm{C}}\,\underline{\mathrm{A}}}_{\Psi}\,\Delta\underline{\mathrm{u}} + \underbrace{\underline{\mathrm{C}}\,\underline{\mathrm{B}}}_{\gamma}\,\bar{x}(k) \tag{29}$$

This expression is used to estimate the future states in the prediction horizon for evaluation of the tracking cost function in Eq. (21).

V. Results

The MPC pressure control strategy for a partial stroke operated DDM is tested by implementation in the non-linear simulation model of the DD motor and transmission. To investigate the influence of the energy cost, the most optimal tracking performance is initially investigated by choosing the scaling parameter $W_1 = 0$. The reference input is chosen as a sine function, such that the motor is operating at both high and low displacements. For a 100 rpm machine the optimization problem has been solved online within the real time sampling period by the Differential Evolution Algorithm [17], but faster and more powerful optimization algorithms for this problem is very likely to exist. This is however not investigated further in this paper. The simulation results is shown in Fig. 11. It is seen that the flow response due to the digital machine behavior is highly fluctuating, but the relatively large fluid capacity of the pressure line smoothens the pressure response and results in a decent pressure reference tracking with only minor ripples. The flow from the non-linear model is seen to have larger spikes than that predicted by the DLTI-model, which is due to the angle averaging approximation which flattens the response as shown in Fig. 7. There is several energy expensive state switchings ($u \approx 0.5$), which at high pressure has a rather significant energy cost.

The optimization problem of finding a combination of the ideal displacement fractions is considered rather complex and is found to have a very large number of local minimum points. This problem has been addressed by running the same simulation 350 times and investigate the variance in the tracking performance. The tracking performance is evaluated by the sum of absolute errors given by

$$e_{\mathrm{rr}} = \sum_{n=1}^{N} |y(n) - y_{\mathrm{ref}}(n)| \tag{30}$$

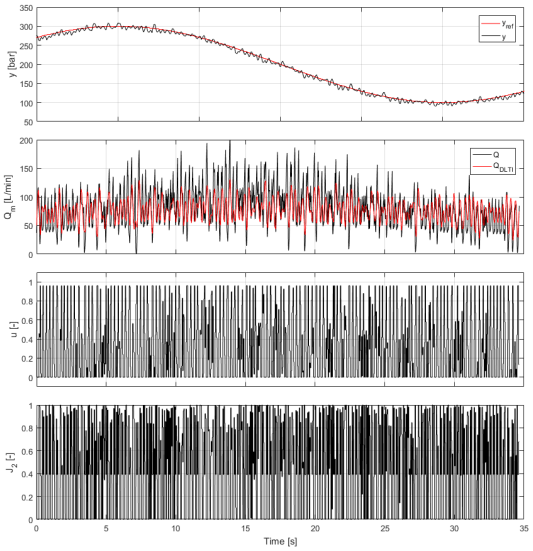

Fig. 11. Simulation results for the MPC strategy in the non-linear simulation model where $W_1 = 0$ and $p_{\mathrm{e}} = 1$.

The resulting error histogram is shown in Fig. 12, together with an estimated normal distribution function of the results.

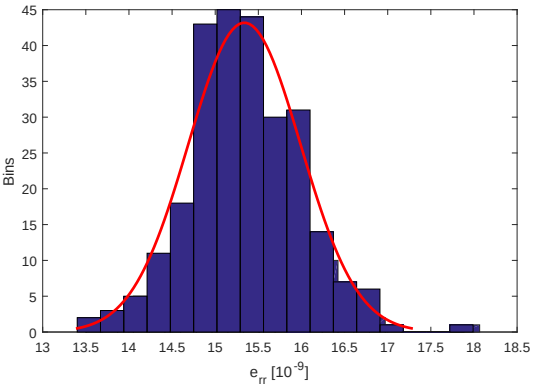

Fig. 12. Histogram of the sum of absolute error running the same optimization problem numerous times.

Since the same problem is solved multiple times, it would be ideal to find the minimum error every time, which is seen to be $e_{rr} \approx$ 13.5e-9 or less. However, a mean error of $e_{rr} \approx$ 15.25e-9 and a maximum error of $e_{rr} \approx$ 18e-9 is observed. This corresponds to a mean deviation of 13% and a maximum deviation of 33% from the optimal set-point. This is considered a quite significant deviation, why it is desired to investigate into better optimization algorithms for this problem.

To investigate the influence of the energy cost function, the weighting parameter is changed to $W_1 = 1e10$. The results of the simulation is shown in Fig. 13.

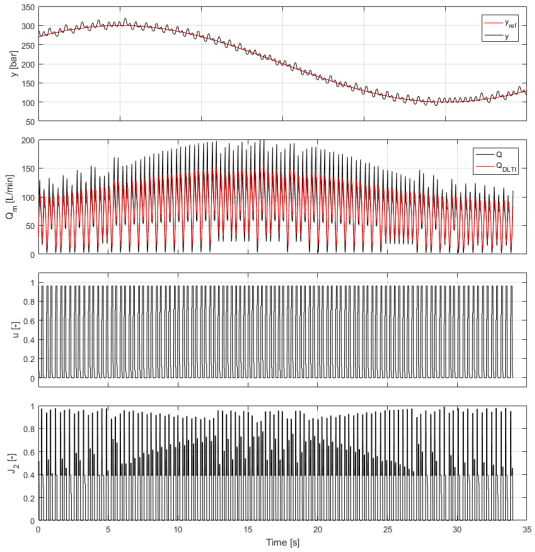

Fig. 13. Simulation results for the MPC strategy in the non-linear simulation model where $W_1 = 1e13$ and $p_e = 1$.

The tracking response is seen to be less accurate and have larger ripples around the set-point compared to the results in Fig. 11. However, the number of expensive state switchings has been reduced significantly and switchings occurs more often at either $\eta = 0$ or $\eta = 0.96$ which corresponds to an idling and a full stroke respectively.

To investigate the influence of the energy cost function, the pressure reference tracking error and the energy cost J_2 is summed over the presented time period and compared. The results are provided in Tab. III.

TABLE III
COMPARING OF RESULTS WITH AND WITHOUT ENERGY COST.

Parameter	w/o. J_2	w. J_2
W_1	0	1e13
Sum of absolute error	2.42e10	7.75e10
Sum of energy	5.33e4	8.08e3

The sum of absolute tracking error is 69 % higher with the energy cost function included, but the energy cost is 85 % higher without the energy cost function. Based on the application and control objective, the parameter W_1 may be determined by a trial-and-error method to yield the best comprise based on control and energy requirements for the specific application.

Even though the presented MPC strategy shows promising results with respect to control of a relatively low speed digital displacement machine, there are several aspects of the strategy that should be improved if possible.

Angle averaging approximation: An angle averaging approach has been used to develop a DLTI-model of the DD motor. An improvement would be to use a time-variant model description, where the model is dependent on the input. However, to describe the output correctly it is required that the input is always unity and as a result it does not fit into classical MPC. However, modified MPC algorithms where only the plant dynamics is updated may possibly increase the performance significantly.

Re-decision of state changing angle: If the optimal state changing angle for a given chamber occurs after the subsequent samples, it would be beneficial to be able to make a re-decision of the angle. In the current implementation, the closing angle is chosen before the stroke is initiated and may not be changed. An improved method would be to enable re-decision of the already decided closing angle if the closing angle has not yet been surpassed at the subsequent samples. This would reduce the decision phase, which is currently up to half of a revolution $2\,\pi/2$, to only be up to the angle between two decisions $2\,\pi/N_c$.

Constraints on state changing angle: In the presented strategy the state changing angle may take any value in the interval $\eta = [0,\ 0.96]$. However, it is considered unfavorable to change the state near 0, since it would provide almost no effective displacement. However, it is very important that $\eta = 0$ may be chosen, since idling mode is the most energy efficient choice.

CONCLUSION

A model predictive control strategy (MPC) for a relatively low speed and partial stroke operated digital displacement machine (DDM) was presented. It was shown that the input to a partial stroke operated DDM changes the width of the response, such that the model order of a discrete model is dependent on the input. To overcome this problem and enable discrete linear time invariant (DLTI) control, a conservative angle averaging approach was presented. The MPC strategy was applied for pressure control of a simplified load transmission system to illustrate the applicability of the strategy. The trade-off between reference tracking and energy efficiency was investigated by simulation in a non-linear simulation model of the complete system with control. The problem of finding the global minimum of the rather complex optimization problem was addressed and it is assessed that improved performance may be obtained with more suitable optimization algorithms. Lastly, several improvement suggestions for better performance was discussed which however gives additional control challenges that are not possible to solve with conventional MPC.

ACKNOWLEDGMENT

This research was funded by the Danish Council for Strategic Research through the HyDrive project at Aalborg

University, at the Department of Energy Technology (case no. 1305-00038B).

REFERENCES

[1] Rampen, W., 2006. "Gearless transmissions for large wind turbines the history and future of hydraulic drives.".

[2] Taylor, J., Rampen, W., Robertson, A., and Caldwell, N., 2011. "Digital displacement hydraulic hybrid - parallel hybrid drives for commercial vehicles". *Paper presented at the annual JSAE congress, Kyoto, Japan, Tech.*

[3] Ehsan, M., Rampen, W., and Salter, S., 1997. "Modeling of digital-displacement pump-motors and their application as hydraulic drives for nonuniform loads". *ASME. J. Dyn. Sys., Meas., Control.*

[4] Payne, G. S., Stein, U. P. P., Ehsan, M., Caldwell, N. J., and Rampen, W. H. S., 2005. "Potential of digital displacement hydraulics for wave energy conversion". *In Proc. of the 6th European Wave and TIdal Energy Conference, Glasgow UK*.

[5] Rampen, W., 2010. "The development of digital displacement technology". *In Proceedings of Bath/ASME FPMC Symposium*.

[6] Heikkila, M., and Linjama, M., 2013. "Displacement control of a mobile crane using digital hydraulic power management system". *Mechatronics, Vol. 23, Issue 4, Pages 452-461*.

[7] Johansen, P., Roemer, D. B., Pedersen, H. C., and Andersen, T. O., 2017. "Discrete linear time invariant analysis of digital fluid power pump flow control". *Journal of Dynamic Systems, Measurement and Control, Transactions of the ASME, Vol. 139(10)*.

[8] Pedersen, N. H., Johansen, P., and Andersen, T. O., 2016. "Lqr feedback control development for wind turbines featuring a digital fluid power transmission system". *Proceedings of the 9th FPNI Ph.D. Symposium on Fluid Power. American Society of Mechanical Engineers*.

[9] Pedersen, N. H., Johansen, P., and Andersen, T. O., 2017. "Optimal control of a wind turbine with digital fluid power transmission". *Nonlinear Dynamics, Volume 91, Issue 1, pp 591607*.

[10] Sniegucki, M., Gottfried, M., and Klingauf, U., 2013. "Optimal control of digital hydraulic drives using mixed-integer quadratic programming". *Proceedings of the 9th IFAC Symposium on Nonlinear Control Systems*.

[11] Roemer, D. B., 2014. "Design and optimization of fast switching valves for large scale digital hydraulic motors". PhD thesis, Department of Energy Technology, Aalborg University. Department of Energy Technology, Aalborg University.

[12] Andersen, T. O., and Hansen, M. R., 2003. "Fluid power systems - modelling and analysis". *Institute of Energy Technology, Aalborg University, Denmark. 2nd Edition*.

[13] Noergaard, C., Christensen, J. H., and Bech, M. M., 2017. "Modeling and validation of moving coil actuated valve for digital displacement machines". *IEEE TRANS. ON INDUSTRIAL ELECTRONICS - INITIAL Submitted for review*.

[14] Noergaard, C., Madsen, E. L., Joergensen, J. M. T., Christensen, J. H., and Bech, M. M., 2017. "Test of a novel moving magnet actuated seat valve for digital displacement fluid power machines". *IEEE/ASME TRANSACTIONS ON MECHATRONICS - Submitted for review*.

[15] Pedersen, N. H., Johansen, P., and Andersen, T. O., 2017. "Event-driven control of a speed varying digital displacement machine". *Proceedings of the 2017 Bath/ASME Symposium on Fluid Power and Motion Control*.

[16] Stephens, M. A., Manzie, C., and Good, M. C., 2013. "Model predictive control for referene tracking on an industrial machine tool servo drive". *IEEE Transaction on Industrial Informatics, vol. 9, No. 2*.

[17] Bech, M. M., Noergaard, C., Roemer, D. B., and Kukkonen, S., 2016. "A global multi-objective optimization tool for design of mechatronic components using generalized differential evolution". *Proceedings of the 42nd Annual Conference of IEEE Industrial Electronics Society*.

Paper H

Model Predictive Control of Low-Speed Partial Stroke Operated Digital Displacement Pump Unit

Niels H. Pedersen, Per Johansen, Anders H. Hansen and Torben O. Andersen

The paper has been published in
Modeling, Identification and Control, 2018, doi:10.4173/mic.2018.3.3.

The layout has been revised.

Modeling, Identification and Control, Vol. 39, No. 3, 2018, pp. 167–177, ISSN 1890–1328

Model Predictive Control of Low-Speed Partial Stroke Operated Digital Displacement Pump Unit

N. H. Pedersen P. Johansen A. H. Hansen T. O. Andersen

Fluid Power and Mechatronic Systems, Department of Energy Technology, Aalborg University, Pontoppidanstraede 111, 9220 Aalborg, Denmark. E-mail: nhp@et.aau.dk, pjo@et.aau.dk, ahh@et.aau.dk, toa@et.aau.dk

Abstract

To enhance the use of the Digital Displacement Machine (DDM) technology as the future solution for low speed fluid power pump and motor units, a Model Predictive Control (MPC) strategy is presented. For a low speed DDM, the conventional full stroke operation strategy is unsuitable, since the control update rate is proportional to the machine speed. This creates an incentive to utilize sequential partial stroke operation where a fraction of the full stroke is used, which thereby increases the control update rate and control signal resolution. By doing this, the energy loss is increased and may become undesirable large if the control objective is purely set-point tracking, why a trade-off is considered advantageous. Discretizing the full stroke based on a chosen update rate results in a Discrete Linear Time Invariant (DLTI) model of the system with discrete input levels. In this paper, the Differential Evolution Algorithm (DEA) is used to determine the optimal control input based on the trade-off between set-point tracking and energy cost in the prediction horizon. The paper presents a flow and a pressure control strategy for a fixed speed digital displacement pump unit and shows the trade-off influence on the optimal solution through simulation. Results show the applicability of the control strategy and indicate that a much higher energy efficiency may be obtained with only a minor decrease in tracking performance for pressure control.

Keywords: Digital Displacement Units, Fluid Power, Control, Non-smooth System, Hybrid Systems

1 Introduction

The Digital Displacement Machine (DDM) technology is a promising alternative to conventional hydraulic pump and motor units, since it provides excellent redundancy and scalability due to its modular construction. Additionally, it provides the possibility of an improved energy efficiency and reliability Linjama (2011). As a result, a large amount of research regarding design and performance optimization of these machines has been published Payne et al. (2005); M. Ehsan and Salter (March 2000); Rampen (2010); Johansen (2014); Roemer (2014); Noergaard (2017); Wilfong et al. (2010, 2011); Merrill et al. (2011).

One important task for successful deployment of the machine technology is the control system, which is a key feature with respect to proper operation and energy efficiency. However, the challenges with respect to control of such non-smooth dynamical system are many and considered to be complicated Pedersen et al. (2018a). Several research papers regarding control strategies of digital displacement machines has been published, but the strategies are often limited to open-loop control at simplified operation conditions M. Ehsan and Salter (March 2000); Heikkila and Linjama (2013); Song (2008); Armstrong and Yuan (June 2006). Control strategies for high speed operated machines have further been exploited to include closed loop control. Sniegucki et al. (2013) presents a mixed logical dynamic programming control structure for a fixed-speed machine. Although the method is limited to offline optimization, promising result is ob-

doi:10.4173/mic.2018.3.3

tained with respect to fluctuations and set-point tracking. A full stroke Pulse-Density Modulation (PDM) technique is proposed by Johansen et al. (2015) in a feedback structure. To allow for model based closed loop control design, a Discrete Linear Time Invariant (DLTI) approximation to the digital machine dynamics is developed by Johansen et al. (2017) for constant speed operation. To expand the use of this method to be applicable for variable speed operation, Pedersen et al. (2017a) transform the DLTI model to the spatial domain, resulting in a fixed angle sampling rate allowing for classical control synthesis. A combination of the PDM technique and the DLTI model is further used for control of a digital fluid power transmission by Pedersen et al. (2017b, 2018b).

This paper proposes a closed-loop control strategy for a slow rotating digital displacement machine with a relatively low number of cylinders. Because of this, full stroke operation is considered unfavorable, since the control update rate is proportional to the speed of the machine and the tracking performance thus suffers heavily. To account for this, a sequential partial stroke operation method is used with a higher control update rate, which increases the control signal resolution and thereby allows for an improved set-point tracking. Since energy loss due to switching may be of major concern using sequential partial stroke, a Model Predictive Control (MPC) strategy is used. This allows for specifying the importance of tracking performance relative to energy consumption, from where the optimal control input is determined based on a prediction model. The MPC control strategy is tested for both flow and pressure control by simulation in a non-linear model representing the physical system. A fixed speed pump unit is considered in this paper, but the strategy is also applicable to variable speed pump-motor units by the spatial domain transformation method presented by Pedersen et al. (2017a).

2 System Description

To evaluate on the performance of the control strategy, a non-linear mathematical model of the digital displacement machine is established. The model hence represents the physical system and is derived based on a description of the machine characteristics. The digital displacement machine under consideration is illustrated in Fig. 1. The illustration to the left shows the digital displacement machine with 10 cylinders being radially distributed around an eccentric shaft. The flow to and from the pressure chambers is regulated by manipulating the state of the fast switching on/off high and low-pressure valves, HPV and LPV respectively illustrated to the right. Maintaining a closed

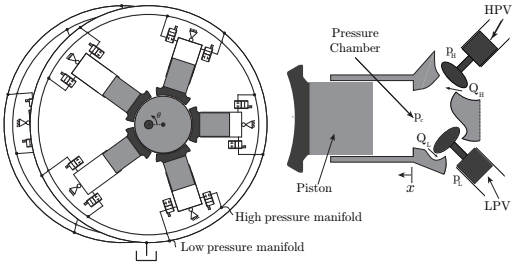

Figure 1: Illustration of the displacement pump-motor unit.

LPV and an open HPV during piston retraction is seen to pressurize the chamber, which result in a flow being pumped to the high pressure manifold. Maintaining the same valve positions results in a motoring mode during piston extension. Using the opposite valve positions results in an idling mode where the chamber pressure remains low. In sequential partial stroke operation, the position of the valves may be changed independently of the cylinder position to obtain a desired volumetric output fraction. However, sequential partial stroke requires that the valves can be opened against high pressure difference. Therefore, larger valves with a higher actuation force are necessary compared to full stroke or conventional partial stroke, where the valve positions may only be altered on a stroke-by-stroke basis.

2.1 Non-linear Simulation Model

To evaluate on the control performance, a non-linear simulation model representing the physical system is made. The local shaft angles for the respective cylinders are given by

$$\theta_{\mathrm{i}} = \theta + \frac{2\,\pi}{N_{\mathrm{c}}}\,(i-1) \quad i \in \{1,..,N_{\mathrm{c}}\} \tag{1}$$

where θ is the shaft angle and N_{c} is the number of cylinders. Since the equations used to describe the different pressure chambers are the same, the following model derivation is made for a single chamber. The piston displacement, x, is seen to be a function of the shaft angle described as

$$x\,(\theta) = r_{\mathrm{s}}\;(1-\cos(\theta)) \tag{2}$$

where r_{s} is the eccentric shaft radius being equivalent to half of the piston stroke length. The stroke volume is thus given by $V_{\mathrm{d}} = 2\,r_{\mathrm{s}}\,A_{\mathrm{p}}$, where A_{p} is the piston area. The pressure chamber volume, V_{c} is then given

by

$$V_c(\theta) = \frac{V_d}{2}(1-\cos(\theta)) + V_0$$
$$\dot{V}_c(\theta) = \frac{V_d}{2}\dot{\theta}\sin(\theta) \tag{3}$$

where V_0 is the minimum chamber volume. Using the continuity equation to describe the pressure dynamics results in

$$\dot{p}_c = \frac{\beta_e}{V_c}\left(Q_H - Q_L - \dot{V}_c\right) \tag{4}$$

The flows through the high and low pressure valve, Q_H and Q_L respectively are modeled by the orifice equation and given by

$$Q_L = k_f\sqrt{|p_c - p_L|}\,\mathrm{sign}(p_c - p_L)\,\bar{x}_L$$
$$Q_H = k_f\sqrt{|p_H - p_c|}\,\mathrm{sign}(p_H - p_c)\,\bar{x}_H \tag{5}$$

where $\bar{x}_L$ and $\bar{x}_H$ are the normalized valve positions of the low- and high-pressure valve respectively and k_f is the valve flow coefficient. To reduce the model complexity significantly, the valve dynamics is simplified to be described as a first order system given by

$$\dot{\bar{x}}_L = \frac{1}{\tau_v}(u_L - x_L) \quad \dot{\bar{x}}_H = \frac{1}{\tau_v}(u_H - x_H) \tag{6}$$

where t_v is the valve time constant, u_L and u_H are the valve inputs. Despite the simple valve description, the important characteristics with respect to machine level control is captured.

2.2 Valve timing and control

The valve actuation is described by considering the hybrid automaton shown in Fig. 2. Two mode switching functions are defined as $\lambda_H = F_H - (p_H - p)\,A_v$ and $\lambda_L = F_L - (p - p_L)\,A_v$ and are used to construct the switching logic. The systems input is hence the valve forces, $u = \begin{bmatrix}F_H & F_L\end{bmatrix}^T$ for the high and low pressure valve respectively. A_v is the effective valve area that the pressure is generating a force on. It is seen that the pressure chambers may operate in three modes namely idling, compression and pressurization. The hybrid automaton shows that a pressure chamber is activated if $\lambda_L < -\alpha$, which results in a transition from idling to compression mode. α represents a static force hysteresis band which has to be surmounted in order to alternate the valve state and avoid numerous subsequently switchings. A further transition to the pressurization mode where the HPV is opened is obtained when $(p_H - p)\,A_v > \alpha$ or a large force, F_H is applied to the HPV. The valve area A_v is hence considered identically on both sides of the valve plunger as a simplification. Similar transitions occur when deactivating

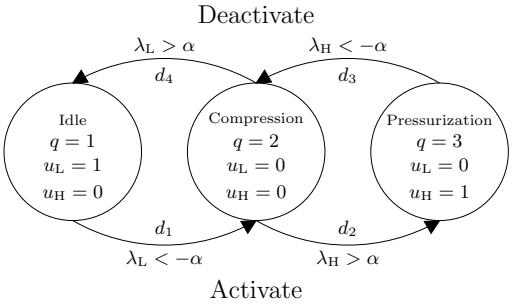

Figure 2: Hybrid automaton representation of valve control of the digital displacement machine.

a pressure chamber, where the HPV is initially closed and the LPV is subsequently opened.

In conventional partial stroke operation, passive opening of the LPV and HPV due to pressure force is used, such that small valves with a low actuation force may be used. However, the control update is made on a stroke-by-stroke basis and is thus proportional to the machine speed. For a very low speed machine with a low number of cylinders, the control update rate is very low and may be troublesome with respect to obtaining the desired control performance. By using a sequential partial stroke strategy, the valves may be opened and closed independent of the chamber pressure level, but requires valves being able to deliver significantly higher actuation force. Such sequential partial stroke strategy is considered in this paper to significantly increase the control update rate and thereby improve the reference tracking performance. However, due to valve opening against a high pressure difference, the energy loss may also be significantly higher and the strategy is thus only considered feasible for very low speed operation.

The total flow and torque of the digital machine is given as the sum of flows and torques from each pressure chamber and are given by

$$Q = \sum_{j=0}^{N_c-1} Q_{H,j} \qquad \tau = \sum_{j=0}^{N_c-1} \tau_j \tag{7}$$

The parameters used in the simulation model is provided in Tab. 1.

3 MPC and DLTI model approximation

Discrete Model Predictive Control (MPC) is characterized as a sample-and-hold feedback control method, where the optimal control input is determined based

Table 1: Parameters of the 5 MW transmission

Parameter	Symbol	Value	Unit
Motor rotation speed	ω, θ	10	rpm
Motor displacement volume	V_d	153.4	cm^3
Motor dead volume	V_0	153.4	cm^3
Maximum bulk-modulus	β_e	16000	bar
Low pressure	p_L	10	bar
Valve flow constant	k_f	1.26	$\mathrm{L}/(\mathrm{min}\sqrt{\mathrm{bar}})$
Valve time constant	t_s	5	ms
Valve effective area	A_v	31.66	mm^2
Force threshold	α	50	N

on an estimation of the future plant states in a prediction horizon. Since the system is discretely actuated, a discrete dynamical model is demanded such that the future states may be predicted and the valve switching energy may be included. Two important parameters in MPC is the sampling time and prediction horizon. The sampling rate should be low enough such that the next optimal control input may be calculated between two samples, but high enough to ensure proper control performance. Similar, a small prediction horizon reduces the solving time for the optimal control input but reduces the control performance.

In this paper the optimal control input is chosen as a trade-off between reference tracking accuracy and energy cost. For a digital displacement machine, it is considered advantageously to use a prediction horizon corresponding to the number of samples during one full stroke, $p = 5$. This allows the controller to know that it is cheaper to switch the valve states during a low flow at the end of a stroke. Similar, since it is an advantage to switch valve states at the beginning of a stroke at a low flow rate, the sampling time is chosen as the time between two cylinders starting a stroke, $T_\mathrm{s} = 2\,\pi/(\omega\,N_\mathrm{c})$. With 10 cylinders this results in 5 samples during a pumping stroke and 5 samples during a motoring stroke, which means that each chamber may switch valve states 5 times during a full stroke.

As long as the valve dynamics is sufficiently fast compared to the machine speed, the switching only takes a neglectable fraction of a full stroke. In this example the valve is switched in $T_\mathrm{v} \approx 5\,\tau_\mathrm{v} = 25$ ms and there is 50 ms from the LPV closing signal is given until the HPV opening signal is given, such that it takes 75 ms from the LPV closing signal is given until the HPV is fully open. At a speed of $\omega = 10$ rpm a single revolution takes 6 s, such that it is considered valid to neglect the valve dynamics.

By neglecting the valve and pressure dynamics, a DLTI-model is constructed where $Q_\mathrm{H} \approx \dot{V}_\mathrm{c}$ during an active stroke. The model is established by considering the change in volume between samples using the relation given by (8) as proposed in Johansen et al. (2017).

$$\begin{aligned} Q_\mathrm{d}[k] &\approx \frac{\Delta V_\mathrm{c}[k]}{\Delta T[k]} \approx \frac{N_\mathrm{c}}{2\,\pi}\,\omega[k]\,\underbrace{(V_\mathrm{c}(\theta[k+1]) - V_\mathrm{c}(\theta[k]))}_{\Delta V_\mathrm{c}[k]} \\ \tau_\mathrm{d}[k] &\approx \frac{\Delta V_\mathrm{c}[k]}{\Delta\theta}\,p_\mathrm{H}[k] \approx \frac{N_\mathrm{c}}{2\,\pi}\,p_\mathrm{H}[k]\,\underbrace{(V_\mathrm{c}(\theta[k+1]) - V_\mathrm{c}(\theta[k]))}_{\Delta V_\mathrm{c}[k]} \end{aligned} \tag{8}$$

where the angle as function of sample number is given by

$$\theta[k] = \frac{2\,\pi}{N_\mathrm{c}}\,k \qquad k \in \{0, \ldots, N_\mathrm{c} - 1\} \tag{9}$$

A simulation has been made where the response of the discrete model is compared to that of the non-linear model and is shown in Fig. 3.

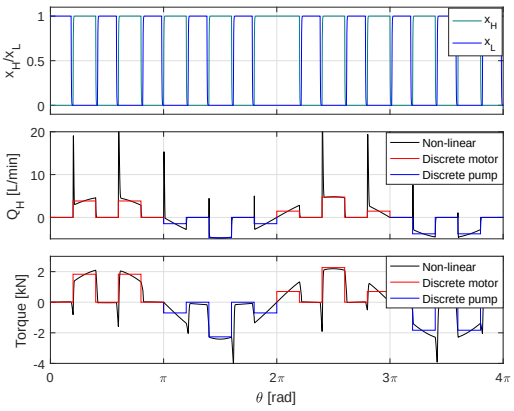

Figure 3: Comparison of non-linear and discrete model of the digital displacement machine.

It is seen that every second decision is to activate the chamber. Although the outputs are approximately matched between samples, large pressure spikes are observed in the non-linear model. These pressure spikes are due to opening against high pressure difference and since the pressure dynamics has been neglected in the discrete model, they are not observed. The severity of the spikes is seen to be larger for higher flow rates and especially high for motoring where the pressure change due to the change in volume is negative. Despite these deviations, the output is matched quite fairly. The total flow and torque throughput of the digital displacement machine is described by a sum of the individual contributions given by

$$Q[k] = \sum_{m=0}^{N_\mathrm{c}-1} Q_\mathrm{d}[k]\,\bar{u}[k] \qquad \tau[k] = \sum_{k=0}^{N_\mathrm{c}-1} \tau_\mathrm{d}[k]\,\bar{u}[k] \tag{10}$$

where $\bar{u} \in \{1, 0\}$ are the binary actuation decision (active or inactive).

3.1 Input combinations

With 10 cylinders, there are 10 pressure chambers that may either be active or inactive for a total of $2^{10} = 1024$ combinations at every sample. However, due to symmetry it makes no sense to motor and pump simultaneous with different cylinders, such that there is $2^5 = 32$ pumping and motoring combinations. The different combination are shown in Fig. 4 and are illustrated as normalized values (displacement fractions). The relations between the displacement fraction to the flow and torque are given by

$$Q[k] = \underbrace{\frac{V_\mathrm{d}\, N_\mathrm{c}}{2\pi}}_{k_\mathrm{q}} \omega[k]\, \alpha[k] \quad \tau[k] = \underbrace{\frac{V_\mathrm{d}\, N_\mathrm{c}}{2\pi}}_{k_\tau} p_\mathrm{H}[k]\, \alpha[k] \tag{11}$$

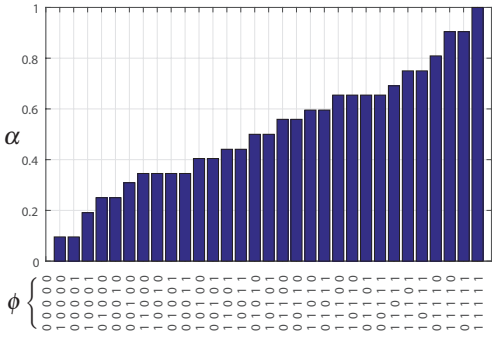

Figure 4: Combinations of discretized displacement fraction.

As expected a displacement fraction of 1 is obtained by activating all five pressure chambers operating in the same mode (motoring or pumping). It is seen that several of the combinations yield the same output, but they may have significantly different energy cost related, since one may require a valve switch while the other may not require a switch. Additionally, it is more energy costly and the flow/pressure spikes are higher when switching at high flow levels.

3.2 Input mapping

Having identified an optimal discrete input at a given sample, the next step is to map the input to a pressure chamber actuation sequence for the 10 cylinders. Let the prediction horizon $p = \mathrm{ceil}(N_\mathrm{c}/2)$ and j be such that $\theta\,[j] = \theta(t)$, where $\theta\,[j] \wedge \theta(t) \in [0\,;\, 2\,\pi]$. Let k and n be defined as $m \in \{0, \ldots, N_\mathrm{c} - 1\}$ and $n \in \{0, \ldots, p-1\}$ then the chamber actuation sequence is given by

$$\Phi[m] = \begin{cases} \phi[n] & \text{for } m = (j-n) \bmod N_\mathrm{c} \\ 0 & \text{otherwise} \end{cases} \tag{12}$$

Φ hence contains information about whether each individual pressure chamber should be active or inactive. If a value in the vector is changed from 0 to 1, the LPV for the given pressure chamber is closed following an opening of the HPV. Inversely, if a value is changed from 1 to 0, the HPV is closed following an opening of the LPV. An example of how the chamber actuation vector Φ is constructed is shown in Fig. 6.

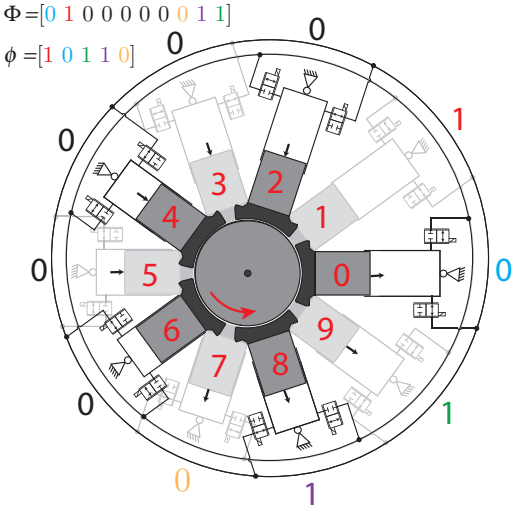

Figure 6: Example of the chamber actuation sequence generation.

In this example cylinder 1 (red) is at Bottom Dead Center (BDC) where a pumping stroke starts. Cylinder 0, 9, 8 and 7 are in the pumping stroke part, while the remaining cylinders are in the motoring stroke part. At this sample, $\phi = [1\ 0\ 1\ 1\ 0]$ is identified as the optimal input sequence. Since the first entry is 1, the current cylinder 1 has to be activated, while the previous cylinder 0 has to be inactive given by the second entry. Similarly, the cylinders 9 and 8 have to be active given by the third and fourth entries in ϕ. Cylinder 7 which has almost completed its pumping stroke should be inactive and the remaining cylinders are inactive as well, since they are in the motoring stroke part. As a result it is seen that $\Phi = [0100000011]$ is the resulting chamber actuation vector, providing information about the state of each pressure chamber.

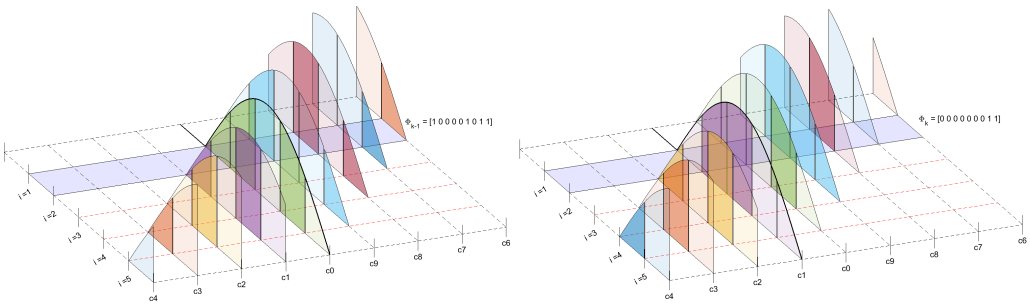

Figure 5: Illustration of the chamber actuation decisions in the prediction horizon for sample $k-1$ and k. Those areas shown with a dark color illustrate an active period.

3.3 MPC flow control

This paper presents a flow and a pressure control method for a low speed DD pump, where the flow control method is relatively simple since no dynamics is present and the future state estimation is thus omitted. The optimization problem of determining the optimal displacement fraction input is found as a combination of reference tracking accuracy and energy cost given as

$$\alpha^* = \underset{\alpha^* \in \alpha}{\operatorname{argmin}} \left\{ J_1^T \, J_1 + W_1 \, J_2^T \, J_2 \right\} \tag{13}$$

$$J_1 = \sum_{i=1}^{p} \left(k_\mathrm{q} \, \omega \, \alpha[i]^* - y_\mathrm{ref}[i] \right) \tag{14}$$

α^* is hence a vector containing the optimal inputs in the prediction horizon. J_1 is the cost function for the reference tracking and J_2 for the switching cost, where W_1 is a scaling parameter between the two cost functions. The tracking error cost function J_1 is seen to be the sum of errors in the prediction horizon. The energy cost function J_2 is defined as

$$J_2 = \sum_{i=0}^{N_\mathrm{c}-1} \left(\frac{\lambda[i]}{\sum_{j=0}^{N_\mathrm{c}-1} \lambda[j]} \; |\Phi[i]_\mathrm{k} - \Phi[i]_\mathrm{k\text{-}1}| \right)$$

$$\lambda[n] = \begin{cases} 1 + W_2 \sin(\theta[n]) & \text{for } m = (j-n) \bmod N_\mathrm{c} \\ 0 & \text{otherwise} \end{cases} \tag{15}$$

The (k)-index and (k-1)-index of the actuation vector Φ indicate the current and previous optimized vector. For every value change in the actuation vector, Φ, the correspondent valves for the given pressure chambers are switched and energy cost is added to the function. Since no specific valve design is considered, the base energy cost of a switch is set to 1 by the function λ, using the same definitions as in (12). The function $\sin(\theta[n])$ takes into account that it costs more to switch at higher flow rates, where also the pressure spikes are larger, and W_2 is again a scaling parameter. The denominator in J_2 is introduced to normalize the function, such that the value of J_2 always has a value between 0 and 1. An illustration of how the energy cost function is evaluated in the prediction horizon is shown in Fig. 5. It is seen that the optimized input α^* corresponds to an actuation sequence for the respective pressure chambers in the prediction horizon. The energy cost function is only evaluated for the current step $i = 1$, since only the actuation vector for the current sample determines which valves are switched. The energy cost could be evaluated in the full prediction horizon, but this has been found to yield slightly worse performance. Alternatively, a weighted sum could be used to penalize the early steps in the prediction horizon more than the later ones.

3.4 Optimization algorithm

In this paper, the optimal solution to the optimization problem is solved by the differential evolution algorithm (DEA), due to its feature of searching a large space and being able to solve discrete valued problems. Better and faster algorithms for the given problem may very well exist, but this is considered out of scope of this paper. The algorithm has previously been successfully applied to a similar problem for discrete force control of a wave energy converter in Hansen et al. (2017). For more information about the DEA, see e.g. Bech et al. (2016). To show the best possible tracking performance with the proposed control strategy, the energy cost function scaling parameter is initially chosen as $W_1 = 0$, while $W_2 = 10$. The optimized result is shown in Fig. 7. For this relatively easy optimization

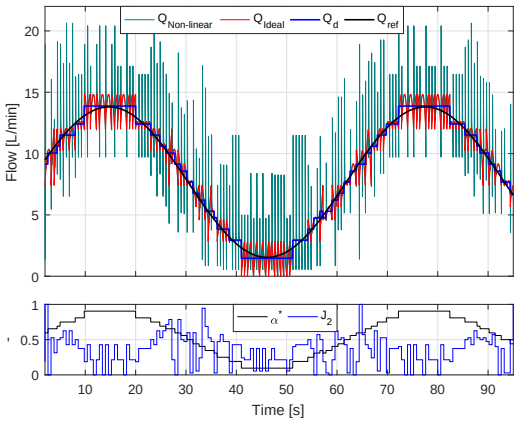

Figure 7: Flow tracking response using the DEA-MPC algorithm without the energy cost function.

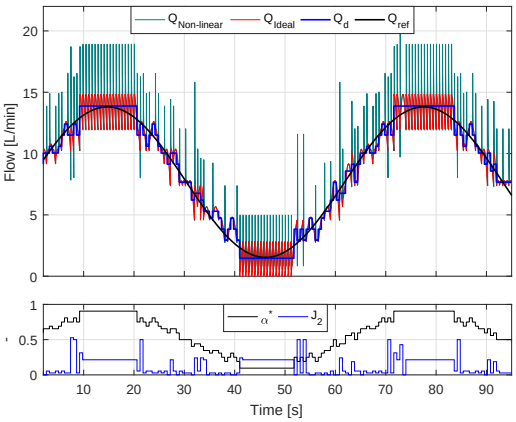

Figure 8: Flow tracking response using the DEA-MPC algorithm with the energy cost function.

problem, the optimal solution could be identified manually by taking the discrete value in Fig. 4 that yields the lowest value when evaluating $|k_q\omega\,\alpha - y_{ref}|$, which gives the same result. $y_{DLTI} = k_q\omega\alpha_1^*$ is the chosen discrete value. y_{ideal} is the ideal flow output considering $Q_H = \dot{V}_c$ and y_{NLM} is the flow output of the non-linear dynamic model. The results are as expected, where the integrated value of y_{DLTI} and y_{ideal} are identically and that of y_{NLM} is a bit higher due to the flow spikes. The bottom part of Fig. 7 shows the optimal input $u = \alpha_1^*$ and the switching cost function value of J_2. It is seen that there are several valve switchings with a high cost that may be unfavorable. When changing the cost scaling parameter to W_1 = 2e-9, results in the optimized solution shown in Fig. 8. It is evident, that the tracking accuracy has been reduced, especially at low and high flow rates. However, it is seen that the switchings with a high cost have been removed completely. Taking the time integral of the absolute tracking error and energy cost yield the results given in Tab. 2.

Table 2: Results with and without energy cost.

Parameter	w/o. J_2	w. J_2
W_1	0	2e-9
Integrated absolute error	1.6 L	2.1 L
Integrated energy (J_2)	96.53	57.17

It is seen that the tracking error is 29 % higher when the energy cost is included in the cost function, but the energy cost is 41 % higher without the energy cost included. This is a simple example to illustrate how the optimal solution changes based on the trade off between tracking and energy. A good choice of the scaling parameter W_1 is of course dependent on the control and energy requirements for the specific application.

3.5 MPC pressure control

A relatively simple system is constructed in this paper to illustrate the applicability of the control structure, but it is expected that the control method is suitable for more advanced fluid power systems comprising low-speed digital displacement machines with a relative low number of cylinders. An illustration of the system considered for pressure control is shown in Fig. 9.

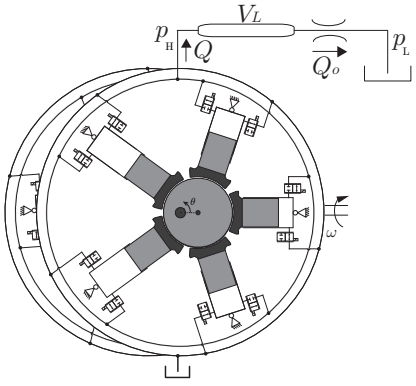

Figure 9: Illustration of the simple load system used for pressure control of the digital displacement machine.

A simple orifice load is considered as a flow restriction, where the objective is to control the pressure in

the high pressure manifold, p_{H}. For pressure control, a DLTI model of the pressure dynamics is derived based on the shown definition of variables. The dynamic equation describing the pressure is given by

$$\dot{p}_{\mathrm{H}}(t) = \frac{\beta_{\mathrm{e}}}{V_{\mathrm{L}}} \left(\underbrace{k_{\mathrm{q}}\, \omega\, \alpha(t)}_{Q(t)} - \underbrace{k_{\mathrm{qo}}\, \sqrt{p_{\mathrm{H}}(t)}}_{Q_{\mathrm{o}}(t)} \right) \tag{16}$$

where $k_{\mathrm{qo}} = 2.2\ \mathrm{L/(min\ \sqrt{bar})}$, $V_{\mathrm{L}} = 0.1\mathrm{m}^3$ is the volume in the pressure line, β_{e} is the effective bulk-modulus and $u = \alpha$ is the input. Due to the non-linear equation describing the flow through the orifice, a linearization by first order Taylor approximation is made and results in

$$\underbrace{\delta\dot{p}_{\mathrm{H}}(t)}_{\dot{x}} = \underbrace{-\frac{\beta\, k_{\mathrm{qo}}}{2\, V_{\mathrm{L}}\, \sqrt{p_0}}}_{A_{\mathrm{c}}} \underbrace{\delta p_{\mathrm{H}}(t)}_{x} + \underbrace{\frac{\beta}{V_{\mathrm{L}}}\, k_{\mathrm{q}}\, \omega}_{B_{\mathrm{c}}} \underbrace{\delta u(t)}_{u} \tag{17}$$

A discretization is made by assuming a zero-order-hold input as approximated by the discrete model having the sampling time $T_{\mathrm{s}} = 2\,\pi/(N_{\mathrm{c}}\,\omega)$. The resulting DLTI model has the standard state-space form given by

$$\begin{aligned} x_{\mathrm{k+1}} &= A\, x_{\mathrm{k}} + B\, u_{\mathrm{k}} \\ y_{\mathrm{k}} &= C\, x_{\mathrm{k}} \end{aligned} \tag{18}$$

It has been identified that integral action added to the control system is necessary to obtain offset-free reference tracking, due to the model inaccuracies caused by linearization and flow discretization. Incorporating integral action within the MPC control structure is done by modifying the state model to a state difference model in accordance with Stephens et al. (2013) and result in

$$\begin{aligned} \Delta x_{\mathrm{k+1}} &= A\, \Delta x_{\mathrm{k}} + B\, \Delta u_{\mathrm{k}} \\ \Delta y_{\mathrm{k+1}} &= C\, \Delta x_{\mathrm{k}} \end{aligned} \tag{19}$$

where $\Delta x_{\mathrm{k}} = x_{\mathrm{k}} - x_{\mathrm{k\text{-}1}}$, $\Delta u_{\mathrm{k}} = u_{\mathrm{k}} - u_{\mathrm{k\text{-}1}}$ and $\Delta y_{\mathrm{k}} = y_{\mathrm{k}} - y_{\mathrm{k\text{-}1}}$. Rewriting the output equation yields the desired result given as

$$\begin{aligned} \Delta y_{\mathrm{k+1}} &= C\, \Delta x_{\mathrm{k}} \\ y_{\mathrm{k+1}} - y_{\mathrm{k}} &= C\, (A\, \Delta x_{\mathrm{k}} + B\, \Delta u_{\mathrm{k}}) \\ y_{\mathrm{k+1}} &= C\, A\, \Delta x_{\mathrm{k}} + C\, B\, \Delta u_{\mathrm{k}} + y_{\mathrm{k}} \end{aligned} \tag{20}$$

It is seen that the output $y_{\mathrm{k+1}}$ is now dependent on the previous output y_{k} similar to a conventional discrete integrator. Forming the new state formulation yields

$$\begin{aligned} \underbrace{\begin{bmatrix} \Delta x_{\mathrm{k+1}} \\ y_{\mathrm{k+1}} \end{bmatrix}}_{\bar{x}_{\mathrm{k+1}}} &= \underbrace{\begin{bmatrix} A & 0 \\ C\,A & I \end{bmatrix}}_{\bar{A}} \underbrace{\begin{bmatrix} \Delta x_{\mathrm{k}} \\ y_{\mathrm{k}} \end{bmatrix}}_{\bar{x}_{\mathrm{k}}} + \underbrace{\begin{bmatrix} B \\ C\,B \end{bmatrix}}_{\bar{B}} \Delta u_{\mathrm{k}} \\ y(k) &= \underbrace{\begin{bmatrix} 0 & I \end{bmatrix}}_{\bar{C}} \bar{x}_{\mathrm{k}} \end{aligned} \tag{21}$$

This state model is then used to predict the future state development by use of recursive evaluation. The recursive discrete state estimation method is given by

$$\begin{aligned} \underbrace{\begin{bmatrix} \bar{x}_{\mathrm{k+1}} \\ \bar{x}_{\mathrm{k+2}} \\ \bar{x}_{\mathrm{k+3}} \\ \vdots \\ \bar{x}_{\mathrm{k+p}} \end{bmatrix}}_{\underline{\mathrm{x}}} &= \underbrace{\begin{bmatrix} \bar{B} & 0 & 0 & \dots & 0 \\ \bar{A}\,\bar{B} & \bar{B} & 0 & \dots & 0 \\ \bar{A}^2\,\bar{B} & \bar{A}\,\bar{B} & \bar{B} & \dots & 0 \\ \vdots & \ddots & & \ddots & \vdots \\ \bar{A}^{p-1}\,\bar{B} & \bar{A}^{p-2}\,\bar{B} & \bar{A}^{p-3}\,\bar{B} & \dots & B \end{bmatrix}}_{\underline{\mathrm{A}}} \underbrace{\begin{bmatrix} \Delta u_{\mathrm{k}} \\ \Delta u_{\mathrm{k+1}} \\ \Delta u_{\mathrm{k+2}} \\ \vdots \\ \Delta u_{\mathrm{k+p}} \end{bmatrix}}_{\Delta\underline{\mathrm{u}}} + \underbrace{\begin{bmatrix} \bar{A} \\ \bar{A}^2 \\ \bar{A}^3 \\ \vdots \\ \bar{A}^p \end{bmatrix}}_{\underline{\mathrm{B}}} \bar{x}_{\mathrm{k}} \\ \underline{\mathrm{y}} &= \underbrace{\begin{bmatrix} \bar{C} & 0 & 0 \dots & 0 \\ 0 & \bar{C} & 0 \dots & 0 \\ 0 & 0 & \bar{C} \dots & 0 \\ \vdots & \vdots & \vdots \ddots & \vdots \\ 0 & 0 & 0 \dots & \bar{C} \end{bmatrix}}_{\underline{\mathrm{C}}} \underline{\mathrm{x}} \end{aligned} \tag{22}$$

In short notation the discretely predicted pressure may thus be written as

$$\underline{\mathrm{y}} = \underbrace{\underline{\mathrm{C}}\,\underline{\mathrm{A}}}_{\Psi}\, \Delta\underline{\mathrm{u}} + \underbrace{\underline{\mathrm{C}}\,\underline{\mathrm{B}}}_{\gamma}\, \bar{x}_{\mathrm{k}} \tag{23}$$

The optimization problem is very similar to that for the flow control problem, except for how the predicted output is used to estimate the tracking error cost function. The optimization problem becomes that given as

$$\begin{aligned} \underline{\mathrm{u}} &= \underset{\underline{\mathrm{u}} \in \alpha}{\operatorname{argmin}} \left\{ J_1^T\, J_1 + W_1\, J_2^T\, J_2 \right\} \\ J_1 &= \sum_{i=1}^{p} \left((\Psi\, \Delta\underline{\mathrm{u}}_{\mathrm{k}}[i] + \gamma\, \bar{x}_{\mathrm{k}}) - y_{\mathrm{ref}}[i] \right) \\ J_2 &= \sum_{i=0}^{N_{\mathrm{c}}-1} \left(\frac{\lambda[i]}{\sum_{j=0}^{N_{\mathrm{c}}-1} \lambda[j]}\ |\Phi[i]_{\mathrm{k}} - \Phi[i]_{\mathrm{k\text{-}1}}| \right) \end{aligned} \tag{24}$$

It should be noticed that the difference input $\Delta u_{\mathrm{k}} = u_{\mathrm{k}} - u_{\mathrm{k\text{-}1}}$ has to be evaluated at each function evaluation using the current and previous optimal input vector.

4 Results

To investigate the influence of the energy cost function, the control strategy is initially implemented with the energy cost function scaling parameter chosen as $W_1 = 0$, while $W_2 = 10$. The results of the optimized problem is shown in Fig. 10.

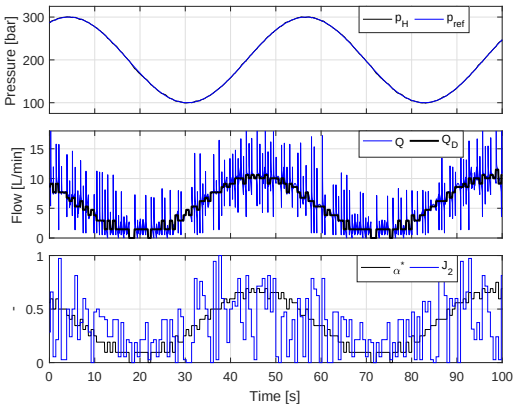

Figure 10: Pressure tracking response using the DEA MPC algorithm without the energy cost function.

It is seen that relative great reference tracking is obtained with a minor amount of ripples around the tracking point due to the non-smooth flow profile. The bottom plot reveals that there is a high number of expensive switchings, where a value of 1 indicates that the maximum of 6 valves are switched simultaneously. When changing the cost scaling parameter to $W_1 = 2e12$, yields the optimized results shown in Fig. 11.

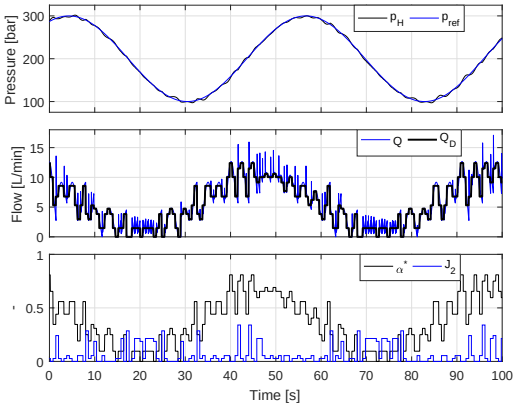

Figure 11: Pressure tracking response using the DEA MPC algorithm with the energy cost function.

As expected the reference tracking error has increased and larger ripples around the set-point is observed. It is also clear that the switching cost has been reduced significantly. Additionally, the large flow spikes due to switching at high flow rates have been removed. Taking the time integral of the absolute tracking error and energy yields the results given in Tab. 3 for the two optimized control problems.

Table 3: Results with and without energy cost.

Parameter	w/o. J_2	w. J_2
W_1	0	2e12
Integrated absolute error	2.27e7	2.95e7
Integrated energy	30.3	6.1

It is seen that the tracking error is 30 % higher when the energy cost is included in the cost function, but the energy cost is 397 % higher without the energy cost included. For this particular example it is clear that it might be beneficial to penalize the energy cost unless there is strict requirement to set-point tracking. Based on the specific application it is considered easy to adjust the cost function scaling parameter W_1 based on the desired trade-off between tracking performance and energy cost. In all of the presented results for both flow and pressure control, the problem has been solved in much less time than the control sampling time, which enables the algorithm to be implemented online. However, MPC control requires the reference trajectory to be pre-specified or at least estimated within the prediction horizon which may cause problems based on the specific application. Also, there is a clear restriction with regard to the maximum speed of the digital displacement machine, both due to the problem solving time and valve switching time. Additionally, an increased sample rate may be beneficial for very low speed machines, but this comes with the cost of an increased number of input decisions, which again increases the problem-solving time.

5 Conclusion

A Model Predictive Control (MPC) method for a sequential partial stroke operated low speed Digital Displacement Machine (DDM) with a relatively low number of cylinders is demonstrated in this work. The method improves the set-point tracking capability compared to full-stroke and conventional partial stroke operated machines, while allowing the designer to specify the importance of energy consumption and reduced flow/pressure/torque pulsations. To solve the discrete valued optimization problem, the Differential Evolution Algorithm (DEA) is used. For a 10-rpm machine with 10 cylinders the algorithm is online capable, since the solving time is much less than the control sampling time. Simulation results for both flow and pressure control show great tracking performance if energy

consumption is not considered, while a minor decrease in tracking performance leads to a large decrease in energy consumption in the case of pressure control. The presented control strategy is however not suitable for fast rotating digital displacement machines due to both solving time and additional energy losses due to excessive switchings compared to a full-stroke control method.

Acknowledgments

This research was funded by the Danish Council for Strategic Research through the HyDrive project at Aalborg University, at the Department of Energy Technology (case no. 1305-00038B).

References

Armstrong, B. S. R. and Yuan, Q. Multi-level control of hydraulic gerotor motor and pumps. *Proceedings of the 2006 American Control Conference Minneapolis, Minnesota*, June 2006. doi:10.1109/ACC.2006.1657450.

Bech, M. M., Noergaard, C., Roemer, D. B., and Kukkonen, S. A global multi-objective optimization tool for design of mechatronic components using generalized differential evolution. *Proceedings of the 42nd Annual Conference of IEEE Industrial Electronics Society*, 2016. doi:10.1109/IECON.2016.7793419.

Hansen, A. H., Asmussen, M. F., and Bech, M. M. Energy optimal tracking control with discrete fluid power systems using model predictive control. *The Ninth Workshop on Digital Fluid Power, September 7-8, Aalborg, Denmark*, 2017.

Heikkila, M. and Linjama, M. Displacement control of a mobile crane using digital hydraulic power management system. *Mechatronics 23(4), pp. 452 - 461*, 2013. doi:10.1016/j.mechatronics.2013.03.009.

Johansen, P. *Tribodynamic Modeling of Digital Fluid Power Motors*. Ph.D. thesis, Department of Energy Technology, Aalborg University, 2014.

Johansen, P., Roemer, D. B., Pedersen, H. C., and Andersen, T. O. Delta-sigma modulated displacement of a digital fluid power pump. *Proceedings of the 7th Workshop on Digital Fluid Power, Linz, Austria*, 2015. The Seventh Workshop on Digital Fluid Power, Linz, Austria.

Johansen, P., Roemer, D. B., Pedersen, H. C., and Andersen, T. O. Discrete linear time invariant analysis of digital fluid power pump flow control. *Journal of Dynamic Systems, Measurement and Control, Transactions of the ASME, Vol. 139, Nr. 10, 101007*, 2017. doi:10.1115/1.4036554.

Linjama, M. Digital fluid power state of the art. *The Twelfth Scandinavian International Conference on Fluid Power, May 18-20, Tampere, Finland*, 2011.

M. Ehsan, W. R. and Salter, S. Modeling of digital-displacement pump-motors and their application as hydraulic drives for nonuniform loads. *ASME, Journal of dynamic system measurement and control, Vol. 122, pp. 210-215*, March 2000. doi:10.1115/1.482444.

Merrill, K., Holland, M., and Lumkes, J. Analysis of digital pump/motor operating strategies. *Proceedings of the 52nd National Conference on Fluid Power*, 2011.

Noergaard, C. *Design, Optimization and Testing of Valves for Digital Displacement Machines*. Ph.D. thesis, Aalborg University, 2017. doi:10.5278/vbn.phd.eng.00013.

Payne, G. S., Stein, U. P. P., Ehsan, M., Caldwell, N. J., and Rampen, W. H. S. Potential of digital displacement hydraulics for wave energy conversion. *In Proc. of the 6th European Wave and TIdal Energy Conference, Glasgow UK.*, 2005.

Pedersen, N. H., Johansen, P., and Andersen, T. O. Event-driven control of a speed varying digital displacement machine. *Proceedings of ASME/BATH FPMC Symposium on Fluid Power and Motion Control, Sarasota, Florida, USA*, 2017a. doi:10.1115/FPMC2017-4260.

Pedersen, N. H., Johansen, P., and Andersen, T. O. Lqr-feedback control development for wind turbines featuring a digital fluid power transmission system. *9th FPNI PhD symposium on fluid power, Florianpolis, Brazil*, 2017b. doi:10.1115/FPNI2016-1537.

Pedersen, N. H., Johansen, P., and Andersen, T. O. Challenges with respect to control of digital displacement hydraulic units. *Modeling, Identification and Control, Vol 39*, 2018a. doi:10.4173/mic.2018.2.4.

Pedersen, N. H., Johansen, P., and Andersen, T. O. Optimal control of a wind turbine with digital fluid power transmission. *Nonlinear Dynamics*, 2018b. doi:10.1007/s11071-017-3896-0.

Rampen, W. The development of digital displacement technology. *In Proceedings of Bath/ASME FPMC Symposium*, 2010.

Roemer, D. B. *Design and Optimization of Fast Switching Valves for Large Scale Digital Hydraulic Motors*. Ph.D. thesis, 2014. Department of Energy Technology, Aalborg University.

Sniegucki, M., Gottfried, M., and Klingauf, U. Optimal control of digital hydraulic drives using mixed-integer quadratic programming. *9th IFAC Symposium on Nonlinear Control System, Toulouse*, 2013. doi:10.3182/20130904-3-FR-2041.00013.

Song, X. Modeling an active vehicle suspension system with application of digital displacement pump motor. *Proceedings of the ASME 2008 International Design Engineering Techical Conference/Computers and Information in Enegineering Conference, Brooklyn, New York*, 2008. doi:10.1115/DETC2008-49035.

Stephens, M. A., Manzie, C., and Good, M. C. Model predictive control for reference tracking on an industrial machine tool servo drive. *IEEE Transactions on Industrial Informatics, Vol. 9*, 2013. doi:10.1109/TII.2012.2223222.

Wilfong, G., Batdorff, M., and Lumkes, J. Design and dynamic analysis of high speed on/off poppet valves for digital pump/motors. *In Proceedings of the 6th FPNI-PhD Symposium*, 2010.

Wilfong, G., Holland, M., and Lumkes, J. Design and analysis of pilot operated high speed on/off valves for digital pump/motors. *In Proceedings of the 52nd National Conference on Fluid Power*, 2011.

Paper I

Control and Performance Analysis of a Digital Direct Hydraulic Cylinder Drive

Niels H. Pedersen, Per Johansen, Lasse Schmidt, Rudolf Scheidl and Torben O. Andersen

The paper has been submitted for publication in
International Journal of Fluid Power, 2018.

INTERNATIONAL JOURNAL OF FLUID POWER

Control and Performance Analysis of a Digital Direct Hydraulic Cylinder Drive

Niels H. Pedersen[a], Per Johansen[a], Lasse Schmidt[a], Rudolf Scheidl[b] and Torben O. Andersen[a]

[a]Department of Energy Technology, Aalborg University, Aalborg, Denmark; [b]Institute of Machine Design and Hydraulic Drives, Johannes Kepler University, Linz, Austria

ARTICLE HISTORY
Compiled June 19, 2018

ABSTRACT
This paper concerns control of a digital direct hydraulic cylinder drive (D-DHCD) and is a novel concept with the potential to become the future solution for energy efficient hydraulic drives. The concept relies on direct control of a differential cylinder by a single hydraulic pump/motor unit connected to each cylinder inlet/outlet. The pump/motor unit in this research uses the digital displacement technology and comprises of numerous individually digital controlled pressure chambers, such that the ratio of active (motoring, pumping or idling) chambers determines the machine power throughput. This feature reduces energy losses to a minimum, since the inactive (idling) chambers has very low losses. A single DDM may provide individually load control for several cylinders without excessive throttling due to various load sizes. Successful implementation of the concept relies on proper control of the DDM, which demands a dynamical model that allows for system analysis and controller synthesis. This is a challenging task, due to the highly non-smooth machine behavior, comprising both non-linear continuous and discrete elements. This paper presents the first feedback control strategy for a D-DHCD concept, based on a discrete dynamical approximation and investigates the control performance in a mathematical simulation model representing the physical system.

KEYWORDS
Digital Displacement Machines; Hydraulics; Fluid Power; Direct Drive; Control; Energy efficient

1. Introduction

Conventional hydraulic cylinder drives are widely used in industry due to their high power-to-weight ratio, but is challenged by their low efficiency, especially at part load operation. The high losses are a result of throttling through utilization of proportional flow control valves used to achieve the desired cylinder operation. Various solutions for improving the efficiency of cylinder drives has therefore been studied, such that hydraulic drives are a viable candidate for future energy efficient actuation systems. One proposed solution where proportional valve flow control is maintained, is through use of an additional valve, allowing for individual pressure chamber control through the separate metering principle Nielsen (2005). Another solution is to introduce an additional intermediate pressure line, allowing for a reduction in throttling losses at lighter

CONTACT Niels H. Pedersen. Email: nhp@et.aau.dk

loads through switching between active pressure lines Dengler *et al.* (2011, 2012). An alternative concept is direct pump/motor flow control, where the throttling losses as a result of proportional flow control valves is omitted. Various solution proposals for achieving proportional direct flow control has been presented which are based on variable displacement units, rectifying bridges and/or accumulator solutions Heybroek *et al.* (2008, 2006), Ivantysynova and Rahmfeld (1998). However, these methods are often either rather complex and/or costly, why low cost alternative solutions has been investigated, e.g. the speed-variable switched differential pump system Schmidt *et al.* (2017, 2015). Recently emerging solutions based on digital hydraulics is another alternative to increase the energy efficiency through direct flow control M. Heikkil (2013). This paper investigates a digital hydraulic solution, where the direct pump/motor flow control is achieved through use of the digital displacement technology. The digital displacement machine (DDM) comprises of numerous displacement chambers in a modular construction, where each chamber is individually controlled by electrically actuated on/off valves. The machine enables utilization of three modes (pumping, motoring and idling), which in full stroke operation may be changed on a stroke-by-stroke basis once per revolution at a fixed angle for each chamber. This way, the committed displacement is determined by the ratio of active cylinders in discrete levels. Since the chamber pressure remains low in idling mode, it entails very low losses and thus high efficiency at part load operation. Additionally, the use of leakage free digital valves provides reliable load holding which is often a major problem for direct drive solutions. For a more detailed description of the digital displacement technology and operation see e.g. Ehsan *et al.* (1997), Payne *et al.* (2005), Rampen (2010)

To enable the technology to be feasible demands a proper feedback control system. However, development of the control system is considered a challenging task due to the non-smooth machine behavior. This may explain why state of the art control strategies are often limited to either neglecting the dynamics or pre-determine the actuation sequence offline Johansen *et al.* (2015), Sniegucki *et al.* (2013), Armstrong and Yuan (2006), Song (2008), Heikkila and Linjama (2013). Model based feedback control strategies has been developed for the digital displacement machine, but has only been considered for a machine either operating solely in pumping or motoring mode Sniegucki *et al.* (2013), Pedersen *et al.* (2016, 2017a,b, 2018). Model based feedback control of a combined pump/motor DDM is complicated by the pump and motor impulse responses being different and the decisions being made out of phase. This paper proposes the first model based control strategy for a DDM that may both use pumping and motoring strokes by use of a discrete angle average approximation method. The performance of the control system is investigated through simulation in a non-linear model representing the physical system.

2. System Description and Mathematical Model

To illustrate the digital direct hydraulic cylinder drive concept and developed control strategy, a simplified load system with a single cylinder is considered. The DDM concept allows each pressure chamber to both act as a pump and a motor unit, such that movement of the main cylinder in both direction is possible with a single fixed speed DDM. The D-DHCD concept under consideration is illustrated in Fig. 1.

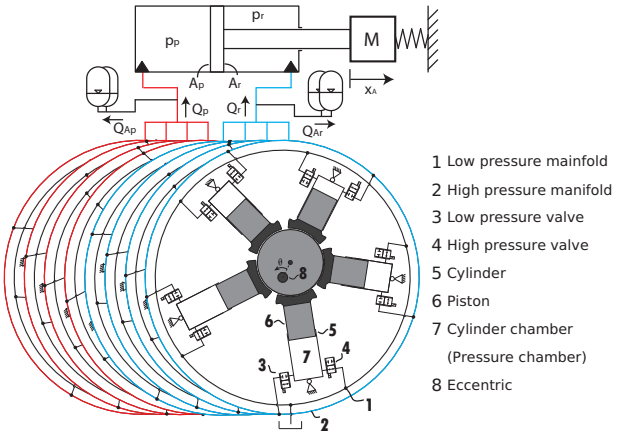

Figure 1.: Conceptional drawing of a digital displacement controlled direct cylinder drive.

The DDM consist of 8 modules with 5 cylinders in each module, for a total of 40 cylinders. The 8 modules are divided into two banks with 20 cylinders in each bank, where one bank is connected to the main cylinder piston side and the other to the main cylinder rod side. The cylinders in each bank are radially distributed around a common eccentric shaft and the two banks are parallel connected. The chamber size of the cylinders in each bank is matched with the main cylinder area ratio, such that the chamber sizes on the piston side is larger than on the rod side. When extending the main cylinder, the piston side bank may be set to pumping mode, while the rod side bank may be set to motoring mode. When reversing the direction of motion, the piston side bank may be set to motoring mode and the rod side bank to pumping mode. This way, the drive torque from the electric rotary machine may be reduced by the generated motor torque. Depending on the size of the load, only a fraction of the cylinders in a bank is active in either pumping or motoring mode, while the remaining chambers are set to idle mode. To smooth out the pressure spikes induced by the digital machine, damping accumulators is placed in the connection lines to the main cylinder chambers. In theory, the system under consideration enables the potential of running the electrical motor in generator mode for energy recovery if the stored potential energy in the spring is large. However, this is not investigated further in this paper where a fixed speed machine is assumed.

2.1. *Dynamic mathematical model*

A non-linear model representing the physical system is set-up to allow for simulation and performance evaluation, since a physical test-setup is not available. However, the presented model for the main cylinder has been experientially validated Schmidt *et al.* (2017). The cylinder motion dynamics is described by Eq. (1) and is obtained by applying newtons 2nd law of motion, resulting in

$$M\,\ddot{x}_{\mathrm{A}} = -K\,x + p_{\mathrm{p}}\,A_{\mathrm{p}} - p_{\mathrm{r}}\,A_{\mathrm{r}} - F_{\mathrm{fric}} \tag{1}$$

Here M is the combined load and piston mass, while K is the spring constant. p_p and p_r is the piston and rod side pressure respectively, while A_p and A_r is the piston and rod side area respectively. The friction force, F_fric is described by a viscous and a static term given as

$$F_\mathrm{fric} = \underbrace{B_\mathrm{c}\,\dot{x}_\mathrm{A}}_{\text{Viscous}} + \underbrace{\left(F_\mathrm{c} + (F_\mathrm{s} - F_\mathrm{c})\right)\, e^{-\left|\frac{\dot{x}_\mathrm{A}}{v_\mathrm{s}}\right|} \tanh\left(\gamma\,\dot{x}_\mathrm{A}\right)}_{\text{Stribeck + Coloumb}} \tag{2}$$

where B_c is the viscous friction coefficient, F_c is the static Coulomb friction and F_s is the Stribeck friction coefficient. γ is a shaping factor which determines the slope of the static friction near zero velocity and v_s is a shaping factor for the Stribeck friction. The pressure in the cylinder pressure chambers are described by the continuity equation and are given by

$$\begin{aligned} \dot{p_\mathrm{p}} &= \left(Q_\mathrm{p} - Q_\mathrm{Ap} - A_\mathrm{p}\,\dot{x}_\mathrm{A}\right)\, \frac{\beta_\mathrm{e}(p_\mathrm{p})}{V_\mathrm{p,0} + A_\mathrm{p}\,x_\mathrm{A}} \\ \dot{p_\mathrm{r}} &= \left(Q_\mathrm{r} - Q_\mathrm{Ar} + A_\mathrm{r}\,\dot{x}_\mathrm{A}\right)\, \frac{\beta_\mathrm{e}(p_\mathrm{r})}{V_\mathrm{r,0} - A_\mathrm{r}\,x_\mathrm{A}} \end{aligned} \tag{3}$$

The pressure dependent effective bulk modulus, β_e is modeled in accordance with Andersen and Hansen (2003) which includes the ratio of air entrapped in the oil and has a maximum value of β_max. $V_\mathrm{p,init}$ and $V_\mathrm{r,init}$ are the initial piston and rod side volumes respectively.

The flows into the damping accumulators are modeled as

$$\begin{aligned} Q_\mathrm{Ap} &= K_\mathrm{v}\,\sqrt{|p_\mathrm{p} - p_\mathrm{Ap}|}\,\mathrm{sgn}(p_\mathrm{p} - p_\mathrm{Ap}) \\ Q_\mathrm{Ar} &= K_\mathrm{v}\,\sqrt{|p_\mathrm{p} - p_\mathrm{Ar}|}\,\mathrm{sgn}(p_\mathrm{r} - p_\mathrm{Ar}) \end{aligned} \tag{4}$$

where p_Ap and p_Ar are the pressures in the damping accumulators on the piston and rod side respectively. The accumulators are modeled relatively simple by considering the ideal adiabatic gas model and is given by

$$p_\mathrm{Ap} = \left(\frac{V_\mathrm{Ap}}{\int Q_\mathrm{Ap}}\right)^{\kappa}\, p_\mathrm{Ap,0} \qquad\qquad p_\mathrm{Ar} = \left(\frac{V_\mathrm{Ar}}{\int Q_\mathrm{Ar}}\right)^{\kappa}\, p_\mathrm{Ar,0} \tag{5}$$

where κ is the adiabatic gas constant, V_Ap and V_Ar are the accumulator volumes and $p_\mathrm{Ap,0}$ and $p_\mathrm{Ar,0}$ are the pre-charge pressures. The parameter values of the main cylinder is provided in Tab. 1.

Parameter	symbol	value	Unit
Load mass	M	1316	Kg
Spring constant	K	81367	N/m
Piston side area	A_p	31.17	cm^2
Rod side area	A_r	21.55	cm^2
Viscous friction coefficient	B_c	6480	Ns/m
Coulomb friction	F_c	1740.8	N
Stribeck friction coefficient	F_s	1790.8	N
Stribeck velocity coefficient	v_s	0.7	cm/s
Friction slope coefficient	γ	1700	-
Initial piston side volume	$V_{\mathrm{p},0}$	0.36	L
Initial rod side volume	$V_{\mathrm{r},0}$	0.54	L
Maximum oil bulk modulus	β_max	7500	bar
Accumulator size, piston	V_Ap	3	L
Accumulator size, rod	V_Ar	3	L
Adiabatic gas constant	κ	1.4	-
Pre-charge pressure, piston	$p_{\mathrm{Ap},0}$	40	bar
Pre-charge pressure, rod	$p_{\mathrm{Ar},0}$	25	bar

Table 1.: Parameter values used in the non-linear simulation model for the main cylinder. The cylinder model has been experimentally validated by Schmidt *et al.* (2017).

The remaining modeling governs the dynamics of the digital displacement machine, where the important characteristics with respect to control of the machine is included. The piston and rod side flows Q_p and Q_r are the sum of flows from the individual pressure chambers of the DDM given by

$$Q_\mathrm{p} = \sum_{i=1}^{N_\mathrm{c}} Q_\mathrm{Hp}(i) \quad Q_\mathrm{r} = \sum_{i=1}^{N_\mathrm{c}} Q_\mathrm{Hr}(i) \tag{6}$$

where $N_\mathrm{c} = 20$ is the number of cylinders. Q_Hp and Q_Hr are the flow through the high pressure valve as shown in Fig. 2 illustrating a pressure chamber of the DDM. Since the dynamics of the rod side cylinder bank is identically to the piston side cylinder bank, the following derivation is made only for the piston side bank.

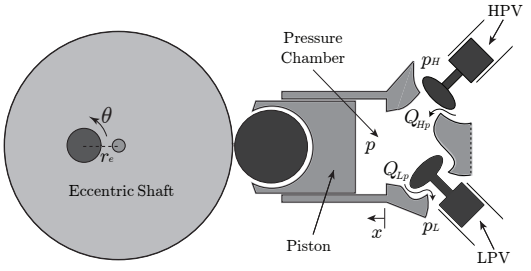

Figure 2.: Illustration of a single cylinder of the radial piston digital displacement machine.

It is seen that the high pressure valve (HPV) controls the flow to and from the high pressure manifold, while the low pressure valve (LPV) controls the flow to and

from the low pressure manifold, such that these in combination controls the chamber pressure. The piston stroke length, x as a function of the shaft angle is given by

$$x_{\mathrm{i}}\left(\theta_{\mathrm{i}}\right) = r_{\mathrm{e}}\ \left(1 - \cos(\theta_{\mathrm{i}})\right) \qquad \theta_{\mathrm{i}} = \theta + \frac{2\,\pi}{N_{\mathrm{c}}}\left(i-1\right)\ \ i \in \{1, ..., N_{\mathrm{c}}\} \tag{7}$$

r_{e} is the eccentric radius and is equal to half of the stroke length and $N_{\mathrm{c}} = 20$ is the number of cylinders. The cylinder chamber volume is then described by

$$\begin{aligned} V_{\mathrm{i}}\left(\theta_{\mathrm{i}}\right) &= \frac{V_{\mathrm{d}}}{2}\ \left(1 - \cos(\theta_{\mathrm{i}})\right) + V_0 \\ \dot{V}_{\mathrm{i}}\left(\theta_{\mathrm{i}}, \dot{\theta}\right) &= \frac{V_{\mathrm{d}}}{2}\,\dot{\theta}\ \sin(\theta_{\mathrm{i}}) \end{aligned} \tag{8}$$

where the chamber volume is given as $V_{\mathrm{d}} = V_0 = 2\,r_{\mathrm{e}}\,A_{\mathrm{c}}$, with A_{c} being the piston area. The pressure dynamics is described by the continuity equation and is given by

$$\dot{p}_{\mathrm{i}} = \frac{\beta_{\mathrm{e}}(p_{\mathrm{i}})}{V_{\mathrm{i}}}\ \left(Q_{\mathrm{Hp,i}} - Q_{\mathrm{Lp,i}} - \dot{V}_{\mathrm{i}}\right) \tag{9}$$

where Q_{Hp} and Q_{Lp} are the flows through the high and low pressure valve respectively and β_{e} is the effective oil bulk modulus. The valve flows are described by the orifice equation yielding

$$\begin{aligned} Q_{\mathrm{Lp,i}} &= \frac{\bar{x}_{\mathrm{Lp,i}}}{k_{\mathrm{f}}}\ \sqrt{|p_{\mathrm{i}} - p_{\mathrm{L}}|}\,\mathrm{sign}\left(p_{\mathrm{i}} - p_{\mathrm{L}}\right) \\ Q_{\mathrm{Hp,i}} &= \frac{\bar{x}_{\mathrm{Hp,i}}}{k_{\mathrm{f}}}\ \sqrt{|p_{\mathrm{H}} - p_{\mathrm{i}}|}\,\mathrm{sign}\left(p_{\mathrm{H}} - p_{\mathrm{i}}\right) \end{aligned} \tag{10}$$

where k_{f} is the valve flow coefficient and $\bar{x}_{\mathrm{Lp}}$ and $\bar{x}_{\mathrm{Hp}}$ are normalized valve plunger positions. The plunger dynamics is modeled as a constant acceleration to yield a smooth plunger position response with a desired switching time. An illustration of the plunger dynamic response is shown in Fig. 3.

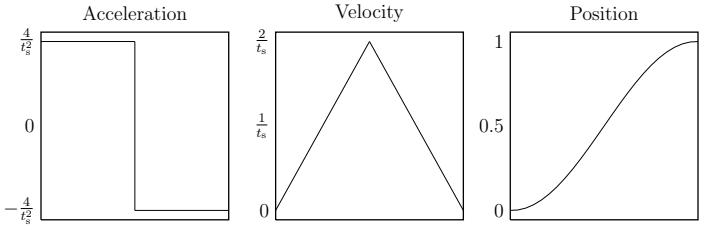

Figure 3.: Dynamics response of the digital valves.

where t_{s} is the valve opening/closing time. The position response is similar to what may be expected if a more detailed valve model with force balance equation had been utilized. Despite the relatively simple valve model, the fundamental dynamical characteristics with respect to the behavior of the machine is included.

Valve control is achieved though active closing and passive opening due to pressure, meaning that the valves are closed at specific angles based on whether a pumping,

motoring or idling decision is desired. Similarly, the HPV is opened when the chamber pressure exceeds the high pressure and the LPV is opened when the chamber pressure drops below the low pressure. Simulation results of a single chamber using the non-linear simulation model is shown in Fig. 4, where all the possible activation combinations of motoring, pumping and idling is conducted.

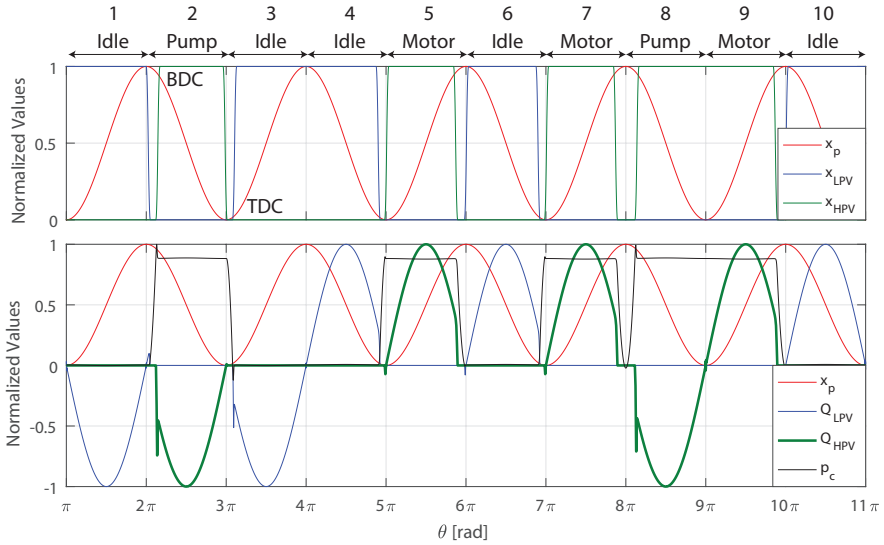

Figure 4.: Simulation of a pumping, idling and motoring strokes of the digital displacement machine.

Four different closing angles are used, namely θ_{LP}, θ_{HP}, θ_{LM} and $\theta_{\mathrm{HM}} \in [0, 2\,\pi]$, which are the closing angles for the LPV during pumping, HPV during pumping, LPV during motoring and HPV during motoring respectively. Going from section 1 to section 2, it is seen that a pumping stroke is initiated by closing the LPV at θ_{LP} located at bottom dead center (BDC), which results in a pressure increase due to chamber compression. As the chamber pressure exceeds the pressure in the high pressure manifold, a passive opening of the HPV due to pressure force is achieved and high pressure fluid is pumped to the high pressure manifold. The HPV is actively closed near top dead center (TDC) at θ_{HP}, following a chamber decompression and a passive opening of the LPV as the chamber pressure decreases below the low pressure. Similarly, a motoring stroke is initiated in the end of section 4 by closing the LPV at θ_{LM}, resulting in a passive opening of the HPV at TDC. The HPV is further closed at θ_{HM} to end the motor stroke in section 5, such that passive opening of the LPV is achieved in ahead of BDC. The later sections 7, 8 and 9 illustrates transitions when going directly between pumping and motoring strokes. Going directly from motoring to pumping is achieved by maintaining the LPV closed and going from pumping to motoring is achieved by keeping the HPV open such that the LPV remains closed. The parameters of the digital displacement machine model is provided in Tab. 2.

Parameter	symbol	value	Unit
DDM speed	$\dot{\theta}$	1500	rpm
Piston side volume	$V_{\mathrm{d,p}}$	1.25	cm^3
Rod side volume	$V_{\mathrm{d,r}}$	0.86	cm^3
Chamber flow coefficient	k_{f}	$5 \cdot 10^6$	$\sqrt{pa}\, s/\mathrm{m}^3$
Valve actuation time	t_{s}	3	ms
LPV motoring closing angle	θ_{LM}	337.7	deg
HPV motoring closing angle	θ_{HM}	152.2	deg
LPV pumping closing angle	θ_{LP}	179.9	deg
HPV pumping closing angle	θ_{HP}	353	deg
Low pressure	p_{L}	1	bar
Maximum bulk-modulus	$\beta_{\max}$	16000	bar

Table 2.: Parameters of the digital displacement machine

The reason that the maximum bulk-modulus in the DDM pressure chambers is much higher than in the main cylinder is that the hydraulic connection to the main cylinder consist of a relative large hose-volume. It is known that the pressure chamber volumes are very small in size and may be physically difficult to realize. However, the combination of chamber volume, number of pressure chambers and speed of the DDM has to be dimensioned such that they match the main cylinder specifications. With respect to control performance, it is desired to have a large number of cylinders and a high rotational speed, such that a high control resolution and update rate is achieved. However, having many small cylinder chambers is costly, why a trade off between cost and performance has to be made. Since the control strategy is the main focus of this paper and it is not effected by how these values are chosen, the above parameter values are accepted.

3. Control strategy and DLTI Model

The mathematical model and description of the D-DHCD revealed that the dynamics of each pressure chamber is described by non-linear continuous differential equations, while the inputs (pumping, motoring or idling) are discrete and may only be updated at fixed shaft angles. To overcome these control complications, this paper proposes an angle average approximation and shows that a discrete linear time invariant (DLTI) model may be sufficient in describing the DDM dynamics. The proposed control strategy is shown in Fig. 5 and is based on pulse-density modulation. Similar strategies has successfully been applied for control of both fixed and variable speed digital displacement machines which may either pump or motor, but not both Pedersen *et al.* (2016, 2017a,b). It is seen that a multi-variable DLTI controller is utilized, which output $u(t)$ is a displacement fraction reference for the piston and rod side DDM banks. This value is converted to an activation sequence for the DDM banks through a two-bit pulse-density modulator. A delta-sigma modulator is chosen, since its output is time averaging equal to the input due to integration of the error. The value of $\bar{u}(t) \in \{-1, 0, 1\}$ hence corresponds to a motoring, an idling and a pumping stroke respectively. Establishing a DLTI description of the system is seen to require a linearization of the pulse-density modulator, as well as a DLTI-approximation of the motor dynamics. Additionally, a linearization and discretization of the application load dynamics is necessary.

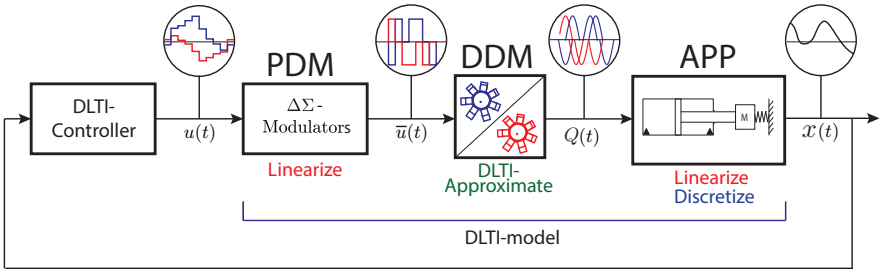

Figure 5.: Illustration of the DLTI control strategy for the digital direct hydraulic cylinder drive.

3.1. *Digital Displacement Machine*

To obtain a synchronous sampled system, the decision to either pump, motor or idle must be synchronized. The synchronization of decisions is made by considering the flow characteristic of the DDM for the individually chambers shown in Fig. 6. The fast dynamics flow spikes seen in Fig. 4 caused by a rapid pressure change is omitted for simplicity of illustration.

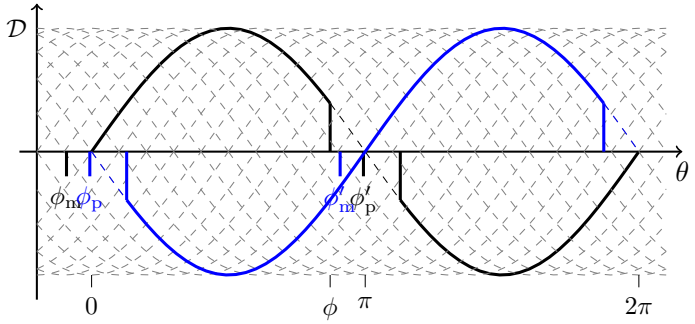

Figure 6.: Two quadrant operated DDM full stroke activation pattern of two opposite located cylinders.

When initiating a motoring stroke the LPV is closed at a local angle, $\theta_{\mathrm{LM}} = \phi_{\mathrm{m}}$ for the specific cylinder and when initiating a pumping stroke, the LPV is closed at a local angle, $\theta_{\mathrm{LP}} = \phi_{\mathrm{p}}$ for the specific cylinder. Considering two cylinders located opposite to each other, one cylinder is in the pumping stroke cycle when the other is in the motoring stroke cycle. For these opposite located cylinders, it is seen that the decision to motor is located ahead of the decision to pump. To significantly reduce the control complexity, the actuation decision for a pumping and a motor stroke is synchronized to be done at ϕ_{m}. The disadvantage of doing this is the minor delay introduced for pumping decisions, but since the speed of the machine is high, this time delay is very low.

To develop a DLTI model of the flow characteristics, it is required that there is a linear relationship between the input and output. It is seen in Fig. 6 that the response of the pumping and motoring stroke is not identically, since a minor part in the beginning of the pumping stroke is not used, while a minor part in the end of the motoring stroke is not used. However, this fraction of unused displacement is approximately identically,

such that the integrated displacement during a full stroke is the same. This compliance is used in the establishment of a DLTI model where the output during a half revolution is matched. The DLTI model is established by considering the flow throughput between samples as proposed by Johansen *et al.* (2017). The displacement fraction between samples is described by Eq. (11) when considering $Q \approx \dot{V}$, which is considered valid due to the fast pressure dynamics.

$$\begin{aligned} Q_{\mathrm{H}}[k] &\approx \frac{V_{\mathrm{d}}}{\theta_{\mathrm{s}}} \left(\bar{V}(\theta[k+1]) - \bar{V}(\theta[k]) \right) \dot{\theta} \\ &\approx \frac{V_{\mathrm{d}}\, N_{\mathrm{c}}}{2\,\pi}\, \dot{\theta}\, \Delta \bar{V}[k] \end{aligned} \tag{11}$$

where $\bar{V}$ is the normalized chamber volume and $\theta_{\mathrm{s}} = 2\,\pi / N_{\mathrm{c}}$ is the sample angle. The samples are made at angles given by

$$\theta[k] = \phi_{\mathrm{m}} + \frac{2\,\pi}{N_{\mathrm{c}}}\,(k-1) \qquad\qquad k \in \{1, \ldots, N_{\mathrm{c}}\} \tag{12}$$

where ϕ_{m} is the local angle where the actuation decision is made. The displacement fractions between samples is determined by Eq. (13) when considering a motoring stroke.

$$\Delta \bar{V}[k] = \begin{cases} 0 & \theta[k], \theta[k+1] \notin [0\,;\pi] \\ \bar{V}(\theta[k+1]) - \bar{V}(\theta[k]) & \theta[k], \theta(k+1) \in [0\,;\pi] \\ \bar{V}(\theta[k+1]) - \bar{V}(0) & \theta[k] < 0 < \theta[k+1] \\ \bar{V}(\pi) - \bar{V}(\theta[k]) & \theta[k] < \pi < \theta[k+1] \end{cases} \tag{13}$$

The flow response may then be written as a convolution sum (sum of impulse responses) given by

$$Q[k] = \underbrace{\frac{V_{\mathrm{d}}\, N_{\mathrm{c}}\, \dot{\theta}}{2\,\pi}}_{k_{\mathrm{m}}}\ \alpha[k] \qquad\qquad \alpha[k] = \sum_{m=0}^{k} \Delta \bar{V}[k-m]\ \bar{u}[m] \tag{14}$$

where α corresponds to the displacement fraction. The resulting impulse response of the discrete displacement model is shown in Fig. 7.

To match the DC-gain of the response, the committed displacement during a full stroke of the DLTI-model has to be scaled with that of the physical system where a minor fraction is not utilized. This is done by calculating the fraction of the full stroke that is utilized by

$$\eta = \frac{V(\phi)}{V(\pi)} = \frac{\frac{V_{\mathrm{d}}}{2}\ (1 - \cos(\phi))}{\frac{V_{\mathrm{d}}}{2}\ (1 - \cos(\pi))} = \frac{(1 - \cos(\phi))}{2} \tag{15}$$

where $\phi = \theta_{\mathrm{HP}}$ is the angle where motoring is stopped as shown in Fig. 6. The resulting DLTI-model transfer function thus becomes that in Eq. (16), when transforming the difference equation representation in Eq. (14) to a transfer function.

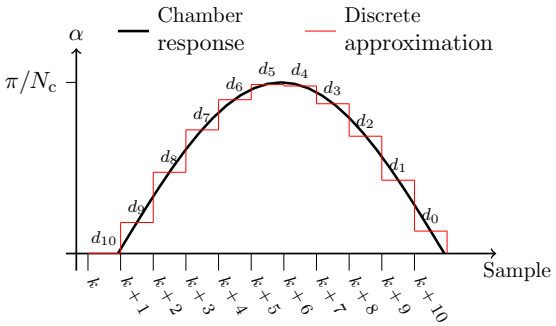

Figure 7.: Discretization of displacement response.

$$G(z) = \frac{Q}{\bar{u}} = \eta\, k_{\mathrm{m}} \frac{d_{10}\, z^{10} + d_9\, z^9 + \cdots + d_1\, z + d_0}{z^{10}} \tag{16}$$

where $d_{\mathrm{i}} = \Delta\bar{V}[10 - i]$. It is seen that the model order is directly determined by the number of cylinders. The flow response of the angle average discrete model is shown in Fig. 8, for both a motoring and a pumping stroke.

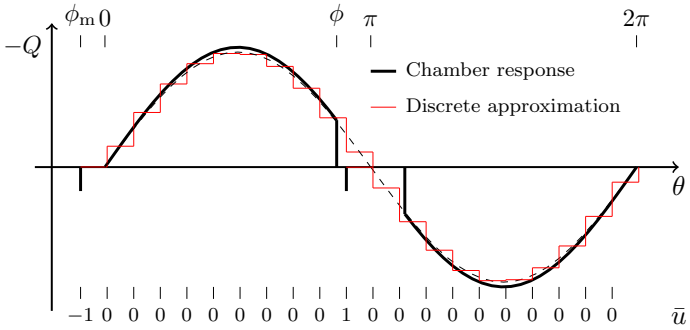

Figure 8.: Two quadrant operated DDM full stroke activation pattern.

The figure shows a motoring and a pumping impulse response of the DLTI-model. A value of -1 (motoring) is given as input at the first sample which output last for the subsequent 10 samples. An input value of 1 (pumping) is then given 10 samples later, which makes the same cylinder do a pumping stroke immediately after. The output is seen to resemble the system response fairly well. As expected, there are minor discrepancies in the end of the motoring stroke and in the beginning of the pumping stroke due to the linear approximation. However, the fundamental characteristics and the committed displacement during a full stroke is identical.

3.2. *Pulse-density modulator*

The input $\bar{u} \in \{-1, 0, 1\}$ is generated by a discrete delta-sigma modulator that comprises of a discrete integrator and a quantizer as shown in Fig. 9a.

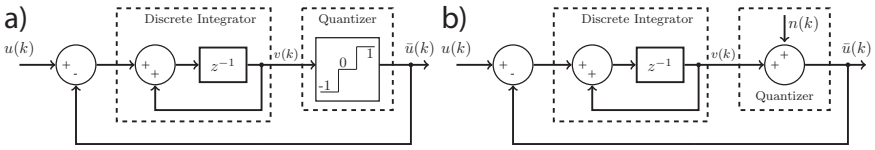

Figure 9.: Two-bit first order Delta-Sigma Modulation diagram and linear representation of it.

The modulator integrates the error between the input and output such that the average value is identical. The quantizer is implemented in the form given by

$$\bar{u}[k] = \begin{cases} 1 & \text{if } v[k] \geq 0.5 \\ 0 & \text{if } -0.5 \leq v[k] < 0.5 \\ -1 & \text{if } -0.5 < v[k] \end{cases} \tag{17}$$

The quantizer is seen to be highly non-linear and thus requires linearization. This is done by considering the quantizer as an additive noise input, n with noise intensity $\mathcal{I} \in [0; 1/2]$ as illustrated in Fig. 9b. Replacing the quantizer with an additive noise input yields the linear discrete model given by

$$\begin{aligned} \bar{U}(z) &= \frac{1}{z}\, U(z) + \frac{z-1}{z}\, N(z) \\ \bar{u}(k) &= u(k-1) + n(k) - n(k-1) \end{aligned} \tag{18}$$

It is seen that the linear model comprises of a single sample delayed input and a discrete differentiated noise term. The result of this linear approximation is illustrated by considering the relationship between the input $u(k)$ and the output $\bar{u}(k)$ as shown in Fig. 10. (The discretization of the response is omitted for simplicity of illustration).

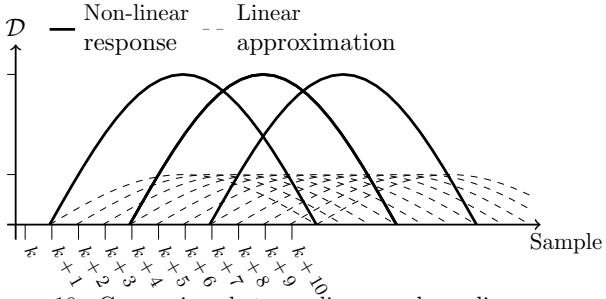

Figure 10.: Comparison between linear and non-linear response.

It is seen that if the input $u(k) = 1/3$, then one third of the cylinders are activated physically. However, if neglecting the quantizer noise term, the DLTI model output results in the sum of dashed line responses. The linear response has all the cylinders

active, but their amplitude is 1/3, such that the average displacement is identically. This linear approximation with neglected noise term is hence less accurate at lower displacement fractions and yields a more smooth response than the actual, which may be a limiting factor with respect to linear deterministic control of such system. The DLTI model of the modulator may then be combined with the DDM model to represent the dynamic behavior of the full stroke operated digital displacement machine.

3.3. *Application load*

To apply DLTI-control of the system, the cylinder drive and load dynamics requires linearization and discretization. The mechanical system is linearized by omitting the static friction resulting in

$$M\,\ddot{x}_\mathrm{A} = -K_\mathrm{eq}\,x + p_\mathrm{p}\,A_\mathrm{p} - p_\mathrm{r}\,A_\mathrm{r} - B_\mathrm{c}\,\dot{x} \tag{19}$$

Linearization of the cylinder drive dynamics is done by specifying a linearization point for the effective bulk-modulus and the pressure chamber volumes, as well as neglecting the accumulator dynamics resulting in

$$\dot{p}_\mathrm{p} = (Q_\mathrm{p} - A_\mathrm{p}\,\dot{x}_\mathrm{A})\,\frac{\beta}{V_\mathrm{p}} \quad \dot{p}_\mathrm{r} = (Q_\mathrm{r} + A_\mathrm{r}\,\dot{x}_\mathrm{A})\,\frac{\beta}{V_\mathrm{r}} \tag{20}$$

The value of bulk-modulus, β, is evaluated at a relatively low pressure of 25 bar where the stiffness is low, while V_p and V_r are chosen as those yielding the lowest eigen-frequency. On state-space form the linearized system dynamics is hence described as

$$\begin{aligned}
\underbrace{\begin{bmatrix}\dot{p}_\mathrm{p}\\ \dot{p}_\mathrm{r}\\ \ddot{x}_\mathrm{A}\\ \dot{x}_\mathrm{A}\end{bmatrix}}_{\dot{\mathbf{z}}_\mathrm{p}} &= \underbrace{\begin{bmatrix} 0 & 0 & -\frac{\beta}{V_\mathrm{p}}A_\mathrm{p} & 0\\ 0 & 0 & \frac{\beta}{V_\mathrm{r}}A_\mathrm{r} & 0\\ \frac{A_\mathrm{p}}{M} & -\frac{A_\mathrm{r}}{M} & -\frac{B_\mathrm{c}}{M} & -\frac{K_\mathrm{eq}}{M}\\ 0 & 0 & 1 & 0\end{bmatrix}}_{\mathbf{A}_\mathrm{c}} \underbrace{\begin{bmatrix}p_\mathrm{p}\\ p_\mathrm{r}\\ \dot{x}_\mathrm{A}\\ x_\mathrm{A}\end{bmatrix}}_{\mathbf{z}_\mathrm{p}} + \underbrace{\begin{bmatrix}\frac{\beta}{V_\mathrm{p}} & 0\\ 0 & \frac{\beta}{V_\mathrm{r}}\\ 0 & 0\\ 0 & 0\end{bmatrix}}_{\mathbf{B}_\mathrm{c}} \underbrace{\begin{bmatrix}Q_\mathrm{p}\\ Q_\mathrm{r}\end{bmatrix}}_{\mathbf{u}_\mathrm{p}}\\
\underbrace{\begin{bmatrix}x_\mathrm{A}\\ p_\mathrm{r}\end{bmatrix}}_{\mathbf{y}} &= \underbrace{\begin{bmatrix}0 & 0 & 0 & 1\\ 0 & 1 & 0 & 0\end{bmatrix}}_{\mathbf{C}_\mathrm{c}} \mathbf{z}_\mathrm{p}
\end{aligned} \tag{21}$$

The plant model is normalized to simplify control synthesis by the state transformation $\mathbf{z}_\mathrm{p} = \mathbf{P}\,\mathbf{x}_\mathrm{p}$ resulting in

$$\begin{aligned}
\dot{\mathbf{x}}_\mathrm{p} &= \underbrace{\mathbf{P}^{-1}\,\mathbf{A}_\mathrm{c}\,\mathbf{P}}_{\mathbf{A}_\mathrm{n}}\,\mathbf{x}_\mathrm{p} + \underbrace{\mathbf{P}^{-1}\,\mathbf{B}_\mathrm{c}}_{\mathbf{B}_\mathrm{n}}\,\mathbf{u}_\mathrm{p}\\
\mathbf{P} &= \mathrm{diag}\begin{bmatrix}\hat{p}_\mathrm{p} & \hat{p}_\mathrm{r} & \hat{\dot{x}}_\mathrm{A} & \hat{x}_\mathrm{A}\end{bmatrix}
\end{aligned} \tag{22}$$

where a hat denotes its maximum value. A discretization of the main cylinder plant dynamics yields the discrete state model given by

$$\begin{aligned} \mathbf{x}_{\mathrm{p}}(k+1) &= \mathbf{A}_{\mathrm{p}}\,\mathbf{x}_{\mathrm{p}}(k) + \mathbf{B}_{\mathrm{p}}\,\mathbf{u}_{\mathrm{p}}(k) \\ \mathbf{y}(k) &= \mathbf{C}_{\mathrm{p}}\,\mathbf{x}_{\mathrm{p}}(k) \end{aligned}$$
$$\mathbf{A}_{\mathrm{p}} = e^{\mathbf{A}_{\mathrm{n}}\,T_{\mathrm{s}}} \qquad \mathbf{B}_{\mathrm{p}} = \int_0^{T_{\mathrm{s}}} e^{\mathbf{A}_{\mathrm{n}}\,\lambda} d\lambda\,\mathbf{B}_{\mathrm{n}} \qquad \mathbf{C}_{\mathrm{p}} = \mathbf{C}_{\mathrm{c}} \tag{23}$$

The discrete transfer function of the DDM flow presented in Eq. (16) may be rewritten into state space form. For the piston side flow the resulting state representation is given by

$$\underbrace{\begin{bmatrix} x_{\mathrm{mp}}(k) \\ x_{\mathrm{mp}}(k-1) \\ x_{\mathrm{mp}}(k-2) \\ \vdots \\ x_{\mathrm{mp}}(k-p+1) \end{bmatrix}}_{\mathbf{x}_{\mathrm{mp}}(k+1)} = \underbrace{\begin{bmatrix} 0 & 0 & \cdots & 0 & 0 \\ 1 & 0 & \cdots & 0 & 0 \\ 0 & 1 & \cdots & 0 & 0 \\ \vdots & \vdots & \ddots & \vdots & \vdots \\ 0 & 0 & \cdots & 1 & 0 \end{bmatrix}}_{\mathbf{A}_{\mathrm{mp}}} \underbrace{\begin{bmatrix} x_{\mathrm{mp}}(k-1) \\ x_{\mathrm{mp}}(k-2) \\ x_{\mathrm{mp}}(k-3) \\ \vdots \\ x_{\mathrm{mp}}(k-p) \end{bmatrix}}_{\mathbf{x}_{\mathrm{mp}}(k)} + \underbrace{\begin{bmatrix} 1 \\ 0 \\ 0 \\ \vdots \\ 0 \end{bmatrix}}_{\mathbf{B}_{\mathrm{mp}}} \bar{u}_{\mathrm{p}}(k)$$
$$Q_{\mathrm{p}}(k) = \underbrace{k_{\mathrm{mp}}\,\eta\,\begin{bmatrix}\Delta\bar{V}_{\mathrm{c}}[1] & \cdots & \Delta\bar{V}_{\mathrm{c}}[p]\end{bmatrix}}_{\mathbf{C}_{\mathrm{mp}}}\,\mathbf{x}_{\mathrm{mp}}(k) + \underbrace{k_{\mathrm{mp}}\,\eta\,\begin{bmatrix}\Delta\bar{V}_{\mathrm{c}}[0]\end{bmatrix}}_{D_{\mathrm{mp}}}\,\bar{u}_{\mathrm{p}}(k) \tag{24}$$

The only difference between the rod side and the piston side flow model of the DDM is the value of k_{m}, which is smaller for the rod side, since V_{d} is smaller to match the differential cylinder area ratio. The DLTI-model for the rod side DDM flow is thus described by

$$\begin{aligned} \mathbf{x}_{\mathrm{mr}}(k+1) &= \mathbf{A}_{\mathrm{mr}}\,\mathbf{x}_{\mathrm{mr}}(k) + \mathbf{B}_{\mathrm{mr}}\,\bar{u}_{\mathrm{r}}(k) \\ Q_{\mathrm{r}}(k) &= \mathbf{C}_{\mathrm{mr}}\,\mathbf{x}_{\mathrm{mr}}(k) + D_{\mathrm{mr}}\,\bar{u}_{\mathrm{r}}(k) \end{aligned} \tag{25}$$

The flow input model to the main cylinder plant is then given as

$$\underbrace{\begin{bmatrix}\mathbf{x}_{\mathrm{mp}}(k+1) \\ \mathbf{x}_{\mathrm{mr}}(k+1)\end{bmatrix}}_{\mathbf{x}_{\mathrm{m}}(k+1)} = \underbrace{\begin{bmatrix}\mathbf{A}_{\mathrm{mp}} & 0 \\ 0 & \mathbf{A}_{\mathrm{mr}}\end{bmatrix}}_{\mathbf{A}_{\mathrm{m}}} \underbrace{\begin{bmatrix}\mathbf{x}_{\mathrm{mp}}(k) \\ \mathbf{x}_{\mathrm{mr}}(k)\end{bmatrix}}_{\mathbf{x}_{\mathrm{m}}(k)} + \underbrace{\begin{bmatrix}\mathbf{B}_{\mathrm{mp}} & 0 \\ 0 & \mathbf{B}_{\mathrm{mr}}\end{bmatrix}}_{\mathbf{B}_{\mathrm{m}}} \underbrace{\begin{bmatrix}\bar{u}_{\mathrm{p}}(k) \\ \bar{u}_{\mathrm{r}}(k)\end{bmatrix}}_{\bar{\mathbf{u}}(k)}$$
$$\underbrace{\begin{bmatrix}Q_{\mathrm{p}}(k) \\ Q_{\mathrm{r}}(k)\end{bmatrix}}_{\mathbf{u}_{\mathrm{p}}(k)} = \underbrace{\begin{bmatrix}\mathbf{C}_{\mathrm{mp}} & 0 \\ 0 & \mathbf{C}_{\mathrm{mr}}\end{bmatrix}}_{\mathbf{C}_{\mathrm{m}}} \underbrace{\begin{bmatrix}\mathbf{x}_{\mathrm{mp}}(k) \\ \mathbf{x}_{\mathrm{mr}}(k)\end{bmatrix}}_{\mathbf{x}_{\mathrm{m}}(k)} + \underbrace{\begin{bmatrix}D_{\mathrm{mp}} & 0 \\ 0 & D_{\mathrm{mr}}\end{bmatrix}}_{\mathbf{D}_{\mathrm{m}}} \underbrace{\begin{bmatrix}\bar{u}_{\mathrm{p}}(k) \\ \bar{u}_{\mathrm{r}}(k)\end{bmatrix}}_{\bar{\mathbf{u}}(k)} \tag{26}$$

The discrete pulse density modulator difference equation in Eq. (18) is rewritten into state space form resulting in

$$\begin{aligned}\underbrace{\begin{bmatrix}x_{\mathrm{dp}}(k+1)\\ x_{\mathrm{dr}}(k+1)\end{bmatrix}}_{\mathbf{x}_{\mathrm{d}}(k+1)} &= \underbrace{\begin{bmatrix}0 & 0\\ 0 & 0\end{bmatrix}}_{\mathbf{A}_{\mathrm{d}}}\underbrace{\begin{bmatrix}x_{\mathrm{dp}}(k)\\ x_{\mathrm{dr}}(k)\end{bmatrix}}_{\mathbf{x}_{\mathrm{d}}(k)} + \underbrace{\begin{bmatrix}1 & 0\\ 0 & 1\end{bmatrix}}_{\mathbf{B}_{\mathrm{d}}}\underbrace{\begin{bmatrix}u_{\mathrm{p}}(k)\\ u_{\mathrm{r}}(k)\end{bmatrix}}_{\mathbf{u}(k)} + \underbrace{\begin{bmatrix}-1 & 0\\ 0 & -1\end{bmatrix}}_{\mathbf{B}_{\mathrm{N}}}\underbrace{\begin{bmatrix}n_{\mathrm{p}}(k)\\ n_{\mathrm{r}}(k)\end{bmatrix}}_{\mathbf{n}(k)}\\ \underbrace{\begin{bmatrix}\bar{u}_{\mathrm{p}}(k)\\ \bar{u}_{\mathrm{r}}(k)\end{bmatrix}}_{\bar{\mathbf{u}}(k)} &= \underbrace{\begin{bmatrix}1 & 0\\ 0 & 1\end{bmatrix}}_{\mathbf{C}_{\mathrm{d}}}\underbrace{\begin{bmatrix}x_{\mathrm{dp}}(k)\\ x_{\mathrm{dr}}(k)\end{bmatrix}}_{\mathbf{x}_{\mathrm{d}}(k)} + \underbrace{\begin{bmatrix}1 & 0\\ 0 & 1\end{bmatrix}}_{\mathbf{D}_{\mathrm{N}}}\underbrace{\begin{bmatrix}n_{\mathrm{p}}(k)\\ n_{\mathrm{r}}(k)\end{bmatrix}}_{\mathbf{n}(k)}\end{aligned} \tag{27}$$

The combined full system DLTI-model then becomes

$$\begin{aligned}\underbrace{\begin{bmatrix}\mathbf{x}_{\mathrm{p}}(k+1)\\ \mathbf{x}_{\mathrm{m}}(k+1)\\ \mathbf{x}_{\mathrm{d}}(k+1)\end{bmatrix}}_{\mathbf{x}_{\mathrm{t}}(k+1)} &= \underbrace{\begin{bmatrix}\mathbf{A}_{\mathrm{p}} & \mathbf{B}_{\mathrm{p}}\,\mathbf{C}_{\mathrm{m}} & \mathbf{B}_{\mathrm{p}}\,\mathbf{D}_{\mathrm{m}}\,\mathbf{C}_{\mathrm{d}}\\ \mathbf{0} & \mathbf{A}_{\mathrm{m}} & \mathbf{B}_{\mathrm{m}}\,\mathbf{C}_{\mathrm{d}}\\ \mathbf{0} & \mathbf{0} & \mathbf{A}_{\mathrm{d}}\end{bmatrix}}_{\mathbf{A}_{\mathrm{t}}}\underbrace{\begin{bmatrix}\mathbf{x}_{\mathrm{p}}(k)\\ \mathbf{x}_{\mathrm{m}}(k)\\ \mathbf{x}_{\mathrm{d}}(k)\end{bmatrix}}_{\mathbf{x}_{\mathrm{t}}(k)} + \underbrace{\begin{bmatrix}\mathbf{0}\\ \mathbf{0}\\ \mathbf{B}_{\mathrm{d}}\end{bmatrix}}_{\mathbf{B}_{\mathrm{t}}}\mathbf{u}(k)\\ &+ \underbrace{\begin{bmatrix}\mathbf{B}_{\mathrm{p}}\,\mathbf{D}_{\mathrm{m}}\,\mathbf{D}_{\mathrm{N}}\\ \mathbf{B}_{\mathrm{m}}\,\mathbf{D}_{\mathrm{N}}\\ \mathbf{B}_{\mathrm{N}}\end{bmatrix}}_{\mathbf{N}_{\mathrm{t}}}\mathbf{n}(k) \qquad \mathbf{y}(k) = \underbrace{\begin{bmatrix}\mathbf{C}_{\mathrm{p}} & \mathbf{0} & \mathbf{0}\end{bmatrix}}_{\mathbf{C}_{\mathrm{t}}}\mathbf{x}_{\mathrm{t}}(k)\end{aligned} \tag{28}$$

Since the DD unit is driven at a constant high speed $\dot{\theta} = 1500$ rpm and it takes half of a revolution to go from minimum to maximum flow rate, the response time of the digital displacement machine is $T_{\mathrm{resp}} \approx 0.02$ s. The DDM actuation dynamics is thus relatively fast compared to the main cylinder dynamics, why it is investigated if the DDM dynamics may be neglected when synthesizing the controller. This is done through analysis of the singular values with and without the DDM dynamics. To be able to compare these values, the input to the discrete main cylinder model in Eq. (23) is normalized to be given by

$$\mathbf{x}_{\mathrm{p}}(k+1) = \mathbf{A}_{\mathrm{p}}\,\mathbf{x}_{\mathrm{p}}(k) + \mathbf{B}_{\mathrm{p}}\,\underbrace{\mathbf{P}_{\mathrm{u}}\,\mathbf{u}_{\mathrm{n}}(k)}_{\mathbf{u}_{\mathrm{p}}(k)} \quad \mathbf{P}_{\mathrm{u}} = \begin{bmatrix}A_{\mathrm{p}}\,\hat{\dot{x}}_{\mathrm{A}}\,\eta & 0\\ 0 & A_{\mathrm{r}}\,\hat{\dot{x}}_{\mathrm{A}}\,\eta\end{bmatrix} \tag{29}$$

where $\mathbf{P}_{\mathrm{u}}$ contains the maximum flow rate for the piston and rod side and $\eta = 0.96$ is the maximum fraction of utilized displacement. The singular values for the state equation for $\mathbf{x}_{\mathrm{p}}$ in Eq. (29) and the complete state equation $\mathbf{x}_{\mathrm{t}}$ in Eq. (28) is shown in Fig. 11. It is seen that the dynamics of the DDM and modulator is so fast compared to the cylinder dynamics that the DDM dynamics may be neglected in the control design if the closed loop dynamics is slower than $\omega_{\mathrm{cl}} = 10$rad/s. This requirement ensures that no phase-shift is introduced to the control system by the digital machine below this frequency threshold. This requirement is easily fulfilled when designing the feedback controller. However, since the DDM states are binary (active or inactive) in reality and it is a duty-cycle ratio when analyzed linearly, neglecting the DDM dynamics might cause a reduction in performance. Therefore it is chosen to perform a simulation study of the control performance both with and without the DDM dynamics included in the control design. Also it is evident, that if the DDM is operated at a relatively low shaft speed it is always necessary to include the DDM dynamics.

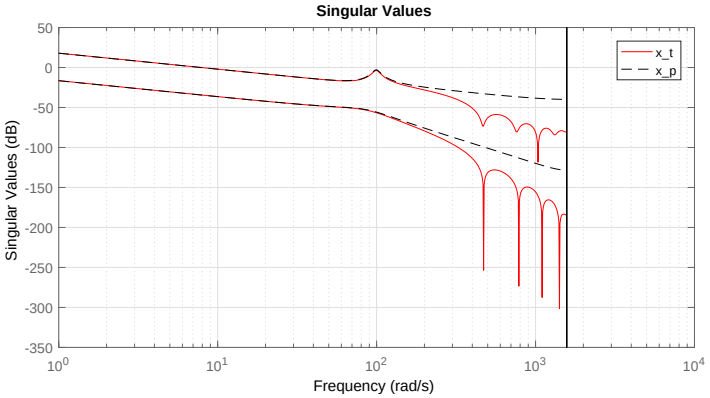

Figure 11.: Comparison of singular values with and without actuator dynamics.

4. Deterministic Optimal Control strategy

Since the system has multiple inputs and multiple outputs, it is considered advantageous to utilize an optimal control strategy. A deterministic control strategy based on linear-quadratic regulator (LQR) is used, since it has earlier been found for a similar system, that control performance is not improved noticeable by using a stochastic method where the disturbances are included in the control design Pedersen *et al.* (2017a). The following section is written for control design of the full system where the DDM dynamics is included, but the same procedure it also applied for the simplified system without the DDM dynamics.

To improve set-point tracking, integral action is added to the system on the form given by

$$\begin{aligned} \mathbf{x}_\mathrm{i}(k+1) &= \mathbf{x}_\mathrm{i}(k) + \mathbf{e}(k) \\ \mathbf{x}_\mathrm{i}(k+1) &= \mathbf{x}_\mathrm{i}(k) + \mathbf{r}(k) - \mathbf{C}_\mathrm{t}\,\mathbf{x}_\mathrm{t}(k) \end{aligned} \tag{30}$$

The resulting state space formulation used for control synthesis then becomes

$$\begin{aligned} \underbrace{\begin{bmatrix} \mathbf{x}_\mathrm{t}(k+1) \\ \mathbf{x}_\mathrm{i}(k+1) \end{bmatrix}}_{\mathbf{x}_\mathrm{s}(k+1)} &= \underbrace{\begin{bmatrix} \mathbf{A}_\mathrm{t} & \mathbf{0} \\ -\mathbf{C}_\mathrm{t} & \mathbf{I} \end{bmatrix}}_{\mathbf{A}_\mathrm{s}} \underbrace{\begin{bmatrix} \mathbf{x}_\mathrm{t}(k) \\ \mathbf{x}_\mathrm{i}(k) \end{bmatrix}}_{\mathbf{x}_\mathrm{s}(k)} + \underbrace{\begin{bmatrix} \mathbf{B}_\mathrm{t} \\ \mathbf{0} \end{bmatrix}}_{\mathbf{B}_\mathrm{s}} \mathbf{u}(k) \\ \mathbf{y}(k) &= \underbrace{\begin{bmatrix} \mathbf{C}_\mathrm{t} & \mathbf{0} \end{bmatrix}}_{\mathbf{C}_\mathrm{s}} \mathbf{x}_\mathrm{s}(k) \end{aligned} \tag{31}$$

The LQR algorithm determines the optimal control input $\mathbf{u}(k)$ that minimizes the discrete quadratic cost function given by

$$\mathcal{J} = \sum_{k=1}^{\infty} \left(\mathbf{x}_\mathrm{s}(k)^T\, \mathbf{Q}\, \mathbf{x}_\mathrm{s}(k) + \mathbf{u}(k)^T\, \mathbf{R}\, \mathbf{u}(k) \right) \tag{32}$$

where $\mathbf{Q} = \mathbf{Q}^T \geq \mathbf{0}$ is the state weighting matrix and $\mathbf{R} = \mathbf{R}^T \geq \mathbf{0}$ is the input

weighting matrix, which specifies the relative importance between driving the states to zero and the control effort to do so. It may be derived that the feedback control law is given by $\mathbf{u}(k) = -\mathbf{K}\ \mathbf{x}_{\mathrm{t}}(k) + \mathbf{K}_{\mathrm{i}}\ \mathbf{x}_{\mathrm{i}}(k)$, where the feedback control gains are determined as

$$\mathbf{K}_{\mathrm{s}} = \left(\mathbf{B}_{\mathrm{s}}^{T}\ \mathbf{S}\ \mathbf{B}_{\mathrm{s}} + \mathbf{R}\right)^{-1}\ \left(\mathbf{B}_{\mathrm{s}}^{T}\ \mathbf{S}\ \mathbf{A}_{\mathrm{s}}\right) \tag{33}$$

where the feedback gain vector is defined as $\mathbf{K}_{\mathrm{s}} = \begin{bmatrix}\mathbf{K} & \mathbf{K}_{\mathrm{i}}\end{bmatrix}$. The unknown matrix $\mathbf{S} = \mathbf{S}^{T} \geq \mathbf{0}$ is solved by the use of the discrete version of the algebraic Ricatti equation given by

$$\begin{aligned}\mathbf{0} &= \mathbf{A}_{\mathrm{s}}^{T}\ \mathbf{S}\mathbf{A}_{\mathrm{s}} - \mathbf{S} + \mathbf{Q} \\ &\quad - \left(\mathbf{A}_{\mathrm{s}}^{T}\ \mathbf{S}\ \mathbf{B}_{\mathrm{s}}\right)\ \left(\mathbf{B}_{\mathrm{s}}^{T}\ \mathbf{S}\ \mathbf{B}_{\mathrm{s}} + \mathbf{R}\right)^{-1}\left(\mathbf{B}_{\mathrm{s}}^{T}\ \mathbf{S}\ \mathbf{A}_{\mathrm{s}}\right)\end{aligned} \tag{34}$$

To exemplify the control strategy presented in this paper, the state weightings are chosen in a relatively simple manner relatively to the input weighting matrix chosen as $\mathbf{R} = \mathrm{diag}\,[1\ \ 1]$. With reference tracking being the main objective, the integral state for the tracking error and pressure error is of high importance. Since position tracking is much more important than pressure tracking, the state weighting matrix is chosen as $\mathbf{Q} = \mathrm{diag}\left\{\begin{bmatrix}0 & 0 & \cdots & 5 & 0.001\end{bmatrix}\right\}$. With the presented method, the control synthesis has been reduced to specifying two parameters, although the system comprises of 26 states.

5. Simulation Results

Since a physical test set-up is not available and the purpose of this paper is to illustrate the potential of the concept and control strategy, only performance evaluation based on simulation results is conducted. In the simulation, a common position tracking reference has been studied and a constant pressure reference is used. Two simulations are made, one which include the digital displacement machine dynamics in the control structure and one which does not. The results of the simulation is shown in Fig. 12 and Fig. 13.

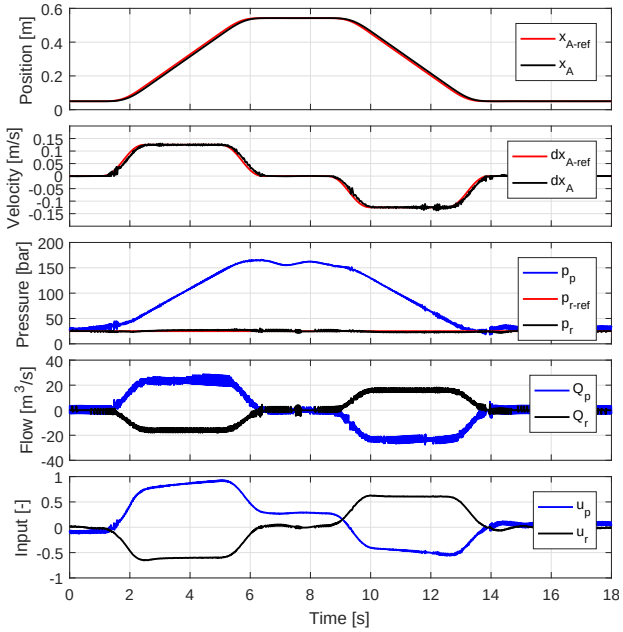

Figure 12.: Without the DDM dynamics in the control structure.

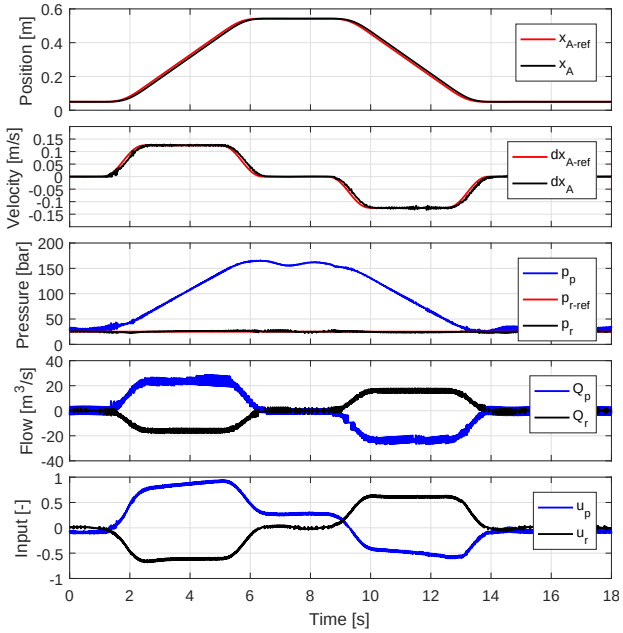

Figure 13.: With the DDM dynamics in the control structure.

The performance of the two control structures are seen to be very similar, but slightly less oscillation is identified in the piston velocity response when the complete system dynamics is included. It is clear that there is a phase-shift between the position reference and response that is undesired. This is caused by the controller gains being tuned rather conservatively. Increasing the controller gains, is found to result in an increasingly oscillating control signals and response. Minor oscillations is already seen for the piston velocity and pressure response at very low displacements, where the digital machine behavior is most clearly observed. The pressure reference tracking is also seen to be good, but as long as the pressure is within ± 10 bar, the performance is considered adequate. The flow responses are actually close to what might be considered ideal, since the amplitude of the fluctuations corresponds to the actuation of a single cylinder chamber.

Although the performance is considered acceptable it is not as good as what may be expected when using a conventional proportional valve controlled cylinder. The digital displacement technology as a direct drive is clearly most suitable for high inertia systems, where the fluctuations are dampened passively. This paper investigates a relatively low inertia system to illustrate the challenges of utilizing such digital system. Therefore, a significantly better performance is expected for high inertia systems, which control performance will be much closer to a conventional proportional valve controlled system. Alternatively, the fluctuations may be reduced by utilizing more pressure chambers with smaller volumes, but this is an expensive solution that might result in unpractical low pressure chamber volumes. Only a minor effort has been put into dimensioning of the accumulators, why optimized accumulators is also expected to increase the performance. The paper shows that the concept is viable for direct cylinder drive control, but still has many challenges that has to solved to make it a viable solution.

Conclusion

This paper proposed a control strategy for a novel energy efficient digital direct hydraulic cylinder drive concept. The highly non-smooth system behavior with both continuous and discrete dynamics challenges feedback control development. To overcome these challenges with respect to having a single machine both utilizing pumping and motoring strokes, an angle average discrete approximation of the system dynamics is established. Since the response time of the machine is proportional to its speed, a linear analysis showed that the DDM dynamics may be neglected for sufficiently high speeds. However, a simulation with the control system implemented showed that there is a slightly increase in performance by including the binary states of the digital machine in the control strategy. The system performance is found to be highly influenced by the inertia mass of the system, since a significant dampening of the digital effect is necessary to obtain smooth performance. Since this paper illustrates the concept and control system on a low mass inertia system, the obtained performance is worse than what may be expected with a conventional hydraulic cylinder drive. However, the potential usage of such system is considered very high, why control strategies like the one presented is important.

Acknowledgments

This research was funded by the Danish Council for Strategic Research through the HyDrive project at Aalborg University, at the Department of Energy Technology (case no. 1305-00038B).

References

Andersen, T.O. and Hansen, M.R., 2003. *Fluid power systems - modelling and analysis*. 2nd edition. AAU.

Armstrong, B.S.R. and Yuan, Q., 2006. Multi-level control of hydraulic gerotor motors and pumps. *Proceedings of the american control conference, minnesota, usa*.

Dengler, P., Geimer, M., and von Dombrowski, R., 2012. Deterministic control strategy for a hybrid hydraulic system with intermediate pressure line. *Proceedings of the fluid power and motion control (fpmc), bath, uk*.

Dengler, P., Groh, J., and Geimer, M., 2011. Valve control concepts in a constant pressure system with an intermediate pressure line. *21st international conference on hydraulics and pneumatics, ostrava, czech republic*.

Ehsan, M., Rampen, W., and Salter, S., 1997. Modeling of digital-displacement pump-motors and their application as hydraulic drives for nonuniform loads. *Asme. j. dyn. sys., meas., control*.

Heikkila, M. and Linjama, M., 2013. Displacement control of a mobile crane using digital hydraulic power management system. *Mechatronics volume 23, issue 4, pages 452-461*.

Heybroek, K., Larsson, J., and Palmberg, J.O., 2006. Open circuit solution for pump controlled actuators. *Proceedings of the 4th fpni-phd symposium. sarasota*.

Heybroek, K., *et al.*, 2008. Evaluating a pump controlled open circuit solution. *Proceedings of the 51th international exposition for power transmission, nevada, usa*.

Ivantysynova, M. and Rahmfeld, R., 1998. Energy saving hydraulic actuators for mobile machinery. *1st bratislavian fluid power symposium*.

Johansen, P., *et al.*, 2017. Discrete linear time invariant analysis of digital fluid power pump flow control. *Journal of dynamic systems, measurement and control, transactions of the asme, vol. 139, nr. 10, 101007*.

Johansen, P., *et al.*, 2015. Delta-sigma modulated displacement of a digital fluid power pump. *The 7th workshop on digital fluid power, linz, austria*.

M. Heikkil, a.M.L., 2013. Displacement control of a mobile crane using a digital hydraulic power management system. *Mechatronics, 23(4), 452461*.

Nielsen, B., 2005. *Controller development for a separate meter-in separate meter-out fluid power valve for mobile applications*. Thesis (PhD). Department of Energy Technology, Aalborg University.

Payne, G.S., *et al.*, 2005. Potential of digital displacement hydraulics for wave energy conversion. *In proc. of the 6th european wave and tidal energy conference, glasgow uk*.

Pedersen, N.H., Johansen, P., and Andersen, T.O., 2016. Lqr feedback control development for wind turbines featuring a digital fluid power transmission system. *Proceedings of the 9th fpni ph.d. symposium on fluid power. american society of mechanical engineers*.

Pedersen, N.H., Johansen, P., and Andersen, T.O., 2017a. Optimal control of a wind turbine with digital fluid power transmission. *Nonlinear dyn.*

Pedersen, N.H., Johansen, P., and Andersen, T.O., 2017b. Event-driven control of a speed varying digital displacement machine. *Proceedings of the 2017 bath/asme symposium on fluid power and motion control*.

Pedersen, N.H., Johansen, P., and Andersen, T.O., 2018. Feedback control of multi-level pulse-density modulated digital displacement transmission. *Ieee/asme transaction on mecatronics, vol. x, no. x*.

Rampen, W., 2010. The development of digital displacement technology. *In proceedings of bath/asme fpmc symposium.*

Schmidt, L., *et al.*, 2017. Position control of an over-actuated direct hydraulic cylinder drive. *Control engineering practice 64, 1-14.*

Schmidt, L., *et al.*, 2015. Speed-variable switched differential pump system for a direct operation of hydraulic cylinders. *Proceedings of asme/bath symposium on fluid power & motion control, chicago, illinois usa.*

Sniegucki, M., Gottfried, M., and Klingauf, U., 2013. Optimal control of digital hydraulic drives using mixed-integer quadratic programming. *Proceedings of the 9th ifac symposium on nonlinear control systems.*

Song, X., 2008. Modeling and active vehicle suspension system with application of digital displacement pump motor. *Proceedings of the asme 2008 international design engineering techical conferences & computers and information in engineering conference, new york, usa.*

Paper J

Non-Linear Hybrid Control Oriented Modelling of a Digital Displacement Machine

Niels H. Pedersen, Per Johansen, Rudolf Scheidl and Torben O. Andersen

The paper has been published in
Proceedings of the 9th Workshop on Digital Fluid Power, Aalborg, Denmark, 2017.

The layout has been revised.

NON-LINEAR HYBRID CONTROL ORIENTED MODELLING OF A DIGITAL DISPLACEMENT MACHINE

Niels H. Pedersen, Per Johansen, Torben O. Andersen, Rudolf Scheidl*
Department of Energy Technology
Aalborg University, Johannes Kepler University*
Pontoppidanstraede 111, 9220 Aalborg East, Denmark
E-mail: nhp@et.aau.dk, pjo@et.aau.dk, toa@et.aau.dk, rudolf.scheidl@jku.at*

ABSTRACT

Proper feedback control of digital fluid power machines (Pressure, flow, torque or speed control) requires a control oriented model, from where the system dynamics can be analyzed, stability can be proven and design criteria can be specified. The development of control oriented models for hydraulic Digital Displacement Machines (DDM) is complicated due to non-smooth machine behavior, where the dynamics comprises both analog, digital and non-linear elements. For a full stroke operated DDM the power throughput is altered in discrete levels based on the ratio of activated pressure chambers. In this paper, a control oriented hybrid model is established, which combines the continuous non-linear pressure chamber dynamics and the discrete shaft position dependent activation of the pressure chambers. The hybrid machine model is further extended to describe the dynamics of a Digital Fluid Power Transmission (DFPT) comprising two variable speed DDM's with asynchronous control sampling schemes. A validation with respect to a non-linear dynamical model representing the physical system, shows the usefulness of the hybrid model with respect to feedback control development.

KEYWORDS: Fluid Power, Digital Displacement, Hybrid system, Control model, Event-driven

1 INTRODUCTION

Digital fluid power is gaining an increased interest as an alternative to its conventional analogue counterpart due to its fast dynamic response and high efficiency [1, 2]. Digital fluid power machines are characterized by delivering a discrete volumetric output determined by the fraction of activated pressure chambers. Fluid power transmissions (drives) is one application with a high potential for the use of these digital hydraulic machines, since robustness, repeatability and redundancy is an appreciated property that digital fluid power brings [3].

The so called digital displacement machine (DDM) is of this type and is the research topic for a high number of papers focusing on design and performance optimization [4, 5, 6, 7, 8, 9, 10, 11]. The machine comprises of several cylinders being radially

distributed around a common shaft (eccentric or cam-ring type). The pressure in each of these cylinder chambers is controlled by electrically actuated on/off valves connected to a common high and low-pressure manifold. Due to these digital valves, the displacement throughput of a full stroke operated DDM cannot be altered continuously, but rather in a stroke-by-stroke fashion once for every reciprocating piston motion. In a full stroke operation, each pressure chamber is either active or inactive during a full stroke, which means that a pump chamber is either pumping or idling and a motor chamber is either motoring or idling. This inherent feature complicates the control of the machine, which is of high importance for obtaining high efficiency and performance with respect to torque ripples and reference tracking.

Control development for digital displacement machines is a complicated task and requires a control oriented model, such that proper feedback controllers can be designed. The development of such dynamical model is not straightforward since the system comprises several dynamically aspects. The dynamics of the machine and its pressure chambers is governed by non-linear continuous differential equations, while the input is binary (active or inactive) and may only be updated discretely at certain fixed shaft angles. Additionally, when an actuation decision (active or inactive) has been made for a cylinder chamber, the output is affected for the next half of the stroke, during where the mentioned actuation decision cannot be changed.

No traditionally control oriented models are able to capture all the mentioned effects, but is instead limited to describe some of these effects or use approximations of them. Both globally asymptotically stabilizing control feedbacks for continuous and discrete linear systems has been widely studied and various approaches exist [12]. In the case of a non-linear sample-and-hold control system, the designer often tend to approximate the system dynamics, often though linearization and discretization, which puts a limiting factor on the obtainable performance [13, 14]. Another obstacle in the control of a DDM, is the position triggered sampling, which contrarily to time triggered sampling is not widely used and therefore remains an undergoing research topic. However, methods of state dependent event-driven sampled control exist, but is in general limited to linear system [15, 16, 17] or focused around minimizing the number of events in networked control systems [18, 19].

Control development for digital displacement machines is an expanding research topic and several results on the subject has been published. Most of these results are however limited to simplified operation conditions under fixed speed and often in an open loop configuration [5, 20, 21, 22]. Promising results regarding feedback control have been published by Sniegucki et. al. [23], which utilizes mixed logical dynamic programming to determine the optimal actuation sequence. Despite yielding promising results with respect to torque fluctuations and tracking, its use has so far been limited to offline optimization due to a large computational effort. Johansen et. al [24] proposes a closed loop structure for fixed speed operation, where the digital control signal is converted to a binary actuation sequence by a Delta-Sigma modulator. The same authors [25] presents a discrete linear time invariant (DLTI) model approximation of the digital machine, allowing for closed loop control development for a fixed speed machine. The work of these two papers has been combined by Pedersen et. al [26, 27] and applied to a digital fluid power transmission for a wind turbine. An event-driven control strategy using the DLTI model and Delta-Sigma modulator to overcome the problem of variable speed operation is presented in [28]. However, all of these approaches are based on discrete linear approximations, which puts limitations to the performance and region of stability. Furthermore,

no control oriented model for a DFPT with two DDM's has so far been developed.

In this study, a hybrid representation of a digital displacement machine is made, followed by a hybrid model of a digital fluid power transmission. Hybrid dynamical models are able to capture both discrete and continuous non-linear effects, as well as irrational state dependent sampling [29, 30]. Furthermore, the theory of hybrid dynamical systems has been well studied in the recent years, which has provided tools for designing globally asymptotically stabilizing feedbacks [29, 31]. This paper is structured as follows, initially as a foundation to deriving the hybrid model, the description of the DFPT is given together with the operation principle of the digital pump and motor. Following this a brief introduction to hybrid system theory in the case of sample and hold systems is provided. Then the hybrid representation of the DDM is given and verified by comparison to a non-linear dynamic simulation model representing the physical system. Lastly, the full DFPT hybrid model is derived and verified.

2 SYSTEM DESCRIPTION

The Digital Fluid Power Transmission (DFPT) under consideration comprises a multi-lobe cam-ring type digital displacement pump and a radial piston type digital displacement motor connected through a high and low pressure line as illustrated in Fig. 1.

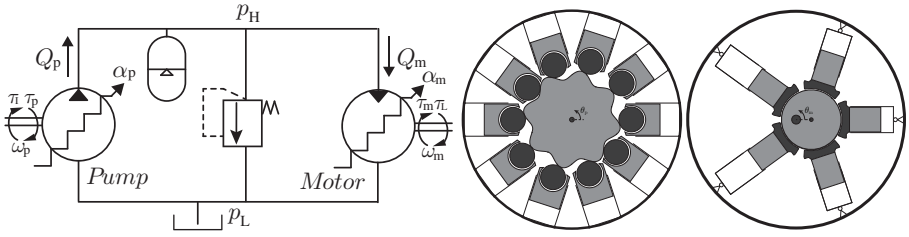

(a) Illustration of the Digital Fluid Power transmission system.

(b) Design illustration of the digital displacement pump (left) and motor (right).

Figure 1: Sketch of a digital fluid power transmission and the pump/motor designs.

The DFPT is shown in a general set-up and is applicable as transmission in e.g. wind turbines, where the turbine rotor drives the pump and the motor is connected to an electrical generator. An input torque τ_I is seen to drive the DFP pump which outputs a pressurized fluid flow Q_p to the high-pressure line having the pressure p_H. The DFP motor intakes a flow Q_m from the high-pressure line and converts it to a shaft rotation through the mechanical torque τ_m. In general, both the pump and motor may be operating at variable speed and torque/flow, which is controlled by the displacement input α_p and α_m for the pump and motor respectively. In this specific case, the machines are dimensioned around a 5 MW transmission. The pump having the design principle illustrated to the left in Fig. 1b is a cam-ring type with radially distributed cylinder pistons attached by use of roller bearings. In correct scale, there are 16 ring cam lobes and 25 cylinders in one module and 4 modules in total, which are radially shifted to avoid simultaneous chamber activations. As a result, the pump consists of 100 cylinders, each going through 16 strokes for every pump revolution. The lobed geometry yields a high displacement and a great flow/torque output resolution for a low speed machine (< 15 rpm) with a compact design. The motor having the design principle illustrated to the right, is a radial piston type with an eccentric

cam connected to a common shaft. In correct scale 7 cylinders are distributed radially around the eccentric cam shaft. A total of 6 modules are radially shifted around the common shaft similar to the pump, such that there is a total of 42 cylinders doing one stroke each for every motor revolution. This design is suited for a high-speed machine (∼1500 rpm) with a relative low displacement per revolution.

Digital displacement machines are characterized by having fast switching electrically actuated on/off valves controlling the flow throughput of the numerous cylinder pressure chambers. A sketch of a single motor cylinder pressure chamber is illustrated in Fig. 2, and is essentially identically for the pump design.

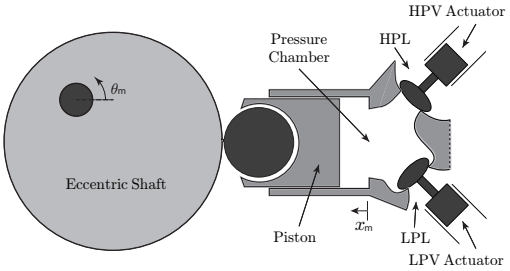

Figure 2: Sketch of a single motor pressure chamber.

Proper operation of the machine requires precisely timed actuation of the high-pressure valve (HPV) and low-pressure valve (LPV). Essential to the underlying framework of developing a control oriented model of the digital displacement machines is the understanding of the operating principle. Considering a full-stroke operation there are three distinct operating modes being idling, pumping and motoring. In a full stroke operation, the mode of each displacement chamber is altered on a stroke-by-stroke basis. Simulation results showing a pumping, idling and motoring stroke is shown in Fig. 3 and is obtained from a non-linear simulation model of the digital displacement machines presented in [26, 28].

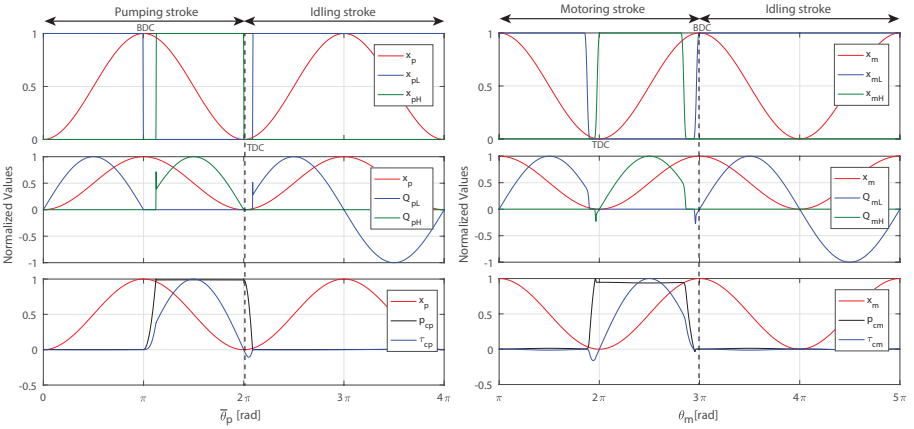

(a) Pumping and idling mode.

(b) Motoring and idling mode.

Figure 3: Simulation results of a pumping, idling and motoring stroke of the digital displacement machines.

The local pumping angle is defined as $\bar{\theta}_\mathrm{p} = \theta_\mathrm{p} N_\mathrm{p,l}$, where $N_\mathrm{p,l} = 16$ is the number of cam lobes. For the pumping mode, the LPV is closed just ahead of Buttom Dead Center (BDC), such that a passive opening of the HPV is obtained due to the chamber pressure exceeding the high pressure. During the active part of the pumping stroke, pressurized fluid is pumped to the high-pressure line. Near Top Dead Center (TDC), the HPV is closed and the LPV is passively opened since the chamber pressure drops below the low pressure. The motoring stroke is seen to be essentially the opposite of the pumping stroke, where pressurized fluid is drawn from the high-pressure line.

3 CONTROL ORIENTED MODEL

Based on the system description, the following things about the digital displacement machines may be stated with respect to development of a control oriented model.

- The dynamics of each pressure chamber is described by non-linear continuous differential equations.
- The actuation input to each pressure chamber is binary (active or inactive).
- An update of the actuation input can only be made at a fixed shaft angle.
- After an actuation input for a pressure chamber has been made, the output is affected for almost half of a piston revolution.

With respect to developing a control oriented model, the system contains non-linear dynamics, as well as both continuous and discrete elements. Additionally, memory effects are necessary, since the output depends on the input decisions after numerous subsequent input decisions. As a result, classical continuous and discrete control methods are not adequate, why a hybrid model is established to include all these different effects. Hybrid theory is very broad and is able to describe most known dynamical processes by combining the analog and digital world.

3.1 SAMPLE AND HOLD HYBRID SYSTEM THEORY

A hybrid system comprises both continuous differential (flow) equations and discrete difference (jump) equations. A hybrid system is in general formulated as that given by (1) in accordance with [32, 30].

$$\mathscr{H}: \quad \begin{cases} \dot{x} & \in F(x,u), & x \in C, \\ x^+ & \in G(x,u), & x \in D \\ y & = h(x,u) \end{cases} \tag{1}$$

$\dot{x}$ denotes the state time derivative and x^+ denotes the state value after a jump. u and y are system input and output respectively. For simplicity, a hybrid system is written as $\mathscr{H} = (F,C,G,D,h)$, where the variables describes the following

- The flow set: C
- The flow map: F
- The jump set: D
- The jump map: G
- The output map h

As long as x belongs to the flow set C, x is described by the differential inclusion given by the flow map F and when x belongs to the jump set D, x is described by the difference inclusion given by the jump map G.

To illustrate the use of hybrid dynamical system theory, a sample-and-hold control system where a continuous plant is feedback controlled by a digital controller may be formulated as a relatively simple hybrid control system given by (2) [32, 30].

Flow map and set:

$$\left.\begin{aligned} \dot{x} &= f(x,u) \\ \dot{\tau} &= 1 \\ \dot{z} &= 0 \end{aligned}\right\} \qquad \tau \in [0, T_s] \tag{2}$$

Jump map and set:

$$\left.\begin{aligned} x^+ &= x \\ \tau^+ &= 0 \\ z^+ &= u = \mathscr{C}_\kappa(z,x) \end{aligned}\right\} \qquad \tau = T_s \tag{3}$$

Where τ is a sawtooth shaped sampling timer that tracks the time since the last sample and resets when a sample occurs at the sampling time T_s. z is the internal controller state, which here represent the zero-order hold input to the plant, u. $\mathscr{C}_\kappa$ is the feedback stabilizing control law. An illustration of a simple sample-and-hold system is given in (4) and the response is shown in Fig. 4. where $\begin{bmatrix} x(0) & \tau(0) & z(0) \end{bmatrix} = \begin{bmatrix} 1 & 0 & 0 \end{bmatrix}$.

$$\left.\begin{aligned} \dot{x} &= -0.1\,x + u \\ \dot{\tau} &= 1 \\ \dot{z} &= 0 \end{aligned}\right\} \quad \tau \in [0,1]$$

$$\left.\begin{aligned} x^+ &= x \\ \tau^+ &= 0 \\ z^+ &= u = -0.4\,x \end{aligned}\right\} \quad \tau = 1 \tag{4}$$

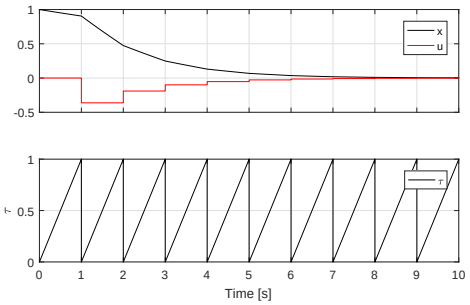

Figure 4: Response of hybrid dynamical sample-and-hold system.

It is seen that the timer state τ is reset when the timer reach the jump map $T_s = 1$, where the input $u = z$ is updated. Between jumps the continuous state evolution occurs in correspondence with the flow map. This method of modeling a sample-and-hold feedback control system is exploited, when modeling the digital displacement machine control system.

3.2 HYBRID FORMULATION OF A DDM

The displacement volume and its derivative of a single pressure chamber may be described by (5) [26, 27, 28].

$$\begin{aligned} V(\theta(t)) &= k_q\,(1 - \cos(\theta(t))) \\ \dot{V}(\theta(t)) &= k_q\,\omega(t)\,\sin(\theta(t)) \end{aligned} \tag{5}$$

where $k_q = \hat{V}/2$, $\omega = \dot{\theta}$ and $\hat{V}$ being the maximum displacement volume. In this study, it is valid to neglect the pressure dynamics during a single stroke as seen in Fig. 3, why the following approximation is valid $Q \approx \dot{V}$. The hybrid model for approximating the flow throughput of the DDM is derived based on the illustrations shown in Fig. 5.

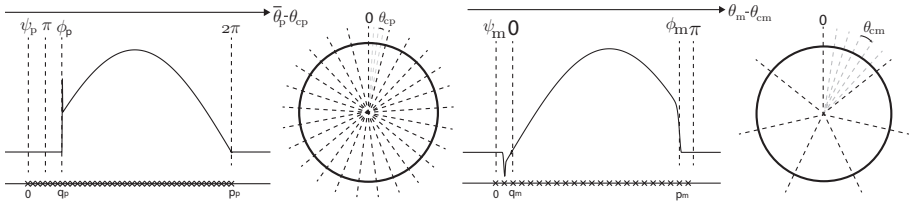

(a) Pump. $\theta_{cp} = 2\pi/N_p = 2\pi/100$ (b) Motor. $\theta_{cm} = 2\pi/N_m = 2\pi/42$

Figure 5: Definitions of angles used to derive the hybrid model.

θ_{cp} and θ_{cm} are the angle between each cylinder on the common shaft. ψ_p is the pump decision angle, where the decision to use a pumping or an idling stroke is made and ψ_m is the motor decision angle, where the decision to use a motoring or an idling stroke is made. ϕ_p indicates where the active part of the pump stroke is initialized and ϕ_m indicates where the active part of the motoring stroke ends. Since the derivation is very similar for the pump and motor, the hybrid approximation to the flow throughput is only derived for the motor in this paper. In a full stroke operation, the motor flow throughput may be described as

$$Q_{mH}(t) \approx \begin{cases} k_{qm}\,\omega_m(t)\,\sin(\theta_m(t)-\theta_{cm}) & if\ \ 0 < \theta_m(t)-\theta_{cm} \le \phi_m \\ 0 & else \end{cases} \tag{6}$$

If a decision of a motoring stroke is made, the active stroke part ends almost half a revolution later, where almost $N_m/2$ numbers of decisions for other cylinders has been made meanwhile. Therefore, a memory state for each input decision in the active part of the motoring stroke is necessary. Additionally, a memory state of the shaft angle θ_m where the sampling occurred is required to describe the flow throughput as function of the shaft angle. As a result an input decision and an angle sampling state vector is defined by

$$z_{mu} = \begin{bmatrix} z_{mu,0} & z_{mu,1} & \cdots & z_{mu,pm} \end{bmatrix}^T \quad z_{m\theta} = \begin{bmatrix} z_{m\theta,0} & z_{m\theta,1} & \cdots & z_{m\theta,pm} \end{bmatrix}^T \tag{7}$$

Since the motoring stroke starts at an angle of $\theta_m = 0$ and the decision angle ψ_m is located ahead of this, the shaft angle memory state is shifted by this delay angle and is defined as $z^+_{m\theta,i} = \theta_m - \psi_m$ The flow throughput of the machine can then be written by use of Fig. 5a and combining (6) and (7). The resulting motor flow model is given by

$$Q_m(t) = \sum_{i=1}^{N_m} Q_{mH,i}(t) \approx k_{qm}\,\omega_m(t) \sum_{i=q_m}^{p_m} \sin\left(\theta_m(t) - z_{m\theta,i}\right) z_{mu,i} \tag{8}$$

Similarly, it may be derived that the torque throughput can be described by

$$\tau_m(t) = \sum_{i=1}^{N_m} \tau_{cm,i}(t) \approx k_{\tau m}\,p_H(t) \sum_{i=q_m}^{p_m} \sin\left(\theta_m(t) - z_{m\theta,i}\right) z_{mu,i} \tag{9}$$

Where k_{qm} and $k_{\tau m}$ are the flow and torque coefficients. It is evident, that the precision of the model will suffer for a low number of cylinders, which will be elaborated on based on a verification of the presented hybrid model.

3.3 HYBRID DDM MODEL VALIDATION

A validation of the hybrid model is made by comparing the impulse response for the flow and torque of the hybrid model to that of the non-linear dynamical model shown in Fig. 3. To simplify the verification process the following sample and hold hybrid model has been used

$$\left.\begin{array}{r} \dot{\theta}_{\mathrm{m}} = \omega_{\mathrm{m}} \\ \dot{\chi}_{\mathrm{m}} = \omega_{\mathrm{m}} \\ \dot{z}_{\mathrm{mu,0}} = 0 \\ \dot{z}_{\mathrm{mu,i}} = 0 \;\; i = [1,..,p_{\mathrm{m}}] \\ \dot{z}_{m\theta} = 0 \\ \dot{z}_{m\theta,\mathrm{i}} = 0 \;\; i = [1,..,p_{\mathrm{m}}] \end{array}\right\} \quad \chi_{\mathrm{m}} \in [0, \theta_{\mathrm{cm}}] \quad \left.\begin{array}{l} \theta_{\mathrm{m}}^{+} = \theta_{\mathrm{m}} \\ \chi_{\mathrm{m}}^{+} = 0 \\ z_{\mathrm{mu,0}}^{+} = u_{\mathrm{m}} \\ z_{\mathrm{mu,i}}^{+} = z_{\mathrm{mu,i\text{-}1}} \;\; i = [1,..,p_{\mathrm{m}}] \\ z_{m\theta,0}^{+} = \theta_{\mathrm{m}} - \psi_{\mathrm{m}} \\ z_{m\theta,\mathrm{i}}^{+} = z_{m\theta,\mathrm{i\text{-}1}} \;\; i = [1,..,p_{\mathrm{m}}] \end{array}\right\} \quad \chi_{\mathrm{m}} = \theta_{\mathrm{cm}} \tag{10}$$

where $y = \begin{bmatrix} Q_{\mathrm{m}} & \tau_{\mathrm{m}} \end{bmatrix}^T$ are calculated by use of (8) and (9). It is evident that the sampling is triggered by the position instead of time as done in conventional sample-and-hold systems. In this validation example with constant rotation speed, the sampling time is constant and the conventional representation could might as well had been used. However, for a variable speed DDM the sampling time is no longer constant but sampling angle is. Therefore, this representation is made to also allow for modeling of speed variable machines.

A description of the sample-and-hold scheme is made below for clarification

- The triggering state reaches $\chi_{\mathrm{m}} = \theta_{\mathrm{cm}}$ and the jump map is triggered. In the jump map the triggering state is reset: $\chi_{\mathrm{m}}^{+} = 0$.
- A motor actuation decision is made, determine whether the current cylinder pressure chamber should be idling $z_{\mathrm{mu,0}}^{+} = 0$ or motoring $z_{\mathrm{mu,0}}^{+} = 1$.
- The previous actuation decisions are shifted a single place, such that the newest decisions states are available.
- The current decision angle θ_{m} is sampled, $z_{m\theta,0}^{+} = \theta_{\mathrm{m}} - \psi_{\mathrm{m}}$. Lastly, the previous decision angles are shifted a single place.

The resulting impulse responses are shown in Fig. 6a and Fig. 6b for the pump and motor respectively. The system has been simulated by use of the Matlab toolbox "Hybrid Equations Toolbox v2.04" by R. Sanfelice. The values of the various parameters used in the model is provided in Tab. 1.

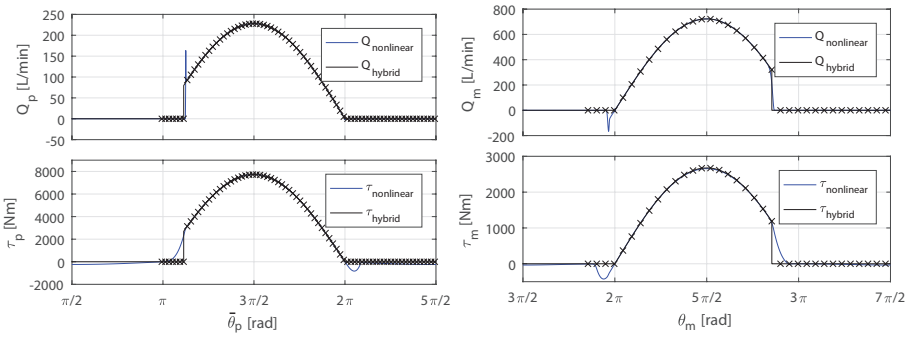

(a) Pump (b) Motor

Figure 6: Validation of hybrid flow and torque model of the DDM.

It is seen that there is a clear coherence between the non-linear model and the hybrid model. However, there are discrepancies at the end of the active stroke part due to valve and pressure dynamics. Since these differences are of relatively minor importance and are complex to model accurately, the hybrid formulation is accepted for system analysis and control development. As mentioned, the model accuracy will suffer for a low number of pressure chambers, since the discretization level will be poor. In that case, the model could be improved by including a different function than the proposed sinus function for the first and last sample of the active stroke part to increase the model precision.

3.4 Hybrid model for a DFPT

Developing a control oriented model for a digital fluid power transmission comprising both a digital displacement motor and pump is considered very problematic with conventional techniques. Considering the DLTI event-driven control strategy proposed by Pedersen et. al. [28] for speed varying digital displacement machines, it is not possible to extend the model to include two machines in a multi-rate sampling scheme, since the update rates are varying independently of each other. However, hybrid theory is able to overcome this problem by utilizing several jump maps.

A non-linear state equations for the continuous plant is given by (11) and is derived with basis in the definitions of variables shown in Fig. 1.

$$\underbrace{\begin{bmatrix} \dot{\theta}_\mathrm{m}(t) \\ \dot{\omega}_\mathrm{m}(t) \\ \dot{\bar{\theta}}_\mathrm{p}(t) \\ \dot{\omega}_\mathrm{p}(t) \\ \dot{p}_\mathrm{H}(t) \end{bmatrix}}_{\dot{x}} = \underbrace{\begin{bmatrix} \omega_\mathrm{m}(t) \\ -\frac{d_\mathrm{m}}{J_\mathrm{m}}\,\omega_\mathrm{m}(t) + \frac{1}{J_\mathrm{m}}\,\tau_\mathrm{m}(t) - \frac{1}{J_\mathrm{m}}\,\tau_\mathrm{L}(t) \\ \omega_\mathrm{p}(t)\,N_\mathrm{p,I} \\ -\frac{d_\mathrm{p}}{J_\mathrm{p}}\,\omega_\mathrm{p}(t) - \frac{1}{J_\mathrm{p}}\,\tau_\mathrm{p}(t) + \frac{1}{J_\mathrm{p}}\,\tau_\mathrm{I}(t) \\ -\frac{\beta}{V_\mathrm{H}}\,k_\mathrm{L}\,p_\mathrm{H}(t) + \frac{\beta}{V_\mathrm{H}}\,Q_\mathrm{p}(t) - \frac{\beta}{V_\mathrm{H}}\,Q_\mathrm{m}(t) \end{bmatrix}}_{f(x,\zeta)} \tag{11}$$

Where $\zeta = \left[Q_\mathrm{m}(t)\;\tau_\mathrm{m}(t)\;Q_\mathrm{p}(t)\;\tau_\mathrm{p}(t)\right]^T$. τ_i and τ_L represents the input torque to the pump shaft and the load torque to the motor respectively. J_p and J_m are the inertia masses, while d_p and d_m are the damping coefficient of the pump and motor shaft, respectively. β is the effective bulk modulus, V_H is the high pressure line volume and k_L is the leakage

coefficient. The hybrid sample-and-hold scheme for the flow map is given by

$$\left.\begin{aligned} \dot{x} &= f(x,\zeta) \\ \dot{\chi}_{\mathrm{m}} &= \omega_{\mathrm{m}} \\ \dot{z}_{\mathrm{mu}} &= 0 \\ \dot{z}_{m\theta} &= 0 \\ \dot{\chi}_{\mathrm{p}} &= \omega_{\mathrm{p}} N_{\mathrm{p,l}} \\ \dot{z}_{\mathrm{pu}} &= 0 \\ \dot{z}_{p\theta} &= 0 \end{aligned}\right\} \quad \begin{matrix} \chi_{\mathrm{m}} \in [0, \theta_{\mathrm{cm}}] \\ \chi_{\mathrm{p}} \in \left[0, \theta_{\mathrm{cp}}\right] \end{matrix} \wedge \tag{12}$$

When both triggering states are below their threshold angle, the flow map is used and when one of them reaches the triggering value a control update is initiated by entering the respective jump map given by

$$\left.\begin{aligned} x^{+} &= x \\ \chi_{\mathrm{m}}^{+} &= 0 \\ z_{\mathrm{mu,0}}^{+} &= u_{\mathrm{m}} \\ z_{\mathrm{mu,i}}^{+} &= z_{\mathrm{mu,i\text{-}1}} \;\; i = [1,..,p_{\mathrm{m}}] \\ z_{m\theta,0}^{+} &= \theta_{\mathrm{m}} - \psi_{\mathrm{m}} \\ z_{m\theta,\mathrm{i}}^{+} &= z_{m\theta,\mathrm{i\text{-}1}} \;\; i = [1,..,p_{\mathrm{m}}] \\ \chi_{\mathrm{p}}^{+} &= \chi_{\mathrm{p}} \\ z_{\mathrm{pu}}^{+} &= z_{\mathrm{pu}} \\ z_{p\theta}^{+} &= z_{p\theta} \end{aligned}\right\} \quad \begin{matrix} \chi_{\mathrm{m}} = \theta_{\mathrm{cm}} \\ \chi_{\mathrm{p}} \in \left[0, \theta_{\mathrm{cp}}\right] \end{matrix} \wedge \quad \left.\begin{aligned} x^{+} &= x \\ \chi_{\mathrm{m}}^{+} &= \chi_{\mathrm{m}} \\ z_{\mathrm{mu}}^{+} &= z_{\mathrm{mu}} \\ z_{m\theta}^{+} &= z_{m\theta} \\ \chi_{\mathrm{p}}^{+} &= 0 \\ z_{\mathrm{pu,0}}^{+} &= u_{\mathrm{p}} \\ z_{\mathrm{pu,i}}^{+} &= z_{\mathrm{pu,i\text{-}1}} \;\; i = \left[1,..,p_{\mathrm{p}}\right] \\ z_{p\theta,0}^{+} &= \bar{\theta}_{\mathrm{p}} - \left(\pi - \psi_{\mathrm{p}}\right) \\ z_{p\theta,\mathrm{i}}^{+} &= z_{p\theta,\mathrm{i\text{-}1}} \;\; i = \left[1,..,p_{\mathrm{p}}\right] \end{aligned}\right\} \quad \begin{matrix} \chi_{\mathrm{m}} \in [0, \theta_{\mathrm{cm}}] \\ \chi_{\mathrm{p}} = \theta_{\mathrm{cp}} \end{matrix} \wedge \tag{13}$$

Based on (8) the flow throughput of the machines may be approximated by

$$\begin{aligned} Q_{\mathrm{m}}(t) &= k_{\mathrm{qm}}\, \omega_{\mathrm{m}}(t) \sum_{i=q_{\mathrm{m}}}^{p_{\mathrm{m}}} \sin\left(\theta_{\mathrm{m}}(t) - z_{m\theta,i}\right) z_{mu,i} \\ Q_{\mathrm{p}}(t) &= k_{\mathrm{qp}}\, N_{\mathrm{p,l}}\, \omega_{\mathrm{p}}(t) \sum_{i=q_{\mathrm{p}}}^{p_{\mathrm{p}}} \sin\left(\bar{\theta}_{\mathrm{p}}(t) - z_{p\theta,i}\right) z_{pu,i} \end{aligned} \tag{14}$$

Similarly based on (9), it may be derived that the torque throughput can be described by

$$\begin{aligned} \tau_{\mathrm{m}}(t) &= k_{m\tau}\, p(t) \sum_{i=q_{\mathrm{m}}}^{p_{\mathrm{m}}} \sin\left(\theta_{\mathrm{m}}(t) - z_{m\theta,i}\right) z_{mu,i} \\ \tau_{\mathrm{p}}(t) &= k_{p\tau}\, N_{\mathrm{p,l}}\, p(t) \sum_{i=q_{\mathrm{p}}}^{p_{\mathrm{p}}} \sin\left(\bar{\theta}_{\mathrm{p}}(t) - z_{p\theta,i}\right) z_{pu,i} \end{aligned} \tag{15}$$

Hereby a dynamic hybrid system model of a digital fluid power transmission comprising two digital displacement machines is developed and may be used for dynamic analysis and feedback control development.

3.5 HYBRID DFPT MODEL VALIDATION

To verify the proposed hybrid formulation of the DFPT, a simulation of the model is made and the results are compared to those obtained by simulation of the non-linear model representing the physical transmission. The equations for the non-linear model are available

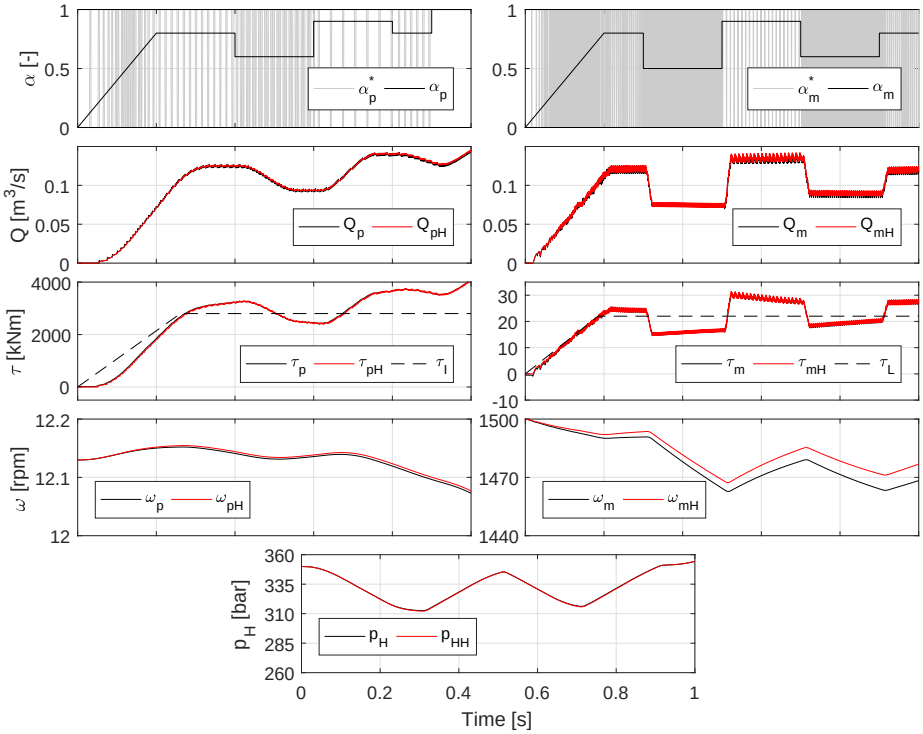

Figure 7: Results for validation of the hybrid DFPT model. Black lines represents the non-linear physical model and red lines represents the hybrid model.

in [26, 28], and the results for a single stroke of the pump and motor has already been shown in Fig. 3. In the validation, both models are given the same inputs (α_p, α_m, τ_I, τ_L). The displacement fractions α_p and α_m are converted to Pulse Width Modulated (PWM) signals α_p^* and α_m^* by a first order discrete Delta-Sigma-Modulator (DSM) [33] describing the cylinder chamber actuation sequence. The results are shown in Fig. 7, where it should be noted that only the generated PWM signals for the non-linear model are shown for clarity. The results are seen to have a great correspondence, which may be expected based on the validation of a single stroke shown in Fig. 6. The only easily identified difference is seen in the motor velocity response where drifting between the two responses is observed, which is due to the low motor inertia mass and damping combined with the minor discrepancy in the motor torque response. Overall, all the relevant system dynamics is captured with the hybrid model, which verifies its applicability with respect to system analysis and feedback control development.

4 CONCLUSION

To enhance the development of feedback stabilizing controllers for hydraulic digital displacement machines, a hybrid dynamical control oriented model of the system dynamics has been derived and verified. The presented digital displacement machine hybrid model avoids the previous model approximations by linearization, allowing for the possibility of an increased performance and enlarged region of stability. Hybrid system theory has

also been proven to be able to describe the dynamics of a digital fluid power transmission system with multiple speed varying digital displacement machines, which is not possible with classical discrete or continuous methods. The next step is thus to design globally asymptotically stable feedback controllers based on well established tools within hybrid dynamical system theory.

5 APPENDIX

Table 1: Parameters values used in the model

Parameter	symbol	value	Unit	Parameter	symbol	value	Unit
Pump lobes in 1 module	$N_{\mathrm{p,l}}$	16	-	Pump flow constant	k_{qp}	249.3	cm^3
Pump cylinders in 1 module	$N_{\mathrm{p,c}}$	25	-	Pump torque constant	$k_{\tau p}$	249.3	cm^3
Number of pump modules	$N_{\mathrm{p,m}}$	4	-	Motor flow constant	k_{qm}	77	cm^3
Motor cylinders in 1 module	$N_{\mathrm{m,c}}$	7	-	Motor torque constant	$k_{\tau m}$	77	cm^3
Number of motor modules	$N_{\mathrm{m,m}}$	6	-	Pump damping coefficient	d_{p}	50e3	$N\,m\,s/rad$
Number of pump cylinders	N_{p}	100	-	Pump inertia mass	J_{p}	38.76e4	$kg\,m^2$
Number of motor cylinders	N_{m}	42	-	Motor damping coefficient	d_{m}	10	$N\,m\,s/rad$
Pump decision angle	ψ_{p}	178.8	deg	Motor inertia mass	J_{m}	534.2	$kg\,m^2$
Pump stroke angle	ϕ_{p}	18.2	deg	Effective bulk modulus	β	16000	bar
Motor decision angle	ψ_{p}	26.3	deg	High pressure line volume	V_{H}	3.92	m^3
Motor stroke angle	ϕ_{p}	161.8	deg				

6 ACKNOWLEDGMENT

This research was funded by the Danish Council for Strategic Research through the HyDrive project at Aalborg University, at the Department of Energy Technology (case no. 1305-00038B).

References

[1] W. Rampen, "Gearless transmissions for large wind turbines - the history and future of hydraulic drives," Artemis IP Ltd., Scotland.

[2] P. Silva, A. Giuffrida, and N. F. et. al., "Performance prediction of a multi-mw wind turbine adopting an advanced hydrostatic transmission," *Energy, Vol. 64, pp. 450 - 461*, December 2013.

[3] M. Linjama, "Digital fluid power state of the art," *The Twelfth Scandinavian International Conference on Fluid Power, May 18-20, Tampere, Finland*, 2011.

[4] G. S. Payne, U. P. P. Stein, M. Ehsan, N. J. Caldwell, and W. H. S. Rampen, "Potential of digital displacement hydraulics for wave energy conversion," *In Proc. of the 6th European Wave and TIdal Energy Conference, Glasgow UK.*, 2005.

[5] W. R. M. Ehsan and S. Salter, "Modeling of digital-displacement pump-motors and their application as hydraulic drives for nonuniform loads," *ASME, Journal of dynamic system measurement and control, Vol. 122, pp. 210-215*, March 2000.

[6] W. Rampen, "The development of digital displacement technology," *In Proceedings of Bath/ASME FPMC Symposium*, 2010.

[7] P. Johansen, *Tribodynamic Modeling of Digital Fluid Power Motors*. PhD thesis, Department of Energy Technology, Aalborg University, 2014.

[8] D. B. Roemer, *Design and Optimization of Fast Switching Valves for Large Scale Digital Hydraulic Motors*. PhD thesis, 2014. Department of Energy Technology, Aalborg University.

[9] G. Wilfong, M. Batdorff, and J. Lumkes, "Design and dynamic analysis of high speed on/off poppet valves for digital pump/motors," *In Proceedings of the 6th FPNI-PhD Symposium*, 2010.

[10] G. Wilfong, M. Holland, and J. Lumkes, "Design and analysis of pilot operated high speed on/off valves for digital pump/motors," *In Proceedings of the 52nd National Conference on Fluid Power*, 2011.

[11] K. Merrill, M. Holland, and J. Lumkes, "Analysis of digital pump/motor operating strategies," *Proceedings of the 52nd National Conference on Fluid Power*, 2011.

[12] T. Chen and B. Francis, *Optimal Sampled-Data Control Systems*. Springer, 1995.

[13] D. Nesic and L. Grune, "Lyapunov-based continuous-time nonlinear controller redesign for sampled-data implementation," *Automatica, Vol. 14, Issur 7*, 2005.

[14] D. Nesic and A. Teel, "A framework for stabilization of nonlinear sampled-data systems based on their approximate discrete-time models," *IEEE TRANSACTIONS ON AUTOMATIC CONTROL, VOL. 49, NO. 7,*, 2004.

[15] J. H. Sandee, W. P. M. H. Heemels, and S. B. F. Hulsenboom, "Analysis and experimental validation of a sensor-based event-driven controller,"

[16] J. H. Sandee, W. P. M. H. Heemels, and S. B. F. Hulsenboom, "Analysis and experimental validation of a sensor-based event-driven controller," *Proceedings of the 2007 American Control Conference*, 2007.

[17] W. P. M. H. Hellems, R. J. A. Gorter, A. van Zijl, P. B. J. vand den Bosch, S. Weiland, W. H. A. Hendrix, and M. R. vonder, "Asynchronous measurement and control: a case study on motor synchronization," *Control Engineering Practice 7, 1467-1482*, 1999.

[18] P. Tabuada, "Event-triggered real-time scheduling of stabilizing control tasks," *IEEE Transactions on Automatic Control (Volume: 52, Issue: 9)*, 2007.

[19] A. Seuret, "Stability of non-linear systems by means of event-triggered sampling algorithms,"

[20] M. Heikkila and M. Linjama, "Displacement control of a mobile crane using digital hydraulic power management system," *Mechatronics 23(4), pp. 452 - 461*, 2013.

[21] X. Song, "Modeling an active vehicle suspension system with application of digital displacement pump motor," *Proceedings of the ASME 2008 International Design Engineering Techical Conference/Computers and Information in Enegineering Conference, Brooklyn - New York, Vol. 5, pp. 749-753*, 2008.

[22] B. S. R. Armstrong and Q. Yuan, "Multi-level control of hydraulic gerotor motor and pumps," *Proceedings of the 2006 American Control Conference, Minneapolis, Minnesota, USA*, June 2006. Proceedings of the 2006 American Control Conference Minneapolis, Minnesota.

[23] K. U. Snieguckl M, Gottfried M, "Optimal control of digital hydraulic drives using mixed-integer quadratic programming," September 2013. 9th IFAC Symposium on Nonlinear Control System, Toulouse.

[24] P. Johansen, D. B. Roemer, H. C. Pedersen, and T. O. Andersen, "Delta-sigma modulated displacement of a digital fluid power pump," *In Proceedings of the 7th Workshop on Digital Fluid Power*, February 2015 2015. The Seventh Workshop on Digital Fluid Power, Linz, Austria.

[25] P. Johansen, D. B. Roemer, H. C. Pedersen, and T. O. Andersen, "Discrete linear time invariant analysis of digital fluid power pump flow control," *Journal of dynamic system measurement and control, ASME, accepted for publication*, 2016.

[26] P. J. Niels H. Pedersen and T. O. Andersen, "Lqr feedback control development for wind turbines featuring a digital fluid power transmission system," 2016.

[27] P. J. Niels H. Pedersen and T. O. Andersen, "Optimal control development of a wind turbine featuring a digital fluid power transmission," 2016.

[28] N. H. Pedersen, P. Johansen, and T. O. Andersen, "Event-driven control of a speed varying digital displacement machine," *Proceedings of ASME/BATH FPMC Symposium on Fluid Power and Motion Control, Sarasota, Florida, USA*, 2017.

[29] R. Goebel, R. G. Sanfelice, and A. R. Teel, "Hybrid dynamical systems," *IEEE control systems magazine*, 2009.

[30] A. R. Teel, R. G. Sanfelice, and R. Goebel, "Hybrid control systems," 2009.

[31] R. G. Sanfelice and A. R. Teel, "Lyapunov analysis of sample-and-hold hybrid feedbacks," 2005+.

[32] R. Goebel, R. G. Sanfelice, and A. R. Teel, "Hybrid dynamical systems," *IEEE control systems magazine*, 2009.

[33] J. D. Reiss, "Understanding sigma-delta modulation: The solved and unsolved issues," *Journal Audio Engineering Society, Vol. 56, No. 1/2*, 2008.

Paper K

Four Qudrant Hybrid Control Oriented Dynamical System Model of Digital Displacement Units

Niels H. Pedersen, Per Johansen and Torben O. Andersen

The paper has been published in
Proceedings of the Bath/ASME Symposium on Fluid Power and Motion Control,
Bath, UK, 2018.

The layout has been revised.

Proceedings of the 2018 Bath/ASME Symposium on Fluid Power and Motion Control
FPMC2018
September 12-14, 2018, Bath, United Kingdom

FPMC2018-8874

FOUR QUADRANT HYBRID CONTROL ORIENTED DYNAMICAL SYSTEM MODEL OF DIGITAL DISPLACEMENT® UNITS

Niels H. Pedersen
Fluid Power and Mechatronic Systems
Department of Energy Technology
Aalborg University
9220 Aalborg East, Denmark
Email: nhp@et.aau.dk

Per Johansen
Torben O. Andersen
Fluid Power and Mechatronic Systems
Department of Energy Technology
Aalborg University
9220 Aalborg East, Denmark
Email: pjo@et.aau.dk; toa@et.aau.dk

ABSTRACT

Proper feedback control of dynamical systems requires models that enables stability analysis, from where control laws may be established. Development of control oriented models for digital displacement (DD) fluid power units is complicated by the non-smooth behavior, which is considered the core reason for the greatly simplified state of the art control strategies for these machines. The DD unit comprises numerous pressure chambers in a modular construction, such that the power throughput is determined by the sequence of activated pressure chambers. The dynamics of each pressure chamber is governed by non-linear differential equations, while the binary input (active or inactive) is updated discretely as function of the shaft angle. Simple dynamical approximations based on continuous or discrete system theory is often inaccurate and is not applicable for such system when it is to operate in all four quadrants. Therefore, a method of applying hybrid dynamical system theory, comprising both continuous and discrete elements is proposed in this paper. The paper presents a physical oriented hybrid model accurately describing the machine dynamics. Since development of stabilizing control laws for hybrid dynamical systems is a complicated task, a simpler hybrid model only including the fundamental machine characteristics is beneficial. Therefore, a discussion and several proposals are made on how a simpler DD hybrid model may be established and used for feedback control development.

1 INTRODUCTION

In recent years, research and development of energy efficient fluid power solutions for both conventional cylinder drives [1, 2] and power take-off systems [3–9] has gained an increasing amount of attention. Digital fluid power is a promising technology, since it has the potential to become the future solution for energy efficient hydraulic systems. The digital displacement machine (DDM) is an emerging technology for energy efficient fluid power pump-motor units, which comprises of numerous independently controlled cylinder pressure chambers. Each pressure chamber is flow controlled by two fast switching on/off valves, connecting the chamber with the high and low pressure manifold. Contrary to conventional fluid power the digital displacement technology yields a non-smooth output based on the ratio of activated pressure chambers. Detailed read regarding the digital displacement technology may be found in several publications [6, 10–15]. Due to the digital nature of the machine, the output is quantized by the ratio of activated pressure chambers and can therefore not be altered continuous. Instead the activation sequence depends on the shaft angle, which for a DD machine operating in both direction of motions results in an asynchronous input activation sequence in both the time and angle domain.

Proper control of digital displacement units is considered a core challenge to be solved for successfully deployment of the technology. However, dynamical feedback control of such non-smooth system, where non-linear continuous dynamics is bi-

nary activated in discrete time/angle varying steps is considered a challenging task [16]. The complicated control task may explain why current state of the art control strategies often neglect the transient behavior. Additionally, the strategies are often limited to an open loop control configuration, where the machine is operated at fixed speed in a greatly simplified load system. Both pulse-density modulation and pulse-width modulation methods has been used to determine the actuation sequence for the pressure chambers [17, 18], similar to control of digital electronics. Control strategies involving a pre-determined actuation sequence through optimization as function of the shaft angle and displacement reference has also been considered [18–21]. A limited amount of control strategies based on dynamical control models has been published. Pedersen et. al [22] presents a continuous approximation of the non-smooth dynamics which is only valid if the number of cylinders and displacement fractions are relatively high, while the excitation frequencies must be relatively low. Johansen et. al. [23] proposes a discrete linear approximation for a fixed speed machine, by considering the committed displacement fraction between samples. The discrete method has been extended to include variable speed operation in [24]. The discrete methods are limited to operation in one direction of motion in either pump or motoring mode and are increasingly inaccurate for a lower number of cylinders. Additionally, for both the continuous and discrete approximations, the use of linear control theory for a highly non-linear system limits the valid operation range.

Since the dynamics of the digital machine comprises both continuous and discrete elements, it belongs to the class of hybrid dynamical systems. To cope with the non-smooth dynamics, Pedersen et. al. [25] proposes a hybrid control oriented model for a full stroke operated digital displacement machine. The model does however only include the fundamental dynamical behavior of the machine and is limited to full stroke operation in either pumping or motoring mode in one direction of motion. Since several fluid power applications (vehicle transmissions, winch drives, ect.) requires operation in all four quadrants (pumping and motoring in both direction of motion), it is considered important to be able ensure stability for such system through control. Neither continuous or discrete approximation methods are considered viable in describing the digital displacement machine dynamics when operating in all four quadrants, due to the discrete sampling effect being input dependent and asynchronous in both the time or the angle domain.

In this paper, a four-quadrant hybrid control oriented model describing the non-smooth dynamics of the digital displacement machine accurately is presented. The model equations and results greatly resembles various experimental validated models of the digital displacement machine [26–30]. The hybrid dynamical model is hence valid independent of how the machine is operated and allows for development of stabilizing feedback control laws. However, although control theory for hybrid system does exist [31–33], control of such systems is considered a complex task even for relatively simple systems. Therefore, this paper discusses and suggest several approaches with respect to establishing a simpler DD hybrid model which only describes the fundamental machine dynamics and thereby simplifies the control task.

2 SYSTEM DESCRIPTION AND MODEL

To set up a mathematical model describing the non-smooth dynamics of the digital displacement machine an illustration of the DD unit under consideration is shown in Fig. 1.

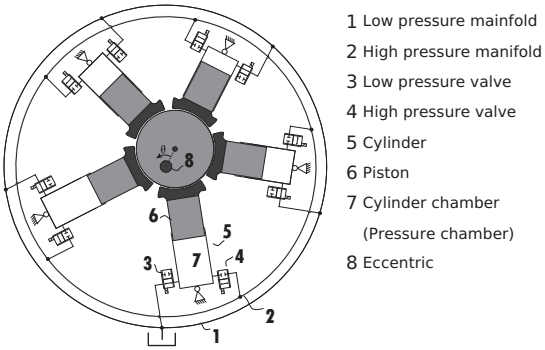

FIGURE 1. Sketch of the radial five piston digital displacement machine under consideration.

The digital displacement machine is seen to comprise 5 radially distributed cylinders connected to an eccentric shaft. Each of these cylinders has a high and a low pressure valve connected to its pressure chamber for controlling the flow to and from the high and low pressure manifold respectively. The eccentric shaft results in a reciprocating piston motion yielding the ability to motor during piston extension and pump during piston contraction. A description of the working principle of a single pressure chamber is based on the illustration shown in Fig. 2, where variables used to set up the mathematical model is defined. It is seen that the high pressure valve (HPV) is of type normally closed and the low pressure valve (LPV) is of type normally open, such that the chamber is passively held in an idling mode at low pressure. The piston stroke length as function of the shaft angle is given by Eq. (1) for the respective cylinders.

$$x_{\mathrm{i}} = r_{\mathrm{e}}\left(1-\cos(\theta_{\mathrm{i}})\right) \quad \theta_{\mathrm{i}} = \theta + \frac{2\pi}{N}(i-1) \quad i \in \{1,..,N\} \quad (1)$$

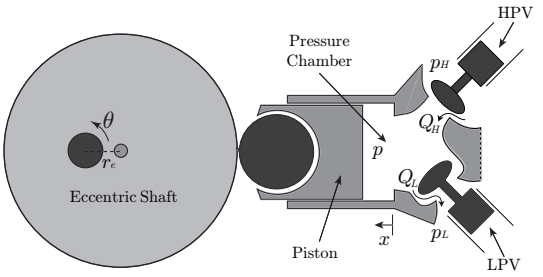

FIGURE 2. Sketch of a pressure chamber of the digital displacement machine used for modeling.

where $N = 5$ is the number of cylinders and r_e is the eccentric radius corresponding to half of the maximum stroke length. The cylinder chamber volume, V is described by

$$\begin{aligned} V_i &= \frac{V_d}{2}\left(1-\cos(\theta_i)\right)+V_0 \\ \dot{V}_i &= \frac{V_d}{2}\sin(\theta_i)\,\dot{\theta} \end{aligned} \tag{2}$$

where the displacement and dead volume are given by $V_d = V_0 = 2\,r_e\,A_p$ and A_p is the piston area. The continuity equation is used to describe the pressure dynamics and is given by

$$\dot{p}_i = \frac{\beta_e}{V_i}\left(Q_{H,i} - Q_{L,i} - \dot{V}_i\right) \tag{3}$$

where β_e is the effective oil bulk modulus and Q_H and Q_L are the flows through the high and low pressure valve respectively. The orifice equation is used to describe the valve flows and results in

$$\begin{aligned} Q_{L,i} &= \frac{\bar{x}_{L,i}}{k_f}\sqrt{|p_i - p_L|}\,\mathrm{sign}\left(p_i - p_L\right) \\ Q_{H,i} &= \frac{\bar{x}_{H,i}}{k_f}\sqrt{|p_H - p_i|}\,\mathrm{sign}\left(p_H - p_i\right) \end{aligned} \tag{4}$$

where $\bar{x}_L$ and $\bar{x}_H$ are normalized valve plunger positions and k_f is the valve flow coefficient. The torque contribution to the eccentric shaft is given by

$$\tau_i = \frac{dV(\theta_i)}{d\theta_i}\,p_i = \frac{V_d}{2}\sin(\theta_i)\,p_i \tag{5}$$

The parameters used for the non-linear simulation model is provided in Tab. 1. However, the value of these parameters does not affect the applicability of the presented hybrid model.

TABLE 1. Parameters of the digital displacement machine

Parameter	symbol	value	Unit
Piston area	A_p	31	cm^2
Piston displacement	r_e	25	mm
Chamber flow coefficient	k_f	$1\cdot10^6$	$\sqrt{pa}\,s/m^3$
Low pressure	p_L	10	bar
Effective Bulk modulus	β_e	16000	bar

The above presented differential equations are seen to all be continuous, however the digital valves may either be open or closed resulting in a non-smooth dynamical behavior, where the output cannot be altered continuously. This dynamical behavior is illustrated by the pressure trajectories as function of the shaft angle in a polar phase plot shown in Fig. 3.

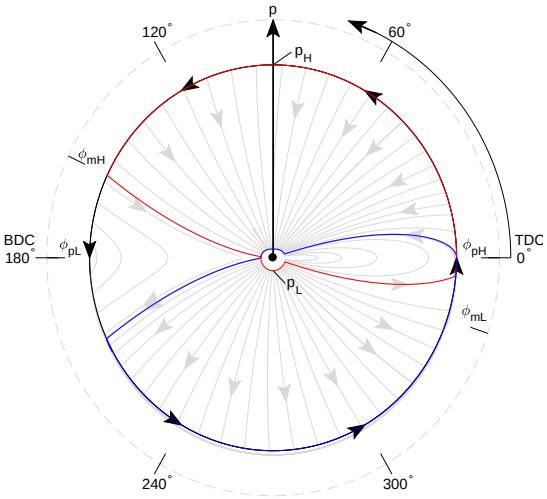

FIGURE 3. Phase portrait of the pressure dynamics as function of the angle. Red trajectory illustrates a full motoring stroke and blue trajectory illustrates a full pumping stroke.

During the down-stroke, $\theta = [0;\pi]$, the high pressure valve (HPV) is initially open and the pressure is equal to the high pressure $p = p_H$. The pressure trajectories are obtained by closing the HPV at varying shaft angles, which results in a de-pressurization. As the pressure goes below the low pressure, $p < p_L$, the low pressure valve (LPV) is passively opened by the pressure force. During up-stroke, $\theta = [\pi;2\pi]$, the LPV is initially open and the

pressure is equal to the low pressure, $p = p_{\mathrm{L}}$. By closing the LPV at varying shaft angles pressurization is seen by the pressure trajectories. When the pressure exceeds the high pressure, $p > p_{\mathrm{H}}$, the HPV is passively opened due to pressure force. The angles ϕ_{mL}, ϕ_{mH} are the angles where a full motoring stroke is initiated by closing the LPV and ended by closing the HPV respectively. Similarly, the angles ϕ_{pL}, and ϕ_{pH} are the angles where a full pumping stroke is initiated by closing the LPV and ended by closing the HPV respectively. A partial stroke is hence obtained by closing the HPV at an earlier angle during the motoring stroke and by closing the LPV at a later angle during the pumping stroke.

It is clear, that the discrete behavior is caused both actively through inputs by closing the valves and passively through state values of the pressure when valves are opened. Hence the discrete effects are both input and state depended. Additionally, the machine may comprise of a high number of cylinders and may therefore be considered a rather complex hybrid system.

3 HYBRID DYNAMICAL SYSTEM THEORY

Hybrid dynamical systems (HDS) are used to describe the dynamics of systems comprising both continuous and discrete elements and may be used for stability analysis, sensitivity analysis and development of stabilizing control algorithms. The investigation of the DD machine dynamics revealed that the pressure dynamics for each chamber is described by non-linear continuous differential equations, while the opening and closing of valves are made discretely. The class of HDS comprises several sub-classes with different structures, which describes the non-smooth interactions differently. The established control methods that are applied to these sub-classes are often different and the chosen modeling and control strategy is often dependent on the type of switching phenomena. Mention-worth classes are switched systems, impulsive systems and hybrid automatons, but all of them may be described through a general notation [31, 32].

A HDS comprises both continuous differential (flow) equations and discrete difference (jump) equations and is in general formulated as that given by

$$\mathcal{H}: \quad \begin{cases} \dot{x} & \in F(x,u), & x \in C, \\ x^{+} & \in G(x,u), & x \in D \\ y & = h(x,u) \end{cases} \tag{6}$$

where $\dot{x}$ is the state time derivative and x^{+} is the state value after a jump. u and y are the system input and output respectively. For simplicity, a HDS is written as $\mathcal{H} = (F, C, G, D, h)$, where the variables describes the following

- The flow set: C
- The flow map: F
- The jump set: D
- The jump map: G
- The output map: h

As long as x belongs to the flow set, C, it is described by the differential inclusion given by the flow map, F and when x belongs to the jump set, D, it is described by the difference inclusion given by the jump map G.

3.1 Single chamber hybrid model

With respect to model based control design it is desired that the model captures all the relevant dynamics, while being as simple as possible. This often leads to omitting the fast dynamics, since these occurs almost instantaneously with respect to the dynamics to be controlled, e.g. neglect the actuator dynamics. Since control theory for hybrid dynamical systems is a complex mathematical task, it is considered crucible with respect to successfully developing stability control laws, that the hybrid model is as simple as possible, while it maintains the important dynamics.

Initially, a rather complex and accurate HDS model is proposed, which include the valve actuation dynamics. Combining the presented continuous dynamical equations for a pressure chamber results in the flow map and set given by Eq. (7).

$$\left.\begin{aligned} \dot{\theta} &= \omega \\ \dot{p} &= \frac{\beta_{\mathrm{e}}}{V}\left(Q_{\mathrm{H}} - Q_{\mathrm{L}} - \dot{V}\right) \\ V &= \frac{V_{\mathrm{d}}}{2}\left(1 - \cos(\theta)\right) + V_0 \\ \dot{V} &= \frac{V_{\mathrm{d}}}{2}\sin(\theta)\,\omega \\ Q_{\mathrm{L}} &= \frac{x_{\mathrm{L}}}{k_{\mathrm{f}}}\sqrt{|p - p_{\mathrm{L}}|}\,\mathrm{sign}\left(p_{\mathrm{i}} - p_{\mathrm{L}}\right) \\ Q_{\mathrm{H}} &= \frac{x_{\mathrm{H}}}{k_{\mathrm{f}}}\sqrt{|p_{\mathrm{H}} - p|}\,\mathrm{sign}\left(p_{\mathrm{H}} - p\right) \\ \dot{x}_{\mathrm{L}} &= \frac{1}{\tau_{\mathrm{v}}}\left(u_{\mathrm{L}} - x_{\mathrm{L}}\right) \\ \dot{x}_{\mathrm{H}} &= \frac{1}{\tau_{\mathrm{v}}}\left(u_{\mathrm{H}} - x_{\mathrm{H}}\right) \\ \dot{u}_{\mathrm{L}} &= 0 \\ \dot{u}_{\mathrm{H}} &= 0 \\ \dot{q} &= 0 \end{aligned}\right\} \quad (x,u) \in \mathbb{R} \setminus D \tag{7}$$

It is seen that the state evolvement is described by the flow map, as long as the states and inputs does not belong to the jump set. The valve dynamics is modeled as a first order system with time constant τ_{v}. The inputs, u_{H} and u_{L}, to the valves are seen to be constant when the system dynamics is governed by the flow map and it may hence only be updated during jumps. Even though the valve model is relatively simple, the model resembles the

$$
\left.\begin{array}{l}\theta^+ = \theta \\ p^+ = p \\ x_{\mathrm{L}}^+ = x_{\mathrm{L}} \\ x_{\mathrm{H}}^+ = x_{\mathrm{H}}\end{array}\right\} \quad (x,u) \in D \qquad D = d_1 \cup d_2 \cup d_3 \cup d_4
$$

$$
\left.\begin{array}{l}u_{\mathrm{H}}^+ = 0 \\ u_{\mathrm{L}}^+ = 1 \\ q^+ = 1\end{array}\right\} \quad (x,u) \in d_4, q = 2
$$

$$
\left.\begin{array}{l}u_{\mathrm{H}}^+ = 0 \\ u_{\mathrm{L}}^+ = 0 \\ q^+ = 2\end{array}\right\} \quad ((x,u) \in d_1, q = 1) \vee ((x,u) \in d_3, q = 3)
$$

$$
\left.\begin{array}{l}u_{\mathrm{H}}^+ = 0 \\ u_{\mathrm{L}}^+ = 1 \\ q^+ = 3\end{array}\right\} \quad (x,u) \in d_2, q = 2 \tag{8}
$$

physical dynamics quite well. The state, q, is introduces to describe which mode the chamber is in (idling, compression or pressurization). The valve actuation dynamics is described by considering the hybrid automaton shown in Fig. 4. Two mode switching functions are defined as $\lambda_{\mathrm{H}} = F_{\mathrm{H}} - (p_{\mathrm{H}} - p)A_{\mathrm{v}}$ and $\lambda_{\mathrm{L}} = F_{\mathrm{L}} - (p - p_{\mathrm{L}})A_{\mathrm{v}}$ and are used to construct the jump maps. The system input is hence the valve forces, $u = \begin{bmatrix} F_{\mathrm{H}} & F_{\mathrm{L}} \end{bmatrix}^T$ for the high and low pressure valve respectively, while A_{v} is the effective valve area that the pressure is generating a force on.

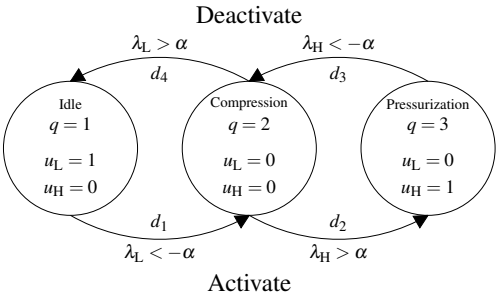

FIGURE 4. Hybrid Automaton representation of valve control of the digital displacement machine.

It is seen there are 3 modes the pressure chamber may operate in, idling, compression and pressurization. A chamber is activated by closing the LPV with a negative actuation force F_{L} that is lower than $-\alpha$ illustrating a spring force tending to open the valve. This results in a compression state and when the pressure force exceeds the spring equivalent force, the HPV is passively opened. Similarly, the chamber is deactivated by closing the HPV by an actuation force F_{H} and when the pressure force decreases below the spring force, the LPV is passively opened. From the hybrid automaton illustration, the jump map and set is described by Eq. (8). The shaft angle, θ, chamber pressure, p and valve plunger position, x_{H}, and x_{L} cannot change instantaneously and thus remains unchanged during jumps. The three remaining sub jump domains is directly obtained by considering the hybrid automaton in Fig. 4. In this study example, the valve parameters in Tab. 2 are used.

TABLE 2. Parameters of the digital on/off valves

Parameter	symbol	value	Unit
Valve time constant	τ_{v}	2	ms
Valve effective area	A_{v}	31.66	mm^2
Force threshold	α	50	N

With these parameter values, it requires a force impulse larger than 50 N to open/close a valve at zero pressure difference and a force of 1000 N to open/close a valve at maximum pressure difference of 300 bar. Since small and fast valves are considered, the maximum actuation force is limited to 60 N, such that it is only possible to open/close the valves at low pressure difference.

4 SIMULATION RESULTS

To validate the hybrid dynamical model, a simulation has been made where a sequence of all possible combinations of motoring, idling and pumping full strokes are conducted. The simulations are made in the Hybrid Equation (HyEQ) Matlab toolbox and the results are shown in Fig. 5. The full strokes are conducted by applying force pulses to the valves are specific angles, resulting in the desired full stroke operation.

It is seen that a pumping stroke is made in section 2, by closing the LPV near ahead of bottom dead center (BDC) resulting in a passive opening of the HPV due to the chamber pressure exceeding the high pressure as the chamber is compressed. Similarly, a motoring stroke is conducted in section 5, by closing the LPV near ahead of top dead center (TDC), resulting in a passive

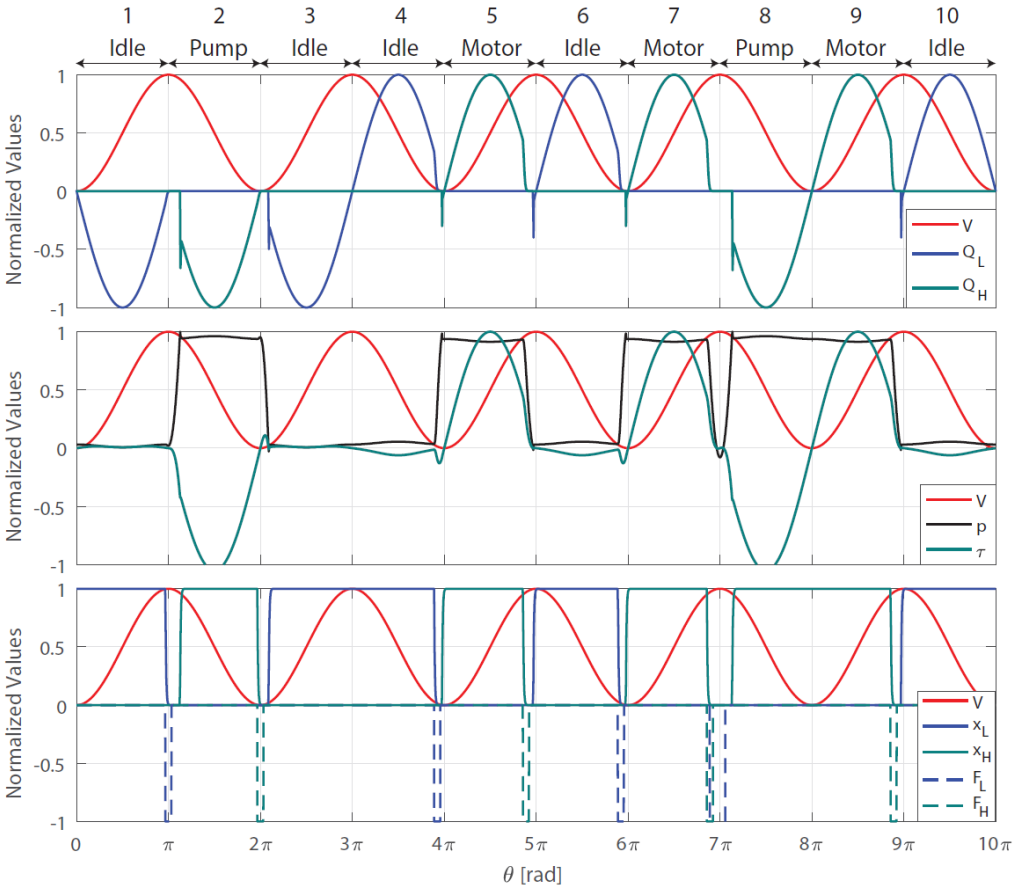

FIGURE 5. Simulation of a pumping, idling and motoring strokes of the digital displacement machine. $\dot{\theta} = 100\,\text{rpm}$, $p_\text{H} = 300\,\text{bar}$ and $p_\text{L} = 10\,\text{bar}$

opening of the HPV due to pressure force.

The main advantage of the presented hybrid model is the physical accuracy of it. The model describes the dynamics of the system independent on how the machine is operated (Full stroke, partial stroke, motoring, pumping, idling and in both direction of motion). A more advanced operation is shown in Fig. 6, where both partial motoring and pumping strokes are committed and the machine is operated in both directions of motion. The simulation shows the effect of changing the direction of motion, where a motoring stroke is initiated in section 3. As the shaft direction of motion is changed, the motoring stroke automatically becomes a pumping stroke and it becomes impossible to close the HPV. The next decision is thus to do another motoring stroke by maintaining the HPV open as seen in section 4, where a full motoring stroke is made. The same is illustrated for a pumping stroke in section 5, where a change of shaft direction results in motoring and two pumping decisions subsequently. However, it is possible to close the HPV during the motoring part in section 5, since the pressure difference across the valve remains low.

5 DISCUSSION

Although the presented hybrid dynamical model of the digital displacement chamber agrees well with the physical machine behavior it is not very practical with respect to development of control. The dynamics of each pressure chamber is described by

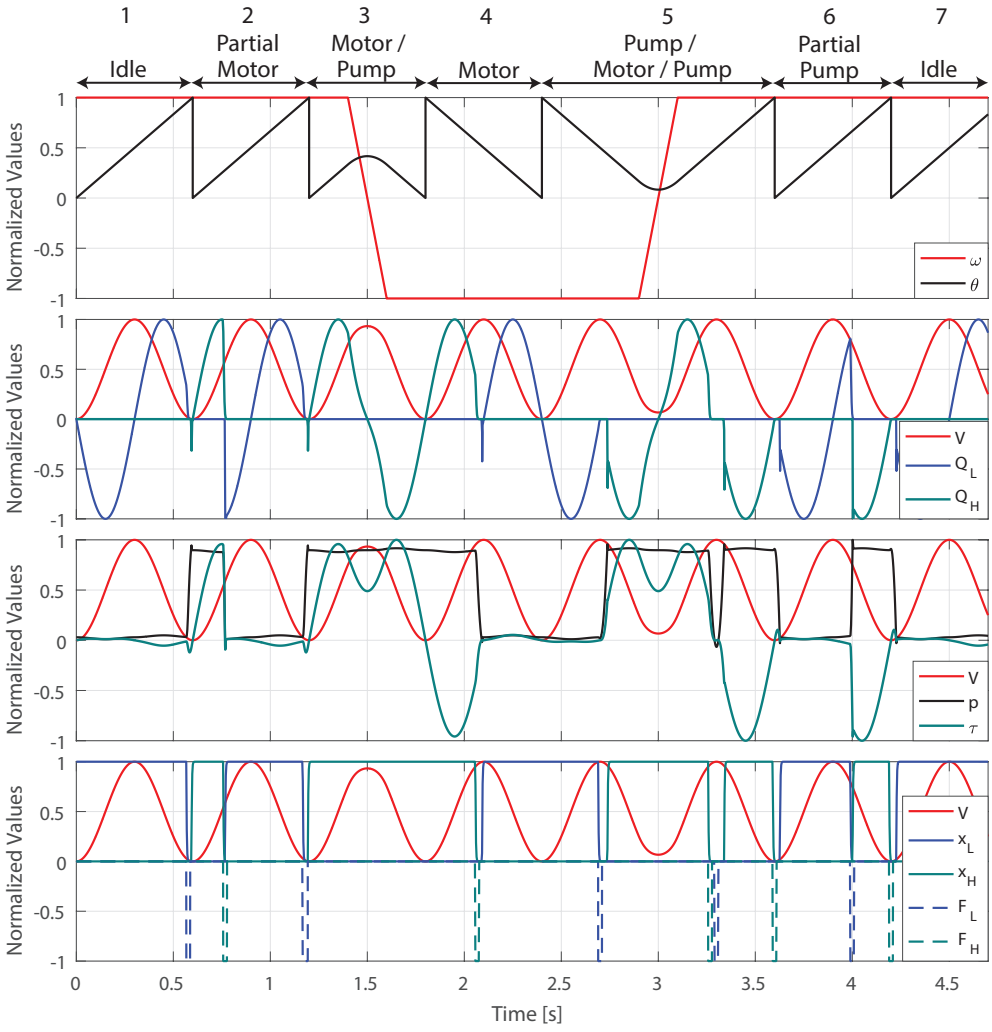

FIGURE 6. Simulation of 4 quadrant operation including partial strokes. Maximum speed: $\dot{\theta} = 100\,\text{rpm}$, $p_\text{H} = 300\,\text{bar}$ and $p_\text{L} = 10\,\text{bar}$

7 states and comprises of three individual sub jump maps. Considering a DD unit with a high number of pressure chambers, the complexity of the hybrid system may become tremendous. An additional drawback of the model, is the inputs being force pulses, where the same response is obtained with many different kinds of input shapes and sizes.

In system wide control, the objective is to control the combined machine output from all pressure chambers and not control each individual pressure chamber separately, which may be considered an internal control objective. With system wide control in mind, it is considered optimal if the hybrid model only comprises the fundamental machine dynamics. Considering the responses in Fig. 5 and Fig. 6, it is seen that the valve dynamics are very fast compared to the remaining dynamics and may therefore be

neglected. Similarly, the pressure build up is relatively fast and by allowing it to jump between the low and high pressure instantaneously, yields a flow and torque output given by

$$Q_{\mathrm{H}} \approx \dot{V} = z\,\frac{V_{\mathrm{d}}}{2}\sin(\theta)\,\omega \quad \tau \approx z\,\frac{V_{\mathrm{d}}}{2}\sin(\theta)\,p_{\mathrm{H}} \tag{9}$$

where $z \in \{0,1\}$ determines whether the pressure chamber is active or inactive. Considering the most simple hybrid representation of the DD unit results in the model given by

$$\begin{aligned} \dot{z} &= 0 && \text{if} \quad u = z \\ z^{+} &= u && \text{if} \quad u \neq z \end{aligned} \tag{10}$$

However, there is a noticeable delay from the angle where the force impulse to close the LPV is applied and the angle where the active stroke starts and an output is generated. Since delays are very important with respect to stability in controlled systems, it is not something that should be neglected. Describing delays in a hybrid system requires timers and since the machine may operate in both direction of motion, several additional states are required to describe the delay. Furthermore, the delay for motoring and pumping decisions are different, such that a significant number of timer related states are necessary. A further complication is due to the activation variable, z, which may not be changed as desired, since the valves cannot be opened/closed against high pressure difference. Also the input remains binary, which is often treated as a duty cycle ratio in control system, but doing this result in a much smoother system which might not be valid. These input delays and constraints may either be implemented in the hybrid dynamical model of the system or in the control law. Nonetheless, the control task for this system remains complex and yet to be solved, even though it is considered crucial with respect to successful deployment of the digital displacement technology.

6 CONCLUSION

This paper presented a hybrid dynamical model of a digital displacement fluid power machine, which includes both the continuous and discrete dynamics of the non-smooth system. The hybrid model resembles the physical behavior of the machine well and allows for operation in all four quadrants, which is not considered possible with simple continuous and discrete approximations. However, since the presented model is rather complex and control of hybrid dynamical systems is a complicated task, it is not deemed suitable for control development. Therefore, a significantly simpler hybrid model structure describing only the fundamental machine dynamics has been proposed. However, to remain reliable with respect to stability, the model requires delay states and are subject to several input constraints, which challenge the design of stabilizing control laws for the system.

ACKNOWLEDGMENT

This research was funded by the Danish Council for Strategic Research through the HyDrive project at Aalborg University, at the Department of Energy Technology (case no. 1305-00038B).

REFERENCES

[1] Schmidt, L., Roemer, D. B., Pedersen, H. C., and Andersen, T. O., 2015. "Speed-variable switched differential pump system for direct operation of hydraulic cylinders". *Proceedings of ASME/BATH 2015 Symposium on Fluid Power and Motion Control, American Society of Mechanical Engineers*.

[2] Jarf, A., Minav, T., and Pietola, M., 2016. "Nonsymmetrical flow compensation using hydraulic accumulator in direct driven differential cylinder application". *Proceedings of the 9th FPNI Ph.D. Symposium on Fluid Power, Florianpolis, Brazil*.

[3] Hansen, A. H., and Pedersen, H. C., 2016. "Optimal configuration of a discrete fluid power force system utilised in the PTO for WECs". *Ocean Engineering,* ***117***, may, pp. 88–98.

[4] Hansen, R. H., Andersen, T. O., Pedersen, H. C., and Hansen, A. H., 2014. "Control of a 420 kN Discrete Displacement Cylinder Drive for the Wavestar Wave Energy Converter". In ASME/BATH 2014 Symposium on Fluid Power and Motion Control, ASME, p. V001T01A021.

[5] Payne, G. S., Kiprakis, A. E., Ehsan, M., Rampen, W., Chick, J. P., and Wallace, A. R., 2007. "Efficiency and dynamic performance of digital displacement hydraulic transmission in tidal current energy converters". *Journal of Power and Energy, Proc. IMechE, Vol. 221, Part A, pp. 207-218.*

[6] Payne, G. S., Stein, U. P. P., Ehsan, M., Caldwell, N. J., and Rampen, W. H. S., 2005. "Potential of digital displacement hydraulics for wave energy conversion". *In Proc. of the 6th European Wave and TIdal Energy Conference, Glasgow UK.*

[7] Pedersen, H. C., Hansen, R. H., Hansen, A. H., Andersen, T. O., and Bech, M. M., 2016. "Design of full scale wave simulator for testing power take off systems for wave energy converters.". *International Journal of Marine Energy, Vol. 13, pp. 130-156.*

[8] Rampen, W., 2006. "Gearless transmissions for large wind turbines the history and future of hydraulic drives.". *Bremen.*

[9] Salter, S. H., Taylor, J. R. M., and Caldwell, N. J., 2002.

"Power conversion mechanisms for wave energy". *Proc. of the Institution of Mechanical Engineers, Part M - Journal of Engineering for the Maritime Environment, pp. 1-27*.

[10] Ehsan, M., Rampen, W., and Salter, S., 1997. "Modeling of digital-displacement pump-motors and their application as hydraulic drives for nonuniform loads". *ASME. J. Dyn. Sys., Meas., Control.*

[11] Rampen, W., 2010. "The development of digital displacement technology". *In Proceedings of Bath/ASME FPMC Symposium*.

[12] Roemer, D. B., 2014. "Design and optimization of fast switching valves for large scale digital hydraulic motors". PhD thesis, Department of Energy Technology, Aalborg University. Department of Energy Technology, Aalborg University.

[13] Noergaard, C., 2017. "Design, optimization and testing of valves for digital displacement machines". PhD thesis, Department of Energy Technology, Aalborg University, Denmark.

[14] Johansen, P., 2014. "Tribodynamic modeling of digital fluid power motors". PhD thesis, Energy Technology, Aalborg University, Denmark.

[15] Johansen, P., Roemer, D. B., Andersen, T. O., and Pedersen, H. C., 2015. "On the Influence of Piston and Cylinder Density in Tribodynamics of a Radial Piston Digital Fluid Power Displacement Motor". In ASME/BATH 2015 Symposium on Fluid Power and Motion Control.

[16] Pedersen, N. H., Johansen, P., and Andersen, T. O., 2018. "Challenges with respect to control of digital displacement hydraulic units". *Modeling, Identification and Control, Vol. 39, No. 2*.

[17] Johansen, P., Roemer, D. B., Andersen, T. O., and Pedersen, H. C., 2015. "Delta-sigma modulated displacement of a digital fluid power pump". *The 7th workshop on digital fluid power, Linz, Austria*.

[18] Sniegucki, M., Gottfried, M., and Klingauf, U., 2013. "Optimal control of digital hydraulic drives using mixed-integer quadratic programming". *Proceedings of the 9th IFAC Symposium on Nonlinear Control Systems*.

[19] Armstrong, B. S. R., and Yuan, Q., 2006. "Multi-level control of hydraulic gerotor motors and pumps". *Proceedings of the american control conference, Minnesota, USA*.

[20] Song, X., 2008. "Modeling and active vehicle suspension system with application of digital displacement pump motor". *Proceedings of the ASME 2008 International Design Engineering Techical Conferences & Computers and Information in Engineering Conference, New York, USA*.

[21] Heikkila, M., and Linjama, M., 2013. "Displacement control of a mobile crane using digital hydraulic power management system". *Mechatronics Volume 23, Issue 4, Pages 452-461*.

[22] Pedersen, N. H., Johansen, P., and Andersen, T. O., 2018. "Feedback control of multi-level pulse-density modulated digital displacement transmission". *Submitted to IEEE/ASME Transaction on Mecatronics, Vol. x, No. x.*

[23] Johansen, P., Roemer, D. B., Pedersen, H. C., and Andersen, T. O., 2017. "Discrete linear time invariant analysis of digital fluid power pump flow control". *Journal of Dynamic Systems, Measurement and Control, Transactions of the ASME, Vol. 139, Nr. 10, 101007*.

[24] Pedersen, N. H., Johansen, P., and Andersen, T. O., 2017. "Event-driven control of a speed varying digital displacement machine". *Proceedings of the 2017 Bath/ASME Symposium on Fluid Power and Motion Control*.

[25] Pedersen, N. H., Johansen, P., Andersen, T. O., and Scheidl, R., 2017. "Non-linear hybrid control oriented modelling of a digital displacement machine". *The Ninth Workshop on Digital Fluid Power, September 7-8, Aalborg, Denmark*.

[26] Christian Noergaard, Michael M. Bech, J. H. C., and Andersen, T. O., 2018. "Modeling and validation of moving coil actuated valve for digital displacement machines". *IEEE Transacton of industrial electronics*.

[27] Christian Noergaard, Jeppe H. Christensen, M. M. B. A. H. H., and Andersen, T. O., 2017. "Test rig for valves of digital displacement machines". *In proc of the Ninth Workshop on Digital Fluid Power, September 8-9, Aalborg, Denmark*.

[28] Christian Noergaard, Esben L. Madsen, J. M. T. J. J. H. C., and Bech, M. M., 2018. "Test of a novel moving magnet actuated seat valve for digital displacement fluid power machines". *Submitted to IEEE/ASME transaction on mechatronics*.

[29] Noergaard, C., Bech, M. M., Roemer, D. B., and Pedersen, H. C., 2016. "Optimization of moving coil actuators for digital displacement machines". *The eighth workshop on digital fluid power, Tampere, Finland*.

[30] Roemer, D. B., Noergaard, C., Bech, M. M., and Johansen, P., 2016. "Valve and manifold considerations for efficient digital digital hydraulic machines". *In proceedings of the eighth workshop on digital fluid power, Tampere Finland*.

[31] Teel, A. R., Sanfelice, R. G., and Goebel, R., 2009. "Hybrid control systems".

[32] Goebel, R., Sanfelice, R. G., and Teel, A. R., 2009. "Hybrid dynamical systems". *IEEE control systems magazine*.

[33] Brogliato, B., 2016. *Nonsmooth Mechanics - Models, Dynamics and Control (third edition)*. Springer.

Paper L

Investigation of Concepts and Operation Strategies for a Wind Turbine with a Digital Fluid Power Transmission

Niels H. Pedersen, Per Johansen and Torben O. Andersen

The paper has not been published

The layout has been revised.

Investigation of Concepts and Operation Strategies for a Wind Turbine with a Digital Fluid Power Transmission

Niels Henrik Pedersen, Per Johansen*, Torben Ole Andersen +

Department of Energy Technology, Aalborg University, 9220 Aalborg, Denmark

nhp@et.aau.dk, *pjo@et.aau.dk, +toa@et.aau.dk

Abstract

Fluid power transmissions has gain increasing attention for use in e.g. wind and wave energy applications, due to high power to weight ratio and being a rugged mechanically decoupled gear. Until recently, fluid power technology has been considered infeasible for use in wind turbine transmissions, because of low part-load efficiencies compared to conventional gearbox drive trains. However, research within digital fluid power (DFP) has led to a successful increase in efficiencies, which makes the technology a competitive alternative. This paper investigates fluid power transmission topologies for a wind turbine application, focusing on the potential of using digital displacement machines. Several transmission concepts are examined, for which possible operation strategies are discussed and performance is compared. With the objective of having a high availability and energy efficiency, as well as low torque pulsations and response time, the outcome is an identification of the most promising fluid power transmission concepts.

1 Introduction

In the offshore wind turbine industry there is a large desire of having a robust and reliable transmission, such that the availability of the turbine is high and the electrical production cost is minimized. A fluid power transmission is known to have these characteristics, while it also provide a mechanical decoupled gear and hydraulic buffering capability. The power transmission in wind turbines has to be rated for peak power throughputs that are significantly higher than average, due to varying wind conditions. Conventional fluid power machines are considered infeasible due to this, since the efficiencies are significantly decreased for diminishing loads.

With the introduction of digital fluid power (DFP) machines, the energy efficiency of hydraulic pumps and motors has been significantly increased, such that the technology is a strong aspirant for use in future large scale power take-off systems. Digital fluid power machines is characterized by having a modular construction with numerous electrical actuated on/off valves controlling the fluid flow throughput of the machine [1].

Artemis Intelligent Power Ltd. has developed the digital displacement machine®, which consist of numerous pressure chambers being flow controlled by these digital valves [2, 3, 4]. The required flow throughput is then determined by specifying the ratio of activated pressure chambers. This way, time averagely any power level may be obtained with a high efficiency, since the losses of inactive chambers are kept very low. Due to the non-smooth behavior of the digital machines, the DFP technology is challenged by the introduced pressure and torque pulsations, as well as the increased complexity.

The performance characteristics of a fluid power transmission is depending on its configuration, whether it is equipped with digital or conventional hydraulic machines and if these are of fixed or variable displacement type. With focus on availability, energy efficiency, torque pulsations and response time, this paper examines fluid power transmission concepts for a variable speed wind turbine. The paper investigates operation strategies and compares performance of the different concepts, for an identification of the most promising fluid power transmission concepts.

2 System Presentation

A fluid power transmission for a variable speed wind turbine comprises of a hydraulic pump and motor. The pump is connected to the turbine rotor shaft and to the hydraulic motor

through pipelines. As a simplification, this study has been limited to investigate a transmission with a single hydraulic pump and motor. Multiple pumps and/or multiple motors and generators may however be used in various combinations and connections to improve the performance. A simplified illustration of a fluid power transmission for a wind turbine is shown in Fig. 1.

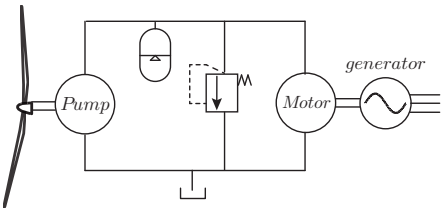

Fig. 1: *Fluid power transmission system for a wind turbine.*

The turbine rotor drives the hydraulic pump, which outputs a pressurized fluid flow driving the hydraulic motor. The motor is further connected to an electrical generator supplying the grid. A hydraulic accumulator may be used to provide buffering capacity and smoothen sudden pressure pulsations. The performance characteristics of the transmission is highly dependent on the choice of pump and motor type, since they may either be fixed or variable displacement, as well as either conventional or digital. To identify the most promising setup, a comparison of the different transmission types are made.

2.1 Hydrostatic transmission types

Independent of the hydraulic machines being conventional or digital, the operation of the transmission is determined by the machine type, whether it is a variable or a fixed displacement machine that is used. With basis in conventional hydraulic machines, there are four different transmission concepts as shown in Fig. 2.

a) *Fixed displacement pump and fixed displacement motor:* Fixed gear transmission similar to a conventional drive train, where a variable speed generator controls the rotor speed. An input to output proportional fixed speed and fixed torque is hence obtained.

b) *Fixed displacement pump and variable displacement motor:* Variable gear transmission, where the motor displacement controls the rotor speed and a fixed speed generator is used. A fixed speed and variable torque output is hence obtained, which allows for use of a synchronous generator.

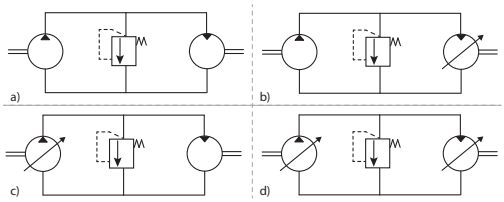

Fig. 2: *a) Fixed displacement pump and motor, b) fixed displacement pump and variable displacement motor, c) variable displacement pump and fixed displacement motor, d) Variable displacement pump and motor.*

c) *Variable displacement pump and fixed displacement motor:* Variable gear transmission, where the pump displacement controls the rotor speed and a variable speed generator controls the pressure. A variable speed and fixed torque output may hence be obtained.

d) *Variable displacement pump and variable displacement motor:* Is the most versatile transmission, since any input/output ratio between torque and speed may be obtained. Again, a synchronous generator may be used in the case of a fixed motor speed. Additionally, alternative control possibilities arises by having an additional controllable input.

To avoid the tediousness of comparing all combinations of fixed and variable type, being either conventional or digital for both the pump and motor, a preliminary selection is conducted. This is done by use of a simple steady state operation analysis of the different fluid power transmissions for a wind turbine. Since the steady state operation is similar regardless of using a conventional or a digital type hydraulic machine, the analysis is simplified to be based on the conventional concepts shown in Fig. 2.

3 Steady state operation

The steady state analysis takes basis in the NREL 5 MW wind turbine, which data is readily available [5]. The rotor power, P_r and torque, τ_r, is statically determined by Eq. 1 and Eq. 2 respectively.

$$P_\mathrm{r} = \frac{1}{2}\, A_\mathrm{r}\, \rho_\mathrm{air}\, C_\mathrm{p}\left(\lambda, \beta\right)\, v^3 \tag{1}$$

$$\tau_\mathrm{r} = \frac{1}{2}\, A_\mathrm{r}\, R_\mathrm{r}\, \rho_\mathrm{air}\, C_\mathrm{q}\left(\lambda, \beta\right)\, v^2 \tag{2}$$

Where A_r, R_r, ρ_air and v is the rotor area, rotor radius, air density and wind speed respectively. $C_\mathrm{p}\left(\lambda, \beta\right)$ and

$C_q(\lambda, \beta)$ are the turbine specific power and torque coefficient respectively. $\lambda = \frac{\omega_r R_r}{v}$ is the turbine tip-speed ratio and β is the blade pitching angle. The turbine rotor speed, ω_r, is described by Eq. 3

$$\dot{\omega}_r = \frac{1}{J_r}\left(\tau_r - d_r\,\omega_r - \underbrace{\frac{\bar{V}_p\,\Delta p}{\eta_p}}_{\tau_p}\right) \tag{3}$$

Where J_r is the combined rotor, hub and shaft inertia mass, d_r is the viscous friction, η_p is the mechanical efficiency, taking the static friction into account. Since efficiency data is not available in the full operation space, it has been considered constant as a simplification, which does not influence the overall operation. The pressure difference between the high and low pressure line, Δp is given in Eq. 4.

$$\dot{\Delta}_p = \frac{\beta_H}{V_H}\left(\underbrace{\bar{V}_p\,\omega_r\,\alpha_p}_{Q_p} - \underbrace{\bar{V}_m\,\omega_m\,\alpha_m}_{Q_m} - \underbrace{k_l\,\Delta_p}_{Q_l}\right) \tag{4}$$

Where $\bar{V}_p$ and $\bar{V}_m$ are the volumetric throughput of the pump and motor respectively. α_p and α_m are the displacement fraction of the pump and motor respectively. β_H is the effective fluid bulk modulus, V_H is the volume in the high pressure line and k_l is the leakage coefficient between the high and low pressure line. The parameter values used in the simulation is provided in Table 3 as an appendix.

In the steady state analysis the dynamics has been omitted, why $\dot{\omega}_r = \dot{\Delta}_p = 0$. The conventional operation strategy for the turbine is utilized, where the reactive drive torque is a function of the rotor speed as shown in Fig. 3.

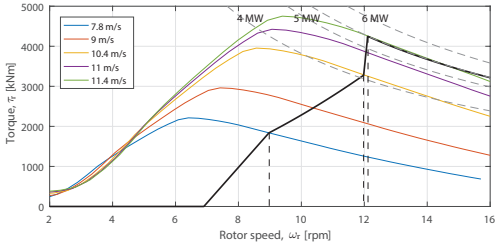

Fig. 3: *Rotor speed versus rotor torque operation curve.*

When rated rotor speed is reached at $\omega_r = 12.1$ rpm, the blade pitching angle is adjusted to yield rated power output at increasing wind speeds. In the simulations of drive train c) and d), the pressure has been controlled to that corresponding to the nominal power output as a simplification. This is however not a necessity, which is elaborated later. The results of the steady state operation analysis is shown in Fig. 4 on plot 1-7.

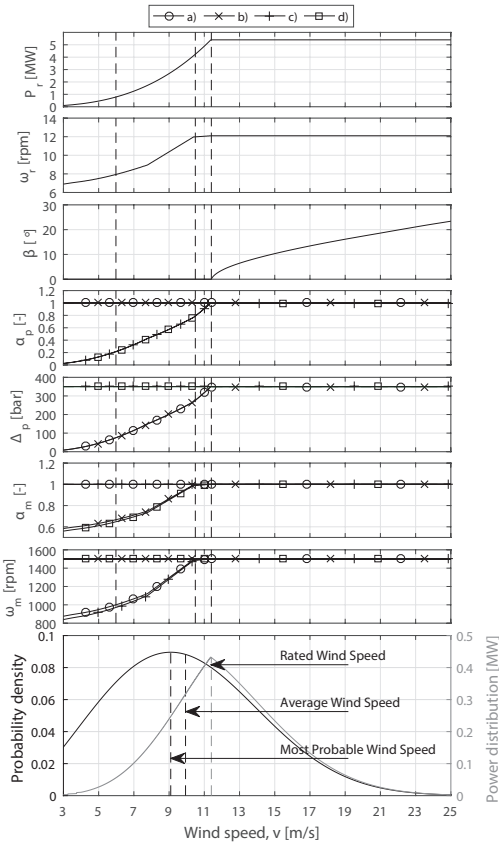

Fig. 4: *Steady state operation of NREL 5 MW wind turbine.*

It is seen that above rated wind speed, all four transmission concepts are operated identically at rated conditions. Below rated wind speed, either the pump displacement or the pressure is varied to control the rotor speed depending on the pump being either variable or fixed. Similar, either the motor displacement or the motor speed is varied to control the pressure depending on the motor type.

To establish a performance characteristic of the different transmission concepts, a wind speed distribution profile has been provided in the bottom plot of Fig. 4. The wind speed probability density is described by a Weibull distribution

function, based on wind data from Horns Rev, Denmark [6]. Furthermore, the bottom plot in Fig. 4 also shows the power distribution function which is the product of the wind speed distribution function and the rotor power shown in the top plot. The power distribution reveals that there is a relative high amount of energy to capture below rated wind speed, why the efficiency of the turbine transmission below rated wind speeds is of high importance.

From Fig. 4 it is seen that drive train c) and d) has low pump displacement fractions for low wind speeds. Conventional variable displacement hydraulic machines are known to have very low part load efficiencies. Fig. 5 shows a typical efficiency maps for a variable bent-axis machine operating at 100 % and 20 % displacement.

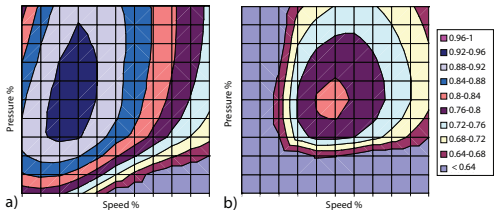

Fig. 5: *Efficiency maps for the bent-axis Rexroth AV6M 250cc machine. a)* 100 % *displacement. b)* 20 % *displacement. Modified from [7].*

Since both the pump speed and displacement is varying when using a variable displacement pump, the efficiency becomes inadequately low at wind speeds having a relatively high power distribution. Having such low part load efficiencies when using a variable displacement pump makes both transmission type c) and d) infeasible. Drive train b) benefits of using a fixed speed generator, thus omitting the necessity of the power converter. Additionally, drive train a) has a slow dynamic performance, since a change in generator speed is not reflected directly in the rotor speed due to fluid compressibility. Therefore, drive train b) is considered the favorable choice when using only conventional hydraulic machines. This is also validated by the major research conducted on use of the transmission type b) concept [8, 9, 10].

Although drive train b) is preferable it still suffers heavily due to low part load efficiency compared to a conventional gearbox transmission. Therefore, it is interesting to investigate the potential of using DFP machines.

4 Digital displacement machines

Replacing the conventional hydraulic machines with digital displacement machines gives alternative topologies, which might be more favorable than the conventional hydraulic drive train type b) (Conv. b)) in Fig. 2. As mentioned in the introduction, the digital displacement machines has a modular construction, where the flow throughput is determined by the ratio of activated pressure chambers. Digital hydraulic machines has several advantages with respect to conventional ones, which could make digital fluid power transmissions the future drive train for wind turbines. Main advantages and disadvantages of the digital displacement machines compared to conventional hydraulic machines are the following:

Advantages:

1. High energy efficiencies both at full and partial load operation, since each pressure chamber may be enabled/disabled on a stroke by stroke basis. Disabled pressure chambers has very low losses and no leakage flow is present due to use of seat valves.
2. Fast dynamic response, since the flow throughput may be changed from minimum to maximum within half a revolution.
3. High availability since the machine functionality persist when single modules fails. (Provided that the valves has a reasonable reliability)
4. Low maintenance cost since failed components may be replaced easily without the use of heavy equipment. (Provided that the valves has a reasonable reliability)
5. Superb scalability due to the modular structure

Disadvantages:

1. Flow and torque throughput contains increased fluctuations due to the non-smooth behavior.
2. Complex system that requires complicated control.
3. Relative new concept that is not commercially available.

The digital displacement machines obviously has some very promising features making them interesting for use in wind turbine drive trains, but is challenged by the non-smooth behavior of the machine.

To be able to compare with the performance of conventional hydraulic machines, Fig. 6 shows the efficiency curve

of a digital displacement machine operating at 100 % and 20 % displacement.

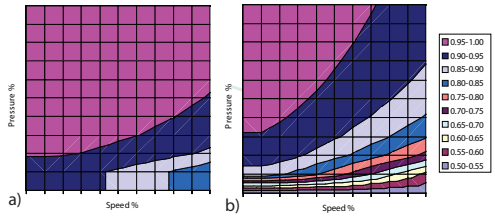

Fig. 6: *Efficiency maps for a digital displacement machine. a)* 100 % *displacement. b)* 20 % *displacement. Modified from [7].*

Due to the machines having almost no leakage flow, the volumetric efficiency of the digital displacement machine is high. Therefore, the efficiency is approximately described by the mechanical losses. The mechanical loss is decreased for increasing pressure difference, while is it is increased for higher speed due to viscous and hydro-kinetic friction. This is seen in the efficiency map, where it is clear that as long as the pressure level is relatively high, the efficiency is above 90 % even at part load operation.

5 Digital fluid power transmission

It has been established that a conventional variable displacement pump is infeasible efficiency wise for a fluid power transmission. As a result only the two drive train topologies using digital displacement machines shown in Fig. 7 are interesting to investigate further.

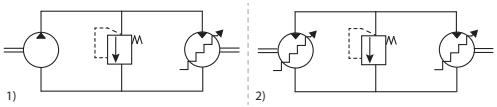

Fig. 7: *1) Conventional fixed displacement pump and digital displacement motor, 2) digital displacement pump and digital displacement motor.*

The digital machines may be operated as either fixed or variable displacement, which has a large influence on the performance characteristics of the transmission. It should be noticed that operating a digital displacement machine with a fixed displacement is not conventional. For a fixed displacement setup, it may be more favorable to utilize mechanical valve actuation instead of electrical, but this is expected to increase the complexity of the machine even further. With the proposed topologies shown in Fig. 7, the transmission concepts given in Table 1 exist. Additionally, a conventional gear box transmission (Ref.) is included for comparison.

Table 1: Combination of components in transmission

		Ref.	Dig. 1		Dig. 2			
			a	b	a	b	c	d
Gearbox:	Multi stage	✓	-	-	-	-	-	-
Pump:	Fixed displacement	-	✓	✓	-	-	-	-
Dig. pump:	Fixed displacement	-	-	-	✓	✓	-	-
	Variable displacement	-	-	-	-	-	✓	✓
Dig. motor:	Fixed displacement	-	✓	-	✓	-	✓	-
	Variable displacement	-	-	✓	-	✓	-	✓
Generator:	Fixed speed	-	-	✓	-	✓	-	✓
	Variable speed	-	✓	-	✓	-	✓	-
Power converter:		✓	✓	-	✓	-	✓	-
Cooling/boost/filter system:		-	✓	✓	✓	✓	✓	✓

To provide an overview of the strengths and weaknesses of the proposed concepts, a comparison based on the five key parameters, availability, torque pulsations, energy efficiency, response time and complexity has been made. The results are provided in Table 2, where $--$ is the worst score and $++$ is the best score.

Table 2: Comparison of transmissions topologies.

Topology	Availability	Torque pulsations	Energy efficiency	Response time	Complexity
Ref.	$--$	$+$	$++$	$++$	$++$
Conv. b)	$-$	$++$	$-$	$+$	$+$
Dig. 1a)	$-$	$+/-$	$+/-$	$-$	$+/-$
Dig. 1b)	$+$	$+/-$	$+/-$	$+$	$+/-$
Dig. 2a)	$+/-$	$-$	$++$	$-$	$+/-$
Dig. 2b)	$++$	$-$	$++$	$+$	$-$
Dig. 2c)	$+/-$	$--$	$++$	$+$	$-$
Dig. 2d)	$++$	$--$	$++$	$++$	$--$

It is seen that topology Dig. 1 using a conventional fixed displacement pump suffers from having significantly reduced efficiencies at partial load operation, while topology Dig. 2 using two digital machines suffers from having increased torque and pressure pulsations. However, using two digital machines also provides the additionally mentioned advantages, like higher availability and lower maintenance cost. Topology Dig. 1a) and 1b) that use a fixed displacement pump and motor, suffers from having a slow

response time and requires the use of a variable speed generator. Since the power converter has a high failure rate, it is considered feasible to use a variable displacement motor coupled with a synchronous generator, which also increases the response time. The conventional fluid power transmission Hyd. b) has over several decades been considered infeasible due to poor efficiencies compared to a conventional gearbox transmission. This results in three potential fluid power topology candidates, being Dig. 1b), Dig. 2b) and Dig. 2d), which all has their clear strengths and weaknesses.

6 Discussion and Conclusion

It is clear that the main challenge of using digital displacement machines is the introduced pressure and torque pulsations, which puts additional requirements to the mechanical structure. It is assessed that a fluid power transmission using both a digital pump and motor is the favorable choice if the torque and pressure pulsations can be kept below an acceptable level. This is justified by the high efficiency and potentially high availability, accepted that the reliability of the digital valves are sufficiently high. Furthermore, having both a variable displacement pump and motor yields the fastest response time of the hydrostatic transmissions, as well as an increased control flexibility.

With the established results, it is considered interesting to further investigate the potential of a fluid power transmission comprising both a digital displacement pump and motor. Specially the attention should be drawn towards using variable displacement machines, since the additional control possibilities might bring the cutting edge compared to the other concepts. From the efficiency curves in Fig. 6, it is seen that it is beneficial to maintain a high operation pressure. However, it is also desired for the grid to be supplied with a uniform power having a high quality (matching voltage, frequency and power factor with respect to the grid). Using both a variable displacement motor and pump, the control objective may be altered continuously based on the operation conditions.

7 Appendix

Table 3: Parameters of the hydrostatic transmission

Parameter	symbol	value	Unit
Pump mechanical efficiency	η_p	0.95	-
Volumetric pump displacement	$\bar{V}_\mathrm{p}$	121.88	L/rad
Viscous friction coefficient	d_r	50	kNm/s
Transmission leakage coefficient	k_l	0.01	$\mathrm{L}/(\mathrm{bar\,s})$
Synchronous motor speed	ω_m	1500	rpm
Volumetric motor displacement	$\bar{V}_\mathrm{m}$	0.89	L/rad

References

[1] Linjama, M., 2011. "Digital fluid power state of the art". *The Twelfth Scandinavian International Conference on Fluid Power, May 18-20, Tampere, Finland*.

[2] Payne, G. S., Stein, U. P. P., Ehsan, M., Caldwell, N. J., and Rampen, W. H. S., 2005. "Potential of digital displacement hydraulics for wave energy conversion". *In Proc. of the 6th European Wave and TIdal Energy Conference, Glasgow UK*.

[3] Ehsan, M., Rampen, W., and Salter, S., March 2000. "Modeling of digital-displacement pump-motors and their application as hydraulic drives for nonuniform loads". *ASME, Journal of dynamic system measurement and control, Vol. 122, pp. 210-215*.

[4] Rampen, W., 2010. "The development of digital displacement technology". *In Proceedings of Bath/ASME FPMC Symposium*.

[5] Jonkman, J. M., Butterfield, S., Musial, W., and Scott, G., 2009. Definition of a 5-mw reference wind turbine for offshore system development.

[6] Feng, J., and Shen, W. Z., 2015. "Modelling wind for wind farm layout optimization using joint distribution of wind speed and wind direction". *Energies 8, pp. 3075 - 3092*.

[7] Rampen, W. "Gearless transmissions for large wind turbines - the history and future of hydraulic drives". Artemis IP Ltd., Scotland.

[8] Dolan, B., and Aschemann, H., 2012. "Control of a wind turbine with a hydrostatic transmission - an extended linearilinear approach". *In 17th International Conference on Methods and Models in Automation and Robotics, 445-450. Miedzyzdroje, Poland*.

[9] Wang, F., and Stelson, K. A., 2013. "Model predictive control for power optimization in a hydrostatic wind turbine". *The 13th Scandinavian International Conference on Fluid Power, Linkping, pp. 155-160*.

[10] Laguna, A. J., Diepeveen, N. F. B., and van Wingerden, J. W., Oct. 2013. “Analysis of dynamics of fluid power drive-trains for variable speed wind turbines: Parameter study”. *IET Renewable Power Generation, vol. 8, no. 4, pp. 398-410.*

ISSN (online): 2446-1636
ISBN (online): 978-87-7210-345-7

AALBORG UNIVERSITY PRESS